Chemical Reaction Engineering—Houston

In Chemical Reaction Engineering—Houston; Weekman, V., et al.;
ACS Symposium Series; American Chemical Society: Washington, DC, 1978.

Chemical Reaction Engineering—Houston

Vern W. Weekman, Jr., EDITOR
Mobil Research and Development Company
Dan Luss, EDITOR
University of Houston

The Fifth International Symposium on Chemical Reaction Engineering co-sponsored by the American Chemical Society, the American Institute of Chemical Engineers, the Canadian Society for Chemical Engineering, and the European Federation of Chemical Engineering, held at the Hyatt Regency Hotel, Houston, TX, March 13–15, 1978.

ACS SYMPOSIUM SERIES 65

AMERICAN CHEMICAL SOCIETY
WASHINGTON, D. C. 1978

Library of Congress CIP Data

International Symposium on Chemical Reaction Engineering, 5th, Houston, Tex., 1978. Chemical reaction engineering—Houston.
(ACS symposium series; 65 ISSN 0097-6156)

Bibliography: p.

Includes index.

1. Chemical engineering—Congresses. 2. Chemical reactions—Congresses.
I. Weekman, Vern W. II. Luss, Dan, 1938- . III. American Chemical Society. IV. Title. V. Series: American Chemical Society. ACS symposium series; 65.

TP5.I67 1978 660.2'9'9 77-25340
ISBN 0-8412-0401-2 ACSMC 8 65 1-619 (1978)

PRINTED IN THE UNITED STATES OF AMERICA

ACS Symposium Series

Robert F. Gould, *Editor*

Advisory Board

In Chemical Reaction Engineering—Houston; Weekman, V., et al.;
ACS Symposium Series; American Chemical Society: Washington, DC, 1978.

FOREWORD

The ACS SYMPOSIUM SERIES was founded in 1974 to provide a medium for publishing symposia quickly in book form. The format of the SERIES parallels that of the continuing ADVANCES IN CHEMISTRY SERIES except that in order to save time the papers are not typeset but are reproduced as they are submitted by the authors in camera-ready form. As a further means of saving time, the papers are not edited or reviewed except by the symposium chairman, who becomes editor of the book. Papers published in the ACS SYMPOSIUM SERIES are original contributions not published elsewhere in whole or major part and include reports of research as well as reviews since symposia may embrace both types of presentation.

In Chemical Reaction Engineering—Houston; Weekman, V., et al.;
ACS Symposium Series; American Chemical Society: Washington, DC, 1978.

PREFACE

The Fifth International Symposium on Chemical Reaction Engineering has, as in past symposia, provided an excellent forum for reviewing recent accomplishments in theory and application. This international symposium series grew out of the earlier European Symposia on Chemical Reaction Engineering which began in 1957. In 1966, as part of the American Chemical Society Industrial and Engineering Chemistry Division's Summer Symposium series, a meeting was devoted to chemical reaction engineering and kinetics. This meeting highlighted the great interest and activity in this field in the United States, and led the organizers to join with the American Institute of Chemical Engineers and the European Federation of Chemical Engineers in organizing International Symposia on Chemical Reaction Engineering. The first symposium was held in Washington in 1970 and was followed by symposia in Amsterdam (1972), Chicago (1974), and Heidelberg (1976).

These meetings consistently attract experts in the field who have submitted many more papers than can be accommodated. This year was no exception with more than 130 papers being submitted, only 48 of which could be accepted. Again, the international flavor was maintained with more than one-half the papers coming from Western Europe, in addition to one each from Russia, Japan, Australia, and Canada.

While industrial participation was not as extensive as anticipated (30%), it did show clearly the increasing and productive application of Reaction Engineering tools to industrial problems.

The meeting format maintained three plenary review lectures each morning and three parallel, original paper sessions in the afternoon. The nine plenary review papers are being published in the American Chemical Society Symposium Series as a separate volume.

We acknowledge financial support from the National Science Foundation, American Chemical Society-Petroleum Research Fund, Shell Oil Co., Mobil Oil Corp., and Exxon Co.

VERN W. WEEKMAN, JR.
Mobile Research Corp.
Princeton, NJ

DAN LUSS
University of Houston
Houston, TX

October 1977

In Chemical Reaction Engineering—Houston; Weekman, V., et al.;
ACS Symposium Series; American Chemical Society: Washington, DC, 1978.

Organizing Committee

for the

Fifth International Symposium on

Chemical Reaction Engineering

Vern W. Weekman, Jr., *Editor*
Dan Luss, *Editor*

Members: Chandler H. Barkelew (Shell Development Co.)
K. B. Bischoff (University of Delaware)
John B. Butt (Northwestern University)
James M. Douglas (University of Massachusetts)
Hugh M. Hulburt (Northwestern University)
Donald N. Miller (Dupont Co.)

In Chemical Reaction Engineering—Houston; Weekman, V., et al.;
ACS Symposium Series; American Chemical Society: Washington, DC, 1978.

1

Design and Operation of a Novel Impinging Jet Infrared Cell-Recycle Reactor

R. LEAUTE and I. G. DALLA LANA

Department of Chemical Engineering, University of Alberta, Edmonton, Alberta, Canada

In the study of chemisorbed species on catalyst surfaces, the application of infrared spectroscopic methods has developed from the early *in situ* studies of Eischens and Pliskin [1] to rather detailed surface kinetics measurements [5]. The variety of techniques which have been described [1,2,3,4,5,6,7,8] increase in their effectiveness with their ability to discriminate between the spectra of adsorbed species which are relevant to the reaction mechanism and spectra of spurious adsorbed species. These approaches may be classified using this criterion as follows:

(i) Intrinsic Rates/Surface Spectra Transients Measured Directly. Under reaction conditions where adsorbed reactants, intermediates, and products display significant IR absorption band intensities, the transient intensities may be quantitatively monitored. Considerable detailed studies are required to correlate these intensities with surface concentrations.

(ii) Global Rates/Surface Spectra Static or Transient. By carrying out studies in an IR cell - circulation flow reactor, a cause-and-effect relation between reactant concentration and specific band intensities may be discerned. Such mechanistic insights may be useful in developing more reliable forms of rate expressions.

(iii) Indirect Studies of Adsorption and Surface Reactions. The observation of selected spectral band intensities attributed to chemisorbed species are assumed to be related to the surface reactions involved. If the spectra are recorded at room temperature, the presence of spurious spectra may occur. Generally, additional experimental evidence is required to demonstrate the relevance of such observations to the kinetics of the catalytic reaction.

In Chemical Reaction Engineering—Houston; Weekman, V., et al.;
ACS Symposium Series; American Chemical Society: Washington, DC, 1978.

This paper describes the development of an improved version of the IR cell-recycle reactor (type (ii)) which is to be used to study the mechanism and kinetics of reactions of 2-propanol on various alumina catalysts. While this reaction does not have direct commercial implications (dehydration or dehydrogenation), it exhibits many of the characteristics which make it very suitable to demonstrate the usefulness of the IR technique.

Design Factors

The *in situ* technique involves catalyst pellets in the form of very thin wafers, about 40 mg/cm^2 alumina content. The high surface area, about 4 m^2/cm^2 of IR beam cross-section, enables sufficient adsorbed species to interact with the IR beam even at relatively low surface coverages ($\sim 10^{17}$ molecules/cm^2 IR beam) that spectra with good resolution may be obtained.

In studying solid-catalyzed gas-phase reactions, the background spectra resulting from the gas-phase are usually eliminated by use of a double-beam IR spectrophotometer, in which the sample cell is matched with an "identical" reference cell without catalyst in it. Variations in pressure and/or temperature between sample and reference cells increase the difficulty of matching the two cells. When the catalyst wafer is placed transverse to the flow of gases through the IR cell-reactor, the flow patterns within the cell lead to concentration gradients along the axis of the IR beam, and between the front and rear surface concentrations on the wafer. Under reaction conditions, these aspects limit the sensitivity of the technique because of low surface coverages at reaction temperatures. The new cell attempts to eliminate many of these objectionable features.

Figure 1a describes a typical geometry for previous cell designs. It should be evident that it is difficult to obtain values of the intrinsic reaction rate because of the uneven contacting between the gas and wafer at various points on the wafer surface. High recirculation rates within such a steady-state recycle reactor provide differential values of the reaction rate, but these global values are unlikely to equal intrinsic rates (neglecting, for the moment, intraparticle diffusion). Compatibility of flow patterns between the IR cell and an ideal continuous stirred-tank reactor are required as a minimum condition. Since the mode of heating the wafer likely involves IR-transparent windows being at temperatures lower than those of the wafer, compensation for temperature gradients may also be required.

Figure 1b describes the proposed geometry of the improved IR cell-reactor. This recycle reactor is to be capable of being operated in either open (flow) or closed (batch) modes of operation. The reactor unit is maintained at the reaction temperature (up to 400°C) and the pump and sampling system are maintained at a constant usually lower temperature (220°C) to ensure maximum

In Chemical Reaction Engineering—Houston; Weekman, V., et al.;
ACS Symposium Series; American Chemical Society: Washington, DC, 1978.

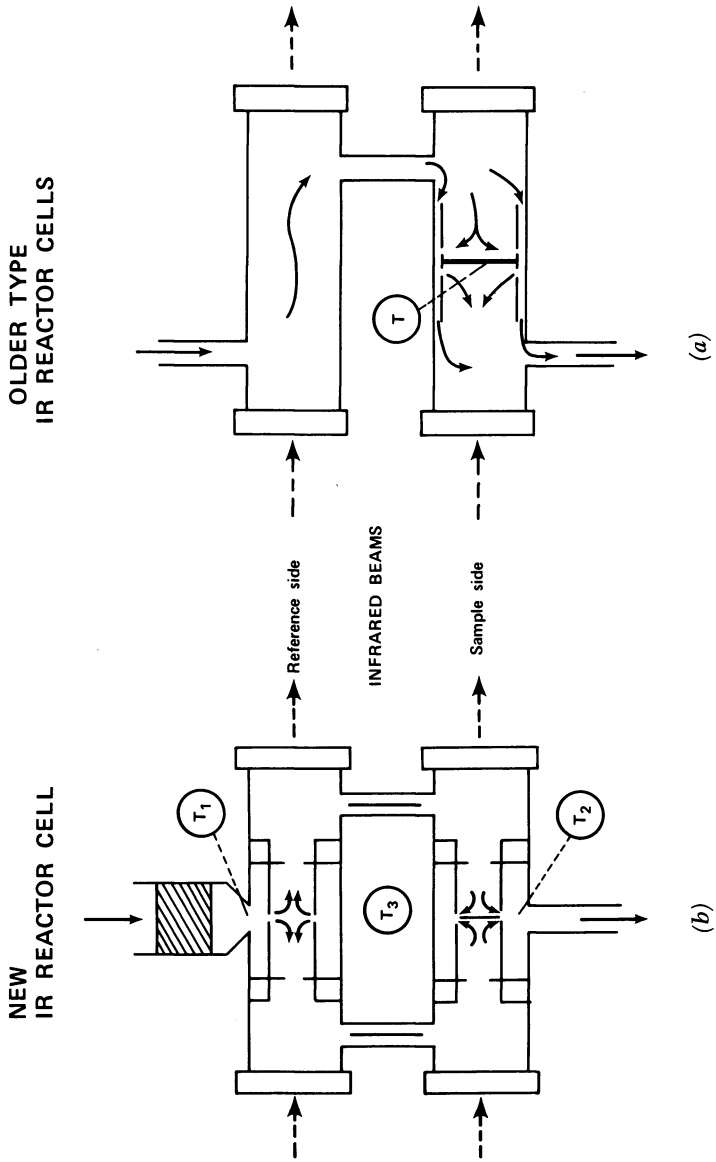

Figure 1. Geometrical arrangement and flow patterns in typical and improved ir cell-reactors

longevity of equipment.

Figure 2 describes the information flow between the IR spectrophotometer and an IBM/1800 computer system which are interfaced. The spectral data are monitored at wave number intervals as low as 0.2 cm^{-1} over the complete spectral scan range of the spectrophotometer (about 700 to 4000 cm^{-1}, corresponding to a maximum of about 16,000 data points). The "% transmission" versus "wave number" points are transmitted in digitized form to the computer from absolute encoders. At present, the complete spectral scan may be monitored and stored in a disk file and retrieved at a later time. The coupled Model 621 spectrophotometer with IBM/1800-compatible interface was purchased some time ago from Perkin-Elmer.

The improved cell utilizes axisymmetric jets of feed gas impinging upon both sides of the wafer to develop a highly turbulent field over most of the wafer surface. This enables global reaction rates to approximate intrinsic reaction rates at high flow-rates and in the absence of pore diffusion.

The new configuration shown in Figure 1 is housed in an oven-type enclosure controlled at the temperature, T_3, by internal air circulation. In addition to the oven heater, a second heater about the inlet section, packed with glass beads, raises the circulating gas temperature from the reduced temperature in the pump compartment to T_1. Because of heat losses from the IR windows, the temperature difference, T_3-T_2, could range as high as 50°C. This not only changes the density of the flowing gas but also results in a considerable deviation of the true temperature of the catalyst wafer from the measured values T_2. Additional heaters placed around the ends of the two cylindrical sections compensated for the window heat losses. In this way, the temperatures, T_2 and T_3, could be matched within 0.5°C, and the wall temperature would be expected to differ from T_2 (or T_3) only if the catalytic reaction exhibited severe thermal effects. With greatly improved mass transfer rates normal to the wafer surface, one would also expect from similarity considerations enhanced heat transfer between the wafer surface and the impinging gas jet. Such adjustments among the three monitored temperatures enabled the reference cell IR beam to compensate nearly exactly for the sample cell gas phase absorption spectra.

By changing the configuration of the two cells in the sample compartment of the IR spectrophotometer this enables the determination of either recirculating gas composition or plotting of the baseline spectrum for the catalyst wafer. With the two cells in the double-beam mode, the catalyst baseline and surface spectra are recorded. If the reference cell was placed in the sample beam and an air gap in the reference beam, quantitative absorption spectroscopy was possible. The IR cells thus provide information leading to both reaction rates and mechanistic insights concerning adsorbed species at reaction conditions.

When used as a recirculating batch reactor, the spectrophotometer-computer interface can monitor but not record the "% trans-

In Chemical Reaction Engineering—Houston; Weekman, V., et al.;
ACS Symposium Series; American Chemical Society: Washington, DC, 1978.

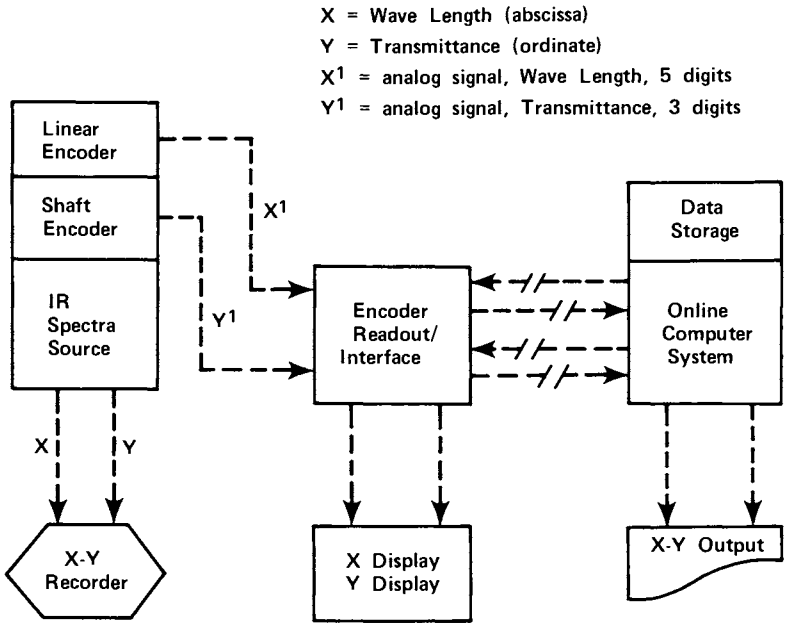

Figure 2. Information flow between ir spectrophotometer and digital computer

In Chemical Reaction Engineering—Houston; Weekman, V., et al.;
ACS Symposium Series; American Chemical Society: Washington, DC, 1978.

mission" at a fixed "spectral frequency" (usually that of a specified absorption band). At present, the drum chart on the IR recorder plots the time - absorption band intensity relation corresponding to transient reaction conditions. The time constant of the spectrophotometer thermocouple sensor was sufficiently small that the transient reaction rates could be recorded.

Experimental Performance

1. Mass Transfer Performance tests were designed to test for micromixing or for mass transfer performance and thus, to facilitate definition of the cell design specifications. Limited reaction data had been recorded for the 2-proposal reaction over alumina.

Figure 3 summarizes the mass transfer characteristics which were observed in a protptype cell with naphthalene used for the wafer material. Air flows between 10 and 50 ℓ/min were passed through the cell and the corresponding sublimation rates, mg/min, were recorded. Since the cell geometry was held constant for a series of flow rates and the temperatures were always at room temperature, the coordinates of Figure 3 show the measured sublimation rates versus flow rate rather than Reynolds number. The exponent of the flow parameter (given by the slope of the line) is seen to remain nearly constant over a wide range of conditions verifying that the turbulent flow regime is maintained. The influence of changing the orifice size used to create the jets, and of the spacing between the orifice and the wafer upon mass transfer rates are also shown.

In addition to the above tests with the new design, mass transfer rates were also observed for cell-reactors of the old type, with wafers positioned both parallel and transverse to flows. These tests suggest that in such geometries much of the stream bypasses the wafer surface making it difficult to obtain intrinsic rates of reaction. Furthermore, contacting of the gas flow with localized portions of the periphery of the wafer resulted in abnormally high local mass transfer rates. Figure 3 demonstrates that old type cell designs provide mass transfer performance inferior to that observed with the impinging jets.

By calculating mass transfer coefficients from the usual equation for the rate of sublimation, gmol/(min)(g catalyst).

$$r_s = k_g a \left(C_{surface} - C_o\right)$$

and using the bulk gas phase concentration, $C_o = 0$, and external area, a=10 cm^2, some experimental coefficients could be compared to values estimated from published correlations. Table 1 shows these results.

In Chemical Reaction Engineering—Houston; Weekman, V., et al.;
ACS Symposium Series; American Chemical Society: Washington, DC, 1978.

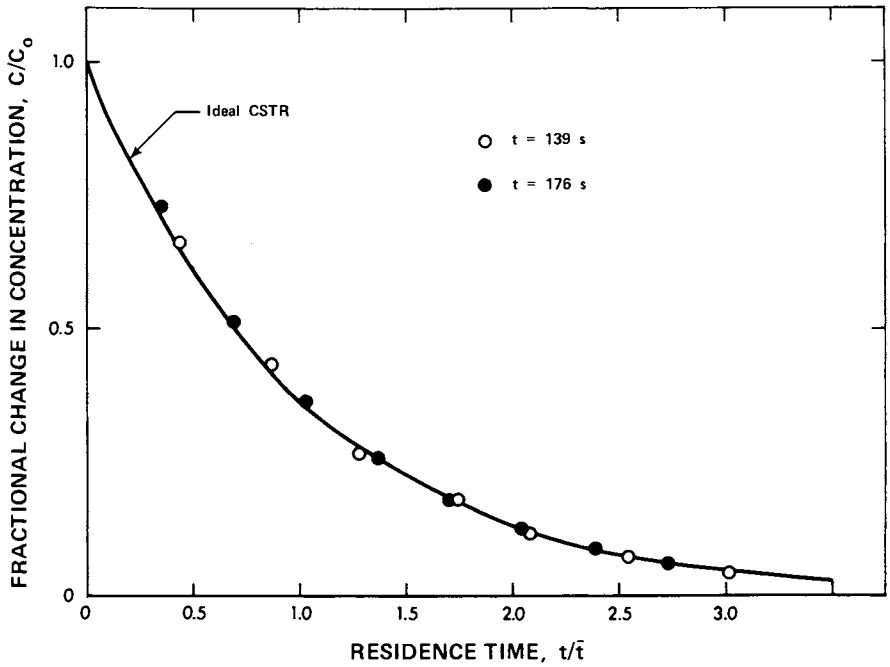

Figure 3. Sublimation rate of naphthalene in various cell-reactor prototypes as influenced by flow-rate through cell

Table 1
Comparison of Mass Transfer Coefficients (cm/sec)

Model	Flow = 10 ℓ/min	Flow = 50 ℓ/min
Flat plate in perpendicular flow	1.3 cm/sec	2.9 cm/sec
Sphere of equal area in a packed bed	2.1	5.4
Experimental wafer, conventional geometry	1.6	3.0
Experimental wafer, new geometry	3.7	9.2

Table 1 and Figure 3 both illustrate the marked superiority of the new IR cell-reactor design in promoting mass transfer at the wafer surface. However, it still remains to be demonstrated that under reaction conditions, intrinsic rates of reaction may be obtained at the flow rates mentioned.

In Chemical Reaction Engineering—Houston; Weekman, V., et al.;
ACS Symposium Series; American Chemical Society: Washington, DC, 1978.

2. Mixing Within Cell The analysis of performance within a differential bed-recycle reactor is usually compared to that of a continuous stirred-tank reactor. By operating the reactor with an inert wafer and by introducing alcohol to the feed as a step change in concentration, the mixing performance of this reactor may be compared to that predicted for an ideal CSTR of comparable volume. Figure 4 illustrates such a comparison and indicates substantial agreement with the ideal behaviour. It may be expected that channelling, stagnation of some flow, etc. are absent from the recycle reactor within the range of performance of the pump.

3. Double-beam Compensation for Gas Phase Absorption When recording IR spectra at reaction temperature, the IR beams are attenuated by the number of molecules in the beam path. Since the gas phase population is likely only one or two orders of magnitude greater than the number of similar molecules adsorbed on the wafer surface, it is important that the gas phase beam attenuation in the two cells be balanced as well as possible. For example, a pressure drop between the two cells necessitates heating the upstream cell to reduce its gas density to that in the downstream cell. Similarly, differences in temperature between the cells must also be compensated.

Such inbalances between reference and sample cell gas phases required calibrations to determine the values of T_1 required, for a fixed value of T_2 ($\simeq T_3$) and given circulation rate at various isopropanol concentrations in the gas-phase, to blank out gas phase absorption spectra. Figure 5 shows how spectral bands in the 1200-1500 cm^{-1} region from gas phase isopropanol can be altered be changing T_1. Curve B represents near-extinction of the background whereas curves A and B represent under- and over-compensation, respectively.

4. Dehydration of 2-Propanol over Alumina The preliminary measurements of spectra for adsorbed species will be used to illustrate how the mechanism of reaction may be clarified. The main feature of the IR cell-flow reactor is its capability of determining spectra at reaction conditions. Most published work on the dehydration of isopropanol by alumina describes *in situ* studies with spectra recorded with the cell at room temperature.

Figure 6 reveals absorption bands in selected regions of the spectrum for several concentration levels of isopropanol vapour. Each curve, A, B, or C, represents a spectral scan at steady-state reaction conditions with all reaction parameters except feed composition of isopropanol being kept constant. If different curves (A, B, and C) result, the adsorbed species associated with the spectra are considered to be germane to the reaction mechanism. In the event that the spectral bands do not change the adsorbed species are considered to be spurious. Subsequently, the reactor may be operated in a batch mode and the questionable band monitored continuously. The failure of this band to change with the extent of reaction would provide extra support to the view that the band is associated with a by product species not involved in the dehydration mechanism.

In Chemical Reaction Engineering—Houston; Weekman, V., et al.;
ACS Symposium Series; American Chemical Society: Washington, DC, 1978.

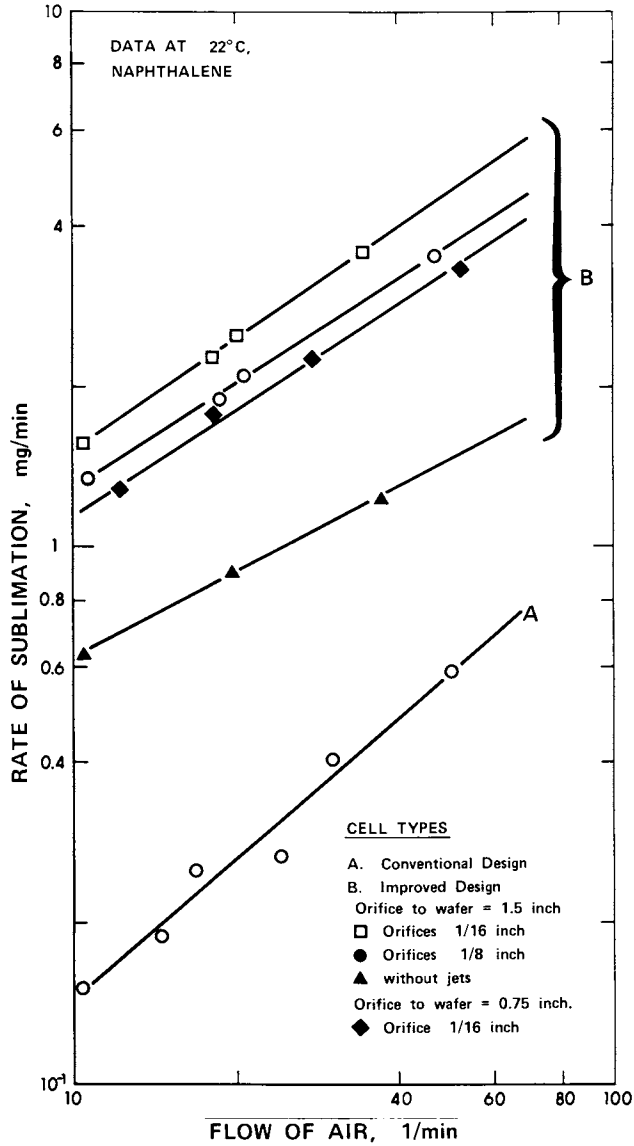

Figure 4. Comparison between ideal CSTR and improved cell-reactor to step change in input concentration

In Chemical Reaction Engineering—Houston; Weekman, V., et al.;
ACS Symposium Series; American Chemical Society: Washington, DC, 1978.

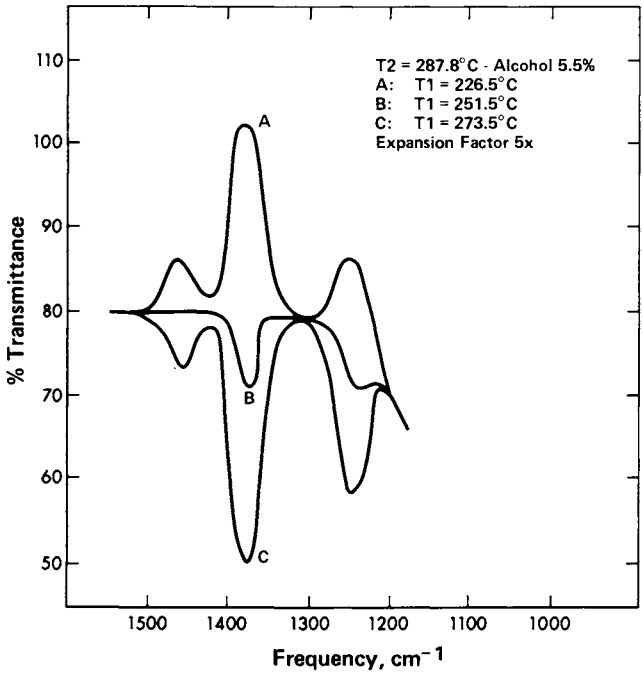

Figure 5. Compensation of gas-phase adsorbance between reference and sample cells

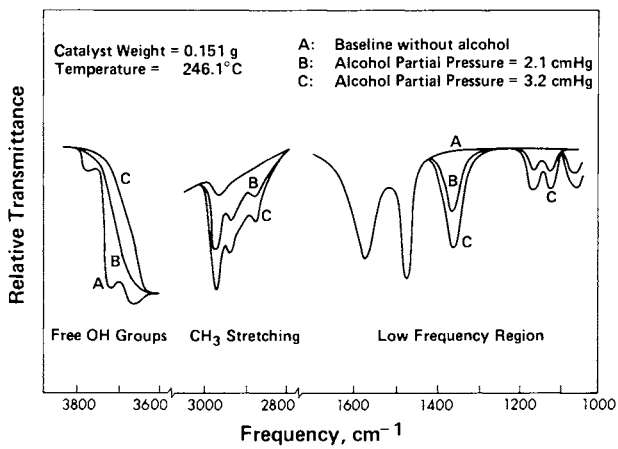

Figure 6. Steady-state spectral scans for dehydration of isopropanol at reaction conditions

The steady-state spectral scans when recorded on the IBM/1000 may be processed.

(i) to subtract the baseline of the catalyst wafer from each spectral scan at varying partial pressures of the isopropanol;

(ii) to subtract one spectral scan at $(P_{alcohol})_1$ from another spectral scan at $(P_{alcohol})_2$ to ascertain the magnitude of the change in band intensities at given band frequencies.

A preliminary interpretation of the spectra shown in Figure 6 would suggest the following observations. The free hydroxyl groups on the surface of alumina progressively disappear, A to B to C, with increasing reactant concentration, isopropanol. This implies that the alcohol hydrogen bonds to these hydroxyl sites but it is not clear whether the alcohol O or H atom in its hydroxyl group is involved.

The stretching vibrations from the methyl groups in isopropanol also display direct correspondence between their surface concentration and that of the isopropanol vapour concentration. This information suggests that isopropanol adsorption on γ-alumina involves more than one adsorption band, i.e. both hydroxyl and emthyl groups are bonded and likely to different sites on the surface of alumina.

In the low frequency region, region I relates to carbon chain skeletal vibrations and region II to symmetrical C-H deformation vibrations in the methyl group. Both of these observations are in accord with a multi-site adsorption model. Region III shows the stretching vibration for a carboxylate species formed on the surface. Since the band intensities in region III do not change with isopropanol vapour concentration, the spectra are considered incidental to the reaction mechanism. With additional experiments, it should be possible to distinguish which surface sites on the alumina are specifically involved and thus to propose a reaction mechanism compatible with such chemical evidence. During the above spectral measurements, steady-state reaction rates in the recirculation reactor were also determined. These rates may then be used to test the kinetic model resulting from observations of the spectra of adsorbed species.

Comments

1. The use of a "single-wafer" catalytic recycle reactor system requires strict attention to operating parameters, if one aspires to obtain intrinsic rates of reaction. By modifying the flow past the wafer to ensure highly turbulent conditions on both sides of the wafer, mass transfer rates may be more than doubled over those observed in the old design of cells in which flow is transverse to the wafer surface. This indicates that the utilization of both sides of the wafer is greatly improved and that the average mass transfer rates are also enhanced.

In Chemical Reaction Engineering—Houston; Weekman, V., et al.;
ACS Symposium Series; American Chemical Society: Washington, DC, 1978.

2. Ideal mixing (CSTR) is obtained with the recirculating rates available from the bellows pump used to this system. The corresponding residence time distribution function is not of value in the analysis of the kinetics since it is anticipated that non-linear rate expressions will be encountered.
3. The usefulness of a combined IR-kinetics study in establishing a more reliable kinetic model is apparent. The processing of such data to ascertain which spectral bands are significant is usually a very tedious chore. By interfacing the IR spectrophotometer to a digital computer, a number of data processing simplifications are evident. Full use of this situation has not yet been attained in this program. Whether or not improved resolution of minor spectral bands results from an online computer facility still remains to be demonstrated for this reaction system.
4. The problem of isolating intrinsic rates of reaction from reaction rates measured in a single-wafer reactor appears to have been reduced but not necessarily solved. If relative intensities of absorption bands exhibited by reactants or reaction intermediates can be ascertained as a function of time, it may be possible to check rate expressions based upon a single step being rate-controlling.
5. Many extensions of this technique (using the new reactor) are evident in the study of catalytic kinetics. Some aspects worth pursuing include:
   (i) a study of pore diffusion under controlled conditions; varying wafer thickness at constant porosity should provide a direct means of calculating the effectiveness factor as a function of wafer thickness.
   (ii) the role of trace amounts of catalyst promoters or inhibitors may be examined using IR techniques and correlated directly with steady-state reaction rates.

Acknowledgements

Financial support of this project by the National Research Council of Canada is gratefully acknowledged.

Literature Cited

1. Eischens, R.P., Pliskin, W.A., Advan. Cata., (1957), 9, 662.
2. Heyne, H., Tompkins, F.G., Proc. Roy. Soc., (1966), A292, 460.
3. Baddour, R.F., Modell, M., and Goldsmith, R.L., J. Phys. Chem. (1968), 72, 3621.
4. Dent, A.L., and Kokes, R.J., J. Phys. Chem, (1970), 74, 3653.
5. Tamaru, K., Onishi, T., Fukada, K., Noto, Y., Trans. Faraday Cos., (1967), 63, 2300.
6. Thornton, R., Ph.D. thesis, University of Delaware 1973,
7. Shih, Stuart Shan San, Ph.D. thesis, Purdue University, 1975.
8. London, J.W., Bell, A.T., J. Cat., (1973), 31, 36-109.

2

Performances of Tubular and Loop Reactors in Kinetic Measurements

GERHARD LUFT, RAINER RÖMER, and FRITZ HÄUSSER

Institut für Chemische Technologie der Technischen Hochschule Darmstadt, 61 Darmstadt, Petersengstrasse 15, West Germany

Industrial reactors in which highly exothermic, heterogenous catalytic reactions are carried out are sensitive if the reaction conditions or the cooling rates are suddenly changed. They can be operated only in a small range in order to avoid damage to the apparatus or to the catalyst by super heating, also to avoid loss in yield by side reactions, favoured at high temperatures.

In addition, poor accuracy in the rate data, as well as in the mass and heat transfer parameters, do not allow to calculate the exact concentration and temperature profiles inside the reactor. This leads to incorrect prediction of the reactor's dynamic behaviour. Therefore these data should be determined as accurately as possible.

For the measurement of reaction rates, differential reactors having extremely short catalyst beds or integral reactors with relative long catalyst beds are often used. In the first type of experimental reactor, the concentration and temperature gradients within the catalyst beds are negligibly small. Due to this fact, the reaction rate point data can be measured, provided the small concentration differences can be accurately analyzed. In the integral reactor, the change in concentration is much higher. There is in general no difficulty analyzing the concentrations of the reacting species but, the reaction rates have to be determined from the concentration curves by calculation and cannot often be related to the fast changing temperature. Because of these obvious disadvantages, the so-called loop reactors are being used more and more in kinetic studies. In loop reactors, the extremely small concentration and temperature gradients desired within the short catalyst bed, along with sufficiently high concentration difference between the reactor inlet and the

© 0-8412-0401-2/78/47-065-015$05.00/0

In Chemical Reaction Engineering—Houston; Weekman, V., et al.;
ACS Symposium Series; American Chemical Society: Washington, DC, 1978.

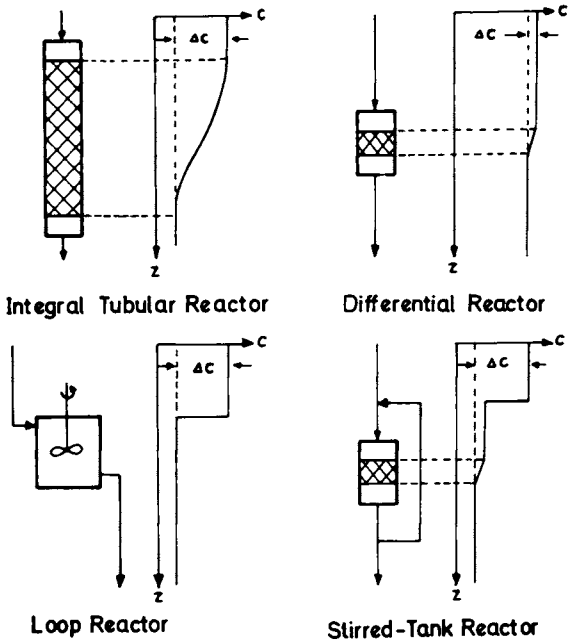

Figure 1. Types of laboratory reactors

In Chemical Reaction Engineering—Houston; Weekman, V., et al.;
ACS Symposium Series; American Chemical Society: Washington, DC, 1978.

outlet, can be realized by recycling a part of the reaction products.

In order to see how these advantages could be realized in practice, the performance of a loop reactor was compared with that of a conventionally-built integral reactor. In this comparison the capability to handle actual industrial catalysts, the settling time of changing experimental conditions, the difficulty of the mathematical evaluation of the measured data were considered. The accuracy of the datas for scale up problems was checked in a pilot plant. For the reaction, the oxidation of o-xylene with a vanadiumpentoxide catalyst, an industrially important process, was chosen.

Apparatus

The design of the loop reactor (Fig. 2) permits changes in the reaction conditions, such as temperature, concentration and throughput in a wide range. Its core is a differential reactor directly coupled to the blower. It sucks the reactants through the catalyst bed and recycles part of it. This design allows only a small dead volume and a small pressure drop across the catalyst bed even at high flow rates. Furthermore, the whole apparatus is compact and therefore it can easily be maintained at constant temperature. The small temperature and concentration gradients within the catalyst bed, necessary for the kinetic measurements, can be realized by recycling part of the gas about 12 m^3/h. It is very large compared to the feed and corresponds to recycle ratios of 1oo to 5oo, also sufficient for the appropriate study of highly-exothermic reactions. The recycle ratio can be changed with respect to the reaction conditions by changing the speed of rotation of the blower.

The blower is driven by an asynchronousmotor whose rotor is fixed to the shaft of the blower. It is separated from the stator by means of a pressure tube in order to exclude any leakage.

The integral apparatus (Fig. 3) consists of a tubular reactor of 1 m-length. In order to measure the concentration, about 2o sampling taps are installed along the tube. Through each sampling tap, a thermocouple is passed to determine the temperature profile. The air is fed through driers, flow meters and heaters before entering vaporizer, where xylene is evaporated. This air-xylene mixture, containing about o.9 Mol% xylene, is fed to the top of the tubular reactor. The phthalicanhydride, leaving the reactor is washed and condensed by water in a spray tower. The reaction heat is removed by an efficient cooling system in which diphenyl (Dow therm) is vaporized.

In Chemical Reaction Engineering—Houston; Weekman, V., et al.;
ACS Symposium Series; American Chemical Society: Washington, DC, 1978.

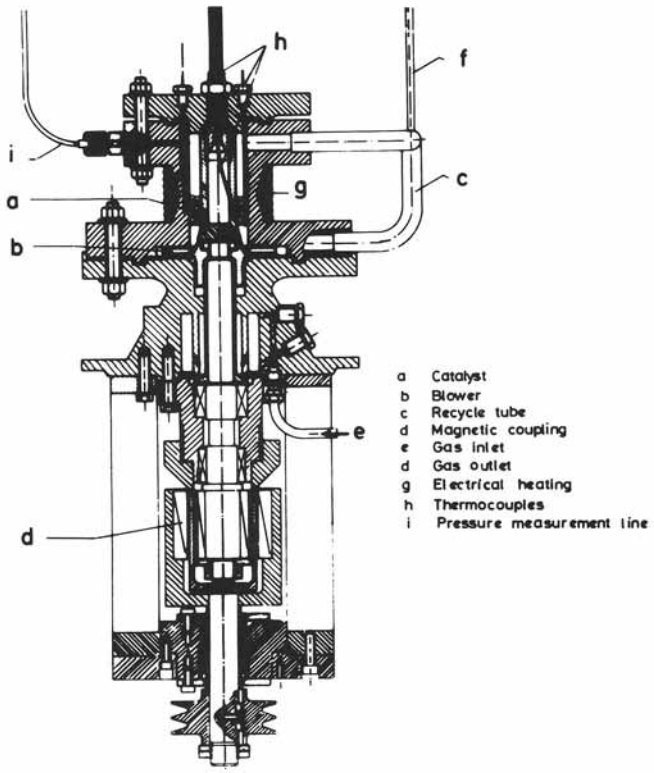

Figure 2. Loop reactor

In Chemical Reaction Engineering—Houston; Weekman, V., et al.;
ACS Symposium Series; American Chemical Society: Washington, DC, 1978.

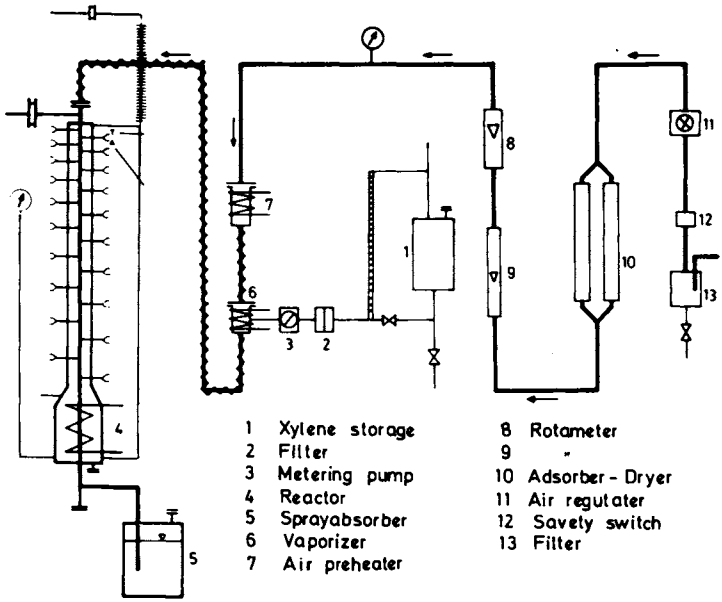

Figure 3. Tubular reactor for the oxidation of xylene

In Chemical Reaction Engineering—Houston; Weekman, V., et al.;
ACS Symposium Series; American Chemical Society: Washington, DC, 1978.

Results and evaluation

The measurements in both reactors were carried out at steady state. The catalyst activity was maintained at all times, testing at regular intervals for any loss in activity.

The results of a typical experiment are shown in Fig.4. The concentration of the reactants is plotted versus a modified residence time. The residence time could be varied along the range 1-1o g.h/mole by changing the throughput and the quantitiy of catalyst.

The temperature was kept constant at 41o°C. The xylene concentration in the feed could be increased up to 1,3 mol %, which is higher than the lower explosion limit. As it can be seen from the curves, the concentration of the xylene feed decreases steadily with increasing residence time. The concentration of the mai reaction product phthalicanhydride (PSA) increases first, then decreases at high residence times due to its oxidation forming CO and CO_2.Also the concentration of the intermediate products tolualdehyde (TOL) and phthalide (PI) which are considered together for simplicity, pass through a maximum.

In the integral reactor, the experiments could not be carried out isothermally (Fig. 5). The temperature (left ordinate) rises steeply in the first part of the catalyst bed, passes through a distinct maximum and decreases again by the cooling.

The xylene is almost completely converted. The concentration of the PSA increases at first steeply, then tends to level off in the lower part of the reactor. Carbonmonoxide (CO) and carbondioxide as well as maleicanhydride which was detected at a low concentration, increase steadily along the catalyst bed whereas the curve of tolualdehyde and phthalide show a maximum similar to the loop reactor experiments.

The evaluation of the experiments in both reactors was based on the mechanism of the oxidation. The concentration profiles measured in the integral reactor, as well as the finite slope in the origin of the concentration-residence time curves from the loop reactor, reveal that, the xylene is converted by simultaneous reactions to the products phthalicanhydride, phthalide, toluylaldehyde, CO and CO_2. The distinct maximum of the phthalide- and tolualdehyde -concentration curve indicates that these are intermediate products which are converted mainly to phthalicanhydride in a consecutive step. From the decrease of the PSA-concentration at high residence times it may be concluded that, this species oxidize to CO, CO_2, as well as water and to a lower extend, to MSA. For the evaluation of the ex-

In Chemical Reaction Engineering—Houston; Weekman, V., et al.;
ACS Symposium Series; American Chemical Society: Washington, DC, 1978.

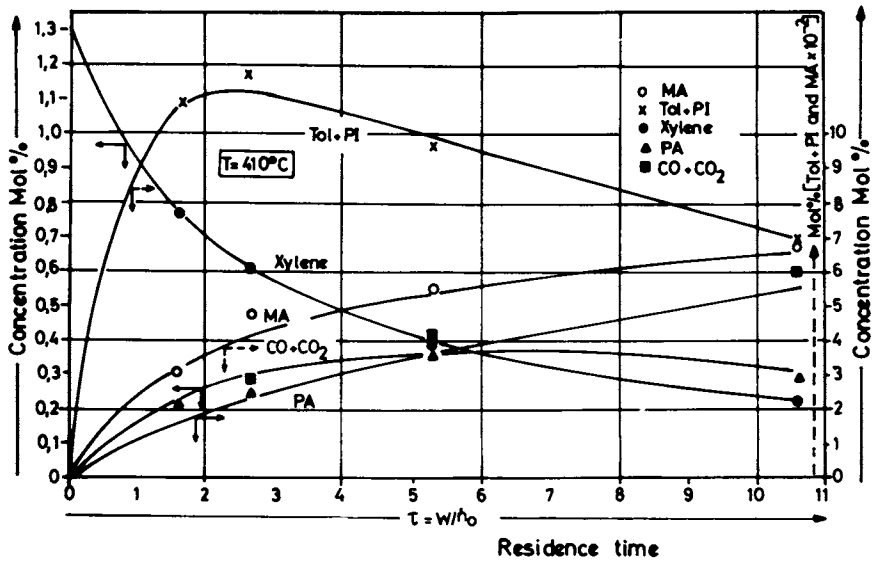

Figure 4. Results of loop-reactor experiments

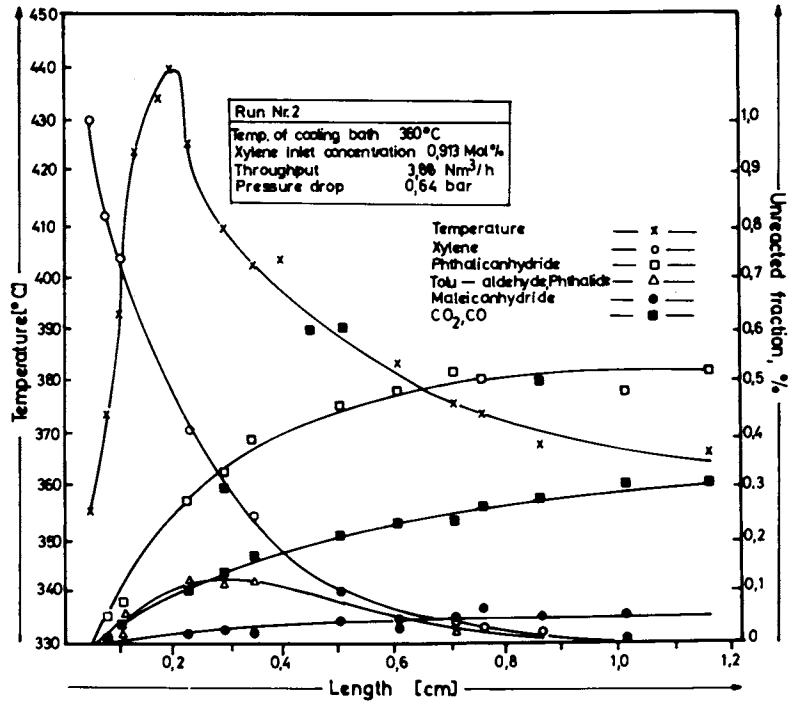

Figure 5. Concentration and temperature distribution in integralreactor

In Chemical Reaction Engineering—Houston; Weekman, V., et al.;
ACS Symposium Series; American Chemical Society: Washington, DC, 1978.

perimental results, it is considered useful to simplify the mentioned reaction scheme; thus, the concentrations of tolualdehyde and phthalide were included together. The small quantities of MSA were neglected.

At the high recycling ratios the loop reactor operates as an ideal stirred-tank reactor. Therefore, the reaction rate can immediately be determined from the difference in concentration between the feed and the outlet, the throughput and the quantity of catalyst.The rate equation, describing the consumption of xylene and the formation of the reaction products, are considered to be pseudo first order. The parameter of the rate equations, which are the frequency factors and the activation energies, are determined by least square methods. In the above function (Fig. 6b) r is the measured rate, $\hat{r}$ is calculated with estimated parameters, w represent appropriate weight factors and N is the number of measured values. Because the rate equations could be differentiated with respect to the unknown kinetic parameters, the objective function was minimized by a stepwise regression.

The steep concentration and temperature profiles in the integral reactor did not allow to determine the reaction rates immediately. Therefore, the objective function contains the measured and the calculated concentrations instead of the reaction rates, also the temperatures because of the nonisothermal reactor behaviour. The kinetic parameters must be obtained by direct search techniques like the derivative free simplex method of Nelder and Mead.

Comparison

Comparing the two laboratory reactors it may be noticed that the loop reactor is more expensive. Although the quantity of catalyst and the volume of the loop reactor is small, compared to the integral reactor, the recycling of a large volume of gas requires a complicated blower.

However, certain advantages and disadvantages result from the different concentration and temperature distribution in both reactors. Because of the uniform concentration and temperature inside the loop reactor, the concentration of the reactants could be measured only in the reactor inlet and outlet to determine the reaction rate. The steep concentration and temperature gradients inside the integral reactor require measurements at many spots along the tube. This becomes rather expensive in time if several components are to be analyzed as in the oxidation of xylene.

In the evaluation of the experimental results the distribution of concentration and temperature appear

In Chemical Reaction Engineering—Houston; Weekman, V., et al.;
ACS Symposium Series; American Chemical Society: Washington, DC, 1978.

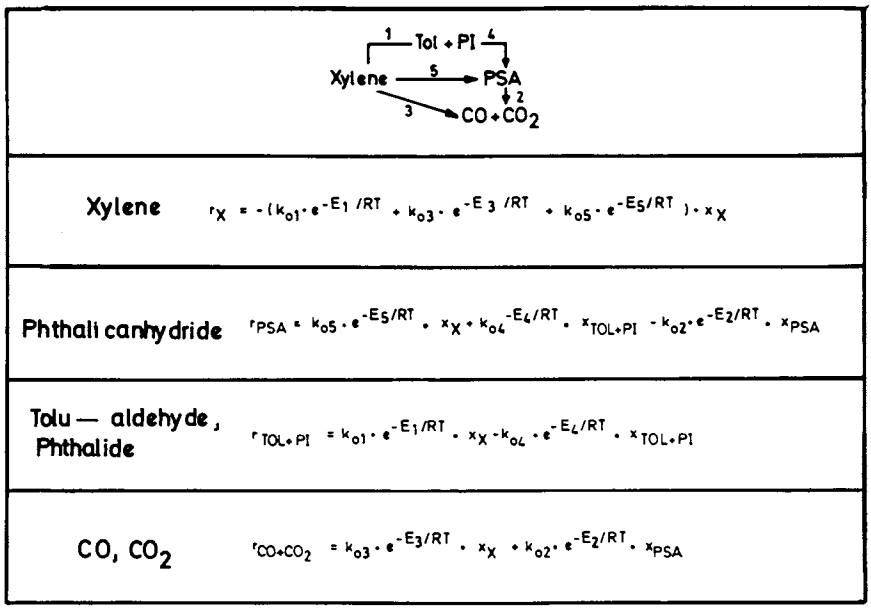

Figure 6a. Rate equations

$$\Phi = \sum^{N} w_X (r_X - \hat{r}_X)^2 + \sum^{N} w_{PSA} (r_{PSA} - \hat{r}_{PSA})^2 + \sum^{N} w_{TOL+PI} (r_{TOL+PI} - \hat{r}_{TOL+PI})^2 + \sum^{N} w_{CO,CO_2} (r_{CO,CO_2} - \hat{r}_{CO,CO_2})^2$$

X	Xylene	N	Number of runs
PSA	Phthalic anhydride	W	Appropriate weight factor
TOL	Tolu — aldehyde	$\hat{r}$	Reaction rate, calculated
PI	Phthalide	r	— " —, measured

Figure 6b. Objective function

In Chemical Reaction Engineering—Houston; Weekman, V., et al.;
ACS Symposium Series; American Chemical Society: Washington, DC, 1978.

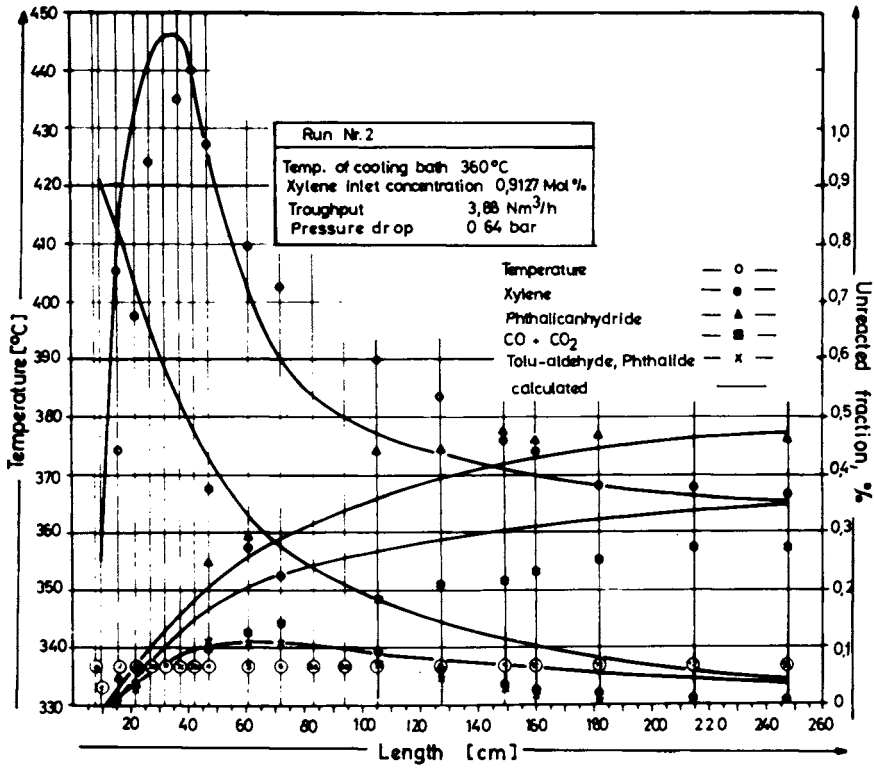

Figure 7. Comparison of the loop-reactor data with pilot plant experiments

In Chemical Reaction Engineering—Houston; Weekman, V., et al.;
ACS Symposium Series; American Chemical Society: Washington, DC, 1978.

to be the basic factors introducing difficulty. The loop reactor can be described by simple algebraic equations of which the coefficients, pertaining to the unknown frequency factors and activation energies, can be obtained by stepwise regression. In the case of the integral reactor, the estimation parameters are more complicated and requires more computation time because of the necessity for numerical integration of a set of differential equations.

In order to check the accuracy of the measured data and collect information for scale-up, additional experiments were carried out in a pilot plant and the results were compared with these previously obtained in the laboratory reactors. The pilot plant reactor consisted of a tube of 25 mm inner diameter and 4 m length taken from an industrial multitube reactor. It was filled with about 1 kg catalyst pellets. The measured temperature- and concentration profiles are plotted in Fig. 7 versus the length of the catalyst bed. The points are experimentally determined whereas the thick-line curves have been calculated using the kinetic constants obtained in the loop reactor experiments. A close agreement between the experimental results of the pilot reactor and the calculated values is apparent. Only the calculated CO and CO_2 concentrations are a little high, causing also a higher temperature maximum.

Recommendations

As the experiments in the loop reactor can be carried out isothermally and at constant concentrations and the influence of mass transfer can be excluded by a high flow rate and small catalyst pellets, the loop reactor is to be recommendated for kinetic studies. Further advantages are the flexibility of the reactor with respect to changes in experimental conditions and last but not least the uncomplicated evaluation of the measured data.

The integral reactor shows some advantages in the study of the product quality and selectivity because technical conditions can easily be incorporated. Furthermore, it is possible to measure simultaneously the heat conductivity in the catalyst bed and the heat transfer coefficient through the reactor wall.

The difficulties in the evaluation of the experiments depend strongly on the mathematical model which has to be chosen. The evaluation is certainly more complicated if the reactor must be described by a two-dimensional model because of steep radial temperature gradients as we have observed it in the phthalic anhydrid reactor.

In Chemical Reaction Engineering—Houston; Weekman, V., et al.;
ACS Symposium Series; American Chemical Society: Washington, DC, 1978.

3

Kinetic Measurements of the Hydrogenation of Carbon Monoxide (Fischer-Tropsch Synthesis) Using an Internal Recycle Reactor

A. ZEIN EL DEEN, J. JACOBS, and M. BAERNS

Lehrstuhl für Technische Chemie, Ruhr-Universität Bochum, Postfach 102148, D-4630 Bochum, West Germany

The Fischer-Tropsch-synthesis has gained renewed interest during the last years. Its goal being nowadays the formation of mainly lower olefins as chemical feedstocks (1-5). From this point of view kinetic measurements on the hydrogenation of CO have been performed in an internal recycle reactor with a differently pretreated catalyst containing oxides of iron, manganese, zinc and potassium. Catalysts containing manganese have been described recently (4,5) as suited for producing short-chain olefins such as ethylene and propylene. The experimental results of this investigation are discussed with respect to product distribution and the rate determining step of the synthesis reaction.

Experimental Procedure

The internal recycle reactor as described elsewhere (6) used for the experiments was charged with about 60 g of catalyst which was thermally pretreated and reduced with hydrogen before the synthesis reaction. During the synthesis recycle ratios (recycled volume per time and weight of catalyst divided by space velocity under operating conditions) of more than 20 were used to establish ideal mixing as well as isothermal operation and to avoid transport limitation due to film resistance.

The measurements were conducted in two different regions of catalyst performance: After reduction and operation of about 5 to 10 hrs under synthesis conditions the activity reached a constant level where it remained for upto 60 to 70 hrs during which the kinetic measurements were performed; thereafter the activity decreased continously.

The analysis of the reaction mixture (H_2, CO, CO_2, and the various C1- to C4-hydrocarbons) was carried out by gaschromatography.

© 0-8412-0401-2/78/47-065-026$05.00/0

In Chemical Reaction Engineering—Houston; Weekman, V., et al.;
ACS Symposium Series; American Chemical Society: Washington, DC, 1978.

Experimental Conditions

The pelletized catalyst (D = 3,7 mm, L = 6,2 mm) was thermally treated for 20 hrs at 300°C and subsequently reduced with H2 for 50 hrs at 300°C (catalyst A) and at 500°C (catalyst C). These treatments resulted in different surface areas S and average pore diameters $\bar{d}_p$:

A: 13,4 m^2/g $\bar{d}_p$ = 4,6 nm (meso-pores)

C: 10,4 m^2/g $\bar{d}_p$ = 3,8 nm (meso-pores)

The total pore volume amounted in both cases to 0.4 cm^3/g. Catalyst C was used in two different forms: First, it was used as pretreated above (C-I); secondly the catalyst (C-II) was further treated under conditions similar to synthesis (T = 258 to 323°C, p(total) = 5; 10 and 15 bar) at a level of conversion of about 40 % resulting in some disintegration before kinetic tests were conducted.

The kinetic measurements with catalysts A, C-I and C-II were performed under the following conditions:

Catalyst	T[°C]	p_{total} [bar]	Space velocity (STP) [1/h]	X_{CO} [%]
A	233-270	5;10;15	366-4480	8-65
C-I	323	5;10	872-3752	8-34
C-II	309-335	10;15	1180-5580	18-45

The feed gas was in all instances composed of 40.1 vol-% CO, 39.3 vol-% H2 and 20.4 vol-% Ar.

Experimental Results

The CO was converted under all conditions to about 45 to 48 % CO2 thus, resulting in a nearly constant ratio of CO-to H2-conversion of 1.4 to 1.6. This means that the water formed during the hydrogenation is mainly reduced to H2. The formation of carbon and/or carbonaceous material insoluble in xylene was almost negligible. The remainder of CO i.e. approximately 52 to 55 % yielded hydrocarbons of which only the C1- to C4-fraction is quantitatively detailed in the following.

Selectivity. The selectivity of the hydrocarbon formation is almost independent on CO-conversion and partial pressure of carbon monoxide and hydrogen in the range studied for the catalysts A and C-I during the period of constant activity as exemplified in Figure 1 A/B; the selectivity is, however, dependent upon the catalyst used, catalyst A producing significantly less C1- to C4-hydrocarbons than catalyst C-I and also a

In Chemical Reaction Engineering—Houston; Weekman, V., et al.;
ACS Symposium Series; American Chemical Society: Washington, DC, 1978.

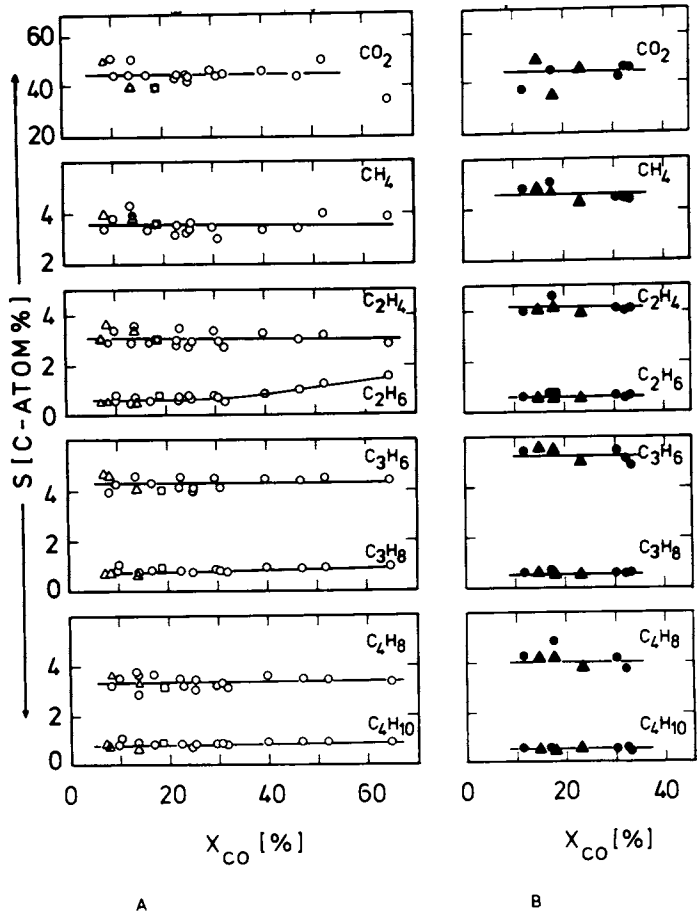

Figure 1. Dependence of selectivity S on CO-conversion X(CO). (A) catalyst A; T = 256°C; P(total) = 15 (□), 10 (○), 5 (△) bar; (B) catalyst C–I; T = 322°C; P(total) = 10 (●), 5 (▲) bar.

In Chemical Reaction Engineering—Houston; Weekman, V., et al.;
ACS Symposium Series; American Chemical Society: Washington, DC, 1978.

smaller portion of olefins. This difference may be, however, due to the different temperatures of reaction; for catalyst C a higher one was necessary to obtain measurable conversions at otherwise comparable conditions. The effect of temperature is discussed later in some more detail. A change of selectivity is, however, observed during catalyst deactivation (Table I); in the

Table I: Effect of operating time on performance of catalyst A with respect to conversion X(%) and selectivity S(C-atom%) at constant temperature (256°C), pressure (10 bar) and space velocity (822 h^{-1} S.T.P).

time [h]	2,42	8,08	11,83	21,52	35,75	47,50	63,67	79,17	95,42
X_{CO}	26,87	31,30	29,10	27,33	28,02	27,75	27,02	25,10	23,20
X_{H_2}	18,00	18,80	18,50	18,50	18,47	18,90	17,72	16,23	15,30
X_{CO}/X_{H_2}	1,49	1,66	1,57	1,48	1,52	1,47	1,52	1,55	1,52
$S(CO_2)$	52,33	46,52	46,67	49,69	48,07	50,81	50,52	47,77	46,59
$S(CH_4)$	2,57	3,45	3,92	4,46	4,71	4,65	4,51	4,98	5,04
$S(C_2H_6)$	0,45	0,73	0,82	0,99	1,11	1,15	1,11	1,27	1,34
$S(C_2H_4)$	2,57	3,77	4,19	4,72	4,75	4,54	4,18	4,50	4,27
$S(C_3H_8)$	0,78	1,12	1,13	1,28	1,28	1,30	1,22	1,27	1,29
$S(C_3H_6)$	3,65	5,30	5,77	6,37	6,53	6,20	5,96	6,29	6,12
$S(i\text{-}C_4)$	0,04	0,13	0,07	0,11	0,11	0,11	0,11	0,12	0,13
$S(n\text{-}C_4)$	0,82	1,09	1,13	1,28	1,25	1,22	1,18	1,27	1,25
$S(1\text{-}C_4^{=}+i\text{-}C_4^{=}+i\text{-}C_5)$	3,01	4,44	4,78	5,16	5,25	4,94	4,77	5,06	4,87
$S(t\text{-}2\text{-}C_4^{=}+n\text{-}C_5)$	0,67	0,86	0,86	0,95	0,96	0,94	0,96	1,00	0,99
$S(c\text{-}2\text{-}C_4^{=}+3\text{-}M\text{-}C_4(1))$	0,33	0,45	0,48	0,51	0,53	0,50	0,52	0,52	0,47
$\sum S_i$	67,21	67,86	69,83	75,52	74,55	76,36	75,05	74,06	72,37

latter case the ratio of olefin to paraffin diminishes although the absolute amount of the various olefinic hydrocarbons stays constant.

Activity. The activity of the catalysts was quantitatively expressed by the rate of reaction as moles of component consumed or formed respectively per time and weight of catalyst which could be measured directly by definition of the recycle reactor. The activity was greatest for catalyst A when compared with C on an equal temperature basis; the activity of C-II was higher than C-I. The latter dependence is probably caused by the smaller particle size of C-II which was obtained during pretreatment. The various overall reaction rates were found to be only slightly dependent on carbon monoxide partial pressure as is shown in Table II for the three catalysts; the dependence on p(CO) is not very

In Chemical Reaction Engineering—Houston; Weekman, V., et al.;
ACS Symposium Series; American Chemical Society: Washington, DC, 1978.

Table II: Correlation between reduced reaction rate r_i/p_{H_2} and partial pressure of carbon monoxide

$r_i/p_{H_2} = k_i \cdot p_{CO}^{n_i}$ mole/(g-cat.·h·bar)

Component i	Catalyst A			Catalyst C-I			Catalyst C-II		
	$k_1 \cdot 10^5$	n_i	$R^2(p_{CO})$	$k_1 \cdot 10^5$	n_i	$R^2(p_{CO})$	$k_i \cdot 10^5$	n_i	$R^2(p_{CO})$
CO	108	-0.22	0.53	116	0.22	0.41	223	0.04	0.03
CH_4	3.64	-0.31	0.88	5.08	0.22	0.63	7.42	0.20	0.39
C_2H_4	1.94	-0.39	0.85	2.73	0.15	0.30	4.22	0.13	0.21
C_2H_6	0.22	+0.18	0.64	0.30	0.43	0.69	0.57	0.27	0.81
C_3H_6	1.72	-0.40	0.65	2.38	0.14	0.28	2.85	0.32	0.47
C_3H_8	0.20	+0.01	0.01	0.24	0.22	0.42	0.27	0.41	0.74
C_4H_8	1.11	-0.46	0.66	1.38	0.09	0.07	1.35	0.45	0.48
C_4H_{10}	0.17	-0.10	0.15	0.15	0.25	0.33	0.14	0.54	0.84
pressure range of CO	1.8 to 5.2 bar			1.8 to 3.8 bar			2.9 to 5.6 bar		
Temperature	$T_R = 255 \pm 1°C$			$T_R = 321 \pm 1°C$			$T_R = 322 \pm 1°C$		

significant as can be derived from the correlation coefficient R^2 [p(CO)] which is also given in this table. This result is in agreement with earlier publications (7,8) assuming that the rate is proportional only to p(H2) and not in any way to p(CO) when the active surface is almost completely covered with CO.

The temperature dependency of the overall reaction rates was derived from Arrhenius plots (Figure 2) for which reaction rates measured at comparable conversions and equal partial pressures of CO and H2 were used. The apparent activation energies E_a and the preexponential reaction rates r_o are listed in Table III for catalysts A and C-II. The activation energies for the individual compounds obtained for the two catalysts are almost equal considering that the accuracy of E_a is approximately 5 to 10 %.

Discussion

Based on the afore communicated experimental results some specific aspects of the reaction scheme and of the rate determining steps of the Fischer-Tropsch-synthesis are discussed in the following.

Product distribution. A relationship between the rate of formation of the individual hydrocarbon and its chain length may be formulated by the following equation when assuming that the carbon skeleton is built up by stepwise addition of one carbon atom to an adsorbed

In Chemical Reaction Engineering—Houston; Weekman, V., et al.;
ACS Symposium Series; American Chemical Society: Washington, DC, 1978.

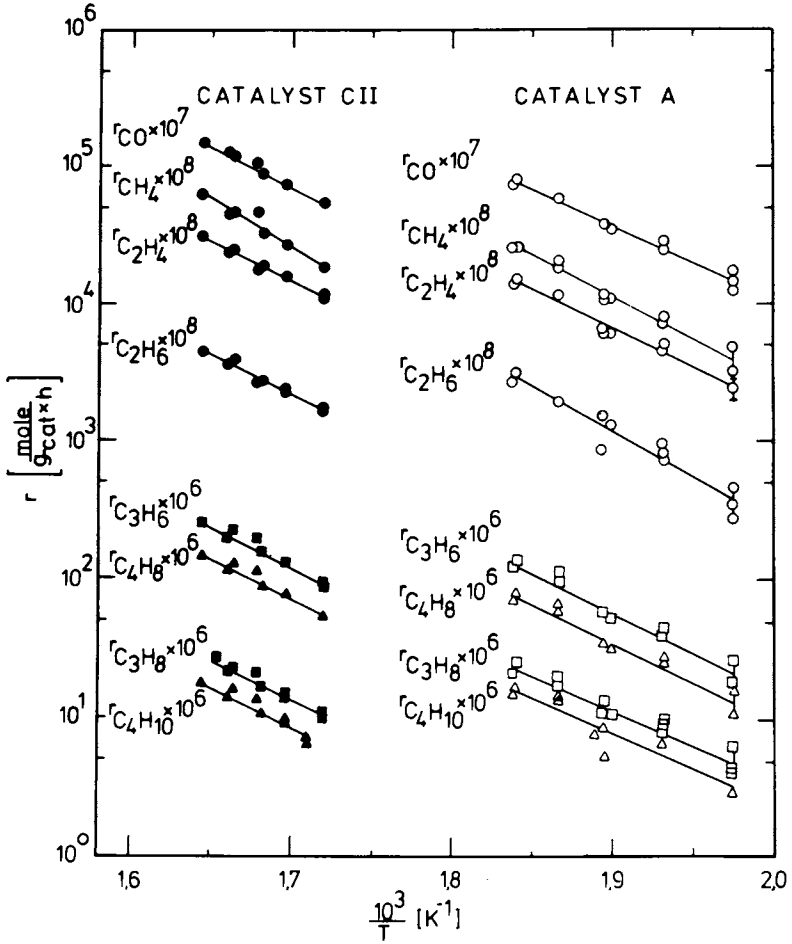

Figure 2. Arrhenius diagram for reaction rates

In Chemical Reaction Engineering—Houston; Weekman, V., et al.;
ACS Symposium Series; American Chemical Society: Washington, DC, 1978.

Table III: Apparent activation energy E_a for rates of CO-consumption and hydrocarbon formation.
$r = r_o \cdot \exp(-E_a/RT)$, $r_o = r_o^o \cdot f(p_{H_2}, p_{CO})$

Compound	Catalyst A		Catalyst C-II	
	r_o [1]	E_a [2]	r_o [1]	E_a [2]
CO	$4.0 \cdot 10^7$	24.1	$5.0 \cdot 10^7$	26.4
CH_4	$8.5 \cdot 10^7$	28.5	$2.6 \cdot 10^8$	32.2
C_2H_4	$3.6 \cdot 10^6$	25.8	$8.8 \cdot 10^5$	26.2
C_2H_6	$4.0 \cdot 10^7$	30.1	$1.5 \cdot 10^5$	26.4
C_3H_6	$5.7 \cdot 10^6$	26.4	$1.4 \cdot 10^6$	27.0
C_3H_8	$2.3 \cdot 10^4$	22.4	$3.4 \cdot 10^4$	25.2
C_4H_8	$1.7 \cdot 10^3$	25.6	$4.3 \cdot 10^5$	26.2
C_4H_{10}	$1.9 \cdot 10^4$	22.5	$4.7 \cdot 10^4$	26.1
p_{CO} bar	3.5 to 3.7		3.4 to 3.6	
p_{H_2} bar	3.6 to 3.7		3.7 to 3.8	
X_{CO} %	12 to 19		22 to 28	
T °C	233 to 271		309 to 335	

[1] mole/(g-catalyst x h) [2] kcal/mole

growing chain and that the probability of chain growth W is independent of chain length:

$$r_n/r_{CO} = A\ W^n$$

r_n is the rate of formation of paraffin plus olefin of carbon number n. As exemplified in Figure 3 the experimental rate data can be represented by the above correlation. The constants A and W have been evaluated for the various experimental conditions and are listed in Table IV; A increases and W decreases slightly with temperature. Postulating that the linear plot can be extended to carbon numbers n>4 the total selectivity for the formation of straight chain paraffins and α-olefins $\sum S_n$[C-atom%] can be calculated:

In Chemical Reaction Engineering—Houston; Weekman, V., et al.;
ACS Symposium Series; American Chemical Society: Washington, DC, 1978.

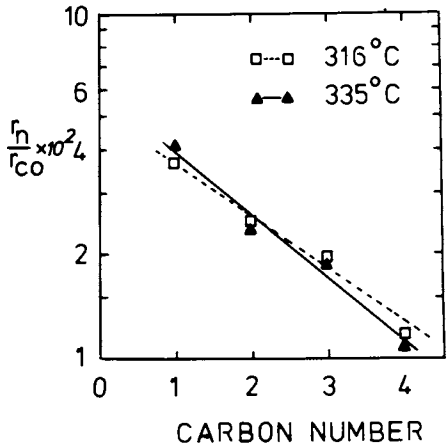

Figure 3. Correlation between the rate of formation of straight chain paraffins plus α-olefins (r_n) and carbon number n *(catalyst C–II,* P*(CO) = 3.5 bar,* P*(H_2) = 3.7 bar)*

$$\sum S_n = \sum n \frac{r_n}{r_{CO}} = \int_{n=0}^{n=\infty} n\, A\, W^n\, dn = A/(\ln W)^2$$

The values of $\sum S_n$ are given in Table IV; the average amounts to about 44 %. Considering that the average selectivity towards CO2 is approximately 48 % the missing 8 % of selectivity are to be contributed to branched hydrocarbons and oxygenated compounds.

Table IV: Parameters A and W of the product distribution correlation and cumulative selectivity $\sum S_n$ of straight chain-hydrocarbons

Catalyst A				Catalyst C II			
T_R °C	$A \cdot 10^2$	W	$\sum S_n$* C-atom %	T_R °C	$A \cdot 10^2$	W	$\sum S_n$* C-atom %
233	3,13	0,776	49	309	4,88	0,697	38
245	3,76	0,776	58	316	5,17	0,704	42
254	4,34	0,755	55	322	5,44	0,687	39
263	4,20	0,732	43	329	5,53	0,679	37
270	4,57	0,724	44	335	6,00	0,655	34

*S_{CO_2} = 45-50 C-atom %

Rate determining step and activation energy. The modified Thiele-modulus Φ is commonly used as a means for evaluating whether a reaction is effected by pore diffusion (9):

$$\Phi = \frac{R_p^2 \cdot r_i \cdot \varrho_p}{C(H_2) \cdot D_{eff}}$$

For the Fischer-Tropsch-synthesis the question arises on what kind of diffusion coefficient to base the calculation. When applying a gas phase diffusion coefficient Φ amounts to about 0,001 to 0,01; hence, pore diffusion should be excluded. It is, however, known that the pores of the catalyst are filled with high boiling liquid hydrocarbons as was also observed in

In Chemical Reaction Engineering—Houston; Weekman, V., et al.;
ACS Symposium Series; American Chemical Society: Washington, DC, 1978.

this study. Therefore it seems appropriate to substitute for the reactands the liquid phase diffusion coefficients and their solubility in the liquid hydrocarbons as a measure of concentration. When using estimated values for the molecular diffusion coefficient based on (10) and for the solubility of H2 (11) moduli are obtained in the order of 20 to 50 resulting in effectiviness factors of 0.3 to 0.1. This clearly suggests that the rate of CO-consumption is strongly influenced by pore diffusion. The magnitude of the apparent activation energies as listed in Table III, however, is comparable to the true activation energies of the synthesis as proposed by (12). It might therefore be assumed that the measured values of E_a are not effected by pore diffusion but correspond to the true values. In this case the transport of the reactands to the active surface would have to occur by another mechanism than pore diffusion; surface diffusion has been suggested earlier (13).

Performance of catalysts A and C-II. Catalyst C-II reduced at 500°C was less active than A reduced at 300 °C. The difference in activity which is exemplified by the reaction rates of CO in Table V is greater than could be explained by the smaller surface area of C-II.

Table V: Effect of catalyst pretreatment on activity calculated according to the kinetic data of Table III.

Temp. °C		250	270	300	330
$10^3 \cdot r_{CO}$ $\frac{\text{mole}}{\text{g-cat.}\cdot\text{h}}$	Cat. A	3.9	9.2	(29.4)+)	(83.8)+)
	Cat.C-II	(0.6)+)	(1.4)+)	5.0	15.6

It is concluded that the number of active sites per unit area decreases by the high temperature reduction. There are minor differences in selectivity of the two catalysts as is shown in Table VI for ethylene and ethane. The selectivity towards ethylene is in the temperature range investigated slightly higher for catalyst C-II as compared with A. Considering ethane its selectivity can be looked at as nearly constant. Hence, the main difference of the two catalysts is their activity.

To elucidate the mechanism of the decrease in activity investigations are presently in progress to determine the number of active sites of the catalysts.

In Chemical Reaction Engineering—Houston; Weekman, V., et al.;
ACS Symposium Series; American Chemical Society: Washington, DC, 1978.

Table VI: Effect of catalyst pretreatment on selectivity (C-atom %) calculated according to the kinetic data of Table III.

Temp. °C	Catalyst A			Catalyst C-II		
	$S(C_2^=)$	$S(C_2)$	$S(C_2^=)/S(C_2)$	$S(C_2^=)$	$S(C_2)$	$S(C_2^=)/S(C_2)$
250	3.5	0.6	5.8	(4.3)+)	(0.6)+)	(7.2)+)
270	3.8	0.8	4.8	(4.2)+)	(0.6)+)	(7.0)+)
300	(4.1)+)	(1.1)+)	(3.7)+)	4.2	0.6	7.0
330	(4.4)+)	(1.4)+)	(3.1)+)	4.1	0.6	6.8

+) catalyst was not operated at this temperature

Acknowledgement

This work was supported by Ruhrchemie AG, Oberhausen and the Ministry for Research and Technology of the Fed. Rep. of Germany.

Literature Cited

(1) Büssemeier B., Frohning C.D., Cornils B., Hydroc. Proc. (1976) 11, 105.
(2) German Patent Applic. DAS 2.536.488 (16.8.1975).
(3) German Patent Applic. DOS 2.518.982 (29.4.1975).
(4) German Patent Applic. DOS 2.518.964 (29.4.1975).
(5) German Patent Applic. DOS 2.507.647 (19.2.1975).
(6) Berty J.M., Chem. Engng. Progr. (1974) 70, 78.
(7) Anderson R.B., Seligmann B., Schultz J.F., Kelly R., Elliot M.A., Ind. Engng. Chem. (1952) 44, 391.
(8) Dry M.E., Shingles T., Boshoff L.J., J. Catal. (1972) 25, 99.
(9) Satterfield C.N., "Mass Transfer in Heterogeneous Catalysis", 138, M.I.T. Press, London 1970.
(10) Weast R.C. (editor) "Handbook of Chemistry and Physics" F59(n-Hexane), CRC-Press, Cleveland/Ohio 1974.
(11) Kölbel H., Ackermann P., Engelhardt F., Erdöl und Kohle (1965) 9 (3), 153.
(12) Anderson R.B., Hofer L.J.E., J. Chem. Eng. Data (1960) 5, 511.
(13) Brötz W., Spengler H., Brennstoff-Chem. (1950) 31, 97.

Thermal and Kinetic Design Data from a Bench-Scale Heatflow Calorimeter

W. REGENASS

CIBA–GEIGY Ltd., Department of Chemical Engineering, Basel, Switzerland

THERMAL AND KINETIC DESIGN DATA FROM A BENCH-SCALE HEATFLOW CALORIMETER

In this paper, a heat flow calorimeter designed for the investigation of industrial organic reactions is presented. This instrument is extensively used for the elucidation of reaction kinetics and for the assessment of thermal hazards. It also permits the determination of heats of reaction, specific heats and heat transfer coefficients, and due to its accurate controls, it is an ideal "mini-pilot-reactor".

Attempts to use heat evolution as an indicator for the kinetics of chemical reactions are as old as thermochemistry. Nowadays thermal methods are firmly established for the investigation of solid/solid, gas/solid and curing reactions, and they are widely used for biochemical reactions. There is an adequate supply of instruments for this type of work. However, it is only in the last few years that calorimeters suited to the requirements of process development have been described in the literature [1,2,3,4], and no such instrument is available commercially to date. Therefore, chemical engineers often are not aware of the potential of thermal methods.

Thermal methods and Instrumentation

As an introduction for the chemical engineer not familiar with thermal methods, a short review on instrumentation is given here.

The most important feature for classifying thermal methods is certainly the treatment of the evolved heat. In accumulation methods (adiabatic and isoperibolic calorimetry), the sample is well insulated from its environment and its temperature change is used as a measure of the extent of conversion. In heat transfer or heat flow methods, the evolved heat flow to the environment in

© 0-8412-0401-2/78/47-065-037$05.00/0

a measurable way, while the sample temperature remains near its set point; here the measured rate of heat flow is proportional to the rate of conversion. For kinetic work and hazards assessment, heat flow methods are to be prefered.

Heat flow calorimeters may be classified further with respect to the method of heat transfer control. In passive systems, heat flow is induced by temperature changes of the sample due to partial accumulation of the evolved heat. In active systems, a heat transfer controller causes heat transfer induced by the slightest deviation of the sample temperature from its set point. Three heat flow control principles are mainly used in active systems:

1) Peltier heat transfer [5]
2) Compensation heating (a constant heat flow is produced by a constant temperature difference across a heat barrier and a controlled electric heater is so adjusted that the sample temperature is kept at its set point, i.e. the heating power is complementary to the heat release of the sample)
3) adjustment of the environment temperature

Heat flow measurement is straight forward with the first two principles; there are two methods in connection with principle 3):

31) use of the temperature difference across the sample wall as a measure of heat flow
32) heat balance on the heat transfer fluid [4] [6].

Another characteristic feature of heat flow calorimeters is sample size.

The micro-methods (differential-thermal analysis = DTA, differential scanning calorimetry = DSC) are quick and require little experimental effort, but they provide no means of adding reactants during measurements, and heterogeneous samples cannot be mixed. All micro-methods use a twin (or differential) design to eliminate disturbing effects, i.e. an inert sample is exposed to the same environment conditions as the sample under investigation and the difference of the two heat flows is recorded.

Laboratory (research type) heat flow calorimeters (with sample sizes of 20 to 200 ml) are available from various suppliers. These instruments are very accurate but they have limited ranges of application with respect to temperature, pressure, corrosion resistence and handling of reactants.

Two bench-scale heat flow calorimeters (with a sample size of 0.3-2.5 litres) have been described: a design of Hub [4], particularly suitable for work under reflux conditions, and the instrument presented in this paper, which is a single sample active heat flow calorimeter, using the heat flow control method 31).

More comprehensive reviews on thermal analysis instrumentation are found in references [7] and [8].

In Chemical Reaction Engineering—Houston; Weekman, V., et al.;
ACS Symposium Series; American Chemical Society: Washington, DC, 1978.

A bench scale heat flow calorimeter [2,3,9,10,11]

For the requirements of process development and process safety investigation, a bench scale heat flow calorimeter has been developed and built. Figure 1 outlines its principle. The stirred tank reactor (A) is surrounded by a jacket in which a heat transfer fluid is circulated at a very high rate. A cascaded controller (B) adjusts the temperature of the circulation loop (C) so that heat transfer through the reactor wall equilibrates the heat evolution in the reactor. Injection of thermostated hot or cold fluid is used to adjust the temperature in the loop.

The rate of heat transfer q (which equals the rate of heat evolution) is related to the observed temperature difference ΔT between the jacket fluid and the reaction mixture by the relation

$$q = U \cdot A \cdot \Delta T = f_c \cdot \Delta T \qquad (1)$$

where the calibration factor f_c is the product of U, the overall heat transfer coefficient, and A the active (= wetted) heat transfer area. Because both A and U depend on the reactor contents and on the stirring conditions, specific calibration is required. This is done by producing a known heat input rate to the reaction mixture by means of an electric heater (D).

The need of frequent calibration is of some inconvenience as compared with heat balance calorimeters. On the other hand, the method chosen permits the use of an uninsulated glassreactor and thus allows visual observation of phase changes, colour changes and mixing conditions. This is a distinct advantage for process development work.

Our standard instrument, which is shown in fig. 2,is equipped with a refrigeration unit, electronic controls for temperature programming; automatic calibration and with feeding systems (not shown) for gases, solids and liquids. Thus, all standards operations carried out with industrial stirred tank reactors canbe performed.

The specifications are as follows:

reactor temperature : -20 to 200°C
temperature programm : ± 1 to 200°/hour
pressure (glass reactor): - 1 to 2 bar
volume of reactor : 0.5/2.5 litres (exchangeable)
volumen of reactant : 0.3-2.5 litres
sensitivity : 0.5 Watts for low viscosity reaction mixtures
heat removal capacity : 500 Watts (for temp. > 30°C)
response time (to a step change of the heat release rate):
20 seconds for 50%, 200 seconds for 99% of the full signal.

Special units for high temperature (250°C), low temperature (-60°C, [11]) and moderate pressure (50 bar) are also in use.

In Chemical Reaction Engineering—Houston; Weekman, V., et al.;
ACS Symposium Series; American Chemical Society: Washington, DC, 1978.

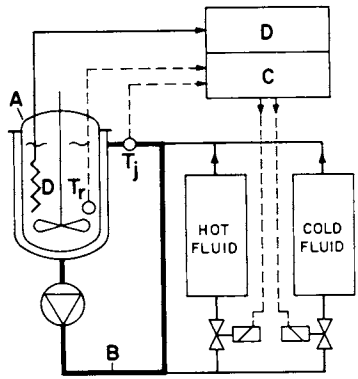

Figure 1. Bench scale heat flow calorimeter

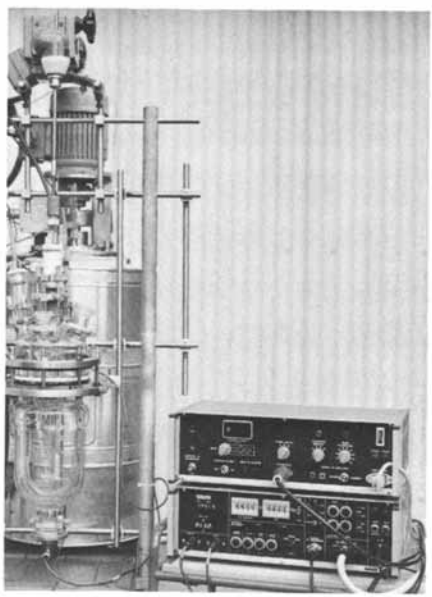

Figure 2. Bench scale heat flow calorimeter

In Chemical Reaction Engineering—Houston; Weekman, V., et al.;
ACS Symposium Series; American Chemical Society: Washington, DC, 1978.

Fig. 3 presents a typical heatflow record of an isothermal run. In the example acetic anhydride was hydrolyzed at 25°. The following events are indicated:

(A) Initiation of the reaction by instantaneous addition of 0.88 moles of acetic anhydride to a large amount of 0.1 n aqueous HCl
(B) dynamic lag (heat flow to the jacket has to equilibrate with heat release in the reactor)
(C) heat evolution decreasing exponentially (first order reaction)
(D) calibration (superimposed on reaction)

Thermal data

The rate of heat evolution which is of primary interest for safety and design considerations, is obtained immediately from the observed temperature difference by calibration.

The total heat of reaction follows by integrating the surface under the heat flow curve.

Heat capacities and specific heats are obtained from temperature programmed runs. When the rate of imposed temperature change $\dot{T}$ is altered, there is a step change in heat flow (S in fig.4):

$$\Delta q = \Delta(\dot{T}) \cdot (w + m_r c_{p,r})$$

In this relation w denotes the proportionate heat capacity of the calorimeter (a quantity which depends on temperature and on the volume of the calorimeter contents and has to be calibrated for a specific reactor), m_r and $c_{p,r}$ are the mass and the specific heat of the mixture under investigation.

The evaluation of heat flow data obtained from the bench scale calorimeter has been treated by Martin [2] and Gautschi [10].

Kinetics

For single reactions, the rate of reaction is directly proportional to the rate of heat evolution observed. The most common objections to the use of thermal methods are related to the facts that most reactions are not single and that heat is a very unspecific information. Therefore the conclusion could be drawn that thermal methods are of little value for kinetic work. However, in the authors experience on several hundred reactions of widely different kinds, this is not the case. In a surprisingly large number of cases, the main reaction is dominating thermally to such an extent, that the influence of concentrations and of temperature on the reaction rate can be obtained by heat flow experiments alone. In most other cases, thermal data provide valuable information additional to the data obtained by classical means, a fact which drastically speeds up kinetic work. Of course, thermal methods are not appropriate for selectivity determinations.

In Chemical Reaction Engineering—Houston; Weekman, V., et al.;
ACS Symposium Series; American Chemical Society: Washington, DC, 1978.

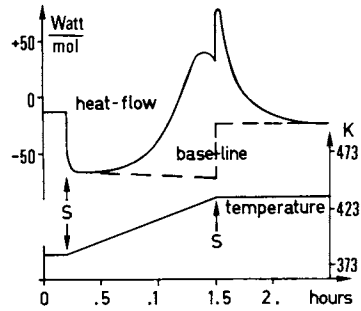

Figure 3. Isothermal run of the hydrolyse of acetic anhydride

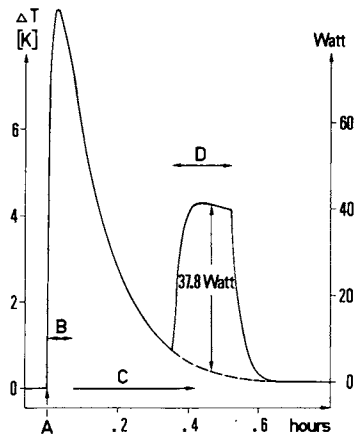

Figure 4. Temperature programmed run of a diazo-decomposition

In Chemical Reaction Engineering—Houston; Weekman, V., et al.;
ACS Symposium Series; American Chemical Society: Washington, DC, 1978.

In order to utilize calorimetry to its full extent, it is important to have different means of reaction initiation at ones disposal. The bench-scale calorimeter described permits the following initiations of reaction:

1) instantaneous addition of a reactant (fig. 3) or a catalyst (fig. 5 and 6)
2) gradual (continuous) addition of liquid, gaseous or solid reactants (fig. 7)
3) gradual rise of temperature (as shown in fig. 4 for the formation of a phenolic compound by the decomposition of the corresponding diazo-salt: $ArN_2^+HSO_4^- + H_2O \longrightarrow ArOH + N_2 + H_2SO_4$)

By temperature programmed operation, heat of reaction, specific heat, frequency factor and activation energy may be obtained from one single run. From the thermogram shown in fig. 4 the following parameters have been obtained 1O : first order rate constant k (433 K) : $1.0 \cdot 10^{-2} s^{-1}$; activation energy E: $2.1 \cdot 10^5$ Joule/mole; heat of reaction ΔH: $2.29 \cdot 10^5$ Joule/mole, with estimated variation coefficients of 7%, 6% and 4% respectively.

Fig. 5 and 6 are taken from an investigation by Martin [2] on the isomerisation of trimethylphosphite (TMP):

$$P(OCH_3)_3 \longrightarrow CH_3\text{-}PO(OCH_3)_2$$

This reaction is catalysed by CH_3J and inhibited by $N(C_2H_5)_3$.

Fig. 5 demonstrates the ease of investigating influences on reaction rate by means of the calorimeter. After catalyst addition (marked C), there is an immediate increase in reaction rate; after the addition of inhibitor (marked I) there is a fast exothermic reaction between the catalyst and the inhibitor and then a decrease of the rate of isomerisation.

Fig. 6 illustrates the value of direct information on reaction rate. After catalyst addition there is at first a marked increase of reaction rate at constant temperature, where one would expect a first order decrease. This is due to a considerable increase in polarity of the reaction mixture as a consequence of conversion. The heat flow record demonstrates this fact more evidently than a classical conversion versus time diagram .

A comprehensive review on the kinetic evaluation of thermal data has been given by Wendtland and coworkers [12], the evaluation procedures specific to heat flow calorimetry have been treated by Becker [12], Martin [2] and Gautschi [10].

Assessment of thermal hazards

Thermal explosions do occur, when the heat evolution rate of a reaction (with a high latent adiabatic temperature rise) exceeds the heat transfer capacity of the reactor. Events of this type which have happened in industry, may be divided into two classes:

In Chemical Reaction Engineering—Houston; Weekman, V., et al.;
ACS Symposium Series; American Chemical Society: Washington, DC, 1978.

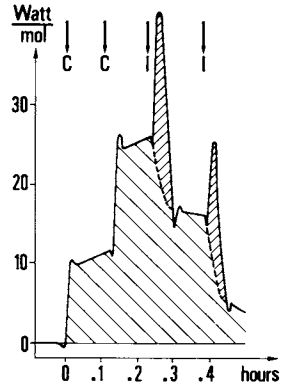

Figure 5. Catalysis and inhibition of the isomerization of $P(OCH_3)_3$

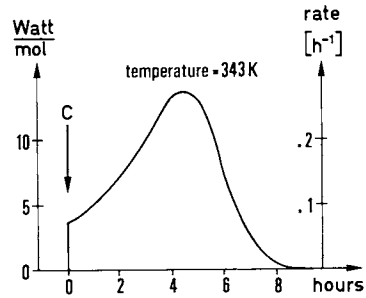

Figure 6. Isothermal run of the isomerization of $P(OCH_3)_3$

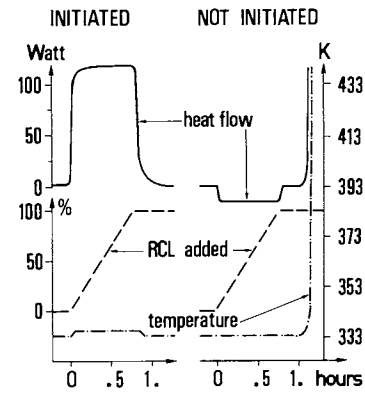

Figure 7. Formation of Grignard compound

1) exothermal decomposition or polymerisation of thermally instable mixtures (e.g. nitro compounds, benzyl-halides, etc.)
2) "run away" of an intended reaction.

Type 1 hazards are easily assessed using well established test methods [14,15], e.g. the thermoanalytical micro-methods DTA or DSC; a test established by Lütolf [16], which is now standard in Swiss firms; or the "Sikarex" [4]. However, the elaboration of safe reaction conditions (which avoid type 2 hazards) is still a problem.

Whenever possible, highly exothermal reactions are performed in such a way, that the reactants disappear by reaction as they enter the reactor (semibatch or continuous operation). Under these conditions, any accumulation of reactants in the reactor is hazardous. It may have several causes, e.g.

21) too low temperature
22) insufficient mixing
23) wrong kinetic assumptions (a case often encountered in process development: the reaction is assumed to be fast and the heat evolved after the addition of the reactants is not noticed on laboratory scale; then at the pilot stage, there is a run away).
24) incorrect initiation

Fig. 7 demonstrates the investigation of a type-24)-hazard during formation of a Grignard-reagent. A halide is added gradually to magnesium suspended in a solvent (RCl + Mg ⟶ RMgCl). After correct initiation (left), the reaction proceeds almost like a neutralisation; without initiation (right), the reaction does not start until far too much halide has been added, and then gets out of control.

Even slightly exothermal reactions may become dangerous, when at a higher temperature an exothermal decomposition is triggered off. For this reason, the potential adiabatic temperature rise of industrial reactions is of general interest. When synthetic work is done in the bench-scale-calorimeter, the required data are obtained without additional effort.

Heat transfer coefficients

Film heat transfer coefficients may be estimated from flow conditions and from physical properties. For forced convection and turbulent flow (i.e. conditions prevailing inside stirred tank reactors), the relation

$$h = a \cdot \frac{\lambda}{d_r} \cdot Re^{2/3} \cdot Pr^{1/3} \cdot \left(\frac{\mu_b}{\mu_w}\right)^{0.14} \qquad (3a)$$

is valid, where a is a geometric factor and d_r is the vessel diameter. Neglecting the ratio of the viscosities in the bulk and at the wall, a rearrangement yields

In Chemical Reaction Engineering—Houston; Weekman, V., et al.;
ACS Symposium Series; American Chemical Society: Washington, DC, 1978.

$$h = a\left\{\frac{d_s^4 \cdot f_o^2}{g\, d_r^3}\right\}^{1/3} \cdot \left(\frac{f_s}{f_o}\right)^{2/3} \cdot \left\{\frac{\lambda^2 \rho^2 \cdot c_p \cdot g}{\mu}\right\}^{1/3} = Z \cdot r_f^{2/3} \cdot \gamma \qquad (3b)$$

with s denoting the stirrer, r_f being the ratio of the actual stirrer frequency f_s to a standard frequency f_o, specific for a given stirrer type and vessel size, and g (the gravitaty acceleration) introduced to make Z dimensionless. In the right hand representation of (3b), first proposed by Jehle and Oeschger [17], Z is a property of the reactor (which can be tabulated for standardized reactors) and γ is a property of the liquid.

For viscous reaction mixtures, where we have a particular interest in knowing h, the physical properties required to determine γ, are not easily accessible. It is much simpler to calculate γ from the overall heat transfer coefficient U in the heat flow calorimeter, which is obtained by the calibration procedure:

$$\frac{\Delta(\Delta T)}{\Delta q} \cdot A = \frac{1}{U} = \frac{1}{h_j} + \frac{d_w}{\lambda_w} + \frac{1}{h_r} = B + \frac{1}{Z_c \cdot r_f^{2/3} \cdot \gamma} \qquad (4)$$

Here the indices denote jacket, wall, reaction mixture and calorimeter vessel, and B is the sum of the resistances of the wall and of the film in the jacket. B is influenced by the heat transfer fluid, by the circulation condition in the jacket and by the reaction vessel chosen. For a given set of equipment, B depends only on temperature and can be calibrated once and for all. This calibration has to be done carefully since B is the dominating term of (4), due to the large resistance of the glass used as reactor wall. Therefore, the procedure outlined here is suggested for typical reaction mixtures (with viscosities similar to sulfuric acid or higher) and not for liquids like methanol or water. For very viscous fluids, where (3) becomes invalid, Zlokarnik [18] has proposed a more general relation. Experimental work in this flow region is in progress.

Fig. 8 compares a few γ-values obtained experimentally in the heat flow calorimeter with the values calculated from physical properties [19]. Table I illustrates the scaling up procedure. One may conclude from this table, that reliable estimates of heat transfer coefficients are not only useful for design purposes, but are also a valuable clue for improving heat transfer in existing equipment. We have often found, particularly in glass lined vessels, that poor circulation in the jacket contributes more to the overall heat transfer resistance than the film of the reaction mixture.

In Chemical Reaction Engineering—Houston; Weekman, V., et al.;
ACS Symposium Series; American Chemical Society: Washington, DC, 1978.

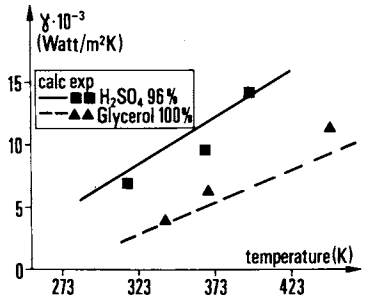

Figure 8. Temperature dependence of the "heat transfer property" γ

Table 1

Liquid mixture	T [K]	(1) γ	Reactor-type	Z_r (2)	h_r (1)	U_{calc} (1)	U_{found} (1)
organic in H_2SO_4	400	6100 ±2000	.6 m^3, (3) (5)	.183	1040 ±370	350 ± 40	150 (7) 320 (8)
nitrobenzene/ $AlCl_3$	380	7100 ±3000	4 m^3, (3) (6)	.153	1090 ±450	370 ± 50	320
naphta, aqu. $ZnCl_2$ solid organic	330	3600 ±1000	10 m^3, (3) (5)	.134	480 ±140	270 ± 30	80 (7) 220 (8)
caustic fusion	470	500 ± 200	4 m^3, (4) (5)	.153	77 ± 30	70 ± 30	85

Remarks: (1) SI-Units: watt/m^2 K (2) anchor at standardized frequency (3) glass lined steel with jacket (4) Ni-clad steel, outside coils (5) cooling by circulated water (6) steam heating (7) before improving circulation (8) after improving circulation in jacket.

Conclusions

There is an obvious need for thermal analysis instruments which are suited to the specific requirements of process development. The bench-scale calorimeter presented in this paper is designed to fill this gap by providing thermal and kinetic information in conjunction with conventional synthetic investigations.

The reaction models obtained from thermal data are as a rule valid over a wide range of experimental conditions and in general permit the elucidation of the thermal safety aspects of a reaction.

Used as a mini-pilot-reactor, the bench-scale-calorimeter in many cases provides data which permits a direct scale-up to plant scale, when conventional means would neccessite a pilot stage. Thus, it is a powerful tool for process development, drastically reducing cost and time required.

Acknowledgment

The author is indebted to many collegues for help, in particular to A. Runser, H.P. Gfrörer, A. Mauerhofer, Dr. H. Martin, Dr. W. Gautschi, Dr. H. Randegger, Dr. P. Finck and Dr. W. Kanert for their contribution to the design of the calorimeter and to Dr. H.U. Meister for fruitful stimulation and generous support. He is also obliged to Prof. M. Brenner and to Prof. D.W.T. Rippin for their support of fundamental work on the method presented.

Nomenclature

A	effective heat transfer area		m^2
c_p	specific heat		$J\ kg^{-1}K^{-1}$
d	diameter (or thickness)		m
g	dimensional constant	9.81	ms^{-2}
h	film heat transfer coefficient		$Wm^{-2}K^{-1}$
f	frequency (of stirring)		s^{-2}
m	mass (of calorimeter contents)		kg
Pr	Prandtl number		-
q	heat flow		W
r	ratio (of frequencies)		-
Re	Reynolds number		-
ΔT	temperature difference (between calorimeter contents and jacket)		K
$\dot{T}$	rate of temperature change		Ks^{-1}
U	overall heat transfer coefficient		$Wm^{-2}K^{-1}$
w	effective heat capacity of calorimeter vessel		JK^{-1}
Z	"heat transfer property" of a stirred tank		-
γ	"heat transfer property" of liquid		$Wm^{-2}K^{-1}$
λ	heat conductivity		$Wm^{-1}K^{-1}$

In Chemical Reaction Engineering—Houston; Weekman, V., et al.;
ACS Symposium Series; American Chemical Society: Washington, DC, 1978.

μ	dynamic viscosity	kg $m^{-1}s^{-1}$
ρ	density	kg m^{-3}

subscripts:
b : bulk, j: jacket, r: reactor contents, s: stirrer, w: wall

Literature cited

1 Köhler, W. et al., Chem.Ing.Techn. 45 (1973), 1289
2 Martin, H., Ph. D.Thesis, Basel, 1973
3 Regenass, W., Gautschi, W., Martin, H. and Brenner, M., Proc. 4th Int.Conf.Thermal Anal. 3, 834, Budapest 1974
4 Hub, L., Ph.D.Thesis, ETH, Zürich, 1975
5 Becker, F. and Walisch, W., Z.Phys.Chem. NF 46 (1965), 279
6 Swiss Patent 455 325
7 Regenass, W., Thermochim. Acta 20 (1977), 65
8 Wendtland, W.W., "Thermal Methods of Analysis", Wiley, 1974
9 US-Patent 3 994 164
10 Gautschi, W., Ph.D.Thesis, ETH, Zürich, 1975
11 Kanert, W., Ph.D.Thesis, Basel, 1977
12 Sestak, J. et al., Thermochim. Acta 7 (1973), 335
13 Becker, F., Chem.Ing.Techn. 40 (1968), 933
14 Coffee, R.D., AIChE-64th-Natl.Meeting (1969), Preprint 25C
15 Eigenmann, K., 2nd Int.Symp. on Loss Prevention (1977)
16 Lütolf, J., Staub, Reinh. Luft 31/3 (1971), 94
17 Jehle, E. and Oeschger, V., Ciba-Geigy, presented at Dechema Jahrestagung 1968, but never printed
18 Slokarnik, M., Chem.Ing.Techn. 41 (1969), 1195
19 Gautschi, W., Ciba-Geigy, unpublished

In Chemical Reaction Engineering—Houston; Weekman, V., et al.;
ACS Symposium Series; American Chemical Society: Washington, DC, 1978.

5

Adsorption Studies at Reaction Conditions—Reactor Development and Evaluation for Transient Studies at Millisecond Rates

RICHARD D. STOLK* and ALDRICH SYVERSON

Department of Chemical Engineering, Ohio State University, Columbus, OH 43210

The role of adsorption in heterogeneous catalysis is not easily evaluated because of the simultaneous occurrence of adsorption and reaction and the difficulty of measuring surface concentrations of reacting species on the catalyst at these conditions. Exploratory research directed toward devising a method for studying adsorption in gas-solid systems by means of a batch adsorber-reactor has been underway in this laboratory for several years. This technique provides an opportunity to examine the "adsorption" and "reaction" steps sequentially at reaction temperatures and pressures. How sharply the individual steps can be separated depends largely upon the magnitude of the differences in rates and upon the data resolution capability of the experimental apparatus. Interpretation of the transient rapid response measurements in terms of steady state operation is needed if these results are to be most useful. Recent studies in this laboratory indicate that this approach holds some promise and it is the purpose of this paper to describe the adsorber-reactor system and its performance capabilities. The most recent design provides rapid gas-solid contact in a constant volume cell with transient rates for temperature and pressure measurements in the millisecond region.

Few adsorber-reactors have been devised to measure adsorption at reaction conditions. Winfield (1) described a high speed apparatus for adsorption studies at low pressure. Macarus (2) reported results on a high speed adsorption-reaction apparatus; his data were correlated with fixed bed catalyst studies of Sashihara (3) with encouraging results. The second generation high speed adsorption apparatus was built by Edwards (4) and Keller (5) and improved by Haering (6) in the early 1960's. They overcame many of the previous limitations by first treating and sealing the catalyst sample in a glass capsule which was then placed in the adsorber-reactor containing gaseous reactants at the desired temperature and

*Present Address: Monsanto Enviro-Chem Systems, Inc. 800 N. Lindbergh Blvd., St. Louis, Missouri 63166

In Chemical Reaction Engineering—Houston; Weekman, V., et al.; ACS Symposium Series; American Chemical Society: Washington, DC, 1978.

pressure. The reaction was initiated by crushing the capsule by remote control using a feedthrough device. This procedure allowed a pretreatment of the catalyst with reactants or products before sealing the capsule. For a binary system either of the gaseous reactants may be adsorbed by the catalyst prior to the reaction. Pretreating the catalyst provides some insight into the effects of multi-component adsorption at reaction conditions.

The reactor described herein may be considered third generation. Data collection was first accomplished by recording the analog signals on a tape recorder. Later a modified PDP-15 dual processor digital computer was directly coupled to the reactor itself. The equipment was completed in 1971 (7). Since that time others including Becher (8), Wolfe (9), and Nash (10) have used the system for high speed transient adsorption/reaction studies.

Reactor Design Features

The primary design consideration was the arrangement of reactor components to insure rapid gas-solid contact. The measuring devices had to be capable of operating at high temperature and have millisecond time constants. The parameters of internal and catalyst volume and their ratio are key elements in a constant volume system. The internal reactor volume must be minimized. Catalyst volume was chosen to cause a detectable pressure change in the system during the experiment.

After evaluating several design concepts to achieve rapid gas-solid contact followed by effective mixing, a combination "flywheel/fan" was designed to crush the glass capsule and to provide gas circulation. An inclined grid and screen were added to separate the catalyst particles from the capsule before contact with the flywheel to reduce attrition. Clear plastic prototypes were built for evaluation at ambient conditions. High speed (4000 fps) motion pictures permitted observation of a capsule being broken inside the reactor. Examination of the pictures showed that gas-solid mixing was effective in the millisecond range and that very little disintegration of the catalyst occurred.

The reactor components and the assembled reactor are shown in Figure 1. Components of the reactor include: (1) capsule holder, (2) flywheel, (3) rotary feedthrough, (4) grid and screen, (5) pressure transducer, and (6) thermocouple. The internal volume was 415 cc and held a 24 cc capsule. The reactor was made of 304 stainless steel and weighed about 35 pounds. Specifications are presented in Table 1 describing the upper limits of temperature and pressure for the major components.

In Chemical Reaction Engineering—Houston; Weekman, V., et al.;
ACS Symposium Series; American Chemical Society: Washington, DC, 1978.

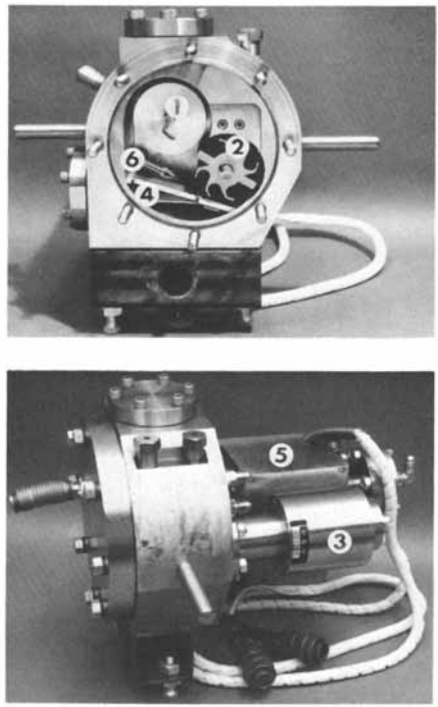

Figure 1. Adsorber–reactor

In Chemical Reaction Engineering—Houston; Weekman, V., et al.;
ACS Symposium Series; American Chemical Society: Washington, DC, 1978.

Table 1. Specifications for the Adsorber-Reactor

A.	(1) Rotary Feedthrough	450°C	60 psia
	(2) Pressure Transducer	485°C	68 psia
	(3) Thermocouple	485°C	-
	(4) Manual Feedthrough Bellows	-	30 psia
B.	Response Time to a Step Change (Time Constant)		
	(1) Pressure Transducer	2-3 milliseconds	
	(2) Thermocouple	2-10 milliseconds	

The capsule holder contained the activated catalyst in a sealed glass capsule at the start of the test. The reaction was initiated by manually rotating the holder 180 degrees releasing the capsule into the flywheel.

High Speed Pressure Transducer. The characteristics of the Datametrics Type 531 Barocel pressure transducer are shown in Table II. It can be operated as a differential or absolute type up to 450°C without cooling.

Table II. Characteristics of Pressure Transducer

A. Sensing Element: capacitive potentiometer
B. Rise Time: 2-3 milliseconds
C. Hysteresis: Less than 0.2%
D. Temperature Coefficient of Sensitivity: 0.01%°C
E. Accuracy at 75°C: 0.2% of Reading plus 0.01%F.S.

High Speed Thermocouple. Micro-miniature chromel-alumel thermocouples having 0.002-0.010 second time constants were purchased from BLH Electronics, Inc. The thermocouple wire is 0.001 inch in diameter. An amplifier with a gain up to 1000 was used to produce a 10 volt signal.

Data Collection and Reduction

In the beginning a tape recorder was used to record the high speed transducer data. However, because of high noise level in the system, the data collection was interfaced with a modified PDP-15 dual processor digital computer. Comparing the signal-to-noise ratio for both schemes, the former had a 14:1 ratio while the latter had a 250:1 ratio. The precision has been improved from about 10 torr for the tape recorder scheme to 0.3 torr for the computer scheme without time averaging the data.

The electrical signals from the measuring devices were transmitted via shielded cable directly into the computer. Internal to

In Chemical Reaction Engineering—Houston; Weekman, V., et al.;
ACS Symposium Series; American Chemical Society: Washington, DC, 1978.

the computer, the analog data were digitized to binary decimal and finally recorded on DEC tape.

The quantity of gas adsorbed was determined from the pressure and temperature changes in the constant volume cell. A fast response pressure transducer and thermocouple monitored continuously at a millisecond frequency provided the basic transient data. Measurement of gas composition in such a rapidly changing system is difficult because of the need to sample at high rates for analysis. However, both initial and final compositions may be sampled when the system is at equilibrium. A provision was made to install a pair of filaments for continuous measurement of the gas thermal conductivity but they were not used in this study.

Computer Program Description. Computer programs were written in both Fortran IV and Macro-15 assembler language. The program used to collect and store the data was written in Macro-15 language to allow a 1000 cycle per second sampling rate. The program can sample three data channels, perform time averages, and make other calculations all within one millisecond. It "waits" until the next millisecond before repeating the calculations and storage of data.

Five data sets were collected during the experiment. Two were at steady state prior to breaking the capsule to evaluate the reactor conditions. Thirty seconds of steady state data were collected at a one second frequency. One hundred data points with a one millisecond separation were recorded to evaluate the noise level on the non-time averaged data. The three remaining data sets were averages based on 16 millisecond values.

After the first second of time had been recorded with millisecond data points, the sampling rate was reduced to ten points per second for a ten second period. It was further reduced to one point per second for the remaining period. A total of 6390 data points were collected during the experiment lasting 15 minutes.

Other computer programs were used to reduce the data to pressure and temperature values. The data in the two steady state data sets were reordered with respect to time since each was collected in a loop which was continuously being rewritten before the capsule broke. A time base was added to the data before being transferred to tape.

Experimental Results

In order to illustrate the capability of this device and possible areas of application to research in catalysis, examples of

In Chemical Reaction Engineering—Houston; Weekman, V., et al.;
ACS Symposium Series; American Chemical Society: Washington, DC, 1978.

results are reported in the following categories: (a) dynamic response of the system to a step pressure change, (b) adsorption rate studies of water on an alumina catalyst, and (c) typical adsorption-reaction results for catalytic dehydration of tertiary butanol on alumina.

Pressure Response Characteristics. A mechanical device was not used to initiate the data collection because a finite time elapsed after the capsule was released from the holder until it contacted the flywheel; instead a voltage change on the transducer signal equivalent to 15 torr within 10 milliseconds was found to be the best way to start data collection. The system response to a step change caused by breaking an empty capsule under vacuum surrounded by air is shown in Figure 2. Time constants were calculated for 63.2% response to the pressure change. The values of 0.9 and 0.8 milliseconds were recorded at 13 and 196 °C respectively. The response time of the pressure transducer was adequate for this mechanical system and for the water and t-butanol studies on alumina. (Prior work showed that a 100 torr pressure change occurred in 20-30 milliseconds after the alumina was exposed to the adsorbate).

Transient Adsorption Studies: Water on Alumina. One eighth inch alumina pellets (Type 100S) supplied by Air Products Corp., Houdry Division were crushed into smaller particles and separated into various fractions from -10 to +200 mesh. The alumina was activated at 300 °C at less than 100 microns pressure for three hours. All calculations were based on sample weight after activation.

A series of samples was tested using the size fractions presented in Table III. Adsorption-time curves of these samples are shown in Figure 3.

Table III Water Adsorption Alumina

-Mesh Size	12/20	20/35	20/35	35/65	65/100
Cat. Weight (g)	5.775	7.421	7.936	7.476	6.382
Initial Conditions					
Pressure (torr)	787	770	784	782	783
Temperature (°C)	193	111	203	196	195
Final Conditions After 15 minutes					
Pressure (torr)	579	357	525	523	545
Temperature (°C)	191	114	199	194	193
Max Temp. Obs. (°C)	223	136	227	215	220
Equilib. (mgm/g)*	0.52	1.06	0.47	0.51	0.54

*mgm/g - milligram moles adsorbed per gram of catalyst

In Chemical Reaction Engineering—Houston; Weekman, V., et al.;
ACS Symposium Series; American Chemical Society: Washington, DC, 1978.

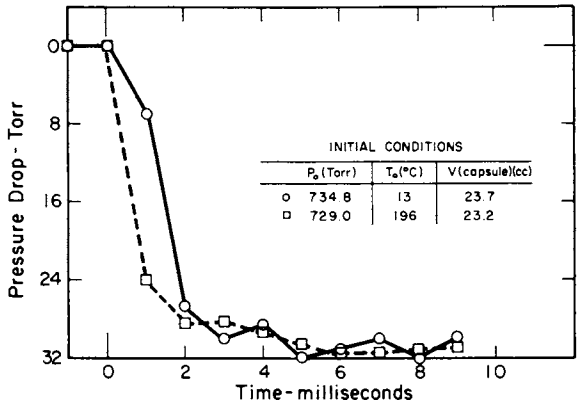

Figure 2. System response to pressure change

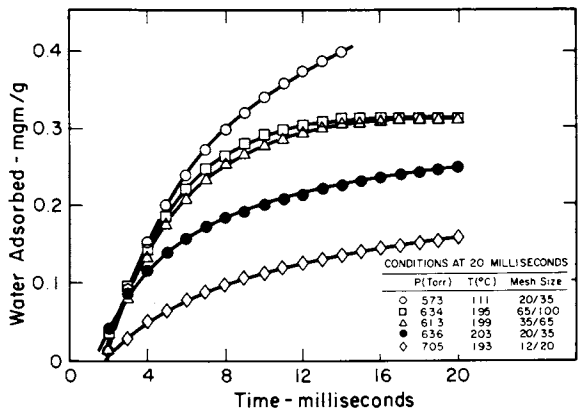

Figure 3. Adsorption of water on 100S alumina

In Chemical Reaction Engineering—Houston; Weekman, V., et al.;
ACS Symposium Series; American Chemical Society: Washington, DC, 1978.

The curves in Figure 3 intersect the time corrdinate at 1 to 2 milliseconds. This time lag arises because of the way the computer corrects for the capsule volume and sets time zero while the capsule is breaking in the first two milliseconds. Since particle size and shape are significant factors in mass transfer considerations and the size and shape distributions within a given mesh size for these experiments are not known, quantitative evaluation of transport properties may not be meaningful. Certainly the potential for such quantitative measurements seems possible. In a qualitative sense, the curves of Figure 3 are in the order expected if mass transfer were a dominant factor.

Adsorption Reaction Studies: Dehydration of t-butanol on Alumina. Previous work in this laboratory has given encouraging results in arriving at Langmuir-Hinschelwood or Hougen and Watson type kinetic models (2,6,8,10) when the amount of adsorption at reaction conditions has been determined. The typical results presented here repeat some earlier experiments with, however, a much superior apparatus.

The basis for this procedure for evaluating the concentration of absorbed species at reaction conditions rests upon being able to measure adsorption while a much slower reaction step takes place. If the study is to go beyond the adsorption step, the reaction must be of the type that produces a change in pressure at constant volume and temperature. Figure 4 shows portions of a typical adsorption reaction history for the catalytic dehydration of t-butanol on Alumina 100S which has been treated or "conditioned" with water (6). The reaction which is endothermic produces one mole of isobutylene and a mole of water for each mole of t-butanol. The steep decrease in pressure during the first second (approximately) was caused by adsorption, then the slow rise resulted from the reaction. The ratio of adsorption rate to reaction rate for this case was about 1700. The temperature rose during the first three seconds as a result of the heat of adsorption then fell because of the endothermic reaction and heat loss to the reactor. The temperature lag may be due in part to the slower response of the thermocouple. The amount of t-butanol which was measured by the drop in pressure from the initial value to the minimum is considered to be the adsorption at reaction conditions.

The technique of confining the catalyst in a capsule permits various treatment or activation procedures as well as examination of multi-component adsorption effects. For a single reactant system reaction products can be preadsorbed at a known quantity to ascertain the effect these might have on reactant adsorption and

In Chemical Reaction Engineering—Houston; Weekman, V., et al.;
ACS Symposium Series; American Chemical Society: Washington, DC, 1978.

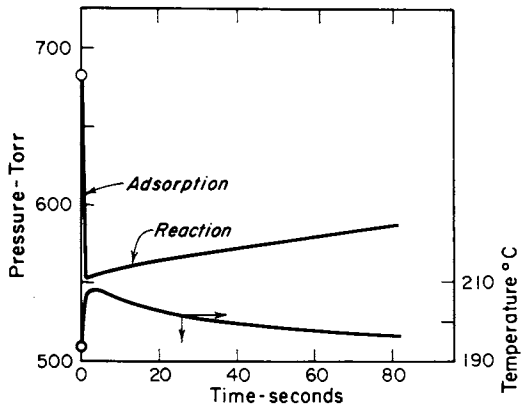

Figure 4. Adsorption–reaction pressure transient for catalytic dehydration of tert-*butanol*

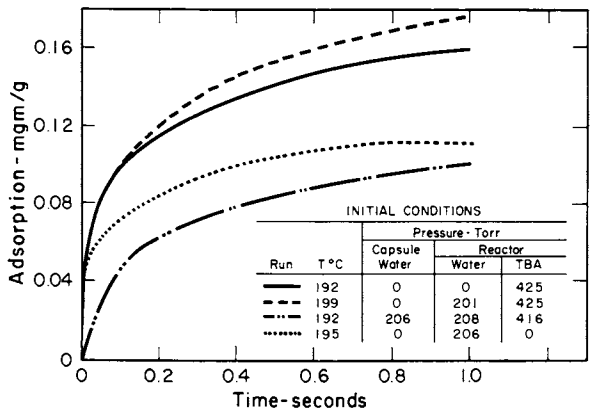

Figure 5. Effect of water on tert-*butanol adsorption*

In Chemical Reaction Engineering—Houston; Weekman, V., et al.;
ACS Symposium Series; American Chemical Society: Washington, DC, 1978.

reaction rate. To avoid transport or desorption the initial partial pressure of the products inside and outside the capsule can be made equal. For reactions with more than one reactant, the binary adsorption effects can also be measured.

Figure 5 shows the effect of water on the adsorption of t-butanol on 100S alumina. All runs involving t-butanol (TBA) had about the same initial partial pressure. Most adsorption-reaction experiments reach the minimum pressure in one second, hence the time scale for Figure 5. The top curve represents the adsorption of 2:1 mixture of TBA and water. This curve is only slightly above the TBA curve, whereas, were the adsorption of the two components independent, the total adsorption would be 60-100% higher as can be seen by adding the two single component curves. The lower curve represents the adsorption of TBA on a surface having absorbed water equivalent to a pressure of 208 torr. The suppression of the adsorption of TBA by preadsorbed water is indeed substantial.

Adsorption measurements at reaction conditions have been coupled with fixed bed kinetic data to arrive at simple kinetic models with one or two adjustable parameters (2 and 6). In recent work (10) the adsorber-reactor has been used as a batch reactor for obtaining kinetic data up to high conversions in addition to its use as an adsorber.

Conclusions

The design and experimental results for some typical applications of a high temperature, high speed constant volume adsorber-reactor have been presented. Preliminary experiments indicate that adsorption studies can provide a better insight into transport mechanisms and the role of adsorption in heterogeneous catalysis thereby assisting the development of improved kinetic models for these complex reactions.

Acknowledgement

The authors thank Professor E.R. Haering for his helpful advice on the t-butanol kinetics, Professor J.T. Heibel for his assistance on the computer data acquisition facilities and programming and Michael Kukla for his help on electronics. Financial support for fellowships and grants-in- aid from The American Oil Company, Exxon Company, E.I. duPont Company, Monsanto Company, Henry Dreyfus Teaching Fellowship Program and the Chemical Engineering Development Fund are gratefully acknowledged.

Literature Cited

1. Winfield, M.E., Aust. J. of Chem., (1953), 6, 221.
2. Macarus, D.P., Syverson, A. I&EC Proc. Design Dev, (1966), 5, 397.
3. Sashihara, T.F., Syverson, A., I&EC Proc. Design Dev., (1966), 5, 392.
4. Edwards, D.C., M.Sc. Thesis (1961), The Ohio State University, Department of Chemical Engineering.
5. Keller, R.M., M.Sc. Thesis (1962), The Ohio State University, Department of Chemical Engineering.
6. Haering, E.R., Syverson, A., (1974). J. of Catalysis, 32, (3), 396-414.
7. Stolk, R.D., PhD. Dissertation, (1971), The Ohio State University, Department of Chemical Engineering.
8. Becher, J.H., PhD. Dissertation, (1972), The Ohio State University, Department of Chemical Engineering.
9. Wolfe, D.B., PhD. Dissertation, (1974), The Ohio State University, Department of Chemical Engineering.
10. Nash, G.L., M.S. Thesis, (1976), The Ohio State University, Department of Chemical Engineering.

In Chemical Reaction Engineering—Houston; Weekman, V., et al.;
ACS Symposium Series; American Chemical Society: Washington, DC, 1978.

6

Methanation in a Parallel Passage Reactor

E. W. DE BRUIJN, W. A. DE JONG, and C. J. VAN DER SPIEGEL

Laboratory of Chemical Technology, Delft University of Technology, Delft, The Netherlands

One of the steps in the process of making SNG via coal gasification, the methanation of carbon oxides, has received considerable attention in recent years. Owing to the highly exothermal nature of the reaction, the temperature control of methanation reactors is difficult. Among the solutions proposed are the application of parallel plate (1) and coated tube (2) reactors. It is also possible to apply recirculation of cold product gas, but when this is done with conventional fixed-bed reactors the resulting high pressure drop is a disadvantage. The *parallel passage reactor* (PPR) recently described in connection with Shell's Flue Gas Desulphurization Process (3) does not have this drawback because it contains shallow beds of solid reactant separated from narrow channels by wire screens, the gaseous reactants flowing through the channels with a relatively low pressure drop. Such reactors could, in principle, be applied in any process in which large volumes of gas must be treated at minimum pressure drop, provided that sufficient capacity for absorption of the heat of reaction is available. Examples of such processes are oxidation reactions, Fischer Tropsch synthesis and, as outlined above, carbon oxide methanation.

This paper describes preliminary results of a study on this reactor using the methanation of carbon dioxide in hydrogen at atmospheric pressure as the test reaction. Moreover, a mathematical model was formulated and used to compare computed conversions with experimental data. The objective of the first phase of this work is to obtain a rough estimate of the applicability of the PPR for methanation purposes.

Experimental

The *test reaction*,

$$CO_2 + 4\ H_2 \rightarrow CH_4 + 2\ H_2O \quad (\Delta H^o_{r,s} = -164.7\ \text{kJ/mole}\ CO_2)$$

has been studied extensively and reliable kinetic data are available (4). Work on the use of this reaction in studying the transient behaviour of an adiabatic methanator indicates that it can be applied as a test reaction between 200 ^{o} and 280 ^{o}C, with good

© 0-8412-0401-2/78/47-065-063$05.00/0

results (5). The kinetic equation used in the present work is given in table I, along with the experimental conditions of the initial phase of the work. The set of conditions being covered in current work is also given in the table, as well as information on the industrial methanation catalyst applied.

Table I

The reaction rate is given by:

$$r_{CO_2} = -\frac{K_\infty \exp.(-E_a/RT)\rho_{CO_2}}{1 + K_{CO_2}\rho_{CO_2}} \quad mol.h^{-1}.g^{-1}$$

Experimental conditions		first phase	current work
Temperature	°C	208, 224, 242	190 - 240
Concentration	vol%	0,19 - 2,56	0,19 - 4
Flow	Nm^3/h	0,05 - 0,45	0,05 - 7
Total pressure	atm.	1	1 - 12
Reactant		H_2, CO_2	H_2, CO, CO_2, H_2O

Catalyst: Girdler G-65 Ni/Al_2O_3; NiO/Al_2O_3 = 3: 3 w/w; particle size = 0,35 - 0,42 mm; S_{BET} = 42,4 m^2/g; S_{Ni} = 6,6 m^2/g

The *equipment* used is similar to that of ref.4, except for the parallel passage reactor and the gas throughput, which is between 0,1 and 0,5 Nm^3/h. It consists of a feed preparation section for metering and controlling the reactant mixture, the PPR immersed in a fluidized bed thermostat and a section for on-line analysis of feed and product gases by gas chromatography. Figure 1 shows a block diagram. The dimensions of the reactor are shown in figure 2. The two catalyst beds are filled with particles of 0.35-0.42 mm; the bottom and top parts of the beds contain inert material of the same dimensions to ensure that the flow regime in the channel is completely established when the gas reaches the catalyst beds.

Reactor Model

Let z be the coordinate in longitudinal direction and y in lateral direction and assume that the concentration changes caused by reaction and mass transport to the catalyst bed are similar to that of figure 3. If the flow regime in the channel is laminar and the reactor isothermal, and supposing that mass transport in channel screen and catalyst bed are entirely due to diffusion, the mass balance for the channel reads:

$$v_y \cdot \frac{\partial C}{\partial z} = \mathbb{D} \frac{\partial^2 C}{\partial y^2} \qquad (1)$$

The equation contains the assumption that the diffusion can be represented by Fick's law, in other words that flow due to the volume change by chemical reaction can be neglected. Furthermore, axial diffusion is not taken into account. Also, the channel is taken to be wide enough to consider it as being bounded by two

In Chemical Reaction Engineering—Houston; Weekman, V., et al.;
ACS Symposium Series; American Chemical Society: Washington, DC, 1978.

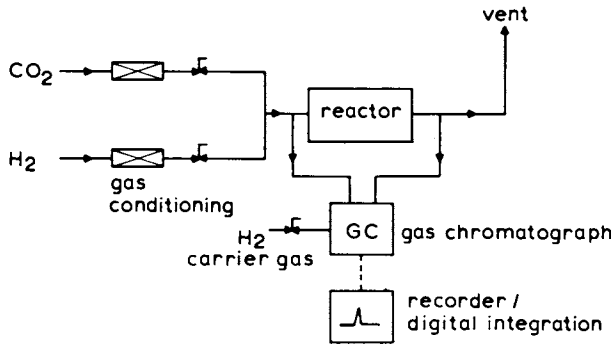

Figure 1. Block diagram of a parallel passage reactor

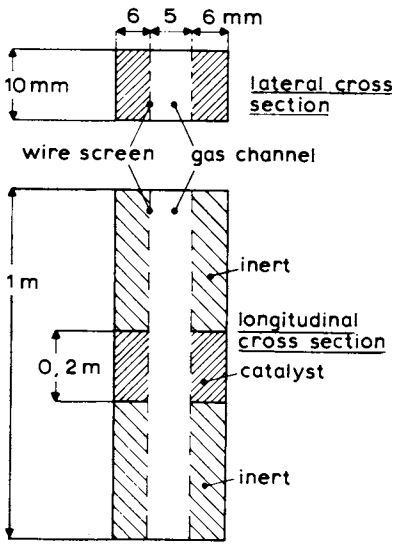

Figure 2. Dimensions of a parallel passage reactor

infinitely wide parallel plates. The boundary conditions are: $\frac{\partial C}{\partial y} = 0$ at $y = 0$ (2); $C = C_o$ at $z = 0$ (3); $\mathbb{D}.\frac{\partial C}{\partial y} = \mathbb{D}_{sc}.\frac{\partial C}{\partial y}$ at $y=\frac{1}{2}a$ (4);

$\mathbb{D}_{eff}.\frac{\partial C}{\partial y} = f(C_k)$ at $y = y_k$ (5) and $v_y = 1 - (y/\frac{1}{2}a)^2$ (6)

The diffusion coefficient in the wire screen ($\mathbb{D}_{sc}$ in eq.4) is taken to be equal to the product of the screen porosity and the diffusion coefficient in the gas channel. Boundary condition (5) must be found by integrating the mass balance over the catalyst bed, which for a volume with thickness dy in the x-z plane reads:

$$\mathbb{D}_{eff}.\frac{\partial^2 C}{\partial y^2} = r_{CO_2}.\rho_{bed} \qquad (7)$$

In this equation, r_{CO_2} represents the rate equation of table I. The effective diffusion coefficient in the catalyst bed is equal to the diffusion coefficient in the channel, corrected for the bed porosity and a factor for the tortuosity of the diffusion path. Both factors are assumed to be $\frac{1}{2}$ according to ref. 6.

Assumptions made in formulating the mass balance over the catalyst bed are that pore diffusion limitation in the catalyst particles can be neglected over the entire concentration range of CO_2 existing in the bed (5), that the bed is isothermal and homogeneous, and that mass transport in the bed is entirely due to diffusion. The boundary conditions are:

$$C = C_k \text{ at } y = y_k \text{ (8) and } \frac{\partial C}{\partial y} = 0 \text{ at } y = y_w \qquad (9)$$

Numerical solution of the mass balance in the catalyst layer is relatively simple. However, a complete solution is superfluous since we are primarily interested in mass transport at $y=y_k$; this transport can be calculated if the first derivative of the concentration in the y-direction is known. It is possible to obtain this derivative analytically from equation (8); if this is done the result is:

$$\frac{\partial C}{\partial y} = \left(\frac{2A}{B^2}(BC - \ln(1 + BC))\right)^{\frac{1}{2}} + \text{integration constant}$$

The integration constant can be determined with boundary condition (9); if C_w is the concentration of reactant at the reactor wall one finds:

$$\frac{\partial C}{\partial y} = \left(\frac{2A}{B^2}(BC - \ln(1 + BC) - BC_q + \ln(1 + BC_w)\right)^{\frac{1}{2}} \qquad (10)$$

The first derivative of the concentration in the y-direction can now be computed by substituting $C = C_k$ in eq (10), provided that the concentration at the reactor wall, C_w, is known. We have assumed that it is equal to 0 to a first approximation, in other words that the catalyst layer is so thick that complete conversion of CO_2 entering it is obtained. This appeared justified on the basis of numerical calculations at the conditions applied in our experiments as well as the calculations reported here. Equation (11) then represents the mass transport into the catalyst bed:

In Chemical Reaction Engineering—Houston; Weekman, V., et al.;
ACS Symposium Series; American Chemical Society: Washington, DC, 1978.

$$\mathbb{D}_{eff} \cdot \left(\frac{\partial C}{\partial y}\right)_{y=y_k} = \mathbb{D}_{eff} \cdot \left(\frac{2A}{B^2} (BC_k - \ln (1 + BC_k))\right)^{\frac{1}{2}} \qquad (11)$$

This means that boundary condition (5) is now known and that the mass balance in the z-direction can be solved, in a way similar to the calculations on the catalytic parallel plate reactor (7). In this first phase of the work the explicit finite differences method of Binder-Schmidt was applied (8); other methods being examined are the method of Dufort and Frankel (9) and orthogonal collocation (10).

Results and discussion

Before making runs with the reactor filled with catalyst, experiments were made with the empty reactor. At first, significant conversions were noted, but it soon appeared that these were due to catalytic activity of the stainless steel wire screen. After replacement by an iron screen no conversion in the empty reactor was found.

Experimental results are shown in figures 4, 5 and 6 for three temperatures, in the form of plots of the conversion against the space velocity at several concentrations of CO_2 in hydrogen. At high space velocities, i.e. at low residence times, the ratio of mass transport by flow through the channel to the mass transport by diffusion into the catalyst bed is relatively high, resulting in low CO_2 conversion. As the flow rate of the gas in the channel is decreased, the above ratio diminishes and a larger proportion of CO_2 is then converted. At very low space velocities the residence time apparently is long enough to give complete conversion.

The figures also indicate a number of encircled conversion points calculated by means of the simple model outlined previously. It is found that the calculated results agree reasonably well with the experimental data at the higher two temperatures (figures 4 and 5); at 208 °C (figure 6), the lowest of the three temperatures, the calculated conversions are invariably higher than the measured values. This is presumably due to the low rate of chemical reaction in the bed at this temperature, which causes the concentration of CO_2 at the reactor wall, C_w, to have a finite value. It is concluded that the model should be improved to incorporate a numerical calculation of the concentration profile in the catalyst bed.

Still, it was thought possible to make a small extrapolation to assess the effect of operating at a higher pressure, at otherwise unchanged conditions. Exploratory calculations indicate that when raising the pressure from 1 to 4 atm at 224 °C and a CO_2 concentration of 0.58 vol%, the space velocity can be increased from about 4000 to about 11000 h^{-1} to obtain the same conversion, 81%, in the two cases. Thus, operation at pressures higher than atmospheric gives improved reactor performance. Further work, both experimental and by improved model calculation, is in progress to evaluate the performance of the reactor for methanation purposes

In Chemical Reaction Engineering—Houston; Weekman, V., et al.;
ACS Symposium Series; American Chemical Society: Washington, DC, 1978.

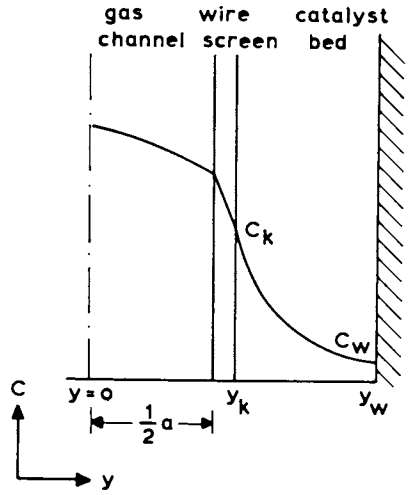

Figure 3. Concentration changes caused by reaction and mass transport to the catalyst bed

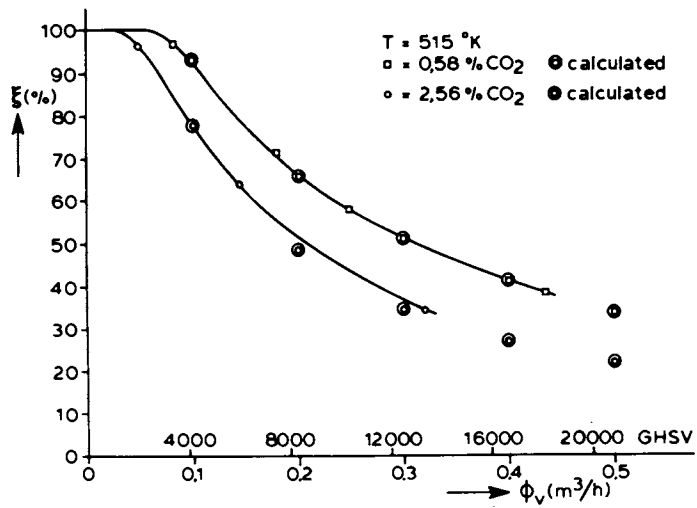

Figure 4. Plot of conversion against the space velocity at $T = 515^{\circ}K$

In Chemical Reaction Engineering—Houston; Weekman, V., et al.;
ACS Symposium Series; American Chemical Society: Washington, DC, 1978.

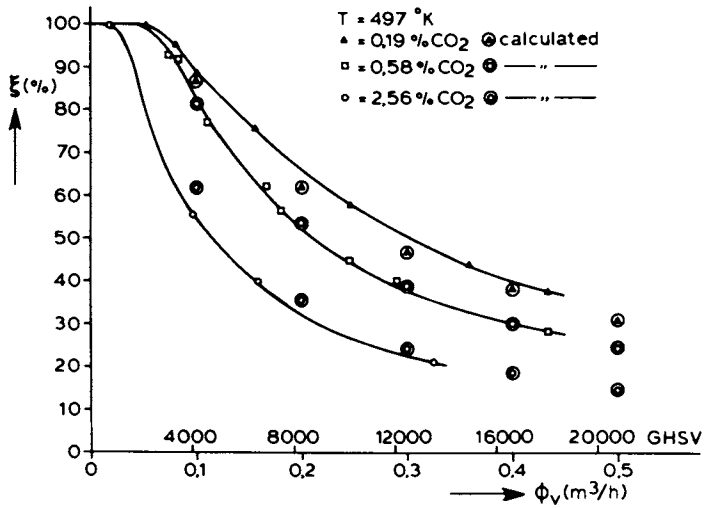

Figure 5. Plot of conversion against the space velocity at T = 497°K

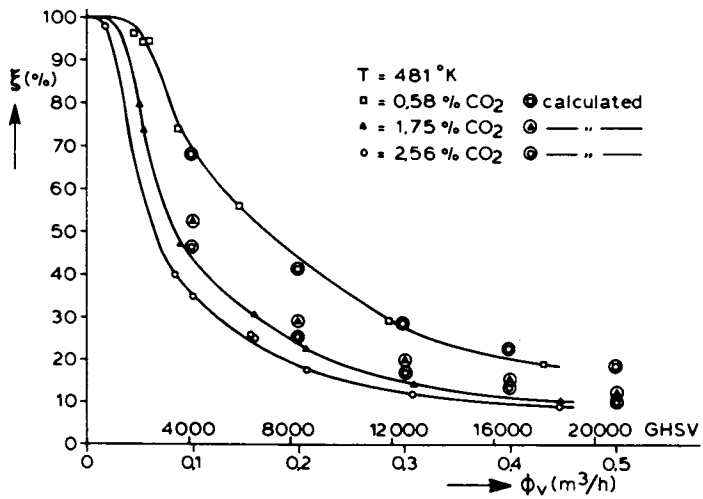

Figure 6. Plot of conversion against the space velocity at T = 481°K

In Chemical Reaction Engineering—Houston; Weekman, V., et al.;
ACS Symposium Series; American Chemical Society: Washington, DC, 1978.

more fully.

If the parallel passage reactor is applied in an industrial methanation operation, it will most probably be followed by a small fixed-bed adiabatic methanator, to enable operation at a certain small concentration of carbon oxides in the product gas of the parallel passage reactor. Moreover, the ratio of the reactor length to the bed depth can be taken much higher in such applications; an industrial reactor would operate at much higher linear velocities in the gas channel than our model reactor. This implies not only that mass transfer from the channel to the bed may be much faster, particularly when the flow in the channel is turbulent, but also that the average CO_2 concentration in the front end of channel as well as in the bed will be rather higher. Thus, catalyst utilization is also expected to be higher.

An advantage of the parallel passage reactor over parallel plate or coated tube reactors is that catalyst poisoning in a PPR will most probably have less effect because it contains a relatively thick catalyst layer. Model calculations are in progress to assess the effects of poisoning more fully. On the basis of the encouraging results obtained so far we are now constructing a reactor system for operation at higher temperatures and pressures in which recycle is possible, in order to study methanation in the parallel passage reactor at conditions more representative of industrial SNG operations.

Acknowledgements

The authors thank the Koninklijke/Shell Laboratorium, Amsterdam, for their generous help in the construction of our experimental reactor, and mrs.J.S.van Regteren for assistance in carrying out measurements and model calculations.

Summary

Exothermic gas/solid reactions involving large quantities of gas, such as carbon oxide methanation with recycle of cold product gas for temperature control, can be carried out in a parallel passage reactor in which the reactants flow through narrow empty channels between shallow beds of solid reactant or catalyst.

A model reactor has been built and studied using the methanation of carbon dioxide as the test reaction. Calculation results of a simple mathematical model agree well with the experimental data except at low temperatures. The conversions obtained are sufficiently promising to warrant further exploration of the parallel passage reactor as a tool in SNG production, the more so because exploratory calculations show that operation at higher pressures results in much improved performance.

In Chemical Reaction Engineering—Houston; Weekman, V., et al.;
ACS Symposium Series; American Chemical Society: Washington, DC, 1978.

List of symbols

a	distance between wire screens	m
A	$\rho_{bed} K_\infty RT \exp(-E_a/RT) D_{eff}$ defined by eq.10	
B	$K_{CO_2} RT$ " " " "	
C	concentration	mole/m^3
C_o	inlet concentration	"
C_k	concentration in catalyst bed at wire screen	"
C_w	concentration at reactor wall	"
D	diffusion coefficient	m^2/s
D_{sc}	" " in wire screen	"
D_{eff}	" " in catalyst bed	"
r_{CO_2}	reaction rate	mole/kg kat s
v_y	gas velocity	m/s
y	running variable perpendicular to direction of flow	m
y_k	y behind wire screen	m
y_w	y at reactor wall	m
z	running variable in flow direction	m
ρ_{bed}	density of catalyst bed	kg/m^3

References

1. Haynes, W.P., Schehl, R.R., Weber, J.K., Forney, A.J. Ind.Eng.Chem.Process Des.Dev. 16(1) 113 (1977)
2. Ralston, R.D., Haynes, W.P., Forney, A.J., Schehl, R.R. Bur.of Mines, Rep. of Invest. 7941 (1974)
3. Helden, H.J.A.van US patent 3.501.897 March 1970 Versluis, R. US patent 3.747.308 July 1973
4. Herwijnen, T.van, Doesburg, H.van, Jong, W.A.de J.Cat 28 391 (1973)
5. Doesburg, H.van Transient behaviour of an adiabatic fixed-bed reactor. Doctoral thesis, Delft University of Technology, 1974
6. Hoogschagen, J. Ind.and Eng.Chem 47 906 (1955)
7. Solbrig, C.W., Gidaspow, D. Ind.Chim. Belge 32 392 (1967)
8. Forsyth, G.E., Wasow, W.R. Finite difference methods for partial differential equations John Wiley & Sons, Inc. 4th ed. 1967
9. Dufort, E.C., Frankel, S.P. Math.Tables Aids Comput. 7 135 (1953)
10. Finlayson, B.A. Cat.Rev. - Sci.Eng. 10 (1) 69 (1974)

In Chemical Reaction Engineering—Houston; Weekman, V., et al.;
ACS Symposium Series; American Chemical Society: Washington, DC, 1978.

7

Experimental and Theoretical Study of the Simultaneous Development of the Velocity and Concentration Profiles in the Entrance Region of a Monolithic Convertor

M. A. M. BOERSMA,* W. H. M. TIELEN, and H. S. VAN DER BAAN

University of Technology, Department of Chemical Technology, Eindhoven, The Netherlands

In catalytic afterburning of waste gases the monolithic or active wall reactor is becoming increasingly important. Most experimental and theoretical studies on this reactor that have been published so far consider the velocity field in the separate channels of the monolith either undeveloped, i.e. plug flow (1-3), or fully developed, i.e. laminar flow (4-7). In reality, however, the velocity profile, which can be assumed to be more or less uniform at the entrance of the channel, will develop into a laminar Poiseuille profile downstream the tube. This implies that the experimental measured conversions will not correspond to the theoretically calculated concentration profiles for either plug flow or laminar flow, i.e. concentration profiles calculated for a uniform velocity profile will result in a conversion which is higher than the actual conversion, while a fully developed profile gives rise to a conversion lower than the actual one. Therefore, to get a more accurate description of the phenomena taking place in the entrance region of the active wall reactor we studied the simultaneous development of the velocity and concentration profiles by numerical analysis of the governing steady state differential equations, i.e. the Navier-Stokes equation of motion and the diffusion equation for incompressible flow of a Newtonian fluid. Some work in this field has been performed earlier by Ulrichson and Schmitz (8). These investigators used the approximate solution of Langhaar (9) for the entrance velocity profiles to provide the velocity data for numerical solution of the component material balance.

The calculations apply to an isothermal reactor, a condition which generally is satisfied in case of low concentration of the waste gas. Further it is assumed that the kinetics of the chemical reaction taking place at the tube wall can be described by

$$r = k\, c_{HC,wall}^{n}$$

* Present address: Koninklijke/Shell-Laboratorium (Shell Research B.V.) Amsterdam, The Netherlands

© 0-8412-0401-2/78/47-065-072$05.00/0

n being the order of the reaction. This rate expression applies to the oxidation of small concentrations hydrocarbon in an excess of air.

To check the calculated concentration profiles in practice we studied the combustion of low concentrations of ethylene and isobutene in a commercial monolithic convertor special made for us by Kali-Chemie Engelhard Katalysatoren GmbH.

Theoretical Part

At first we tried to solve the problem in study by a simultaneous numerical analysis of the Navier-Stokes equations and the mass transport equation. Since by this method serious numerical instabilities were encountered we choose an alternative procedure. This consists of calculating first, at each grid point in the tube, the axial and radial velocities, after which these values are used to solve the mass transport equation. In solving this equation care is taken that the grid used is identical to that for solving the velocity field.

The Entrance Velocity Field For an isothermal, steady state, incompressible flow of a Newtonian fluid being symmetrical in the azimuthal direction, the governing equations are the Navier-Stokes equations and the steady state continuity equation. In dimensionless form the equations are:

$$V\frac{\partial V}{\partial r} + U\frac{\partial V}{\partial z} = -\frac{1}{U_m^2\rho}\frac{\partial P}{\partial r} + \frac{2}{Re}\left(\frac{\partial^2 V}{\partial r^2} + \frac{1}{r}\frac{\partial V}{\partial r} - \frac{V}{r^2} + \frac{\partial^2 V}{\partial z^2}\right) \quad (1)$$

$$V\frac{\partial U}{\partial r} + U\frac{\partial U}{\partial z} = -\frac{1}{U_m^2\rho}\frac{\partial P}{\partial z} + \frac{2}{Re}\left(\frac{\partial^2 U}{\partial r^2} + \frac{1}{r}\frac{\partial U}{\partial r} + \frac{\partial^2 U}{\partial z^2}\right) \quad (2)$$

$$\frac{\partial V}{\partial r} + \frac{V}{r} + \frac{\partial U}{\partial z} = 0 \quad (3)$$

The pressure dependent terms in equations (1) and (2) can be removed by differentiating equations (1) and (2) with respect to z and r, respectively, and subtracting the resultant equations from each other (10,11). According to the method outlined by Vrentas et.al.(11) now a stream function Ψ is introduced which is defined as:

$$U = -\frac{\partial \Psi}{r\partial r} \qquad V = \frac{\partial \Psi}{r\partial z} \quad (4)$$

We further recall that the only non zero component of the vorticity vector is the azimuthal physical component, which is given by:

$$\omega = \frac{\partial V}{\partial z} - \frac{\partial U}{\partial r} \quad (5)$$

With the aid of equations (4) and (5) we finally get the following

In Chemical Reaction Engineering—Houston; Weekman, V., et al.;
ACS Symposium Series; American Chemical Society: Washington, DC, 1978.

equations:

$$-\frac{\omega}{r^2}\frac{\partial\Psi}{\partial z}+\frac{1}{r}\frac{\partial\Psi}{\partial z}\frac{\partial\omega}{\partial r}-\frac{1}{r}\frac{\partial\Psi}{\partial r}\frac{\partial\omega}{\partial z}=\frac{2}{Re}\left(\frac{\partial^2\omega}{\partial r^2}+\frac{1}{r}\frac{\partial\omega}{\partial r}-\frac{\omega}{r^2}+\frac{\partial^2\omega}{\partial z^2}\right) \quad (6)$$

$$\omega r=\frac{\partial^2\Psi}{\partial z^2}+\frac{\partial^2\Psi}{\partial r^2}-\frac{1}{r}\frac{\partial\Psi}{\partial r} \quad (7)$$

When in these equations the second partial derivatives of Ψ and ω with respect to z are neglected, which is justified because in the monolithic convertor the convective transport of vorticity in the axial direction is greater than the axial diffusive transport, the elliptic differential equations change into parabolic equations.

Solution of the equations is carried out with the following initial and boundary conditions:

$$r=0,\ z>0:\ \frac{\partial U}{\partial r}=V=\omega=0,\ \Psi=\tfrac{1}{2} \quad (8)$$

$$0\leq r\leq 1,\ z=0:\ \omega=0,\Psi=\tfrac{1}{2}\ (1-r^2) \quad (9)$$

$$r=1,\ z>0: U=V=\Psi=\frac{\partial\Psi}{\partial r}=0,\ \omega=\frac{\partial^2\Psi}{\partial r^2} \quad (10)$$

In the numerical analysis the radial and axial derivatives of the parabolic equations are replaced by the central difference approximations and the backward difference approximations, respectively. Thus N-1 sets of finite parabolic difference equations are obtained, N being the number of radial steps. The number of equidistant grid points in radial direction amounted to 40, while for the finite difference increment of $\zeta(=2z/Re)$ a value of $1.25\ 10^{-4}$ was used. Details of the numerical solution procedure are given elswhere (12). Figure 1 is a graphical representation of the development of the axial velocity obtained by the numerical solution procedure. This result agrees quite well with that obtained by Vrentas et.al. (11).

The Tube Wall Catalyzed Reaction Assuming incompressible flow of a Newtonian fluid and no contributions in the azimuthal direction a mass balance for a differential element in the entrance region of the tube yields the following steady state dimensionless differential equation:

$$\frac{\partial^2 C}{\partial r^2}+\frac{\partial C}{r\partial r}+\frac{\partial^2 C}{\partial z^2}=\frac{Pe}{2}\ \frac{\partial UC}{\partial z}\ +\frac{Pe}{2r}\frac{\partial(rVC)}{\partial r} \quad (11)$$

Since in the monolith the convective transport will overwhelm the diffusion transport (Pe>25) the term $\partial^2C/\partial z^2$ may be neglected. The initial and boundary conditions are then given by:

$$r=0, z>0:\ \frac{\partial C}{\partial r}=0,\ \lim_{r\to 0}\frac{\partial C}{rdr}=\frac{\partial^2 C}{\partial r^2} \quad (12)$$

In Chemical Reaction Engineering—Houston; Weekman, V., et al.;
ACS Symposium Series; American Chemical Society: Washington, DC, 1978.

$$0 \leq r \leq 1,\ z = 0:\ C = 1 \tag{13}$$

$$r = 1, z > 0:\ \frac{\partial C}{\partial r} = \frac{KRc_o^{n-1}}{D}\ C^n = -\ DaC^n \tag{14}$$

As the radial concentration gradient at the tube wall determines the mass flux supplied by diffusion a good approximation of this gradient is necessary to obtain an accurate description of the concentration profiles in the tube. In the numerical analysis this is effected by reduction of the radial step width near the tube wall. During the calculations it turned out, however, that a non equidistant radial grid resulted in persistent numerical instabilities. We, therefore, used an equidistant grid, which was identical to that applied for the volocity profile.

For a fully developed and for an undeveloped velocity profile the radial velocity is independent of the axial distance while also the radial velocity may be neglected.
Equation (11) then reduces to

$$U\frac{\partial C}{\partial z} = \frac{2}{Pe}\left(\frac{\partial^2 C}{\partial r^2} + \frac{1}{r}\frac{\partial C}{\partial r}\right) \tag{15}$$

Equation (11) and (15) have been solved numerically together with conditions (12)-(14) for various values of the reaction order (n), Damköhler number (Da) and Schmidt number (Sc)*. Figure 2 shows for a first order reaction and Da = 1.28 the average and tube wall concentrations obtained numerically for three flow conditions, i.e. undeveloped, developing and fully developed flow. We see that indeed the average concentration for developing flow lies between that for fully developed and undeveloped flow. Similar pictures were obtained for other combinations of n, Sc and Da.

Experimental Part

Methods The reaction system used for the oxidation experiments consists of a gas mixing part, a reactor and an analysis system. In the gas mixing part mixtures of air and the hydrocarbon to be oxidized can be prepared in all desired compositions. After leaving the mixing room, the feed gas enters a preheater. Both the mixing room and the preheater are filled with glass Raschig rings.

The reactor shell, which is made from glass, has a hexagonal cross section, in which the commercial honeycombs fit snugly. It consists of a preheating section, about 15 cm in length, which is filled with packing material, and a reaction zone containing the monolith. The temperature of both sections can be controlled separately with Eurotherm Thyristor controllers. Temperature of the gas stream entering and leaving the monolith is measured by means of chromel-alumel thermocouples.

To determine the inlet and outlet hydrocarbon concentrations, gas samples are taken just before and after the reaction zone by means of an eight way Becker gas sampling valve. For hydrocarbon analysis we use a Pye series 104 gas chromatograph with flame ionization detector.

* Details of the numerical solution procedure are given elswhere (12)

In Chemical Reaction Engineering—Houston; Weekman, V., et al.;
ACS Symposium Series; American Chemical Society: Washington, DC, 1978.

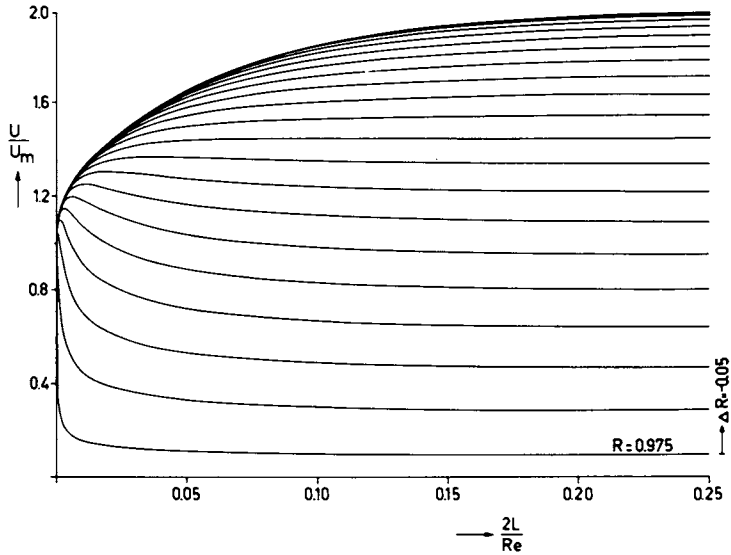

Figure 1. Development of the axial velocity field obtained by numerical solution of the parabolic differential equations

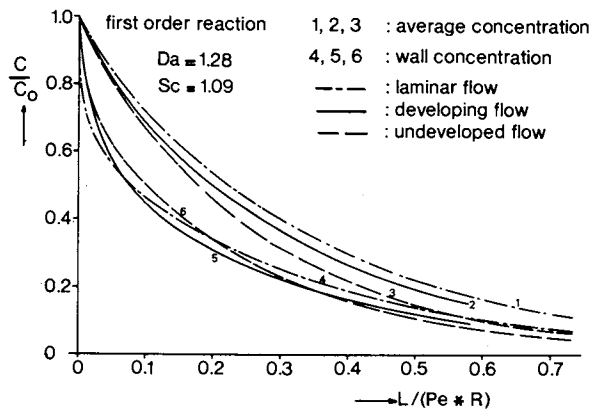

Figure 2. Numerical solutions of equations 11 – 15 for a first order reaction with Da = 1.28 and Sc = 1.09

In Chemical Reaction Engineering—Houston; Weekman, V., et al.;
ACS Symposium Series; American Chemical Society: Washington, DC, 1978.

The experiments have been executed partly with a commercial (WK 220, supplied by Kali-Chemie Engelhard Katalysatoren GmbH, Hannover) honeycomb reactor, and partly with a highly active honeycomb, especially made for us by Kali-Chemie Engelhard. The WK 220 honeycomb is 10 cm in length and contains 169 tubes each of which are 2.4 mm in diameter. In both monoliths the active component was platinum.

Results When we assume that the catalyzed wall reaction takes place homogeneously and can be described as being first order in the hydrocarbon concentration, while the gas flow through the tubes is supposed to be ideal plug flow, an impression of the magnitude of the rate constant can be obtained by using the relation:

$$\ln \frac{c_e}{c_o} = - k\tau \qquad (16)$$

Since the dimension of k in this equation does not correspond to that of K, figuring in equation (14), the experimental measured rate constant, k, has to be transformed in the wall rate constant, K, by the relation:

$$K = (\frac{d}{4}) \cdot k \qquad (17)$$

Determination of K by relation (17) assumes that the tube wall concentration equals the cup mix concentration. Since it is expected that concentration gradients are present in the tubes of the monolith the rate constant from equation (17) will always be lower than its real value.

The kinetics of the ethylene combustion (c_o = 200 - 300 ppm) was studied in the commercial honeycomb reactor. The temperatures of the gas entering and leaving the reactor were almost equal (within 1-2 °C). The oxidation appeared to be first order in ethylene. Changing the temperature gave the result shown in figure 3. Below 500 K the oxidation takes place in the reaction controlled region. The activation energy then amounts to 42 kJ/mol. Above this temperature, however, a transition to the film diffusion limitation region occurs. The activation energy now amounts to only 8 kJ/mole. The existence of the diffusion limitation region is also illustrated by the excellent agreement between the temperature dependence of the diffusion coëfficient of ethylene in air, as determined by the Lennard-Jones expression, and the temperature dependence of the rate constant in this region. Figure 4 shows for the various temperatures the relation between the outlet concentration and reactor length. We see that the position of the curves relative to each other is determined by the Da number. In the reaction limited region (< 500 K) the Da number increases with temperature. In the film diffusion limited region, however, the Da number decreases with increasing temperature due to the slight temperature dependence of K in this region. In the film diffusion region a modified form of the Leveque equation holds (13), i.e.

In Chemical Reaction Engineering—Houston; Weekman, V., et al.;
ACS Symposium Series; American Chemical Society: Washington, DC, 1978.

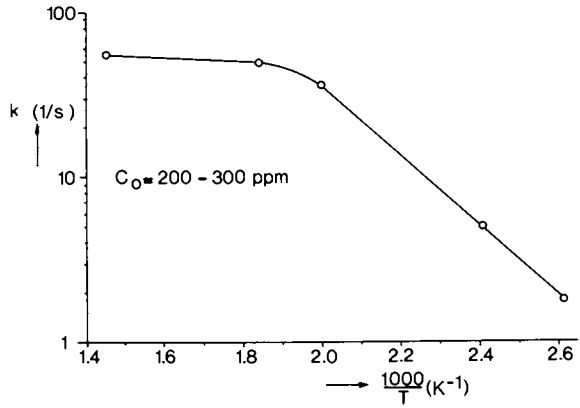

Figure 3. Arrhenius plot for the oxidation of ethylene in the commercial honeycomb reactor (WK 220)

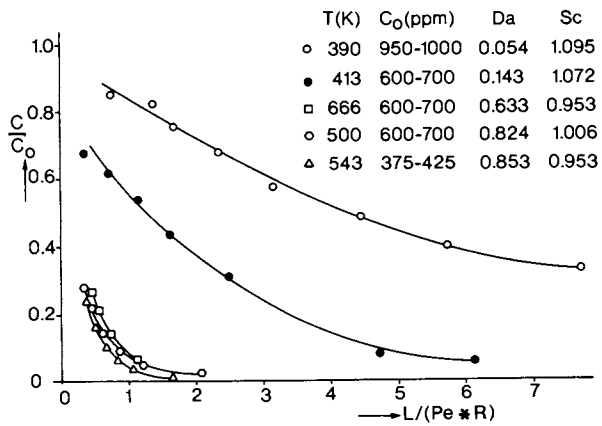

Figure 4. Oxidation of ethylene in commercial (WK 220) honeycomb reactor

In Chemical Reaction Engineering—Houston; Weekman, V., et al.;
ACS Symposium Series; American Chemical Society: Washington, DC, 1978.

$$F \text{ (conversion)} = \text{constant } \frac{(D\tau)^{2/3}}{R^{4/3}} \qquad (18)$$

It appears that for the experiments at 666 K this equation gives a good description of the measurements up to F = 80 - 90%.

Hereafter we studied the entrance effect by using a honeycomb convertor which consisted of a non-impregnated and an impregnated (highly active) part, both about 5 cm in length. When the feed gas enters the non-impregnated part firstly, the velocity profile will be fully developed when entering the impregnated part. By turning around the convertor 180° in the reactor we have the situation of developing flow combined with chemical reaction at the tube wall. This procedure allows to measure the entrance effect experimentally. The results of the measurements are shown in figure 5. It turns out that indeed the conversion for developing flow is higher than for fully developed flow. The Da number calculated for these measurements with a K value from equation (17) amounts to 1.28. The calculated profile for fully developed flow with this Da number, however, does not correspond with the experimental points for this flow condition, indicating that indeed the average concentration does not equal the tube wall concentration. With Da = 2.7, however, the agreement between the theoretical profiles for fully developed flow and the experimental measured conversions for this flow condition is excellent. This indicates that the tube wall concentration is roughly two times as low as the average concentration. The agreement between the theoretical profile for developing flow (Da = 2.7) and the experimental points is somewhat worse than for fully developed flow, indicating that for developing flow the Da number will be somewhat lower.

With the highly active convertor used for studying the entrance effect all experiments in the temperature range 400-680 K are run in the film diffusion region. This allows to study the validity of the Leveque equation in more detail. From figure 6 we may conclude that at all three investigated temperatures the Leveque equation gives a good description of the experiments up to F = 80 - 90%.

Besides the oxidation of ethylene we also paid attention to the combustion of 1-butene. This reaction was found to be 1.3 order in 1-butene and has an activation energy of 6.7 kJ/mole (500-713K), indicating that the reaction runs also in the film diffusion limitation region. Like in the case of ethylene oxidation the relative situation of the curves in the c/c_o vs L/RPe plane is solely determined by the value of Da. Also here the Leveque equation proves to be a good description of the experimental results.

Discussion

From the preceding paragraph it has become clear that the experimental determined rate constant, K, always will be less than its real value. Therefore, it looks appropriate to deal more specific with the ratio between the tube wall and cup mix concentration, since this ratio determines how far the rate constant K, as

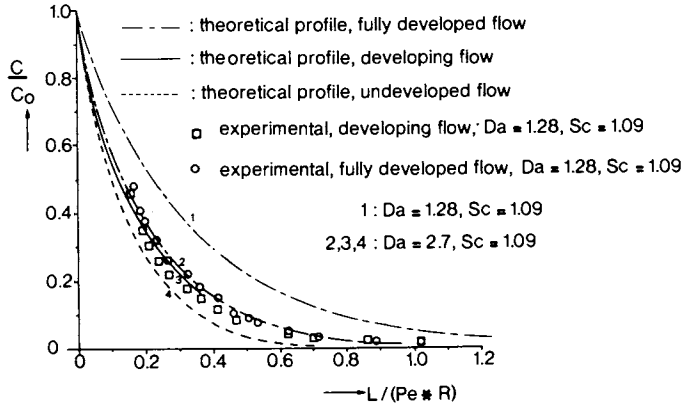

Figure 5. Entrance effect in highly active monolith. Oxidation of ethylene (C_o = 300–350 ppm) at 400 K.

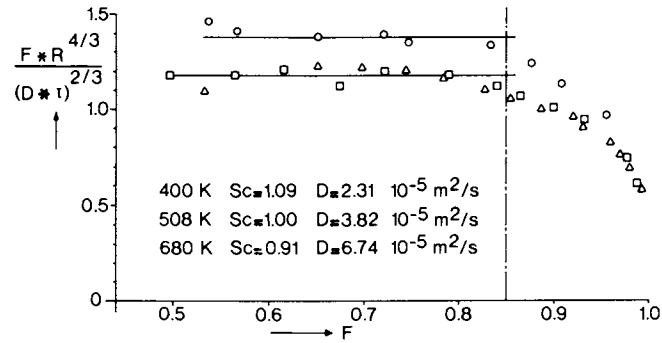

Figure 6. Verification of the Leveque equation for the oxidation of ethylene in the diffusion limitation region

In Chemical Reaction Engineering—Houston; Weekman, V., et al.;
ACS Symposium Series; American Chemical Society: Washington, DC, 1978.

determined from a homogeneous description of the wall reaction, deviates from the real rate constant. Table I gives for three flow conditions, i.e. fully developed, developing and undeveloped flow, this ratio as a function of the axial distance, reaction order, Da number and Sc number.

No	L / (Pe * R)	Undeveloped			Developing			Fully developed		
		0.1	0.2	0.3	0.1	0.2	0.3	0.1	0.2	0.3
1	Da=1.7; Sc=0.97; n=1	0.68	0.675	0.673	0.57	0.545	0.544	0.564	0.557	0.565
2	Da=2,7; Sc=1.09; n=1	0.564	0.557	0.557	0.442	0.424	0.423	0.438	0.432	0.432
3	Da=5.5; Sc=1,19; n=1.3	0.488	0.528	0.572	0.38	0.397	0.426	0.373	0.397	0.43
4	Da=10; Sc=1; n=1	0.238	0.234	0.234	0.166	0.16	0.16	0.162	0.16	0.16
5	Da=10; Sc=1; n=2	0.56	0.635	0.722	0.459	0.516	0.578	0.447	0.506	0.572

Table I Ratio between tube wall and cup mix concentration for various conditions.

We see that the ratio between tube wall concentration and cup mix concentration is highest for undeveloped flow and lowest for a fully developed velocity profile. It further follows that under our experimental conditions (no 1, 2, 3 Table I) for all three flow conditions the average concentration is roughly two times as high as the wall concentration. This implies that also the rate constant roughly spoken has to be two times as high as the experimental value. In the preceeding paragraph we saw that for the fully developed velocity field this indeed is the case.

The calculations further have shown that the concentration profiles for developing flow agree better with the fully developed velocity field than with the undeveloped flow condition. This agreement becomes even better with increasing Da number. Therefore, in practice one should use the Poiseuille profile for calculating the conversion in the monolith reactor.

Finally, it has become clear that as a result of diffusion limitation Da values greater than 10 are hardly realistic in active wall reactors in which the reactants are in the gas phase.

Acknowledgement It is a pleasure to thank Kali-Chemie Engelhard Katalysatoren GmbH, Hannover, Germany, for supplying the monoliths used in this study. We also want to thank Dr.G.J. Visser of the Computer Centre for his valuable advice during the computational work.

Notation

C	dimensionless concentration	ρ	density
c_e	exit concentration	μ	dynamic viscosity
c_o	inlet concentration	τ	residence time

d	diameter tube	Ψ	dimensionless stream function
D	molecular diffusion coëfficient	ζ	dimensionless axial coordinate (= 2 z/Re)
F	relative conversion	ω	dimensionless azimuthal component of the vorticity vector
k	rate constant homogeneous reaction	Da	Damköhler number $\frac{KRc_o^{n-1}}{D}$
K	rate constant for wall reaction	Pe	Péclet number $\frac{Ud}{D}$
L	length of tube	Re	Reynolds number $\frac{\rho Ud}{\mu}$
n	reaction order	Sc	Schmidt number $\frac{\mu}{\rho D}$
P	pressure		
r	radial distance/radius of tube		
R	radius of tube		
U	velocity axial direction		
U_m	axial velocity at r = 0		
V	velocity radial direction		
z	axial distance/radius of tube		

Literature Cited

1. Baron, Th., Manning, W.R., and Johnstone, H.F., Chem. Eng. Prog., (1952), 48, 125.
2. Johnstone, H.F., Houvouras, E.T., and Schowalter, W.R., Ind. Eng. Chem., (1954), 46, 702.
3. Brauer, H., and Schlüter, H., Chemie-Ing.-Techn., (1966), 38, 279.
4. Bräuer, H.W., and Fetting, F., Chemie-Ing.-Techn., (1966), 38, 30.
5. Seifert, A., and Schmidt, H., Chemie-Ing.-Techn., (1967), 39, 593.
6. Koch, H., and Kirchner, K., Dechema Monografiën, (1973), 75, 145.
7. Young, L.C., and Finlayson, B.A., Adv. Chem. Ser., (1974), 133, 629.
8. Ulrichson, D.L., and Schmitz, R.A., Ind. Eng. Chem., Fundam., (1965), 1, 1.
9. Langhaar, H.L., J. Appl. Mech., (1942), 9, A-55.
10. Wang, Y.L., and Longwell, P.A., A.I.Ch.E. Journal, (1964), 10, 323.
11. Vrentas, J.S., Duda, J.L., and Bargeron, K.G., A.I.Ch.E. Journal, (1966), 12, 837.
12. Tielen, W.H.M., "An experimental and theoretical study of the active wall reactor", MSc-Thesis, Eindhoven, The Netherlands, (1976).
13. Cowherd, C., and Hoelscher, H.E., Ind. Eng. Chem, Fundam., (1965), 4, 150.

In Chemical Reaction Engineering—Houston; Weekman, V., et al.;
ACS Symposium Series; American Chemical Society: Washington, DC, 1978.

Monolithic Reactor-Heat Exchanger

T. F. DEGNAN, JR. and J. WEI
University of Delaware, Newark, DE 19711

A novel monolithic reactor-heat exchanger has been constructed and operated in five different modes. Experiments were conducted with the oxidation of carbon monoxide over copper chromite pelleted catalysts. The experimental temperatures of reactants and coolants, and concentrations agree with computations with a cell model. Virtually flat temperature profiles can be obtained in the co-current mode.

Equipment

A novel chemical reactor has been constructed of four crossflow monoliths arranged in series to act as reactor-heat exchangers. Every second pass of each crossflow is packed with a pelleted catalyst or has catalyst deposited on the monolith walls. The remaining passes are empty to facilitate the flow of heat exchange medium. A pelleted crossflow monolith is shown in Fig. 1, and its dimensions are shown in Table I. For the coated monolith, the heights of the two passes are the same. Note the large heat transfer area to volume ratio achieved in the crossflow design, which leads to a high number of transference units for heat exchange.

Arranging the crossflows in series approximates true cocurrent or countercurrent flow. Mathematical analyses of simple heat transfer were published on cocurrent or countercurrent behavior for a series of crossflows (1,2). This paper deals with the mathematical modeling and experiments for simultaneous reaction and heat transfer.

The oxidation of carbon monoxide over a base metal catalyst was selected because it is a highly exothermic reaction whose rate has an approximate first order dependence on the concentration of

© 0-8412-0401-2/78/47-065-083$05.00/0

Table I

Physical Dimensions of Crossflow Monoliths

	Pellet Filled Monoliths	
	Reaction Pass	Coolant Pass
Cross Sectional Area of Flow, A^x	2.326 in^2	0.867 in^2
Heat Transfer Area, A	86.2 in^2	67.82 in^2
Height Between Flats, b	0.315 in	0.125 in
Thickness of Flats, a'	0.0336in	0.0336in
Volume of Pass, V	4.652 in^3	1.735 in^3
Hydraulic Radius, r	0.054 in	0.026 in
Heat Transfer Area to Volume Ratio, a	18.49 in^{-1}	39.10 in^{-1}

CO (3,4,5); pelleted copper chrome "aero ban" catalyst provided by American Cyanamid Co. was characterized, using a 1.25 cm OD integral reactor in a constant temperature sand bath. First order kinetics were obtained in the range of 425 to 1000°F. The following kinetic parameters were obtained:

$$\frac{E}{R} = 6{,}300\ °R^{-1}$$

$$k_\infty = 1.194 \times 10^4\ sec^{-1}.$$

The pelleted copper chrome catalyst was metered into each of the large sinusoidal ducts of the reaction pass of each of the four monoliths comprising the reactor-heat exchanger. A ¼" layer of quartz chips at each of the reaction pass faces of the cross-flows guaranteed that the reaction was confined to the volume of the monolith where heat exchange could take place.

In a separate set of four crossflow monoliths, a catalyst of similar composition (1.442% Cu and 0.966% Cr) and density was coated exclusively on the walls of the reaction pass. No attempt was made to keep the catalyst from adhering to the section of wall adjacent to which no heat transfer medium flowed.

In both cases, the four cordierite monoliths were positioned in a steel manifold shown in Fig. 2.

In Chemical Reaction Engineering—Houston; Weekman, V., et al.;
ACS Symposium Series; American Chemical Society: Washington, DC, 1978.

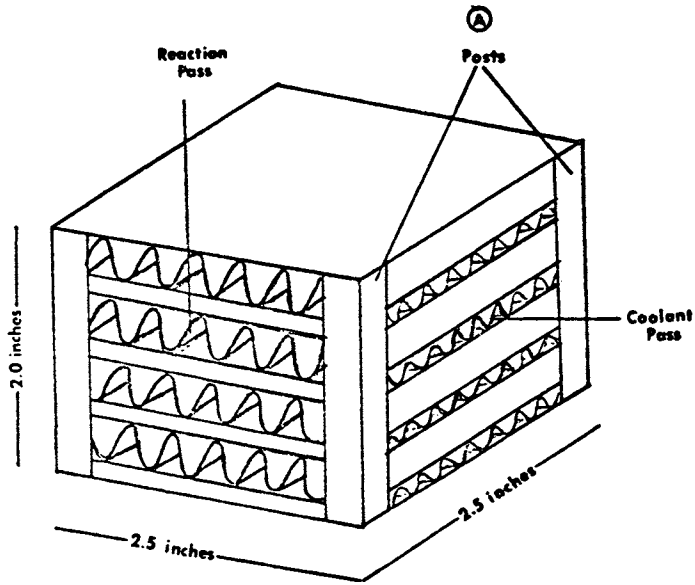

Figure 1. Pellet-filled crossflow monolith

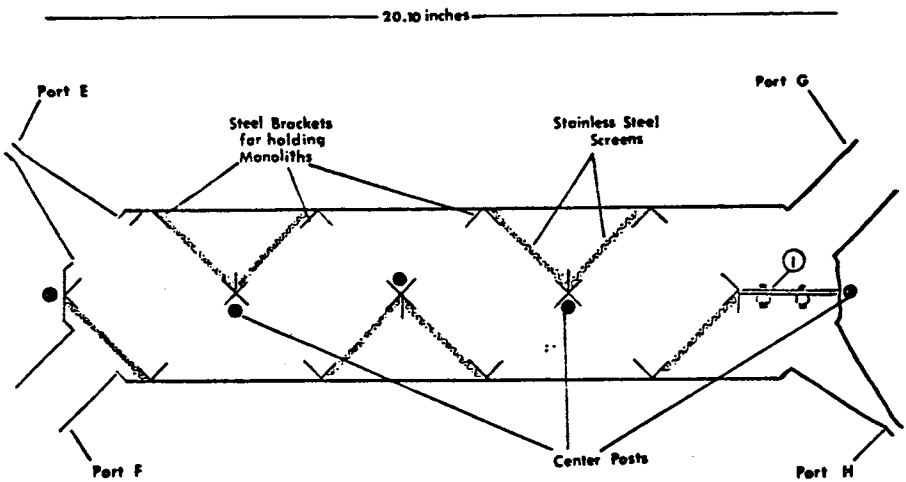

Figure 2. Top view of MRHE

In Chemical Reaction Engineering—Houston; Weekman, V., et al.;
ACS Symposium Series; American Chemical Society: Washington, DC, 1978.

Fifty-seven chromel-alumel thermocouples measured the temperatures within the reactor. A Doric multipoint digital recorder monitored the thermocouple readings and printed these readings on paper tape.

A conversion profile along the reaction pass was obtained by measuring the composition in each of the triangular shaped empty volumes between the monoliths. Fifteen centimeters long pieces of stainless steel were welded into the center of each of the ten triangular shaped volumes for use as gas sample ports. Sample analysis was performed using a gas chromatograph.

Cocurrent, Countercurrent and Autothermal Operation

By feeding the inlet reactant and coolant streams into separate ports of the reactor, it was possible to achieve five different flow schemes, shown in Fig. 3. An adiabatic reactor was simulated by feeding a stream of preheated air and CO to the catalyst containing reaction pass and by sealing off the coolant pass. Similarly, the cocurrent and countercurrent schemes were approximated by flowing coolant and reactant streams either into adjacent ports or into ports which lie at opposite ends of the reactor-heat exchanger respectively.

Finally, autothermal cocurrent and countercurrent schemes were approximated by feeding a cool stream of CO in air into the coolant pass and feeding the heated stream leaving this pass to the catalyst containing reaction pass. For the autothermal countercurrent run, the partition between ports G and H was removed, the ports were sealed, and the CO containing stream was fed to port E. For the autothermal cocurrent case this partition was restored, and the mixture of CO in air was fed into Port G. An insulated stainless steel flex hose was used to carry the gas stream from port E to port H. The reacted stream exited at port F.

Mathematical Models

The cell model (6,7) is particularly well suited to describing the two dimensional temperature and concentration profiles in crossflow, including axial dispersion in these short passes ($L/D_D<25$ for the monoliths and catalyst used in this study). After neglecting the radial and interphase concentration and temperature gradients, we can write the modelling equations for a first order reaction with simultaneous

In Chemical Reaction Engineering—Houston; Weekman, V., et al.;
ACS Symposium Series; American Chemical Society: Washington, DC, 1978.

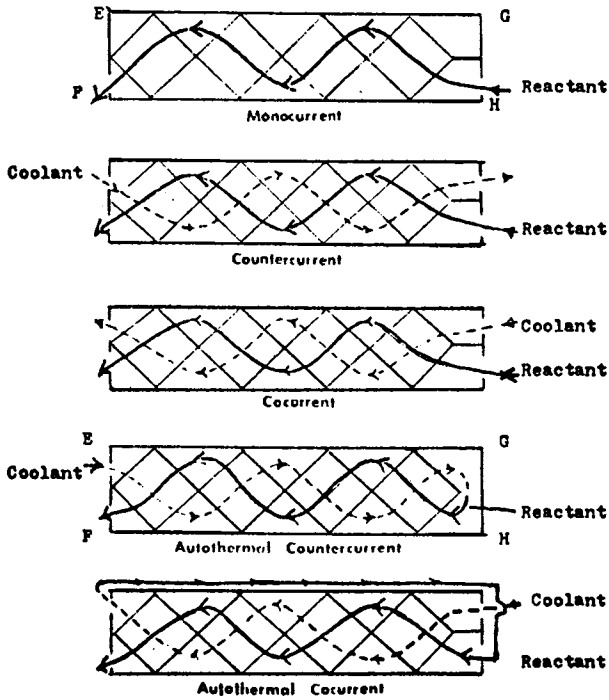

Figure 3. Five MRHE flow modes

In Chemical Reaction Engineering—Houston; Weekman, V., et al.;
ACS Symposium Series; American Chemical Society: Washington, DC, 1978.

heat transfer and heat loss in a single crossflow as:

$$\theta^R_{i,j}-\theta^R_{i-1,j} = -NTU^R(\theta^R_{i,j}-\theta^C_{i,j})-NTU^{AR}(\theta^R_{i,j}-\theta^{AM}) + \beta Y_{i,j}\exp(-\alpha/\theta^R_{i,j})(\theta^R_o/\theta^R_{i,j}) \quad (1)$$

$$\theta^C_{i,j}-\theta^C_{i,j-1} = NTU^C(\theta^R_{i,j}-\theta^C_{i,j})-NTU^{AC}(\theta^C_{i,j}-\theta^{AM}) \quad (2)$$

$$Y_{i,j}-Y_{i-1,j} = -\beta Y_{i,j}\exp(-\alpha/\theta^R_{i,j})(\theta^R_o/\theta^R_{i,j}) \quad (3)$$

An explanation of the terms used in the above equations can be found in the nomenclature. These equations are applicable for i>2 and j>2. The first set of points in each direction, i.e., i=1, j=1, 2, ..., N and j=1, i=1, 2, ...M are for the specification of the boundary conditions. The boundary conditions are thus

$$\begin{aligned} Y_{1,j} &= Y_o \qquad j = 2,3,....N \\ \theta^R_{1,j} &= \theta^R_o \qquad j = 2,3,....N \\ \theta^C_{i,1} &= \theta^C_o \qquad i = 2,3,....N \end{aligned} \quad (4)$$

where N-1 is the number of cells in the j-direction and M-1 is the number of cells in the i-direction.

To solve for the dimensionless temperatures θ^C, and θ^R and the fraction remaining Y over the entire grid, a marching method is used in which the Newton-Raphson algorithm solves for $\theta^C_{i,j}$, $\theta^R_{i,j}$ and $Y_{i,j}$ at each point until the grid is completely specified.

Extension of the proposed cell model for one crossflow monolith to any number of crossflows is relatively straightforward. Each monolith is assigned an NXM grid while the triangular shaped chambers between the monoliths are treated as continuous stirred volumes. The stream entering each of the chambers has a temperature and composition that are the average of the streams leaving the crossflows.

To obtain the inlet temperatures to the next monolith in the direction of flow, a heat balance must be drawn around the chambers to account for heat loss. Heat transfer coefficients needed to obtain NTU^C, NTU^R, NTU^{AC}, NTU^{AR}, NTU^{CR} and NTU^{CR} are obtained from analysis of steady state and stop flow heat transfer data.

By alternately solving the set of equations describing the NXM grid and the heat balances around the chambers, it is possible to compute the temperature and concentration profiles over the entire reactor.

In Chemical Reaction Engineering—Houston; Weekman, V., et al.;
ACS Symposium Series; American Chemical Society: Washington, DC, 1978.

The countercurrent, autothermal cocurrent, and autothermal countercurrent schemes require an iterative approach since the boundary conditions are split in each of these cases.

The hydrodynamic entrance effect is important on the heat transfer coefficient in the coolant pass of each crossflow. Under the experimental conditions, the entrance effect may penetrate more than halfway into the crossflow. Approximations to the Graetz problem for flow entering a sinusoidal duct are available (8) although many of these are in the form of infinite series. Hawthorn (9) has proposed an analytical approximation to the Graetz problem of the form,

$$\frac{hd}{kg} = B(1+0.078(dRePr/x)^{0.45} \qquad (5)$$

where d is the hydraulic diameter, x is the distance, and B is the asymptotic nusselt number (NU=2.12) for flow in a sinusoidal duct.

Results

Experimental analyses of the heat transfer characteristics of the monolithic reactor-heat exchanger were carried out in the absence of reaction to define the NTU values in equations (1), (2), and (3). Experiments were performed in which the coolant pass flow rate was varied independently of the reaction pass flow rate, to produce j-factors vs Reynolds number, in good agreement with both the Graetz solution and data from an experimental study by Kays et al (10) of a crossflow of similar design.

Heat transfer coefficients of the reaction pass in which the pelleted catalyst filled the sinusoidal volume was satisfactorily described by the correlation proposed by Leva (1950) for large d_p/d ratios:

$$\frac{hd}{kg} = 0.125\ \left(\frac{dp\ \rho g\ v}{M}\right)^{0.75} \qquad (6)$$

The NTU values in equations (1) and (2) describing the heat loss from the monolithic reactor-heat exchanger chambers and crossflow shapes were evaluated using data obtained in stop flow experiments. Overall heat transfer coefficients based on the chamber wall area varied from 0.3 BTU/hr. ft^2 °F to 0.55 BTU/hr. ft^2 °F depending on the position in the reactor.

The monolithic reactor-heat exchanger was run successively as an adiabatic reactor, a countercurrent reactor-heat exchanger and a cocurrent reactor-heat

In Chemical Reaction Engineering—Houston; Weekman, V., et al.;
ACS Symposium Series; American Chemical Society: Washington, DC, 1978.

exchanger. Measured temperature and conversion data are shown as points in Fig. 4, 5 and 6. Each of these runs was made using identical inlet conditions. Table II lists these running conditions and provides comparison of the maximum and minimum temperatures and conversion measured in the three individual runs.

The vertical lines through the data points indicate the range of temperatures measured in each of the blocks and chambers (up to 9 thermocouples) per block. In the cocurrent and countercurrent runs, the largest spread in temperatures occurs in the block that the reaction stream first enters since the reaction rate is greatest at this point. The adiabatic run has a small distribution of temperatures in each of the four blocks because the system is essentially one dimensional with only a small radial temperature gradient attributable to heat loss from the reactor.

The cocurrent run has the flattest reaction pass temperature profile of the three shown. Indeed, it is possible to obtain an absolutely flat reaction pass temperature profile in a reactor-heat exchanger in which the reactant and coolant streams flow cocurrently (11).

Theoretical profiles calculated by the cell model described previously are also shown in Fig. 4 through 6. The solid lines are obtained with a plug flow model, and the dotted lines are obtained with a cell model. The simulated profiles fit the average values of the temperature and conversions calculated for each monolith and chamber. A seven x seven grid used to simulate the two dimensional profiles in the cocurrent and countercurrent runs produced the best agreement between experiment and theory.

To simulate the adiabatic run shown in Fig. 4, equations (1) and (3) were solved simultaneously. The same seven grid point (i.e., six cell) model was used to calculate the reaction and coolant pass profiles so that the effect of the axial pellet number on the temperature and concentration distributions could be evaluated. A one dimensional plug flow model of the adiabatic reactor was then formulated and solved using a fourth order Runge-Mutta technique. A comparison of the two models, shown in Fig. 4, indicates that the effect of axial dispersion on the conversion or temperature obtained is not significant.

Autothermal cocurrent and countercurrent runs for the pellet filled reactor-heat exchanger were also made and were correlated with theory. As in the above three cases the results showed good agreement with theory. A more detailed description of the autothermal

In Chemical Reaction Engineering—Houston; Weekman, V., et al.;
ACS Symposium Series; American Chemical Society: Washington, DC, 1978.

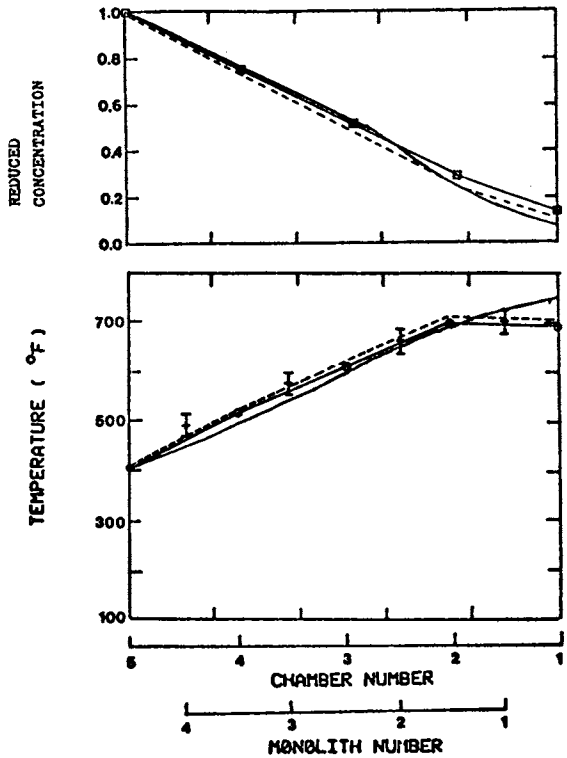

Figure 4. Adiabatic run; reactant flows from left to right

In Chemical Reaction Engineering—Houston; Weekman, V., et al.;
ACS Symposium Series; American Chemical Society: Washington, DC, 1978.

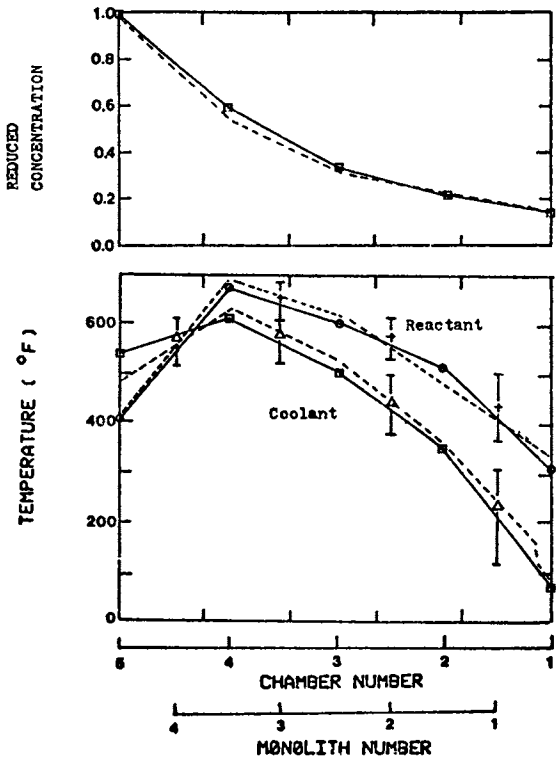

Figure 5. Counter-current run; reactant flows from left, coolant from right

In Chemical Reaction Engineering—Houston; Weekman, V., et al.;
ACS Symposium Series; American Chemical Society: Washington, DC, 1978.

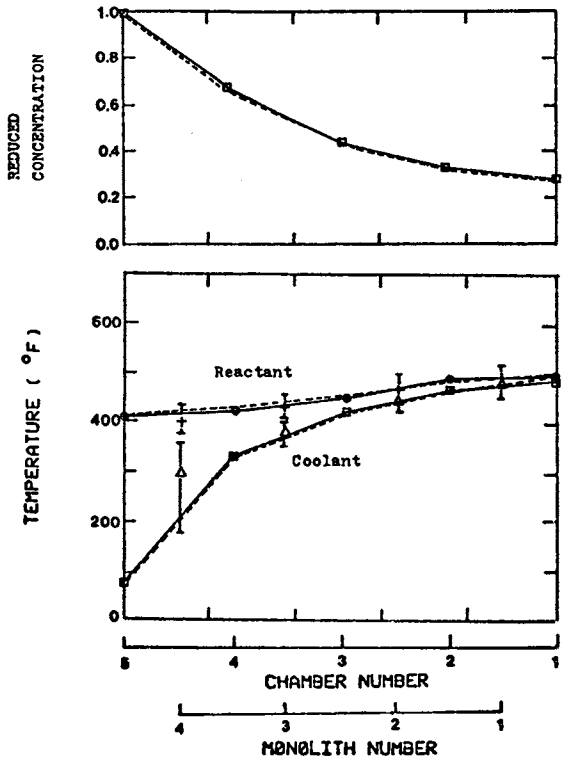

Figure 6. Cocurrent run; both streams flow from left

In Chemical Reaction Engineering—Houston; Weekman, V., et al.;
ACS Symposium Series; American Chemical Society: Washington, DC, 1978.

Table II

Reaction Run Data

a) Reactor Run Conditions

Mass Flow Rate Reaction Pass	21.38 lbm/hr.
Mass Flow Rate Coolant Pass	5.67 lbm/hr.
Gas Composition Reaction Pass	2.7% CO in air
Inlet Reaction Pass Temperature	403°F
Inlet Coolant Pass Temperature	75°F

b) Run Comparison

	Adiabatic	Counter-Current	Co-Current
Maximum Reaction Pass Temperature	693°F	673°F	504°F
Minimum Reaction Pass Temperature	403°F	304°F	403°F
Maximum Coolant Pass Temperature	-----	607°F	496°F
Reaction Pass Exit Temperature	691°F	304°F	497°F
Coolant Pass Exit Temperature	-----	535°F	500°F
Conversion	0.880	0.864	0.731
Position of Maximum Reaction Pass Temperature	R-4	R-2	R-4

In Chemical Reaction Engineering—Houston; Weekman, V., et al.;
ACS Symposium Series; American Chemical Society: Washington, DC, 1978.

reaction schemes and the multiplicity of steady states encountered in these schemes can be found in a previous reference (11).

Several runs were also made using monoliths that had reaction pass walls coated with copper chrome catalyst. The catalyst coated monoliths have much higher overall heat transfer coefficients, so that there is equalization of the coolant and reactant temperatures in three out of four monoliths.

Conclusions

A novel reactor, consisting of a series of crossflow monoliths for a coolant stream and a reactant stream, has been designed and run with a highly exothermic first order reaction. This reactor-heat exchanger is versatile and can be run in five modes: (1) as an adiabatic reactor, (2) with coolant and reacting schemes flowing cocurrently, (3) with coolant and reacting streams flowing countercurrently, (4) with autothermal cocurrent flow and (5) with autothermal countercurrent flow.

Temperature and concentration profiles from adiabatic, cocurrent and countercurrent runs compare favorably with a cell model used to simulate the crossflows in series design.

Acknowledgements

The authors would like to thank the Minnesota Mining and Manufacturing Company for supporting this investigation and supplying the ceramic crossflow monoliths. The American Cyanamid Company supplied the catalyst.

Nomenclature

Roman.

A	Heat transfer area of crossflow monolith
A^x	Cross sectional area of crossflow monolith
A^{fr}	Facial area of crossflow monolith
a	Area to volume ratio
a'	Thickness of ceramic flats
b	Distance between crossflow flats
C	Concentration
C_p	Heat capacity
d	Hydraulic diameter
d_p	Effective diameter of particle
E	Activation energy
h	Film heat transfer coefficient

k_g	Thermal conductivity of gas
k_∞	Catalyst preexponential factor
NTU	Number of transfer units

$$= \frac{Ua\tau}{LC_p}$$

R	Gas constant
r	Hydraulic radius
U	Overall heat transfer coefficient
V	Monolith volume
v	Gas velocity
x	Denotes axial position in the duct
Y	Fraction remaining

Greek.

α	Activity coefficient

$$= \left(\frac{E}{R}\right)\left(\frac{\rho\ C_p}{-\Delta H\ Co}\right)$$

β	Reaction parameter ($=k_\infty\tau$)
ΔH	Enthalpy of reaction
σ	Ratio of free flow area in monolith to frontal area
θ	Dimensionless temperature

$$= T\left(\frac{\rho\ C_p}{-\Delta H\ Co}\right)$$

μ	Viscosity
ρ	Density
τ	Space time based on superficial velocity

Dimensionless Groups

Re	Reynolds number ($\rho dv/\mu$)
Pr	Prandtl number ($C_p\mu/kg$)
j-factor	$(h/vA^xC_p)(C_p\mu/kg)^{2/3}$

Subscripts and Superscripts

AC	Denotes ambient-coolant pass relationship
AM	Ambient
AR	Denotes ambient-reaction pass relationship
C	Coolant pass
CC	Denotes chamber-coolant pass relationship
CR	Denotes chamber-reaction pass relationship
C-L	Chamber designation (coolant pass)
H	Hot pass (noncatalytic)
O	Inlet condition
R	Reaction pass
R-K	Chamber designation (reaction pass)

In Chemical Reaction Engineering—Houston; Weekman, V., et al.;
ACS Symposium Series; American Chemical Society: Washington, DC, 1978.

Literature Cited

1. Nusselt, W., Tech. Mech. Thermod. (1930), 1, 417.
2. Stevens, R. A., Fernandez, J. and Woolf, J. R., Trans. ASME (1957), 79, 287.
3. Harned, J. L., paper presented at Soc. Auto. Eng., SAE paper No. 720520, Detroit, May, 1973.
4. Hertl, W. and Farrauto, R. J., J. Catal. (1973), 28, 352.
5. Yu-Yao, Y., J. Catal. (1975), 39, 104.
6. Deans, H. A. and Lapidus, L., AIChE J. (1960), 6, 663.
7. Kuo, J. C. W., Morgan, C. R. and Lassen, H. G., paper presented to Soc. Auto. Eng. Meeting, Detroit, SAE paper No. 710289 (1971).
8. Shah, R. K. and London, A. L., Tech. Report #75, Dept. Mech. Eng. Stanford University (1971).
9. Hawthorn, R. D., paper presented at AIChE National Meeting (1972).
10. Kays, W. M., London, A. L. and Johnson, D. W., ASME Publication, New York, April 1951.
11. Degnan, T. and Wei, J., to be published (1978).

In Chemical Reaction Engineering—Houston; Weekman, V., et al.;
ACS Symposium Series; American Chemical Society: Washington, DC, 1978.

9

Hysteresis and Multiplicity in Wall-Catalyzed Reactors

BRUCE A. FINLAYSON

Department of Chemical Engineering, University of Washington, Seattle, WA 98195

A mathematical model of a wall-catalyzed reactor is used to elucidate the effects of inlet velocity and concentration, geometry of the duct, and axial conduction on the hysteresis, multiplicity and parametric sensitivity. The monolith reactor for carbon monoxide oxidation is the prototype considered, with wall catalyst being platinum on alumina on a ceramic substrate. Previous models have dealt with only a single tube of the monolith. Two adjacent ducts are examined to see the effect of heat exchange between them when the velocity in each is different.

1. Hysteresis

The term hysteresis refers to a multiplicity of steady states, and the actual steady state depends on the past history of operation of the reactor. In particular, different outlet conversions are obtained for the same inlet temperature depending on whether the device starts out hot or cold. This effect is illustrated in Figure 1, which was obtained experimentally by Hlaváček and Votruba (1) and Mostercky, et al. (2) in the following manner. Beginning with a cold reactor, desired inlet conditions are maintained at a low temperature until steady state has been reached, giving one data point on the top part of the curve. Then the inlet temperature is raised, and the experiment again proceeds to steady state, giving another data point. This procedure is followed giving the curve denoted by →. At the ignition temperature light off occurs and the concentration of carbon monoxide out of the reactor decreases drastically. Almost complete conversion is obtained for any higher inlet temperature. Then the inlet temperature is lowered, step by step, giving rise to the curve marked ←. At the extinction temperature the exit concentration suddenly increases and little reaction takes place. For a given temperature between the extinction and ignition temperatures it is possible to have two different outlet conditions; thus there is a multiplicity of steady states. When the inlet temperature is near the extinction or ignition temperature, a small change in operating conditions - inlet concentration or temperature or velocity - can cause a large

© 0-8412-0401-2/78/47-065-098$05.00/0

In Chemical Reaction Engineering—Houston; Weekman, V., et al.;
ACS Symposium Series; American Chemical Society: Washington, DC, 1978.

change in the outlet conditions. This phenomena is parametric sensitivity. The hysteresis curve illustrated in Figure 1 thus includes information about the multiplicity of steady state solutions and the regions of parametric sensitivity. What it does not show, however, is whether the two steady states shown are stable, and if there are any other steady states between those shown (probably unstable ones). Judging from studies of packed beds (3) it is probable that both the steady states shown are stable, and any other ones are unstable.

A model developed earlier (4,5) used the collocation method to solve the equations for heat, mass and momentum transfer in a single, adiabatic channel of the monolith. The basic model is the one described as Model II-A(5): a square duct with axial conduction of heat longitudinally in the solid walls, but with infinitely fast conduction peripherally around the square, and including the diffusion of heat and mass in the transfer direction in the fluid (See 5 for a discussion of the importance of including this effec.) Nusselt and Sherwood numbers are not assigned a priori, but are derived from the solution. The reaction rate expression P2 in (5) with a basic form

$$\text{rate} = \frac{Dy_{O_2}\, y_{CO}\, e^{-A/T}}{\left[1 + Cy_{CO}e^{B/T}\right]^2} = \frac{k_o(E + y)y}{(1 + \alpha y)^2}$$

This is the expression derived by Voltz, et al. to fit their data (6). Here however, we allow diffusion limitations in the very thin catalytic layer. The temperature is assumed constant within the layer since the primary heat transfer resistance occurs in the fluid. The effectiveness factor curve is generated using a one-term collocation method for small Thiele modulus and the asymptotic solution for large Thiele modulus (7). The base case, unless otherwise noted, is for a Reynolds number 160, $y_{CO,inlet} = 0.04$, P2 kinetics, square geometry, $k_f/k_s = 0.04$, $D_f/D_s = 20$. Other parameters are given elsewhere (4,5), and the parameters are characteristic of an Englehard PTX-4 converter.

The theoretical hysteresis curve is shown in Figure 2 for three different inlet CO mole fractions. The correct qualitative trends are exhibted: the hysteresis is wider (greater difference between the ignition and extinction temperatures) for larger concentrations of carbon monoxide. Other calculations (7) indicate the ingnition and extinction temperatures depend on flow rate, too, reflecting the experimental observations: the hysteresis is wider for the lower flow rates.

As in the case of packed beds, the higher velocities tend to blow the reaction zone out the downstream end of the duct, whereas lower velocities lead to ignition that moves upstream towards the inlet. The effect of geometry is examined in Ref. 8, and ducts

In Chemical Reaction Engineering—Houston; Weekman, V., et al.;
ACS Symposium Series; American Chemical Society: Washington, DC, 1978.

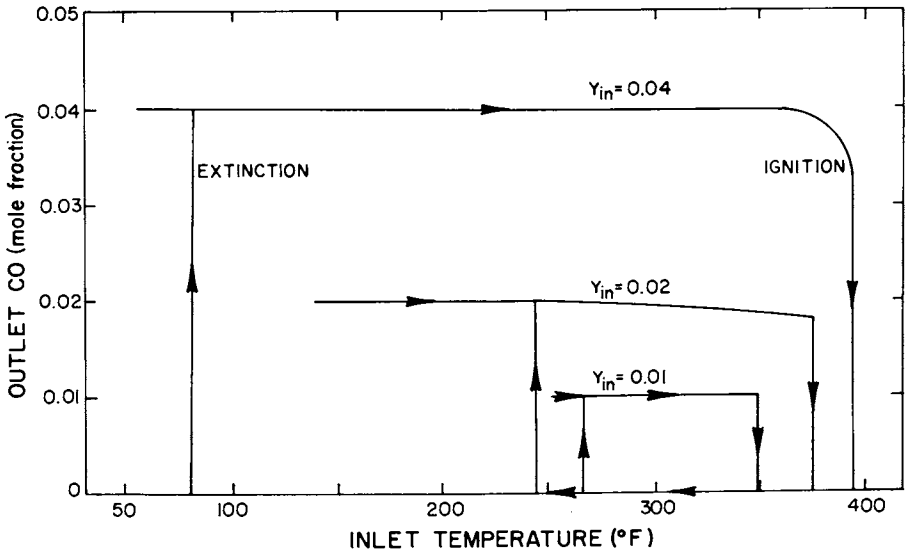

Figure 1. Experimental hysteresis curve, Re = 152, Refs. 1, 2

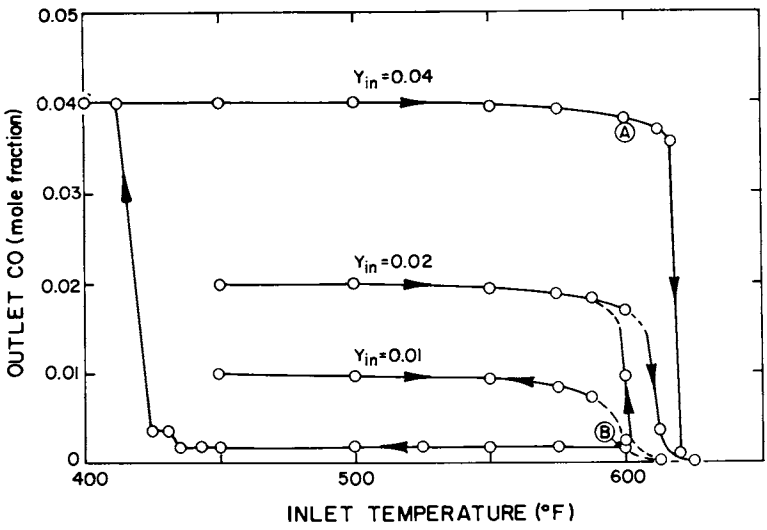

Figure 2. Theoretical hysteresis curves, Re = 160

In Chemical Reaction Engineering—Houston; Weekman, V., et al.;
ACS Symposium Series; American Chemical Society: Washington, DC, 1978.

with four different shapes (square, circle, trapezoid, rectangle) have almost identical hysteresis properties. Consequently it is possible to do calculations with the geometry that leads to the most convenient computations.

The most important effect of the model is the axial conduction of heat in the solid tube wall. Figure 3 shows the temperature and mole fraction profiles for different values of the solid thermal conductivity. The inlet mole fraction of CO is 0.04 and the inlet temperature is 600°F. Figure 2 indicates that for these conditions there are multiple steady state solutions, one with essentially complete reaction, and one with essentially no reaction. The curves marked A and B correspond to the conditions giving the points A and B in the hysteresis curves in Figure 2. The extinguished state has very little reaction and the mole fraction and wall temperature change very little down the length of the duct. This is the same curve obtained if the axial thermal conductivity is set to zero, i.e. the axial conduction of heat is absent, Model II in (5). The ignited state has a sharp rise in temperature inside the duct at z/L = 0.65. The oscillations in the solution are due to numerical error caused by using too few elements, 10, rather than the 20 used earlier (5).

The importance of axial conduction of heat is emphasized by the other curves in Figure 3. Shown there are the ignited states for different solid thermal conductivities, and as the solid thermal conductivity decreases the ignition zone moves to the end of the reactor, and for a small enough value only the extinguished state is possible. The hysteresis is thus much enhanced by a large value of k_s, or by thicker walls. This is further demonstrated in Table I.

Table I. Ignition and Extinction Temperatures for Different Wall Thermal Conductivities (from 7)

k_f/k_s	T_{ex}(°F)	T_{ig}(°F)	ΔT(°F)
0.04	418	618	200
1.0	560	619	59
100.	615	615	0

Since the mechanism for hysteresis is due to the axial conduction of heat in the wall, the hysteresis should decrease as k_s or the wall thickness decrease, as illustrated by the parameter affecting the rate of axial conduction

$$\frac{k_s}{k_f} \frac{2r_h^2}{L^2} \frac{1-\epsilon}{\epsilon} .$$

In Chemical Reaction Engineering—Houston; Weekman, V., et al.;
ACS Symposium Series; American Chemical Society: Washington, DC, 1978.

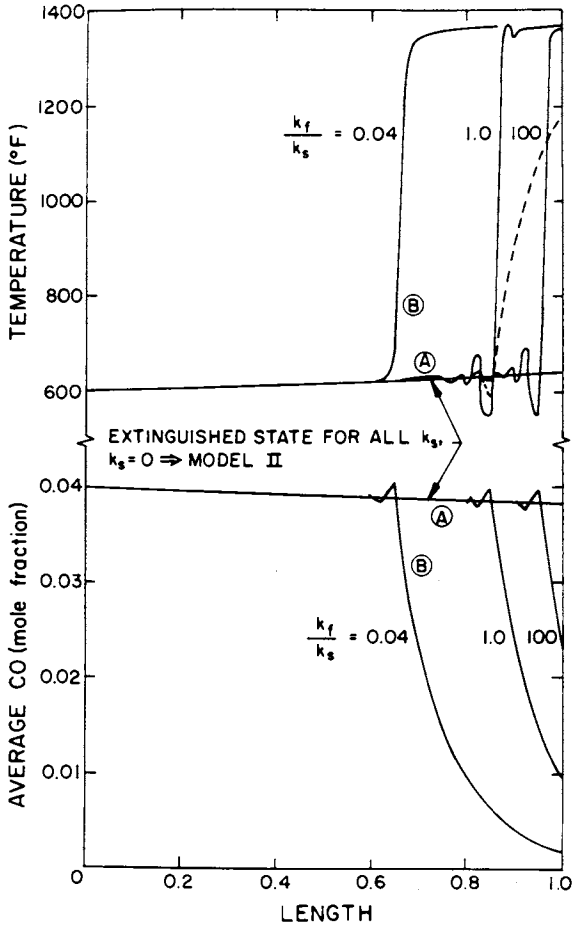

Figure 3. Axial temperature and mole fraction profiles for different thermal conductivities

In Chemical Reaction Engineering—Houston; Weekman, V., et al.;
ACS Symposium Series; American Chemical Society: Washington, DC, 1978.

2. Effect of Multiple Channels

The calculations reported above were for a single, adiabatic channel of a duct in a multi-channel monolith. If each channel is not the same it is possible that further complications can arise. We investigate this possibility in a preliminary way. Since the material entering all the channels is the same (coming from the same larger channel originally), it is likely that the inlet concentration and temperature are identical in the adjacent channels. We thus focus on the effect of velocity differences in adjacent channels. To simplify the computational task we consider only two channels which share the same solid wall. We saw above that the behavior of the hysteresis curve was not influenced by the shape of duct, and here we use a circular duct for computational convenience. The combined geometry is then a checkerboard effect, with every other cell being the same. We still assume that there is infinitely fast peripheral conduction of heat, so that at any axial position the wall temperature is everywhere the same. For this preliminary situation we also assume that the axial conduction of heat is negligible, even though we know this is not the case. However, since the wall temperature is everywhere the same at a given axial location, it should be possible to study the effect of velocity variations in adjacent channels and axial conduction of heat separately, and the results add credence to this supposition. Such a drastic, but plausible, assumption was made for computational convenience.

The computations for multiple channels were made with a revised version of the program REACOLL. This program converts a set of parabolic partial differential equations into a larger set of ordinary differential equations by using the orthogonal collocation method (9,10). Previous versions of REACOLL have used a fifth order Runge-Kutta variable step size integration routine to integrate in the axial direction. We modified the program to use Gear's algorithm (11,12). Gear's algorithm is a collection of multi-step methods, with the step and order of the method automatically controlled to achieve a user-specified accuracy within a minimum computation time. We chose the option of an implicit method with the nonlinear algebraic equations solved with the Newton-Raphson method, with a numerical generation of the Jacobian at each Δz step. The Jacobian is not reevaluated at each Δz step, but is evaluated if the iteration cannot converge in three iterations. If the iteration still does not converge, a smaller Δz is chosen and the calculation is repeated. The advantageous feature of the method is that it will always work for a small enough Δz, but the computational cost may be high. For these problems comparisons were made with a fifth-order Runge-Kutta integration in Δz, too, and Gear's algorithm was about twice as fast for the same user-specified accuracy.

In Chemical Reaction Engineering—Houston; Weekman, V., et al.;
ACS Symposium Series; American Chemical Society: Washington, DC, 1978.

The model equations can be written as

$$v(r)\frac{\partial c_i}{\partial z} = \alpha_i \frac{1}{r}\frac{\partial}{\partial r}\left(r\frac{\partial c_i}{\partial r}\right)$$

with the first two variables as the mole fraction and temperature in the first channel, and the third and fourth variable being the mole fraction and temperature in the second channel. The conditions at the wall require that the diffusion of mass towards the wall equal the generation of mass by the wall-catalyzed reaction, and the same is true for heat. We thus have the boundary conditions

$$-\left.\frac{\partial c_i}{\partial r}\right|_{r=1} = \beta_1 R(c_1, T), \quad -\left.\frac{\partial c_3}{\partial r}\right|_{r=1} = \beta_3 R(c_3, T)$$

$$-\left.\frac{\partial c_3}{\partial r}\right|_{r=1} - \left.\frac{\partial c_4}{\partial r}\right|_{r=1} = \beta_2 R(c_1, T) + \beta_4 R(c_3, T)$$

$$c_2 = c_4 = T \text{ at } r=1$$

The mathematical structure of the problem is thus a set of partial differential equations which are coupled with a set of nonlinear algebraic equations at each axial position. The algebraic equations are solved using a Newton-Raphson iteration with the derivatives calculated numerically. The same reaction rate expression (P2)was used.

The first case corresponds to a case which has not "lit off." We note first that without axial conduction of heat in the wall the solution has to be unique (5), and there is no hysteresis curve. For an inlet temperature of 600°F the wall temperature profile is shown in Figure 4 for different average velocities. The three solid curves are for cases in which the velocity in each channels is the same, but the magnitude of the average velocity is different. In all cases a parabolic velocity distribution is taken as a function of radius of the duct, since the flow is laminar and only the average velocity is changed. The solid curves then represent three separate unrelated cases, in which the average velocity is increased. The calculation for multiple channels is made with the velocity in one channel being 0.8 the normal velocity (giving Re = 128) and the velocity in the other channel being 1.2 times the normal velocity (giving Re = 192). The multiple channel results are denoted by the ■ in the Figure 4, and it is seen that they are very close to the results expected from two channels with the same average velocity in each

In Chemical Reaction Engineering—Houston; Weekman, V., et al.;
ACS Symposium Series; American Chemical Society: Washington, DC, 1978.

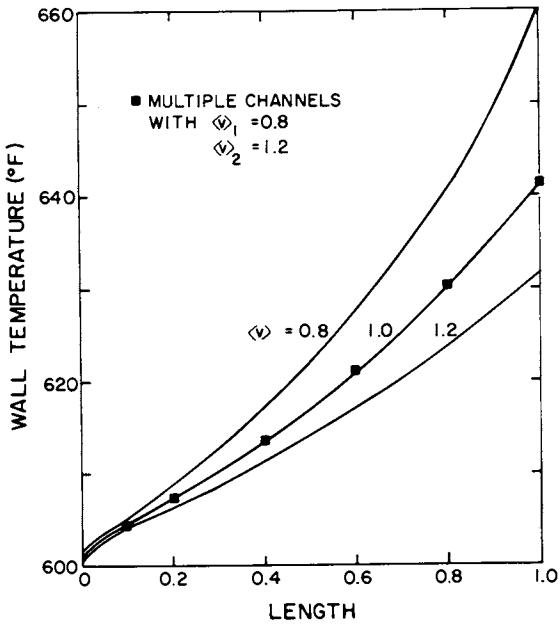

Figure 4. Wall temperature in multiple channels, $T_{inlet} = 600°F$

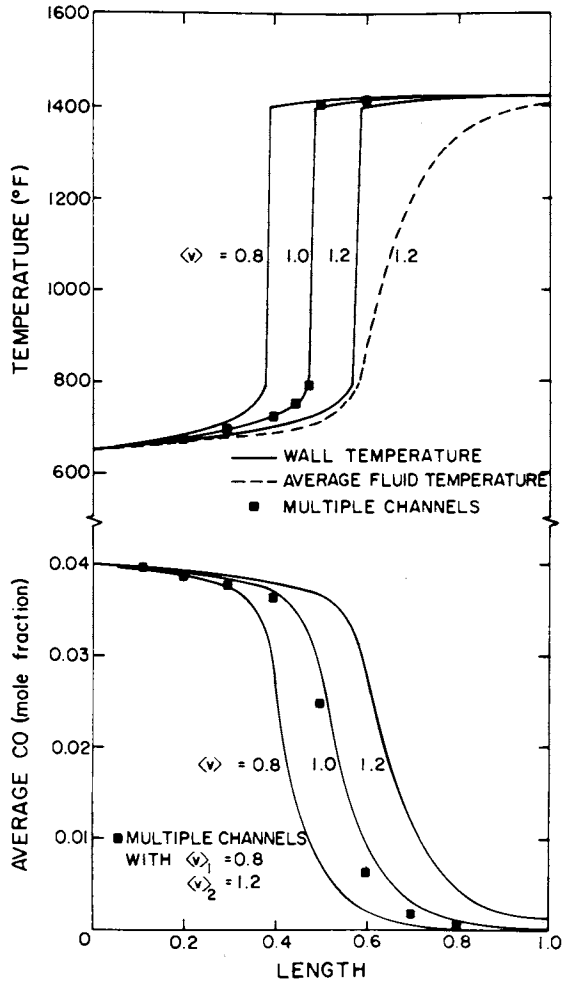

Figure 5. Wall temperature in multiple channels, T_{inlet} = 650°F

In Chemical Reaction Engineering—Houston; Weekman, V., et al.;
ACS Symposium Series; American Chemical Society: Washington, DC, 1978.

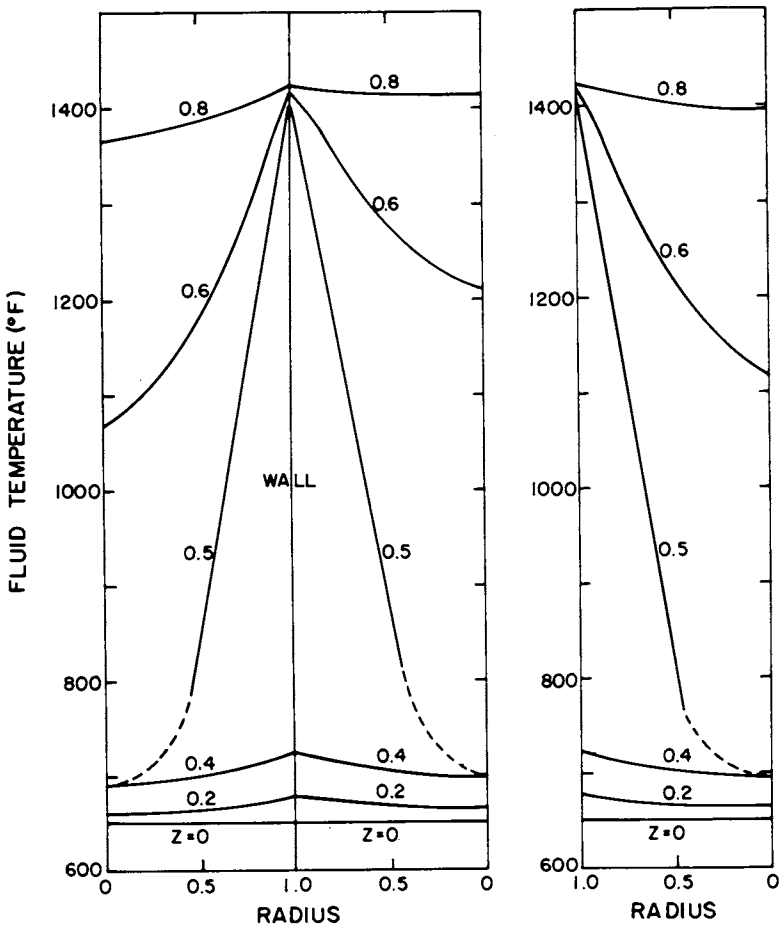

Figure 6. Radial temperature profiles in multiple channels, $T_{inlet} = 650°F$

In Chemical Reaction Engineering—Houston; Weekman, V., et al.;
ACS Symposium Series; American Chemical Society: Washington, DC, 1978.

channel. Here the effect of different velocities in different channels is minimal.

The effect of different velocities may be more pronounced for a case which has "lit off", and this is examined in Figure 5. The nomenclature is the same as in Figure 4 and we see that even at light off the multiple channel with different velocities gives results which are almost identical to the two channels with the same average velocity. The temperature profiles in the radial direction are shown in Figure 6. For the multiple channel case, with different velocities, the fluid temperature profiles are different but with the same wall temperature (since that is shared); despite that discrepancy the overall effects are very similar to the average case shown at the right.

We thus conclude that the effect of different velocities in adjacent channels is not great. This conclusion was reached, however, for a model which excludes axial conduction of heat. However, we have made calculations for three different types of transverse conduction: different geometries of the duct (7), peripheral conduction around the duct (5), and now different velocities in adjacent ducts. In the first two cases the inclusion or exclusion of axial conduction had little effect on the qualitative conclusion as to the importance of the effect, and there is no reason to assume that the multiple channel analysis will be any different. The inclusion of axial conduction will have a dramatic effect on the hysteresis but that hysteresis should not be greatly affected by any of the three transverse phenomena: different geometries, peripherical conduction, or multiple channels with different velocities. We thus conclude that analyzing a single channel suffices.

3. Conclusions

The hysteresis of a wall-catalyzed reactor for oxidizing carbon monoxide, as illustrated in Figures 1 and 2, is greatly affected by axial conduction of heat in the solid. This can be influenced by changing either the wall material or the wall thickness. Having different velocities in adjacent channels does not change the results: they are very similar to those for a single channel under the average conditions. The theoretical model displays hysteresis of the same qualitative features as experiments: the hysteresis is enhanced by higher CO concentrations, lower velocities, and higher solid thermal conductivity. The geometry of the duct has minimal impact.

4. Acknowledgments

Acknowledgment is made to the donors of the Petroleum Research Fund, administered by the American Chemical Society, for support of this research under Grant PRF No. 7698-AC7.

5. Literature Cited

1. Hlaváček, V. and Votruba, J., "Chemical Reaction Engineering-II," pp. 545-558, M.M. Hulburt (ed.), Am. Chem. Soc. Ser. 133 (1974).

2. Mostecky, J., Hlaváček, V. and Votruba, J., Erdöl and Kohle (1974) 27, 261.
3. Eigenberger, G., Chem. Eng. Sci. (1972) 27, 1909, 1917.
4. Young, L.C. and Finlayson, B.A., A.I.Ch.E. J. (1976) 22, 331.
5. Young, L.C. and Finlayson, B.A., A.I.Ch.E. J. (1976) 22, 343.
6. Voltz, S.E., Morgan, C.R., Liederman, D. and Jacob, S.M., Ind. Eng. Chem. Prod. Res. Devel. (1973) 12, 294.
7. Young, L.C. and Finlayson, B.A., paper presented at A.I.Ch.E. meeting, Nov. 13-17, 1977.
8. Young, L.C. and Finlayson, B.A., "Second International Symposium on Finite Element Methods in Flow Problems," Santa Margherita Ligure, Italy, June 14-18, 1976, pp. 623-634.
9. Finlayson, B.A., Chem. Eng. Sci. (1971) 26, 1081.
10. Finlayson, B.A., "The Method of Weighted Residuals and Variational Principles," Academic Press (1972).
11. Gear, C.W. 1971 "Numerical Initial Value Problems in Ordinary Differential Equations," Prentice-Hall.
12. Hindmarsh, A.C. 1975 "GEARB: Solution of Ordinary Differential Equations Having Banded Jacobian," Report UCID-30059, Rev. 1, Lawrence Livermore Laboratory, U.S. AEC W-7405-Eng-48, March, 1975.

In Chemical Reaction Engineering—Houston; Weekman, V., et al.;
ACS Symposium Series; American Chemical Society: Washington, DC, 1978.

10

Poisoning in Monolithic Catalysts

SHENG-TAI LEE and RUTHERFORD ARIS

Department of Chemical Engineering and Materials Science,
University of Minnesota, Minneapolis, MN 55455

Almost all catalytic converters have to contend with the decay or poisoning of the catalyst in some form and the catalytic monolith is no exception. Indeed this is notorious in the automotive application where the catalytic converter must survive 50,000 miles of operation and still perform adequately. Although we shall use the kinetics of carbon monoxide oxidation over a platinum catalyst as an obvious and important example, our main objective is to develop a model which can handle any catalyst decay question and to point out the differences in two types of poisoning. Thus our study comes within the third main division of the subject as laid out by Butt (1) in 1972; not the mechanism or rate determination but the effect of deactivation on the operation of the reactor.

The pertinent work before 1972 has been reviewed by Butt (1). Since then Hegedus and Petersen (2) have considered various kinetic alternatives and Hegedus (3) has extended some of these results to include mass transfer effects. Becker and Wei (4) have considered the effect of non-uniform catalyst activity in a sphere and its advantages and disadvantages with respect to poisoning, and there have been several studies of the fixed bed (5,6,7). Wei (8) has discussed deactivation of the catalyst in the automotive context and with Heck and Katzer (9) has considered the modelling of the monolith following the pioneer work of Finlayson and Young (10).

The generally accepted kinetics of the oxidation of CO over a Pt catalyst imply the adsorption of CO and oxygen with reaction between adsorbed species. The rate is therefore proportional to the square of the active site concentration and leads, when oxygen is in excess, to a kinetic expression of the form

$$r = k_r c_{CO}/(1+k_a c_{CO})^2 \qquad (1)$$

where c_{CO} is the concentration of CO. By non-selective poisoning we mean (as in Wei and Becker (2)) that the poison is deposited randomly on the remaining unpoisoned sites, whether or not these

In Chemical Reaction Engineering—Houston; Weekman, V., et al.;
ACS Symposium Series; American Chemical Society: Washington, DC, 1978.

be catalytically active. Thus $\hat{c}_w$, the total amount of poison precursor deposited, will be governed by

$$\frac{\partial \hat{c}_w}{\partial t} = \hat{k}_p c_{ps} (1 - \frac{\hat{c}_w}{\hat{L}_\infty}) = \hat{k}_p c_{ps} \theta \tag{2}$$

where $\hat{L}_\infty$ is the total amount that could be adsorbed at saturation, c_{ps} the concentration of poison precursor in the gas at the surface and θ the unpoisoned fraction. If $f = \hat{L}/\hat{L}_\infty$ is the catalytically active fraction of total sites then we assume that since the poison is non-selective an amount $f\hat{c}_w$ is effective in blocking active sites. A balance of active sites is $\hat{L} = \hat{c}_{CO} + \hat{c}_O + f\hat{c}_w + \hat{c}_a$, where $\hat{c}_{CO}$ and $\hat{c}_O$ are the concentrations of these occupied by CO or O and $\hat{c}_a$ is that of the available active sites. But if the adsorptions of CO and O_2 are at equilibrium and the latter is dissociative $\hat{c}_{CO} = K_{CO} c_{CO} \hat{c}_a$, $\hat{c}_O = (K_O c_{O_2})^{\frac{1}{2}} \hat{c}_a$ so that

$$\hat{c}_a = \hat{L}\theta / \{1 + (K_O c_{O_2})^{\frac{1}{2}} + K_{CO} c_{CO}\} ; \tag{3}$$

here c_{CO} and c_{O_2} are the concentrations in the gas near the surface and K_{CO} and K_O adsorption equilibrium constants. The surface reaction is at a rate

$$\begin{aligned} \hat{k}_r \hat{c}_{CO} \hat{c}_O &= \hat{k}_r K_{CO} c_{CO} (K_O c_{O_2})^{\frac{1}{2}} \hat{c}_a^2 \\ &= \hat{k}_r K_{CO} (K_O c_{O_2})^{\frac{1}{2}} \hat{L}^2 \theta^2 c_{CO} / \{1 + (K_O c_{O_2})^{\frac{1}{2}} + K_{CO} c_{CO}\}^2 \\ &= k_r \theta^2 c_{CO} / (1 + k_a c_{CO})^2 , \end{aligned} \tag{4}$$

which is of the form (1) with a factor of θ^2 if the concentration of oxygen is constant. The equation for the rate of poisoning (2) can be written

$$\frac{\partial \theta}{\partial t} = - \hat{k}_p' c_{ps} \theta \tag{5}$$

By selective poisoning we mean that adsorption of the poison takes place only on to available catalytically active sites. Thus θ declines at a rate proportional to $\hat{c}_a$ (rather than itself) and by (3) and the assumed excess of oxygen

$$\frac{\partial \theta}{\partial t} = - \hat{k}_p c_{ps} \theta / (1 + k_a c_{CO}) . \tag{6}$$

The Assumptions of the Model and its Equations

It is assumed that a typical single passage of the monolith can be represented as an equivalent circular cylinder through which

the reactants pass in a fully developed laminar flow. Axial conduction and diffusion are ignored but the radial transport processes are considered. The wall of the cylinder is coated with a thin, porous, catalytically active layer which offers some diffusional resistance so that the equations for diffusion and reaction have to be solved in it; it is however sufficiently thin that its curvature is unimportant. Hegedus and Baron (11) observed that poisoning and sintering had opposite effects on the diffusivities in the porous layer so that we will assume that they remain constant for the life of the catalyst. It is assumed that the deactivation is slow so that given any distribution of activity the temperature and concentration have steady state behavior. It is assumed that the active catalyst layer is at the same temperature as the wall and that the relatively high conductivity of the ceramic keeps this uniform in a radial direction. However since the longitudinal gradients can be very large the longitudinal conduction of heat in the walls is considered; radiation is ignored.

Only the dimensionless form of the equations will be given. All symbols are defined in the nomenclature and related to the physical variables, here we need only say that u, v and w refer to concentration of CO, temperature and concentration of poison precursor, the suffixes f and s apply to fluid and solid phases respectively where ξ and $\bar{\xi}$ are the radial coordinates, ζ is the axial coordinate and τ the time. Then in the fluid:

$$2P(1-\xi^2)\frac{\partial u_f}{\partial \zeta} = \frac{1}{\xi}\frac{\partial}{\partial \xi}\left(\xi \frac{\partial u_f}{\partial \xi}\right) , \tag{7}$$

$$2P'(1-\xi^2)\frac{\partial v_f}{\partial \zeta} = \frac{1}{\xi}\frac{\partial}{\partial \xi}\left(\xi \frac{\partial v_f}{\partial \xi}\right) , \tag{8}$$

$$2P''(1-\xi^2)\frac{\partial w_f}{\partial \zeta} = \frac{1}{\xi}\frac{\partial}{\partial \xi}\left(\xi \frac{\partial w_f}{\partial \xi}\right) , \tag{9}$$

At the entrance

$$u_f(\tau,0,\xi) = v_f(\tau,0,\xi) = 1 , \quad w_f(\tau,0,\xi) = w_o , \tag{10}$$

on the axis

$$\partial u_f/\partial \xi = \partial v_f/\partial \xi = \partial w_f/\partial \xi = 0 , \tag{11}$$

while at the wall

$$\left.\begin{aligned} u_f(\tau,\zeta,1) &= u_s(\tau,\zeta,0) , \\ v_f(\tau,\zeta,1) &= v_s(\tau,\zeta,0) , \\ w_f(\tau,\zeta,1) &= w_s(\tau,\zeta,0) . \end{aligned}\right\} \tag{12}$$

In Chemical Reaction Engineering—Houston; Weekman, V., et al.;
ACS Symposium Series; American Chemical Society: Washington, DC, 1978.

The other conditions at the wall state that the CO which diffuses to the wall, passes into it and there reacts, and that the poison is deposited:

$$-\frac{\partial u_f}{\partial \xi}\bigg|_{\xi=1} = -\frac{1}{\Delta}\frac{\partial u_s}{\partial \bar{\xi}}\bigg|_{\bar{\xi}=0} = \gamma\phi^2 E(v_s)\int_0^1 \frac{\theta^2 u_s\, d\bar{\xi}}{(1+\omega u_s)^2} \tag{13}$$

$$-\frac{\partial w_f}{\partial \xi}\bigg|_{\xi=1} = -\frac{1}{\Delta''}\frac{\partial w_s}{\partial \bar{\xi}}\bigg|_{\bar{\xi}=0} = \gamma\phi_p^2 E''(v_s)\int_0^1 \frac{\theta w_s\, d\bar{\xi}}{(1+\omega u_s)} \tag{14}$$

where $E(v) = \exp \varepsilon(v-1)/v$, $E''(v) = \exp \varepsilon''(v-1)/v$.
In the catalyst layer $0 < \bar{\xi} < 1$,

$$\frac{\partial^2 u_s}{\partial \bar{\xi}^2} = \phi^2 E(v_s)\frac{\theta^2 u_s}{(1+\omega u_s)^2} \tag{15}$$

$$\frac{\partial^2 w_s}{\partial \bar{\xi}^2} = \phi_p^2 E''(v_s)\frac{\theta w_s}{(1+\omega u_s)} \tag{16}$$

$$\frac{\partial \theta}{\partial \tau} = -\phi_p^2 E''(v_s)\frac{\theta w_s}{(1+\omega u_s)} \tag{17}$$

The last expression holds for selective poisoning: for nonselective ω is set equal to zero in (14), (16) and (17). We note in passing that ω is a function of v_s. At $\bar{\xi} = 1$,

$$\partial u_s/\partial \bar{\xi} = \partial w_s/\partial \bar{\xi} = 0 \ . \tag{18}$$

Finally, v_s, the solid temperature, is governed by the transport from the fluid, the longitudinal conduction and the heat generated by reaction and adsorption:

$$\frac{\partial v_f}{\partial \xi}\bigg|_{\xi=1} = \frac{1}{Q}\frac{\partial^2 v_s}{\partial \zeta^2} + \beta E(v_s)\int_0^1 \frac{u_s\theta^2 d\bar{\xi}}{(1+\omega u_s)^2} + \beta'' E''(v_s)\int_0^1 \frac{w_s\theta\, d\bar{\xi}}{(1+\omega u_s)} \tag{19}$$

Method of Solution

The method employed was a development of our earlier technique (12) which uses the series expansion for the solution of eqns. (7)-(9). If u_f, v_f and w_f are assumed to be known as functions of ζ for ξ=1, the eigenfunction expansion in terms of Kummer's hypergeometric function allows us to calculate the derivatives needed in eqns. (13), (14) and (19). Since $u_s = u_f$, etc. at

the interface $\xi=1$, $\bar{\xi}=0$, the same assumed values allow eqns.(15), (16) and (18) to be solved. Only the first and third terms of eqns.(13) and (14) are needed (since the equality of the second and third is a consequence of (15) and (16)) so in eqns.(13), (14) and (19) we have three equations for the three assumed functions.

The values of the functions u_f, v_f, and w_f have to be calculated at discrete points and 10 elements with 6 collocation points per element were found to suffice. Rather than solve (15) and (16) separately it was found best to use collocation on these also, using four radial collocation points. This gives 459 simultaneous nonlinear algebraic equations which were solved by a modified Newton-Raphson iteration. The modifications were the use of under-relaxation and less frequent evaluation of the Jacobian. Even so 30-40 seconds of CDC 6600 time were needed for the computation of all quantities at each point in time. The Sherwood and Nusselt numbers and the effectiveness factor, or ratio of the actual reaction rate to the rate at stream conditions, were also calculated.

Results and Conclusions

Values of the parameters were taken to be approximately those that might be applicable to lead poisoning of a CO oxidation monolith, though it should be emphasised that the method is applicable to any slow poisoning situation and that our objective is to show the possibilities rather than to match data—modelling rather than simulation to use Smith's distinction (13). The values used are given in the table of nomenclature.

The results for non-selective poisoning are much what one would expect and are shown in Figure 1. The amount of poison on the catalyst (proportional to $1-\theta$) is seen to decrease along the monolith and this agrees qualitatively with measurements that have been made. Curves for $1-\theta$ are given for the surface of the catalytic layer and at depths of 0.2 and 0.8 of the thickness of the layer. The profiles of the poisoning with depth (shown at the right) suggest that something like pore mouth poisoning is the order of the day. Curves are only given for one value of time, since the results for other times showed that over the range considered θ was approximately linear with time.

The results for selective poisoning are presented using $\theta(0,\zeta)$ the fraction of active sites at the fluid-wall interface for various times (Figure 2). In contrast to non-selective poisoning for which θ would increase monotonically ($1-\theta$ decreased), the sites are virtually untainted at the inlet of the bed and the poison builds up only after the reaction light-off zone when the CO is virtually all oxidized. Figure 3 shows that θ does not vary much with depth into the catalyst so that the surface value is typical and we do not have pore mouth poisoning under these conditions. The top three curves apply to a point ($\zeta=.491$) at the head of the light-off zone, the other curves being for a point beyond the zone ($\zeta=.625$) and at the exit. The profile of wall

In Chemical Reaction Engineering—Houston; Weekman, V., et al.;
ACS Symposium Series; American Chemical Society: Washington, DC, 1978.

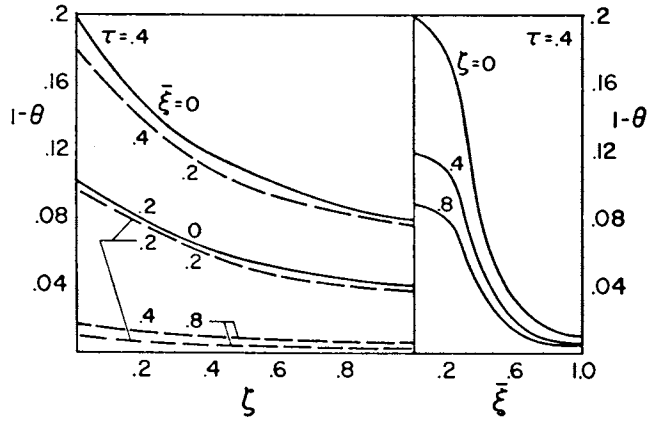

Figure 1. Axial and radial distributions of poison deposition. Nonselective poisoning. ϵ =19.4, ϵ'' = 27.7, ϕ = 4, ϕ_p = 1, ω = 2.62 exp (1.48/v_s), corresponding to T_o = 377°C, $\tau = (D_{pe}c_{CO,o})/(L_\infty S_v l^2)$.

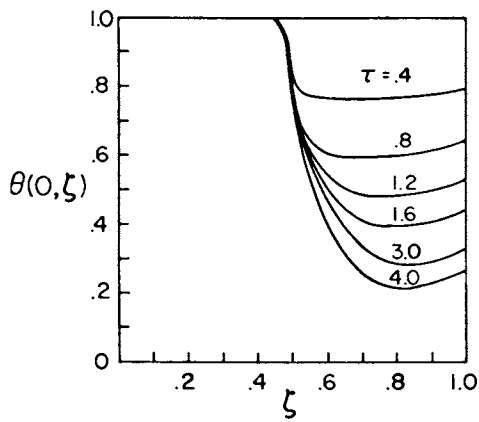

Figure 2. Axial distribution of fractional active sites at fluid–solid interface, $\theta(\tau,\zeta,0)$. Selective poisoning. ϕ = 2.0, ϕ_p = 0.2, ϵ = 21, ϵ'' = 30, ω = 2.62 exp (1.6/v_s), corresponding to T_o = 327°C, $\tau = (D_{pe}c_{CO,o})/(LS_v l^2)$ t.

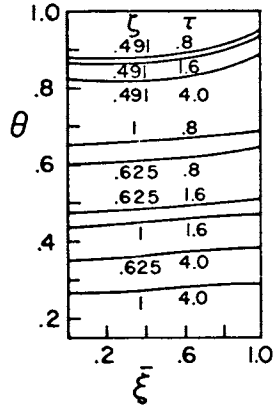

Figure 3. Radial distribution of fractional sites, $\theta(\tau,\zeta,\bar{\xi})$. Inlet conditions as in Figure 2.

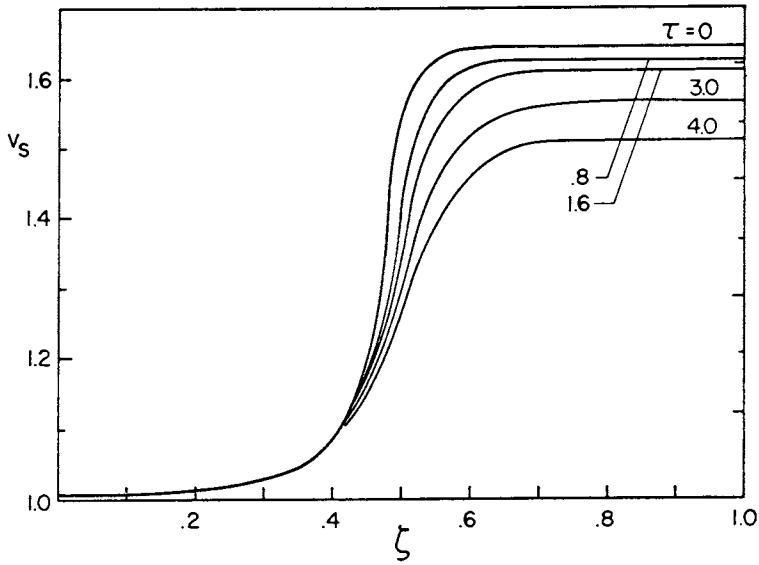

Figure 4. Solid temperature profiles at different τs. Inlet conditions as in Figure 2.

In Chemical Reaction Engineering—Houston; Weekman, V., et al.;
ACS Symposium Series; American Chemical Society: Washington, DC, 1978.

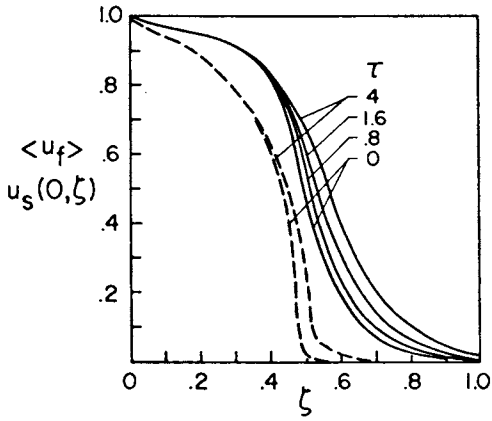

Figure 5. Axial distributions of emission breakthrough, $\langle u_f \rangle$, and the interface CO concentration, $u_s(\tau,\zeta,0)$. (——) $\langle u_f \rangle$, (– – –) u_s. Inlet conditions as in Figure 2.

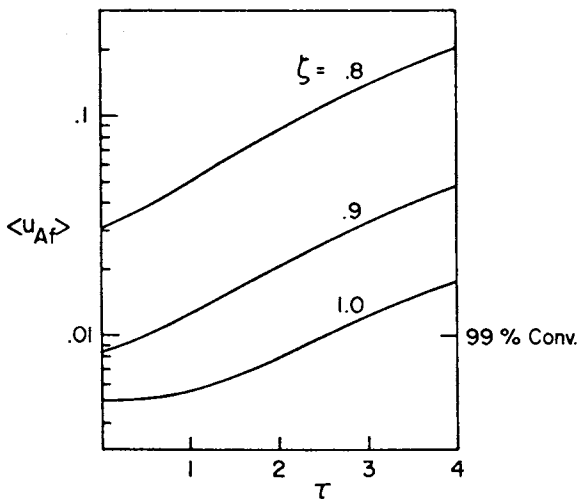

Figure 6. Emission breakthrough, $\langle u_f \rangle$, as a function of τ at different axial positions. Inlet conditions as in Figure 2.

In Chemical Reaction Engineering—Houston; Weekman, V., et al.;
ACS Symposium Series; American Chemical Society: Washington, DC, 1978.

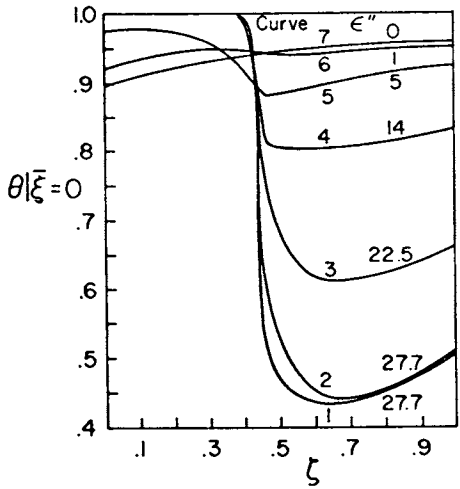

Figure 7. Effects of solid temperature (ϵ'') and CO inhibition (ω) on the axial distribution of θ. ω as in Figure 2 for curve 1; $\omega = 0$ for other curves.

In Chemical Reaction Engineering—Houston; Weekman, V., et al.;
ACS Symposium Series; American Chemical Society: Washington, DC, 1978.

temperature is shown in Figure 4 where the effect of poisoning is seen to bring the exit temperature down. The CO concentrations, both $\langle u_f \rangle$ the cup-mixing mean in the flow and the concentration at the solid-fluid interface are shown in Figure 5 and the all-important emission as a function of τ in Figure 6. From the last it is clear that the original 99.5% conversion deteriorates to 99% by $\tau = 2.5$.

From these figures the reason for the strikingly different behavior with non-selective poisoning becomes evident. At the entrance of the monolith before the light-off zone is reached the low temperature and high CO concentration suffice to cover the surface so well that the laying down of the poison precursor is inhibited. It is only after the reaction is largely spent with the resulting increase in temperature and decrease of CO that the poison can be appreciably laid down.

In a series of further studies some evidence of greater poisoning near the interface was found in the light-off zone. Elsewhere the penetration of the poison was fairly uniform. Finally the question of whether temperature or CO inhibition was the more important was resolved by the results shown in Figure 7. The lowest curve is for selective poisoning as calculated before with $\varepsilon'' = 27.7$. The curve close to it is for poisoning with no CO inhibition (i.e. $\omega \equiv 0$) but the same temperature dependence ($\varepsilon'' = 27.7$). It is evident that there is little difference outside the light-off zone. By reducing the activation energy for the poisoning through the sequence of curves 3-7 the non-selective poisoning condition is attained.

Acknowledgement

This part of the research on monoliths has not had the benefit of consistent funding but it is integral with the long-term work which has had the support of the NSF (GK 39001 and GP 43923) at various times and we are most grateful for this.

Nomenclature

a	passage radius, 0.06205 cm
c_{ps}	concentration of poison precursor in the gas near the solid surface, gmole/cm^3
$\hat{c}_a$	available active sites, gmole/cm^2
$\hat{C}_p$	heat capacity at constant pressure per unit mass, cal/gm°K
$\hat{c}_w$	amount of poison precursor deposited, gmole/cm^2
c	specie molar concentration, gmole/cm^2
$c_{CO,0}$	inlet CO concentration, 8.53×10^{-7} gmole/cm^3 at $T_o = 327°C$
D_{if}	effective molecular fluid diffusivity for component i, cm^2/sec
D_{ie}	effective porous solid diffusivity for component i, cm^2/sec, $D_{is} = D_{if}/20$
$E(v)$	dimensionless Arrhenius rate constant, $\exp \varepsilon(v-1)/v$

In Chemical Reaction Engineering—Houston; Weekman, V., et al.;
ACS Symposium Series; American Chemical Society: Washington, DC, 1978.

f	catalytically active fraction of total sites, $\hat{L}/\hat{L}_\infty$
$(-\Delta H)_{CO}$	molar heat of reaction, 9.04×10^4 cal/(gmole CO + 1/3 gmole H_2)
K	adsorption equilibrium coefficient
k_r	reaction rate constant for main reaction, 1/sec, defined in eqn. (1)
k_a	adsorption coefficient, 1/(gmole/cm^3), defined in eqn.(4)
$\hat{k}_p, \hat{k}_p'$	poison deposition rate constants, defined in eqns. (2), (6) and (5) respectively
L	length of monolith, 8.1 cm
$\hat{L}$	total catalytically active sites, gmole/cm^2
$\hat{L}_\infty$	total amount that could be adsorbed at saturation, gmole/cm^2
ℓ	thickness of catalytic layer, 0.0025 cm
P, P''	fluid-phase Peclet number for CO and poison precursor respectively, $P_i = S_{c_i} Re[(a/2)/L]$, $P = 0.4$, $P'' = 0.15$
P'	fluid-phase Peclet number for heat, $PrRe[(a/2)/L]$, 0.4
Q	dimensionless parameter of solid phase conductivity, $[(2\pi a L k_f)/(k_s S_c)] \cdot [L/a]$, 2500
Re	Reynolds number, 150
r	rate of reaction gmole/cm^{3}sec, also radial coordinate, cm
S_v	effective surface area of catalytic layer per volume of catalytic layer, cm^2/cm^3
S_c	cross-section area for solid phase, catalytic layer plus the ceramic region, cm^2
t	time, sec
t_∞	time to saturate available site, if the poison deposited immediately, sec, $2\pi a L \ell S_v \hat{L}_\infty / \pi a^2 V c_{pf}$
T	temperature, °K
u	dimensionless concentration for CO, $c_{CO}/c_{CO,0}$
v	dimensionless temperature, T/T_o
w	dimensionless concentration for poison precursor, $c_p/c_{CO,0}$, $w_o = 0.0002$
z	axial coordinate, cm

Greek Symbols

β	thermicity parameter for CO, $[k_{CO,0}(-\Delta H)_{CO} c_{CO,0} a\ell]/[k T_o]$, 0.16
β''	thermicity parameter for poison precursor, $[k_{p,o}(-\Delta H)_p c_{CO,0} a\ell]/[k T_o]$, 0
γ	a/ℓ, 25
ϵ, ϵ''	Arrhenius numbers for CO oxidation and selective poison deposition respectively, E_{CO}/RT_o, E''/RT_o
Δ	diffusivity ratio, D_{if}/D_{ie}
ζ	dimensionless axial coordinate, z/L
θ	unpoisoned fraction of adsorption sites, $(1 - \hat{c}_w/\hat{L}_\infty)$, and $(1 - \hat{c}_w/\hat{L})$ respectively for non-selective and selective poisoning
$\underline{\xi}$	dimensionless radial coordinate for fluid phase, r/a
ξ	dimensionless radial coordinate for solid phase, $(r - a)/\ell$
τ	dimensionless time, $[(D_{pe} c_{CO,0})/(\hat{L} S_v \ell^2)]\, t$ and $[(D_{pe} c_{CO,0})/(\hat{L}_\infty S_v \ell^2)]\, t$ for selective and non-selective

In Chemical Reaction Engineering—Houston; Weekman, V., et al.;
ACS Symposium Series; American Chemical Society: Washington, DC, 1978.

poisoning respectively, approx. $0.2t/t_\infty$

ϕ, ϕ_p Thiele moduli for CO and poison precursor, $\ell\sqrt{k_{CO,0}/D_{CO,e}}$, $\ell\sqrt{k_{po}/D_{pe}}$ respectively

ω dimensionless adsorption coefficient, $65.5\, y_{CO,0} \exp(961/T_o v_s)$, $y_{CO,0} = 0.04$, T_s, °K

Subscripts

- CO carbon monoxide
- f fluid-phase value
- o reference value, i.e. inlet value
- p poison precursor
- ps poison precursor at the solid surface
- s solid-phase value
- w poison deposited

Superscripts

- " poison precursor
- ^ value appropriate to the catalytic surface
- $\langle\rangle$ cup-mixing value

Literature Cited

1. Butt, J. B., Adv. Chem. Ser., (1972), 109, 259.
2. Hegedus, L. L. and Petersen, E. E., Chem. Engng. Sci., (1974), 28, 345.
3. Hegedus, L. L., Ind. Eng. Chem. Fundls., (1974), 13, 3, 190.
4. Becker, E. R. and Wei, J., 4th ISCRE, Heidelberg (April 1976).
5. Froment, G. F. and Bischoff, K. B., Chem. Engng. Sci., (1961), 16, 189.
6. Luss, D. and Erwin, M. A., AIChE Jl., (1970), 16, 979.
7. Olson, J. H., Ind. Eng. Chem. Fundls., (1968), 7, 185.
8. Wei, J., Adv. in Catalysis, (1975), 24, 57.
9. Heck, R. H., Wei, J., and Katzer, J. R., AIChE Jl., (1976), 22, 477.
10. Finlayson, B. A. and Young, L. C., AIChE Jl., (1976), 22, 331.
11. Hegedus, L. L., Baron, K., Jl. Catalysis, (1975), 37, 127.
12. Aris, R. and Lee, S.-T., Chem. Engng. Sci., in press.
13. Smith, J. M., "Models in Ecology," Cambridge University Press, Cambridge, 1974.

In Chemical Reaction Engineering—Houston; Weekman, V., et al.;
ACS Symposium Series; American Chemical Society: Washington, DC, 1978.

11

Micromixing Phenomena in Continuous Stirred Reactors Using a Michaelis-Menten Reaction in the Liquid Phase

EDUARD PLASARI, RENÉ DAVID, and JACQUES VILLERMAUX

Laboratoire des Sciences du Génie Chimique, CNRS-ENSIC 1, rue Grandville, 54042 Nancy Cedex, France

Micromixing phenomena have been the subject of much academic work in recent years. Their importance is now recognized from both pratical and fundamental points of view. In practice, micromixing plays an important role when two streams of reacting fluids are put into contact and react rapidly before achieving perfect mixing on the molecular scale (e.g. combustion and precipitation reactions), or when complex reactions are carried out in viscous media (e.g. continuous polymerization reactions). On the fundamental side, the study of coupling between reaction and mixing may yield valuable information on the mechanism of turbulent mixing. In spite of the publication of many papers on the subject, micromixing processes are far from being clearly understood. In one category of models, micromixing is described in the age space. These models are often abstract and they obviously lack a clear physical meaning. In a second category, interaction is supposed to take place in the physical space between neighbouring fluid aggregates.

Three mechanisms have been invoked :

1) Random coalescence processes (1) characterized by the interaction frequency ω_i, or the interaction time $t_I = 1/\omega_i$.

2) mass-transfer between one particular aggregate and a bulk made up of all other aggregates that are statistically interacting with it (2)(3)(4). The parameter is here a fictitious mass transfer coefficient or its reciprocal, the micromixing time t_m (I.E.M. model).

3) molecular diffusion of species into the aggregates (5)(6)(7) of characteristic dimension ℓ. The diffusion time t_D is proportional to ℓ^2/D.

Let $t_R = 1/(kc_o^{n-1})$ be the chemical reaction time. As t_I/t_R, t_m/t_R or t_D/t_R are increased, concentration gradients in the aggregates gives rise to partial segregation, due to the well-known coupling between reaction and mass transfer. The above ratios are analogous to squared Thiele moduli or Hatta numbers. That rapid reactions may create a variable state of segregation in a given

© 0-8412-0401-2/78/47-065-125$05.00/0

In Chemical Reaction Engineering—Houston; Weekman, V., et al.;
ACS Symposium Series; American Chemical Society: Washington, DC, 1978.

hydrodynamic pattern has been demonstrated experimentally (5) (7) (8). However, all the parameters of the above models (ω_i, t_m, $\bar{l}$) remain essentially phenomenological. To date, no general correlation is available to predict the importance of micromixing from the operating parameters of the reactor (e.g. stirring energy input) and the physicochemical properties of the fluid.

The aim of this paper is to provide well established experimental data, and to propose a new and tentative interpretation of micromixing in stirred reactors, with the hope of bridging the gap between phenomenological models and classical results of the theory of turbulence.

With this object, we have chosen experimental conditions in which micromixing effects were expected to be a maximum i.e. a continuous stirred reactor and a rapid liquid phase reaction close to zero order with unmixed feed of reactants. Experimental parameters were adjusted to such values that the space time, the reaction time and the micromixing time was of the same order of magnitude, ranging from 1 to 10 seconds. Micromixing effects were thus clearly and reliably observed.

Experimental :

The small 196 cm^3 reactor is made of "plexiglass" and glass according to Holland and Chapman standards (9) with four baffles and a six blade turbine. The two inlet ports at the bottom are provided with caps in order to break up the incoming jets. At short space times, the kinetic energy of the entering fluid is not negligible and is sufficient to ensure perfect macromixing in the reactor. The fluid flows out of the reactor at the top and passes through a spectrophotometer cell where product concentrations are continuously monitored. Details of the construction and hydrodynamic behaviour of the reactor are given elsewhere (10) (11).

Perfect macromixing is achieved in the reactor for all viscosities and stirring speeds, even without mechanical stirring (N=0), as can be checked by RTD measurements.

After reviewing many reactions, we finally selected the iodination of acetone. The reaction kinetics were carefully redetermined in batch experiments (12). The rate of iodine consumption globally obeys a Michaëlis-Menten law :

$$r = \frac{k_o[I_2]}{k_m + [I_2]} = \frac{k_o c}{k_m + c} \qquad (1)$$

k_o and k_m are given by the following expressions

$$k_o = k[CH_3COCH_3][H^+] = kc_A c_H \qquad (2)$$

$$k_m = k'[H^+]\frac{1+K[I^-]}{1+\alpha K[I^-]} = k'c_H \frac{1+Kc_I}{1+\alpha Kc_I} \qquad (3)$$

In Chemical Reaction Engineering—Houston; Weekman, V., et al.;
ACS Symposium Series; American Chemical Society: Washington, DC, 1978.

As a consequence, k_o and k_m can be varied at will in fixing the concentration of acetone, H^+ and I^-. In particular, the reaction can be made close to zero order (low k_m) in order to enhance sensitivity to micromixing. Moreover, this reaction may conveniently be used for the simulation of biological or enzymatic reactions. Typical values of experimental parameters are reported on table I below. As can be seen, acetone is in large excess and the iodine concentration is small but easily measured by spectrophotometry. The viscosity of the aqueous solution can be varied by addition of polyethylene glycol (Emkapol 6000). For each Emkapol concentration, the viscosity μ, the iodine diffusivity D and the kinetic rate constants were redetermined. The reactants are fed into the reactor as two unmixed streams containing respectively I_2, KI (flowrate Q_1) and CH_3COCH_3, H_2SO_4, KI (flowrate Q_2). Concentrations in table I are expressed as mixing concentrations.

Table I : Experimental conditions

Concentration ranges :	
acetone	0.25 - 0.5 M
H_2SO_4	0.15 - 0.3 M
KI	5×10^{-4} M
I_2 (c_o)	$1.7 \times 10^{-5} - 5 \times 10^{-5}$ M
space time	1.15 - 8 seconds
reaction time $t_R = c_o/k_o$	1.15 - 10 seconds
temperature	20 - 32°C
viscosity μ	0.8 - 6.7 centipoises
stirring speed N	0 - 3000 R.P.M.
flowrate ratio $m = Q_1/(Q_1+Q_2)$	0.1 - 0.9

Treatment of experimental data

Let $\bar{y} = c/c_o$ be the experimental value of reduced iodine concentration measured at the reactor outlet.

Set $K_1 = k_o\tau/c_o$ and $K_3 = k_m/c_o$. A straightforward mass balance gives the maximum mixedness outlet concentration :

$$\bar{y}_M = \left(1 - K_1 - K_3 + \sqrt{(1-K_1-K_3)^2 + 4K_3}\right)/2 \qquad (4)$$

The feed streams being unmixed, the fully segregated concentration would be $\bar{y}_s = 1$.

The experimental concentration lies somewhere between $\bar{y}_M$ and 1, as shown on figure 1 where theoretical lines are drawn together with some experimental points. How can we calculate a micromixing parameter from these observations ? The simplest approach is to define an empirical segregation index as (5) (8) :

$$X = (\bar{y} - \bar{y}_M)/(1 - \bar{y}_M) \qquad (5)$$

In Chemical Reaction Engineering—Houston; Weekman, V., et al.;
ACS Symposium Series; American Chemical Society: Washington, DC, 1978.

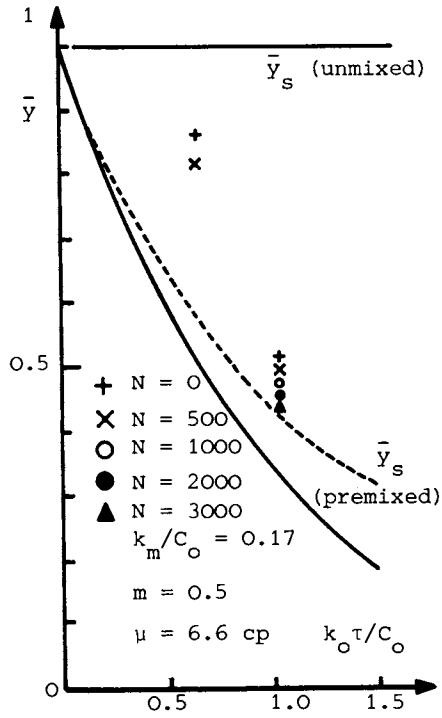

Figure 1. Residual iodine concentration against Damköhler number according to segregation state. Theoretical lines and experimental points.

In Chemical Reaction Engineering—Houston; Weekman, V., et al.;
ACS Symposium Series; American Chemical Society: Washington, DC, 1978.

A micromixing time t_m may also be calculated in applying the I.E.M. model (2)(3) to each entering stream. This model states that the iodine concentration decreases in fluid aggregates according to

$$\frac{dc}{dt} = \frac{\bar{c}-c}{t_m} - \frac{k_o c}{k_m+c} \qquad (6)$$

where t is the age of the aggregate and $\bar{c}$ the mean iodine concentration averaged over the whole reactor content. More precisely, the calculation has to be made for the two streams, the first one containing initially iodine and no acetone nor acid, and the second one being initially free of iodine but containing acid and acetone. Moreover, k_o and k_m are both dependent on acid (c_H) and acetone (c_A) concentrations. Preliminary calculations have shown that k_m could be considered as a function only of C_A and C_H during the course of the reaction so that the rate of reaction may be written

$$r = \frac{k c_A c_H c}{k_m + c} = \frac{k_o y_A y_H c}{k_m + c} \qquad (7)$$

where $k_o = k\bar{c}_A\bar{c}_H$ and $y_A = c_A/\bar{c}_A$, $y_H = c_H/\bar{c}_H$.

Applying the IEM model to acid and acetone (in large excess), the concentrations of these reactants can be calculated as a function of $\theta = t/\tau$, $K_2 = t_m/\tau$ and m.

Similarly, the dimensionless equations for iodine are :

$$\text{Stream 1} : \frac{dy_1}{d\theta} = \frac{\bar{y}-y_1}{K_2} - \frac{K_1 y_1}{K_3+y_1}\left(1 - e^{-\theta/K_2}\right)^2 \qquad (8)$$

$$\text{Stream 2} : \frac{dy_2}{d\theta} = \frac{\bar{y}-y_2}{K_2} - \frac{K_1 y_2}{K_3+y_2}\left(1 + \frac{m}{1-m} e^{-\theta/K_2}\right)^2 \qquad (9)$$

$$y_1(0) = 1/m \; ; \; y_2(0) = 0 \qquad (10)$$

Averaging over all ages and both streams :

$$\bar{y} = \int_0^\infty \left[m y_1 + (1-m) y_2\right] e^{-\theta} d\theta \qquad (11)$$

Since K_1, K_3 and m are given, the solution of equations (11)(12)(13) by iteration gives $\bar{y}$ as a function of $K_2 = t_m/\tau$. The micromixing time t_m can thus be obtained for each experiment.

Results

A few examples of results are reported on table II below. The whole set of data (142 experiments) can be found elsewhere (10).

Table II - Experimental results

n°	m	$C_o.10^5$ M	K_1	K_3	Emk %	$\nu.10^6$ m^2/s	N RPM	τ sec	$\bar{y}$	t_m sec	X	ε_1 m^2/s^3	ε_2 m^2/s^3
1	0.5	3.2	0.55	0.07	0%	0.88	0	2.2	0.58	1.2	0.14	2.4	0
2	0.5	3.2	0.40	0.07	0%	0.88	0	1.6	0.77	2.6	0.36	6.9	0
3	0.1	3.1	0.95	0.12	0%	0.92	0	3.4	0.45	1.0	0.20	2.0	0
4	0.9	3.1	0.90	0.11	0%	0.95	0	3.4	0.40	0.7	0.01	2.0	0
5	0.5	9.1	1.05	0.17	15%	6.55	0	2.9	0.52	2.8	0.30	1.7	0
6	0.5	4.7	1.22	0.23	5%	2.05	0	2.6	0.46	1.1	0.23	1.9	0
7	0.5	4.7	1.22	0.23	5%	2.05	500	2.6	0.43	0.8	0.17	1.9	0.07
8	0.5	4.7	1.22	0.23	5%	2.05	1000	2.6	0.40	0.7	0.14	1.9	0.64
9	0.5	4.7	1.22	0.23	5%	2.05	2000	2.6	0.39	0.6	0.12	1.9	6.0
10	0.5	4.7	1.22	0.23	5%	2.05	3000	2.6	0.38	0.5	0.11	1.9	20.8

The importance of segregation may be estimated in looking at the magnitude of t_m (as compared to τ) or at the segregation index X. Qualitatively, segregation increases with decreasing space time τ (see n° 1,2), with decreasing flowrate ratio m (see n° 3, 4), with increasing viscosity ν (see n° 5,6) and with decreasing stirring speed N (see n° 6-10). These last two results are not unexpected. The influence of τ is much more difficult to understand.

The decrease of t_m vs τ for aqueous solutions without Emkapol at N=0 RPM leads to : $t_m \sim \tau^{-5/3}$ (fig. 2) (12)

This experimental result rules out any explanation based on a reaction/diffusion mechanism, in which the diffusion time t_D varies as l^2_m/D given by the classical expression of CORRSIN (13). In effect, if we assume that the energy input ε is due to the kinetic energy of jets which varies roughly as τ^{-3}, CORRSIN'S expression leads to an increase of t_D with τ. An alternative explanation is proposed below.

The "shrinking aggregate" model (S.A. model)

Let us start from Beek and Miller's description of mixing in three successive stages (18) viz. 1) Distribution of one fluid through the other and a uniform average composition without a decrease in local concentration. 2) Reduction of size of the regions of uniform composition and correlative increase of the areas of contact between regions of different composition. 3) Mixing by molecular diffusion. In experiments with long space times, micromixing occurs mainly during stage 3) and may be explained on the basis of established homogeneous turbulence theory (5) (14). Conversely, at short space times with rapid reactions, micromixing is essentially controlled by stage 2) processes. The fresh fluid is assumed to enter into the reactor in the form of aggregates which are gradually "peeled off" and lose their matter toward a maximum mixedness environment. The shrinking aggregates remain fully segregated and the reaction takes place only in the perfect-

In Chemical Reaction Engineering—Houston; Weekman, V., et al.;
ACS Symposium Series; American Chemical Society: Washington, DC, 1978.

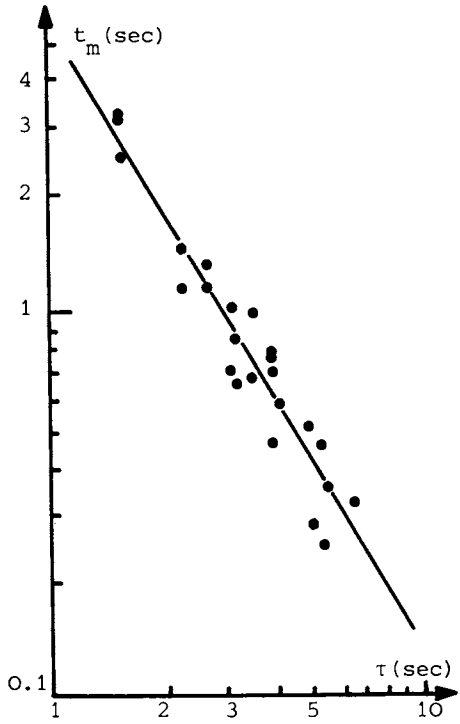

Figure 2. Variation of micromixing time as a function of space time (no mechanical stirring)

In Chemical Reaction Engineering—Houston; Weekman, V., et al.;
ACS Symposium Series; American Chemical Society: Washington, DC, 1978.

ly micromixed volume fraction.

The peeling off process causes the aggregate volume to decrease according to $-dv/dt = hs$, or in terms of the spherical aggregate diameter l :

$$dl/dt = -2h \qquad (13)$$

h is a mass transfer coefficient which is assumed to be given by a general correlation established by Calderbank et al. (15) for small particles in turbulent media :

$$hl/D = 0.13\ l\ (\varepsilon/\nu^3)^{1/4}(Sc)^{1/3} \qquad (14)$$

The aggregate diameter is thus found to decrease linearly with time. The aggregate disappears after the time :

$$t_e = \frac{l_o}{2h} = \frac{l_o}{0.26\ D\ (\varepsilon/\nu^3)^{1/4}(Sc)^{1/3}} \qquad (15)$$

What is the value of the initial diameter l_o ? The only assumption leading to the observed decrease of segregation with increasing τ is that l_o varies as τ^{-1}. This heuristic assumption is supported by an observation of Gunkel et al. (16) who have found that the integral of the autocorrelation function of velocity fluctuations in stirred reactors was a constant independent of reactor size and operating conditions. This integral is proportional to l_o/u_o (17). l_o is thus proportional to u_o, which in turn varies as τ^{-1}. In expression (15), the effective energy input per unit mass may be expressed as $\varepsilon = \eta_1\varepsilon_1 + \eta_2\varepsilon_2$, where ε_1 and ε_2 are the jet kinetic energy and mechanical stirring energy dissipations, respectively. η_1 and η_2 are the corresponding efficiencies of these kinds of energies in the production of micromixing. Finally, setting $l_o = p/\tau$, one obtains from (17) :

$$\tau/t_e = (0.26/p)\ \eta_1^{1/4}\ D(\varepsilon_1+\eta\varepsilon_2)^{1/4}\ \nu^{-3/4}\ Sc^{1/3}\ \tau^2 = A.G \qquad (16)$$

where $A = (0.26/p)\ \eta_1^{1/4}$ and $G = D(\varepsilon_1+\eta\varepsilon_2)^{1/4}\ \nu^{-3/4}\ Sc^{1/3}\ \tau^2$ (17)

$\eta = \eta_2/\eta_1$ is the relative efficiency of the two energies.

Assuming that A, i.e. η_1 may in turn be a function of G, (16) writes :

$$\tau/t_e = B.G^n \qquad (18)$$

The segregated volume fraction β is easily calculated from t_e in averaging over the aggregate distribution of ages.

$$\beta = \frac{1}{\tau}\int_o^{t_e} \frac{v}{v_o}\, e^{-t/\tau} dt = \frac{1}{\tau}\int_o^{t_e} \left(1 - \frac{t}{t_e}\right)^3 e^{-t/\tau} dt \qquad (19)$$

The result of integration is

In Chemical Reaction Engineering—Houston; Weekman, V., et al.;
ACS Symposium Series; American Chemical Society: Washington, DC, 1978.

$$\beta = 1 - 3(\tau/t_e) + 6(\tau/t_e)^2 - 6(\tau/t_e)^3\left[1 - e^{-t_e/\tau}dt\right] \quad (20)$$

$$\text{which is very close to } \beta = (1 + 4\tau/t_e)^{-1} \quad (21)$$

The β fraction of the reactor volume remains fully segregated while the 1-β fraction reacts in a state of maximum mixedness. Accordingly, β is nothing but the segregation index X which finds here its physical interpretation. β is thus known for each experiment. ε_1 is deduced from the pressure drop through the reactor. ε_2 is easily calculated from a classical correlation ($\varepsilon_2=\phi N^3 D_T^2/\nu$).

The unknown parameters of the model are B, n and η. Treating firstly experiments without mechanical stirring ($\varepsilon_2 = 0$), parameters B and n are ajusted by least square optimal fitting on β using (17) (18) and (20). The best fit is obtained for $B = 4000\ m^{-4/3}\ s^{-4/3}$ and $n = 4/3$.

In a second stage, experiments with mechanical stirring are considered. Fixing B to its N = 0 value, η is then determined for each value of the stirring speed N in order to obtain the best grouping of points around the $\beta(\tau/t_e)$ curve. Figure 3 shows this general correlation where all experimental points have been grouped together. The agreement between the data and the model is quite satisfactory. The corresponding values of η as a function of N are reported on figure 5.

Equivalence between the SA model and the IEM model

The basic interaction mechanisms of the two models are different. However, a correspondence may be sought between the micromixing parameters t_m and β or t_e in order to arrive at similar representations. The equivalence may be established on three basis as will be explained more in detail in a further paper :

1) in matching the relative amount of matter lost by a non-reacting aggregate toward the environment. This leads to $t_m = t_e/4$

2) in matching the variances of concentration distributions in the presence of two unmixed tracer feed-streams (concentrations 0 and 1) (2) (3). We obtain $t_m \sim t_e/2$.

3) in matching chemical conversion for instantaneous reactions (unmixed feed, m = 0.5) (2) (3). This leads again to $t_m \sim t_e/4$

Accordingly, we may expect the equivalence for :

$$2t_m < t_e < 4t_m \quad (22)$$

Coming back to the interpretation of experimental data based on the IEM model, an alternative correlation may be sought between t_m and G in analogy to (23). Following a similar procedure as above, the numerical analysis of data shows that experimental results are represented in an optimal way by :

$$\tau/t_m = C.G^{4/3} \quad (23)$$

with $C = 8200\ m^{-4/3}s^{-4/3}$. A new set of η values is determined

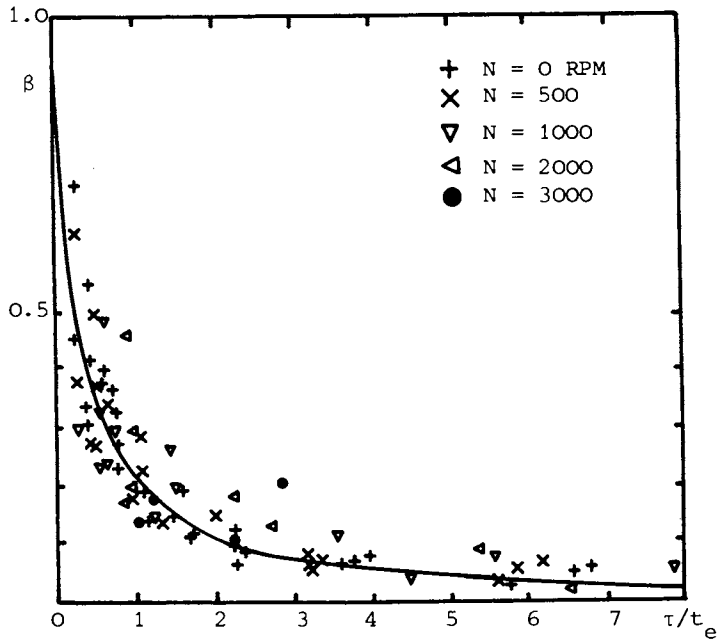

Figure 3. Segregated volume fraction as a function of τ/t_e. General correlation.

In Chemical Reaction Engineering—Houston; Weekman, V., et al.;
ACS Symposium Series; American Chemical Society: Washington, DC, 1978.

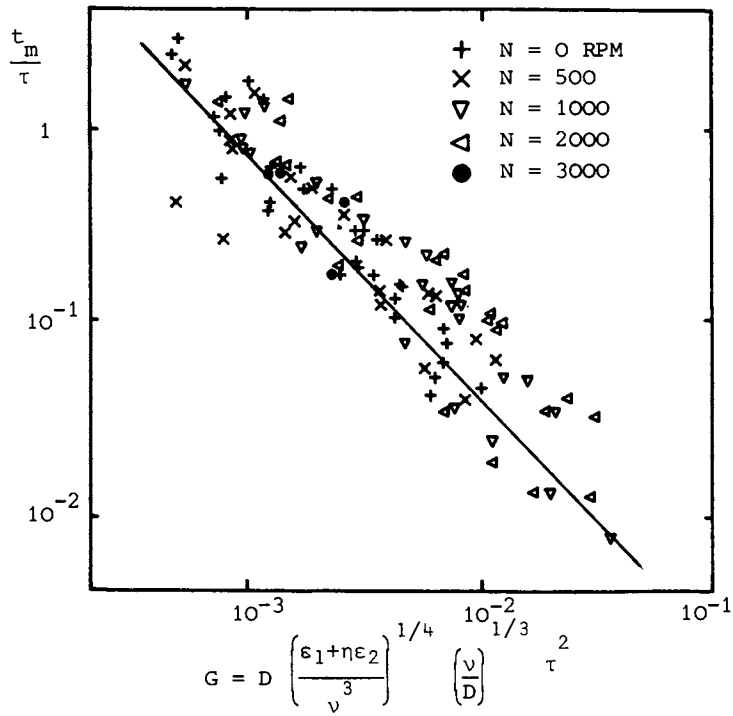

Figure 4. Relative micromixing time t_m/τ as a function of parameter G. General correlation.

In Chemical Reaction Engineering—Houston; Weekman, V., et al.;
ACS Symposium Series; American Chemical Society: Washington, DC, 1978.

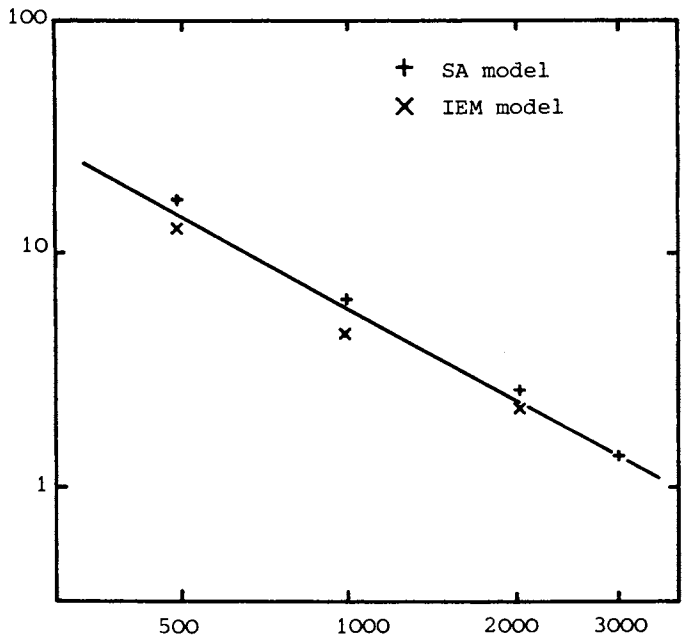

Figure 5. Relative efficiency of mechanical stirring referred to jet stirring as a function of stirring speed

In Chemical Reaction Engineering—Houston; Weekman, V., et al.;
ACS Symposium Series; American Chemical Society: Washington, DC, 1978.

for each stirring velocity. Figure 4 shows the experimental points according to correlation (29). The variation of η against N is also reported on figure 5. Here again, good agreement and consistency between model and experiment are obtained.

Discussion and conclusion

The comparison between (18) and (23) yields an independant evaluation of the relationship between t_e and t_m :

$$t_e/t_m = C/B = 2.1 \qquad (24)$$

This falls within the range predicted in (22).

The initial aggregate size may be estimated from (18), (16) and (15)

$$\ell_o = p/\tau = \frac{0.26\ \eta_1^{1/4}}{BG^{1/3}\tau} \qquad (25)$$

Taking into account the range of variation of G and τ and setting $\eta_1 = 1$ we find as an upper bound, $50\ \mu m < \ell_o < 500\ \mu m$, a reasonable value as compared to previous estimations for laminar eddies (3) and turbulent mixing (5) which led to $\ell_m \approx 10$ to 30 µm.

The most interesting feature is the dependency of $\eta = \eta_2/\eta_1$ on N (figure 5). The excellent agreement between η values coming from both SA and IEM models must be noticed as a check on the consistency of interpretation. η is found to decrease as $N^{-1/2}$. At low stirring speed the efficiency of mechanical stirring is more than 10 times that of jet stirring whereas at high stirring speed, the relative efficiency is close to unity.

In conclusion, several interesting points have been established in this paper.

1) A new micromixing (shrinking aggregate) model has been proposed, which describes the first stages of mixing in stirred tanks.

2) The equivalence of this model with the IEM model has been established, providing an interpretation of the micromixing time t_m.

3) Intermediate micromixing parameters have been shown to depend essentially on the group $G = D(\varepsilon_1+y\varepsilon_2)^{1/4}\ \nu^{-3/4}\ Sc^{1/3}\ \tau^2$. A general correlation has been established and successfully checked with experimental results.

4) The initial size of segregated domains has been estimated.

5) At low stirring speed, mechanical stirring is much more efficient than jet stirring but this relative efficiency strongly decreases as stirring speed is increased.

These results constitute a first attempt at a comprehensive theory of micromixing in stirred reactors based on experimental facts.

Notation

A,B,C parameters of the general correlation

In Chemical Reaction Engineering—Houston; Weekman, V., et al.;
ACS Symposium Series; American Chemical Society: Washington, DC, 1978.

c, c_o, c_A, c_H, c_I concentrations (iodine, initial, acetone, acid, iodide)
D, D_T molecular diffusivity, turbine diameter
$G = D\left(\frac{\varepsilon_1 + \varepsilon_2}{\nu^3}\right)^{1/4} Sc^{1/3} \tau^2$ parameter of the general correlation
h mass transfer coefficient
k, k_o, k_m, k', K kinetic parameters in the rate law
K_1, K_2, K_3 reduced kinetic or micromixing parameters
l, l_o, l_m aggregate diameter (current, initial, final)
m feedflowrate ratio
n, α numerical constants
N stirring speed (rotation frequency RPM)
p parameter
Q_1, Q_2 feedflowrates
r reaction rate
s aggregate external surface
$Sc = \nu/D$ Schmidt number
t, t_I, t_R, t_D aggregate age, interaction time, reaction time, diffusion time
t_e life duration of aggregates
t_m micromixing time (IEM model)
u_o initial jet velocity (entering streams)
v, v_o aggregate volume, initial volume
V reactor volume
X segregation index
Y, Y_M, Y_s, Y_A, Y_H reduced concentrations (iodine, maximum mixedness, fully segregated, acetone, acid)
β segregated fraction of the reactor volume
$\varepsilon, \varepsilon_1, \varepsilon_2$ energy dissipation per unit mass (efficient, from the jets, from the stirrer)
η_1, η_2, η efficiencies (kinetic energy of jets, mechanical stirring, relative)
$\theta = t/\tau$ reduced age
μ, ν viscosity (dynamic, kinematic)
ν_2 kinematic viscosity
$\tau = V/(Q_1+Q_2)$ space time
ϕ power number
ω_i interaction frequency

Acknowledgement : Mathematical treatments of models on the computer were carried out with the help of Bernard Antoine. His valuable contribution to this work is gratefully acknowledged.

Lit erature cited

(1) Ritchie B.W. and Tobgy A.H. Adv. Chem. Series, (1974), 133, 376
(2) Villermaux J. and Devillon J.C. 2nd Symp. Chem. React. Eng. B-1-13 (1972)
(3) Aubry C. and Villermaux J. Chem. Eng. Sci. (1975), 30, 457
(4) David R. and Villermaux J. Chem. Eng. Sci. (1975), 30, 1309

In Chemical Reaction Engineering—Houston; Weekman, V., et al.;
ACS Symposium Series; American Chemical Society: Washington, DC, 1978.

(5) Zoulalian A. and Villermaux J. Adv.Chem.Series(1974),133,348
(6) Nauman E.B. Chem. Eng. Sci. (1975), 30, 1135
(7) Nabholz F., Ott R.J. and Rys P. Second European Conference on mixing, Cambridge 1977
(8) Truong K.T. and Methot J.C. The Canad.J.Chem.Eng. (1976), 54, 572
(9) Holland F.A. and Chapman F.S. Liquid mixing and processing in stirred tanks. Reinhold Pub. Co. New-York 1966
(10) Plasari E. Thèse de Doctorat ès Sciences, INPL, Nancy 1976
(11) Plasari E., David R. and Villermaux J. Chem. Eng. Sci.,(1977) 32, 1121
(12) Plasari E., David R. and Villermaux J., Nouv. J. de Chimie, (1977), 1, 49
(13) Corrsin S. A.I.Ch.E. J. (1964), 10, 870
(14) Evangelista J.J., Katz S. and Shinnar R. A.I.Ch.E. J. (1969) 15, 843
(15) Calderbank P.H. and Moo-Young M.B.,Chem.Eng.Sci.(1961),16,39
(16) Gunkel A.A. and Weber M.E. A.I.Ch.E. J.(1975),21, 931
(17) Reynolds A.J. Turbulent flows in engineering, 95, Wiley, New-York, (1974)
(18) Beek J. Jr and Miller R.S. Chem.Eng.Prog. Symp. Ser. (1959) 55 (25), 33

In Chemical Reaction Engineering—Houston; Weekman, V., et al.;
ACS Symposium Series; American Chemical Society: Washington, DC, 1978.

12

Laminar Flow Polymerization of EPDM Polymer

J. F. WEHNER

Elastomer Chemicals Department, E. I. Du Pont de Nemours and Co., Inc., Deepwater, NJ 08023

The study of polymerization in a tubular reactor involves simultaneous consideration of the velocity profile, heat release and conduction, as well as the kinetics of the polymerization. This work was undertaken to determine the effect of this type of reactor upon the molecular weight distribution of the polymer produced. The system studied was the copolymerization of an elastomer from ethylene, propylene, and 1,4-hexadiene in solution using Ziegler catalysis. Laminar flow polymerization similar to previously described work involving polymerization of sytrene in tubular reactors (1, 2, 3, 4) was analyzed, but the numerical techniques are based on unpublished work and appear to be an efficient method in this application.

Model

The monomers, dissolved in hexane and mixed with catalyst, enter a tubular reactor in parabolic flow. The polymerization releases heat, induces heat transfer by conduction, increases viscosity, and depletes monomers. Heat conduction is considered in the radial direction only. Diffusion of both monomers and polymer has been neglected.

The solution viscosity is calculated by the following expression (Reference 5).

$$\eta = 3.58 \times 10^{-7} C^{5.7} \eta_{inh}^{5.3} \exp.(2380/T - 8.04) + \eta_o$$

$$\eta_{inh} = 1.38 \times 10^{-4} \times \left(\sum_i w_i M_i\right)^{0.811}$$

The reaction rate for a vanadium ion/aluminum alkyl catalyst of the Ziegler type is obtained from the kinetic scheme given in Table I.

Various physical properties of the system are tabulated in Table II.

© 0-8412-0401-2/78/47-065-140$05.00/0

TABLE I

Reference 7

$$R_1 = -(a_{11}x_{s1} + a_{12}x_{s2} + a_{13}x_{s3})x_1$$

$$R_2 = -(a_{21}x_{s1} + a_{22}x_{s2})x_2$$

$$R_3 = -a_{31}x_{s1}x_3$$

$$x_{s1} = [Va^{+++}] \,/\, \left(1 + \frac{x_2}{x_1}\frac{a_{21}}{a_{12}} + \frac{x_3}{x_1}\frac{a_{31}}{a_{13}}\right)$$

$$x_{s2} = x_{s1} \cdot \frac{x_2}{x_1}\frac{a_{21}}{a_{12}}$$

$$x_{s3} = x_{s1} \cdot \frac{x_3}{x_1}\frac{a_{31}}{a_{13}}$$

$$a_{11} = k_2 \cdot a_{21}$$

$$a_{12} = (504/x_2)\ f\ (T)$$

$$a_{13} = (0.79/x_3)\ f\ (T)$$

$$a_{31} = a_{11}/k_3$$

$$a_{21} = 184\ f\ (T)$$

$$a_{22} = k_1 a_{12}$$

$$k_1 = 0.0489 + 3.8\ (x_3/x_2)^{1.63}$$

$$k_2 = 20.46 + 32.2\ (x_3/x_1)^{1.29}$$

$$k_3 = 0.62\ k_2$$

$$f\ (T) = \exp\ (-3220/T + 10.27)/3600$$

In Chemical Reaction Engineering—Houston; Weekman, V., et al.;
ACS Symposium Series; American Chemical Society: Washington, DC, 1978.

TABLE II

The following parameters for the reaction mixture were assumed constant at the values shown:

Liquid density:

Propylene - 0.52 g/cc
Ethylene - 0.45 g/cc
Hexadiene - 0.70 g/cc
Hexane - 0.66 g/cc
Polymer - 0.84 g/cc

η_o - hexane viscosity - 0.0005 poise

Heat of reaction:

Propylene - 488 cal/g
Ethylene - 796 cal/g
Hexadiene - 262 cal/g

Liquid heat capacity - 0.3 cal/°C-cm^3

Thermal conductivity - 2.4 x 10^{-4} cal/sec-cm-°C

In Chemical Reaction Engineering—Houston; Weekman, V., et al.;
ACS Symposium Series; American Chemical Society: Washington, DC, 1978.

Mathematical Analysis

The flow model was taken from an unpublished report described in the Appendix. The reactor is considered to consist of a set of annuli each containing an equal portion of the volumetric flow. The axial distance is broken into subdivisions whose size is dependent upon the stability analysis of the numerical technique. The physical properties at the entrance of each annular section are considered constant in the radial direction. At each axial point, these properties are calculated and the radial coordinate is resubdivided into new annuli. The heat balance is then obtained from the differential equation in cylindrical coordinates transformed into a difference equation of tridiagonal form which was solved by the method of L.H. Thomas (Reference 6).

The differential equation

$$k\left(\frac{1}{r}\frac{\partial T}{\partial r} + \frac{\partial^2 T}{\partial r^2}\right) - \Sigma(\Delta H_i R_i) = \rho C_p v(r) \frac{\partial T}{\partial Z}$$

is transformed into this difference equation:

$$A(J+1)T(N,J)+B(J+1)T(N,J+1)+C(J+1)T(N,J+2) = D(J+1)$$

where

$$A(J+1) = X/\ln \frac{r(J)}{r(J+1)} - \frac{\rho C_p v(r(J))}{\Delta Z}$$

$$B(J+1) = X/\ln \frac{r(J+1)}{r(J+2)} - X/\ln \frac{r(J)}{r(J+1)}$$

$$C(J+1) = X/\ln \frac{r(J+1)}{r(J+2)}$$

$$D(J+1) = -\left[\frac{\rho C_p v(r(J))T(N-1,J)}{\Delta Z} - \sum_i \Delta H_i R_i (T(N-1,J))\right]$$

$$X = K/(r(J)(r(J)-r(J+1)))$$

Special provision was made for J = 0 (adiabatic) and J = JM (symmetrical) (wall and centerline, respectively). Note that the axial subscript is suppressed for the radial distance although at each axial interval the radial subdivision was changed to give volumetric elements of equal flow.

The polymer concentration and monomer disappearance were incremented by simple trapezoidal integration in the axial direction.

The calculations were performed for reactors broken into 200 or 1000 annuli with up to 20 axial points. The size of the subdivisions depends on the stability analysis of the Thomas method. The method is stable to round off errors except in the region of the centerline of the tube where the coefficient A (J)

In Chemical Reaction Engineering—Houston; Weekman, V., et al.;
ACS Symposium Series; American Chemical Society: Washington, DC, 1978.

changes sign. This sign change depends on the axial increment ΔZ. If ΔZ is too small, the unstable region extends beyond the first radial increment from the center. Using increments of equal volumetric flow adjusts the radial increment so that when the flow is forced to the center of the tube by the increasing viscosity at the wall, the subdivision is not too large at the point of most rapid change. This feature minimizes the difficulty with stability as well as permitting relatively larger radial increments where they can be tolerated. In practice, the instability was observed only for the reactor of largest diameter which is the least interesting physically.

Results

The calculations were performed for tubes of a diameter practical for laboratory work (1 cm), for semi-works (5.0 cm) and for plant scale (30 cm). The initial velocity profile is gradually distorted as polymerization preferentially occurs near the wall of the reactor increasing viscosity there. The bulk of the flow gradually is forced to the center of the tube, and beyond a certain point the reactor is effectively bypassed as far as polymerization is concerned. By trial and error it was found that this occurred when the outermost 10% of the flow occupied about 2/3 of the reaction area or the space beyond the radial position of 0.6 of the radius. This situation is equivalent to a plugged reactor and represents the practical limit of reactor length. The output of the reactor is considered to be the product formed up to this point. The computer program was designed to terminate at this point and output the results in the form of polymer concentration, molecular weight, residence time, velocity, and temperature as a function of radial coordinate. Figures 1 to 5 show the velocity profiles, molecular weight distribution and temperature traverses for the various reactor diameters studied. The velocity profiles for all three cases were similar when superposed so that only one case is shown in Figure 1 which shows the inlet velocity profile as well as the exit profile for Case 5. The temperature profiles show the effect of reactor diameter. For the small-scale reactor at any axial distance the temperature gradient is not severe. The wall temperature is at the most 3°C above the axial temperature. For the larger diameter there is a considerable gradient near the wall which appears to have the nature of a hot spot in the 30 cm diameter (20 to 90°C wall temperatures are seen with only a degree or two rise in the center of the reactor).

Table III shows some of the average reactor results for various cases studied. As the reactor increases in diameter the pluggage situations occur for a lower average molecular weight. These molecular weights are somewhat lower than that of a practical polymer although practical molecular weights could be obtained in a yet smaller diameter tube.

In Chemical Reaction Engineering—Houston; Weekman, V., et al.;
ACS Symposium Series; American Chemical Society: Washington, DC, 1978.

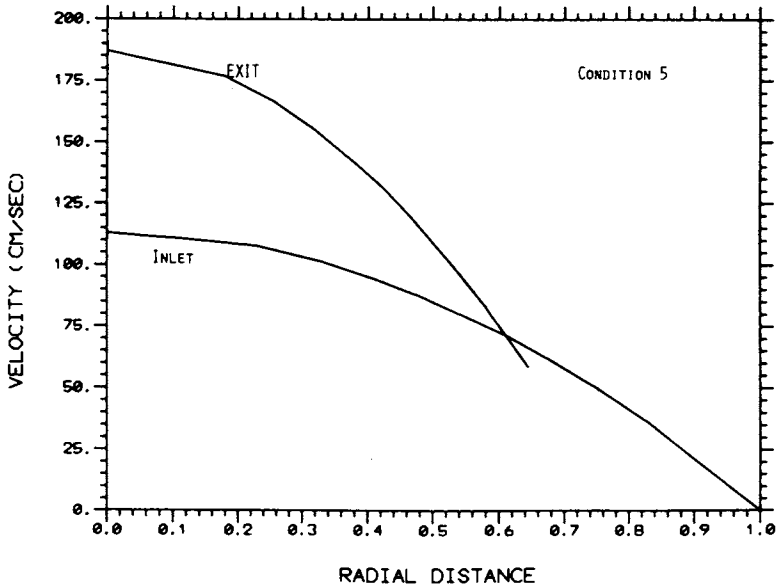

Figure 1. Velocity profile

In Chemical Reaction Engineering—Houston; Weekman, V., et al.;
ACS Symposium Series; American Chemical Society: Washington, DC, 1978.

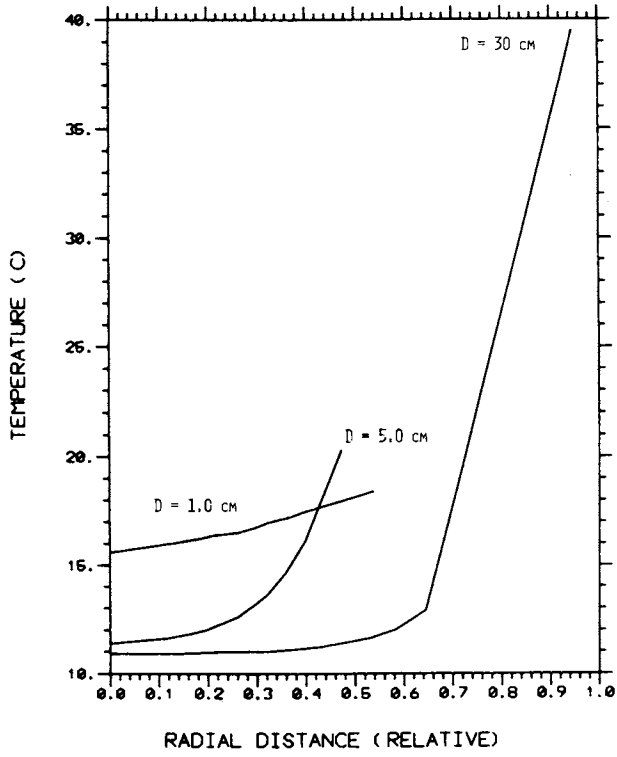

Figure 2. Temperature profile

In Chemical Reaction Engineering—Houston; Weekman, V., et al.;
ACS Symposium Series; American Chemical Society: Washington, DC, 1978.

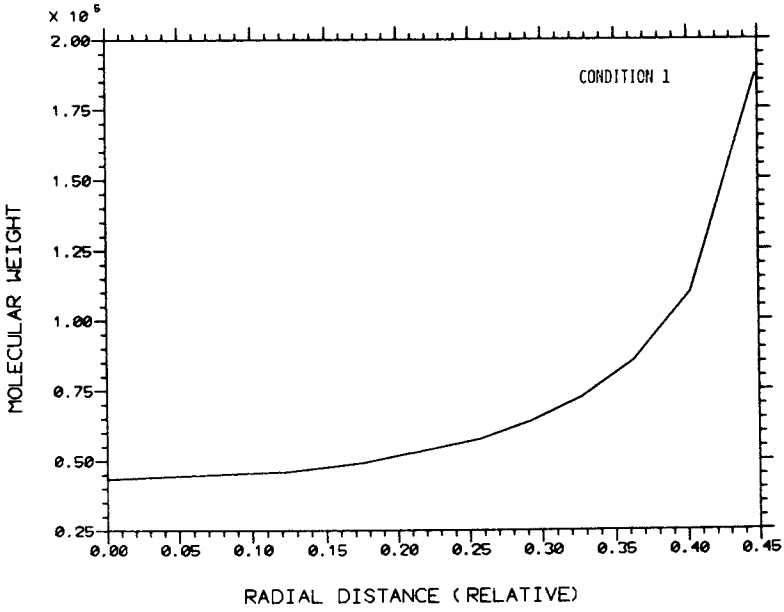

Figure 3. Molecular weight traverse

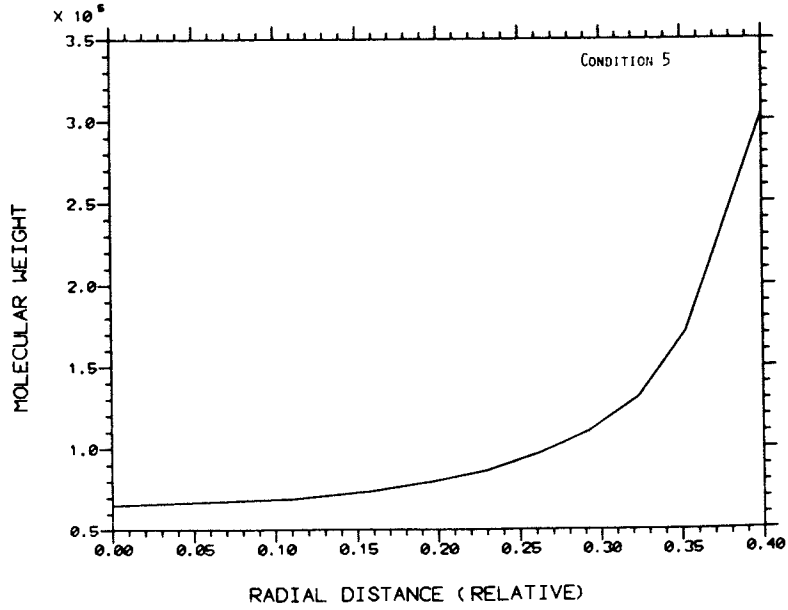

Figure 4. Molecular weight traverse

In Chemical Reaction Engineering—Houston; Weekman, V., et al.;
ACS Symposium Series; American Chemical Society: Washington, DC, 1978.

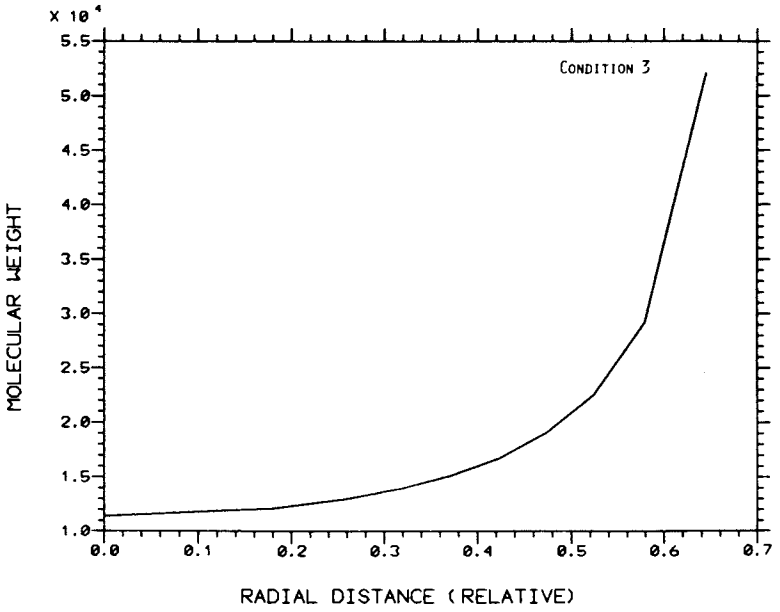

Figure 5. Molecular weight traverse

TABLE III

RESULTS OF LAMINAR FLOW INTEGRATION

Condition	R cm	(Va^{+++}) mmol/l	$\overline{MW}_v$ -	θ min	L m	η_{inh} -	MWD -
1	0.50	0.035	77,000	1.97	2.1	1.5	1.27
2	2.5	0.035	72,300	1.77	2.1	1.42	1.33
3	15.0	0.035	22,600	0.55	3.6	0.54	1.32
4	0.50	0.01	126,000	3.30	3.5	2.25	1.29
5	2.5	0.01	123,000	3.11	9.6	2.2	1.32
6	15.0	0.015	23,000	0.96	67.2	0.7	-
7	15.0	0.07	11,600	0.28	17.9	0.3	-

Inlet Condition

$T = 10°C$; $x_1 = 0.083$, $x_2 = 0.50$, $x_3 = 0.028$

In Chemical Reaction Engineering—Houston; Weekman, V., et al.;
ACS Symposium Series; American Chemical Society: Washington, DC, 1978.

Discussion

As applied to copolymerization with Ziegler catalysis, tubular reactors are limited in conversion for two principal reasons. The reaction is highly exothermic and high temperatures are detrimental to the catalyst. In addition, since the monomers have differing reactivity, polymer of varying composition is obtained as the monomers are depleted. Useful EPDM elastomers have a restricted compositional range. The material produced in these studies have compositions of 55 to 70% ethylene, 30 to 45% propylene and about 3% hexadiene by weight.

An important feature of this work is the localization of the bulk of the reaction near the wall of the tube distorting the velocity profile. Contrary to expectations, this feature does not produce a product with a broad molecular weight. The ratio of weight average divided by number average molecular weight is almost constant at 1.3 for all the cases studied. The above-mentioned compositional variation near the wall limits molecular weight because of depletion of the most rapidly reacting species (ethylene). A previous work (8) with butadiene solution polymerization included reactors long enough for essentially complete reaction which showed nearly monodisperse polymer at the exit of the reactor. This is possible at the expense of a very high temperature and a large pressure drop when high viscosity material fills the reactor. Lynn (9) recently published a strong argument against the feasibility of tubular reactors in polystyrene production.

In Table III, it may be seen that the largest diameter reactor produces the lowest molecular weight. This reactor suffers also from an apparent hot spot at the wall (see also Reference 2). A third limitation is that the model fails at this diameter since the entrance flow is turbulent. It would not be worth the effort to develop a model for this case since high molecular weight polymer can only be produced in small diameter reactors.

This paper is Contribution 418 from the Elastomer Chemicals Department.

APPENDIX

VELOCITY PROFILE ANALYTIC SOLUTION FOR NONUNIFORM VISCOUS FLOW

(A Method Derived by R. L. Turner and E. D. Wohlsen)

Conceptually, the flow is divided or lumped into a number of annular streams each representing a fraction of the flow. Equal fractions are most convenient, but the treatment is general. All conditions within an annulus which affect viscosity are assumed to be uniform. (This is true of shear rate also. This means that non-Newtonian fluids cannot be handled directly. In actual practice, the method has shown itself to

be even more helpful in non-Newtonian situations. In all such cases, the shear rate contribution is corrected after each "Newtonian" solution and the whole solution scheme repeated until the velocity profile is stabilized.)

Examination of "Newtonian" considerations for a single-flow annulus between outside radius r_J and inside radius r_{J+1} carrying ΔQ_J units in a pipe of radius r_W shows that the shear stress at the mid-point is

$$\tau_J = \frac{\tau_w}{r_w}\left(\frac{r_{J+1} + r_J}{2}\right)$$

The average shear rate in an element is

$$\left(\overline{\frac{dv}{dr}}\right)_J = -2\,\frac{\bar{v}_J - v_J}{r_{J+1} - r_J}$$

The average velocity is

$$\bar{v}_J = \frac{\Delta Q_J}{\pi(r_J^2 - r_{J+1}^2)}$$

The definition of viscosity yields

$$\tau_J = \eta_J\left(\overline{\frac{dv}{dr}}\right)_J$$

Utilizing these four equations, a rather lengthy derivation gives analytical working equations for the velocity (v_n) and the radius (r_n) at the outside of each annulus.

$$v_n = \left(\alpha\,\tau_w \sum_{J=1}^{n-1} \frac{\Delta Q_J}{\eta_J}\right)^{1/2}$$

$$r_n = \left(r_w^2 - \frac{1}{\tau_w^{1/2}} \sum_{J=1}^{n-1} \ell_J\right)^{1/2}$$

Where:

$$\alpha \equiv \frac{1}{r_w \pi}$$

$$h_n \equiv \frac{\Delta Q_n}{\pi}$$

$$\ell_J \equiv \frac{h_J}{g_J}$$

In Chemical Reaction Engineering—Houston; Weekman, V., et al.;
ACS Symposium Series; American Chemical Society: Washington, DC, 1978.

$$g_n = \tfrac{1}{2}\alpha^{\frac{1}{2}} \left[\left(\sum_{J=1}^{n-1} \frac{\Delta Q_J}{\eta_J} \right)^{\frac{1}{2}} + \left(\sum_{J=1}^{n} \frac{\Delta Q_J}{\eta_J} \right)^{\frac{1}{2}} \right]$$

$$\tau_w = \frac{1}{r_w 4} \left(\sum_{J=1}^{JM} \ell_J \right) 2$$

JM = the total number of annuli
η_J = average viscosity of the Jth annulus

Nomenclature

C	is	polymer concentration (gm/deciliter)
η	is	solution viscosity (poise)
η_{inh}	is	inherent viscosity
η_o	is	viscosity of hexane at reactor entrance
W_i	is	weight fraction
M_i	is	molecular weight
$\overline{MW}_v$	is	viscosity average molecular weight
θ	is	reactor residence time
R_i	is	the rate of reaction of the i^{th} monomer
ΔH_i	is	the heat of polymerization for this monomer
k	is	thermal conductivity
r	is	radial distance
ρ	is	liquid density
C_p	is	liquid heat capacity
v	is	velocity in the Z direction
Z	is	the distance along the axis of the reactor
T	is	temperature (absolute when appropriate)
J	is	the index for the radial distance
N	is	the index for the axial distance
x_1, x_2, x_3		are mole fractions of ethylene, propylene, and hexadiene respectively
V_a^{+++}	is	vanadium ion concentration (millimole/liter)
τ	is	shear stress
Q	is	volumetric flow
α, h, ℓ, and g		are defined in the text

Acknowledgement:

The author is grateful to R. L. Turner for discussions of his work on laminar velocity distributions and for pointing out the method of L. H. Thomas.

REFERENCES

1. Husain, A. and A. E. Hamielec, CEP Symposium Series (1976) 160 112
2. Sala, R., F. Valz-Griz and L. Zanderighi, Chemical Eng. Sci. (1974) 29 2205
3. Wyman, C. E. and L. F. Carter, CEP Symposium Series (1976) 160 1
4. Ghosh, M., D. W. Foster, J. P. Lenczyk and T. H. Forsyth, CEP Symposium Series (1976) 160 102
5. Shih, Chi-Kai, Unpublished
6. von Rosenberg, D. V, "Methods for the Numerical Solution of Partial Differential Equations," P-8, American Elsevier, New York, 1969
7. Petersen, R. E. A. and R. E. Tarney, Unpublished
8. Lynn, S. and J. E. Huff, AIChE Journal (1971) 17 475
9. Lynn, S. AIChE Journal (1977) 23 389

In Chemical Reaction Engineering—Houston; Weekman, V., et al.;
ACS Symposium Series; American Chemical Society: Washington, DC, 1978.

13

Comparison of the Performances of Various Fermentors and Selection Criteria

J. P. EUZEN, P. TRAMBOUZE, and H. VAN LANDEGHEM

Institut Francais du Petrole, C.E.D.I., B.P. 3, 69390,Vernaison, France

For several decades now, fermentation has been an important industrial operation. Systematic research began only some 20 years ago, chiefly at the time of the development of processes whose main objective was the production of biomass. Our own research was carried out in this context, and accompanied the development of fermentation processes using as substrate either hydrocarbons or methanol.

Our pre-occupation was to improve the economics of the process : it was therefore necessary to find appliances which could operate with a minimum fermentor volume and low energy consumption. Our criteria of choice were therefore essentially based on biomass productivity (weight of biomass/unit of volume and time) and energy consumption per kg of dry material produced.

The acquisition of comparative values for different appliances is very difficult. In fact it became apparent that the nature of the strain and fermentation conditions noticeably affected the conditions of mass transfer and consequently the overall kinetics of the cell growth.

A priori oxygen and hydrocarbons are in the same situation, that means that mass transfer phenomena between two fluid phases will limit free cell growth, but we shall see that hydrocarbons have a special behaviour.

In fact since 1967, several authors (1, 2) have confirmed that the transfer of paraffins was far too rapid to be explained like O_2 transfer by a transfer via the aqueous phase : diffusion and solubility coefficients are far too low. In the same way a direct transfer between the cells and the hydrocarbon drops seems highly unlikely. It was A.AIBA who in 1969 (2) introduced the idea of pseudo-solubility or "accomodation" of the hydrocarbon in sub-micronic drops. The validity of this idea has been demonstrated on several occasions (3, 4, 5, 6) which now allows to treat hydrocarbons as a soluble substrate with, however, this particularity that the value of the saturation constant depends not only on the nature of the strain but also on the previous history of

© 0-8412-0401-2/78/47-065-153$05.00/0

the culture. It has in fact appeared that this accomodation occurs only thanks to the presence in the culture medium of a certain number of still not clearly identified surfactants. Consequently a limitation by hydrocarbons is not more likely to occur than that of other soluble substrats, so that in a well-conducted fermentation, oxygen has every chance of being the only growth limiting substrate.

We know moreover that surfactant substances influence mass transfers, even gas-liquid transfers, as a result of modifications of the interfacial area and of the transfer coefficient (among others (7)).

Conclusions which might be drawn on the transfer kinetics from chemical or physico-chemical measurements are therefore suspect, and only direct comparison of fermentation results can give rise to valid conclusions, on condition that the strain is well-known and controlled. In what follows we shall refer however to some experimental results obtained by the oxidation of sodium sulphite method.

Experimental Methods.

a) - Oxydation of sodium sulphite. The method and the physico-chemical constants, were borrowed from REITH (8).

b) - Fermentations. The fermentations were carried out in an aqueous nutritive medium with optimization for the essential constituents (N, K, P, oligo-elements, vitamins) taking care to avoid any deficiency of soluble substrates. The carbon source was a n-paraffin commercial cut with 12-20 carbon atoms. The strain used was a Candida Tropicalis ; air provided the oxygen while the nitrogen supply and pH control (pH $\approx$ 3,5) was made by ammonia injection. Some evolution of the strain characteristics allowed a small increase of the fermentation temperature in the last experiments (30 to 35 °C).

Experimental Results and Interpretation .

We were interested in 3 types of fermentors during this study :
- mechanically stirred fermentors
- air-lift fermentors
- loop fermentors.

The last-one, still undergoing experimentation will thus only be referred to briefly.

Concerning interpretation of the results we have adopted the following simplifications :
- the oxygen consumption is of 2 kg/kg of cells
- in our stirring conditions the transfer coefficient k_L will be taken as a constant equal to 1,80 m/h; this approximation has frequently been confirmed (7, 8).

In Chemical Reaction Engineering—Houston; Weekman, V., et al.;
ACS Symposium Series; American Chemical Society: Washington, DC, 1978.

a) - Mechanically stirred fermentors. Figure 1 shows diagrams of 3 fermentors studied.

The flat-blade turbine may be surrounded by a cylinder pierced with openings between the turbines and with small holes at the level of the turbines. It was the version without a cylinder which was preferably used in the fermentation tests, while different geometries were studied more systematically by the oxydation of sodium sulphite.

Results obtained are summarized in figure 2 in the form suggested by REITH (9). The powers and interfacial areas are thus expressed per unit volume of non-expanded liquid phase. The power P is the sum of the one resulting from the isothermic expansion of the injected gas and the mechanical power absorbed by the liquid phase.

The interfacial areas were either measured by the chemical method, or else calculated from fermentation results.

The following comments might be made :
- the cylindrical baffles fitted to provoke a strong shearing action at turbine level have a negative effect for oxygen transfer, and serve no purpose for the transfer of hydrocarbons, which with a good strain are pseudo-solubilized by the surfactants ;
- the energy supply is more efficiently used if it is provided by air, rather than by stirrers ;
- for a given energy source and for a given strain the results can be expressed approximatively as follows :

$$A = KZ^{\alpha} \quad (1) \quad \text{with} \quad \begin{cases} Z = P/V_L \\ 0,6 < \alpha < 0,7 \\ 100 < K < 200 \text{ for the systems used} \end{cases}$$

A good choice of fermentor should therefore be able to give a K value of at least 200 ($\alpha = 0,65$), which implies a k_LA value calculated as follows :

$$k_LA = 1,8 * 200\ Z^{\alpha} = 360\ Z^{\alpha} \qquad (h^{-1}) \qquad (1')$$

b) - Airlift fermentors. Two types of fermentors were used (fig.3). Five dimensions, from 60 to 1 900 liters, were tested for type A. The experimental data (table I and figures 4 & 6) were, once more, correlated by a law of the form suggested by WANG (12) $A = KZ^{\alpha}$ with $0,6 < \alpha < 0,7$

The K factor is influenced by the geometry of the system, by operating conditions, and by the nature of the strain. Moreover successive selections modified the nature of the strain between certain test series on airlifts. This explains why different performances may have been noted on similar fermentors. Thus the strain used in the type A 850 l air lift reactor is probably less oxygen demanding, which would bring the value of A down to a level approwimately 40 % lower (arrows on figure 4). The outputs being non-ambiguous magnitudes, taking energy consumption per kg

In Chemical Reaction Engineering—Houston; Weekman, V., et al.;
ACS Symposium Series; American Chemical Society: Washington, DC, 1978.

Liquid volume	A 5 l	B 200 l	C 1000 l
Ratio liquid height at rest / fermentor diameter	1,2	1,9	2,1
Ratio baffle diameter / fermentor diameter	1/2,3	1/2,8	1/3,1
Ratio outer baffle cross section area / inner	4,4	6,7	8,5
Ratio height between turbines / turbines diameter	1,1	1,5	1,3

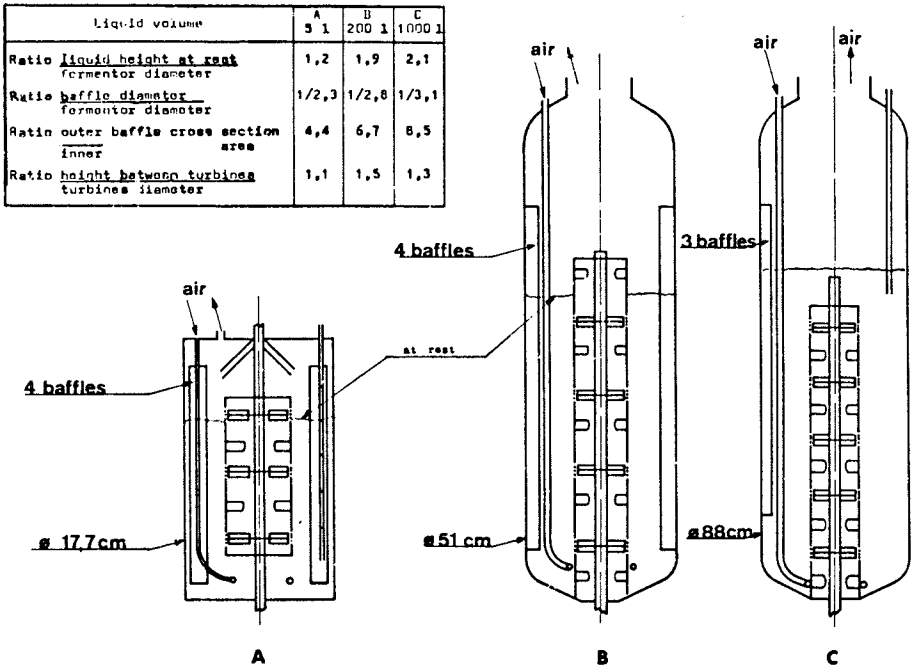

Figure 1. Three mechanically-stirred fermentors

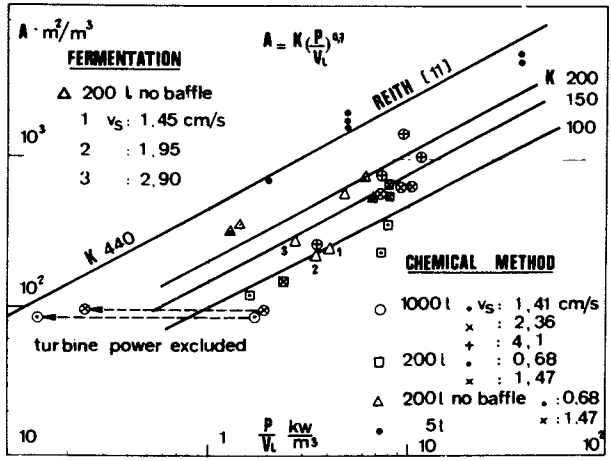

Figure 2. Mechanically-stirred fermentors

In Chemical Reaction Engineering—Houston; Weekman, V., et al.;
ACS Symposium Series; American Chemical Society: Washington, DC, 1978.

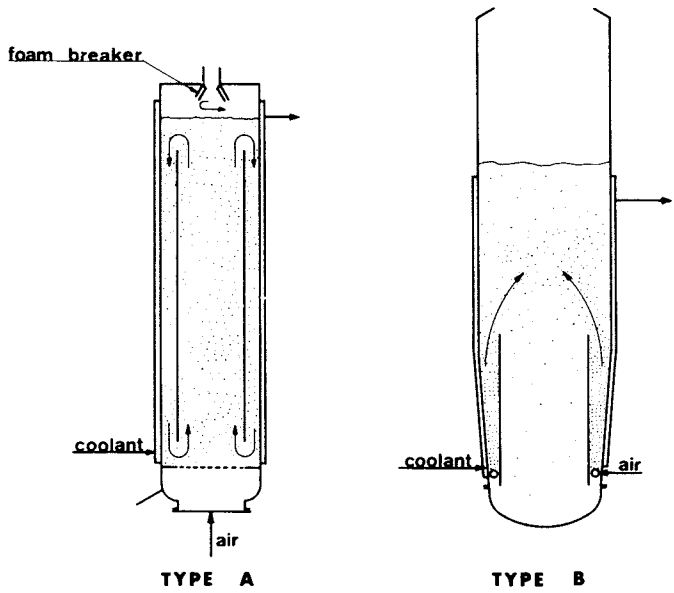

Figure 3. Two types of airlift fermentors

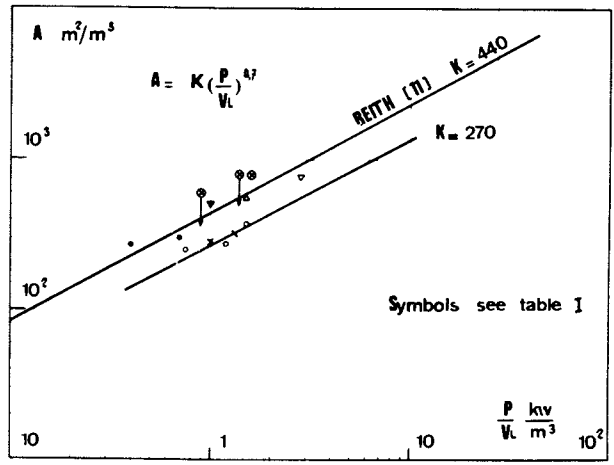

Figure 4. Air lift fermentors

TABLE I

Performances of some fermentors

Volume V_L l	v_S cm/s	$Z = \frac{P}{V_L}$ kW/m^3	Mechanical energy fraction (%) ϕM	Interfacial area A m^2/m^3	Productivity $\frac{XF}{YoV_1} = \pi$ kg O2/m^{3}h	Energy Consumption E kWh/kgO_2	1 - ε	Symbols of fig. 4, 5
A - MECHANICAL STIRRING - (1 000 rev/min)								
450	1,45	3,60	86	236	2,6	1,38	-	□
450	1,95	3,40	79	220	2,4	1,42	-	□
450	2,90	2,60	55	280	3,0	0,87	-	□
B - AIR LIFT -								
Type A								
60	5	0,4	-	287	1,55	0,26	-	●
	8	0,7	-	315	1,70	0,41	-	●
160	12	1	-	287	1,55	0,65	0,09	x
	15	1,33	-	333	1,80	0,74	0,17	x
235	9	0,75	-	250	1,35	0,56	-	o
	13,5	1,15	-	278	1,50	0,77	-	o
	18	1,50	-	370	2,00	0,75	-	o
850	8	0,89	-	590	3,2	0,28	-	⊠
	12,5	1,40	-	800	4,30	0,33	0,29	⊠
1 900	19	1,5	-	590	3,20	0,47	0,13	△
Type B								
3 300	26	2,75	-	780	4,20	0,65	0,58	▽
C - LOOP FERMENTOR -		3,5				0,5		⊙

In Chemical Reaction Engineering—Houston; Weekman, V., et al.; ACS Symposium Series; American Chemical Society: Washington, DC, 1978.

of oxygen consumed against $Z = P/V_L$ seems more suitable.

This representation avoids the ambiguity on the O_2 concentration in the bulk of the liquid. Indeed, the presence of hydrocarbons in the medium provokes an important drift on the O_2 measurements with dissolved O_2 probes.

If, as a first approximation, the oxygen productivity π is proportional to the interfacial area $\pi \simeq A = K Z^{\alpha}$ (2)
we can state as specific energy consumption

$$E = Z/\pi = K_1 Z^{1-\alpha} \quad (3)$$

This relationship is respected (fig.6), and K_1 depends on the strain and on the fermentation system. All our previous conclusions are, of course, confirmed by this representation. It does clearly appear that, as the fermentor which has the lowest $Z = P/V_L$ is more worthy of interest, it will of course be more bulky. The compromise between these two contradictory factors which, in the absence of other requirements, will go to make up the criteria for fermentor choice.

c) - Loop fermentors. Figure 5 shows the basic designs of a loop fermentor (10, 11).

The important recirculation ensures a good broth homogeneity and permits interesting heat and mass transfers.

The sole operational point available for an industrial plant, is located close to the results observed for the other fermentors (fig. 6).

Conclusions.

Apart from a certain number of requirements, the relationship developed so far enable us to draw some useful conclusions regarding the choice of the fermentation system and its operating conditions. It is thus that mechanical systems, showing up badly in figures 2 and 6, are not to be retained, and that, among air lift type equipment, a compromise should be sought between reactional volume and energy consumption. The factors on which this compromise might be based are in fact available. The hourly cost of operation fermentation equipment producing X kg/h of yeasts might be stated :

$$\text{cost} = a_0 X + a_1 + a_2 EXY_0 + P_R + P_C \ (F/h) \quad (4)$$

Where :

a_0	nutrient price	F/kg of yeast
a_1	fixed expenditure	F/h of operation
a_2	cost of air compression energy (taking into account yield)	F/kWh
P_R	cost of reactor (amortization)	F/h of operation
P_C	cost of compressor idem	

These two latter terms could be written as follows :

In Chemical Reaction Engineering—Houston; Weekman, V., et al.;
ACS Symposium Series; American Chemical Society: Washington, DC, 1978.

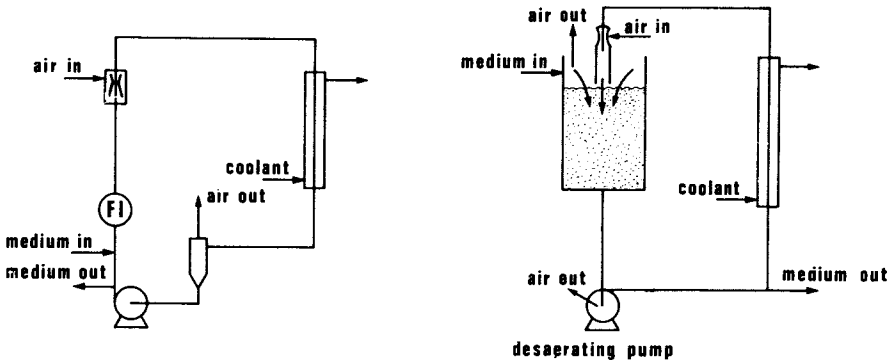

Figure 5. Loop fermentors

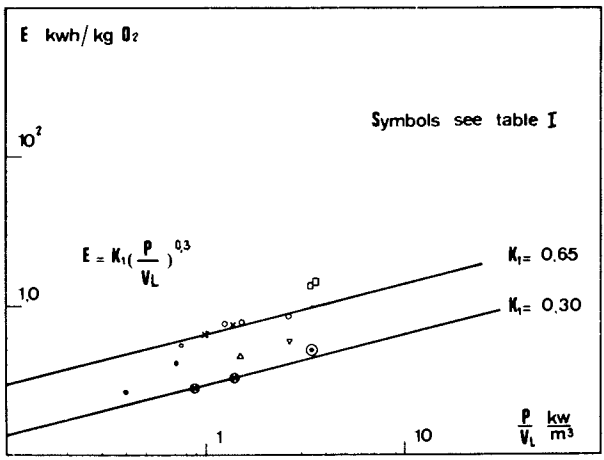

Figure 6. Final comparison of the various studied fermentors

In Chemical Reaction Engineering—Houston; Weekman, V., et al.;
ACS Symposium Series; American Chemical Society: Washington, DC, 1978.

$P_R = a_3 (V_L)^{\beta}$ supposing the price of the reactor depends on its liquid volume

$P_C = a_4 P^{\gamma}$

a_3 specific operating cost of fermentor

a_4 specific operating cost of compressor.

Thus the price of the yeast in F/kg would come to :

$$\text{price} = a_0 + a_1/X + a_2 E Y_0 + a_3 (V_L)^{\beta}/X + a_4 P^{\gamma}/X \ (\text{F/kg}) \quad (5)$$

For big compressors γ is in the range of 0.8 to 1 (13). If for the sake of simplicity we take $\gamma = 1$, we obtain :

$$\text{price} = a_0 + a_1/X + K_1 Y_0 (a_2 + a_4) Z^{(1-\alpha)} + a_3 K_1^{\beta} X^{(\beta-1)} . Y_0^{\beta} . Z^{-\alpha\beta} \ \text{F/kg} \quad (6)$$

owing to $V_L = P/Z$, $P/X = EY_0$ and $E = K_1 Z^{(1-\alpha)}$.

Then the optimal Z value is obtained when :

$$Z_{opt} = \left[\frac{\alpha\beta}{1-\alpha} \cdot \frac{a_3}{a_2+a_4} \cdot (K_1 X Y_0)^{\beta-1} \right]^{\frac{1}{1+\alpha\beta-\alpha}} \quad (7)$$

As we have seen α is close to 2/3, while β is somewhere between 0,6 and 1.

It can be pointed out that a big size fermentor has to be operated with a lower P/V_L value than a small size one.

We can also see that the optimum P/V_L for large appliances which, in 1969, was in the region of 1.5 kW/m^3, is tending to evolve as a result of changes in relative energy/investment costs, towards less productive units with a lower specific energy consumption.

An ambiguity does however persist for air lift fermentors: the volume which we calculated above is a liquid volume. However there is no means by which, in these appliances, we can predict and control the expansions. As a result, in industrial practice, a very high "expansion volume" is to be expected, while adapting the gas velocity to the foaming propensities of the culture is an in situ operation. It is this absence of precision in the design stage, involving as it does the danger of a certain lack of homogeneity, which is the weak point of these appliances. Loop fermentors, easier to control from this point of view, could thus represent a step foreward on condition however that their unit volume and their energy consumption prove to be competitive. In any case they will always have an advantage in terms of the heat transfer coefficients in the re-circulation loop.

It should also be noted that the criteria of productivity and energy consumption alone are insufficient criteria on which to base a choice of fermentor. The importance of maintaining a homogeneous "broth" could, in fact, be decisive if, for example, the functioning were to be disturbed by excessive sedimentation or foaming. On the other hand, while substrate yield depends on

In Chemical Reaction Engineering—Houston; Weekman, V., et al.;
ACS Symposium Series; American Chemical Society: Washington, DC, 1978.

the fermentor productivity, some oversimplification has been made in this study and more experimental work is needed to find out the true overall optimum for the process.

In this respect it must never be forgotten that, while a fermentor is certainly a chemical reactor, it is also one in which the presence of living substances disturbs the traditional working of the equipment, in particular as far as transfer and expansion factors are concerned.

It is therefore only by comparing equipments, in the presence of the strain whose industrial use is being considered, that it would be possible to obtain truly representative conclusions.

List of Symbols

A	interfacial area	m^2/m^3 of liquid
E	specific energy consumption	kWh/kg O_2 transf.
k_L	mass transfer coefficient	m/h
P	total power	kW
V_L	liquid volume in fermentor	m^3
V_S	superficial gas velocity	cm/s
X	ponderal broth flow rate	kg/h
Y_O	weight oxygen consumed/weight cells produced	
Z	total power per unit of liquid volume	kW/m^3
ε	liquid volume fraction in fermentor	
ϕM	mechanical energy fraction	%
π	productivity expressed as kg O_2/m^3 of liquid.h	

Literature Cited

(1) B. ERDSIECK, Thesis, Eindhoven (The Netherlands) (1967)
(2) A. AIBA et alii, J. Ferment. Technol, 47, 211 (1969)
(3) F. YOSHIDA and alii, Bioeng.& Biotechn, XIII, 215(1971); ibid XV, 257 (1973) ; ibid XVI, 635 (1974)
(4) M. CHAKRAVARTY et alii,ibid, XIV, 61 (1972) ; ibid XVII, 399, (1975)
(5) D.A. WHITWORTH et alii,ibid, XV, 649 (1973)
(6) G. GOMA et alii, J. Ferment. Technol., 51, 616 (1973)
(7) A. BENEDECK et alii, Bioeng.& Biotechn., XIII, 663 (1971)
(8) T. REITH, Thesis, Delft (1968)
(9) T. REITH, Brit.Chem. Eng. 15, 1562 (1970)
(10) H. ZIEGLER et alii., Bioeng. & Biotechn., XIX, 507 (1977)
(11) K. SCHEIER, Chem. Rundschau, 38, 18 (1976)
(12) D.I.C. WANG et alii,8e World Petroleum Congress, Panel discussion "Petroleum and Microbiology" P.152(1971)
(13) P. LEPRINCE et alii, Manuel d'Evaluation économique de procédés. Ed. Technip. Paris (1976)

In Chemical Reaction Engineering—Houston; Weekman, V., et al.;
ACS Symposium Series; American Chemical Society: Washington, DC, 1978.

14

Kinetic Analysis of Unbalanced Bacterial Growth in Temperature Shift

TATSURO SAWADA and TETSUJI CHOHJI
Department of Chemical Engineering, Faculty of Technology, Kanazawa University, Kanazawa 920, Japan

SIGERU KUNO
Department of Biochemistry, School of Medicine, Kanazawa University, Kanazawa 920, Japan

Attempts to assess quantitatively the bacterial growth and their physiological state have long been pursued by many investigators. Bacteria can be cultivated in a virtually unchanging environment for long periods during which they simply repeat the same cycle of mass increase and division. Depending on culture conditions, however, a large number of physiological states exists, each of which is characterized by a particular size and chemical composition of the cells (1, 2). In balanced growth with a sufficient amount of substrate, a simple relationship exists between the growth rate and the average mass or macromolecule content of the cells, and thus the state of the balanced growth can be characterized by either the growth rate or the average mass or macromolecular content.

In utilization of microorganisms for sanitary and industrial purposes, it is difficult to maintain a constant environment for microbial growth. Since a change in environment results usually in a change in the growth rate as well as the size and the chemical composition of the cells, a plausible conjecture as to the mode of growth is difficult. We have studied a method to evaluate quantitatively the unbalanced growth in response to shifts in environmental condition. For practical reasons we chose growth temperature for environmental change. Although the cell size and composition were almost independent of the growth temperature in a given medium containing a sufficient amount of substrate (1), it was found that a shift in the growth temperature brought changes in the physiological state in a medium containing a lower concentration of substrate. In the present communication, we will present the behavior and formular expression of the bacterial growth in this unbalanced state.

Materials and Methods

Organism and Growth Medium. The strain used throughout the

© 0-8412-0401-2/78/47-065-163$05.00/0

experiments was *Escherichia coli* BB. A basal medium contained 0.25 % $(NH_4)_2HPO_4$, 0.15 % NaCl, and 0.01 % $MgSO_4 \cdot 7H_2O$. To this basal medium, various concentrations of glucose (maximum 0.5 %) were added. The pH of the media was maintained at 7.0 throughout the experiment.

Experiment in Batch Culture. In a batch culture, the cell concentration was less than 10^4 cells/ml so that a change in glucose concentration was negligible during the experiments. At intervals, samples were withdrawn and viable cells were measured by the double agar layer method.

Experiment in Continuous Culture. An aliquot of overnight culture was added in a T-shaped tube (working volume = 100 ml) containing 90 ml of the fresh medium and shaken at 37 °C. When the optical density at 660 nm of the culture reached to 0.2, the culture was poured into a fermentor (working volume = 500 ml) containing 400 ml of the fresh medium. After 5 to 6 hrs cultivation, a supply of the medium which contained 0.5 mg/ml glucose and had been stored in a reservoir was initiated to start a continuous run. The schematic diagram of the fermentor is shown in Figure 1. Agitation was provided by means of a magnetic stirrer and a removable baffle. Air flow rate was 2 vvm. The air from the compressor was saturated with water vapor by passing it through a humidifier to protect evaporation of the medium.

When the effect of a temperature was studied, the fermentor was immersed in a vessel containing isopropyl alcohol and dry ice. When the temperature of the medium reached the desired value, the fermentator was quickly transferred into a new water-bath which had been adjusted to the desired temperature. This method made it possible to change the culture temperature within one minute.

The concentration of glucose in the culture was determined according to the method of Park and Johnson (3), after centrifugation (3,500 rpm, 5 min) to remove cells.

Reaction Model

The Monod's equation (4, 5), which was obtained on the basis of Michaelis-Menten's equation for enzymatic reaction, has been one of the most widely accepted models, for a quantitative assessment of microbial growth. If bacteria are grown in media in which excess inorganic nutrients but a limiting amount of glucose (carbon source) are present, a specific growth rate, μ, of the bacteria is specified as a function of the concentration, y, of glucose in the medium, and can be expressed by the following Monod's equation:

$$\mu = \mu_m \, y/(K_S + y) \qquad (1)$$

where μ_m and K_S are the maximum value of μ and a saturation con-

In Chemical Reaction Engineering—Houston; Weekman, V., et al.;
ACS Symposium Series; American Chemical Society: Washington, DC, 1978.

stant (numerically equal to the glucose concentration at 1/2 μ_m), respectively. It is well known that μ_m is a function of temperature. Since K_S is apparently equivalent to the dissociation constant in the Michaelis-Menten's equation, $1/K_S$ appears to show degree of utilizability of substrate by cells and to be also a function of growth temperature. Thus, μ_m and $1/K_S$ may be given by following Arrhenius' equations.

$$\mu_m = A_1 \exp(-E_1/RT) \quad (2), \quad 1/K_S = A_2 \exp(-E_2/RT) \quad (3)$$

In our previous study (1), it was demonstrated that a content of macromolecule, such as DNA, RNA and protein, per cell was expressed by an exponential function of specific growth rate:

$$C_i = C_{i0} \exp(\alpha_i \mu) \quad (4)$$

where C_i is a content of macromolecule, i, per cell, C_{i0} is a content of macromolecule per cell at the zero growth rate, and α_i is a function of temperature and a gradient in the plots of logarithmic values of C_i against μ. The value of C_{i0} was shown to be constant and independent of temperature. From equations (1) and (4),

$$C_i/C_{i0} = (C_{im}/C_{i0})^{y/(K_S + y)} \quad (5)$$

where C_{im} is the macromolecular content per cell at the maximum growth rate, μ_m. Since the maximum growth rate is obtained in the presence of a sufficient amount of glucose (thus $y >> K_S$), C_{im} is a constant regardless of growth temperature. However, C_i at a limiting concentration of glucose may be varied by growth temperature, unless E_2 value in equation (3) is zero. This relationship is illustrated in Figure 2. The solid lines in the figure represent a relationship between μ and DNA content per cell at a given temperature calculated from equation (4). The broken lines indicate a relationship between μ and DNA content per cell at a given concentration of glucose, and are obtained by calculation of equations (1), (3) and (5).

Results and Discussion

Effect of Temperature on μ_m and K_S. Figure 3 shows the relationship between the specific growth rate and substrate (glucose) concentration. In the figure, $1/\mu$ has been plotted against a reciprocal of glucose concentrations in media for seven different growth temperatures. It is clear from the equation (1) that the intercepts on the vertical axis and the base line give $1/\mu_m$ and $-1/K_S$, respectively, and that both μ_m and K_S are functions of temperature. In Figure 4, the logarithms of μ_m and K_S are plotted against 1/T. These Arrhenius plots give straight lines, and the activation energies for μ_m and K_S were calculated from the slopes as 8.51 and 15.7 kcal/g-mole, respectively. It is obvious that

In Chemical Reaction Engineering—Houston; Weekman, V., et al.;
ACS Symposium Series; American Chemical Society: Washington, DC, 1978.

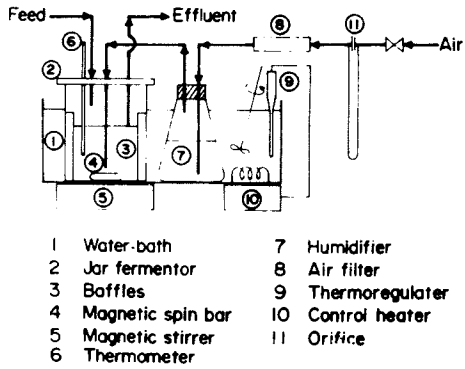

Figure 1. Apparatus for continuous culture

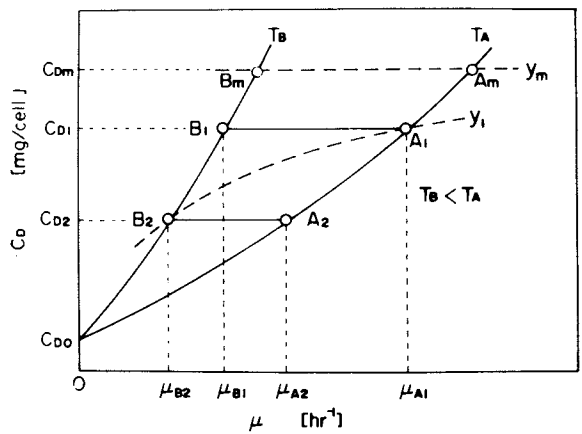

Figure 2. DNA contents per cell as a function of specific growth rate at temperatures T_A and T_B. The broken lines represent the relationship at a glucose concentration of y_m or y_1.

In Chemical Reaction Engineering—Houston; Weekman, V., et al.;
ACS Symposium Series; American Chemical Society: Washington, DC, 1978.

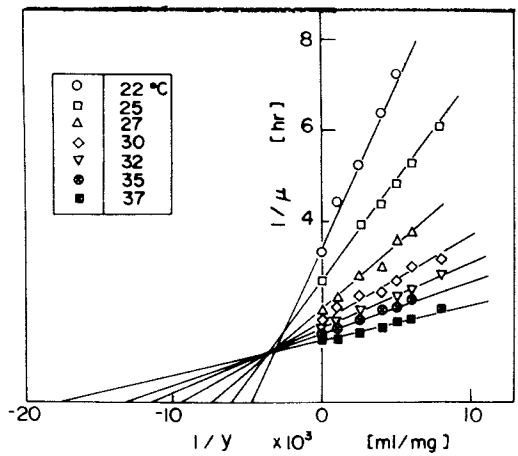

Figure 3. Reciprocal plots between the specific growth rate and glucose concentrations as a function of temperature

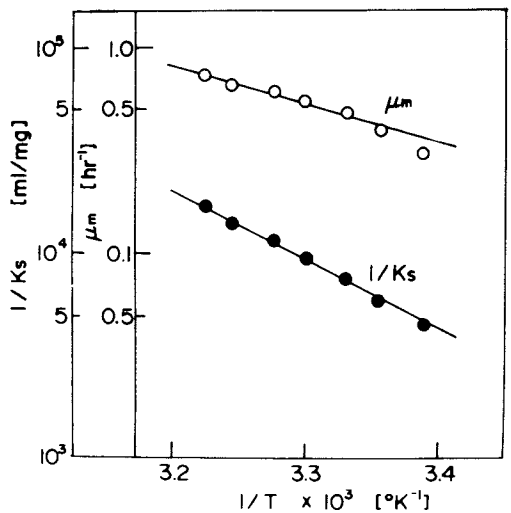

Figure 4. Temperature dependency of parameters μ_m and $1/K_S$

In Chemical Reaction Engineering—Houston; Weekman, V., et al.;
ACS Symposium Series; American Chemical Society: Washington, DC, 1978.

the extrapolated points of the lines to $1/T = 0$ give $A_1 = 7.31 \times 10^5$ hr^{-1} and $A_2 = 1.99 \times 10^{15}$ ml/mg of equations (2) and (3).

Relationship between Average DNA Content and μ. In Figure 5, the DNA content per cell was plotted against μ. The solid lines in the figure were calculated from equations (1), (2), (3) and (5), using $C_{D0} = 4.1 \times 10^{-12}$ mg/cell and $C_{Dm} = 8.5 \times 10^{-12}$ mg/cell obtained in our previous report (1). The broken lines in the figure were obtained by calculation of equations (1), (2) and (5). The experimental data were in agreement with the calculated value. As expected from Fig. 2, it was shown that the DNA content per cell was independent of growth temperature at higher glucose concentrations, while the DNA content decreased with a lowering of the growth temperature at suboptimal concentrations of glucose.

Effects of Temperature Shift on Growth in Batch Culture. As reported previously (1), when the bacteria are grown in a sufficient amount of substrate, the bacteria are capable of adapting without any lag to a sudden change in growth temperature because the physiological state of the bacteria is independent of growth temperature under this condition. However, in an insufficient supply of glucose, the sudden upward or downward shift in temperature will cause the bacteria to lag in adapting to a new condition, because the physiological state of the cell differs by growth temperature in this case. When the medium contains a limiting amount of glucose, y_1, physiological states of the bacteria are B_2 state at temperature T_B, and A_1 state at T_A (Fig. 2). When the growth temperature of the steady state culture is suddenly shifted from T_B to T_A, the physiological state of the cells will move from B_2 to A_2 and to A_1. Similarly a temperature shift from T_A to T_B will cause a change in the physiological state from A_1 to B_1 and to B_2. Therefore, a change in growth rate (as measured by cell number, N) may occur after some time lag in temperature shift-up, and an initial overshot growth may be observed in temperature a shift-down. These situations are probably similar to those observed in shift-up to an enriched medium or a shift-down to a poorer medium (6). These conjectures were verified in the shift-up and shift-down experiment with the batch culture, as shown in Figure 6. Although the temperature shift in the batch culture brought qualitatively expected results, it was difficult to measure cell mass and macromolecule content, because the cell density in the culture had to be kept very low to maintain the culture at the fixed and much lower concentration of glucose. Therefore, a continuous culture was carried out to follow changes in the physiological state of cells at the temperature shift.

Effects of Temperature Shift on Growth in Continuous Culture. At the steady state in the continuous culture, the culture population density is maintained constant, and the specific growth rate is equal to the dilution rate, D (the influent volume per hr

In Chemical Reaction Engineering—Houston; Weekman, V., et al.;
ACS Symposium Series; American Chemical Society: Washington, DC, 1978.

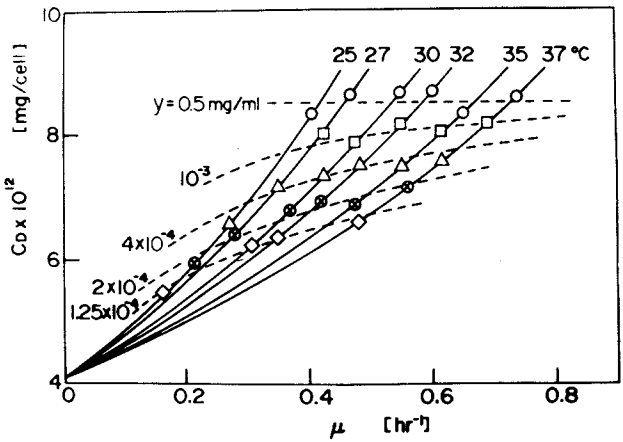

Figure 5. Relationship between DNA contents per cell and the specific growth rate at various glucose concentrations and temperatures. Solid and broken lines represent the calculated curves at isothermal conditions and those at the same glucose concentrations, respectively.

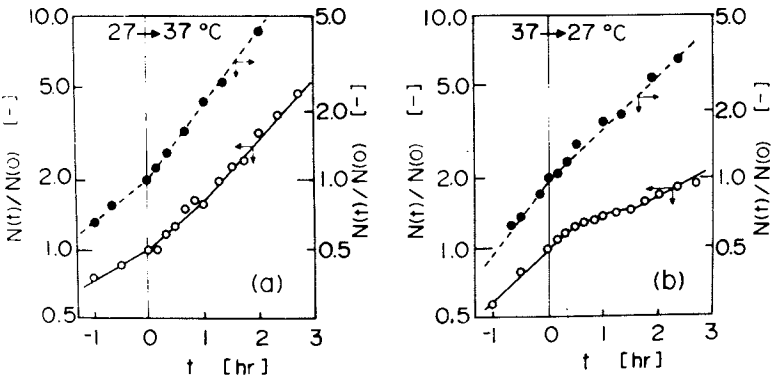

Figure 6. Increment in cell number after a shift in temperature. Filled circles and open circles show increments in cell number with 0.5 mg/mL and 2 × 10⁻⁴ mg/mL glucose, respectively. (a) Growth temperature was shifted up from 27°–37°C at t = 0. (b) Growth temperature was shifted down from 37°–27°C at t = 0.

In Chemical Reaction Engineering—Houston; Weekman, V., et al.;
ACS Symposium Series; American Chemical Society: Washington, DC, 1978.

per the total volume of medium in the growth vessel). The concentration of glucose (y) in the growth vessel is also maintained constant in the balance between the input and the output plus consumption by bacteria. Thus, it is possible to measure cell mass and chemical components of cells in the steady state culture under extremely low glucose concentration. However, the upward or downward shift in growth temperature under the condition causes inevitably a change in the consumption rate of glucose by bacteria as well as a change in growth rate, and therefore it is difficult to maintain the fixed concentration of glucose in the medium before and after the temperature shift. If the temperature of the steady state culture is suddenly lowered without changing the dilution rate, the glucose concentration will increase. And if the specific growth rate is much lower than the dilution rate, the cell concentration will diminish with time as the culture "washesout" from the vessel, and the physiological state of bacteria will finally reach to the state with maximal supply of glucose at that temperature (e.g. B_m state in Fig. 2). Therefore the temperature shift in the continuous culture will cause an unbalanced growth which is more complicate than that in the batch culture. During this unbalanced growth, the net change in concentration of organisms (x) and in glucose concentration (y) can be expressed on the basis of Monod's model as follows:

$$dx/dt = \mu_m \, x \, y/(K_S + y) - D \, x \tag{6}$$

$$dy/dt = -(1/\eta)\mu_m \, x \, y/(K_S + y) + D(y_0 - y) \tag{7}$$

where t is the time after the shift, η is a yield conversion, and y_0 is a influent substrate concentration. However, these equations do not involve a proper consideration of the differences in the physiological state of cells before and after the temperature shift. Fig. 7 illustrates the experiment in which the steady state cultures with the dilution rate of 0.500 hr^{-1} (a) and 0.529 hr^{-1} (b) were shifted from 37 to 27 °C. The filled and open circles indicate cell mass (measured by optical density), x, and glucose concentration, y, respectively. The broken curves show the time course of x and y obtained by calculation of equations (6) and (7). It is apparent that the calculated curves deviate enormously from the experimental data. These deviations can probably be attributed to time lag for attaining to the new physiological state. From this viewpoint, equations (6) and (7) were modified as follows, though the modification is entirely outside the scope of physiological implication.

$$dx/dt = \{t/(K_L + t)\}\mu_m \, x \, y/(K_S + y) - D \, x \tag{8}$$

$$dy/dt = -(1/\eta)\{t/(K_L + t)\}\mu_m \, x \, y/(K_S + y) + D(y_0 - y) \tag{9}$$

where K_L is a constant. The solid lines in the figure were ob-

In Chemical Reaction Engineering—Houston; Weekman, V., et al.;
ACS Symposium Series; American Chemical Society: Washington, DC, 1978.

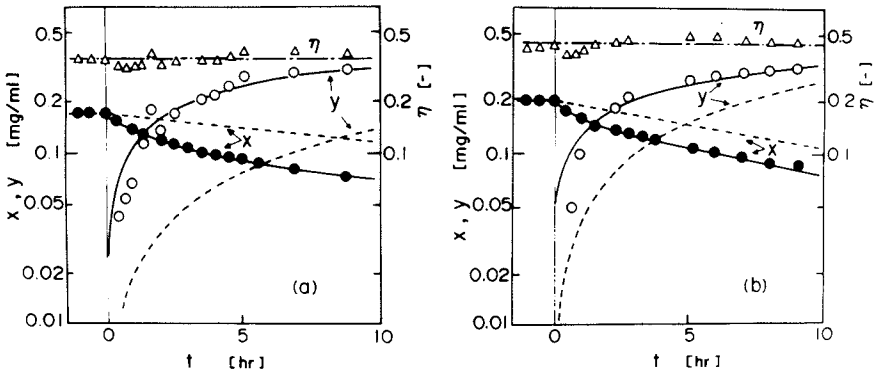

Figure 7. Time course of cell mass and glucose concentrations after the growth temperature was shifted down from 37 –27°C in the continuous culture at dilution rate = 0.500 hr^{-1} (a), and 0.529 hr^{-1} (b). Filled circles and open circles show cell mass and glucose concentrations, respectively. Triangles show the yield to be almost constant after and before the shift. Broken and solid lines represent calculated lines from Equations 6 and 7 and from Equations 8 and 9, respectively.

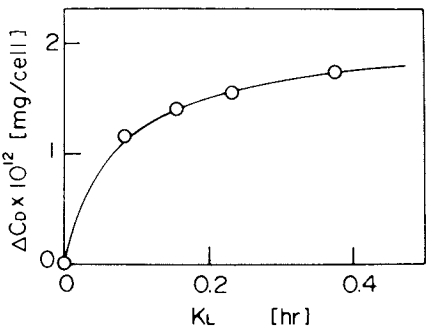

Figure 8. Relationship between a difference in DNA content per cell and K_L

tained by calculation of equations (8) and (9) as K_L = 0.38 hr (a) and 0.23 hr (b), and show satisfactory agreement with the data. K_L shows a time constant of delay and should be dependent on a difference in the states before and after the temperature shift. Figure 8 illustrates the relationship between a difference in DNA content per cell and K_L. ΔC_D represents a difference in DNA content per cell before and after the temperature shift.

In a steady state of bacterial growth, the physiological state of cells, such as cell mass, and macromolecular content per cell, is primarily defined by the culture medium and is an exponential function of the growth rate at a fixed temperature. When an environment of bacterial growth is changed to another state, the bacteria can adapt immediately to the new environment, provided that the physiological states in two environmental conditions are identical, such as temperature shift in a medium containing a sufficient amount of nutrients. However, if the bacteria are transferred to a new condition in which a different physiological state is given, they require some time lag to accommodate to the new condition. In the present investigation, it has been shown that a quantitative expression of growth was possible with temperature shifts in a suboptimal nutrient supply, by using the parameter K_L, the function of the difference in physiological states.

Nomenclature

A_1, A_2 = frequency factors	[hr^{-1}], [ml/mg]
C_D = DNA content per cell	[mg/cell]
D = dilution rate	[hr^{-1}]
E = activation energy	[cal/g-mole]
K_L, K_S = constants	[hr], [mg/ml]
N = cell number	[cells/ml]
R = gas constant	[cal/°K·g-mole]
T = temperature	[°K]
t = time	[hr]
x, y = cell mass and glucose concentrations	[mg/ml]
α = constant	[hr]
η = yield	[-]
μ = specific growth rate	[hr^{-1}]

Literature Cited

(1) Chohji, T., Sawada, T., and Kuno, S., Appl. Environ. Microbiol., (1976), 31, 864.
(2) Schaechter, M., Maaløe, O., and Kjeldgaard, N. O., J. gen. Microbiol., (1958), 19, 529.
(3) Park, J. T., and Johnson, M. G., J. Biol. Chem., (1949), 181, 149.
(4) Monod, J., Ann. Rev. Microbiol., (1949), 3, 371.
(5) Monod, J., Ann. Inst. Pasteur, (1950), 79, 390.
(6) Kjeldgaard, N. O., Maaløe, O., and Schaechter, M., J. gen. Microbiol., (1958), 19, 607.

In Chemical Reaction Engineering—Houston; Weekman, V., et al.;
ACS Symposium Series; American Chemical Society: Washington, DC, 1978.

15

Nonisothermal Behavior and Thermal Runaway Phenomena in Chain Addition Copolymerization

DONALD H. SEBASTIAN and JOSEPH A. BIESENBERGER

Department of Chemistry and Chemical Engineering, Stevens Institute of Technology, Hoboken, NJ 07030

The condition of thermal runaway (RA) in polymerization reactors has been characterized (1,2) by rapidly increasing temperatures ($dT/dt >> 0$) and an upward concavity in the temperature profile ($d^2T/dt^2 > 0$). When runaway additionally exhibits parametric sensitivity it is termed thermal ignition (IG). Beyond the obvious consequence of large temperature rises and possible instability, RA could cause a sharp reduction in polymer molecular weight and an increased spread in molecular weight distribution.

Runaway Analysis of Polymerizations and Copolymerizations

A study of RA in chain polymerizations was undertaken in our laboratories with the aim of developing quantitative criteria for predicting the onset of both RA and IG. A modification of Semenov-type dimensional analysis, together with computer simulation and experimentation, have shown (1,2) that 5 independent parameter groupings characterize the thermal behavior of chain homopolymerizations: $a, B, b, \varepsilon, \varepsilon E_d'$. The approach of Semenov deals with the thermal energy balance. Putting temperature and concentration in dimensionless form the thermal energy balance for homopolymerization appears as (1):

$$\frac{dT'}{dt} = \frac{mm_o^{1/2}}{\lambda_G} \exp(E'T'/1 + T') - \frac{1}{\lambda_R}(T' - T_R') \qquad (1)$$

The first term of the RHS of Eq. 1 can be interpreted as the rate of heat generation function while the second term as heat removal. The Semenov technique locates the critical temperature for RA at the point where heat generation and removal are not only equal, but their change with temperature (i.e., derivative with respect to T') is also equal. Applying these steps to the generation and removal terms of Eq.1 eliminates T', with resulting criteria formed as functions of 'a' and ε. The effect of the remaining parameters was investigated through numerical simulation. The important criteria for RA is $a < 2$, and for parametrically sensitive RA, $B > 20$ and $b > 100$. Parameters B and b are dimensionless

In Chemical Reaction Engineering—Houston; Weekman, V., et al.;
ACS Symposium Series; American Chemical Society: Washington, DC, 1978.

groupings appearing in the monomer and initiator component balances respectively.

The analytical methods employed in the RA analysis of homopolymerization are not immediately applicable to chain addition copolymerization. The equivalent expression to Eq. 1 is

$$\frac{dT'}{dt} = \left\{ \lambda_{G11}^{-1} m_1^2 \exp E'_{11} T'/1 + T' + (\lambda_{G12}^{-1} + \lambda_{G21}^{-1}) m_1 m_2 \exp E_{12} T'/1+T' \right.$$
$$\left. + \lambda_{G22}^{-1} m_2 \exp E'_{22} T'/1 + T' \right\} \left\{ m_o^{1/2} H' - \lambda_R^{-1} (T' - T'_R) \right. \qquad (2)$$

The basic kinetic equations for chain addition copolymerization are given in Table I for three termination models: geometric mean (GM), phi factor (PF) and penultimate effect (PE). It is important to note the symmetry in form created by confining the effect of choice of termination model to a single factorable function H.

A Semenov-type analysis cannot be applied to Eq. 2. The presence of four exponential terms with different activation energies, and the complicated functional form of $H' \equiv H/H_o$ preclude explicit solution for a critical T'. A more general technique based upon physical interpretation of RA parameters has led to copolymerization analogs for the groupings a,B,b,ε and $\varepsilon E'_d$. Each such parameter can be expressed as the ratio of appropriate time constants. While appearing as coefficients in the balances, time constants serve also as initial values for the balance. For example in Eq.1, note that the reciprocal of λ_G, the characteristic time for heat generation, is also the value of the heat generation function when dimensionless concentrations and temperature take on their initial values of one. The second interpretation, when applied to the generation portion of Eq. 2, defines an overall Λ_G for copolymerization. Similar attack on the total monomer balance yields an expression for Λ_m, the characteristic time for monomer decay.

In homopolymerization analysis (1) the time constant $\lambda_{ad} = \varepsilon\lambda_G$ is crucial to the formulation of runaway parameters a, B,b, ε and $\varepsilon E'_d$. It does not appear explicity in any of the dimensionless balances, but rather is a consequence of a Semenov-type analysis. In the process of taking the temperature derivative of the heat generation function of Eq. 1 the product $E'/\lambda_G = 1/\varepsilon\lambda G$ arises. Because this analysis could not be applied to copolymerization, an alternate means was required. The RA parameter 'a' is more than a mere by-product of a Semenov approach. It is the ratio of initial values of the temperature derivative of the heat removal and generation functions of Eq. 1. Expressed in terms of time constants this ratio is λ_{ad}/λ_R, and thus the interpretation of λ_{ad} as the initial temperature derivative of the heat generation function serves to define an analog, Λ_{ad} for copolymerization. By making use of Λ_{ad} in combination with other overall time constants, a set of RA parameters for copolymerization corresponding to its homopolymerization

In Chemical Reaction Engineering—Houston; Weekman, V., et al.;
ACS Symposium Series; American Chemical Society: Washington, DC, 1978.

counterpart (1), was defined. The parameters are given in Table II. It is important to note that the homopolymerization criteria evolved from combined seni-analytical and numerical solutions to specific kinetic equations. In this work, physical significance has been attached to each parameter in a manner that permits extension of the RA analysis, independently of the kinetic form.

The utility of the runaway and sensitivity parameters a,B, and b has been demonstrated through both numerical simulation and experimentation (3,4). Numerical simulations employed literature values for the kinetic constants for the monomer pairs of Styrene-Methyl Methacrylate (SMMA), Styrene-Acrylonitrile (SAN) and, Acrylonitrile-Methyl Methacrylate (ANMMA). Phi-factor kinetics were generally used, however both geometric mean and recently-advanced penultimate effect kinetics (6) were tested as well. Experiments were confined to the Styrene-Acrylonitrile comonomer system, however, the full range of compositions was studied. An extensive initial rate study was performed on this system to develop the kinetic constants needed to evaluate the runaway parameters (4,5).

A convenient way to illustrate the effect of the RA parameters is through the use of RA boundaries. Kinetic constants associated with real polymer systems limit the values of B to a narrow range (generally 30 - 60) and this is above the region where monomer sensitivity effects become important. Furthermore, initiator consumption with its stronger temperature dependence plays a far greater role in reducing sensitivity than monomer consumption does. Totally unrealistic values of initiator concentration (on the order of 100 m/l) are needed if monomer sensitivity limitations are to be exhibited in the absence of initiator limitations. Thus the most meaningful way to represent runaway boundaries is to show a_{cr} vs b with other dimensionless groups as constant parameters. Detailed studies of homopolymerization have illustrated this dependence (2). What is noteworthy is that the copolymer systems follow the same quantitative behavior. Figure 1 shows dimensionless runaway boundaries for several copolymer systems shown along with the associated homopolymerization boundary. All boundaries are not perfectly coincident due to the effects of composition drift in the copolymerizations. The deviations are rather small although the drift associated with SAN and ANMMA systems for B = 41 is significant.

In Table III values for RA parameters at the transition point are presented for various comonomer-initiator systems. Note that RA parameter 'a' consistently takes on values near the expected value of two when RA occurs. As in homopolymerizations, the critical value of 'a' becomes depressed as 'b' decreases. This effect is a by-product of the decreasing sensitivity of the copolymerization correctly characterized by the declining value of 'b'. Figures 2 and 3 illustrate initiator-limited sensitivity more clearly. At a value of b = 195 there is a sharply defined transition from non-runaway to runaway behavior, and this is

In Chemical Reaction Engineering—Houston; Weekman, V., et al.;
ACS Symposium Series; American Chemical Society: Washington, DC, 1978.

TABLE I

RATE FUNCTIONS AND BALANCES FOR COPOLYMERIZATION

Balance equations

Initiator

$$-\frac{d[m_o]}{dt} = k_d[m_o]$$

Co-monomers

$$-\frac{d[m_1]}{dt} = R_{p11} + R_{p12}$$

$$-\frac{d[m_2]}{dt} = R_{p12} + R_{p22}$$

$$-\frac{d[m]}{dt} = -\frac{d[m_1]}{dt} - \frac{d[m_2]}{dt}$$

Thermal energy

$$\rho C_p \frac{dT}{dt} = \sum_i \sum_j (-\Delta H_{ij}) R_{pij} - (U/\ell)(T - T_R)$$

$$= \left[-\Delta H_{11} k_{p11} k_{p21} [m_1]^2 - (\Delta H_{12} + \Delta H_{21}) k_{p12} k_{p21} [m_1][m_2] - \Delta H_{22} k_{p22} k_{p12} [m_2]^2\right] \left(\frac{f k_d}{k_{t11} k_{t22}}\right)^{1/2} [m_o]^{1/2} H - (U/\ell)(T - T_R)$$

where $\ell \equiv V/A_w$

Rate functions for propagation

$$R_{p11} = k_{p11} k_{p21} \left(\frac{f k_d}{k_{t11} k_{t22}}\right)^{1/2} [m_1]^2 [m_o]^{1/2} H$$

$$R_{p12} = k_{p12} k_{p21} \left(\frac{f k_d}{k_{t11} k_{t22}}\right)^{1/2} [m_1][m_2][m_o]^{1/2} H = R_{p21}$$

$$R_{p22} = k_{p22} k_{p12} \left(\frac{f k_d}{k_{t11} k_{t22}}\right)^{1/2} [m_2]^2 [m_o]^{1/2} H$$

and H is :

In Chemical Reaction Engineering—Houston; Weekman, V., et al.;
ACS Symposium Series; American Chemical Society: Washington, DC, 1978.

for geometric mean (GM) model

$$H = \left[\frac{k_{p21}[m_1]}{(k_{t22})^{1/2}} + \frac{k_{p12}[m_2]}{(k_{t11})^{1/2}} \right]^{-1}$$

for phi factor (PF) model

$$H = \left\{ \left[\frac{k_{p21}[m_1]}{(k_{t22})^{1/2}} \right]^2 + 2\phi \frac{k_{p21}k_{p12}[m_1][m_2]}{(k_{t22}k_{t11})^{1/2}} + \left[\frac{k_{p12}[m_2]}{(k_{t11})^{1/2}} \right]^2 \right\}^{-1/2}$$

for penultimate effect (PE) model

$$H = \left\{ \frac{k_{p21}[m_1]}{(k_{t22})^{1/2}} \left[\frac{r_1[m_1] + \left(\frac{k_{t21}}{k_{t11}} \right)[m_2]}{r_1[m_1] + [m_2]} \right] + \frac{k_{p12}[m_2]}{(k_{t11})^{1/2}} \left[\frac{r_2[m_1] + \left(\frac{k_{t12}}{k_{t22}} \right)[m_1]}{r_2[m_2] + [m_1]} \right] \right\}^{-1}$$

TABLE II

DIMENSIONLESS RUNAWAY PARAMETERS

$$a = \frac{\Lambda_{ad}}{\lambda_R} = \left\{ (E'^{-1}_{11}\gamma^{-1}_{T11} + E'^{-1}_{12}\gamma^{-1}_{T12} + E'^{-1}_{12}\gamma^{-1}_{T21} + E'^{-1}_{22}\gamma^{-1}_{T22}) + \frac{\partial H}{\partial T'} \frac{\lambda_R}{\Lambda_G} \right\}^{-1}$$

$$B = \frac{\Lambda_m}{\Lambda_{ad}} = \frac{(E'^{-1}_{11}\lambda^{-1}_{G11} + E'^{-1}_{12}\lambda^{-1}_{G12} + E'^{-1}_{12}\lambda^{-1}_{G21} + E'^{-1}_{22}\lambda^{-1}_{G22}) + \frac{\partial H}{\partial T'} \Lambda_G^{-1}}{(\lambda^{-1}_{m11} + \lambda^{-1}_{m12} + \lambda^{-1}_{m21} + \lambda^{-1}_{m22})}$$

$$b = \frac{\lambda_1}{\Lambda_{ad}} = \left\{ (E'^{-1}_{11}\lambda^{-1}_{G11} + E'^{-1}_{12}\lambda^{-1}_{G12} + E'^{-1}_{12}\lambda^{-1}_{G21} + E'^{-1}_{22}\lambda^{-1}_{G22}) + \frac{\partial H}{\partial T'} \Lambda_G^{-1} \right\} \lambda_1$$

$$\epsilon = \frac{\Lambda_G}{\Lambda_{ad}} = \left\{ \frac{(E'^{-1}_{11}\lambda^{-1}_{G11} + E'^{-1}_{12}\lambda^{-1}_{G12} + E'^{-1}_{12}\lambda^{-1}_{G21} + E'^{-1}_{22}\lambda^{-1}_{G22})}{(\lambda^{-1}_{G11} + \lambda^{-1}_{G12} + \lambda^{-1}_{G21} + \lambda^{-1}_{G22})} + \frac{\partial H}{\partial T'} \right\}^{-1}$$

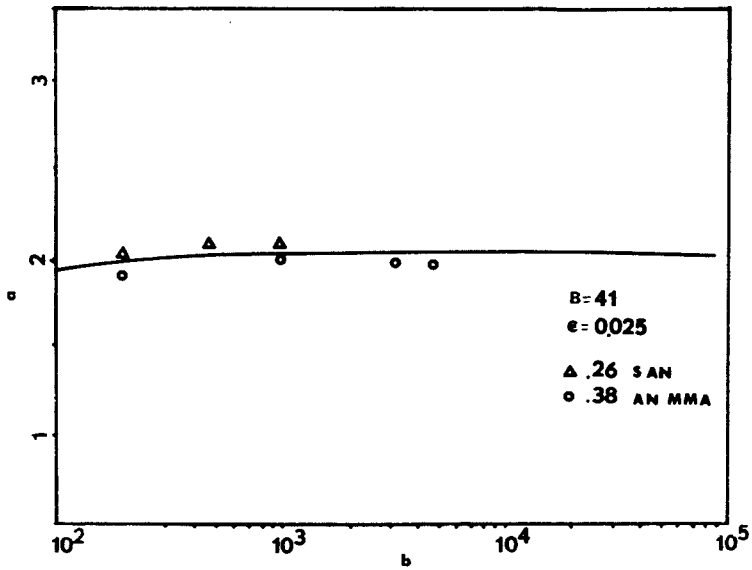

Figure 1. Simulated RA boundary for two copolymer systems

TABLE III
SIMULATION RESULTS

System	x_1	T_o °K	$[I]_o$ mol/l	u/ℓ cal/cc sec °K	B	E'	b	a	RA
AN/MMA/BP	.2	322	1.33×10^{-4}	1.57×10^{-5}	45	28.6	300	2.025	No
				1.55				1.998	Yes
	.8	378	.119	1.61×10^{-2}	45	23.5	300	1.998	No
				1.60				1.985	Yes
S/MMA/BP	.2	318	1.21×10^{-3}	8.99×10^{-6}	45	31.3	300	2.075	No
				8.88				2.05	Yes
	.8	306	7.44×10^{-4}	1.54×10^{-6}	45	33.5	300	2.05	No
				1.52				2.026	Yes
S/AN/DTBP	.7	403	.05	1.04×10^{-2}	36	30	400	1.985	No
				1.03				1.975	Yes
S/AN/BP	.7	373	.025	4.86×10^{-3}			136	1.915	No
				4.82				1.90	Yes
			.01	3.01×10^{-3}			86	1.875	No
				2.97				1.85	Yes
S/AN/AIBN	.7	373	.10	3.55×10^{-2}	36.0	28.0	42	1.77	No
				3.49				1.74	Yes
			.05	2.37×10^{-2}			30	1.67	No
				2.34				1.65	Yes

In Chemical Reaction Engineering—Houston; Weekman, V., et al.;
ACS Symposium Series; American Chemical Society: Washington, DC, 1978.

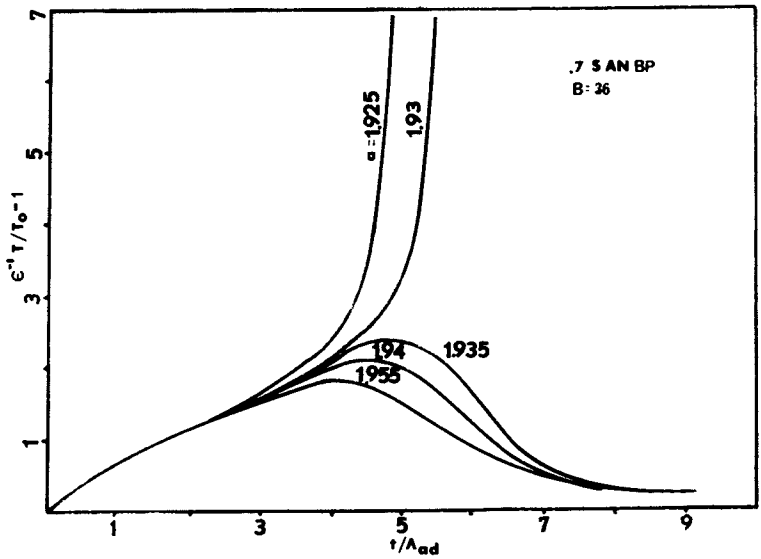

Figure 2. RA transition, b = 195

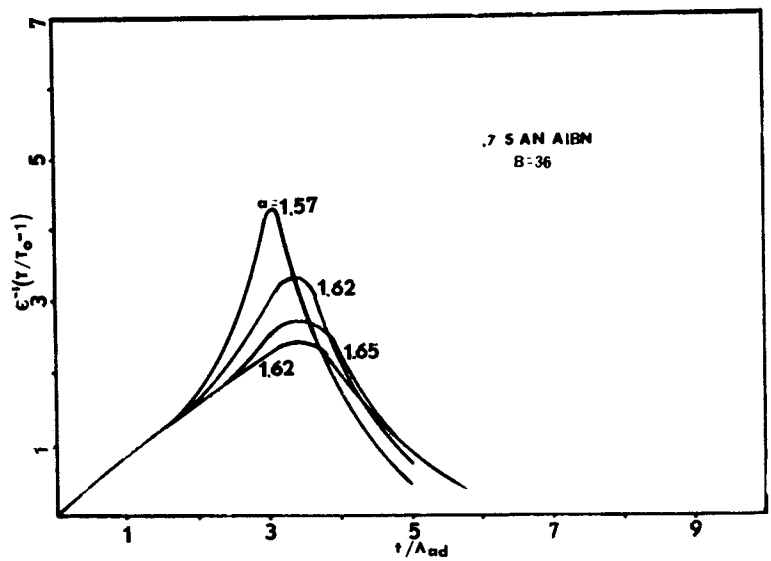

Figure 3. RA transition, b = 30

caused by a 0.3% change in 'a'. When b is decreased to 30 the RA point is not clearly defined. A continuous spectrum of profiles fills the transition region. Changes in parameter 'a' are an order of magnitude greater than in the previous case to bring about similar changes in the thermal histories. In addition, the value of 'a' in the region of transition has been significantly decreased from the nominal value of two.

The Copolymer Approximate Form (CPAF)

The fact that copolymer and homopolymer runaway envelops agreed both qualitatively and quantitatively suggests that perhaps complex copolymerization kinetics might be successfully approximated by simpler kinetics, similar to the homopolymer form. It is proposed that be replacing parameters in the homopolymer balances by their copolymer analogs, i.e., λ_m, λ_G and $\varepsilon = \lambda_{ad}/\lambda_G$ by Λ_m, Λ_G, and $\varepsilon = \Lambda_{ad}/\Lambda_G$ respectively, and subsequently integrating them we will obtain conversion and thermal histories that match the histories of the exact kinetic form. Indeed, this was the case. Thus Eq. 2 would be approximated by the far simpler form:

$$\frac{dT'}{dt} = \Lambda_G^{-1}\, mm_o^{1/2} \exp \frac{E'\,T'}{1+T'} - \frac{1}{\lambda_R}(T' - T_R') \qquad (3)$$

Indeed, it can be shown that if concentration changes are not considered, the remaining temperature dependent portion of Eqs. 2 and 3 are numerically equivalent. Under isothermal conditions the conversion histories match provided that one of the comonomers is not exhausted prior to the completion of the reaction. Under nonisothermal conditions, composition drift influences the agreement between the two forms. When drift is towards the more reactive comonomer, the approximate form underestimates the thermal trajectory (See Fig. 4). Conversely, when drift is towards the less reactive of the pair, the approximate form overestimates the trajectory. Similar behavior is noted in the RA boundaries of Fig. 1. Points for the SAN system lie above the homopolymer boundary, and drift is towards high AN content compositions. Points for the ANMMA boundary lie below the homopolymer boundary, and drift is towards the less reactive of the pair, MMA. As conditions become either more adiabatic or more isotherm, spread between the forms narrows. The poorest agreement of the forms occurs at the parametrically sensitive point of the RA transition.

Experimental Tests of the Runaway Parameters

The SAN copolymer system was chosen for experimental study due to its growing industrial importance. There is a lack of published rate data for this system, as well as broad disagreement among the data reported for homopolymerization of AN. Without kinetic data there would be no way to evaluate the dimensionless parameters associated with experimental runs. Therefore copolymerization kinetic studies were conducted via the technique of Differential Scanning Calorimetry, which had previously been used

In Chemical Reaction Engineering—Houston; Weekman, V., et al.;
ACS Symposium Series; American Chemical Society: Washington, DC, 1978.

by others for homopolymerization studies. The copolymer approximate kinetic form (CPAF) provided the means for separating reaction rate from heat of reaction required by the use of this technique. It should be noted that under initial conditions the exact and approximate kinetic forms are numerically equivalent, thus there is no error involved in applying the approximate form to initial rate studies.

The initial rates for SAN systems with styrene content of ten to ninety mole percent were determined with both benzoyl peroxide and azo-bis-isobutyronitrile initiators. These rates were used to calculate the termination parameters for both PF and PE models of copolymer termination. No single, composition-independent value of the PF adequately fit the initial rate data. The PE model provided fair agreement. High styrene content copolymers showed the widest scatter in the correlation of the model parameters. If the average value of the PF is chosen ($\phi \simeq 25$), this model predicts qualitatively higher rates than the PE model.

Experimental studies of thermal runaway in the homopolymerization of styrene have been conducted in these laboratories. The Thermal Ignition Point Apparatus (TIPA) developed for this work (7) was used for the experimental study of runaway in SAN copolymerization. The compositions of 90, 80, 70, 60, 40, and 20% styrene were provoked from non-runaway to runaway conditions at the feed temperature of 373°K by manipulating the initial concentration of initiator azo-bis. The 90, 80, and 70% compositions were also tested at 363°K and the 70% composition was tested with benzoyl peroxide as initiator. (Furthermore, an ignition envelope of T_o vs $[I]_o$ was constructed for the 70% SAN system initiated by benzoyl peroxide) (4).

Values of the runaway parameters a,B, and b for the experimental RA transitions using each of the three popular termination mechanisms, are presented in Table IV. They reflect the trends observed in the behavior of the experimental runs. All RA's were of the type classified as non-sensitive. The values of parameter b clearly are in agreement with this observation. Lowering feed temperature resulted in heightened sensitivity, and again an increased value of b is in agreement with this observation. Figures 5 and 6 illustrate this behavior for 80% SAN at 363°K and 373°K respectively. They are computer graphs of experimental data which are not curve-fitted, but rather are point-to-point connections of the data. The curves in both figures appear very similar to the non-sensitive transition in Fig. 3 obtained from numerical simulation. The parameters in Table IV reflect the decrease in sensitivity caused by increased temperature. As characterized by 'b' the effect of temperature on the rate of initiation is responsible for the decreased sensitivity as initial temperature rises (4).

At a constant initiator level, runaway can be caused by manipulating the initial styrene content. With initial initiator concentration fixed at 0.03 m/l and initial temperature T_o = 373°K, running the range of compositions from 90 to 20% causes the onset

In Chemical Reaction Engineering—Houston; Weekman, V., et al.;
ACS Symposium Series; American Chemical Society: Washington, DC, 1978.

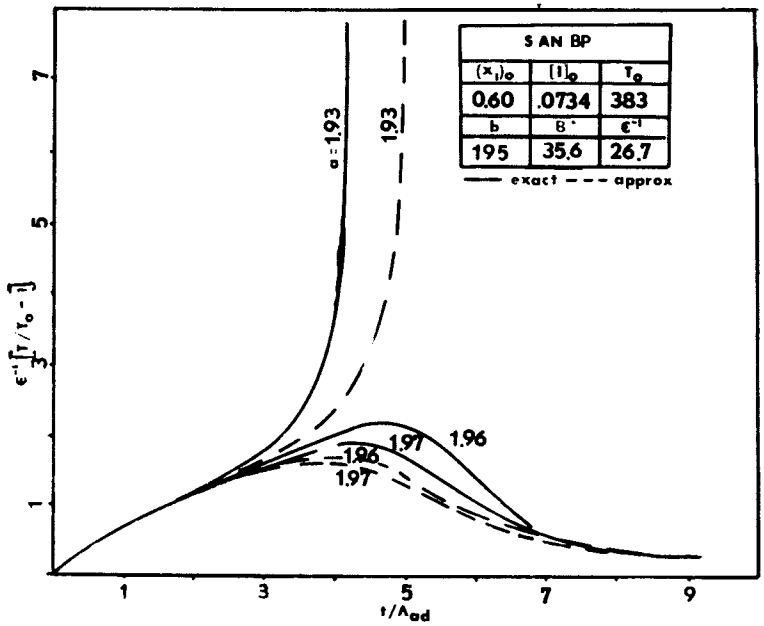

Figure 4. Exact and Cpaf nonisothermal histories, 60% SAN

TABLE IV

DIMENSIONLESS PARAMETERS FOR EXPERIMENTAL RUNS

System	T_o	$[I]_o$	GM a	GM B	GM b	PF a	PF B	PF b	PE a	PE B	PE b	Typ
.9 SAN/AIBN	363	.09	0.87	35	34	0.94	36	31	0.98	34	30	N
			0.79	35	35	0.86	36	32	0.89	34	31	R
	373	.04	0.71	33	16	0.75	34	15	0.79	32	14	N
		.05	0.58	33	17	0.62	34	16	0.65	32	15	R
.8 SAN/AIBN	363	.05	0.80	36	30	0.94	38	26	0.99	34	24	N
		.06	0.76	36	34	0.89	38	29	0.94	34	27	R
	373	.015	0.80	35	12	0.91	36	10	1.00	33	9	N
		.02	0.64	35	13	0.73	36	11	0.80	33	10	R
.7 SAN/AIBN	363	.0425	1.03	39	44	1.37	42	33	1.41	36	32	N
		.05	0.87	39	45	1.14	42	35	1.19	36	33	R
	373	.015	0.95	36	11	0.85	38	12	0.95	33	10	N
		.0175	0.57	36	16	0.71	38	13	0.78	33	11	R
.6 SAN/AIBN	373	.0075	0.72	39	12	0.98	42	9	1.12	34	8	N
		.01	0.63	39	14	0.85	42	11	0.97	34	9	R
.4 SAN/AIBN	373	.0035	0.71	44	12	1.19	49	7	1.44	34	6	N
		.005	0.69	44	16	1.18	49	9	1.39	34	8	R
.2 SAN/AIBN	373	.0035	0.55	51	17	1.32	57	7	1.99	27	4	N
		.005	0.39	51	19	0.92	57	8	1.44	27	5	R

In Chemical Reaction Engineering—Houston; Weekman, V., et al.;
ACS Symposium Series; American Chemical Society: Washington, DC, 1978.

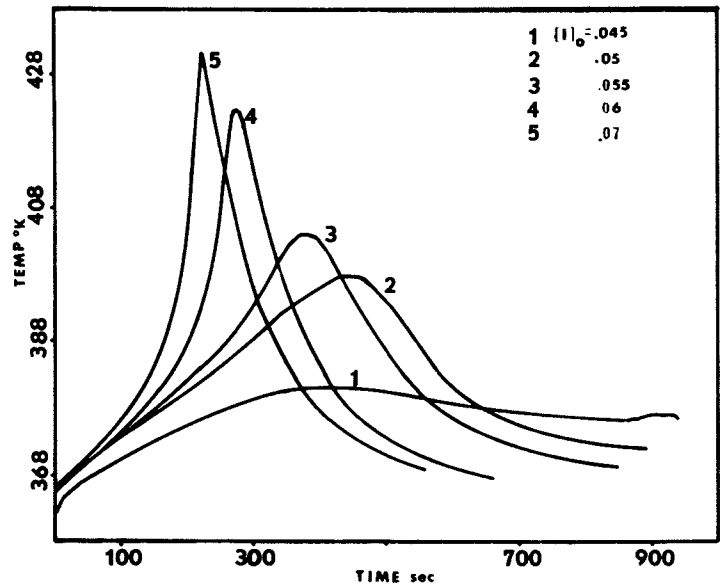

Figure 5. Experimental RA transition, 80% SAN/AIBN, $T_o = 363°C$

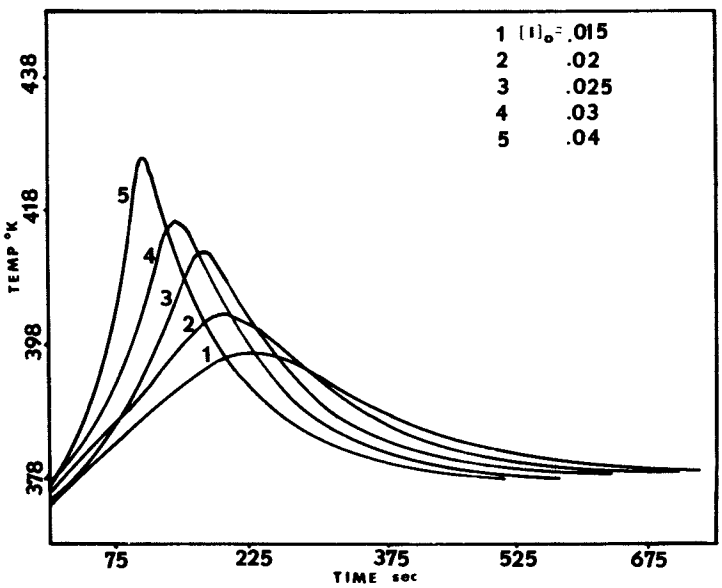

Figure 6. Experimental RA transition, 80% SAN/AIBN, $T_o = 373°C$

In Chemical Reaction Engineering—Houston; Weekman, V., et al.;
ACS Symposium Series; American Chemical Society: Washington, DC, 1978.

of RA at the 80% level.

It should be noted that the values of 'a' associated with experimental RA transitions are somewhat low. The extremely insensitive nature of the reactions would depress the value of a_{cr} considerably. Scatter in the data used to determine the parameters for termination was sufficient that in order to fit the entire range of compositions with a single model, error was introduced in the rates. The critical values of 'a' should lie more in the vicinity of 1.4 than 1.0. Although there is an offset it is important to note that the experimental systems respond in the same manner as the parameters predict. When experiments indicate decreasing sensitivity the parameters change in the same direction. When the experiments show thermal trajectories becoming increasingly more non-isothermal, the parameter 'a' decreases accordingly.

The parameters seem to describe a more reactive system than is observed, and thus RA transition would be predicted at lower values of T_o for a given $[I]_o$. Certainly, the results using the kinetic constants developed satisfy the engineering accuracy expected of them. The strong qualitative agreement suggests that more precise determinations would cause predictions and experimentation to merge. Furthermore, the criteria were formulated in such a way that should a more appropriate termination mechanism be determined or should the heterogeneous kinetic mechanism of acrylonitrile polymerization and acrylonitrile - rich copolymerization be successfully modelled, the resulting parameters could be easily adapted.

Symbols

a	=	R-A parameter defined in reference 1 for homopolymerizations and Table III for copolymerizations
b,B	=	IG parameters defined in reference 1 for homopolymerizations and Table III for copolymerizations
C_p	=	specific heat
E	=	activation energy (with appropriate subscript)
E'	=	E/R_gT_o = dimensionless activation energy (with appropriate subscript)
ε	=	$1/E'$
E_{jk}	=	$(E_{pjk} - E_{p\ell j}) + 1/2\ (E_d - E_{tjj} - E_{t\ell\ell}) = E_{kj}$ for copolymerization
f	=	initiator efficiency factor
H	=	a function defined in Table I
ΔH_{jk}	=	heat of reaction between free radical with end unit j and monomer k
I	=	free-radical initiator
k	=	reaction rate constant
ℓ	=	heat transfer length = V/A_w, reactor volume/wetted heat transfer area
m_j	=	comonomer j or dimensionless concentration of comonomer j, $[m_j]/[m_j]_o$

In Chemical Reaction Engineering—Houston; Weekman, V., et al.;
ACS Symposium Series; American Chemical Society: Washington, DC, 1978.

m_o = initiating species or dimensionless concentration of initiating species, $[m_o]/[m_o]_o$; for initiators used in this study, $I \rightarrow 2m_o$

R = reaction rate point function with units moles/volume/time (and with appropriate subscripts)

R_g = universal gas constant

T = temperature (K)

T' = $(T - T_o)/T_o$

t = time

U = overall heat transfer coefficient

x_j = mole fraction of comonomer j

λ, Λ = time constants or characteristic times (with appropriate subscripts)

$$\Lambda_{ad} = \sum_{j=1}^{2} \sum_{k=1}^{2} E'_{jk}/\lambda_{Gjk} + \frac{\partial H}{\partial T'} \Lambda_G^{-1} \quad \text{for copolymerization}$$

$$\lambda_G = \rho C_p T_o/(-\Delta H)(k_{ap})_o [m]_o [m_o]_o^{1/2} \quad \text{for homopolymerization}$$

$$\lambda_{Gjk} = \rho C_p T_o/(-\Delta H_{jk})(R_{pjk})_o \quad \text{for copolymerization}$$

$$\Lambda_G = \sum_{j=1}^{2} \sum_{k=1}^{2} (1/\lambda_{Gjk})^{-1} \quad \text{for copolymerization}$$

$$\lambda_j = 1/(k_{pjj})_o [f(k_d)_o / (k_{tjj})_o]^{1/2} [m_o]_o^{1/2}$$

$$\lambda_{mjk} = [m_k]_o / (R_{pjk})_o$$

$$\Lambda_m = \sum_{j=1}^{2} \sum_{k=1}^{2} (x_k/\lambda_{mjk})^{-1}$$

ρ = density

[ ] = molar concentration

$\gamma_{T\gamma k} = \lambda_{Gjk}/\lambda_R$

Subscripts

ap = apparent or lumped

d = decomposition of initiator

G = generation of heat

i = initiator depletion or initiation

j,k = comonomer or repeat unit of type j or k, where j = 1,2 and k = 1,2

ℓ = index which takes on values ℓ = 1,2 but always such that ℓ = j

m = monomer depletion

o = feed conditions (except in m_o)

p = propagation

R = reservoir (thermal) or removal of heat

t = termination

In Chemical Reaction Engineering—Houston; Weekman, V., et al.;
ACS Symposium Series; American Chemical Society: Washington, DC, 1978.

Acknowledgment

This work was supported in part by a Grant from the National Science Foundation (ENG-7605053). The authors also wish to thank Union Carbide for supplying the styrene monomer at no cost.

Literature Cited

1. Biesenberger, J. A., Capinpin, R., and Sebastian, D., Appl. Polymer Symp. (1975), 26, 211.
2. Biesenberger, J. A., Capinpin, R., and Yang, J., Polymer Eng. Sci., (1976), 16, 101.
3. Sebastian, D. H. and Biesenberger, J. A., submitted to J. Appl. Polym. Sci.
4. Sebastian, D. H., Ph.D. Thesis, Stevens Institute of Technology (1977).
5. Sebastian, D. H. and Biesenberger, J. A., submitted to J. Polymer Sci.
6. Russo, S., Munari, S., J. Macromol. Sci-Chem., (1967), A-1,5, 2159.
7. Sebastian, D. H. and Biesenberger, J. A., Polymer Eng. Sci., (1976), 16, 117.

16

Comparison of Different Determination Methods for Effective Thermal Conductivity of Porous Catalysts

U. HOFFMANN, G. EMIG, and H. HOFMANN

Institut fur Technische Chemie I, University of Erlangen—Nuremberg, 8520 Erlangen, West Germany

For the design and analysis of fixed-bed catalytic reactors as well as the determination of catalyst efficiency under nonisothermal conditions, the effective thermal conductivity of the porous pellet must be known. A collection of thermal conductivity data of solids published by the Thermophysical Properties Research Centre at Purdue University [1] shows "a disparity in data probably greater than that of any other physical property ". Some of these differences naturally can be explained, as no two samples of solids, especially porous catalysts, can be made completely identical. However, the main reason is that the assumed boundary conditions for the Fourier heat conduction equation

$$\frac{\partial T}{\partial t} = a\nabla^2 T \qquad (1)$$

never can be met experimentally exactly. On the other hand, the magnitude of values predicted by pore structure models differ up to 40 % [2] and there is therefore a need for experimental measurement. In order to come as close as possible to the required boundary conditions, different authors have developed different static and dynamic methods for the experimental determination of the thermal conductivity of solids. A review of these methods has been given recently by J.E. Parrot and A.D. Stuckes [2]. For porous particles in particular much less information is available [3,4,5,6,7,8,9,10,11].

The aim of this paper is to compare results from different experimental methods for several types of catalysts in order to explore their advantages and disadvantages.

© 0-8412-0401-2/78/47-065-189$05.00/0

Experimental Methods

Among the static methods the linear heat flux methods seem to be most commonly used for porous particles . In this case, it is assumed that the transport of heat through the specimen is mainly in one direction thus the Fourier law given by Eqn. (1) becomes one dimensional and λ_p can be calculated according to

$$\lambda_p = \frac{L\,\Phi}{A(T_1-T_2)} = \frac{L}{A\,R_p} \qquad (2)$$

To get correct values of λ_p from this equation, the heat losses from the periphery of the sample have to be negligible. This condition is reached to a considerable extent in the so called conductometer, originally developed by J. Schröder [12] and now commercially available through Colora Meßtechnik GmbH. The principle of the quick and simple, yet elegant and accurate method (Ia in Table 3) consists in contacting a cylindrical sample with two boiling liquids L_1 and L_2 of different boiling points T_1 and T_2 (ΔT=10 to 20 K). Figure 1 shows that the liquid of higher boiling point is contained in the lower vessel B_1, the other in the upper one B_2. The contact between the sample P and the vessels is provided by two silver stoppers at the top of the lower S_1 and the bottom of the upper vessel S_2 to avoid radial temperature gradients. The heat flow from the lower vessel through the sample causes the liquid in B_2 to boil at a constant rate under stationary conditions. A constant temperature difference T_1-T_2 is reached between the two silver plates. The vapor from the upper vessel is condensed in a condenser C and the condensate is collected in a measuring burette B. The time t needed for the evaporation of a certain amount of liquid is measured.

The effective thermal conductivity of the sample then can be calculated according to Eqn. (2) with the known specific heat of vaporisation $(-\Delta H_v)_2$ by setting

$$\Phi = \frac{(-\Delta H_v)_2 \cdot \rho_{f_2} \cdot V}{t} \qquad (3)$$

To avoid systematic errors, e.g. caused by radial heat losses, a relative measurement instead of an absolute determination is recommended in which the thermal conductivity of the sample is compared with that of a reference material. In addition, this eliminates

In Chemical Reaction Engineering—Houston; Weekman, V., et al.;
ACS Symposium Series; American Chemical Society: Washington, DC, 1978.

the necessity of knowing the exact value of $(-\Delta H_v)_2$ and the boiling temperature of the lower boiling liquid. High purity copper, Armco iron, nickel alloys and particular glasses are commonly used as reference material. The method is generally suitable for (i) the whole temperature range for which one can find stable liquids with well defined boiling points, and (ii) nearly all solids with the exception of those with very high thermal conductivity like copper and silver, because in this case heat losses ($\propto 1/L$) are too great or measuring times ($\propto L$) are too small.

With catalyst particles a problem arises that samples normally are not available in the required dimension (e.g. 2x18mm) and repelleting of the ground particles results in most cases in a different pore structure which mainly determines the thermal conductivity of a pellet. In this case, embedding of the original particles (method Ib in Table 3) in a quick hardening plastic can overcome this difficulty for regular shaped as well as irregular shaped pellets. Then the thermal conductivity of the sample can be calculated by

$$\lambda_t = \lambda_m f_m + \lambda_p f_p = \lambda_m (1-f_p) + \lambda_p f_p \quad , \tag{4}$$

assuming the additivity of parallel heat conductivities and invariant cross sections along the distance L for the two materials. If it is impossible to determine the fractional surface f_m and f_p of the two materials because of the irregular shape of the pellets, these values can be approximated by means of the densities (method Ic in Table 3) as

$$f_p = \frac{\varrho_t - \varrho_m}{\varrho_p - \varrho_m} \tag{5}$$

The ASTM- (or DIN-) standard method for low conducting solid material ($\lambda < 1$) is the two plate method with an electrical main heater between two cylindrical sample plates having a small length to diameter ratio and two heat sinks as well as a cylindrical guard heater (Figure 2). For better temperature control each heat sink consists of an electrical driven auxiliary heater and a water cooler. In this case the heat flow rate to each of the two samples is given by

$$\Phi = \frac{1}{2} \frac{U^2}{R_e} \tag{6}$$

In the present investigation the L91 Linseis equipment

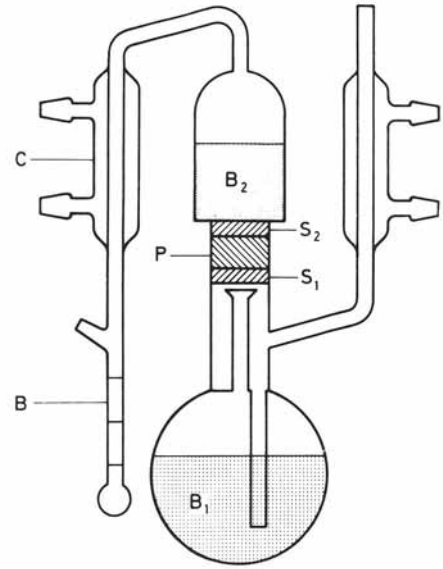

Figure 1. Principle of the COLORA conductometer

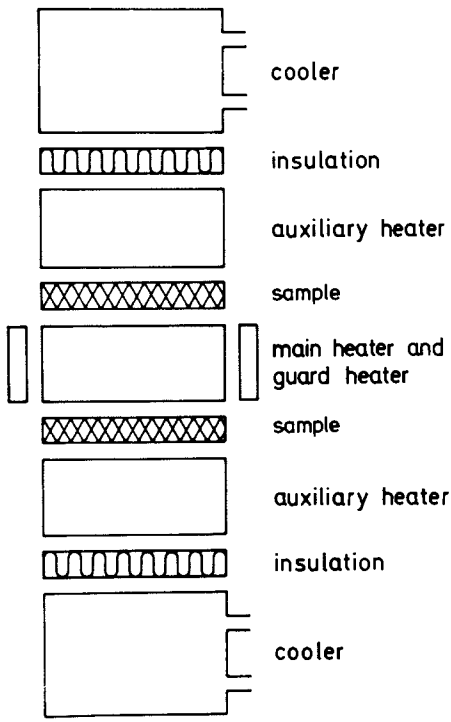

Figure 2. Principle of the LP91 LINSEIS conductometer

In Chemical Reaction Engineering—Houston; Weekman, V., et al.;
ACS Symposium Series; American Chemical Society: Washington, DC, 1978.

was used, operating according to the ASTM method (IIa in Table 3), at least with the reference material. With porous catalyst particles, it is normally not possible to produce samples of 80-120mm diameters. Therefore, in order to use this equipment catalyst particles were embedded also in a quick hardening plastic (method IIb in Table 3).

In order to use this unit also for catalyst particles of any shape, the standard method was modified (method IIc in Table 3) in the same way as described for the determination of the thermal conductivity of nonporous plastic powders in [13]. The concept is to compare the thermal conductivity of the catalyst pellet λ_p with the conductivity of a binary liquid mixture λ_{fm}. If the liquid mixture can be adjusted such that it has the same conductivity as the pellet, the conductivity of a fluid/solid system λ_t (consisting of catalyst particles and the liquid mixture) will be independent of the solid content, and

$$\lambda_t = \lambda_{fm} = \lambda_p \quad . \tag{7}$$

This equation can be satisfied experimentally by varying the thermal conductivity of the binary liquid mixture systematically through varying its composition. This variation is shown in Figure 3 for the system methanol/water used in this study. Figure 4 shows one of the two probe chambers, filled with the liquid mixture (left) and with the added catalyst (right). The bottom and the top of the chamber consist of stainless steel, the cylindrical wall is made of Teflon. If equation (7) holds, then $T_1=T_1'$, $T_2=T_2'$ and $\Phi = \Phi'$.

Method IIc requires that: (i) the thermal conductivity of the catalyst pellets be within the range of the thermal conductivities of the pure liquid components; (ii) the thermal conductivity of the liquid mixture be known as a function of its composition. This means that catalysts with a thermal conductivity greater than water can not be tested in this way, e.g. catalysts A and E in this study. Naturally this method can also be used to determine the thermal conductivity of solid catalyst material if the pellets are so finely ground that the liquid can penetrate into all pores. This value is then the basis for determining the effective thermal conductivity of the porous pellet using known models [3,9].

Dynamic methods for the determination of thermal conductivity of porous catalyst pellets normally consist of experiments in which a spherically or cylindri-

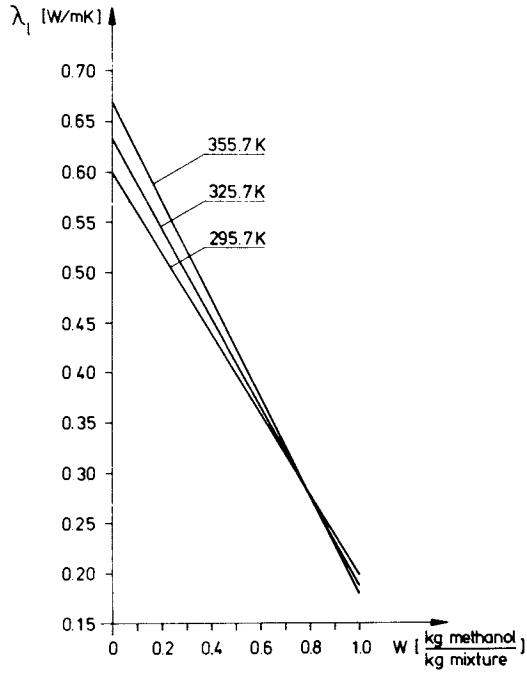

Figure 3. Thermal conductivity of methanol/ water mixtures

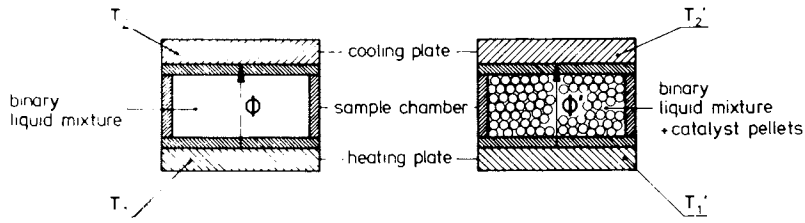

Figure 4. Sample chambers of the modified plate method

In Chemical Reaction Engineering—Houston; Weekman, V., et al.;
ACS Symposium Series; American Chemical Society: Washington, DC, 1978.

cally shaped particle, equipped with a central and a peripherical thermocouple, is immersed in an ambient fluid of constant or linearly changing temperature [4, 8][1]. In the first case one follows the temperature rise or fall in the centre of the particle, in the second case one determines the so called limiting temperature difference between the centre and the surface of the particle.

To compare static and dynamic methods, in this study the second method (III in Table 3) was applied (Figure 5), using a gas. A gas offers the advantage that the particles can be used in their original shape and in the actual reaction mixture (e.g. as a single pellet reactor).

It can be shown theoretically [15] that for spherical particles 99 % of the limiting temperature difference

$$\Delta T_{lim} = \frac{C}{6a} \left(\frac{d}{2}\right)^2 \qquad (8)$$

can be reached at times

$$t > \frac{0.25}{a} \left(\frac{d}{2}\right)^2 . \qquad (9)$$

On the basis of experimental results it has been demonstrated furthermore [16] that with cylindrical particles, having a length to diameter ratio of 1, the limiting temperature difference reached is 1.203 times larger than that for spherical particles, which means that

$$\Delta T_{lim} = \frac{1.203\ C}{6a} \left(\frac{d}{2}\right)^2 \qquad (10)$$

The additional information (density and heat capacity of the pellet), needed in order to calculate the thermal conductivity from a, can be gained by standard routine methods.

Experimental Results

Table 1 shows the properties of the catalysts used in this study.

Values of the thermal conductivity in W/m,K of different nonporous reference and embedding materials are given in Table 2.

Values of the effective thermal conductivity in W/m,K, determined according to the described methods are given in Table 3.

---

[1] Methods with a periodic variation of temperature [14] are not discussed here.

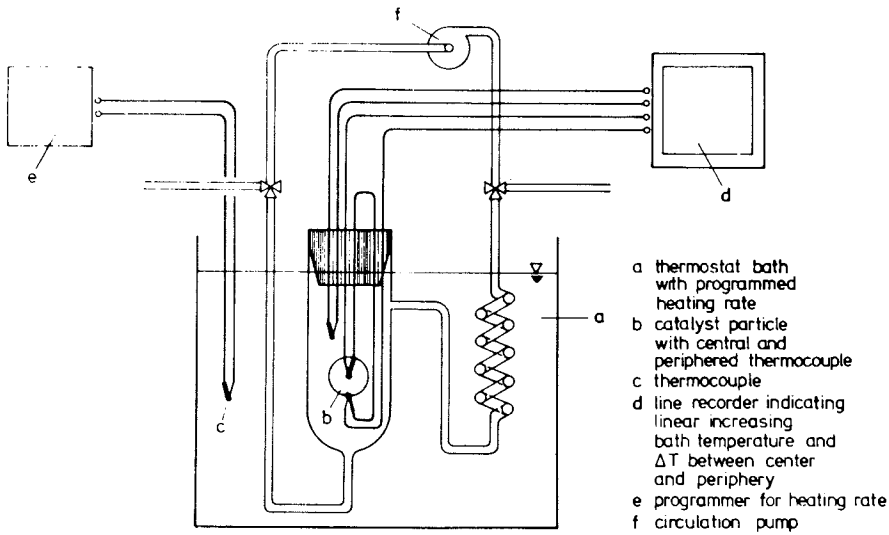

Figure 5. Principle of the apparatus for the dynamic method

In Chemical Reaction Engineering—Houston; Weekman, V., et al.;
ACS Symposium Series; American Chemical Society: Washington, DC, 1978.

Discussion and Conclusion

The data given in Table 1 show that in this study a broad spectrum of catalyst properties has been covered. All of the catalysts are of technical importance. The results given in Table 3 and the experience gained during the investigation permit the following statements:

1) For the determination of the effective thermal conductivity of porous catalyst pellets no standardized method exists and probably will never be developed. On the contrary, the most suitable method depends strongly on the properties of the catalyst. In this connection size and form of the pellet as well as its pore structure, its solubility, hygroscopicity, thermal conductivity of the solid material and reaction mixture are most important. As a general rule, that method should be prefered in which the catalyst can be applied as used in the reactor. This is not always possible. Often the catalyst must be specially prepared for the measurement by grinding and repelletizing, coating, embedding, etc., in order to produce a more or less suitable sample. The influence of the catalyst preparation is seen most clearly from the values for catalyst A in Table 3. The catalyst was used in its original form only in methods Ib and III.

2) Among the commercially available units, the Colora conductometer seems technically fully developed and can be readily adapted for conductivity measurements on catalyst pellets. The design minimizes the uncontrollable heat loss and assures nearly constant temperature in any horizontal plane through the sample. The time necessary for one measurement is about 3 hours. If the reference method is used, no additional information is needed for the determination of the effective thermal conductivity.

Other commercially available units, mainly designed for determination of the thermal conductivity of building materials in the form of plates, like the Linseis L91 unit, suffer from the shortcoming that in order to minimize heat losses, the sample diameter is 80 to 120mm. This large diameter makes it difficult to obtain good contact between the heaters and the catalyst sample. Furthermore, with electric heaters it is difficult to realize a constant temperature across the entire cross section of the probe. Finally the sample size demands a rather large amount of catalyst.

The dynamic method (III) used in this study has the advantage of a short measuring time (0.5 hours),

Table 1 Sample Properties

	catalyst	specific surface area (m^2/kg)	density (kg/m^3)	specific heat ($kJ/kg,K$)	pellet porosity (m^3/m^3)
A	25%Ni on Al_2O_3	56900	1950	1.07	0.468
B	Ca/Ni-phosphate	145000	1350	1.98	0.570
C	Fe/Mo-oxid	7500	2260	0.66	0.448
D	Zeolite	253000	1040	2.15	0.490
E	6%Zn-acetate on active carbon	33100	1150	1.66	0.410

Table 2 Properties of Reference and Embedding Materials

method	acrylic glass	Hostaform C 9021	Technovit 4071	Relopal GK
Ia	0.21		0.24	0.15
IIa	0.18			
IIc	-	0.42		
III	0.20			

Table 3 Effective Thermal Conductivities of Porous Catalysts, Determined by Different Methods

method	mean measuring temperature(K)	catalysts				
		A	B	C	D	E
Ia	367	0.57 [1]	0.18	0.30	0.22	-
Ib		1.60	0.19	0.63	0.37	0.67
Ic		0.82 [2]	0.26	0.68	0.40	0.52
IIb IIc	313	-		0.51		-
III	333-353	1.19	0.24 [3]	0.29	0.22	0.63

1)ground a.repclletized, 2) broken pellets, 3) pelletized under high pressure

In Chemical Reaction Engineering—Houston; Weekman, V., et al.;
ACS Symposium Series; American Chemical Society: Washington, DC, 1978.

provided a proper balance between pellet diameter, heating rate and thermal diffusity of the pellet can be reached. In this study pellet diameters of 6 to 20mm and heating rates between 100 and 300 K/h had been found suitable. The apparatus for this method is easy to build using standard laboratory equipment. If available, a DTA unit could also be used for this special purpose.

3) The embedding of catalyst particles in quick hardening plastic Technovit 4071 (Kolzer) causes no problems, provided the pellets have a constant cross sectional area across the sample height L. With irregular shaped particles the determination of the densities needed in Equation 5 and gas bubbles included in the sample lead to uncertain results. Additionally, with a large sample diameter (method IIa) it is difficult to obtain a perfectly plane contact surface.

Coating of regular shaped pellets with a suitable two component polyurethene varnish (Flügger u. Boecking K.G.) caused no problems if a methanol-water or glycerine-water mixture is used as in method IIc. If carbon tetrachloride must be used to reach a low enough value for the thermal conductivity, another coating system has to be found. Irregular shaped particles could not be coated satisfactorilly in this study as no way was found to make the varnish film thin enough.

To suppress the thermal convection of the liquid mixture in the voids between the pellets (as another source of error) the coated particles should be as small as possible and fill up the measuring chamber completely.

4) The standard deviation of the measurement determined for catalyst C with method Ia was 0.013 for a mean value of 0.30 which is very satisfactory as this value includes both the variation in the catalyst preparation as well as the experimental errors.

Symbols

A	cross-sectional area (m^2)
$a=\lambda_p/\varrho_p c_p$	thermal diffusivity of the catalyst pellet (m^2/s)
C	temperature gradient in the ambient fluid (K/s)
c	specific heat (kJ/kg K)
D	probe diameter (m)
d_p	pellet diameter (m)
f^p	fractional area (m^2/m^2 total)
$(-\Delta H_v)$	heat of evaporation (kJ/kg)
L	distance (m)
R	thermal resistance (K/W)
R_e	electrical resistance (V/A)

In Chemical Reaction Engineering—Houston; Weekman, V., et al.;
ACS Symposium Series; American Chemical Society: Washington, DC, 1978.

T temperature (K)
ΔT_{lim} limiting temperature difference (K)
t time (s)
U voltage (v)
V volume of L_2 condensed (m^3)
w weight fraction (kg/kg total)
λ thermal conductivity (W/mK)
ϱ density (kg/m^3)
Φ heat flow rate (W)

Indices

f fluid
fm liquid mixture
p pellet
m plastic matrix
t total

Literature

[1] Touloukian,Y.S. (Ed.), 1970, Thermophysical Properties of Ma ter. The Thermophysical Properties Research Centre Data Series, Volumes 1 und 2 (IFI/Plenum Press, New York)
[2] Parrot,J.E. and Stuckes,A.D., Thermal Conductivity of Solids Pion Limited, 207 Brondsbury Park, London NW2 5JN
[3] Sharma,C.S. and Hughes,R., Can.J.Chem.Engng. 54 (1976)538-36
[4] Sehr,R.A., Chem.Engng.Sci 9 (1958) 145
[5] Satterfield,C.N., Mass Transfer in Heterogeneous Catalysis, M.I.T. Press, Cambridge, Mass./USA, 1970
[6] Butt, J.B., A.I.Ch.E.J. 11 (1965) 106
[7] Masamune,S. and Smith,J.M., J.Chem.Engng.Data 8 (1963) 54
[8] Cunningham, R.S., Carberry, J.J. and Smith,J.M., A.I.Ch.E.J. 11 (1965) 636
[9] Harriott,P., Chem.Engng.J., 10 (1975) 65-71
[10] Sharma,C.S., Harriott,P. and Hughes,R., ibid., 10 (1975) 73-80
[11] Saegusa,T., Kamata,K., Iida,Y. and Wakao,N., Int.Chem.Engng. 14 (1974) 169-173
[12] Schröder,J., Review of Scientific Instruments, 34 (1963) 615-621
[13] Ritter,J., Helm,E. and Fürst,H., Chem.Techn. 28 (1976) 232-621
[14] Gunn,D.J. and De Souza,J.F.C., CES 29 (1974) 1363-1371
[15] Carslaw,H.S. and Jaeger,J.C., Conduction of Heat in Solids, Oxford, Clarendon Press, 1959
[16] Jirátová,K. and Horák,J., Chem.Techn. 28 (1976) 550-553

In Chemical Reaction Engineering—Houston; Weekman, V., et al.;
ACS Symposium Series; American Chemical Society: Washington, DC, 1978.

17

Interpretation of Catalyst Deactivation by Fouling from Interactions of Pore Structure and Foulant Deposit Geometries

C. C. HUGHES and REGINALD MANN

Department of Chemical Engineering, University of Manchester Institute of Science and Technology, Manchester, England

Deactivation is a term of general designation and encompasses several distinct, though sometimes poorly defined processes, that give rise to a lowering of catalyst activity. Poisoning, ageing, sintering and fouling are particular examples of deactivation and these terms ought in principle to clearly indicate and discriminate the mechanisms involved. In practice, probably due to the potential complexity if these processes take place simultaneously, there is often some overlap and confusion in their use.

Levenspiel [1] has referred to fouling as being primarily rapid, accompanied by deposition and a physical blocking of surface. He then defines poisoning as a slow modification of activity by chemisorption on the active sites, the poison being characterised by difficulty of removal. It is our view that rate of loss of activity is not a sufficiently meaningful discriminant. Instead, we propose that poisoning should refer to active site deactivation by monolayer type adsorption at the site, and thereafter no further poison adsorption takes place at that location. In this way, a very great loss of activity can take place with the adsorption of very small amounts of poison. If, however, successive adsorption on the surface can take place, such that significant amounts of material accumulate, then this represents fouling of the catalyst.

The classical treatments of activity loss by poisoning by Thiele [2] and Wheeler [3], support the above distinctions, since the poison was not considered to have any influence upon the pore geometry or effective diffusivity. Uniform, non-uniform and anti-selective poisoning do give rise to a wide spectrum of deactivation behaviour, but the non-comprehensive capability of a theory of poisoning to explain deactivation when significant accumulation takes place, requires that new approaches be made. This is confirmed by several more recent observations.

Thus, Butt's [4] measurements of a very non-uniform coke profile, indicate that ultimate penetration of a coke type foulant into a catalyst particle is very quickly attained, and sybsequent deposition occurs entirely within an outer shell.

© 0-8412-0401-2/78/47-065-201$05.00/0

There remains an uncoked central core, apparently never contacte(by reactant. The work of Rostrup-Nielsen 5 and Levintner 6 also suggests that pore mouth closure by coke plugs may be theoretically required, and a simplified theory has been recently proposed by Newson 7.

There is therefore a good deal of evidence to support the idea that the effect of foulant deposits on activity, selectivit; and pellet macroscopic properties is sensitive to both the pore structure and the foulant deposit structure. Such an approach should improve upon the more empirically based methods used by Voorhies 8 and Wojciechowski 9, which have traditionally attempted to describe deactivation when fouling occurs.

Outline of the Theory

The nature of the interaction of the pore structure and foulant deposit geometries is determined from two basic assumptions. Firstly, that the pore structure may be represente(by a set of idealised parallel sided non intersecting pores of variable radius, but each of a certain length L. This is the so called 'parallel bundle' model. Secondly, that the foulant accumulates by simultaneous penetration and thickening, giving rise to successive laying down of foulant. We call this the 'wedge layering' model of foulant deposition.

The qualitative features of the subsequent interaction are depicted in Fig. 1. The smallest pore A blocks first as thickening proceeds and thereafter the remaining surface within pore A is rendered inaccessible and thus catalytically inactive. If the desired non-fouling reaction is taking place without diffusion influence, the loss in activity is equal to this loss of area in pore A. This is shown in Fig. 2. As penetration and thickening continue at the same relative rate, additional losses in activity take place, as the remaining larger pores become plugged. It is clear that in the absence of a theory of plugging, the activity loss would be erroneously interpreted as being caused by poisoning with diffusional resistance.

Total foulant content as a function of pellet activity is perhaps the most important characteristic in analysing fouling behaviour, since it is fairly simply observed by experiment. Fig. 3 shows some qualitative aspects. It is clear that at any given foulant content two possibilities exist for the distribution of foulant that give rise to the same activity. Thi is illustrated in Figs. 3(a),(c). If the foulant has a small thickness and large penetration as in (a), this can be viewed as a poisoning mode of deactivation. On the other hand, the same amount of foulant could be present as a large thickness small penetration wedge as in Fig. 3(c), and this would be a pore mouth plugging mode of deactivation. A further observation is that at a certain level of the parameter β defined by

β = rate of foulant thickening/rate of foulant penetration

In Chemical Reaction Engineering—Houston; Weekman, V., et al.;
ACS Symposium Series; American Chemical Society: Washington, DC, 1978.

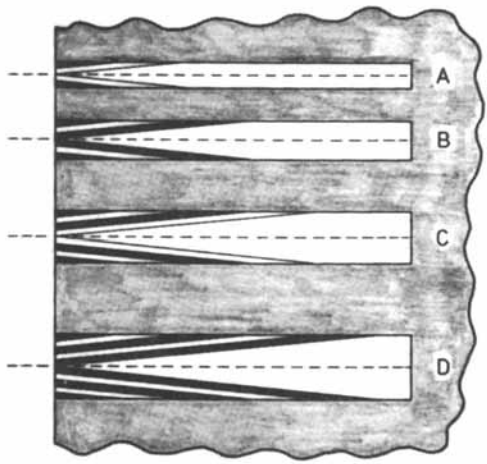

Figure 1. Fouling by "wedge layering" in a parallel bundle pore structure model

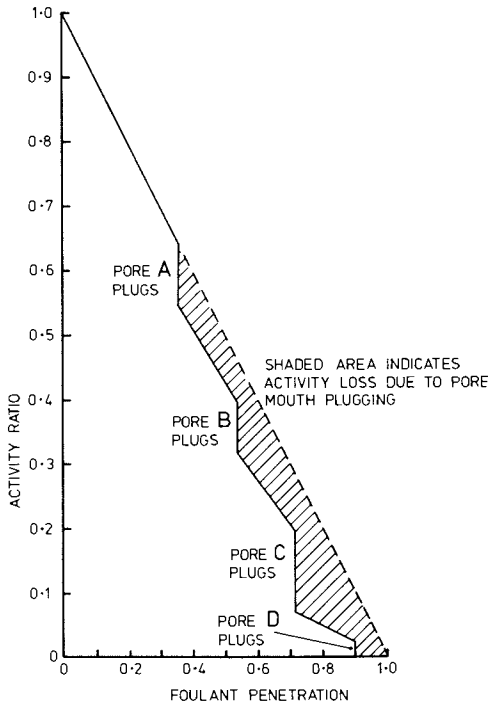

Figure 2. Activity losses as foulant penetrates and accumulates

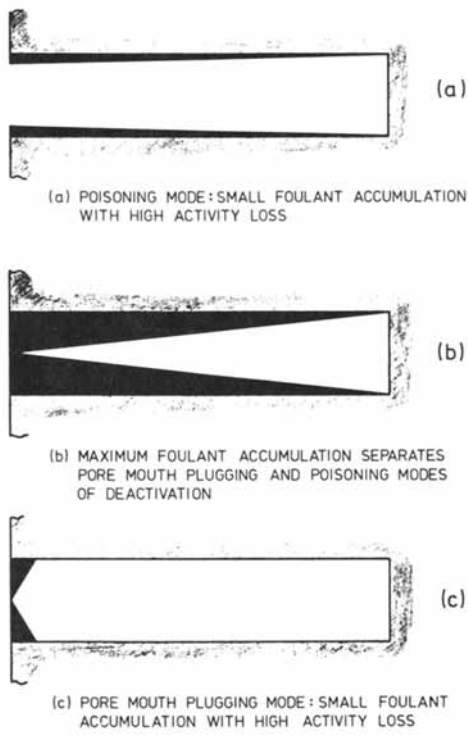

Figure 3. Illustration of differing modes of deactivation

In Chemical Reaction Engineering—Houston; Weekman, V., et al.;
ACS Symposium Series; American Chemical Society: Washington, DC, 1978.

which is here assumed to be a constant irrespective of degree of penetration or thickening, a pore of a given size reaches a maximum foulant content as β increases from zero (pure poisoning) to infinity (pure pore mouth plugging). This is indicated in Figs. 4(a) and (b). This characteristic of maximum foulant accumulation at some critical value β_{crit} has been deduced with respect to pores of a single size. In order for the theory to find general applicability, it requires extension to pellets with distributed pore sizes.

For a unit mass of catalyst, if $f_s(r)dr$ is the surface area contained in pores of size between r and r+dr, then

$$\int_0^\infty f_s(r)dr = S_g \qquad (1)$$

where S_g is the specific surface area of the catalyst. If pure pore mouth poisoning were to take place under non-diffusion influenced conditions, the reduced activity at a given penetration x is given by

$$F = (1 - \frac{x}{L}) \int_0^\infty f_s(r)dr/S_g = 1 - \frac{x}{L} \qquad (2)$$

where L is the length dimension of the parallel pore bundle. Now, if fouling takes place by wedge layering such that $\beta = h/x$, pores will remain unplugged, and their interior surface will be accessible and catalytically active, provided that $r>h$. Therefore the reduced activity at a given penetration x will be given by

$$F = (1 - \frac{x}{L}) \int_h^\infty f_s(r)dr/S_g \qquad (3)$$

The dimensionless activity is therefore identified with non-fouled pore surface that succeeds in remaining accessible. As mentioned previously, this effect due to mouth plugging can be spuriously identified as pore diffusional resistance accompanying poisoning.

In calculating the corresponding volume or mass of accumulated foulant, those pores which have already become sealed have to be distinguished from those that yet remain to be plugged. For unplugged pores, if $f_N(r)dr$ is the number fraction of pores sized between r and r+dr, the foulant volume in this category of pores at a potential mouth thickness h is given by

$$V_f'(h) = \int_h^\infty \tfrac{1}{2}\pi(r^2 - \beta^2x^2)xNf_N(r)dr \qquad (4)$$

where N is the total number of pores constituting the parallel bundle within a unit mass of catalyst.

For the category of plugged pores, a pore becomes plugged and thereafter remains plugged at the instant when $h = \beta x = r$, and hence all the pores between 0 and h are blocked off for a

In Chemical Reaction Engineering—Houston; Weekman, V., et al.;
ACS Symposium Series; American Chemical Society: Washington, DC, 1978.

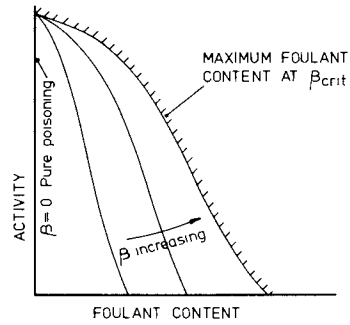

(a) FOR $0<\beta<\beta_{crit}$ ACTIVITY LOSS IS POISONING DOMINANT

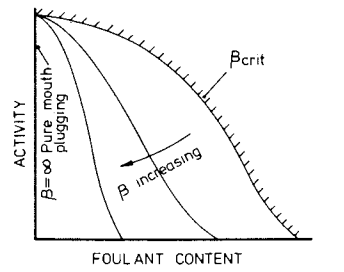

(b) FOR $\beta_{crit}<\beta<\infty$ ACTIVITY LOSS IS MOUTH PLUGGING DOMINANT

Figure 4. Activity foulent content behavior during deactivation

In Chemical Reaction Engineering—Houston; Weekman, V., et al.;
ACS Symposium Series; American Chemical Society: Washington, DC, 1978.

particular penetration x. The volume of foulant in plugged pores is given by

$$V''_f(h) = \int_o^h \tfrac{1}{2}\pi\beta^2 x^3 \, N \, f_N(x) \, dx \qquad (5)$$

The total foulant volume is obtained from

$$V_f(h) = V'_f(h) + V''_f(h) \qquad (6)$$

so that

$$V_f(h) = \frac{S_g}{4L}\left[\beta^2\int_o^h r^2 f_s(r)dr + \int_h^\infty (\frac{hr^2}{\beta} - \frac{h^3}{\beta})\frac{f_s(r)\,dr}{r}\right] \qquad (7)$$

which is now conveniently given in terms of the pellet specific surface, pellet/pore length dimension and the pellet surface area distribution function.

Comparison of Theory and Experiment for a HDS Catalyst

The theory can now be applied for the interpretation of some experimental results obtained for the vapour phase hydrodesulphurisation of thiophene over a commercial alumina supported cobalt-molybdate catalyst, COMOX 1661 manufactured by Laporte Industries Ltd., General Chemicals Division, Widnes, U.K., available in the form of cylindrical extruded pellets of dimensions 10 mm x 1.5 mm. These pellets were formed into a small fixed bed containing 2 gm of dry oxide catalyst held in place by quartz wool plugs in a 1.5 cm I.D. glass tubular reactor. The reactor feed was a vapour mixture of thiophene and hydrogen, formed by bubbling hydrogen through liquid thiophene kept at 0°C in an ice bath. The reactor operated at atmospheric pressures and was controlled by an electric furnace at 300°C. Conversions of thiophene were determined by on-line sampling using a gas-liquid chromatograph. Presulphiding of the catalyst which is supplied in the oxide form, was carried out in accordance with procedures recommended by the supplier. The conversion - feed rate behaviour of the pretreated unfouled catalyst is presented in Fig. 5.

Separate catalyst samples were then subjected to fouling by coke deposition using a sequential technique with ethylene. This coking was carried out at 500°C by passing a mixture of 50 cm^3/min of ethylene and 187.5 cm^3/min of oxygen free nitrogen over the 2 gm catalyst bed, after presulphiding and checking the activity. The extent of coke deposition was changed by altering the time of coking, using otherwise identical conditions for each coking run. After coking, the conversion of thiophene hence the reaction rate, was determined in the usual way. The complete set of runs with coking time varied from 5 to 120 min is presented in Fig. 5. The continuous lines shown are the fitting of the kinetic rate equation based upon

In Chemical Reaction Engineering—Houston; Weekman, V., et al.;
ACS Symposium Series; American Chemical Society: Washington, DC, 1978.

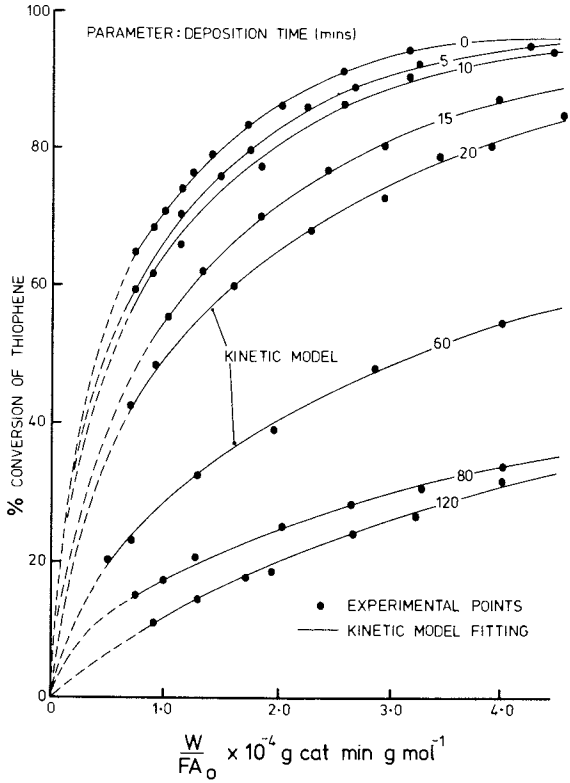

Figure 5. Effect of increasing sequential fouling coke deposition time on HDS catalyst activity at 300°C

In Chemical Reaction Engineering—Houston; Weekman, V., et al.;
ACS Symposium Series; American Chemical Society: Washington, DC, 1978.

$$(-r_A) = \frac{k_1 C_A}{1 + K_1 C_A} \qquad (8)$$

using an assumption of plug flow in the reactor. This kinetic equation is a reduced form of a more complete Langmuir-Hinshelwood equation.

The values of model parameters at 300°C are listed in Table I. The negative values of the apparent adsorption constant K_1 indicate that the product butanes and hydrogen sulphide are more strongly adsorbed than thiophene.

TABLE I: The Effect of Coke Deposition on Apparent Rate Constants

	300°C	
q_c °/w coke	k_1 gmoles.min /gcat x10^3	$-K_1$ gmoles /gmole
0.00	2.30	31.5
0.70	1.93	30.14
1.90	1.67	32.07
2.20	1.19	30.17
2.50	0.86	32.00
4.26	0.25	33.36
5.84	0.07	35.38
8.47	0.10	29.69

Analysis of diffusion and reaction for generalised kinetics 10, shows that the present results give reaction rates in the non-diffusion influence regime 11. Thus, the activity loss that is observed is due to surface area loss, and is not due to diffusional resistance accompanying poisoning. This is borne out by Table I, where the impact of fouling is seen in the decrease of k_1, with K_1 being independent of coke content.

The coking procedure that has been used is arbitrary, but serves the purpose of separating fouling mechanism from the activity measurement. Parallel fouling by using mixed feeds of thiophene and ethylene at 300°C produced no coke deposition. However, this sequential technique did give uniform coking throughout the catalyst bed. The coke contents were determined using burnoff with oxygen on a horizontal thermobalance, and again full details are given in 11.

The reaction rates predicted from the kinetic model at 10% conversion increments from 21% to 91% conversion of thiophene, have been used to construct Table II. At each conversion level the global reaction rate has been normalised to a fraction of the reaction rate for the unfouled catalyst. Only results falling within the experimental range have been included. The activity

In Chemical Reaction Engineering—Houston; Weekman, V., et al.;
ACS Symposium Series; American Chemical Society: Washington, DC, 1978.

ratio seems to be constant over wide ranges of conversion for a given coke content. Therefore the average activity at each coke content is taken to represent the effect of coke deposition upon catalyst activity, and these results form the basis of comparing theory and experiment.

TABLE II: Experimental Coked Catalyst Activities

	300°C							
Conversion Level X_A%	Coke Content wt %							
	0.00	0.70	1.90	2.20	2.50	4.26	5.84	8.47
21	1.00	-	-	-	-	.133	.044	.040
31	1.00	-	-	-	-	.125	.039	.042
41	1.00	-	-	-	.394	.121	-	-
51	1.00	-	-	.518	.391	.117	-	-
61	1.00	.846	.755	.523	.388	-	-	-
71	1.00	.848	.750	.525	.385	-	-	-
81	1.00	.853	.748	.524	.385	-	-	-
91	1.00	.852	.754	-	-	-	-	-
Average Activity*	1.00	.850	.752	.521	0.390	.124	0.042	0.041

The final element in the analysis is the pore size distribution function of the experimental catalyst COMOX 1661. The manufacturers pore size data has been fitted with a log-normal distribution with $r = 54$ Å and $\sigma = 0.30$. Using $r_{min} = 10$ Å and $r_{max} = 2000$ Å and $L = 6.5 \times 10^8$ Å, a pellet surface area of 323.3 m gm^{-1} and pore volume of 0.606 cm^3 gm^{-1} are predicted. These compare with 300 and 0.60 quoted by the manufacturer as typical values.

The consequent comparison of theory and experiment as the thickening/penetration parameter β increases from zero to infinity is presented in Figs. 6(a), (b). The experimental results show a clear inflexion tendency, and therefore the monotone decreasing prediction for poisoning dominated foulant accumulation suggests that this mechanism is not correct. On the other hand, the results do comply with a β value between 3×10^{-5} and 5×10^{-5}, placing the behaviour in the pore mouth plugging dominant regime. In constructing Figs. 6(a),(b) a coke density of 1.0 gm cm^{-3} has been chosen as intermediate between the value of 0.8 quoted by Beuther and Schmid 12 and 1.7 gm cm^{-3} use by Levitner 6. This converts coke volume to coke wt% in the pellet.

The discrimination of the correct deactivating mechanism is of more than academic importance. Thus, if in a particular case, as here, pore mouth plugging is the most important deactivating mechanism, attention should be concentrated on changing the physical pore structure of the catalyst in order to alleviate the deactivation. The striking of a correct balance between poisoning and fouling pore mouth closure when they are both

In Chemical Reaction Engineering—Houston; Weekman, V., et al.;
ACS Symposium Series; American Chemical Society: Washington, DC, 1978.

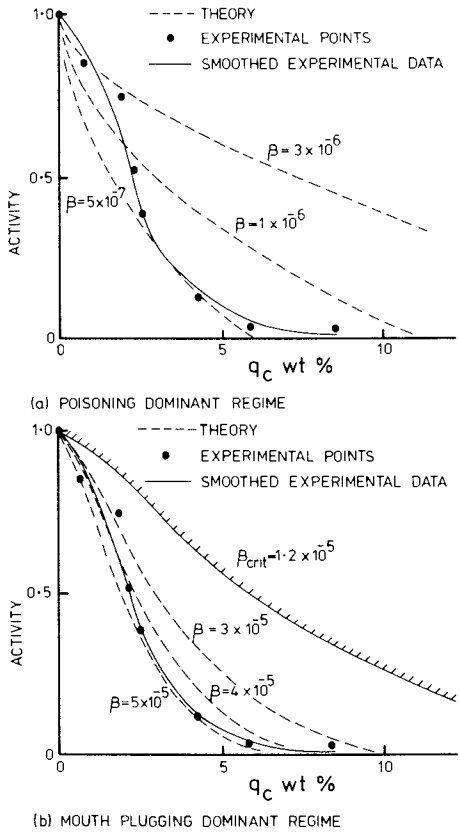

Figure 6. Comparison of wedge layering model with experimental results

inevitable, by rational design of the pore structure, remains a challenging task for the chemical reaction engineer.

Conclusions

A new theory of fouling, based upon the way in which the structure of the pores and the geometric form of the foulant deposit interact together, has been developed. This theory is comprehensive in scope and predicts the activity-foulant content behaviour together with the spatial distribution of foulant within the pellet pore structure, and has the potential to predic porosity, permeability and effective diffusivity changes during fouling. Experiments on the activity behaviour of a commercial HDS catalyst in desulphurising thiophene fouled by a sequential technique using ethylene, showed the deactivation to be in the pore mouth plugging dominated regime.

Nomenclature

β	foulant thickening/penetration rate parameter
C_I	concentration (A=thiophene, H=hydrogen, S=hydrogen sulphide)
F	fractional activity during deactivation
F_{A_0}	molar feed rate of thiophene
$f_N^{A_0}(r)$	number-pore radius distribution function
$f_N^s(r)$	surface area-pore radius distribution function
$f_v^s(r)$	volume-pore radius distribution function
h^v	pore mouth foulant thickness
K_1	adsorption constant
k_1	reaction rate constant
L^1	pellet length dimension
N	number of pores per gm of catalyst
r	pore radius
$\hat{r}$	most frequent pore radius
S	pellet specific surface
$V_f^g(h)$	total volume of foulant at a mouth thickness h
V^f	pore volume of pellet
W^p	weight of catalyst in reactor bed
X_A	conversion of thiophene
x^A	penetration of foulant
σ	variance

Acknowledgement

We wish to thank the S.R.C. for provision of a research studentship for CCH. We are also indebted to Laporte Industries Ltd., General Chemicals Div., Widnes, U.K. for the donation of catalyst samples and for many helpful discussions.

Literature Cited

1. Levenspiel, O., "Chemical Reaction Engineering", 2nd Ed., Wiley, New York (1972).
2. Thiele, E.W., Ind. Eng. Chem. (1939) 31, 916
3. Wheeler, A., Adv. in Catalysis (1951) 8, 250
4. Butt, J.B., J. Catalysis (1976) 41, 190
5. Rostrup-Nielsen, J.R., J. Catalysis (1974) 33, 184
6. Levintner, M.E., Panchenkov, G.M., Tanaterov, M.A., Int. Chem. Eng. (1967) 7, 23
7. Newson, E., Ind. Eng. Chem. Proc. Des. Dev. (1975) 14, 27
8. Voorhies, J.R., Ind. Eng. Chem. (1945) 37, 318
9. Wojciechowski, B.W., Cat. Rev. - Sci. Eng. (1974) 9, 79
10. Roberts, G.W., Satterfield, C.N. Ind. Eng. Chem. (1965) 4, 288
11. Hughes, C.C., Ph.D. Thesis, University of Manchester Institute of Science and Technology (1977)
12. Beuther, H., Schmid, B.K., Proc. 6th World Petroleum Congress (1964) III, 297.

In Chemical Reaction Engineering—Houston; Weekman, V., et al.;
ACS Symposium Series; American Chemical Society: Washington, DC, 1978.

18

Operational Flexibility Consideration in the Design of Multitubular Reactors

C. McGREAVY
Department of Chemical Engineering, Leeds University, Leeds, LS2 9JT, England
B. R. DUNBOBBIN
Union Carbide Corporation, Chemicals and Plastics, Bound Brook, NJ 08805

Multitubular reactor design methods based on the assumption that the tube bundle can be represented by a single, typical tube are adequate when the operating conditions are remote from regions of high performance, and where maldistribution of the feed to the tubes cannot occur. In other circumstances, significantly different conditions are found in the tubes depending on their position in the bundle. Moreover, when optimal performance is being sought, it is often the case that the preferred operating state is in a region where it is no longer possible to make simplifying assumptions, since it is essential to have reliable information on the detailed behaviour of the system. This is required not only to ensure that adequate flexibility of operation is possible, but also to be able to evaluate what potential hazardous conditions might arise. To do this, it is essential to take account of the multitubular characteristics explicitly and to examine the effects of the coolant flow because significantly different patterns of behaviour are possible both in respect to stability as well as having an important bearing on the economic attractiveness of using certain reactor configurations. At the design stage, the decisions to be taken in respect of the latter are obviously of some importance. These considerations will necessarily be influenced by the particular operations, reaction scheme and many other specific factors. Nevertheless, it would be useful to be able to suggest general guide-lines as to how to select initial configurations so as to realise particular operational characteristics.

Despite its importance, very little work has been done in this area, perhaps because of the considerable amount of information on shell and tube heat exchangers. Unfortunately, this expertise is not directly applicable. For example, for highly exothermic reactions of the type to be considered here, it is better to avoid counter-current flow between coolant and reactants because of operational difficulties which can arise. For this reason, it is the intention of this work to explore the general operating characteristics of both co- and counter-current

© 0-8412-0401-2/78/47-065-214$05.00/0

In Chemical Reaction Engineering—Houston; Weekman, V., et al.;
ACS Symposium Series; American Chemical Society: Washington, DC, 1978.

units to enable criteria for design to be established. The insight gained from this can be used to devise alternative arrangements which is able to take advantage of each of the above modes while allowing adequate flexibility of operation. In addition, valuable information can be obtained as to how to deal with control problems.

As with the simple heat exchanger systems, the counter-current reactor will generally require a smaller heat transfer area than a co-current system for the same thermal loading. In this sense, comparison of the two systems is not straightforward. But for convenience, the following discussion will be based on the assumption that a common shell and tube arrangement is being used and the different arrangements are obtained by changing connections at the inlet and outlet nozzles, where appropriate. As already indicated, the principal concern is with flexibility and operability, which would obviously have to be considered in relation to capital cost. Although this will not be explored further, it can be incorporated into the procedure outlined here, when more detailed studies are being carried out (1).

Model of the Multitubular Reactor

The formulation of a mathematical description of a multi-tubular reactor poses no special problems, although the computational effort needed to solve the equations can be very considerable, particularly where extreme operating conditions are being explored. It is under these circumstances that significant interaction occurs between the tubes as a result of the distribution of the coolant in the shell. Dunbobbin (1) and Adderley (2) have shown that unless these effects are accounted for in the heat balances,the results are of limited value.

Clearly, it would be desirable to have a general analytical framework which could be used to indicate when difficult conditions might arise and how they could be handled. At the present time, this is not possible, so a technique must be developed which can demonstrate the broad characteristics of systems and enable the relevant insight to be gained. As a step in this direction, a case study of a representative of a class of important problems offers a suitable compromise, and will be the approach adopted here. The particular system to be considered belongs to the important class of catalytic partial oxidation reactions, as represented by the production of maleic anhydride from benzene. Although these are basically complex reaction schemes, in their limiting behaviour, where temperature runaway and other instabilities develop, the kinetic equations approximate a single irreversible reaction to the complete oxidation products. As far as heat effects are concerned, it is then possible to display all the important pathological features. The following analysis assumes that such an approximation is acceptable for the purposes of

In Chemical Reaction Engineering—Houston; Weekman, V., et al.;
ACS Symposium Series; American Chemical Society: Washington, DC, 1978.

illustration, but in no way restricts the validity of the procedure. More complex schemes would merely require a much more detailed analysis.

An approximation which adequately represents a continuum version of the system shown in figure 1 can be obtained by replacing the equation for the heat balance on the coolant by a series of mixing cells (1), where a volume element of the coolant, together with a small group of reactor tube sections, is considered in one of the passes. The dimensionless heat balance for a typical cell are given by the appropriate equations (1) and (2) below:

Co-current flow.

$$T_{c(i)} = T_{c(i-1)} + \frac{Nu_w^*}{G_c} \int_{z_2}^{z_1} (T-T_{c(i)})dz \qquad (1)$$

Counter-current flow.

$$T_{c(i)} = T_{c(i-1)} - \frac{Nu_w^*}{G_c} \int_{z_2}^{z_1} (T-T_{c(i-1)})dz \qquad (2)$$

Figure 1 indicates the nomenclature used in describing the reactor. The subscript i refers to the ith cell, numbered from the coolant inlet (co-current case), or outlet (counter-current).

The solution of the model is obtained by coupling the tubeside reactor equations with equation (1) or (2) as appropriate, and using a marching procedure to pass through the assembly from cell to cell, iteration around a guessed outlet coolant temperature being necessary in the counter-current case.

For the reaction inside the tube, the dimensionless mass and energy balances, with the usual assumptions, become (1, 2, 3) for the single main reaction:

Fluid Field.

$$\frac{dc}{dz} + G_2 \theta^2 \eta \exp\left(-\frac{1}{T}\right) c = 0 \qquad (3)$$

$$\frac{dT}{dz} - G_4 (t-T) + \frac{2Nu_w^*}{G_3} (T-T_c) = 0 \qquad (4)$$

with initial conditions:

$$T = T\Big|_{z=0}$$

$$c = c\Big|_{z=0}$$

Reaction on the Solid. The reaction rate on the catalyst can be easily calculated if the pellet is assumed to be isothermal (1, 2, 3), at a temperature given by:

$$t = T + \frac{B\ Sh_A\ (r-g)}{(sg + r)} \qquad (5)$$

This equation must be solved iteratively to find the solid temperature and hence the reaction rate.

Details of the method of the solution can be found elsewhere (4), but the resulting profiles give detailed information on the coolant temperature and conditions in the reactor tubes. It is also possible to see how heat is effectively passed between tubes and hence which are most vulnerable to the development of instabilities. Each case requires careful scanning of the results, but the findings can be summarized in the manner indicated below. Nevertheless, it should be noted that it is not possible in general to predict, a priori, which part of the bundle contains the critical tube. It will also depend on whether maldistribution effects are present.

The number of cells used will clearly depend on the nature of the problem, but for the system considered here, and to carry out a reasonable detailed survey, it is necessary to use about 10 cells for each of the coolant side passes. Typical results for the dimensionless profiles for tubes at opposite sides of the bundle are shown in figure 2 i.e. identified as tubes 1 and 50: these are for the row of tubes across the diameter. The very different conditions inside the tubes at these positions is apparent.

Comparison of Reactor Configurations

The data in table I are for the partial oxidation of benzene and can be used to explore how alternative mechanical configurations affect the operation. In adopting this approach, it will be appreciated that a number of different bases for the comparison are possible. For convenience attention will be confined to those factors affecting the operability of a given, fixed size reactor unit. Alternative configurations are easily derived from this by appropriate changes at the inlet and outlet, together with any associated relocation of the baffle plates.

In Chemical Reaction Engineering—Houston; Weekman, V., et al.;
ACS Symposium Series; American Chemical Society: Washington, DC, 1978.

Table I Data used in the case studies

G_2	= 0.0849;	0	= 10^6 ;	$G_{(inlet)}$	= 1.0
G_3	= 0.84 ;	B_o	= 4.602×10^{-5};	G_c	= 98.25
G_4	= 76.85 ;	Nu_w	= 14.6 ;	T_o	= 0.03884
Sh_A	= 500.0 ;	Total No. of tubes = 2,500.			

The obvious difference between the heat transfer mechanism of the co- and counter-currently cooled reactors is that the former operates with a feed-forward and the latter a feed-back of heat along the reactor tubes. Thus,co-current reactors introduce the cold coolant where there is a high reactant concentration and heated coolant promotes reaction in the lean reactant regions towards the tubeside exit. Counter-current reactors on the other hand have pre-heated coolant affecting high reactant concentrations and cold coolant in the exit regions of the tubeside. Thus, the reaction is essentially restricted to the initial portions of the bed. Also, because of the higher coolant temperatures in the region of the tube-side hotspots, the counter-current reactor gives higher peak temperatures and conversions. However, because of the small zone available for high reaction, high conversion often results in temperature runaway on the tubeside, making the co-current system more attractive in many circumstances. Thus, while counter-current flow may reduce the size of reactor to achieve a given conversion, it has undesirable features which can lead to difficult operation.

The above observations suggest an alternative configuration might make it possible to improve designs. Thus, if an arrangement such as that shown in figure 3 is used, it requires no complex shell-side modifications and is achieved very simply by having the coolant entering at pass 2 and leaving at passes 1 and 4, at the cost of a small amount of extra piping. With this scheme the counter-current stream is heated by coolant pass 2 before entering pass 1, so that the incoming reactant is contacted by warm coolant. Since the flowpath is not as long as in a conventional counter-current reactor, the coolant is not heated as much and so the very large temperature peaks of these reactors can be avoided. The co-current stream is also heated and causes reaction in the lower concentration regions of the bed. It therefore makes it possible to take advantage of both the co- and counter-current systems, so that the incoming reactants are contacted by warm coolant, thus ensuring that a useful amount of reaction takes place early in the bed, and any reactants left in the latter half of the reactor are also contacted with warmer coolant, which will thus increase the reaction rate. In effect,

In Chemical Reaction Engineering—Houston; Weekman, V., et al.;
ACS Symposium Series; American Chemical Society: Washington, DC, 1978.

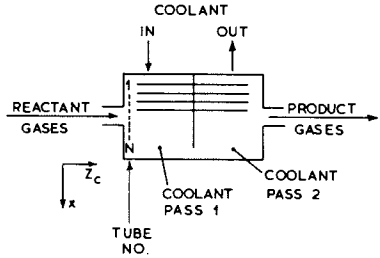

Figure 1. General representation of the reactor indicating the notation used in describing it

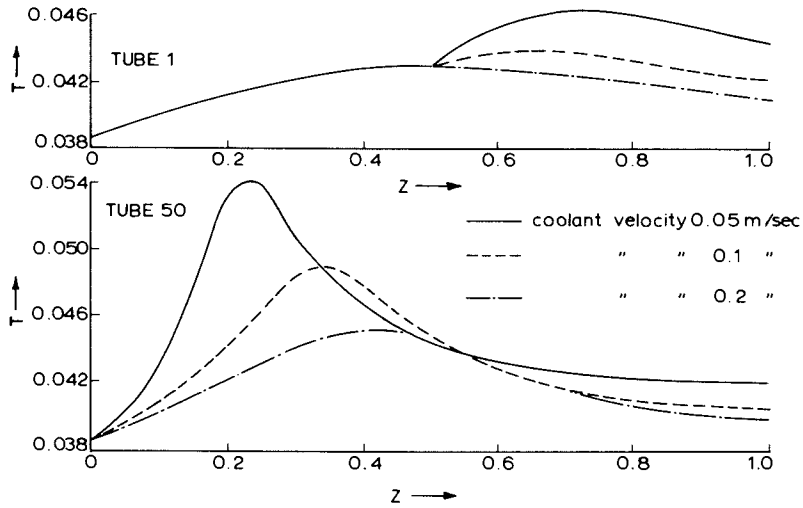

Figure 2. Typical temperature profiles in reactor tubes at positions 1 and 50 for various flows

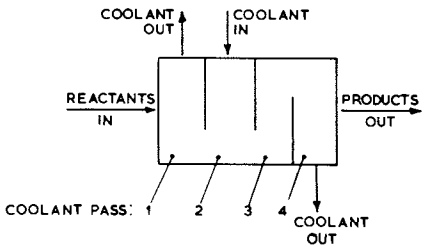

Figure 3. Mixed flow reactor

In Chemical Reaction Engineering—Houston; Weekman, V., et al.;
ACS Symposium Series; American Chemical Society: Washington, DC, 1978.

this mixed-flow configuration introduces the coldest coolant in the position where it is most effective, namely at the tubeside hotspot, and it also provides a reasonable degree of flexibility.

Other methods of increasing the heat transfer in the region of the hotspot do not tend to have the same degree of adaptability during operation. Paris and Stevens (4) devised a complex shell-side arrangement for a single tube reactor and several workers (5, 6, 7) have considered using various sized packings or inert spheres at different points in the tubes. These methods, while often successful, assume that design specifications can, and will be maintained. An advantage of the above method is that it can be used even with existing tube bundles with very little structural change.

Mixed Flow Configurations

To see the inherent advantages of the mixed flow system, it is useful to compare systems for each of the main distributions in each loop, at constant total mass flowrate of coolant. The units are also taken to be the same size, the only difference being the routing of the coolant flow. This means that although the residence time of the coolant is the same in the co- and counter-current reactors, it will be smaller in the mixed flow configuration. Control can be exercised by adjusting the relative flow rates in the circuit, and this is illustrated by using the following distributions:

1. ½ the coolant flow from pass 2 flows counter-currently into pass 1.

2. ⅔ the coolant flow from pass 2 flows counter-currently into pass 1.

3. ¾ the coolant flow from pass 2 flows counter-currently into pass 1.

The flowrate through coolant pass 2 is always the same as in the co- and counter-current cases.

The tubeside temperature profiles of tube 1 for the three types of mixed flow system, together with the profile for the co- and counter-current reactors, are given in figure 4. In all cases, the tube in the bundle representing the 'worst' conditions has been used. An important observation is that it is not always the same one. The lowest, and most stable, temperature profile is obtained from the co-current reactor, with the largest temperature peak being given by the counter-current. The three mixed flow profiles are intermediate to these, with the type 3 giving the flattest profile. Figure 5 uses the T versus B stability plots proposed by McGreavy and Adderley (8) to examine the co-

In Chemical Reaction Engineering—Houston; Weekman, V., et al.;
ACS Symposium Series; American Chemical Society: Washington, DC, 1978.

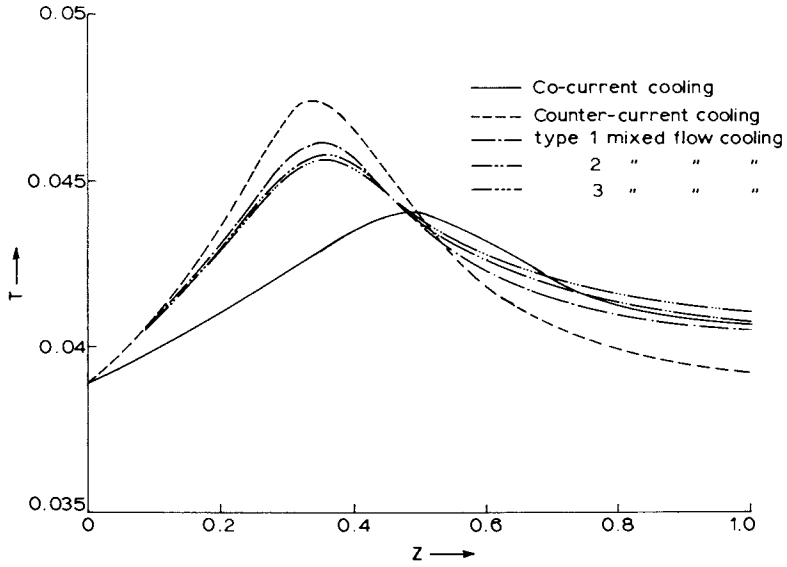

Figure 4. The co-current, counter-current, and mixed-flow tubeside temperature profiles for tube 1 in a four-coolant pass reactor

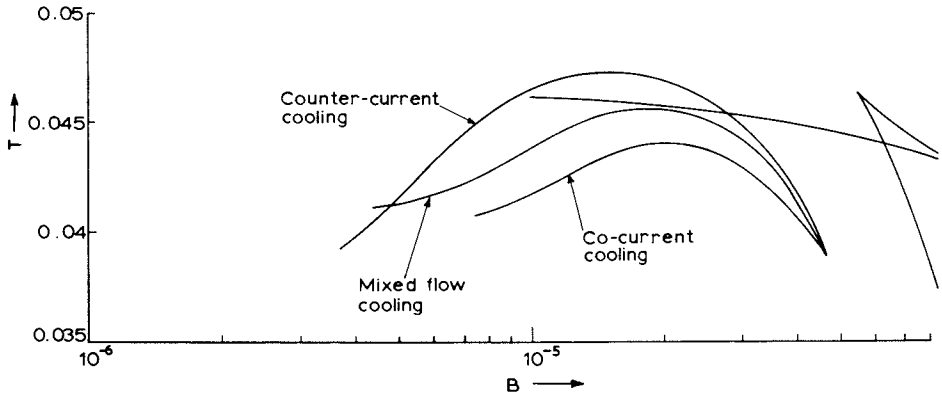

Figure 5. T vs. B stability plot comparing the co-current, counter-current, and mixed-flow four-coolant pass reactors

In Chemical Reaction Engineering—Houston; Weekman, V., et al.;
ACS Symposium Series; American Chemical Society: Washington, DC, 1978.

current, counter-current and type 3 mixed flow systems at a constant coolant flowrate expressed by the dimensionless parameter GG = 4.0. At this value, the latter configuration is at the limit of stability with respect to temperature runaway. To compare performance, it is sufficient to look at the conversions in each case which correspond to the limit of stability, since this indicates the most favourable conversions. Making use of plots similar to figure 5, it may be shown that for the same parameter values and operating conditions, the limit of stability of the counter-current reactor is GG = 5.0 and the co-current GG = 2.0 (1). These would correspond with a maximum temperature rise of 25.1K in the mixed flow type 3 reactor at GG = 4.0. Hence, at these conditions, the coolant temperature rise is much higher for the co-current reactor, being over twice that for the counter-current system, but with a much lower coolant flowrate for the same conversion.

The co-current reactor, with its low coolant flowrate (low value of GG) exhibits the best behaviour of all the configurations. The disadvantage is the high coolant temperature rise (up to 30K). The main advantage of the mixed flow system is that, with coolant flowrates lower than those for the counter-current system, conversions of comparable magnitude can be obtained, which, though they result in higher coolant temperature rises, are still less than those for co-current systems. Furthermore, although this study is in terms of a particular system, with only adjustment in the coolant flow paths, further flexibility is possible by a suitable choice of the position of the baffles, but this must be regarded as a design rather than an operational variable.

The need to introduce some co-current flow for the coolant, despite its unfavourable effect on the size of the reactor is to ensure that the resulting axial temperature profile in the tubes is flatter, and so cause the thermal loading to be more evenly distributed along the length. This is an important advantage of the mixed flow arrangement. The detailed model must be solved to identify the tube which is subject to the greatest risk of damage, however. Unfortunately, it is not always possible to assume it will be the same one, as the operating conditions change. Once identified, the information can be summarized in diagrams such as figure 5. Other plots can also be prepared which give valuable information regarding the influence of the coolant flow rate parameter, GG (1).

Conclusions

A comparison of co- and counter-currently cooled has demonstrated that, although co-current flow has some advantages, the temperature rise of the coolant is greater, because of the lower flow rates which are possible. There is also greater scope for adjusting operating conditions. Using a mixed flow

In Chemical Reaction Engineering—Houston; Weekman, V., et al.;
ACS Symposium Series; American Chemical Society: Washington, DC, 1978.

system, however, it is possible to take advantage of relatively low coolant pumping costs (lower flow rates) without excessive temperature rises. At the same time, a more even temperature distribution can be achieved with the additional benefit of greater operational flexibility.

Nomenclature

A^o = Arrhenius pre-exponential factor.
B = $B_o C$
b = radius of pellet.
C_o, C_f = reference concentration and fluid concentration respectively.
C_p, C_{pc} = specific heats of fluid and coolant respectively.
D_p = effective radial diffusivity within catalyst pellet.
E = activation energy of reaction.
e, e_c = voidage of fixed bed and tube bundle respectively.
h = pellet to fluid heat transfer coefficient.
g = tanh (r).
K_f = effective interstitial radial conductivity in fluid phase.
K_c = thermal conductivity of coolant.
k_g = fluid to pellet mass transfer coefficient.
L_c = diameter of tube bundle.
L_B = distance between baffle plates.
L = length of reactor tube.
M_c = mass flowrate of coolant.
R = reactor tube radius.
R_g = gas constant.
r = $\theta \exp\left(-\frac{1}{(2t)}\right)$
s = $(Sh_A/2 - 1)$
T_c', T_f, T_p = Temperature of coolant, fluid and pellet respectively.
U = overall fluid to coolant heat transfer coefficient.
u, u_c = fluidand coolant interstitial velocity respectively.
ρ, ρ_c = density of fluid and coolant respectively.
$(-\Delta H)$ = heat of reaction.
ϕ = $\theta \exp(-1/(2T))$.
θ = $b\sqrt{(A_o/D_p)}$.
= $1.5\ Sh_A\ (r - g)/(\phi^2\ (sg + r))$

In Chemical Reaction Engineering—Houston; Weekman, V., et al.;
ACS Symposium Series; American Chemical Society: Washington, DC, 1978.

Dimensionless Groups

$B_o = (-\Delta H)\ D_P\ C_o\ R_g\ /(2bhE).$

C = concentration = C_f/C_o.

$$G_c = \frac{m_c\ C_{pc}}{4\pi K_f e\ L_B}$$

$GG = G_c/G_{c\ \text{reference}}$; $G_{c\ \text{reference}} = 98.25.$

$G_2 = (1 - e)\ L\ D_p/(b^2\ ue)$

$G_3 = R^2\ up\ C_p/(L\ K_f)$

$G_4 = (1 - e)\ 3hL/(bpue\ C_p)$

$Nu_w = RU/(K_f\ e).$

$Nu_w^* = 4\ Nu_w/(4 + Nu_w)$

$Sh_A = 2bkg\ /D_p$

T, T_c, t = fluid, coolant and pellet temperature respectively, $T_f\ R_g/E$, $T_c\ R_g/E$, $T_p\ R_g/E$.

z = Axial position in reactor.

Literature Cited

1. Dunbobbin, B.R. Ph.D. Dissertation, University of Leeds (1976).
2. Adderley, C.I. Ph.D. Dissertation, University of Leeds (1973).
3. Thornton, J.M. Ph.D. Dissertation, University of Leeds (1970).
4. Paris, J.R. and Stevens, W.F. Fourth European Symposium on Chemical Reaction Engineering, Brussels (1968), 73, Pergamon Press (1971).
5. Brusset, H. et al, Chem.Eng.Sci. (1972), 27, 1945.
6. Calderbank, P.H. et al. Fourth European Symposium on Chemical Reaction Engineering, Brussels (1968), 93 Pergamon Press (1971).
7. Stewart, W.E. and Sorensen, J.P. Fifth European/Second International Symposium on Chemical Reaction Engineering, Amsterdam (1972), B8-75.
8. McGreavy, C. and Adderley, C.I., Chem.Eng.Sci. (1973) 28, 577.

In Chemical Reaction Engineering—Houston; Weekman, V., et al.;
ACS Symposium Series; American Chemical Society: Washington, DC, 1978.

19

Pore Plugging Model for Gas-Solid Reactions

JAMES W. CHROSTOWSKI and CHRISTOS GEORGAKIS

Department of Chemical Engineering, Massachusetts Institute of Technology, Cambridge, MA 02139

In the past few years a variety of mathematical models have been proposed in order to quantitatively account for the interactions between kinetic and diffusional resistances in gas-solid reactions (1-7). Most of the proposed models are categorized as grain models which assume the reactant solid exists in the form of small grains dispersed uniformly throughout the volume of the solid particle. In the most general of these models (3,5), three major resistances are taken into account: a) diffusional resistance through the pores of the particle, b) diffusional resistance through the solid product and c) kinetic resistance. Solid-solid diffusion and variation of grain size and porosity with conversion were allowed in (6).

An important gas-solid reaction for which porosity decreases with time of exposure to the reactant gas is the absorption of SO_2 by calcined limestone (CaO) or dolomite (CaO/MgO) to produce calcium sulfate ($CaSO_4$ or $CaSO_4$/MgO), which has a larger molar volume than the reactant solid. If diffusional limitations in the pores are important, the porosity decrease will be greater near the surface of the solid particle and pores will plug, limiting access to part of the reactant solid. As a consequence, conversion will be less than 100 percent. Hartman and Coughlin (5) extended previous grain models to account for such porosity changes. They were able to predict that the maximum amount of conversion can be less than 100 percent and compared their model's prediction with their experimental data for the reaction of SO_2 with limestone. However, they only accounted for average porosity changes.

In order to examine in more detail the effect of local porosity changes and quantitatively account for pore plugging, Georgakis et al. (8) and quite independently Ramachandran and Smith (7) focused attention on

© 0-8412-0401-2/78/47-065-225$05.00/0

a single pore.

In the present communication, a brief description of the pore plugging model is presented and its differences with that of Ramachandran and Smith (7) are examined. An analytical calculation of the time required to plug the pore is presented. In addition, a perturbation solution for small times is used to motivate the formulation of a semianalytical version of the collocation method for two point boundary value problems with steep concentration profiles.

1. Pore Plugging Model

In order to examine the interplay between kinetic and diffusional resistances in gas-solid noncatalytic reactions when the molar volume of the product solid (e.g., $CaSO_4$) is larger than the molar volume of the reactant solid (e.g., CaO), attention is focused on a simple case of a cylindrical pore of initial radius r_0 and length L (Figure 1a). As gaseous reactant (e.g., SO_2) is absorbed to form a product layer of $CaSO_4$, the geometry of the pore changes with time (Figure 1b). After some time the pore mouth will plug and reaction will cease.

Assuming isothermal conditions and neglecting bulk flow, radial concentration gradients in the pore and external mass transfer resistance, the following dimensionless form of the pore plugging model is derived (8).

a. Pore Diffusion

$$\beta \frac{\partial}{\partial t} (g_1^2 c) = \frac{\partial}{\partial x} \left[g_1^2 D(g_1) \frac{\partial c}{\partial x} \right] + 2\sigma G(x,t) \tag{1}$$

where

$$G(x,t) = g_1 \frac{\partial \hat{c}}{\partial r} (g_1,t) \tag{2}$$

and with the following initial and boundary conditions

$$c(x,0) = 0;\ c(1,t) = 1;\ c_x(0,t) = 0 \tag{3}$$

b. Product Layer Diffusion

$$\frac{\beta}{\sigma} \frac{\partial \hat{c}}{\partial t} = \frac{1}{r} \frac{\partial}{\partial r} \left(r \frac{\partial \hat{c}}{\partial r} \right) \tag{4}$$

with the following initial and boundary conditions

$$\hat{c}(x,0)=0;\ \hat{c}(g_1 t)=c(x,t);\ -\hat{c}_r(g_2,t)=K\hat{c}(g_2,t) \tag{5}$$

In Chemical Reaction Engineering—Houston; Weekman, V., et al.;
ACS Symposium Series; American Chemical Society: Washington, DC, 1978.

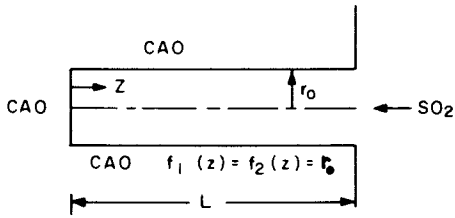

a) Initial Pore Geometry

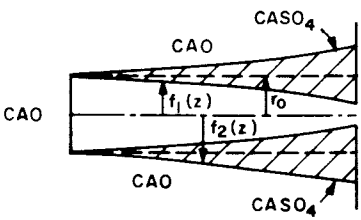

b) Pore Geometry after some reaction has occured (t>0)

Figure 1. Geometric changes of cylindrical pore because of the large molar volume of solid product

In Chemical Reaction Engineering—Houston; Weekman, V., et al.;
ACS Symposium Series; American Chemical Society: Washington, DC, 1978.

c. Reaction Front Change

$$\frac{\partial g_2}{\partial t} = \frac{1}{2}\,\hat{c}\,(g_2,t) \quad \text{with } g_2(x,0) = 1 \tag{6}$$

and the following equation relating the gas-solid interface to the solid-solid interface

$$g_1^2 = \alpha + (1-\alpha)g_2^2 \tag{7}$$

Definition of all symbols is given in the Notation section.

Since the value of β is usually quite small, the pseudo-steady-state hypothesis is justified with respect to the diffusional processes, and eq. (4) can be solved for $\hat{c}(r,x,t)$

$$\hat{c}(r,x,t) = c(x,t)\,\frac{1 + Kg_2\ln(g_2/r)}{1 + Kg_2\ln(g_2/g_1)} \tag{8}$$

Then the overall model reduces to

$$\frac{\partial}{\partial x}\left[g_1^2 D(g_1)\frac{\partial c}{\partial x}\right] = 2\sigma K\,\frac{g_2 c}{1 + Kg_2\ln(g_2/g_1)} \tag{9}$$

with boundary conditions given by eq. (3), and

$$\frac{\partial g_2}{\partial t} = \frac{1}{2}\,\frac{c}{1 + Kg_2\ln(g_2/g_1)} \qquad g_2(x,0) = 1 \tag{10}$$

Here the dimensionless diffusion coefficient $D(g_1)$ is assumed to depend on g_1 in the following way

$$D(g_1) = \mathcal{D}g_1/(1 + \mathcal{D}g_1) \tag{11}$$

since Knudsen diffusion is taken to be equally important as molecular diffusion.

Ramachandran and Smith (7) recently presented a similar model, but assumed that the diffusion coefficient is not changing as the geometry of the pore changes.

2. Analytical Evaluation of the Plugging Time

If attention is focused on the changes taking place at the mouth of the pore (x = 1) where the dimensionless concentration is unity, eq. (10) leads to

$$\frac{dg_2(1,t)}{dt} = \frac{1}{2}\,\frac{1}{1 + Kg_2\ln(g_2/g_1)} \tag{12}$$

In Chemical Reaction Engineering—Houston; Weekman, V., et al.;
ACS Symposium Series; American Chemical Society: Washington, DC, 1978.

Eq. (12) can be integrated to yield

$$(g_2 - 1) + \frac{K}{4}\{g_2^2 \ln g_2^2 + \frac{g_1^2}{\alpha - 1} \ln g_1^2\} = t/2 \quad (13)$$

where g_1 and g_2 imply $g_1(1,t)$ and $g_2(1,t)$.

At the time, t_p, that the pore mouth will plug, g_1 becomes zero. Letting the corresponding value of g_2 be denoted by w from eq. (7) it follows that

$$g_2^2 \equiv w^2 = \frac{\alpha}{\alpha - 1} \quad (14)$$

Then eq. (13) can be rearranged so that

$$t_p = 2(w - 1) + Kw^2 \ln w \quad (15)$$

which gives the dimensionless time required to plug the pore as a function of the dimensionless parameter K.

3. Perturbation Solution for Small Times

In order to obtain analytical solutions for the nonlinear model given in section 1, valid for small times, a Taylor series expansion is assumed for $g_2(x,t)$:

$$g_2(x,t) \doteq 1 + th_1(x) + t^2 h_2(x) + \ldots \quad (16)$$

It then follows that

$$g_1(x,t) \doteq 1 + (1 - \alpha)th_1(x) + \ldots \quad (17)$$

and

$$\frac{1}{1 + Kg_2 \ln(g_2/g_1)} \doteq 1 - \alpha K t h_1(x)$$

provided that $\alpha Kt \ll 1$. Similarly it follows that

$$H(g_1) \equiv g_1^2 D(g_1) = \frac{\mathcal{D} g_1^3}{(1 + \mathcal{D} g_1)} \doteq D_1(1 - D_2 th_1)$$

$$D_1 \equiv \frac{\mathcal{D}}{1 + \mathcal{D}} \qquad D_2 \equiv (\alpha - 1)\frac{3 + 2\mathcal{D}}{1 + \mathcal{D}}$$

By assuming that

$$c(x,t) \doteq c_0(x) + tc_1(x) + \ldots \quad (18)$$

eq. (9) results in the following two-point boundary value problems

In Chemical Reaction Engineering—Houston; Weekman, V., et al.;
ACS Symposium Series; American Chemical Society: Washington, DC, 1978.

$$\frac{d^2c_0}{dx^2} = \phi^2 c_0 \qquad \phi^2 = 2K\sigma/D_1;\ c_0'(0)=0;\ c_0(1)=1 \tag{19}$$

$$\frac{d^2c_1}{dx^2} - \phi^2 c_1 = \phi^2(1-\alpha K+D_2)h_1(x)c_0(x) + D_2\frac{dh_1}{dx}\frac{dc_0}{dx} \tag{20}$$

$$c_1'(0)=0; \quad c_1(1)=0$$

By making similar substitutions in eq. (10) describing the reaction front change, it follows that

$$\frac{d}{dt}[1+th_1(x)+t^2h_2(x)] = \frac{1}{2}(c_0 + tc_1)(1-\alpha K t h_1)$$

which leads to

$$h_1(x) = \frac{1}{2}c_0(x); \quad h_2(x) = \frac{1}{8}[2c_1(x)-\alpha K c_0^2(x)] \tag{21}$$

Equations (19) and (20) can now be solved to give

$$c_0(x) = \cosh\phi x/\cosh\phi \tag{22}$$

and

$$c_1(x) = B_0 + B_1\cosh\phi x + B_2\cosh 2\phi x \tag{23}$$

with

$$B_0 = \frac{-1}{4\cosh^2\phi}(1-\alpha K) \qquad B_1 = \frac{1-\alpha K}{4\cosh^3\phi} - \frac{B_2}{\cosh\phi}$$

$$B_2 = (2D_2+1-\alpha K)\frac{\cosh 2\phi}{12\cosh^2\phi} \tag{24}$$

By utilization of eq. (21) one writes

$$g_2(x,t) = 1+\tfrac{1}{2}c_0(x)t+\tfrac{1}{8}[2c_1(x)-\alpha K c_0(x)h_1(x)]t^2 \tag{25}$$

and at x = 1

$$g_2(1,t) = 1 + \tfrac{1}{2}t - \tfrac{1}{8}\alpha K t^2 \tag{26}$$

The above approximate solutions for the concentration profiles as well as the variation of g_1 and g_2 with time will be accurate when the value of K is small which implies that kinetic resistance is dominating.

In Chemical Reaction Engineering—Houston; Weekman, V., et al.;
ACS Symposium Series; American Chemical Society: Washington, DC, 1978.

When kinetic resistance is not dominating, the full set of equations (9) and (10) need be solved numerically.

4. Comparison with Experimental Data for Sulfation of Fully Calcined Limestone

The pore plugging model for gas-solid reactions given by eqs. (9) and (10) is integrated numerically by the use of orthogonal collocations (9). The values of c, g_1, g_2, are evaluated at the collocation points as functions of time. In order to evaluate conversion as a function of time, an outer radius, r_w, is defined so that for each pore the volume of the available solid reactant is given by $2\pi(r_w^2 - r_0^2)L$. The value of r_w is chosen so that the initial porosity is given by $\varepsilon_0 = r_0^2/r_w^2$. Then the local conversion of reactant solid is given by

$$y(x,t) = \frac{f_2^2 - r_0^2}{r_w^2 - r_0^2} = \frac{1}{\gamma^2 - 1}\left(g_2^2(x,t) - 1\right) \qquad (27)$$

and the overall conversion by

$$Y(t) = \int_0^1 y(x,t)dx = \frac{1}{(\gamma^2-1)}\left(\int_0^1 g_2^2(x,t)dx - 1\right) \qquad (28)$$

where $\gamma = 1/\sqrt{\varepsilon_0}$.

Ramachandran and Smith (7) assumed the surface area per unit volume of the pore, given by $r_0/2$, is equal to that of the solid particles from which the experimental data are obtained. Furthermore the effective length of the pore L is chosen so that the Thiele modulus at zero time given by eq. (19) is equal to that characterizing reaction and diffusion in a sphere of radius R with first order kinetics. It then follows that

$$r_0 = 2V_g/S_g \qquad L = R/3\sqrt{\varepsilon_0} \qquad (29)$$

The additional parameters that remain to be defined in the single pore model are k and D_s. The rate constant can be estimated from initial reaction rate data and the appropriate value of D_s determined by matching the above model to actual experimental data.

The pore plugging model predictions are now compared with experimental data obtained by Hartman and Coughlin (6,10) on the sulfation of calcined limestone.

In Chemical Reaction Engineering—Houston; Weekman, V., et al.;
ACS Symposium Series; American Chemical Society: Washington, DC, 1978.

Reaction conditions and pertinent stone properties are listed below:

$T=1123°K$; $P=1$ atm; $C_B=3.147\times10^{-8}$ gr-mole/cm^3 (0.29%SO_2); $\varepsilon_0=0.535$; $r_0\doteq1.02\times10^{-4}$cm; $R_p=2.82\times10^{-2}$cm; $\alpha=3.09$.

From the initial rate data and effective pore properties, the following single pore parameters are estimated.

$r_w=1.39\times10^{-4}$cm; $L=1.284\times10^{-2}$cm; $k=0.10$cm/sec

Predictions of the pore plugging mode for different values of D_s and k are compared with the experimental data in Figures (2) and (3) respectively.

For this particular limestone the maximum theoretical conversion (i.e., total pore blockage) is estimated to be 55 percent; the maximum conversion obtained experimentally was only 44 percent. Predictions of the pore plugging model are seen to be moderately accurate except for the upper limit on conversion. It should be noted that the single pore model results given in (7) compare more favorably with the experimental data; we have not been able to match these results. Ramachandran and Smith do not consider the variation of the pore diffusion coefficient with changing pore radius; however, for the cases presented in Figures (2) and (3), this effect is not significant because pore diffusion is not limiting until about 75 percent of the pore plug time is reached.

5. Perturbation -- Collocation Method of Solution

For values of the process parameters that yield high values of ϕ ($\phi>5$), the pore diffusional resistance becomes significant and the method of orthogonal collocations requires a very large number of collocation points in order to accurately calculate the resulting stiff concentration profiles. In section 3, it was shown that at time equal to zero the initial concentration profile was equal to $\cosh\phi x/\cosh\phi$. In order to improve calculations for stiff profiles for all times $c(x,t)$ is written as

$$c(x,t) = c_o(x)u(x,t) \qquad (30)$$

where $c_o(x)$ is given by eq. (22). Introduction of eq. (23) into eq. (9) yields

$$\frac{\partial^2 u}{\partial x^2} + \left[2\phi\tanh\phi x + \frac{1}{H(g_1)} \frac{\partial H(g_1)}{\partial x} \right] \frac{\partial u}{\partial x}$$

In Chemical Reaction Engineering—Houston; Weekman, V., et al.;
ACS Symposium Series; American Chemical Society: Washington, DC, 1978.

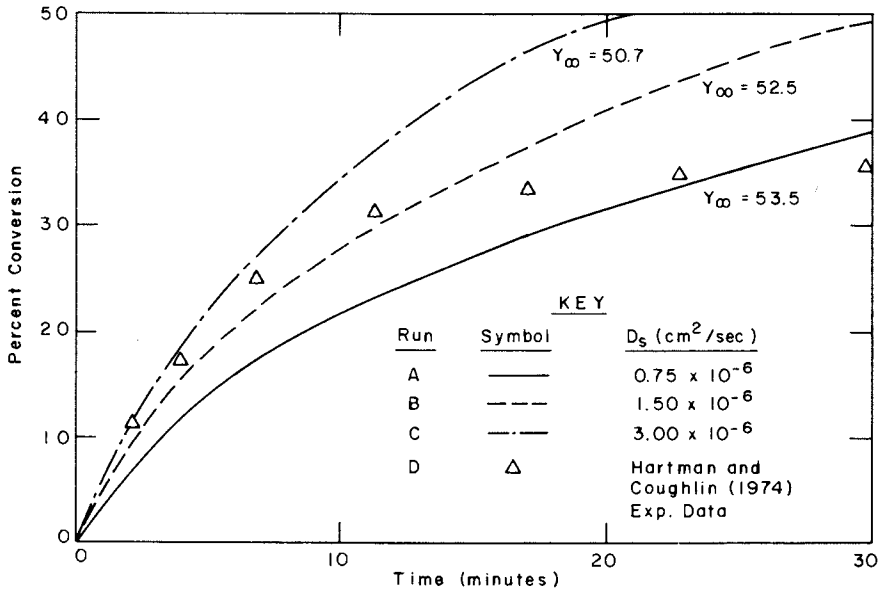

Figure 2. Pore plugging model predictions of the % total conversion change with time for different values of D_s. $k = 0.1$ *cm/sec,* $\alpha = 3.09$, $r_0 = 1.02 \times 10^{-4}$ *cm,* $L = 0.129$ *cm,* $\gamma = 1.367$, $D_m = 1.02$ cm^2/sec, $\vartheta = 4.53$.

In Chemical Reaction Engineering—Houston; Weekman, V., et al.;
ACS Symposium Series; American Chemical Society: Washington, DC, 1978.

$$+ [\phi^2 - \phi^2 D_1 \frac{F(g_2)}{H(g_1)} + \frac{\phi \tanh\phi}{H(g_1)} \frac{\partial H(g_1)}{\partial x}] u = 0 \qquad (31)$$

with initial and boundary conditions:

$$g_2(x,0)=g_1(x,0)=1;\ u(x,0)=1;\ u_x(0,t)=0;\ u(1,t)=1 \qquad (32)$$

In Figure 4, c(x,t) profiles are given for the case where $\phi^2=2$ $K/D_1=176$ obtained through the proposed perturbation/collaction method with only 4 collocation points. Efforts to solve eqs. (9) and (10) by the regular collocation method failed to give accurate results with as many as 10 collocation points. Accuracy was determined by examining whether negative concentrations, however small, were calculated at any collocation point.

6. Conclusions

A generalized gas-solid reaction model for a single pore was presented. It accounted for changes in the pore geometry and diffusion coefficient when the molar volume of the solid product is different from that of the solid reactant. The change with time of the radius of the mouth of the pore and the plugging time were analytically obtained, and a qualitative agreement with experimental data was observed. A perturbation solution for small times was utilized in order to introduce a novel approach for the solution of two point boundary value problem. This new method called perturbation/collocation method was found very successful for high values of the Thiele modulus where the regular collocation method was found unsatisfactory.

7. Notation

A_1 $(1-\varepsilon_R)r_0(w-1)c_B V_R a$; cm

A_2 $(1-\varepsilon_R)r_0^2 w^2 \ln w/2c_B V_R a$; cm^2

a moles of reactant solid reacted per mole of gas reacted

b moles of product solid produced per mole of gas reacted

c c_*/c_B

$\hat{c}$ $\hat{c}_*/c_B$

c_* concentration of gaseous reactant in the pore; gr-mole/cm^3

In Chemical Reaction Engineering—Houston; Weekman, V., et al.;
ACS Symposium Series; American Chemical Society: Washington, DC, 1978.

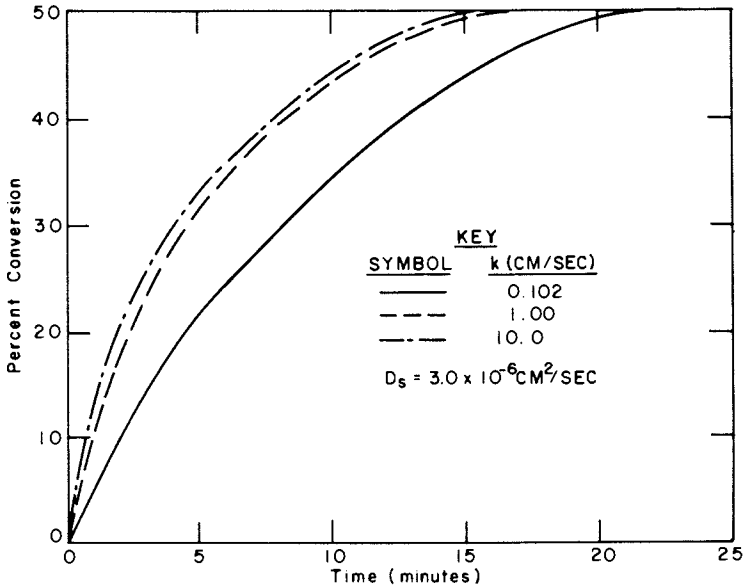

Figure 3. Pore plugging model prediction of the % total conversion change with time for different values of k. *Same constants as in Figure 2 except* k *and* D_s.

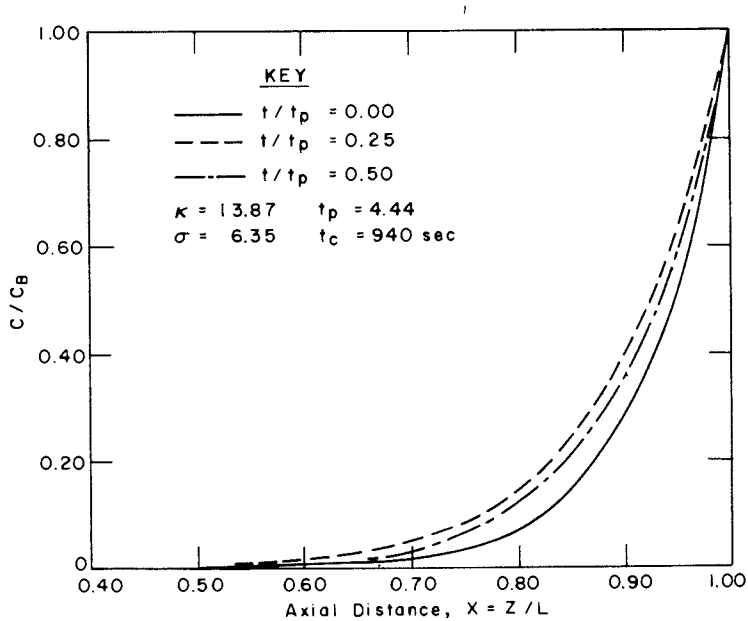

Figure 4. Steep axial concentration profiles for different times obtained by the perturbation/collocation method

In Chemical Reaction Engineering—Houston; Weekman, V., et al.;
ACS Symposium Series; American Chemical Society: Washington, DC, 1978.

$\hat{c}_*$	concentration of gaseous reactant in solid product layer; gr-mole/cm^3
c_B	bulk concentration of gaseous reactant outside the pore; gr-mole/cm^3
$D(g_1)$	$D_*(f_1)/D_m = \mathcal{D}g_1/(1+\mathcal{D}g_1)$
$D_*(f_1)$	$(1/D_m+1/D_K(f_1))^{-1}$ overall diffusion coefficien in pore; cm^2/sec
D_m	molecular diffusion coefficient of reactant gas; cm^2/sec
$D_K(f)$	Knudsen diffusion coefficient = $9700f_1\sqrt{T/MW}$; cm^2/sec
D_K°	$D_K(r_0)$
D_s	gaseous reactant diffusion coefficient through solid product layer; cm^2/sec
$\mathcal{D}$	D_K°/D_m
f_1	radial distance of the gas-solid interface from the pore center; cm
f_2	radial distance of the solid-solid interface from the pore center; cm
g_1	f_1/r_0
g_2	f_2/r_0
$H(g_1)$	$g_1^2D(g_1)$
k	reaction rate constant; cm/sec
L	length of pore;cm
MW	molecular weight of diffusing gas; gr/gr-mole
r	r_*/r_0
r_*	radial distance from the center of the pore;cm
r_0	initial pore radius; cm
R_p	radius of spherical particle; cm
r_w	outer radius of the solid reactant available to a given pore; cm
T	temperature; °K
t	t_*/t_c
t_*	time; sec
t_c	characteristic time = $(1-\varepsilon_R)r_0/2kV_Rc_Ba$
t_f	pore plugging time; sec
t_p	t_f/t_c (dimensionless pore plugging time)
V_p	molar volume of solid product; cm^3/gr-mole
V_R	molar volume of reactant solid; cm^3/gr-mole
y	local conversion
Y	overall conversion

In Chemical Reaction Engineering—Houston; Weekman, V., et al.;
ACS Symposium Series; American Chemical Society: Washington, DC, 1978.

Y maximum conversion at time of pore blockage
x z/L
w $\sqrt{\alpha/(\alpha-1)}$
z distance from the end of the pore; cm

Hellenic Letters

α $(1-\varepsilon_R)V_p b/(1-\varepsilon_p)V_R a$
β $L^2/D_m t_c$
γ r_w/r_0
ε_0 initial porosity
ε_p microporosity of solid product
ε_R microporosity of reactant solid
K $r_0 k/D_s$
σ $L^2 D_s/r_0^2 D_m$

8. Literature Cited

(1) Pigford, R.L., Sliger, G., Ind. Eng. Chem. Process Des. Develop. (1973)12, 85.
(2) Szekely, J., Evans, J.W., Chem. Eng. Sci.(1970) 25, 1091.
(3) Szekely, J., Evans, J.W., Chem. Eng. Sci. (1974) 29, 630.
(4) Sohn, H.Y., Szekely, J., Chem. Eng. Sci. (1974) 29, 630.
(5) Hartman, M., Coughlin, R., AIChE J. (1976) 22, 490.
(6) Howard, J.B., Williams, G.C., Ghazal, F.P.H., "Mathematical Model of the Reaction Between Sulfur Dioxide and Calcine Particles," Final Report on Task No. 2 of HEW-NAPCA Services Contract No. CPA-22-69-44, Department of Chemical Engineering, Massachusetts Institute of Technology, September 1971.
(7) Ramachandran, P., Smith, J., AIChE J.(1977)23,353.
(8) Georgakis, C. et al., "Modelling of Fluidized Bed Combustion of Coal" Quarterly Technical Progress Report to ERDA (No. 3) Nov. 1, 1976 - Jan. 31, 1977, J.R. Louis, Principal Investigator, p. 145-187.
(9) Finalyson, B.A., "The Method of Weighted Residuals and Vanational Principles" Academic Press, 1972.
(10) Hartman, M., Coughlin, R., Ind. Eng. Chem. Process Des. Develop. (1974) 13, 248.

In Chemical Reaction Engineering—Houston; Weekman, V., et al.;
ACS Symposium Series; American Chemical Society: Washington, DC, 1978.

20

Heat Transfer in Packed Beds of Low Tube/Particle Diameter Ratio

A. G. DIXON and W. R. PATERSON
Department of Chemical Engineering, University of Edinburgh, Edinburgh, Scotland
D. L. CRESSWELL
Systems Engineering Group, E. T. H. Zentrum, CH-8092 Zürich, Switzerland

1. Introduction

In spite of much research (1-7), identification of the relevant heat transfer parameters in packed beds and their subsequent estimation continue to provide challenging problems, especially so for beds having a small tube to particle diameter ratio, where so few experimental data are reported.

The aims of this paper are as follows:

(1) to rigorously evaluate homogeneous continuum models as applied to heat transfer in beds of low tube to particle diameter ratio (typically $d_t/d_p \simeq 5\text{-}12$).
(2) to examine the effect of gas flow rate, particle size and conductivity on the estimated heat transfer parameters.
(3) to progress towards *a priori* prediction of the important parameters by modelling the underlying heat transfer mechanisms.

2. Experimental Equipment and Procedure

The experimental apparatus is similar to that used by Gunn and Khalid (7), although temperature measurement is different.

The bed consisted of two sections of internal diameter 70.8 mms, insulated at the plane z=0 by a sandwich of rubber and PVC gaskets (see fig. 1). Twelve thermocouples were inserted radially through the central PVC gasket to provide duplicate temperature measurements at six radial positions, distant 12,16,23,28,31 and 34 mms. from the central axis.

Both sections were packed with similar solid particles to provide a continuous length of packing. The experiments consisted of measuring the temperature distribution in the air stream leaving the top of the packing in the heated section (b) for a range of gas velocities by means of 32 Cr/Al thermocouples (30 SWG) supported at 8 radial positions (r=9,11,13,18,24,29,31 and 33 mms) and at 90^0 intervals by a brass cross, similar to that used by

© 0-8412-0401-2/78/47-065-238$05.00/0

deWasch and Froment (6). The procedure was repeated for a range of bed heights.

The temperature uniformity of the air stream entering the calming section (a) and of the heated wall (b) was checked by additional thermocouples. Altogether, 107 separate experiments were performed (plus several repeats) covering the range of variables shown in Table 1.

Table 1: Ranges of Experimental Variables

d_p (mms)	d_t/d_p	$N_{Re}=(\frac{Gd_p}{\mu})$	Bed Height (L) (cms)
ceramic beads k_s=0.23 w/m ^oK			
12.7	5.6	35-535	5-35
9.5	7.5	65-375	5-25
6.4	11.2	45-275	3-25
mild steel spheres k_s = 38 w/m ^oK			
9.5	7.5	75-470	5 - 25

3. Some Important Overall Observations

Typical measured radial temperature profiles are shown in Fig. 2. These show two particularly interesting features:

(1) There is a significant, but apparently random, variation of temperature with angular position. In some instances, this variation is comparable to the total radial temperature change.

(2) There is a reproducible "hump" in the radial temperature profile roughly 0.5 dp from the wall. The hump is particularly noticeable in shallow beds, but tends to be smoothed out with increasing depth.

De Wasch and Froment (6) also observed a hump, although at a somewhat greater distance from the wall.
Neither of these phenomena are accounted for by existing models.

4. Homogeneous Continuum Heat Transfer Models

We shall confine our study to homogeneous continuum models of heat transfer, since these have been the most widely used in practice.

(A) The Axially Dispersed Plug Flow Model

In this model the gross heat transfer behaviour is characterized by effective thermal conductivities k_a and k_r for heat transfer

In Chemical Reaction Engineering—Houston; Weekman, V., et al.;
ACS Symposium Series; American Chemical Society: Washington, DC, 1978.

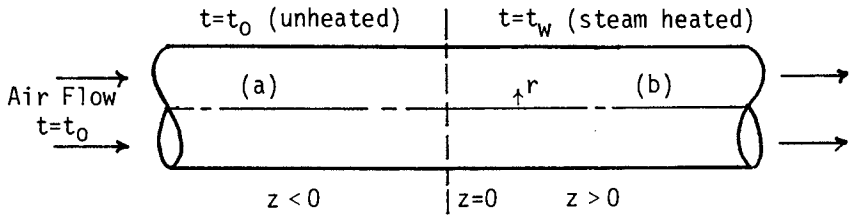

Figure 1. Schematic description of test column

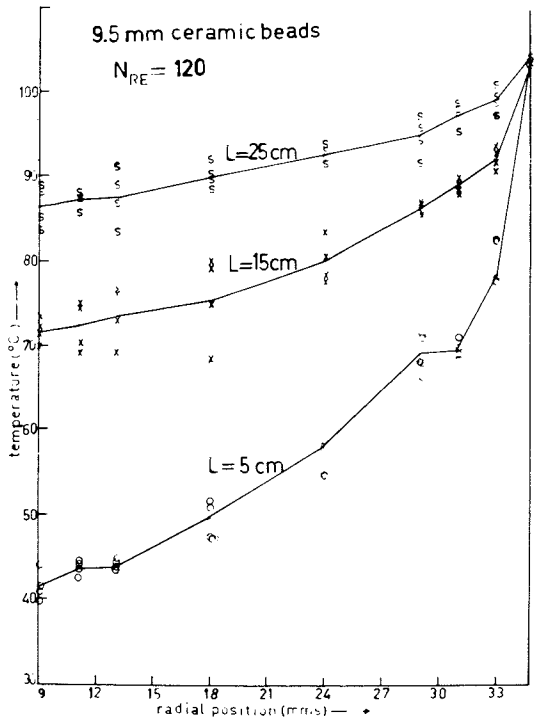

Figure 2. Typical observed temperature profiles

In Chemical Reaction Engineering—Houston; Weekman, V., et al.;
ACS Symposium Series; American Chemical Society: Washington, DC, 1978.

in the axial and radial directions, and a wall heat transfer coefficient h_w, introduced to account for the increased thermal resistance of the wall region.

Heat balances are required on both sections of the column and boundary conditions are needed at both ends and at the adjoining plane z=0. For the heated section, the heat balance takes the form of an elliptic P.D.E.

$$Gc_p \frac{\partial t}{\partial z} = k_r \left(\frac{\partial^2 t}{\partial r^2} + \frac{1}{r}\frac{\partial t}{\partial r}\right) + k_a \frac{\partial^2 t}{\partial z^2} \quad (z>0) \tag{1}$$

A similar equation applies for the calming section if we replace z>0 by z<0 and t by t_c. In the radial direction the equations are subject to the boundary conditions

$$\left.\frac{\partial t}{\partial r} = \frac{\partial t_c}{\partial r} = 0 \quad \text{at } r=0 \right\diagup \begin{array}{l} -k_r \frac{\partial t}{\partial r} = h_w (t-t_w), \; r=R, \; z>0 \\ -k_r \frac{\partial t_c}{\partial r} = h_w (t_c-t_o), \; r=R, \; z<0 \end{array} \tag{2}$$

Boundary conditions in the axial direction follow readily for the long calming section and the adjoining plane (z=0):

$$t_c \to t_o \; ; \qquad z \to -\infty \tag{3}$$

$$t_c = t; \qquad \frac{\partial t_c}{\partial z} = \frac{\partial t}{\partial z} \; ; \qquad z=0 \tag{4}$$

The boundary condition at the bed exit (z=L) is much less certain. If the bed were long we might use the condition

$$t \to t_w; \qquad z \to +\infty \qquad \text{(IBC)} \tag{5}$$

as was done by Gunn and Khalid (7). However, in many of our experiments the beds were necessarily quite short ($L \ll 50\, d_p$), otherwise it would have been impossible to observe significant radial temperature gradients. In these cases, an alternative condition would be

$$\frac{\partial t}{\partial z} = 0; \qquad z=L \qquad \text{(FBC)} \tag{6}$$

which assumes plug flow in the space above the packing. We have analyzed our data using both boundary conditions.

For the infinite bed boundary condition (IBC) the equations can be integrated to give for the test section (7)

$$\left(\frac{t_w-t}{t_w-t_o}\right) = \sum_{n=1}^{\infty} \frac{Bi(1+A_n)\, J_o(\alpha_n y)}{A_n(Bi^2+\alpha^2_n).\, J_o(\alpha_n)} \exp\left\{\frac{-Pe_a(A_n-1)z}{2\, d_p}\right\} \tag{7}$$

where $A_n = (1+16\, \alpha^2_n / \beta^2 Pe_r\, Pe_a)^{\frac{1}{2}}$

In Chemical Reaction Engineering—Houston; Weekman, V., et al.;
ACS Symposium Series; American Chemical Society: Washington, DC, 1978.

Pe_a, $Pe_r = \frac{Gc_p dp}{k_a}$, $\frac{Gc_p d_p}{k_r}$ (axial and radial Peclet numbers)

$Bi = h_w R/k_r$ (wall Biot number), $y = r/R$, $\beta = d_t/d_p$

and α_n are the roots of $\alpha_n J_1(\alpha_n) = Bi\ J_o(\alpha_n)$, $n = 1, 2 \ldots \infty$

For the (FBC), the solution becomes

$$\left(\frac{t_w - t}{t_w - t_o}\right) = \sum_{n=1}^{\infty} \frac{Bi(1+A_n)\, J_o(\alpha_n y)}{A_n(Bi^2+\alpha_n^2)J_o(\alpha_n)} \times \left\{\exp\left\{\frac{-Pe_a(A_n-1)z}{2d_p}\right\}\right. \quad (8)$$

$$\left. + \left(\frac{A_n-1}{A_n+1}\right) \exp\left\{\frac{-Pe_a}{2d_p}\{A_n\,(2L-z)-z\}\right\}\right\}$$

(B) The Plug Flow Model ($Pe_a = \infty$)

A special case which has received much attention (1-2, 4-6) is the plug flow model, resulting from Eqn (7) in the limit $Pe_a \to \infty$:

$$\left(\frac{t_w - t}{t_w - t_o}\right) = 2 \sum_{n=1}^{\infty} \frac{Bi\ J_o(\alpha_n y)}{(Bi^2+\alpha_n^2)J_o(\alpha_n)} \exp\left(\frac{-4\alpha_n^2 z}{\beta^2 d_p Pe_r}\right) \quad (9$$

5. Data Analysis

The models were subjected to two stages of analysis:

(A) Overall Analysis

A stringent test of the models is provided by fitting them simultaneously to data measured at several bed depths. In the axial dispersion model, the parameters Pe_a, Pe_r and Bi were est ated by minimising the sum of squares of residuals on the 32 be exit temperatures:

$$F = \sum_{1}^{N} \sum_{1}^{32} (t_{exp,0} - t_{calc,0})^2 \quad (10$$

where N is the number of bed depths; $t_{calc,o}$ is calculated from either Eqn. (7) or (8), depending upon which boundary condition is adopted at the bed exit, at the appropriate radial measuring points for z=L.

(B) Depth by Depth Analysis

The ability of the models to fit the data at individual bed depths (N=1) was next examined in order to detect any trend in t parameters with bed depth.

The non-linear function minimisations of Eqn.(10) and its simpler cases were carried out by the Marquardt search algorithm

In Chemical Reaction Engineering—Houston; Weekman, V., et al.;
ACS Symposium Series; American Chemical Society: Washington, DC, 1978.

(Fortran sub-routine E04 FBF NAG library, NAG Ltd., Oxford). A preliminary grid search was made to check for irregularities in the sum of squares surface and provide a starting point for the search.

Previous analysis of experimental errors (8) substantiated the validity of the unweighted least squares criterion (10) for estimation of the model parameters.

6. Evaluation of Models

Results of Depth by Depth Analysis

Neither model showed significant lack of fit to the data at the 95% confidence level. However, the plug flow model parameters were found to decrease systematically with increasing bed depth. Fig. (3) shows this effect quite clearly in the case of the effective radial conductivity. No such effect was observed with the axial dispersion model, as is apparent from Fig. (4).

DeWasch and Froment (6) also noted the dependence of the plug flow model parameters with bed depth. They therefore only correlated their data obtained on the longest beds hoping to minimize axial dispersion effects. However, if Figs. (3) and (4) are superimposed, the estimates of k_r obtained from the axial dispersion model are significantly greater than those obtained on the longest bed using the plug flow model, even at the quite large Reynolds numbers of industrial practice. The two sets of estimates ultimately merge at large Reynolds numbers. No doubt the differences would have been even greater had a larger bed been used.

This behaviour of the plug flow model may be a significant factor in explaining some of the scatter in literature correlations obtained on beds of different length.

Results of Overall Analysis

When all the bed depths were analysed simultaneously, the plug flow model was clearly rejected for all the different particles and Reynolds numbers considered. The ratio $F_{calc}/F_{0.05}$ was found to be between 1.5 and 8, where F_{calc} is the estimated F ratio from analysis of variance and $F_{0.05}$ is the appropriate statistic at the 5% significance level.

For all the beads the axial dispersion model (Eqn. 7) showed no significant lack of fit at any Reynolds number, $F_{calc}/F_{0.05}$ lying between 0.4 and 0.9. Fig. (5) shows a typical fit of this model. Fig. (5), however, is unusual in that the calculated and experimental entrance profiles (z=0) agree well. In the majority of cases this was not so, which we attribute in part to unsatisfactory measurements at the entrance.

In Chemical Reaction Engineering—Houston; Weekman, V., et al.;
ACS Symposium Series; American Chemical Society: Washington, DC, 1978.

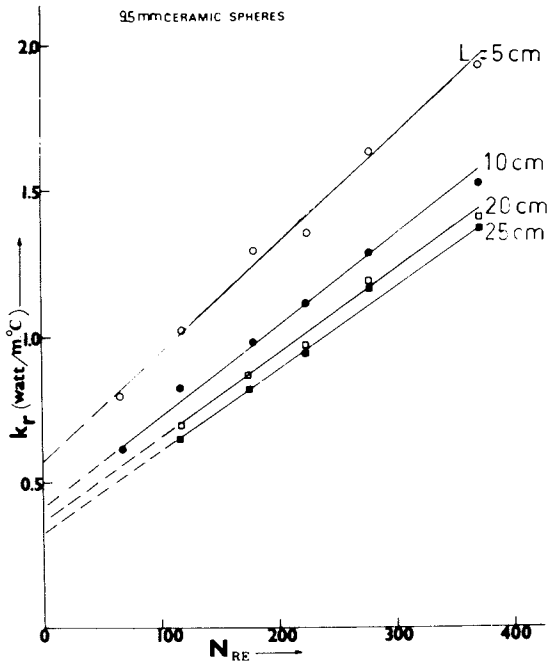

Figure 3. Correlation of k_r with bed depth for the plug flow model

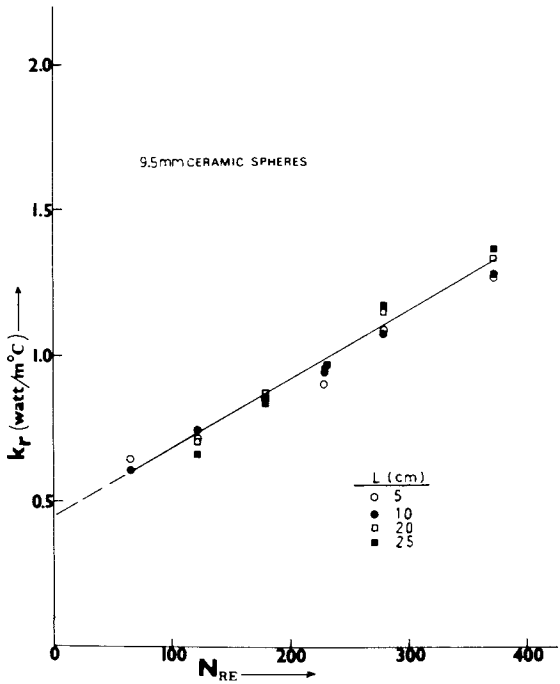

Figure 4. Independence of k_r with bed depth for the axial dispersion model

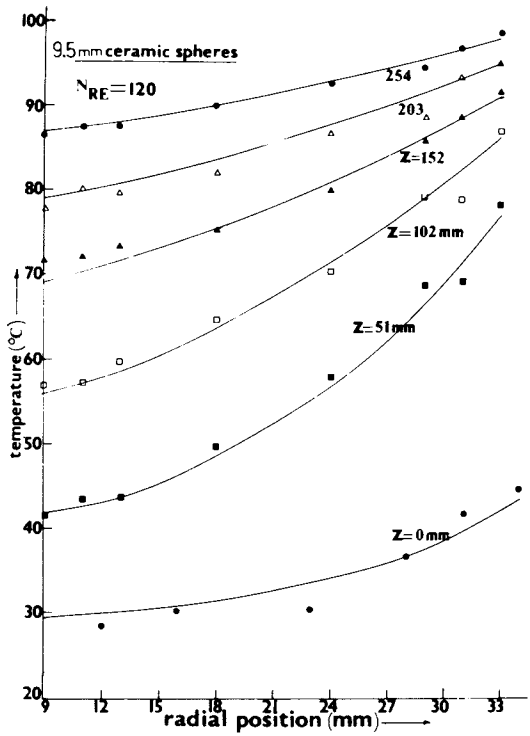

Figure 5. Fit of axial dispersion model to angular smoothed radial temperature profiles

In Chemical Reaction Engineering—Houston; Weekman, V., et al.;
ACS Symposium Series; American Chemical Society: Washington, DC, 1978.

Incorporation of the finite bed boundary condition into the model (Eqn. 8) generally led to a poorer fit, in many cases leading to a significant lack of fit. Its main effect was to increase estimates of Pe_a by some 10-20%, the other parameters Pe_r and Bi remaining virtually unaffected.

It was observed that, in general, the model fit is worst at low Reynolds number and improves progressively as the Reynolds number increases. This is probably due to the difficulty of measuring the development of the radial temperature profile, since at low Reynolds number the bed attains the wall temperature within a few particle diameters of the entrance (z=0).

A typical cross-section of the parameter cross correlations is shown in Table 2.

Table 2: Typical Parameter Cross-Correlations: 12.7 mm Ceramic Beads: Bed Depth 17.5 cms.

N_{Re}	$\rho\hat{k}_r,\hat{h}_w$	$\rho\hat{k}_r,\hat{k}_a$	$\rho\hat{k}_a,\hat{h}_w$
535	-0.72	-0.10	-0.11
430	-0.77	-0.05	-0.07
290	-0.82	+0.06	-0.07
140	-0.91	+0.34	-0.26

Estimates of (k_r,k_a) and (k_a,h_w) are virtually uncorrelated except possibly at low Reynolds number; those for (k_r,h_w) are strongly correlated at all Reynolds numbers. While k_r is not a conductivity in the true sense, it nevertheless has a sound theoretical basis, as proposed by Argo and Smith (9); h_w on the other hand is perhaps no more than an empirical parameter needed in the model to account for a decreasing k_r near the wall.

7. Correlation of Heat Transfer Data

Analysis of the data revealed that the radial conductivity (k_r) is of particular importance. It would be desirable, therefore, to develop a model which gives *a priori* prediction of this parameter in terms of flow rate, particle diameter and conductivity and compare the predictions with our experimental data.

7.1 A Model for Prediction of the Radial Conductivities

Starting along the lines of Argo and Smith (9), the radial conductivity is given by

$$k_r = k_q + k_{td} + k_{series} \qquad (11)$$

where k_g, k_{td} and k_{series} represent the molecular conductivity of the fluid, the turbulent conductivity and the effective conductivity of the solid, all based on unit of void + non-void area.

The turbulent conductivity k_{td} is given in terms of the Reynolds, Prandtl and Peclet numbers by

$$k_{td} / k_m = N_{Re} N_{Pr} / Pe_{rm} \qquad (12)$$

where k_m is the molecular conductivity of the fluid. From turbulent mixing data (10), $Pe_{rm} \simeq 10$ for $N_{Re} > 40$, and for air $N_{Pr}=0.72$. Thus, Eqn. (12) simplifies to

$$k_{td} / k_m = 0.072\ N_{Re} \qquad (N_{Re} > 40) \qquad (13)$$

Heat transfer between contacting particles is assumed to occur by a static process controlled by conduction across stagnant gas fillets at the point of contact, and a dynamic process involving a series mechanism of solid conduction, film convection and turbulent mixing, as in Fig. (6). The static and dynamic processes occur in parallel, thus

$$k_{series} = k_{st} + k_{dyn} \qquad (14)$$

The static contribution can be measured experimentally (11) or estimated from the model of Kunii and Smith (12). The dynamic term is obtained by first integrating the heat flux over the hemispherical surface between $\theta=0$ and $\theta=90^0$ in Fig. (6). After some algebra, the total heat flow is given by

$$Q_T = - \frac{2\pi R_p^2 k'_{td} \beta}{(\beta-1)} \left\{ \frac{\beta}{\beta-1} \ln\beta - 1 \right\} \cdot \left(\frac{dT}{dr}\right)_{fluid} \qquad (15)$$

where $\beta = hk_s/k'_{td}\ (h+k_s/R_p)$ and $(dT/dr)_{fluid}$ is the temperature gradient in the fluid in the direction of heat flow (assumed linear). Eqn. (15) enables an effective conductivity k'_{dyn} to be defined, based on solid projected area πR_p^2,

$$k'_{dyn} = \frac{2\ k'_{td}\ \beta}{(\beta-1)} \left(\frac{\beta}{\beta-1} \ln\beta - 1 \right) \qquad (16)$$

For a packed bed, Eqn. (16) must be modified to account for the bed voidage and for the number of contacts (n) a pellet makes with its neighbours, corrected for the cross-sectional areas normal to the direction of heat flow and for the frequency of the orientations. Assuming an actual bed is a composite of loose and close packings then, according to Kunii and Smith (12), $n \simeq 2$ for beds of voidage $\varepsilon=0.44$ to 0.46, as measured in our studies. Thus,

$$k_{dyn} = 4\ k_{td} \frac{\beta}{(\beta-1)} \left\{ \frac{\beta}{\beta-1} \ln\beta - 1 \right\} \qquad (17)$$

In Chemical Reaction Engineering—Houston; Weekman, V., et al.;
ACS Symposium Series; American Chemical Society: Washington, DC, 1978.

Eqns. (11), (13), (14) and (17) permit a priori prediction of k_r in terms of the underlying heat transfer processes. No adjustable parameters are involved. A comparison of this model with our data is shown in Fig. (7). Static conductivities were measured separately using Sehr's electrical heating method (11) and the correlation of DeAcetis and Thodos (13) was used to estimate h.

The results show an encouraging agreement over a wide range of flow rate, particle size and conductivity. In particular, it is found that

(a) k_r increases linearly with N_{Re} for $N_{Re}>40$ but does not extrapolate linearly to the static results.
(b) k_r is virtually independent of pellet diameter.
(c) k_r is only weakly dependent on pellet conductivity (k_s) - a 100-fold increase in k_s produces a 50% increase in k_r

Also shown in Fig. (7), for comparison, is the contribution to k_r due to turbulent conduction (k_{td}). It is apparent that heat transfer through the solid forms a significant, if not dominant, fraction of the total radial heat transfer within the Reynolds number range of interest.

7.2 The Wall Biot Number

If the data are plotted as $(Bi) \times (d_p/d_t)^{\frac{1}{2}}$ vs. N_{Re} then the results for different particle sizes and conductivity are brought together on a single curve, at least to within the scatter of the data. The results show that the Biot number decreases with Reynolds number, according to (see Fig. 8).

$$(Bi)\ (d_p/d_t)^{\frac{1}{2}} = 5.3\ N_{Re}^{-0.262} \qquad (18)$$

which correlates the data to within 15% in the range $100<N_{Re}<500$. At lower Reynolds numbers, the uncertainty regions of the estimates become large, reflecting the insensitivity of the model to changes in the wall heat transfer coefficient, h_w. The fact that Biot numbers for steel packing are similar to those for ceramic packing, yet k_r is some 30-50% greater, shows that the wall heat transfer coefficient (h_w) depends on the particle conductivity (k_s). Thus, a significant fraction of the heat transferred at the wall is through solid/wall contacts, possibly by a series mechanism, as suggested in Section (7.1) for k_r. This result could also explain some of the scatter in correlations of h_w vs. N_{Re}, which is particularly bad for $N_{Re}<10^3$, where various workers have used particles of widely differing conductivity in their experiments.

7.3 The Axial Conductivity (k_a)

The axial Peclet numbers (Pe_a) are not well-determined; they fall within the range 0.2 ± 0.05 to 1.0 ± 0.5, in broad agreement

In Chemical Reaction Engineering—Houston; Weekman, V., et al.;
ACS Symposium Series; American Chemical Society: Washington, DC, 1978.

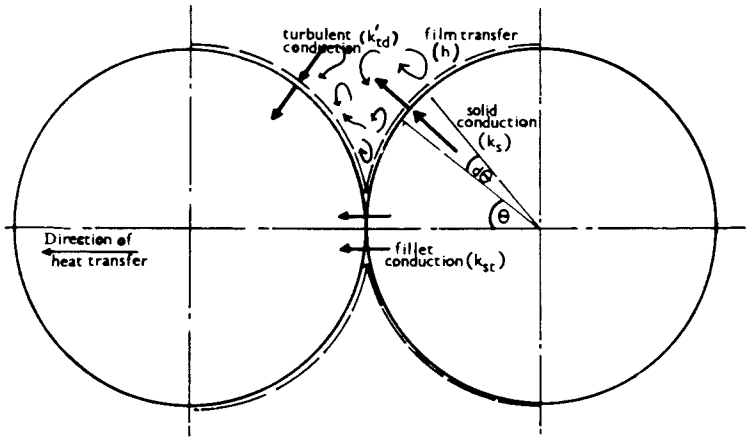

Figure 6. Heat transfer mechanisms for solid/solid heat transfer in a packed bed

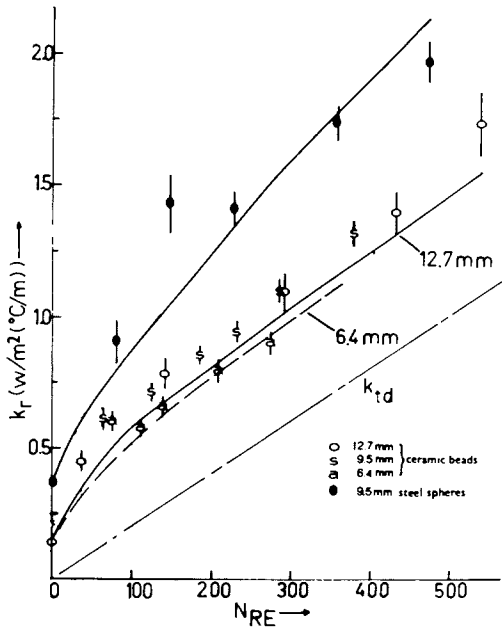

Figure 7. Correlation of effective radial conductivity data

In Chemical Reaction Engineering—Houston; Weekman, V., et al.;
ACS Symposium Series; American Chemical Society: Washington, DC, 1978.

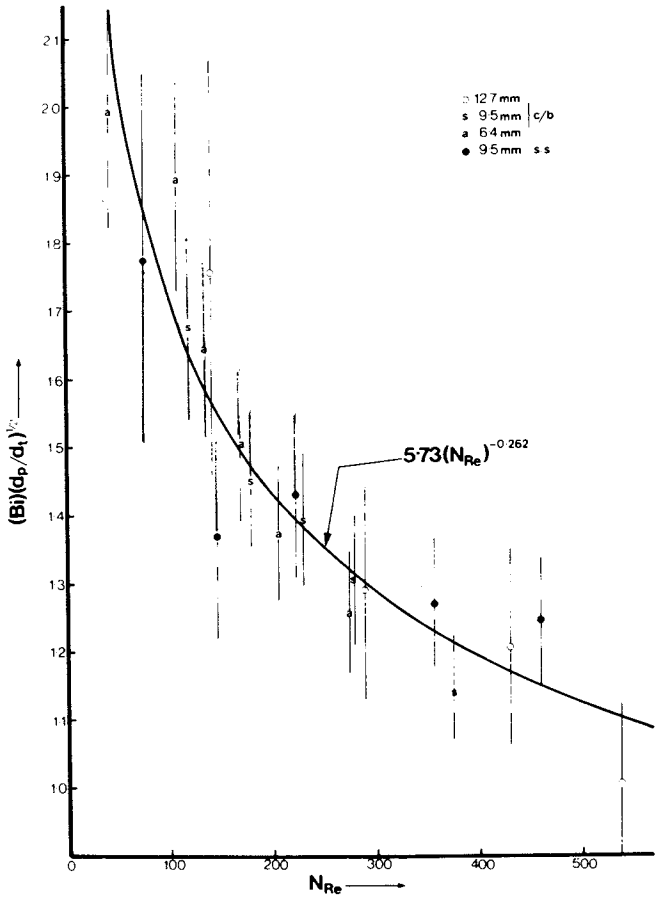

Figure 8. Correlation of wall biot number data

In Chemical Reaction Engineering—Houston; Weekman, V., et al.;
ACS Symposium Series; American Chemical Society: Washington, DC, 1978.

with the results of Votruba et al (14), amongst others. There is no clear dependence on either particle diameter or material, but there does appear to be a tendency for k_a to increase with N_{Re}. More reliable estimates could be obtained only by devising a satisfactory method of taking measurements at the plane z=0.

Summary

An experimental evaluation of homogeneous continum models of steady state heat transfer in packed beds of low tube/particle diameter ratio has been carried out. It was found that both axial and radial conduction effects were important in such beds for $N_{Re} \leq 500$, which covers the flow range in many industrial reactors. Heat transfer resistance at the wall was significant, but of secondary importance.

A model containing no adjustable parameters was developed for a priori prediction of the effective radial conductivity in terms of Reynolds number, particle size and conductivity. This model gave reliable prediction of the effects of these variables over a wide range. Measured radial temperature profiles contained significant, apparently random, angular variations and indicated the existence of a "hump", roughly 0.5 dp from the wall. Neither of these observations are predictable using existing heat transfer models.

Nomenclature: (Symbols not defined in text)

c_p	specific heat	kj/kg °C
G	superficial mass flow velocity	kg/m^2 hr.
J_o	zero-th order Bessel function, first kind.	
J_1	first order Bessel function, first kind.	
k_{td}	turbulent conductivity (based on unit solids area)	w/m °C

Greek Symbols:

ε	bed voidage	
μ	fluid viscosity	kg/m.hr.

Dimensionless Groups:

$N_{Pr} = (\mu c_p/k_m)$	Prandtl number
$N_{Re} = (Gd_p/\mu)$	Reynolds number
$Pe_{rm} =$	Peclet number for radial dispersion of mass.

Literature Cited:

1. Coberly, C.A., Marshall, W.R., Chem. Eng.Prog. (1951),47, 141.
2. Calderbank, P.H., Pogorsky, L.A., Trans. Inst. Chem. Eng., (1957) 35, 195.
3. Yagi, S., Wakao, N., A.I.Ch.E.J. (1959), 5, 79.
4. Yagi, S., Kunii, D., A.I.Ch.E.J. (1960), 6, 71

In Chemical Reaction Engineering—Houston; Weekman, V., et al.;
ACS Symposium Series; American Chemical Society: Washington, DC, 1978.

5. Agnew, J.B. Potter, O.E., Trans. Inst. Chem. Eng., (1970), 48, T15.
6. DeWasch, A.P., Froment, G.F., Chem.Eng.Sci., (1972), 27, 567.
7. Gunn, D.J., Dhalid, M., Chem.Eng.Sci., (1975), 30, 261.
8. Paterson, W.R., Ph.D. Thesis, University of Edinburgh (1975).
9. Argo, W.G., Smith, J.M., Chem.Eng.Prog. (1953), 49, 443.
10. Bernard, R.A., Wilhelm, R.H., Chem.Eng.Prog. (1950), 46, 233.
11. Sehr, R.A., Chem.Eng.Sci. (1958) 9, 145.
12. Kunii, D., Smith, J.M., A.I.Ch.E.J. (1960), 6, 71.
13. DeAcetis, J., Thodos, G., Ind.Eng.Chem. (1960), 52, 1003.
14. Votruba, J., Hlavacek, V., Marek, M. Chem.Eng.Sci. (1972) 27 1845.

In Chemical Reaction Engineering—Houston; Weekman, V., et al.;
ACS Symposium Series; American Chemical Society: Washington, DC, 1978.

21

Catalyst Deactivation through Pore Mouth Plugging during Residue Desulfurization

F. M. DAUTZENBERG, J. VAN KLINKEN, K. M. A. PRONK, S. T. SIE, and J-B. WIJFFELS*

Koninklijke/Shell-Laboratorium, Shell Research B.V., Badhuisweg 3, Amsterdam, The Netherlands

I. Introduction

Hydrodesulfurization of residual feedstocks with a high metals content is a commercial proposition today (1,2). Based on previous work of many investigators (e.g. ref. 3 through 9) Shell's major efforts were focussed on the development of a suitable catalyst, for which a better understanding of the ageing phenomena occurring in the catalyst particle was needed.

The present paper deals with the development of a simple two-parameter model describing the deactivation behaviour of residue-desulfurization catalysts. The validity of the model is being checked against the results of a large number of experiments with a variety of catalysts, two feedstocks and under different operating conditions.

II. Experimental

A. Equipment and Test Conditions Most experiments were performed at a fixed standard temperature and pressure in bench-scale equipment (about 100 ml catalyst volume) provided with facilities for recycle of H_2S-free liquid product (recycle ratio: 10 volumes of liquid product per volume of fresh feed). This mode of operation was adopted to ensure good catalyst wetting in small-scale reactors. It has been established that in this way reproducible and meaningful results can be obtained. At the high recycle ratios applied, the kinetics of the system approach that of a continuous stirred-tank system. An essential feature of this system is that the catalyst deactivates uniformly, i.e., catalyst properties are constant throughout the bed at any time during a run. This is in contrast with the non-uniform deactivation occurring in a plug-flow reactor (fixed bed without recycle). In the latter system, a deactivation front gradually proceeds through the catalyst bed.

In most experiments we used a space velocity of 4.35 kg fresh feed per kg catalyst per hour, while an exit gas rate of 250 Nl H_2 per kg fresh feed was maintained. In a few cases we used different laboratory test conditions. These differences have been indicated in the figures and tables.

* Present address: Shell Internationale Petroleum Mij B.V., The Hague

© 0-8412-0401-2/78/47-065-254$05.00/0

In Chemical Reaction Engineering—Houston; Weekman, V., et al.; ACS Symposium Series; American Chemical Society: Washington, DC, 1978.

B. Feedstocks Properties of the Caribbean long residue (Feed I) and the Middle East long residue (Feed II) used as feedstocks in these studies are listed in Table I.

C. Catalysts Commercial as well as experimental catalysts were tested. In Table II we have listed the compositions of the various catalysts. Details on shaping and preparation are also included in this table. Catalyst A has been tested as 1.5-mm extrudates, but also as 0.5- and 0.8-mm broken particles. Similarly, Catalyst J was tested as 1.5-mm extrudates and as 0.8-mm particles. Before testing, all the catalysts were presulfided in situ.

D. Catalyst Activity It has been found that hydrodesulfurization of heavy gas-oil fractions in fixed-bed operation with a large product recycle (simulated stirred-tank operation) can be described as pseudo one-and-a-half order in sulfur concentration, whereas vanadium removal can be described as pseudo first order in vanadium concentration. We therefore used the following formula to calculate catalyst activity for desulfurization and metal removal:

$$k_s = \frac{S_f - S_p}{S_p^{1.5}} \cdot SV \qquad k_v = \frac{V_f - V_p}{V_p} \cdot SV$$

III. The Mechanism of Catalyst Deactivation

A major problem in the catalytic hydrodesulfurization of residual oils is the deactivation of the catalyst by metal-containing asphaltenic species in the feed. As can be seen from the results of a typical desulfurization experiment presented in Fig. 1, the catalyst shows a rapid initial decline which is attended with a fast build-up of coke on the catalyst. At a relatively low catalyst age Θ, as defined in Section IV, a stationary coke level is reached. In contrast, the deposition of the inorganic remnants of the hydrocracked asphaltenes (mainly vanadium and nickel sulfides) continues and gradually clogs the pores in the outer zone of the catalyst particles, as confirmed by electron microprobe analyses of spent catalyst samples (see Fig. 2). This causes a slow further loss in desulfurization activity over a longer period of time. Ultimately, the catalyst becomes totally inactive for desulfurization because the - still active - inner core has become completely inaccessible to the sulfur-bearing molecules.

IV. Deactivation of a Single Catalyst Particle

Since the deposition of metal compounds determines catalyst life we developed a model in which we used the deposition of metals as the principal parameter to describe the deactivation phenomena for equilibrium-coked catalyst. When coke deposition becomes over-

In Chemical Reaction Engineering—Houston; Weekman, V., et al.;
ACS Symposium Series; American Chemical Society: Washington, DC, 1978.

TABLE I

PROPERTIES OF FEEDSTOCKS

Feed	I	II
Origin	Caribbean	Middle East
UOP distillation		
5 %v at °C	352	315
10 %v at °C	372	337
20 %v at °C	398	372
30 %v at °C	423	408
40 %v at °C	451	443
50 %v at °C	487	483
Density, d 70/4, g/ml	0.9184	0.9183
Mol. weight	527	488
Chemical analysis,		
C, %w on feed	85.88	84.25
H, %w on feed	11.58	11.32
S, %w on feed	2.06	3.86
N, %w on feed	0.312	0.211
Ni, ppm w on feed	25	14
V, ppm w on feed	208	48
Na, ppm w on feed	7	3

TABLE II

CATALYST PROPERTIES

Catalyst ref. no.	Composition	Metal load %w on support	Particle size/shape	Bulk density	Support	
					Type	Particle size/shape
A	Co/Mo	4.3/10.9	1.5 mm extrudates	0.77 g/ml	Al_2O_3	-
B	Co/Mo	4.3/10.9	0.8 mm extrudates	0.78 g/ml	Al_2O_3	-
C	Ni/Mo	4.3/10.9	0.8 mm crushed beads	0.58 g/ml	Sol-gel Al_2O_3	1.5 mm beads
D	Ni/Mo	4.3/10.9	1.5 mm beads	0.62 g/ml	Sol-gel Al_2O_3	1.5 mm beads
E	Ni/Mo	4.3/10.9	1.5 mm extrudates	0.65 g/ml	Al_2O_3	1.5 mm extrudates
F	Co/Mo	4.3/10.9	1.5 mm extrudates	0.66 g/ml	Al_2O_3	1.5 mm extrudates
G	Co/Mo	4.3/10.9	1.6 mm extrudates	0.72 g/ml	Al_2O_3	1.6 mm extrudates
H	Ni/Mo	4.3/10.9	1.7 mm beads	0.58 g/ml	Al_2O_3	1.7 mm beads
I	Ni/Mo	4.3/10.9	1.7 mm beads	0.58 g/ml	Al_2O_3	1.7 mm beads
J	Ni/Mo	2/16	1.5 mm extrudates	0.58 g/ml	$SiO_2.Al_2O_3$	1.5 mm extrudates
K	Ni/Mo	1/8	0.8 mm crushed extrudates	0.41 g/ml	$SiO_2.Al_2O_3$	1.5 mm extrudates
L	Ni/Mo	2/16	0.8 mm crushed extrudates	0.47 g/ml	$SiO_2.Al_2O_3$	1.5 mm extrudates
M	Ni/Mo	2/16	0.9 mm extrudates	0.48 g/ml	$SiO_2.Al_2O_3$	-
N	Ni/Mo	2/16	1.2 mm extrudates	0.49 g/ml	$SiO_2.Al_2O_3$	partly dried gel
O	Ni/Mo	2/16	1.2 mm extrudates	0.48 g/ml	$SiO_2.Al_2O_3$	partly dried gel
P	Ni/Mo	1/8	1.2 mm extrudates	0.48 g/ml	$SiO_2.Al_2O_3$	partly dried gel
Q	Ni/Mo	1/8	1.5 mm extrudates	0.44 g/ml	$SiO_2.Al_2O_3$	partly dried gel
R	Co/Mo	4.3/10.9	1.5 mm extrudates	0.61 g/ml	Al_2O_3	1.5 mm extrudates
S	Co/Mo	4.3/10.9	1.5 mm extrudates	0.58 g/ml	Al_2O_3	1.5 mm extrudates

Catalysts A, B, and S have been commercially prepared.
Catalysts C through I plus catalyst R have been prepared in the laboratory on commercial supports.

In Chemical Reaction Engineering—Houston; Weekman, V., et al.;
ACS Symposium Series; American Chemical Society: Washington, DC, 1978.

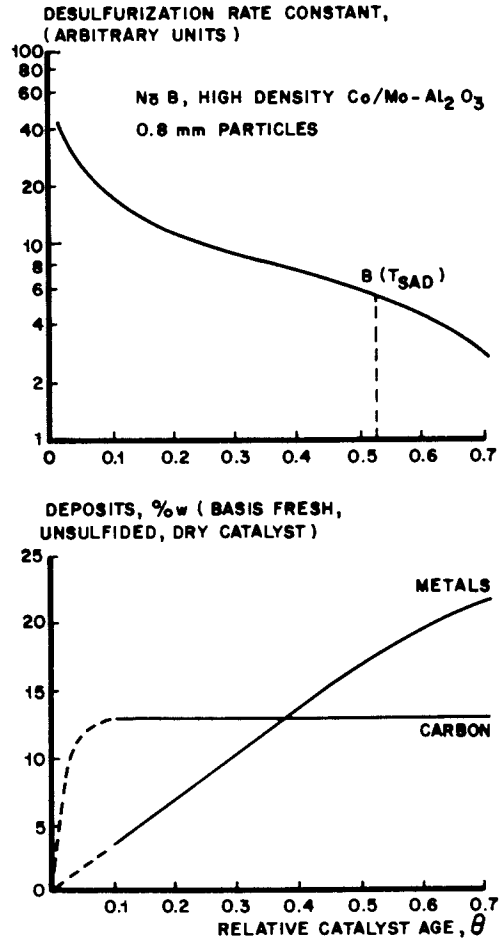

Figure 1. Hydrodesulfurization of a Caribbean long residue (feed I)

In Chemical Reaction Engineering—Houston; Weekman, V., et al.;
ACS Symposium Series; American Chemical Society: Washington, DC, 1978.

ruling, the model cannot be used. This situation may arise with a catalyst operating at too low hydrogen partial pressures. For simplicity we therefore assume that in residue hydrodesulfurization (the initial build-up of coke will not be taken into account) only two reactions take place in parallel: metal removal and hydrodesulfurization. Sulfur is removed as H_2S and ends up in the gas stream; the product of the metal-removal reaction is a metal sulfide that is deposited on the wall of the catalyst pores. These metal sulfides reduce the original desulfurization activity, but leave the metal-removal activity unaffected; hence, new deposits are formed on top of old layers. As in most residual feedstocks vanadium predominates over other metals, it is considered to represent total metals. Furthermore, both the desulfurization and the devanadization reaction are diffusionally controlled inside a catalyst particle.

According to this line of thought, the concentrations of the metal-bearing compounds decrease towards the inside of the catalyst particle, and thus the rate of deposit formation is highest precisely at the pore entrance. As time proceeds, new deposits are formed on top of old layers, increasing their thickness. Thus, the pore radius in the periphery of the catalyst particle is reduced. As the pore radius decreases (which means that the surface area per unit pore volume is enlarged), the metal-removal reaction zone further recedes to the outer surface region of the catalyst particle and a "diaphragm" of metal sulfides is constructed in the mouths of the pores.

We will now describe these effects in quantitative terms. At any point in a pore*, the rate at which the thickness of the deposit layer increases (or the rate at which the pore radius is reduced) is proportional to the volume deposited per unit surface area per unit time:

$$-\frac{\partial r}{\partial t} = k.C.V_{dep} \qquad (1)$$

Since the vanadium concentration is highest at the outside of the catalyst particle (C_o), the pore radius at the entrance r_o is reduced fastest and, after integration of the above equation, is given by:

$$r_o = r_i(1 - \Theta), \qquad (2)$$

in which r_i denotes the pore radius of the fresh catalyst. The "relative catalyst age" Θ, which characterizes the degree of deactivation of the catalyst, is then defined by:

$$\Theta = \frac{k.V_{dep}}{r_i} \int_0^t C_o dt, \qquad (3)$$

and is numerically equal to the fraction of the pore mouth radius blocked by metal-sulfide deposits.

* For reasons of simplicity the pores are considered to be cylinders of equal size and circular cross section.

In Chemical Reaction Engineering—Houston; Weekman, V., et al.;
ACS Symposium Series; American Chemical Society: Washington, DC, 1978.

One has to look the catalyst into its pore mouth in order to tell its age. With a fresh catalyst* the pore mouth is fully open and $\theta = 0$. As soon as $\theta = 1$, the catalyst has obviously died through complete closure of the "diaphragm" of metal deposits.

A catalyst that is exposed to the full metal concentration of the feed (C_F) will have a life which we will define as the "minimum life". The minimum lifetime T_{min} is found from eq. (3):

$$T_{min} = \frac{r_i}{k.C_F.V_{dep}} \tag{4}$$

A catalyst that is in contact with a liquid of lower metal concentrations will remain active for a longer period.

Since the deactivation is a relatively slow process, the vanadium mole balance for the pore can be written as:

$$\frac{\partial}{\partial l}\left\{r^2 D \frac{\partial C}{\partial l}\right\} = 2 r k C, \tag{5}$$

where l denotes the length of the pore measured from the outer surface of the particle, $l = \tau y$, where y is the superficial length of the pore and τ the tortuosity. D denotes the diffusion coefficient of the vanadium-bearing molecules in the pore. The curvature of the shell in which the metal removal takes place has been neglected for simplicity.

For a fresh catalyst $r = r_i$ and eq. (5) may be solved directly to yield:

$$C = C_o \, e^{-\phi \frac{y}{R}}, \tag{6}$$

where ϕ is the Thiele modulus defined by:

$$\phi = \tau R \sqrt{\frac{2k}{r_i D}}$$

and R is the characteristic particle radius. If, now, expression (6) is introduced into eq. (1) we find as a first approximation for the pore radius of an aged catalyst:

$$r = r_i\left(1 - \theta e^{-\phi \frac{y}{R}}\right), \tag{7}$$

and if in turn this expression is introduced into the vanadium balance (5), the vanadium concentration inside the pores of an aged catalyst is found after integration as:

$$C = C_o \left\{ e^{-\phi \frac{y}{R}} + \theta\left(e^{-2\phi \frac{y}{R}} - e^{-\phi \frac{y}{R}}\right)\right\}. \tag{8}$$

* Since we neglected the initial build-up of coke this refers to a fictitious state of the catalyst where coke has reached its steady-state level, but where no significant metals have been deposited yet, so that the pores are considered to be still fully open, $\theta = 0$.

In Chemical Reaction Engineering—Houston; Weekman, V., et al.;
ACS Symposium Series; American Chemical Society: Washington, DC, 1978.

By this method of perturbation using the relative catalyst age Θ as the perturbation parameter the equation for the rate of change of the pore radius can be solved to any desired degree of accuracy, together with the mole balance of the vanadium-bearing molecules over the pore. Expression (8) is an approximation for the exact profile neglecting terms of order Θ^2 and higher. The concentration on the outside of the catalyst particle C_o serves as a link between the "inside" and the "outside happening".

The effectiveness for metal removal of the catalyst decreases with increasing age owing to the plugging of the pore mouths. The effectiveness factor is defined as the ratio of the rate of metal removal for the aged catalyst to that for fresh catalyst:

$$\eta_m = \frac{\pi r_o^2 D \left(\frac{\partial C}{\partial l}\right)_{l=0}}{\pi r_i^2 D \left(\frac{\partial C}{\partial l}\right)_{l=0,\ \Theta=0}} \qquad (9)$$

and can be calculated directly from the solution (expressions (7) and (8)) to give:

$$\eta_m = 1 - \Theta \qquad (10)$$

if terms of order Θ^2 and higher are neglected*.

V. Metal Removal and Catalyst Life in a (Simulated) Stirred-Tank Reactor

The decline in metal-removal activity of catalyst used in simulated stirred-tank reactor experiments may now be evaluated using the vanadium weight balance:

$$SV.(V_f - V_p) = \eta_m . k_v^o . V_p \qquad (11)$$

If the effectiveness factor is approximated by $\eta_m = 1 - \Theta$, expression (11) can be integrated with respect to time using relations (3) and (4) to yield:

$$\frac{t}{T_{min}} = \left(1 + \frac{k_v^o}{SV}\right).\Theta - \tfrac{1}{2}.\frac{k_v^o}{SV}.\Theta^2 \qquad (12)$$

By means of expressions (10), (11) and (12) it can be derived that the metal content of the product (for instance, V_p) as a function of the actual on-stream time t (in hours) is given by:

$$\left(\frac{V_f}{V_p}\right)^2 = \left(\frac{V_f}{V_p^o}\right)^2 - 2.\frac{V_f - V_p^o}{V_p^o} \cdot \frac{t}{T_{min}} \qquad (13)$$

According to eq. (13), a plot of $(V_f/V_p)^2$ against run time should be linear, which indeed proved to be true for all our experimental data obtained so far. Figure 3 shows a few typical examples.

* From a more elaborate solution we found $\eta_m = 1 - \Theta + \frac{1}{8}\Theta^2$ up to order Θ^4. As Θ values of practical interest are smaller than 0.5 (see section V), the simple solution represents an excellent approximation.

In Chemical Reaction Engineering—Houston; Weekman, V., et al.;
ACS Symposium Series; American Chemical Society: Washington, DC, 1978.

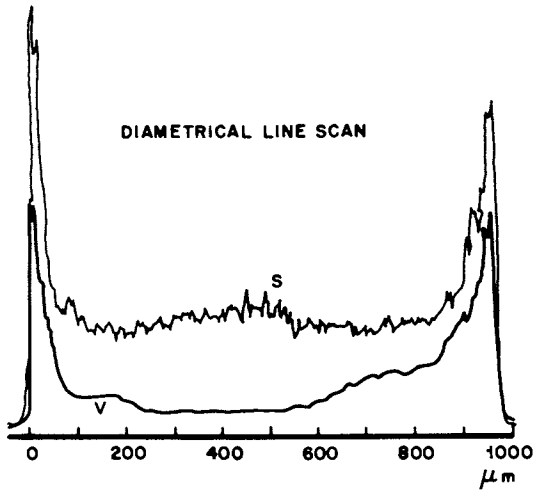

Figure 2. Electron-probe microanalyses of a deactivated catalyst; semiquantitative vanadium and sulfur concentration profiles

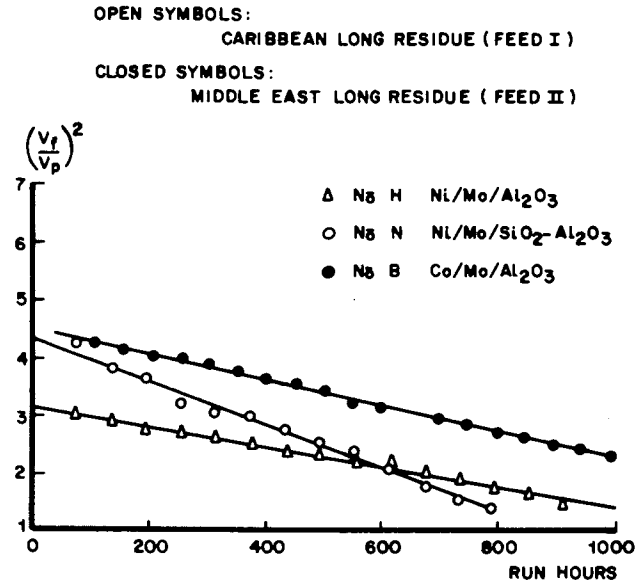

Figure 3. Vanadium removal during hydrodesulfurization of Caribbean and Middle East long residues

In Chemical Reaction Engineering—Houston; Weekman, V., et al.;
ACS Symposium Series; American Chemical Society: Washington, DC, 1978.

From the intercept of the plot with the ordinate k_v^o can be calculated, using the vanadium balance (eq. 11) at time zero:

$$k_v^o = \frac{V_p^o}{V_f - V_p^o} \cdot SV \qquad (14)$$

Furthermore T_{min}, the minimum lifetime, can now be calculated from the slope of the linear plot.

It will be clear that the relative catalyst age ϑ can now be determined using expression (12), introducing T_{min} and k_v^o, two parameters which have been measured experimentally by following the vanadium content of the liquid product.

Long before the catalyst has lived through its active period the desulfurization activity has decreased considerably, reaching a point where finally the desulfurization activity is seen to drop rapidly to a very low level (point B in Fig. 2). At this point the catalyst has reached an age (T_{SAD}) which will be referred to as the start of accelerated decline.

As illustrated in Fig. 4, a catalyst will reach T_{SAD} when the effectiveness for metal removal η_m has dropped to 0.5. In Fig. 4 we have plotted the values of η_m at T_{SAD} for various catalysts and tests conditions as a function of experimentally estimated T_{SAD} from the desulfurization performance. On the basis of these observations we used $\eta_m = 0.5$ as a new definition of T_{SAD}. For simulated stirred-tank experiments the following expression can then be derived, which allows us to calculate T_{SAD} for desulfurization, using experimental metal-removal data:

$$T_{SAD} = T_{min} \cdot \left[0.53 \frac{V_f}{V_p^o} - 0.14 \frac{V_f - V_p^o}{V_p^o} \right] \cdot SV \qquad (15)^*$$

The validity of expression (15), based on the catalyst pore-mouth plugging model, has been demonstrated in many experiments performed with Caribbean as well as Middle-East long residues as feeds, irrespective of the conditions used.

VI. Effect of Metal Deposition on the Desulfurization Activity

According to the proposed model the decline of the desulfurization activity of a catalyst is governed by the deposition of metals present in the feed. Therefore it is expected that catalyst desulfurization activity is a function of the relative catalyst age ϑ. This thesis was tested for a set of experiments in which the Caribbean long residue (feed I) was processed over 1.5-mm Co/Mo/Al_2O_3 extrudates (catalyst no. R) at various space velocities, viz. 4.35, 2.0 and 1.0 $kg.kg^{-1}.h^{-1}$.

* In this expression the more elaborate expression for η_m has been used.

In Chemical Reaction Engineering—Houston; Weekman, V., et al.;
ACS Symposium Series; American Chemical Society: Washington, DC, 1978.

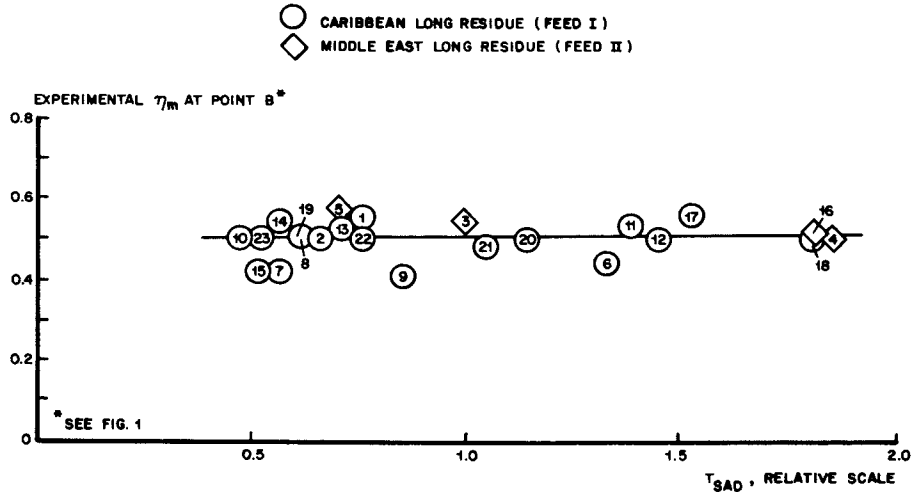

Exp.	Catalyst		Particle		Remarks
	Ref.	Composition	diam., mm	shape	
1	A	$Co/Mo/Al_2O_3$	0.5	granules	-
2	A		0.8	granules	-
3	A		1.5	Extr.	-
4	B	$Co/Mo/Al_2O_3$	0.8	Extr.	low-pressure experiment
5	B		0.8	Extr.	high-pressure experiment
6	C	$Ni/Mo/Al_2O_3$	0.8	granules	-
7	D	$Ni/Mo/Al_2O_3$	1.5	Beads	-
8	E	$Ni/Mo/Al_2O_3$	1.5	Extr.	-
9	F	$Co/Mo/Al_2O_3$	1.5	Extr.	-
10	G	$Co/Mo/Al_2O_3$	1.6	Extr.	-
11	H	$Ni/Mo/Al_2O_3$	1.7	Beads	-
12	I	$Ni/Mo/Al_2O_3$	1.7	Beads	-
13	J	$Ni/Mo/SiO_2.Al_2O_3$	0.8	granules	SV = 4.0 $kg.kg^{-1}.h^{-1}$
14	J		1.5	Extr.	SV = 4.0 $kg.kg^{-1}.h^{-1}$
15	J		1.5	Extr.	-
16	J		1.5	Extr.	-
17	K	$Ni/Mo/SiO_2.Al_2O_3$	0.8	granules	SV = 4.0 $kg.kg^{-1}.h^{-1}$
18	L	$Ni/Mo/SiO_2.Al_2O_3$	0.8	granules	SV = 4.0 $kg.kg^{-1}.h^{-1}$
19	M	$Ni/Mo/SiO_2.Al_2O_3$	0.9	Extr.	-
20	N	$Ni/Mo/SiO_2.Al_2O_3$	1.2	Extr.	-
21	O	$Ni/Mo/SiO_2.Al_2O_3$	1.2	Extr.	-
22	P	$Ni/Mo/SiO_2.Al_2O_3$	1.3	Extr.	-
23	Q	$Ni/Mo/SiO_2.Al_2O_3$	1.6	Extr.	-

Figure 4. Effectivity of vanadium removal at point B for various catalysts and test conditions*

In Chemical Reaction Engineering—Houston; Weekman, V., et al.;
ACS Symposium Series; American Chemical Society: Washington, DC, 1978.

For all three space velocities we plotted $(V_f/V_p)^2$ versus t and found straight lines in agreement with eq. (13) from which we subsequently calculated the initial vanadium content, V_p^o, the overall first-order rate constant, k_v^o, and the minimum lifetime of catalysts, T_{min}. These were found to be constant within about 10 %, which is about the experimental uncertainty. We therefore conclude that the pore-mouth plugging model is useful as a tool to predict for instance T_{SAD} at low space velocities from experiments at rather high space velocity.

Since we know the initial vanadium in product, V_p^o, for each space velocity and T_{min}, we can calculate the relative catalyst age, Θ, as a function of run time t using eq. (12). In order to compare the desulfurization activities on a common scale, we will define a relative catalyst activity for desulfurization:

$$\eta'_s = \frac{k_s}{k_s(\Theta = 0.25)}. \qquad (16)$$

Since the initial desulfurization rate constant is rather difficult to determine accurately the desulfurization activity at $\Theta = 0.25$ has been chosen as reference activity. For all three space velocities we subsequently plotted the relative catalyst activity for desulfurization as a function of Θ (see Fig. 5A). The figure shows that irrespective of the space velocity applied the same plot is obtained.

Encouraged by these results, we analysed in the same way runs performed at different pressures and temperatures. We also compared different feedstocks. The results have been plotted in Fig. 5B through 5D. Figure 5 clearly shows that, although the pore-mouth plugging model does not provide a theoretical expression for the dependance of η_s on Θ, it is possible to derive a unique relation between η'_s and Θ, which appears to be independent of space velocity, pressure, temperature and pressure. This not only confirms our thesis, but it also demonstrates that Θ is the correct life parameter to describe catalyst ageing behaviour.

List of Symbols

r	= actual pore radius	m
r_o	= pore mouth radius	m
r_i	= pore radius in fresh catalyst	m
C	= molar vanadium concentration, inside the pore	$kmol.m^{-3}$
C_o	= ibid, outside the catalyst particle	$kmol.m^{-3}$
C_f	= ibid, in the feed	$kmol.m^{-3}$
V_{dep}	= deposition volume per mole vanadium	$m^3.kmol$
k	= first-order surface reaction rate constant for vanadium removal	$m.s^{-1}$
k_v	= pseudo first-order reaction rate constant for vanadium removal at relative catalyst age Θ	$kg.kg^{-1}.h^{-1}$

In Chemical Reaction Engineering—Houston; Weekman, V., et al.;
ACS Symposium Series; American Chemical Society: Washington, DC, 1978.

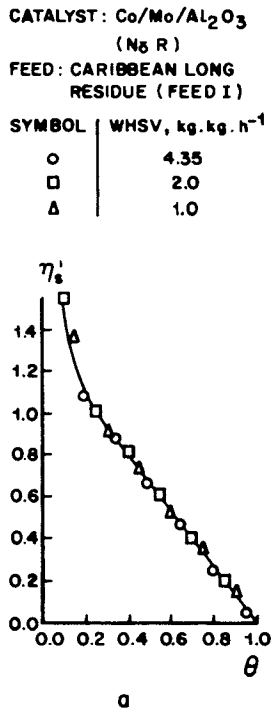

Figure 5a. Relationship between relative catalyst activity for desulfurization and relative catalyst age. Runs at various space velocities.

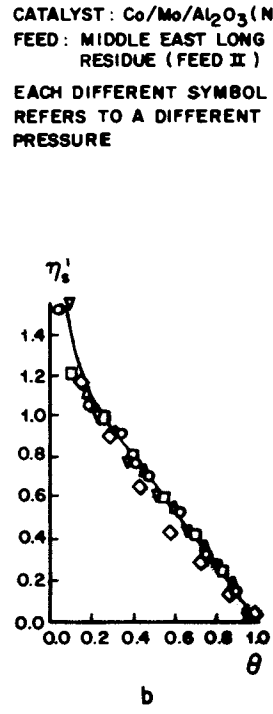

Figure 5b. Relationship between relative catalyst activity for desulfurization and relative catalyst age. Runs at different pressures.

In Chemical Reaction Engineering—Houston; Weekman, V., et al.;
ACS Symposium Series; American Chemical Society: Washington, DC, 1978.

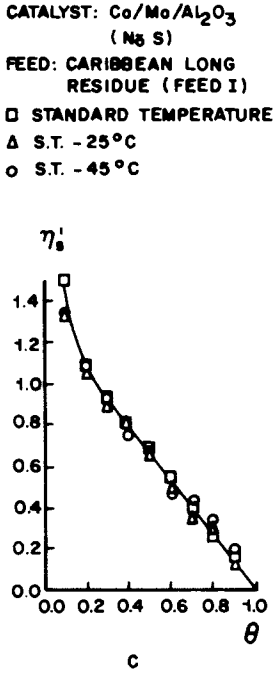

Figure 5c. Relationship between relative catalyst activity for desulfurization and relative catalyst age. Runs at various temperatures.

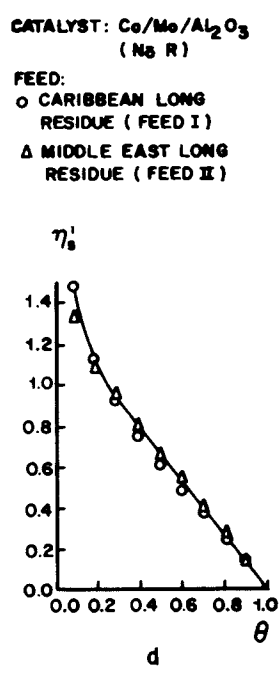

Figure 5d. Relationship between relative catalyst activity for desulfurization and relative catalyst age. Runs with different feedstocks.

In Chemical Reaction Engineering—Houston; Weekman, V., et al.;
ACS Symposium Series; American Chemical Society: Washington, DC, 1978.

k_S = pseudo 1.5th-order reaction rate constant for sulfur removal at relative catalyst age Θ — $kg.kg^{-1}.h^{-1}(\%wS)^{-\frac{1}{2}}$
t = run time — h
Θ = relative catalyst age — $-$
T_{min} = minimum lifetime of catalyst — h
T_{SAD} = catalyst age at the start of accelerated decline — h
SV = space velocity — $kg.kg^{-1}.h^{-1}$
V_f = vanadium content of the feed — $ppm(w)$
V_p = vanadium content of the product at catalyst age Θ — $ppm(w)$
S_f = sulfur content of the feed — $\%w$
S_p = sulfur content of the product at catalyst age Θ — $\%w$
η_m = catalyst effectivity for metal removal
η'_s = relative catalyst activity for desulfurization

Literature Cited

(1) Van Ginneken, A.J.J., van Kessel, M.M., Pronk, K.M.A., and Renstrom, G., Oil and Gas Journal, April 28, 1975, p. 59-63.
(2) Yamamoto, M.D., Oil and Gas Journal, May 16, 1977 p. 146-165.
(3) Hoog, H., Klinkert, H.G., and Schaafsma, A., Petrol. Refin., (1953) 32 (No. 5), 137.
(4) Le Nobel, J.W., and Choufoer, J.H., 1st World Petroleum Congress (1959), Section III, p. 233 paper 18.
(5) Van Zoonen, D., and Douwes, C.Th., J. Inst. of Petr., (1963) 49 383.
(6) Van Deemter, J.J., Proc. 3rd Eur. Symp. Chem. Reaction Eng., (1964) 215.
(7) Larson, O.A., and Beuther, H., Div. Petr. Chem. ACS Preprints, Pittsburg, (1966) B-95.
(8) Newson, E.J., Div. Petr. Chem. ACS Preprints, Chicago, (1970) A141.
(9) Moritz, K.H. et. al., Japan Petr. Inst. Fuel Oil Desulfurization Symposium Tokyo, Japan, March (1970).

In Chemical Reaction Engineering—Houston; Weekman, V., et al.;
ACS Symposium Series; American Chemical Society: Washington, DC, 1978.

22

Simulation of Thermal Cracking Furnaces

H. A. J. VERCAMMEN and G. F. FROMENT

Laboratorium voor Petrochemische Techniek Rijksuniversiteit, Krijgslaan 271, Gent, Belgium

Until now the simulation of a thermal cracking coil has generally been uncoupled from that of the fire box by imposing either a tube wall temperature profile or a heat flux profile. It is then checked a posteriori whether or not the fire box permits such profiles to be attained. The fire box calculations generally proceed along the Lobo & Evans approach (1), although more recently zone methods have been applied, thus permitting a temperature distribution in the fire box to be calculated (2, 3, 4, 5).

In the work reported here the coil and the fire box were simulated simultaneously by means of an optimized computer package in which the design of the radiant section of the furnace is an extension and refinement of Hottel's zone method (3). In this paper the approach is applied to the simulation of an industrial ethane cracking furnace. The only adaptable parameter left in the simulation model is a burner design factor, namely the fraction of the heat generated in the burner that is transferred to the burner cup. The parameter is determined by matching the exit conversion.

1. Cracking coil design equations

The continuity-, energy- and pressure drop equations for the tubular cracking reactor are well known :

$$\frac{dF_k}{dz} = -\Omega \sum_{l=1}^{L} a_{lk} r_l \qquad (1.1)$$

© 0-8412-0401-2/78/47-065-271$05.00/0

$$\frac{dt}{dz} = \frac{1}{\sum F_k c_{p_k}} \left[\pi d_t Q(z) - \Omega \sum_{l=1}^{L} r_l \Delta H_l \right] \qquad (1.2)$$

$$\frac{dp_t}{dz} = \frac{\frac{1}{v}\frac{dv}{dz} + \frac{1}{t}\frac{dt}{dz} + \zeta}{\frac{1}{p_t} - \frac{\Omega}{\beta G \Lambda}} \qquad (1.3)$$

with inlet conditions $F_k=(F_k)_o$ $T=T_o$ and $p_t=(p_t)_o$ at z=o

In (1.1) $r_1 = k_1 (\frac{F_1}{\Lambda})^{a_1} (\frac{F_2}{\Lambda})^{a_2}$

Table I
Molecular reaction scheme and kinetic parameters

A set of reactions has to be considered to predict the product distribution. The following set of molecular reactions was adopted :

	Order	Frequency Factor	E (Kcal/Kmol).10^{-3}
$C_2H_6 \rightarrow C_2H_4+H_2$	1	8.10^{16}	82
$C_2H_6 \rightarrow \frac{1}{2}C_2H_4+CH_4$	1	8.10^{12}	67
$C_2H_4 \rightarrow C_2H_2+H_2$	1	7.10^{13}	76
$C_2H_2+2H_2O \rightarrow 2CO+3H_2$	$2(H_2O)$	1.10^{13}	104.6
$C_3H_8 \rightarrow C_3H_6+H_2$	1	5.10^{13}	63.3
$C_3H_8 \rightarrow C_2H_4+CH_4$	1	$3.2.10^{13}$	63
$2C_2H_2 \rightarrow C_4$	2	$3.2.10^{11}$	45
$2C_2H_4 \rightarrow C_4$	2	4.10^{13}	60

Since the feed contained some propane the above scheme also contains decomposition reactions for this component.

In (1.3) the symbol ζ stands for :

$$\zeta = \frac{0.092}{d_t} Re^{-0.2} + \left[\frac{0.0227 R_b + 0.0847 d_t}{R_b^2} \right] \qquad (1.4)$$

In (1.4) the additional pressure drop in the return bends of the horizontal cracking coil are also accounted for.

In Chemical Reaction Engineering—Houston; Weekman, V., et al.;
ACS Symposium Series; American Chemical Society: Washington, DC, 1978.

2. Fire box heat transfer

2.1 Non radiative heat fluxes. The furnace considered in this work, schematically represented in Fig. 1, is fired by 60 radiant burners, placed in the side walls. A small fraction only of the heat of combustion is transferred to the radiant burner cup itself. The major fraction of the released heat enters the fire box with the combustion gases through radiation and convection. The exact value of this split, represented by γ, is not given in the technical literature, however. It will, therefore, be the only adaptable parameter left in the design model outlined here.

The simulation model is limited to the radiant section. The convective heat transfer to the tubes and to the refractory walls in that section was calculated by means of the usual correlations (6, 7, 8). Heat loss by conduction through the refractory walls and by natural convection at the outside of the furnace walls was also accounted for.

2.2 Radiative heat transfer. To obtain a representative temperature distribution in the radiant section of the furnace the fire box and the outside wall of the coil were divided into a number of isothermal zones as shown in Fig. 2.

The set of heat balances on the zones can be written concisely in matrix notation as shown in (2.1). In each zone Z_i (volume or surface) the net radiation captured is equated to the net non-radiative flux leaving the zone Q'_i. The radiative flux from Z_j to Z_i is given by $Z_i Z_j E_j$, where $E_j = \sigma T_j^4$ and where $Z_i Z_j$ is the total exchange area between Z_j and Z_i, in other words the fraction of the heat radiation emitted by Z_j that is absorbed by Z_i :

$$\begin{vmatrix} Z_1Z_1 - \sum_i Z_iZ_1 & Z_1Z_2 \cdots\cdots\cdots Z_1Z_n \\ Z_2Z_1 & Z_2Z_2 - \sum_i Z_iZ_2 \cdots Z_2Z_n \\ \vdots & \\ Z_nZ_1 & Z_nZ_2 \quad Z_nZ_n - \sum_i Z_iZ_n \end{vmatrix} \begin{vmatrix} E_1 \\ E_2 \\ \vdots \\ E_n \end{vmatrix} = \begin{vmatrix} Q'_1 \\ Q'_2 \\ \vdots \\ Q'_n \end{vmatrix} \quad (2.1)$$

The solution of this set of equations yields the temperatures in the volume and surface zones. Since the set is non linear it has to be solved by iteration. A Newton-Raphson procedure was found to be very efficient for this.

The total exchange areas are obtained in several

In Chemical Reaction Engineering—Houston; Weekman, V., et al.;
ACS Symposium Series; American Chemical Society: Washington, DC, 1978.

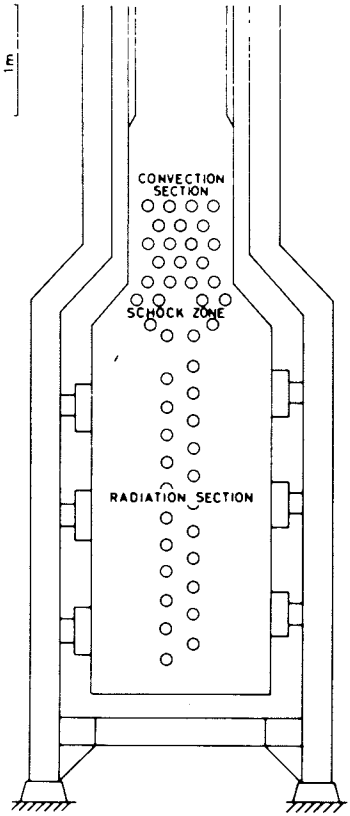

Figure 1. Representation of thermal cracking furnace

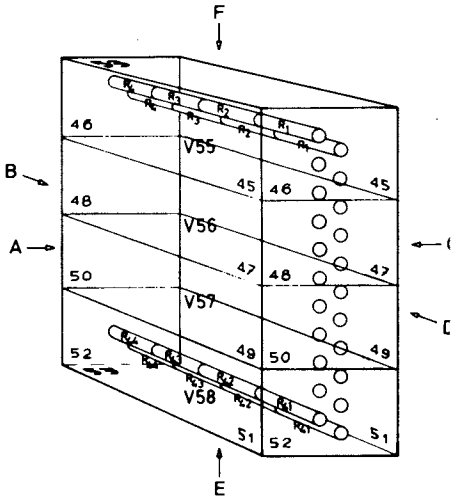

Figure 2. Subdivision of fire box and outs wall of coils into zones

In Chemical Reaction Engineering—Houston; Weekman, V., et al.;
ACS Symposium Series; American Chemical Society: Washington, DC, 1978.

steps. The first step is the calculation of the view factors i.e. the fraction of the radiation leaving an emittor that is emitted in the direction of a receptor. The multiple integrals involved in this were obtained by Monte-Carlo simulation, based upon a sample of 20000 emitted beams. To permit the calculation of viewfactors using other viewfactors obtained in different Monte Carlo integrations and still ascertain that the sum of the view factors for each emittor equals one, Vercammen & Froment (9) developed a regression technique eliminating the inherent statistical errors.

The view factors f_d obtained in this way are valid for a diathermic medium only. The view factor f between surface zones in a real, absorbing medium follows from :

$$f = f_d \, \tau^* \qquad (2.2)$$

where τ^* is the mean transmission coefficient, given by :

$$\tau^* = \int_{S_{min}}^{S_{max}} \tau(S) \; DDF(y) \; dS \qquad (2.3)$$

In (2.3) $\tau(S)$ is the transmission for a beam having a lenght S and DDF(y) is the dimensionless beam lenght distribution function, with $y = (S-S_{min}) \; (S_{max}-S_{min})$. Vercammen and Froment (9) proposed the following form for DDF(y) :

$$DDF(y) = \sqrt{y}(1-\sqrt{y})(-\ln y)^n (a+by+cy^2+\ldots)/n! \qquad (2.4)$$

This form has been found to be quite convenient for widely varying configurations of the surface zones. The temperature dependent transmission coefficient $\tau(S)$ is related to the absorption factor k^* by :

$$\tau(S) = e^{-k^* S} \qquad (2.5)$$

According to Echigo e.a. (10) the mean absorption factor k^* is calculated from :

$$C_F \Delta\omega_o (1-e^{-k^* S}) = \int_{\Delta\omega} (1-e^{-k(\omega) S}) \, d\omega \qquad (2.6)$$

When the viewfactor is multiplied by the surface of the emittor the so-called direct exchange area is obtained. The direct exchange areas between surface zones and volume zones are calculated from those related to all the surface zones bouding the volume zones, fictitious zones included.

In Chemical Reaction Engineering—Houston; Weekman, V., et al.;
ACS Symposium Series; American Chemical Society: Washington, DC, 1978.

The total exchange area takes into account the direct radiation, the absorbed radiation and in addition multiple reflection on the surface zones. Matrices of total exchange areas were set up for CO_2 and H_2O absorption bands and another one for the domain in the absorption spectrum in which no radiation was absorbed. The matrices were weighted with respect to the emitted energy associated with the domain of the frequency spectrum being considered and summed up, yielding the total exchange area matrix shown in (2.1).

3. Simulation procedure

The simulation discussed here is limited to the radiant section of the furnace, where the reaction is taking place. The simulation of the convection zone of the furnace is straight forward.

The subdivision shown in Fig. 2 yielded 110 independent non zero view factors. Fifty four real surface zones were considered, together with 3 fictitious, horizontal surface zones and 4 volume zones. Opposite parts of the side walls (e.g. A_1 and C_1) are considered to be one zone only. Sections of the two parallel coils located at an equal distance of the inlet (R_1 e.g.) are also lumped into one zone. Finally, a 58x58 matrix for the calculation of the total exchange areas was obtained.

It should be added that for the heat transfer aspects the coils were straightened to include on each side half of the bend. The furnace lenght was correspondingly adapted.

To illustrate the calculation procedure the complete mathematical model is summarized as follows :

$$\varphi_n(\bar{T}) = Q_n \tag{3.1}$$

$$\varphi_m(\bar{\bar{T}}) = Q'_m \tag{3.2}$$

$$\varphi_n(\bar{T}_n, h^*_n, t^*_n) = Q_n \tag{3.3}$$

$$\varphi_k(t, \bar{F}) = \frac{dF_k}{dz} \tag{3.4}$$

$$\varphi(t, \bar{F}, \bar{Q}) = \frac{dt}{dz} \tag{3.5}$$

$$\varphi(t, \bar{F}) = \frac{dp_t}{dz} \tag{3.6}$$

$$\varphi(t) = t^*_n \tag{3.7}$$

$$\varphi(h) = h^*_n \tag{3.8}$$

The first two equations symbolize heat balances for the zones at the flue gas side. The balances for the coil

In Chemical Reaction Engineering—Houston; Weekman, V., et al.;
ACS Symposium Series; American Chemical Society: Washington, DC, 1978.

surface (3.1) contain the heat fluxes to the reactor, represented here by Q_n to distinguish them from the other fluxes, Q'_n. The balances for the other surfaces and for the volumes (3.2) contain the non radiant fluxes $\underline{Q}'_m$ which are linear functions of the temperature vector $\underline{T}_m$ at the flue gas side, so that (3.2) could also be written as $f_m(\underline{T}) = 0$. In (3.3) those fluxes are related to the flue gas temperatures T_n, to the mean temperatures in the coil sections, t^*_i and to the heat transfer coefficients for the reactor walls, h^*_i. Equations (3.4)-(3.6) are the conservation equations for the reacting mixture inside the coil, already detailed as (1.1)-(1.3). Equations (3.7) and (3.8) aloow t^*_i and h^*_i to be calculated. A simplified flow diagram of the calculations is given in Fig. 3.

The simulation program comprises a number of modules, grouped in overlay phases. To save computation time the calculation of the matrix of total exchange areas was kept out of the inner iteration loop. This did not significantly affect the speed of convergence of the outer iteration cycle. With realistic starting estimates for Q_i and $\underline{T}$ only 5 to 10 iterations were required. The C.P.U. time per iteration amounted to 50 sec on a Siemens 4004-150, a machine which is 14 times faster than the IBM 360-30 e.g.

4. Results

The results of the simulation are given in Table II and Fig. 4. As mentioned already the only adaptable parameter in the model is the split factor γ. This factor was varied untill the simulated exit conversion matched the experimental. The agreement of the calculated product distribution with the industrial results simply reflects the reliability of the kinetic scheme of Table I. The value of 0.076 for γ is considered to be realistic. From this value a burner cup temperature of 1230°C was calculated in agreement with industrial values. In further support of this γ-value the effluent gas temperature was found to be 820°C, as compared with 830°C for the plant. Also, the flue gas temperatures are close to those observed in such a furnace. Notice that the flue gas temperatures are not too different between the four horizontal volume zones. The heat flux is seen to tend rapidly from 23Kcal/m^2 sec to a constant value of about 14Kcal/m^2 sec, again a plausible value.

To conclude a flexible and reliable modular computer package, incorporating recent progress in radiant heat transfer theory, has been developed and tested

In Chemical Reaction Engineering—Houston; Weekman, V., et al.;
ACS Symposium Series; American Chemical Society: Washington, DC, 1978.

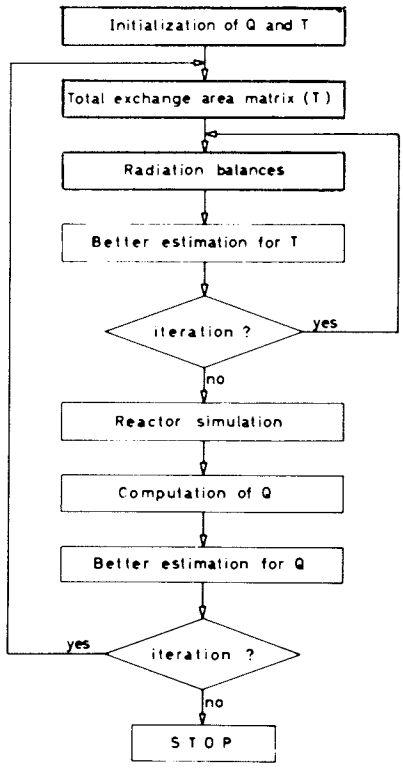

Figure 3. Flow diagram of the calculations

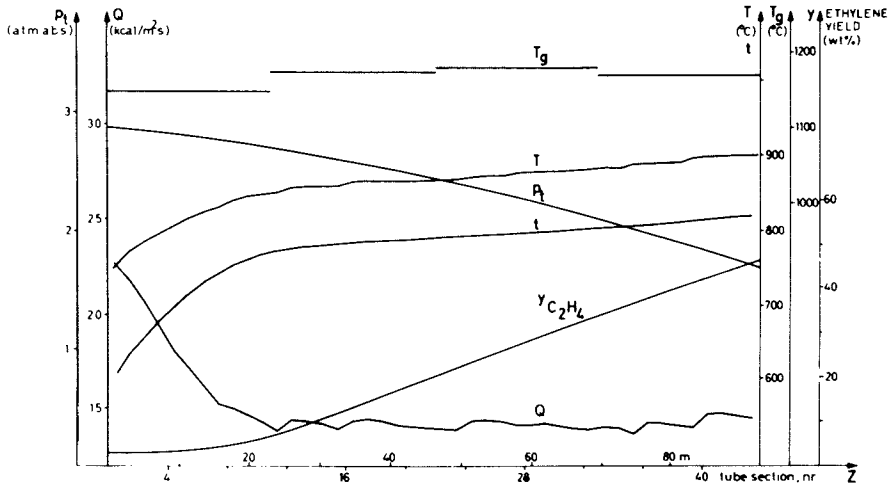

Figure 4. Results of simulation

against industrial data. Further tests on furnaces with different configurations and different cracking reactions are underway. They will provide a check for the adaptable parameter of the model.

Table II
Configuration, operating conditions and results of simulation

Reactor feed :
Feed flow rate : 45 T HC/day/coil
Dilution : 0.40 kg steam/kg HC
Composition (wt%) : C_2H_6:94.3; C_2H_4:3.2; C_3H_8:2.4; C_4:0.2
Inlet temperature in radiation section : 933°K

Reactor coil :
External diameter : 0.126 m
Internal diameter : 0.106 m
Pitch : 0.252 m
Distance between tube planes : 0.180 m
Total length : 92.5 m

Fuel gas :
Composition : CH_4:95%; H_2:5%
Feed rate : $1.5.10^5$ Kcal/hr/burner
Air excess : 15%
Number of burners : 60

Emissivities of :
Walls : 0.60
Coil : 0.96

Furnace dimensions :
Length : 8.40 m
Width : 1.63 m
Height : 3.02 m

Results :

Yields (wt%)	Industrial	Simulated
H_2	2.9	2.9
CH_4	5.5	5.7
C_2H_2	0.2	0.2
C_2H_2	45.4	45.4
C_2H_4	42.4	42.4
C_2H_6	1.3	1.3
C_3	1.9	1.9
C_4	0.25	0.14
$CO+CO_2$		
Outlet temperature (°C) :	830	820

In Chemical Reaction Engineering—Houston; Weekman, V., et al.;
ACS Symposium Series; American Chemical Society: Washington, DC, 1978.

Nomenclature

a_{lk}	stoechiometric coefficient
c_{p_k}	specific heat (Kcal/Kmol °C)
C_F	correction factor for the shape of the band profile
d_t	internal coil diameter (m)
E^j	emissive power (Kcal/m^2s)
F^k	molar flow rate (Kmol/s)
G	mass flow rate (kg/m^2s)
h	global heat transfer coefficient (Kcal/m^2s°C)
$-\Delta H_l$	heat of reaction (Kcal/Kmol)
k	absorption factor (1/m)
k_l	rate coefficient (s^{-1}) or (m^3/Kmol s)
p_t	total pressure (atm.abs.)
Q'_m	non radiant heat flux (Kcal/m^2hr)
Q_n	heat flux to reactor (Kcal/m^2s)
r_l	reaction rate (Kmol/m^3s)
R_b	radius of return bend (m)
Re	Reynolds number
S	beam lenght
t	temperature of reaction mixture (°K or °C)
$\overline{T}$	temperature vector, furnace side
z	axial reactor coordinate (m)
Z_i	zone i
$Z_i Z_j$	total exchange area for radiation from zone Z_j to zone Z_i (m^2)

Greek Letters

β	conversion factor (9.86E-6 atm m s^2/kg)
ζ	friction factor (1/m)
Λ	volumetric flow rate (m^3/s)
ν	molar flow rate (Kmol/s)
τ	transmission coefficient
φ	function
$\omega = 1$	wave number (1/m)
$\Delta\omega$	bandwidth of ω at gas temperature T and path length S
$\Delta\omega_o$	bandwidth of ω at gas temperature T and path length S = 0
Ω	reactor cross section (m^2)

Subscripts

k	: reacting component k = 1,...,K
l	: reaction index l = 1,...,L
n	: relative to reactor outer surface zone

In Chemical Reaction Engineering—Houston; Weekman, V., et al.;
ACS Symposium Series; American Chemical Society: Washington, DC, 1978.

m : relative to zones other than reactor outer surface zones

i,j : general indexes relative to zone Z_i, resp. zone Z_j

Superscript

$\bar{x}$: mean value

Literature Cited

1. Lobo, W.E., Evans, J.E., Trans. A.I.Ch.E., (1939) 35, 743.
2. Hottel, H.C., Radiant Heat Transmission, in McAdams, W.H. (ed) "Heat Transmission" Chap. 4 McGraw Hill, New York, 1954.
3. Hottel, H.C., Cohen, E.S., A.I.Ch.E.J., (1958) 4, 3.
4. Hottel, H.C., Sarofim, A.F., "Radiative Heat Transfer" McGraw Hill, New York, 1967.
5. Petryschuk, W.F., Johnson, A.I., Can.J.Chem.Engng., (1968) 46, 172.
6. Knudsen, J.G., Katz, D.L., "Fluid Dynamics and Heat Transfer" McGraw Hill, New York, 1958.
7. McAdams, W.H., "Heat Transmission" McGraw Hill, New York, 1954.
8. Holland, F.A.,et al., "Heat Transfer" Heineman Educ. Books, London, 1970.
9. Vercammen, H.A.J., Froment, G.F., to be published.
10. Echigo, R., et al., J.S.M.E., (1967) 46, 172.

In Chemical Reaction Engineering—Houston; Weekman, V., et al.;
ACS Symposium Series; American Chemical Society: Washington, DC, 1978.

23

Determining the Realtime Activity Parameters of a Pseudomonomolecular Kinetic Reforming Model

KENNETH R. GRAZIANI and MICHAEL P. RAMAGE

Mobil Research and Development Corporation, Research Department, Paulsboro, NJ 08066

The start-of-cycle (fresh catalyst) kinetics for a pseudomonomolecular reforming reaction system may be determined in two steps (1):

(1) the determination of the selectivity kinetic rate constants, followed by
(2) the determination of the activity kinetics.

The selectivity kinetics describe the rates of production of the chemical species relative to the rate of production of a reference compound. The activity kinetics modify the selectivity kinetics to describe the absolute rate of production of each chemical species on a "realtime" or actual catalyst contact time basis.

Predictions of reforming catalyst activity, such as the reactor inlet temperature (RIT) required to make a specific octane, are determined by the activity kinetics. In the monitoring of Mobil's commercial reformers, inlet temperatures are continually compared to model predicted start-of-cycle (SOC) RIT's to assess commercial catalyst SOC activity and catalyst activity loss over a reformer cycle. Accurate predictions of activity are therefore essential.

In this paper, a simple mathematical procedure requiring the integration of the selectivity transformation is developed to determine reforming activity kinetics and adsorption equilibria coefficients. The method is similar to that reported earlier (2) but is more rigorously applied to the reforming system. Only experimental C_5^- (methane to pentane, inclusive) vs. residence time data and a priori knowledge of the reforming selectivity kinetics are required for the procedure.

Theory

The reforming reaction system may be described by the pseudomonomolecular (1) kinetic interactions of an appropriately defined set of hydrocarbon component lumps. That is, the rates of change of the various species are given by first-order mass action

© 0-8412-0401-2/78/47-065-282$05.00/0

kinetics with the same adsorption isotherm being applicable to each reaction step. For the purpose of this paper, the reforming system will be discussed in terms of N arbitrarily defined component lumps obtained from the C_1 to C_{12} hydrocarbon species in the gasoline boiling range.

In matrix notation, the steady state differential material balance over the differential catalyst volume $d\nu$ is

$$\frac{d\bar{a}}{d\nu} = \phi \bar{\bar{K}} \bar{a} \tag{1}$$

where

$$\phi = \frac{\left\{\frac{P_T V_C}{FRT}\right\} k_\phi}{\left[1 + K_{H_2} P_{H_2} + \frac{P_T F_C}{F} \bar{K} \cdot \bar{a}\right]} \tag{2}$$

P_T, P_{H_2} = total and hydrogen pressures
V_C = total catalyst volume
T = temperature
F = total molar flow
F_C = mass flow rate hydrocarbon charge
K_{H_2}, $\bar{K}$ = adsorption equilibria coefficients

Equation 1 is derived for a fixed bed catalytic reformer assuming plug flow and constant catalyst bed void fraction. A nondissociative Langmuir-Hinschelwood adsorption mechanism is employed with the hydrocarbon partial pressures redefined as

$$P_i = \frac{P_T F_C (1-H) a_i}{F M_i} \tag{3}$$

M_i is the molecular weight of component i. The hydrocarbon weight fractions a_i are defined on a H_2-free basis, i.e., $\sum_{i=1}^{N} a_i = 1$, where H_2 is not included in the summation. In addition, since the hydrogen weight yield based on reformer charge, H, is typically .01 to .02, $1-H \approx 1$ may be assumed in these derivations.

ϕ is the catalyst activity function incorporating the adsorption equilibria effects. $\bar{\bar{K}}$ is the pseudomonomolecular selectivity rate constant matrix whose elements are k_{ji}/k_ϕ. k_ϕ is defined as the realtime activity rate constant to which all rate constants in $\bar{\bar{K}}$ are made relative. Thus, one rate constant in $\bar{\bar{K}}$ is equal to 1.0 and it may be chosen arbitrarily. k_ϕ will therefore be the rate constant for this chosen reaction.

Determining the reforming kinetics may then be separated into a selectivity problem (determine $\bar{\bar{K}}$) and an activity problem (determine ϕ). This is accomplished by defining the selectivity

time, τ, by the following transformation

$$d\tau = \phi d\nu \tag{4}$$

Substituting equation 4 into 1, we obtain

$$\frac{d\bar{a}}{d\tau} = \bar{\bar{K}}\,\bar{a} \tag{5}$$

whose solution upon integration is

$$\bar{a}(\tau) = \bar{\bar{\chi}}\ \mathrm{EXP}\ (\bar{\bar{\Lambda}}\tau)\ \bar{\bar{\chi}}^{-1}\,\bar{a}\ (o) \tag{6}$$

$\bar{\bar{\chi}}$ and $\bar{\bar{\Lambda}}$ are the eigenvectors and eigenvalues of the selectivity matrix $\bar{\bar{K}}$. Since one of the selectivity rate constants in $\bar{\bar{K}}$ is 1.0, we do not need to know τ in order to determine $\bar{\bar{K}}$. $\bar{\bar{K}}$ can be determined from composition data alone without regard to reaction time (1). For this report, the selectivity matrix $\bar{\bar{K}}$ has been previously determined but will be left unspecified for proprietary reasons at this time.

With $\bar{\bar{K}}$ known, only the activity function ϕ containing the realtime rate constant (k_ϕ) and the adsorption equilibrium constants remains to be determined. These may be found employing a method that requires the integration of the selectivity time transformation equation 4.

$$\int_0^{\tau_f} \frac{1}{\phi}\, d\tau = \int_0^1 d\nu = 1 \tag{7}$$

The integration is taken over the total catalyst bed. With equation 2, the integration implied in equation 7 may be more specifically represented as

$$\frac{1}{k_\phi}\int_0^{\tau_f} \frac{RTF}{P_T V_c}\, d\tau + \frac{K_{H_2}}{k_\phi}\int_0^{\tau_f} \frac{RTF}{P_T V_c} P_{H_2}\, d\tau + \frac{\bar{K}}{k_\phi}\cdot\int_0^{\tau_f} \frac{RTF_c}{V_c}\,\bar{a}\, d\tau = 1 \tag{8}$$

Note that $F_c/V_c = S_v\rho_c$ and the total hydrogen molar flow may be represented equivalently as

$$\frac{FP_{H_2}}{P_T} = F_c\left[\frac{H}{2} + \frac{\gamma_R}{M_c}\right]$$

In Chemical Reaction Engineering—Houston; Weekman, V., et al.;
ACS Symposium Series; American Chemical Society: Washington, DC, 1978.

where: ρ_c = hydrocarbon charge density
S_v = liquid hourly space velocity (volume hydrocarbon charge/volume catalyst-time)
γ_R = molar hydrogen-to-hydrocarbon feed ratio
M_c = molecular weight hydrocarbon charge

Equation 8 can then be rearranged to be linear in the realtime parameters:

$$\bar{\bar{K}} \cdot \bar{I}_1 + I_2 + K_{H_2} I_3 = k_\phi \tag{9}$$

where:

$$\bar{I}_1 = S_v \rho_c RT \int_0^{\tau_f} \bar{a}\, d\tau \tag{10a}$$

$$I_2 = \frac{S_v \rho_c RT}{P_T} \int_0^{\tau_f} \frac{F}{F_c}\, d\tau \tag{10b}$$

$$I_3 = S_V \rho_C RT \int_0^{\tau_f} \frac{F P_{H_2}}{F_c P_T}\, d\tau$$

$$= S_v \rho_c RT \int_0^{\tau_f} \left[\frac{H}{2} + \frac{\gamma_R}{M_c}\right] d\tau \tag{10c}$$

The left-hand side integration limit, τ_f in equation 7, is the selectivity time at the end of the catalyst bed, v = 1. Since the selectivity time is the result of the independent variable transformation represented by equation 4, it does not have physical meaning in the sense of catalyst contact time. The selectivity time can only be found by employing the predetermined selectivity kinetics. τ_f is determined by a trial and error matching of the selectivity solution from equation 6 to experimental yields at the outlet of the catalyst bed. That is, a value of τ_f is converged on when the C_5^- yield (methane to pentane, inclusive) as predicted by equation 6 agrees with the experimental C_5^- yield. The value of τ_f so determined relates the known selectivity kinetics to the reactor realtime behavior.

$\bar{I}_1$ is determined using the selectivity kinetics. Substituting the selectivity solution (equation 6) for $\bar{a}$ into equation 10a, we obtain

$$\bar{I}_1 = (S_v \rho_c RT)\, \bar{\bar{X}} \left\{ \int_0^{\tau_f} \mathrm{EXP}(\bar{\bar{\Lambda}}\tau)\, d\tau \right\} \bar{\bar{X}}^{-1} \bar{a}_o \tag{11}$$

As a result of irreversible reforming cracking reactions, the selectivity rate constant matrix, $\bar{\bar{K}}$, contains one column of zeros. $\bar{\bar{K}}$, therefore, will always yield one zero eigenvalue. Let $\lambda_N = 0$, arbitrarily. Realizing that $\lambda_N = 0$, the integration of the exponential diagonal matrix of equation 11 is done term-by-term. Expressing the results in matrix notation, the integration yields

In Chemical Reaction Engineering—Houston; Weekman, V., et al.;
ACS Symposium Series; American Chemical Society: Washington, DC, 1978.

$$\bar{I}_1 = (S_v \rho_c RT)\, \bar{\bar{\chi}}\, \bar{\bar{\Lambda}}^* \left(\bar{\bar{I}}^* - \mathrm{EXP}\left[\bar{\bar{\Lambda}}\, \tau_f\right]\right) \bar{\bar{\chi}}^{-1}\, \bar{a}_o \qquad (12)$$

$\bar{\bar{\Lambda}}^*$ is a diagonal matrix whose elements are $1/\lambda_1, \ldots, 1/\lambda_{N-1}, \tau_f$.
$\bar{\bar{I}}^*$ is a diagonal matrix whose elements are $1, 1, \ldots, 2$.

The analytical integrations for I_2 and I_3, equations 10b and 10c, are complicated by the dependence of F and H on τ through the dependence of the composition on τ. For a single-pass hydrogen reformer configuration, i.e., 100% H_2 introduced with naphtha feed instead of recycle gas, the total molar flow is given by

$$F = F_c \left(1 + \frac{1}{2} H\right)\left(\sum_{i=1}^{N} \frac{a_i(\tau)}{M_i} \right) + F_c \left(\frac{H}{2} + \frac{\gamma_R}{M_c} \right) \qquad (13)$$

A hydrogen balance over the reactor gives the hydrogen weight yield as

$$H = \frac{\sum_{i=1}^{N} n_i (a_{io} - a_i)}{1 - \sum_{i=1}^{N} n_i a_i} \qquad (14)$$

The n_i's represent the weight fraction of combined hydrogen for the ith kinetic lump. a_{io} represents feed composition.

It is necessary to determine I_2 and I_3 numerically. A five-point Simpson's integration rule (3) has been used with the following definition

$$\int_0^{\tau_f} y\, d\tau = \frac{\tau_f}{288} \left| 19\, y(0) + 75\, y(.2\,\tau_f) + 50\, y(.4\,\tau_f) + 50\, y(.6\,\tau_f) + 75\, y(.8\,\tau_f) + 19\, y(\tau_f) \right| \qquad (15)$$

For I_2, $y = \dfrac{S_v \rho_c RTF(\tau)}{P_T F_c}$ and for I_3, $y = S_v \rho_c RT \left[\dfrac{H(\tau)}{2} + \dfrac{\gamma_R}{M_c} \right]$.

In evaluating the numerical approximation to I_2 and I_3, the selectivity solution, $\bar{a}(\tau)$ from equation 6 must be determined at each incremental value of τ. Using equation 13 and 14, F, H, and subsequently y, may be calculated at each increment of τ. Integrals I_2 and I_3 are then determined by the appropriate form of equation 15.

The integrals $\bar{I}_1$, I_2, and I_3 in equation 9 can be determined for any isothermal reforming experiment from the experimental results and predetermined selectivity matrix ($\bar{\bar{K}}$) without knowledge of the activity parameters. The selectivity time, τ_f, can also be obtained with the same information. Thus, if we develop a set of reforming data which covers a wide range of charge stocks and process conditions, the integrals can be calculated explicitly

In Chemical Reaction Engineering—Houston; Weekman, V., et al.;
ACS Symposium Series; American Chemical Society: Washington, DC, 1978.

for each data point. The activity parameters k_ϕ, K_{H_2}, and $\bar{K}$ can then be obtained from equation 9 using parameter estimation techniques. Note that what we have done is to convert one highly non-linear problem (equation 1) into two linear problems (equations 6 and 9). Not only are the linear problems easier to solve, the results are more accurate due to decreased confounding between the kinetic parameters.

Experimental Data

Data used in this study were obtained on an isothermal fixed-bed reforming pilot plant. The reactor section was equipped with five sampling taps spaced along the length of the reactor. On-line gas chromatograph analyses of the axial reformate samples provide composition profiles of 285 hydrocarbon components with increasing residence time through the catalyst bed.

All the data were taken on fresh reforming catalyst. C_6-360°F Nigerian naphtha (naphthenic stock), C_6-360°F Arab light naphtha (paraffinic stock) and C_6-360°F and C_6-290°F Mid-Continent naphtha (intermediate stock) were employed. Reactor pressures of 400 psia and 197 psia and isothermal temperatures ranging from 850°F to 970°F were studied. Hydrocarbon partial pressure was 20 psia. In each case, 100% hydrogen was introduced as recycle (single-pass hydrogen). The experimental conditions were chosen to span the wide variation in charge stocks and process conditions found in commercial reforming. In all, 75 data sets were used.

Determination of the Realtime Activity Kinetics

The set of integrated data, $\bar{I}_1$, I_2 and I_3 were determined for each of the 75 data sets. The activity parameters and their temperature and pressure dependencies were found using Rosenbrock's parameter search technique (4) which minimized the sums of squares deviation as calculated from equation 9. The temperature and pressure dependence of the activity parameters were determined relative to base conditions of 900°F (756°K) and 177 psia H_2. The parameters are expressed in terms of process conditions as

$$k_\phi = k_\phi^{\circ} \text{ EXP} \left[-E_{act} \left(\frac{1}{T} - \frac{1}{756} \right) \Big/ R \right] \left(P_{H_2} / 177 \right)^n \qquad (16a)$$

$$K_i = K_i^{\circ} \text{ EXP} \left[-H_{ads_i} \left(\frac{1}{T} - \frac{1}{756} \right) \Big/ R \right] \qquad (16b)$$

$$K_{H_2} = K_{H_2}^{\circ} \text{ EXP} \left[- H_{H_2} \left(\frac{1}{T} - \frac{1}{756} \right) \Big/ R \right] \qquad (16c)$$

where E_{act} = activation energy (cal/mole)
H_{ads_i}, H_{H_2} = heat of adsorption (cal/mole)
$k_\phi^{\circ}, K_i^{\circ}, K_{H_2}^{\circ}$ = pre-exponential realtime and adsorption constants. (Parameters at base conditions.)
n = hydrogen partial pressure exponent

In Chemical Reaction Engineering—Houston; Weekman, V., et al.;
ACS Symposium Series; American Chemical Society: Washington, DC, 1978.

The activity constants so determined are presented in Table I. The adsorption of hexanes, heptanes and C_8^+ aromatics are seen to have the dominant effect on catalyst activity. The adsorption of benzene, toluene and hydrogen occur to a lesser extent. These adsorption effects may be explained by the dual functional nature of reforming catalysts. It has been shown (5) that species that readily undergo hydrogenolysis (hexanes and heptanes) are strongly chemisorbed on the metal sites while experience with zeolite cracking catalysts (6) indicates a strong adsorption of heavier aromatics on acidic sites.

Table I

Realtime Activity Parameters

	Pre-exponential Term (Ko)	Activation Energy or Heat of Adsorption (cal/mole)	H_2 Pressure Exponent (n)
k_ϕ	0.258	24,380	-0.2
K_{H_2}	3.2×10^{-5}	-43,726	-
K_{A8+}	0.0456	-39,713	-
K_{A_7}	2.2×10^{-5}	-39,610	-
K_{A_6}	4.9×10^{-6}	-14,743	-
K_{P_7}	0.0125	-25,000	-
K_{P_6}	0.05	-25,000	-

Realtime Activity Predictions

With the activity parameters given in Table I, isothermal reformer realtime behavior may be simulated using the differential material balance of equation 1. Figures 1 and 2 show predicted vs. actual composition profiles for two of the data sets used in the fitting. Figure 1 presents C_7 paraffin and toluene compositions vs. catalyst contact time for reforming a 120-380°F Arab Light naphtha. Figure 2 similarly presents C_6 paraffin and benzene composition profiles for reforming a 120-370°F Mid-Continent naphtha. Very good agreement between the simulated and experimental reaction profiles is observed over the wide range of conditions represented by both examples.

In adiabatic reformer simulations, the activity parameters determine the reactor inlet temperature (RIT), required to make a specified reformate octane. With the activity parameters incorporated into Mobil's kinetic reforming model, inlet temperature predictions were compared to numerous adiabatic reforming pilot plant studies (Figure 3). The data used in these comparisons covered a wide range of charge stock types and process conditions commonly encountered in commercial reforming. The predicted RIT's are in good agreement with the reported experimental RIT's. An average deviation of ± 6.8°F is observed.

In Chemical Reaction Engineering—Houston; Weekman, V., et al.;
ACS Symposium Series; American Chemical Society: Washington, DC, 1978.

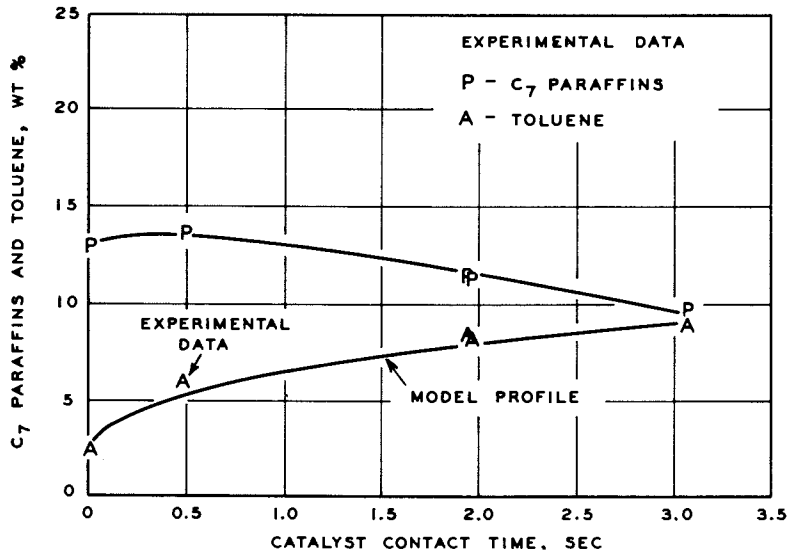

Figure 1. Isothermal reforming reactor profiles for a C_6-370°F Arab light naphtha. Reformer conditions: 949°F, 380 psia H_2, 20 psia hydrocarbon.

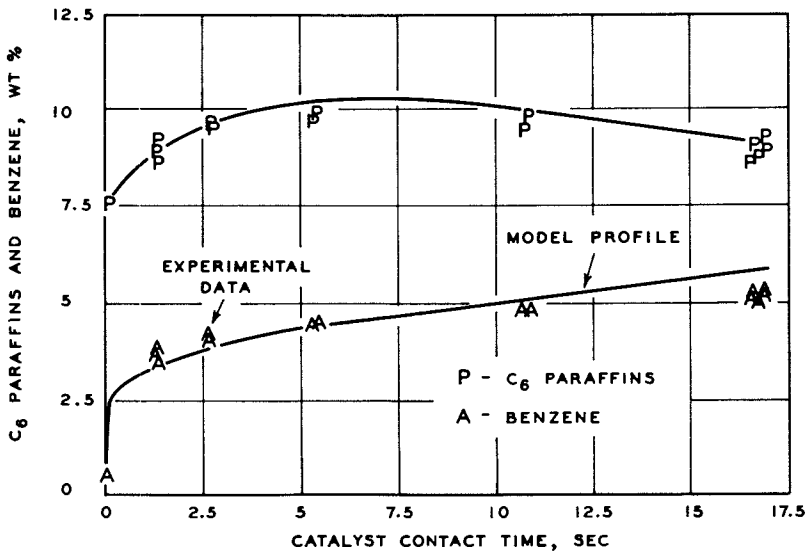

Figure 2. Isothermal reforming reactor profiles for a C_6-370°F Mid-Continent naphtha. Reformer conditions: 898°F, 177 psia H_2, 20 psia hydrocarbon.

In Chemical Reaction Engineering—Houston; Weekman, V., et al.;
ACS Symposium Series; American Chemical Society: Washington, DC, 1978.

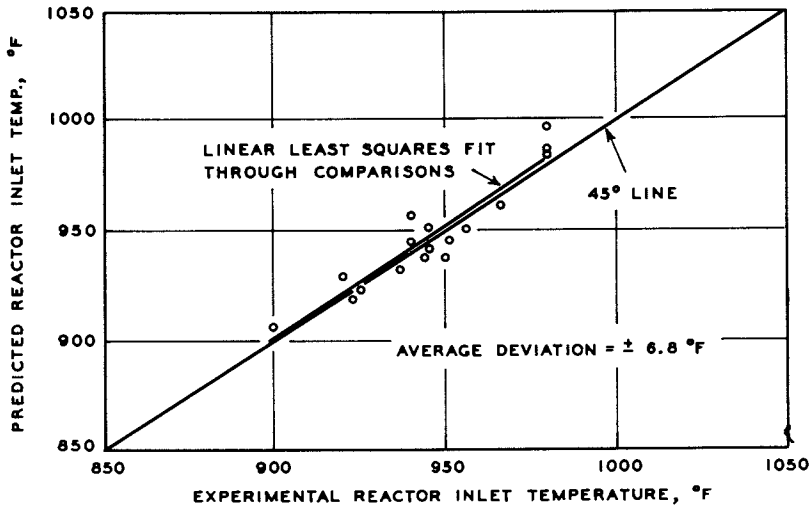

Figure 3. Comparison of activity kinetics predictions to adiabatic pilot plant data

In Chemical Reaction Engineering—Houston; Weekman, V., et al.;
ACS Symposium Series; American Chemical Society: Washington, DC, 1978.

Also, a linear least squares fit through the comparisons shows no bias to the predictions. This degree of accuracy is very reasonable considering the sensitivity of catalyst activity to start-up conditions, environmental control, and the difficulty in defining a precise start-of-cycle RIT due to initial temperature transients.

Thus, the activity kinetics found using the method of integration of the selectivity transformation are seen to accurately model reformer catalyst activity.

Literature Cited

(1) Wei, J., and C. D. Prater, Advances in Catalysis (1962), 13 203.
(2) Kugelman, A. M., and J. C. Bonacci, J. of Cat. (1975), 39, 10-21.
(3) Lapidus, L., "Digital Computation for Chemical Engineers", McGraw-Hill, New York (1962).
(4) Rosenbrock, H. H., Comp. J. (October, 1960), 3 (3), 175-184.
(5) Sarkany, A., L. Guczi and P. Tetenyi, J. of Cat. (1975), 39, 181-189.
(6) Jacob, S. M., B. Gross, S. E. Voltz, and V. W. Weekman, AIChE J. (July, 1976), 22 (4), 701-713.

In Chemical Reaction Engineering—Houston; Weekman, V., et al.;
ACS Symposium Series; American Chemical Society: Washington, DC, 1978.

24

Heuristic Approach to Complex Kinetics

J. B. CROPLEY

Research and Development Department, Union Carbide Corporation, Chemicals and Plastics Division, P.O. Box 8361, South Charleston, WV 25303

Non-linear reaction rate expressions that are adequate for reactor design frequently contain more unknown parameters than can be evaluated by either classical kinetics or non-linear statistical methods. Such expressions are encountered in both heterogeneous and homogeneous catalysis, and in biochemistry. Fifteen or more non-linear parameters are not uncommon in rate models for complex industrial reactions.

The heuristic approach described in this paper utilizes linear statistical methods to formulate the basic hyperbolic non-linear model in a particularly useful dimensionless form. Essential terms are identified and others rejected at this stage. Reaction stoichiometry is combined with the inherent mathematical characteristics of the dimensionless rate expression to reduce the number of unknown parameters to the critical few that must be evaluated by non-linear estimation. Typically, only four or five parameters remain at this point, and initial estimates are available for these. The approach is equally applicable to cases where the rate-limiting mechanism is known and where it is not.

The heuristic approach is illustrated by an example that utilizes the fictitious but realistic catalytic vapor-phase oxidation of dammitol to valualdehyde and water. Some carbon dioxide is also produced. It will be assumed that water is known to have no effect on the reaction, but the effects of the other components and temperature are unknown. No knowledge of the rate-limiting step is available.

The first step in the development of the model is to obtain a set of suitable experimental data. In this case suitable means that the necessary information is actually latent in the data, that the ranges of the variables are realistic, and so on. The experimental reactor should be specifically designed to obtain data

© 0-8412-0401-2/78/47-065-292$05.00/0

for the kind of reaction kinetics one is working with. The experimental plan should be carefully drawn so that the primary, interactive, and curvilinear effects of the variables can be observed. Usually this will mean some sort of statistically-designed experimental array.

For most vapor-phase catalytic reactions, use a gradientless reactor like the back-mixed catalyst autoclave developed by J. M. Berty (1). This reactor permits the independent variation of mass- and space-velocities and the direct observation of reaction rates.

For the experiment array, I prefer an orthogonal central-composite design (2), (3), which consists of three main parts, as shown in Table I. The first is a conventional 16-experiment fractional factorial design for five variables at two levels. The second comprises three identical experiments at the average, or center-point, conditions for the first 16 experiments. The final part comprises two out-lier experiments for each variable. These augment the basic two level design to provide an estimate of curvature for the response to each variable. The overall effect of the design is to saturate effectively the multi-dimensional variable space. It is more effective than the conventional "one-variable-at-a-time" approach.

For purposes of illustration, the "observed" rates in Table I were developed from an assumed "true" rate expression by applying random error as follows;

$$(\text{Rate})_{\text{observed}} = (\text{Rate})_{\text{true}} \times N_R$$

where N_r is a random normal number from a set with a mean of 1.0 and a standard deviation of 0.20. Thus, the "observed" data contain 20 percent random error. This error level is not inordinately high for complex situations that may involve difficult analytical methods and multiple products.

The "true" rate expression used in this example is

$$r = \frac{4.67(10^{11})e^{\frac{-20000}{RT}}(P_{O2})^{.5}(P_D)^{1.0}}{1+5.52(10^{-4})e^{\frac{5000}{RT}}(P_{O2})^{.5}+7.64(10^{-4})e^{\frac{5000}{RT}}(P_v)^2}$$

where r is reaction rate, gmols/valualdehyde/kg catalyst/hr; T is temperature, ^{O}K; R is the gas constant; P is partial pressure, psia; and subscripts 02, D, and v refer to oxygen, dammitol, and valualdehyde, respectively. This rate expression implies that the rate-

In Chemical Reaction Engineering—Houston; Weekman, V., et al.;
ACS Symposium Series; American Chemical Society: Washington, DC, 1978.

TABLE I

A SUMMARY OF SYNTHETIC DATA

THE OXIDATION OF DAMMITOL TO VALUALDEHYDE

#	OBSERVED RATE GMOL/KG/HR	TEMPERATURE, °C	PARTIAL PRESSURES, PSIA OXYGEN	DAMMITOL	VALUALDEHYDE	CO2
THE BASIC FRACTIONAL FACTORIAL SET						
1	4.07	105	7	10	3	3
2	8.70	105	7	10	1	1
3	2.29	105	7	4	3	1
4	5.69	105	7	4	1	3
5	1.58	105	3	10	3	1
6	10.58	105	3	10	1	3
7	1.40	105	3	4	3	3
8	4.63	105	3	4	1	1
9	1.25	95	7	10	3	1
10	4.34	95	7	10	1	3
11	0.62	95	7	4	3	3
12	1.65	95	7	4	1	1
13	1.15	95	3	10	3	3
14	3.66	95	3	10	1	1
15	0.63	95	2	4	3	1
16	1.44	95	3	4	1	3
THE CENTER-POINTS						
17	2.92	100	5	7	2	2
18	3.16	100	5	7	2	2
19	2.72	100	5	7	2	2
THE "OUT-LIERS"						
20	1.66	91.7	5	7	2	2
21	3.57	108.3	5	7	2	2
22	1.96	100.	1.67	7	2	2
23	4.11	100.	8.33	7	2	2
24	1.15	100.	5	2	2	2
25	4.70	100.	5	12	2	2
26	4.12	100.	5	7	0.34	2
27	0.91	100.	5	7	3.66	2
28	2.95	100.	5	7	2	0.34
29	3.16	100.	5	7	2	3.66

In Chemical Reaction Engineering—Houston; Weekman, V., et al.;
ACS Symposium Series; American Chemical Society: Washington, DC, 1978.

limiting step is the surface reaction between chemisorbed oxygen and unadsorbed dammitol. Two molecules of valualdehyde chemisorb (perhaps as a dimer) on a single catalyst site, and carbon dioxide does not influence the reaction.

Hyperbolic equations like the above are typically used to describe rate phenomena in both heterogeneous and homogeneous catalysis, biochemistry, and in many homogeneous reactions in which chemical equilibria are important. They are more descriptive of the reaction chemistry than is the usual exponential rate expression, and they avoid the problems encountered in the exponential models if one of the components is absent. In this paper, we will use the exponential expression as a stepping-stone to the more rigorous and useful hyperbolic model. The following rules comprise the heuristic approach:

Rule 1:

Develop a modified exponential rate model of the following type, using linear regression methods:

$$\ln(r) = f\left[\ln X_i, (\ln X_i)^2, (\ln X_i)(\ln X_j)\right]$$

where the X_i are process variables of the form:

$$e^{-\frac{E}{R}\left(\frac{1}{T} - \frac{1}{T_{cp}}\right)} \quad \text{and} \quad \frac{P}{P_{cp}}$$

The subscript cp refers to the center-point conditions of Table I and E is the apparent activation energy in cal/gmol. The exponential form of the model developed from the data in Table I is:

$$r = 2.77e^{-\frac{23295}{R}\left(\frac{1}{T}-\frac{1}{373}\right)}\left(\frac{P_{O2}}{5}\right)^{.32}\left(\frac{P_D}{7}\right)^{.73}\left(\frac{P_v}{2}\right)^{\left(-.59\ln\frac{P_v}{2} - 1.23\right)}$$

The "true" and "observed" rates are compared with the rates predicted by this model in Table II. The standard deviation of the error with respect to the "observed" data is 22 percent, or very little more than the random error in the data. The model also acts as a filter for the random error, in the sense that the standard deviation with respect to the "true" values is only 14 percent. All in all, it is not a bad model, but we can do better, particularly for design purposes where the concentration of valualdehyde at the entrance

In Chemical Reaction Engineering—Houston; Weekman, V., et al.;
ACS Symposium Series; American Chemical Society: Washington, DC, 1978.

TABLE II

A COMPARISON OF RESULTS

#	DATA "TRUE" RATES	DATA "OBSERVED" RATES (c)	MODEL PREDICTIONS EXPONENTIAL	HEURISTIC #1	HEURISTIC #2
1	4.50	4.07	3.34	4.13	4.24
2	12.34	8.70	10.68	10.28	10.54
3	1.80	2.29	1.71	2.05	1.85
4	4.94	5.69	5.48	5.45	5.31
5	3.11	1.58	2.54	2.76	2.91
6	9.43	10.58	8.14	7.58	7.76
7	1.24	1.40	1.31	1.37	1.27
8	3.77	4.63	4.17	4.10	4.05
9	1.86	1.25	1.44	1.78	1.83
10	5.32	4.34	4.60	4.43	4.54
11	0.75	0.62	0.74	0.88	0.80
12	2.13	1.65	2.36	2.35	2.29
13	1.29	1.15	1.10	1.19	1.25
14	4.11	3.66	3.50	3.26	3.34
15	0.52	0.63	0.56	0.59	0.55
16	1.64	1.44	1.80	1.77	1.74
17	3.00	2.92	2.77	2.93	2.93
18	3.00	3.16	2.77	2.93	2.93
19	3.00	2.72	2.77	2.93	2.93
20	1.44	1.66	1.35	1.43	1.43
21	6.05	3.57	5.49	5.81	5.81
22	1.92	1.96	1.95	1.80	1.85
23	3.63	4.11	3.26	3.62	3.58
24	0.86	1.15	1.11	1.13	0.95
25	5.14	4.70	4.10	4.29	4.48
26	6.56	4.12	3.79	5.89	6.03
27	1.30	0.91	1.06	1.32	1.31
28	3.00	2.95	2.77	2.93	2.93
29	3.00	3.16	2.77	2.93	2.93
MEAN	3.47	3.13	3.08	3.24	3.25
MEAN ERROR(a)			0.07	0.01	0.02
S_{obs} (b)			0.22	0.26	0.27
S_{true} (b)			0.14	0.12	0.08

NOTES: (a) Error is defined as (Data-Pred.)/Data.

(b) S_{obs} and S_{true} are standard deviations of the error as defined above, based on the "observed" and "true" data, respectively.

(c) "Observed" rates were derived from "true" rates by imposing a 20 percent random normal error. Models are based on "Observed" Rates.

In Chemical Reaction Engineering—Houston; Weekman, V., et al.;
ACS Symposium Series; American Chemical Society: Washington, DC, 1978.

to the catalyst bed may be zero. We will use some of the information in this model in the development of the hyperbolic model.

If temperature and the concentrations of all the chemical species in the study were important in both the numerator and denominator of the hyperbolic model, there would be, for n species, (4n+2) unknown parameters in the model. In the example study, there would be 18 parameters. In the "true" expression, there are 10 parameters, because not all species are important in both numerator and denominator. Even if the "true" mechanism were known, there would be too many parameters to estimate simply by tossing the data into a non-linear estimation program.

The heuristic process is one of scaling the problem down to a size that is manageable and of changing the form of the equation a bit to permit good values of the parameters to be calculated. The problem of finding initial estimates is completely eliminated.

Rule 2:

Eliminate from consideration any variable that was not significant in the exponential model. In the example, the partial pressure of carbon dioxide is thus eliminated.

Rule 3:

Eliminate the temperature terms in the denominator. If they are indeed necessary, they can be added later. Usually a change of three or four kilocalories in the apparent activation energy compensates adequately for their absence.

Rule 4:

Develop the hyperbolic equation in terms of the dimensionless variables of Rule 1. By doing so one breaks the interdependence of exponential and pre-exponential terms, and one of the big problems of non-linear estimation is minimized. (See Rule 7.)

Rule 5:

Arbitrarily assign exponents to the terms in the denominator. Here one utilizes his knowledge of the chemistry and the stoichiometry of the assumed adsorption equilibria. These may be changed later, but for now use values of 1/2, 1.0, or 2.0. (The 1/2 is

In Chemical Reaction Engineering—Houston; Weekman, V., et al.;
ACS Symposium Series; American Chemical Society: Washington, DC, 1978.

characteristic for chemisorption of diatomic gases like oxygen, the 2.0 for molecules that adsorb as dimers.)

Rule 6:

Use the value for E, the activation energy, that was obtained in the exponential model.

Rule 7:

Determine the pre-exponential term in the numerator by observing that the concentration and temperature terms are all unity at the center-point levels. Hence, the hyperbolic expression becomes, for the average rate at the center point, merely:

$$\bar{r}_{cp} = \frac{A}{1 + \Sigma K_i}$$

or,

$$A = \bar{r}_{cp}(1 + \Sigma K_i)$$

where A is the pre-exponential factor and the K_i are the adsorption equilibrium constants.

At this point, the hyperbolic model is ready for non-linear estimation and looks like this for our example:

$$r = \frac{\bar{r}_{cp}(1+K_{O2}+K_D+K_v)e^{\frac{-23295}{R}\left(\frac{1}{T}-\frac{1}{373}\right)}\left(\frac{P_{O2}}{5}\right)^a\left(\frac{P_D}{7}\right)^b}{1 + K_{O2}\left(\frac{P_{O2}}{5}\right)^{.5} + K_D\left(\frac{P_D}{7}\right)^{1.0} + K_v\left(\frac{P_v}{2}\right)^{2.0}}$$

There are five parameters to estimate: a, b, K_{O2}, K_D, and K_v. Valualdehyde was eliminated from the numerator because its exponent in the exponential equation was strongly negative, which also suggested the denominator exponent of 2.0.

Rule 8:

Set the non-linear search ranges for the numerator exponents between 0 and 2.0. They will seldom be found outside that range.

Set the search ranges for the denominator K's

In Chemical Reaction Engineering—Houston; Weekman, V., et al.;
ACS Symposium Series; American Chemical Society: Washington, DC, 1978.

between 0 and 5. The logic for this rule is quite simple. At the center-point conditions, the values for all the dimensionless variable terms will be unity, and the denominator will be, as noted before in Rule 7:

$$1 + \Sigma K_i$$

In order to have influence on the rate, each of the K's must be significant with respect to the 1.0, and, at the same time, not overwhelm it. Most K's will be found in the 1.0 to 3.0 range.

Rule 9:

Utilize computerized non-linear estimation of the numerator exponents and the denominator K-values. The final result in our example is:

$$r = \frac{20.18e^{\frac{-23295}{R}\left(\frac{1}{T}-\frac{1}{373}\right)}\left(\frac{P_{O2}}{5}\right)^{.55}\left(\frac{P_D}{7}\right)^{.81}}{1 + 1.74\left(\frac{P_{O2}}{5}\right)^{.5} + 0.59\left(\frac{P_D}{7}\right)^{1.0} + 3.56\left(\frac{P_v}{2}\right)^{2.0}}$$

The predicted values using this model are shown in Table II under Heuristic Model #1. The standard deviations of the error for the "observed" and "true" data are about 26 and 12 percent, respectively. Thus the heuristic model predicts the "true" data slightly better than the exponential model does, but doesn't fit the "observed" data as well. It is actually the better model, although the comparison seems to pose a paradox. Actually, the heuristic model is the more constrained of the two, because it has been structured to reflect a particular chemistry. It is less likely to be influenced by the error structure of the data than is the exponential model, which is more general.

Rule 10:

Examine the heuristic model for any clues or suggestions that may improve the form of the model. Two possibilities are immediately apparent. The numerator exponent for the oxygen is very close to 0.5, and it is therefore a good idea to simply set it to 0.5 to agree with the exponent in the denominator. Likewise, the exponent for dammitol in the numerator is not far removed from 1.0 (its exponent in the denominator) and so we will set it to 1.0. The search variables have

In Chemical Reaction Engineering—Houston; Weekman, V., et al.;
ACS Symposium Series; American Chemical Society: Washington, DC, 1978.

been narrowed to three: the equilibrium constants in the denominator. After re-fitting, the result is

$$r = \frac{27.72e^{\frac{-23295}{R}\left(\frac{1}{T}-\frac{1}{373}\right)}\left(\frac{P_{O2}}{5}\right)^{.5}\left(\frac{P_D}{7}\right)^{1.0}}{1 + 1.83\left(\frac{P_{O2}}{5}\right)^{.5} + 1.62\left(\frac{P_D}{7}\right)^{1.0} + 5.0\left(\frac{P_v}{2}\right)^{2.0}}$$

The results of the predictions of this model are shown in Table II as Heuristic Model #2. The standard deviation of the error with respect to the "observed" data is not quite as good as either of the other models, but it predicts the "true" values markedly better -- the standard deviation for the "true" values is only about 8 percent. Once again we see the paradox. The best model of the three for prediction and design purposes actually fits the data from which it was developed the poorest. It is, therefore, the least likely to be used in practice. This happens quite frequently with error-containing data, and is, in the author's judgment, a frequent cause for the failure of models to predict designed performance adequately.

The obvious question is how to tell when a model is adequate for design and when it is not -- or which is the best of several. One obviously cannot use a model merely because it conforms to a mechanism of some sort and doesn't fit the data very well. But just fitting the data well is obviously not enough.

There are three answers to the above question. The first is to improve the accuracy of the data to the extent practicable. Ten percent data is difficult to produce, but the problems cited here are usually not serious with data of that quality.

The second answer is to test the model extensively against data that were not used in its development, and preferably in a reactor of different geometry. If a fixed-bed catalytic reactor is to be used, then the model should be tested in a test reactor of similar design -- a single plant-scale tube makes an excellent test reactor.

The third answer is to utilize non-kinetic means to discern the true mechanism of the reaction. It is possible to determine, for example, whether a species like dammitol chemisorbs to an appreciable extent on a catalyst. Had such information been available in the study of the example, dammitol would have been eliminated from the denominator and the standard deviation of the error for the "true" data would have been

In Chemical Reaction Engineering—Houston; Weekman, V., et al.;
ACS Symposium Series; American Chemical Society: Washington, DC, 1978.

only about two percent. But the paradox would still remain -- the standard deviation for the "observed" data would have been about the same as for the other heuristic models, and not as good as that for the exponential model. But the ability of the heuristic models to predict "true" values is typically better than that of the more flexible power-series model for complex reactions.

A Comparison With Modern Statistical Methods

There has been substantial progress over the past twenty years in the use of modern statistical methods to develop non-linear kinetic models. Generally, these approaches emphasize the placement of experiments to narrow the confidence intervals of the estimated parameters and techniques to discriminate between rival mechanisms. There is an extensive literature on the subject, and the reader is referred to one or two excellent review articles as starting points (4), (5).

In general, these approaches have not met with wide-spread success in industry because they are virtually limited to non-linear models of fewer than four or five unknown parameters. As the number of parameters is increased to describe complex chemistry more adequately, the ranges of the reaction conditions required for the estimation of unique parameter values correspondingly widen. It often happens that the required ranges are unrealistic because the rate-limiting mechanisms change before such ranges can be reached.

The heuristic approach was developed to blend mathematics with a knowledge of chemistry to accomplish for complex systems what neither is able to alone.

Conclusions

In this paper I have attempted to demonstrate a method for the development of hyperbolic rate models that are adequate for the design of chemical reactors. The method is rapid and overcomes most of the problems that historically have hampered the development of such models for complex reactions. I have shown that the quality of fit of a model to error-containing data is a poor criterion for model discrimination, and that several models may predict almost equally well. This, of course, has been known for a long time, but it has not been widely recognized that the model that fits the data least well may be the best model, and that the converse also may be true. In the final analysis

In Chemical Reaction Engineering—Houston; Weekman, V., et al.;
ACS Symposium Series; American Chemical Society: Washington, DC, 1978.

a model must be tested thoroughly before reactor design is fixed. Because of its rapidity and simplicity, the heuristic approach permits the investigator more time for critical testing and modification.

Literature Cited

(1) Berty, J., Chem. Eng. Prog., (1974), 70(5).
(2) Box, G.E.P., Biometrics, (1954), 10, 16-60.
(3) Davies, O.L., "Design and Analysis of Industrial Experiments", 534-5, Hafner Publishing Company, New York, 1960.
(4) Reilly, P.M., and Blau, G.E., Can. J. Chem. Eng., (1974) 52, 289-299.
(5) Kittrell, J.R., and Mezaki, R., "Applied Kinetics and Chemical Reaction Engineering", 119-32, American Chemical Society Publications, Washington, D.C., 1967.

In Chemical Reaction Engineering—Houston; Weekman, V., et al.;
ACS Symposium Series; American Chemical Society: Washington, DC, 1978.

25

Kinetics of Catalytic Liquefaction of Big Horn Coal

Y. T. SHAH, D. C. CRONAUER, H. G. McILVRIED, and J. A. PARASKOS

Gulf Research and Development Co., Pittsburgh, PA 15230

A number of coal liquefaction processes, including Gulf CCL, are being developed to help counter the coming liquid fuel shortages. In most coal liquefaction processes, coal is liquefied in the presence of a solvent. In addition, the coal-oil slurry may be contacted by a hydrogen-rich gas, and a catalyst may also be present. The process of liquefaction produces a wide boiling range liquid, as well as light gases (C_1-C_4) and by-products, such as water, ammonia, hydrogen sulfide, etc.

Data for the kinetics of coal liquefaction have been published in the literature (1-11). A review of the reported studies has recently been given by Oblad (12). The reported data were mostly obtained in bench-scale reactors. Guin et al. (7) studied the mechanism of coal particle dissolution, whereas Neavel (7), Kang et al. (8), and Gleim (10) examined the role of solvent on coal liquefaction. Tarrer et al. (9) examined the effects of coal minerals on reaction rates during coal liquefaction, whereas Whitehurst and Mitchell (11) studied the short contact time coal liquefaction process. It is believed that hydrogen donor solvent plays an important role in the coal liquefaction process. The reaction paths in a donor solvent coal liquefaction process have been reviewed by Squires (6). The reported studies examined both thermal and catalytic liquefaction processes. So far, however, very little effort has been made to present a detailed kinetic model for the intrinsic kinetics of coal liquefaction.

The primary purpose of this paper is to describe the kinetics of coal liquefaction derived from a pilot-scale unit. The specific coal studied was Big Horn subbituminous coal. The experimental data were obtained in a pilot-scale Gulf patented (13) reactor. The data illustrate the effects of reactor space time and temperature on the product distribution. Since the reactor behaves as a bubble column, the intrinsic kinetics of the liquefaction process can be extracted by means of a kinematic model of the reactor. The experimental data were found to be

© 0-8412-0401-2/78/47-065-303$05.00/0

adequately correlated by a simple reaction mechanism.

Experimental

A schematic of the experimental unit is shown in Figure 1. This unit primarily consisted of a feed tank, charge pump, preheater, reactor and product receivers. A separate hydroclone unit was used to prepare recycle solvent. The reactor was 6 cm I.D. by 122 cm long. The unit was operated with a cocurrent upflow coal slurry rate of 1.8 kg/hr, the feed slurry consisted of mixture of 40% coal and 60% hydroclone overflow. Big Horn (WY) subbituminous coal was used for the experiments. It was pulverized and screened to minus 20 mesh, but was not predried; therefore, the moisture level of the feed coal was typically 22 wt%. The ash content was 3.4 wt%. On a moisture-free basis, carbon, hydrogen and oxygen contents of the coal were 69.34, 4.6 and 19.9 wt%, respectively. All runs were made at 24.1 MPa pressure and a gas rate of 2575 dm^3/hr. A Gulf developed catalyst was used.

Sufficient analyses were made to obtain detailed material balances over the liquefaction reactor. Solvation of the coal organic matter on a moisture and ash-free (maf) basis was calculated using the following equation:

$$\% \text{ Solvation} = \frac{\text{maf coal feed - maf undissolved coal}}{\text{maf coal feed}} \times 100$$

Reactor. The reactor used in this study was a pilot plant version of the Gulf patented (13) segmented bed reactor. The catalyst was held in tubes of 17 mm I.D. by 114 cm length constructed of 10-mesh (U.S.) stainless steel screen. In many of the runs, the catalyst charge was placed in four of the above tubes which typically held 750 g of the catalyst. Some runs were made using only one or two catalyst tubes by blocking off a portion of the reactor cross section.

Glass model studies (14) with an upflow air-water system have shown that gas flow plays a significant role in achieving axial mixing in the open spaces between the catalyst tubes and radial mixing within the catalyst tubes; both axial and radial mixing increased with an increase in the hydrogen flow rate.

It is believed that the reaction process involves depolymerization and solvation of the coal, with these reactions occurring primarily in the open spaces between the catalyst tubes. Once the coal fragments are liberated, they are either stabilized by hydrogen or repolymerized. Thus, the molecular weight of the liquefaction products is determined by a combination of coal properties and hydrogenation activity within the reactor. The process of solvation is improved as the hydrogen donor capacity of the liquid phase is increased. In order to improve the availability of the catalyst surface to the reactants, entrapment

In Chemical Reaction Engineering—Houston; Weekman, V., et al.;
ACS Symposium Series; American Chemical Society: Washington, DC, 1978.

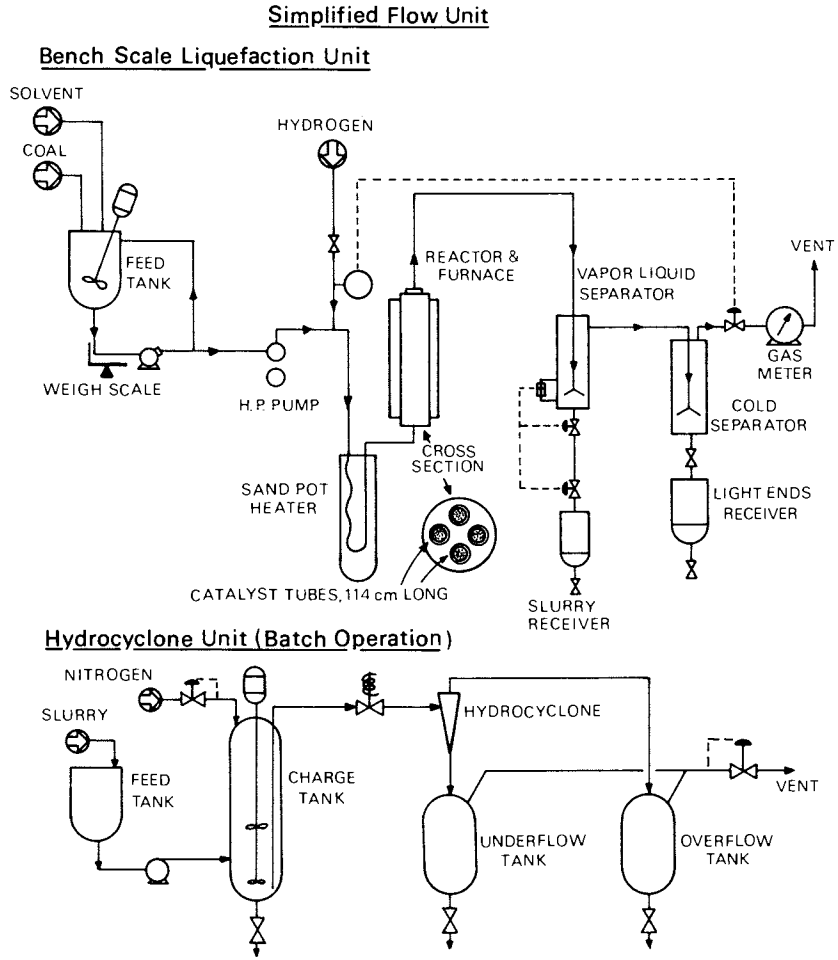

Figure 1. Experimental set-up

of coal particles within the catalyst tube must be minimized, and a high degree of radial mixing within the catalyst tubes must be achieved. Both of these can be improved by increased hydrogen and oil flow rates. Upgrading of the product oil occurs primarily within the catalyst tubes.

The dissolved hydrogen required for both solvation and upgrading is continuously supplied from the gas phase. Both the literature and available experimental data on hydrogen solubility in coal liquids at reaction temperature and pressure indicate that mass transfer of hydrogen from the gas into the liquid phase is not a limiting factor in the reaction process.

Reactor Model. The intrinsic kinetic information for the liquefaction process can be evaluated from the data by accounting for mass transfer effects. The operation of the present reactor system was modeled by making the following assumptions: (1) Coal and liquid flow as a uniform slurry within the reactor. Based on the study of Kato et al., (15) it is reasonable to assume that the backmixing characteristics of coal and oil are about the same. (2) There are no radial concentration or temperature gradients within the reactor. (3) The concentration of hydrogen in the slurry is always in excess of that required for reaction, and (4) The axial dispersion effect within the reactor is significant.

In the present study, we have assumed a simple reaction mechanism for coal solvation illustrated by Equation (1).

$$\begin{array}{l} \text{Gaseous Products } (H_2O, \text{ light gases, } NH_3, H_2S, \text{ etc.}) \\ \quad \uparrow k_2 \\ \text{Coal} \xrightarrow{k_1} \text{Oils } (\text{naphtha, furnace and heavy fuel oils, etc.}) \end{array} \qquad (1)$$

This mechanism is consistent with our understanding of the low severity catalytic liquefaction process. More complex reaction mechanisms which include hydrocracking (i.e., degeneration of higher boiling hydrocarbons into lower boiling components) and hydrogen donor reactions may be important under high severity thermal process.

Gas and slurry flow cocurrently upwards through the open spaces between the catalyst tubes. The gas flow is the primary cause of backmixing in the slurry phase. Literature on hydroprocessing operations indicates that the mass transfer resistance for the transfer of hydrogen from the gas to the liquid phase can be neglected. Furthermore, very high solubility of hydrogen in coal liquids dictates that, for all practical purposes, the mass transfer resistance of hydrogen at the gas-liquid interface can be neglected. This does not mean, however, that the rate of diffusion of hydrogen through the liquid is negligible compared with the rate at which hydrogen is consumed at the catalyst surface. However, because of the reasons mentioned later, it is

In Chemical Reaction Engineering—Houston; Weekman, V., et al.;
ACS Symposium Series; American Chemical Society: Washington, DC, 1978.

assumed that the hydrogen concentration is in excess and constant for all pertinent reactions.

The coal depolymerizes, dissolves in the liquid, and forms various gaseous and liquid products. The simplified mechanism assumes that both gaseous and liquid products are directly formed from coal. The catalyst within the catalyst tubes continuously supplies hydrogen-rich solvent for hydrogen transfer reactions. The solvation of coal is undoubtedly accompanied by some hydrocracking reactions (degeneration of higher boiling hydrocarbons into lower boiling components), but these appear to be relatively unimportant, and in the present study, they were not included in the mechanism.

The reactor feed includes a moisture- and ash-free coal component designated "C_i" and a carrier solvent. Feed hydrogen and flush oil are included in the solvent for simplicity.

The product stream is composed of a "p" fraction (light gases C_1-C_4, H_2O, CO, CO_2, H_2S, NH_3), a "C" fraction (unconverted moisture- and ash-free coal), and an "ℓ" fraction (coal liquids plus solvent, i.e., C_4+).

The concentrations of the above-defined feed and product components are expressed in terms of dimensionless weight fractions; material balance feed and product quantities have been normalized with respect to feed moisture- and ash-free coal; i.e., $p_o = P_o/C_i$, $c_o = C_o/C_i$, and $\ell_o = L_o/C_i$, where P_o, etc., are the concentrations by weight of components p, etc., in the product, and C_i is the concentration of the maf coal at the reactor inlet.

Differential mass balances based on the standard axial dispersion model can be expressed as:

$$\frac{1}{Pe}\frac{d^2c}{dx^2} - \frac{dc}{dx} - (R_1 + R_2)\,c = 0$$

$$\frac{1}{Pe}\frac{d^2p}{dx^2} - \frac{dp}{dx} + R_2\,c = 0$$

$$\frac{1}{Pe}\frac{d^2\ell}{dx^2} - \frac{d\ell}{dx} + R_1 c = 0 \qquad (2)$$

The independent variable "x" is the dimensionless reactor length, i.e., $x = z/\xi$, where z is the distance from the reactor inlet and ξ is the total reactor length. R_1 and R_2 are the dimensionless rate constants. They can be expressed as:

$$R_1 = k_1\Gamma,\ R_2 = k_2\Gamma \qquad (3)$$

In Chemical Reaction Engineering—Houston; Weekman, V., et al.;
ACS Symposium Series; American Chemical Society: Washington, DC, 1978.

where k_1 and k_2 are intrinsic rate constants which include catalyst void fraction and dilution effects. The quantity Γ is defined as the reciprocal of slurry space velocity (g slurry/g cat/hr), i.e., slurry space time. Pe is the Peclet number defined as $U\xi/D_a$, where U is the superficial velocity of liquid slurry and D_a the axial dispersion coefficient measured in a glass model under the present reactor configuration (14).

Equation (2) assumes that the Peclet numbers for all species are equal. The magnitude of the Peclet number characterizes the extent of backmixing within the reactor. At the limiting conditions, an infinite Peclet number means plug flow, while a Peclet number of zero means completely backmixed flow, i.e., the reactor operates just like a continuous stirred tank reactor.

Equation (2) is subjected to the standard boundary conditions:

$$1 = c - \frac{1}{Pe}\frac{dc}{dx}$$

$$0 = p - \frac{1}{Pe}\frac{dp}{dx} \qquad (4)$$

$$\ell_i = \ell - \frac{1}{Pe}\frac{d\ell}{dx}$$

and

$$\frac{dc}{dx} = \frac{dp}{dx} = \frac{d\ell}{dx} = 0 \qquad \text{at } x = 1- \qquad (5)$$

Equation (2) assumes that the feed contains only coal and solvent.

An analytical solution to Equations (2)-(5) can be obtained in a straightforward manner. The solution for the coal concentration is

$$c = \alpha_1 e^{\frac{Pe}{2}(1-q)x} - \alpha_2 e^{\frac{Pe}{2}(1+q)x} \qquad (6)$$

where

$$q = \sqrt{1 + \frac{4(R_1 + R_2)}{Pe}}, \qquad \alpha_1 = \frac{2(1+q)}{(1+q)^2 - (1-q)^2 e^{-Peq}} \qquad (7)$$

$$\alpha_2 = \frac{(1-q)}{(1+q)} e^{-Peq} \alpha_1$$

Similar solutions for "p" and "ℓ" can be obtained.

In Chemical Reaction Engineering—Houston; Weekman, V., et al.;
ACS Symposium Series; American Chemical Society: Washington, DC, 1978.

Results and Discussion

The best values of the rate constants were obtained by non-linear least square fitting of the data to the analytical equations (16). Experimental coal solvations and the yields of gases and oils are compared with model predictions in Figure 2. As shown by this figure, the model correlates the experimental data quite well.

From the experimental data, rate constants for two reactions were obtained at three temperature levels. The Arrehenius plots for the rate constants are shown in Figure 3. Interestingly, the activation energies for all the reactions were found to be considerably higher than normally encountered in first order catalytic reactions. This offers further evidence that the catalyst is not directly involved in the solvation reaction.

The major difference between the kinetic model presented in this study and those presented in the literature is that, here, coal liquefaction is assumed to occur in a parallel reaction mechanism. All the products, light or heavy, are assumed to be formed directly from coal. The models proposed in the literature assume a series reaction mechanism, wherein only heavy components (i.e., high boiling oil fractions) are formed directly from coal, and the lighter components (i.e., low boiling oil fractions) and the gases are produced by the cracking of the heavy components. The present model also assumes that the catalyst provides an excess of hydrogen donor solvent required for the coal liquefaction. A more rigorous model (which would also take catalyst aging effects into account) should include the role of hydrogen donor solvent.

Separate measurements of water, light gases (C_1-C_4) and by-products as functions of space time and temperature were also carried out. These data were correlated by a kinetic model which assumes that water, light gas and by-products all are produced directly from coal by first-order irreversible reactions. This type of "shooting star" mechanism correlated the separate data for water, light gases and by-products as functions of space time as well as the data for the total gas shown in Figure 2. Furthermore, the activation energies for the reactions coal --> water, coal --> by-product and coal --> light gases were found to be 53,500, 63,500 and 85,200 cal/g mole.

In a backmixed reactor, the gas flow rate should have a significant effect on the product distribution. High gas flow is important for eliminating possible resistances to the transfer of hydrogen from the gas phase to the catalyst surface. Two important resistances in the present case are the gas-liquid interface resistance and the inter-particle diffusional resistance within the catalyst tube. A large gas flow would, however, also give significant backmixing in the open portion of the reactor,

In Chemical Reaction Engineering—Houston; Weekman, V., et al.;
ACS Symposium Series; American Chemical Society: Washington, DC, 1978.

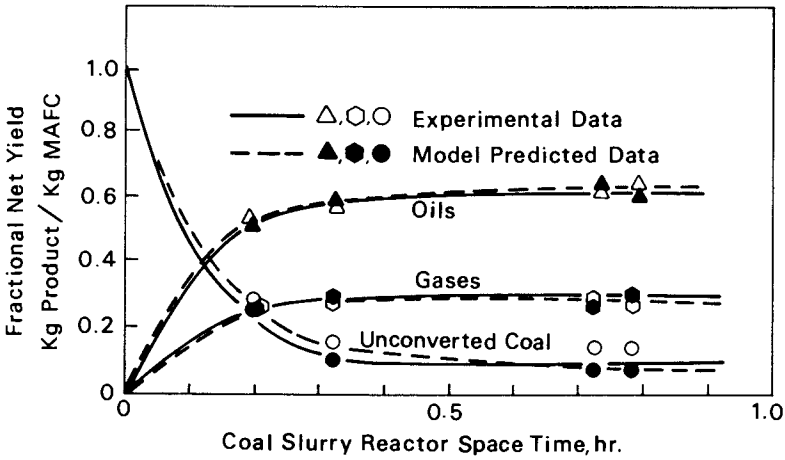

Figure 2. Experimental and model predicted data for reactor space time effect on coal solvation and productions of oils and gases

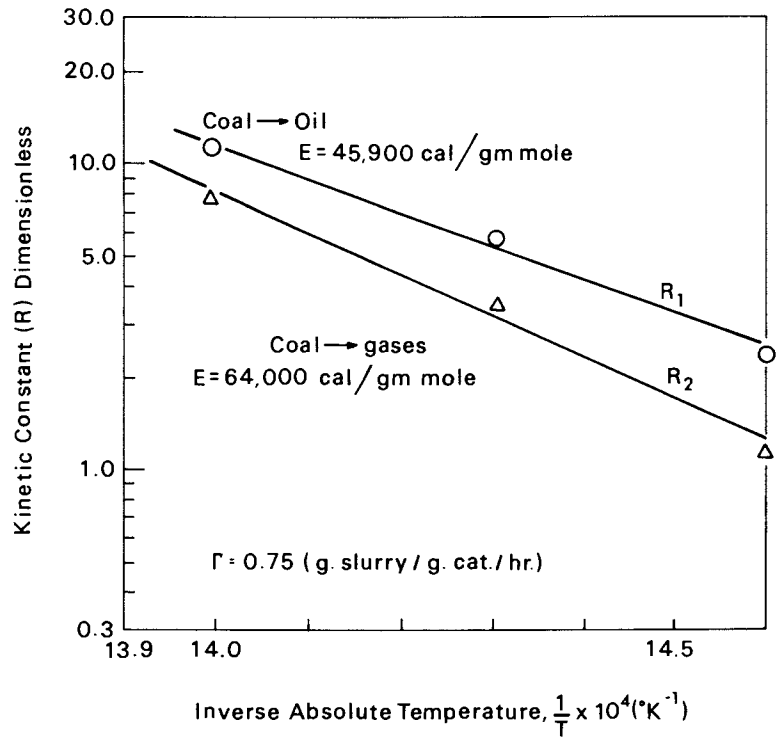

Figure 3. Arrhenius plots for reaction rate constants

as well as significant evaporation of the liquid products, both of which would give a poorer product distribution.

In the present study, the gas-liquid mass transfer coefficients under the prevailing experimental conditions were estimated using the correlations of Akita and Yoshida (17). The radial dispersion coefficients within the catalyst tubes were measured as a function of gas flow rate in a glass model of the reactor. The details of these measurements will be released in a subsequent publication. Based on this knowledge and an estimated value of the catalytic kinetic constant for solvent hydrogenation at the highest temperature and pressure conditions examined in this study, the minimum gas flow rate required to permit neglecting mass transfer resistances was obtained. This value of the gas flow rate was used in all experiments.

Conclusions

As a result of the present study, the following conclusions are drawn.

1. The simple kinetic model for coal liquefaction presented here appears to correlate well the experimentally observed effects of space time and temperature on coal solvation and the production of oils. The model must be refined further to account for hydrogen donor and hydrocracking reactions and to properly explain the effect of pressure on the liquefaction process.
2. It appears that after a relatively short space time, the product distribution during a catalytic coal liquefaction process run remains essentially unchanged.
3. The conversion of coal into gases and oils appears to be a very temperature-sensitive reaction.
4. Since the liquefaction of coal in a regular packed bed catalytic reactor would cause plugging problems, the data illustrate the feasibility of using a novel type of reactor to continuously operate a three-phase gas-liquid-solid (reactant) reaction in the presence of a catalyst.

Literature Cited

1. Neavel, R. C., Fuel (1976), 55, 237.
2. Plett, E. G., Alkidas, A. C., Roger, F. E., Mackiewicz, A. Z., and Summerfield, M., a paper presented at University-ERDA Contractors Conference, (October 22-23, 1975), Salt Lake City, UT.
3. Curran, G. P., Struck, R. T., and Gorin, E., Proceedings, Symposium on Pyrolysis Reactions of Fossil Fuels," Div. Petroleum Chem., ACS (March 23-26, 1966), Pittsburgh, PA, C-130.
4. Guin, J. A., Tarrer, A. R., Pitts, W. S., and Prather, J. W., Proceedings for "Symposium on Coal Liquefaction," Div. Petroleum Chem., ACS (August 1976), San Francisco, CA, 170.

In Chemical Reaction Engineering—Houston; Weekman, V., et al.;
ACS Symposium Series; American Chemical Society: Washington, DC, 1978.

5. Fu, Y. C. and Batchelder, R. F., Proceedings of Div. Fuel Chemistry, ACS (August 29-September 3, 1976), 21 (5), 78.
6. Squires, A. M., "Reactor Paths in Donor Solvent Coal Liquefaction," a paper presented at conference on coal gasification/liquefaction, Moscow, U.S.S.R. (October 1976), sponsored by U.S.-U.S.S.R. Trade and Economic Council, Inc.
7. Guin, J., Tarrer, A., Taylor, L., Jr., Prather, J., and Green, S., Jr., I&EC Process Design and Dev. (1976) 15 (4), 490.
8. Kang, C. C., Nongbri, G., and Stewart, N., Proceedings of Div. Fuel Chemistry, ACS (August 29-September 3, 1976), San Francisco, CA, 21 (5), 19.
9. Tarrer, A. R., Guin, J. A., Pitts, W. S., Henley, J. P., Prather, J. W., and Styles, G. A., Proceedings of Div. Fuel Chemistry, ACS (August 29-September 3, 1976), San Francisco, CA, 21 (5), 59.
10. Gleim, W. K. T., Proceedings of Div. Fuel Chemistry, ACS (August 29-September 3, 1976), San Francisco, CA, 21 (5), 91.
11. Whitehurst, D. D. and Mitchell, T. O., Proceedings of Div. of Fuel Chemistry, ACS (August 29-September 3, 1976), San Francisco, CA, 21 (5), 127.
12. Oblad, A. G., Catalysis Reviews, Science and Engineering (1976), 14 (1), 83.
13. Chun, S. W., Cronauer, D. C., and Leslie, T. W., U.S. Patent No. 3,957,619 (1976).
14. Shah, Y. T., Ratway, C. A., and McIlvried, H. G., British Trans. Inst. of Chem. Engrs. (in press).
15. Kato, Y., Nishiwaki, A., Fukuda, T., and Tanaka, S., J. of Chem. Engineer. of Japan (1972), 5 (2), 112.
16. Paraskos, J. A., Shah, Y. T., McKinney, J., and Carr, N. L., I&EC Process Design and Dev., (1976), 15, 165.
17. Akita, K. and Yoshida, F., Ind. Eng. Chem. (1974), 13 84.

In Chemical Reaction Engineering—Houston; Weekman, V., et al.;
ACS Symposium Series; American Chemical Society: Washington, DC, 1978.

26

Development of Reaction Models for Complex Gas Phase Reactions

K. H. EBERT, H. J. EDERER, and P. S. SCHMIDT

Institut für Angewandte Physikalische Chemie der Universität,
Im Neuenheimer Feld 253, D-6900 Heidelberg, West Germany

Gas phase reactions are generally complex and setting up a reaction mechanism to evaluate an applicable kinetic scheme does not seem very promising. In particular, this concerns thermal decomposition reactions of hydrocarbons, in which the number of reactive and stable species is large. The effort to accomplish 'master set' kinetics is huge and usually does not justify the results obtainable.

We have tried to develop a generally applicable method to find out the 'relevant' elementary reactions, which mainly contribute to the overall reactions and put them together to a consistent reaction mechanism. In a semi-quantitative analysis we have tried to determine the different species and their relative abundance at low pressure in a certain temperature range. Starting at low temperatures at which the number of species is small a reaction mechanism consisting of elementary reactions is set up, and calculations based on this mechanism should be verified by comparison with experiments at normal pressure. In developing the mechanism to higher temperatures and conversions one expects that more elementary steps have to be added to the mechanism, but the number should be kept to a minimum.

In the present paper we have tried to describe our development of a reaction scheme for the pyrolysis of ethylbenzene. It seemed to us that this reaction was complicated enough to get sufficient details and some of them with more general significance. On the other hand, we hoped that, due to a single initiation reaction within a fairly wide temperature range, the reaction would be relatively easily covered by the methods applied.

© 0-8412-0401-2/78/47-065-313$05.00/0

Experimental Methods

Low Pressure Apparatus (LPA). The low pressure experiments have been carried out in a flow apparatus made of quartz and depicted in Figure 1. The reaction took place in a reaction zone, which had a length of approx. 10cm, the reaction zone being heated with a tantalum wire. The apparatus was suitable for temperatures up to 1000^0C, the limiting factor being the heating of the ionisation source.

At the end of the reaction zone a sample flow of the reaction products was led through a nozzle directly into the electron impact ionisation chamber of a time of flight (TOF) mass spectrometer. The main flow of the products was pumped off.

The pressure in the reaction zone was from 1 to $10x10^{-2}$ mm. We adjusted the pressure in the reactor to such a level that the pressure in the ionisation source of the TOF was less then 10^{-4}mm. Variation of the pumping speed allowed to choose reaction times between 0.001 and 1 sec. To keep fragmentation in the ion chamber low we used an electron energy of 12eV in most experiments.

As a result a survey pattern was obtained on all species contained in the reaction, including free radicals. By changing the temperature of the reaction zone we obtained information on the temperature dependence of the abundances of the reaction products and radicals. The results are of a semi-quantitative character because the ionisation probabilities of the species and their mass discrimination in the flow system are not known.

Normal Pressure Apparatus (NPA). To verify our calculations based on the reaction scheme from the LPA experiments we set up a reactor which allowed us to carry out accurate quantitative measurements on the pyrolysis of ethylbenzene. This apparatus was made of quartz and is depicted in detail in Figure 2. The reaction in this flow reactor starts in the mixing chamber in which overheated argon joins the ethylbenzene flow. The temperature of the argon flow was kept at a specific value in order that the reaction temperature was obtained simply by the mixing of the two streams. The reaction zone of 10cm length was kept at a constant temperature by independent control of several coils. The reaction gas was quenched with cold argon at the end of the reaction zone. The temperature in the reactor was continuously controlled with a moveable thermocouple along the center of the reactor. The re-

In Chemical Reaction Engineering—Houston; Weekman, V., et al.;
ACS Symposium Series; American Chemical Society: Washington, DC, 1978.

action time was adjusted by the rate of the argon flow through the reactor.

A sample of the reaction products was passed to the injection loop of a gas chromatograph for analysis. Argon was used as carrier gas for the gas chromatograph. Thus, the carrier gas in the reactor was of no influence on the separation. We used two separation columns in parallel, one for the gases (H_2,CH_4,C_2H_6, C_2H_4) and the other for the liquids (ethylbenzene, styrene, toluene, benzene). Flame ionisation and thermal conductivity were used as detectors. Great care was taken to ensure high sensitivity and reproducibility of the analytical method.

Mathematical Methods

The differential equations which arise in almost all chemical kinetic studies of complex reaction schemes are "stiff differential equations". In chemical kinetics the stiffness is caused by the huge differences in the reaction rate constants of the various elementary reactions. It is impossible to solve such a system of differential equations by the usual Rung-Kutta methods. Therefore we used a program, described by Gear (1) as a special multi step predictor-corrector method with self adjusting optimum step size control.

The program needs not only the subroutine for the derivatives of the dependent variables, i.e. concentrations of the chemical species involved over time, which constitutes a system of m stiff differential equations, but also a subroutine which evaluates the partial derivatives of the differential equations with respect to the concentrations of the different species, resulting in m^2 equations.

Because it is very cumbersome to set up the m differential equations and the m^2 equations for the partial derivatives, we have developed a program which directly generates the two subroutines from the chemical reaction scheme and the assigned kinetic parameters. The output of the program gives the concentration of each chemical species in dependence on time. We also obtained information on the contribution of each elementary reaction on the overall reaction. These calculations must be repeated for different preselected reaction temperatures. The effort required for the computation of the reaction kinetics at a particular temperature was approx.10 sec of CPU time on an IBM 370.

In Chemical Reaction Engineering—Houston; Weekman, V., et al.;
ACS Symposium Series; American Chemical Society: Washington, DC, 1978.

Results and Discussion

Experimental results on the pyrolysis of ethylbenzene obtained in the low pressure apparatus (LPA) are shown in Figure 3, in which the distribution of the various species is shown in dependence on the reaction temperatures as an analog plotting. 72 different species were detected. Those with an abundance smaller than 2% are suppressed in Figure 3.

Up to temperatures of 750°C the following 9 species are obtained: methane, ethylene, toluene, styrene, ethylbenzene, dibenzyl, methyl, benzyl and ethylbenzyl. The most simple reaction scheme involving these consists of seven elementary reactions:

(1) $\phi\text{-}CH_2CH_3 \rightarrow \phi\text{-}CH_2 + CH_3$

(2) $CH_3 + \phi\text{-}CH_2\text{-}CH_3 \rightarrow \phi\text{-}CH\text{-}CH_3 + CH_4$

(3) $\phi\text{-}CH\text{-}CH_3 \rightarrow \phi\text{-}CH{=}CH_2 + H$

(4) $H + \phi\text{-}CH_2\text{-}CH_3 \rightarrow \phi\text{-}CH\text{-}CH_3 + H_2$

(5) $H + \phi\text{-}CH_2 \rightarrow \phi\text{-}CH_3$

(6) $CH_3 + CH_3 \rightarrow C_2H_6$

(7) $2\phi\text{-}CH \rightarrow \phi\text{-}CH_2CH_2\text{-}\phi$

Ethylbenzene is disintegrated in the well-known initiation reaction (1). Methyl initiates the reaction chain in which styrene and hydrogen are formed. Toluene is formed in the transfer reaction (5), while in the two reactions (6) and (7) recombination of radicals occurs.

Kinetic parameters (preexponential factors and activation energies) have been allocated to the particular reaction steps. For reaction (1),(2) and (6) the values were taken from the literature, for the other reactions values have been estimated from analogous approximations (2)-(6). These are listed in Table I. Calculations of the reaction based on the scheme were made and the results compared with the experimental results obtained from the runs carried out in the NPA. Good agreement was obtained for the decrease in ethylbenzene and the increase in styrene and hydrogen concentrations. In the NPA experiments relatively large amounts of ethylene and benzene were formed at temperatures below 760°C. To take

In Chemical Reaction Engineering—Houston; Weekman, V., et al.;
ACS Symposium Series; American Chemical Society: Washington, DC, 1978.

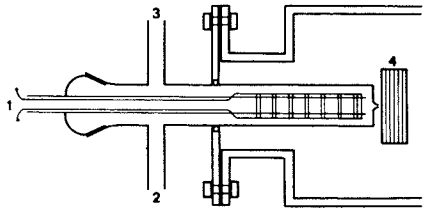

Figure 1. Low pressure apparatus. (1) inlet, (2) vacuum pump, (3) manometer, (4) ion source of mass spectrometer.

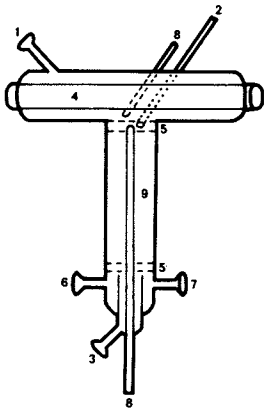

Figure 2. Normal pressure apparatus. (1) inlet argon carrier, (2) inlet ethylbenzene, (3) inlet argon quench, (4) silit heater housing, (5) mixing chamber, (6) sampling line to GC, (7) outlet, (8) thermocouple, (9) reaction zone.

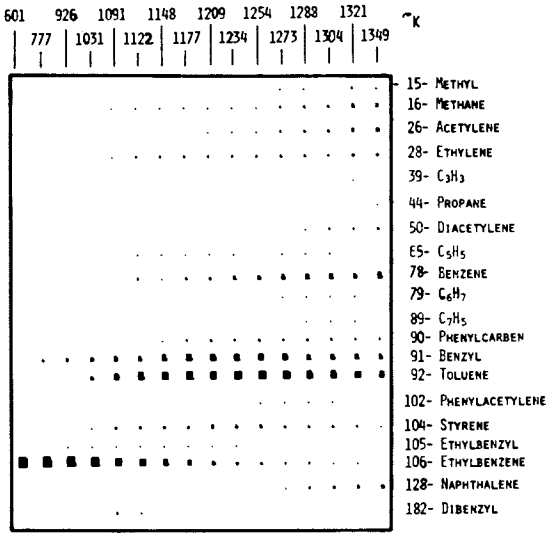

Figure 3. Survey pattern of LPA experiments. Abundances of various species at different temperatures.

these two species into account the following steps were set up and have been added to the reaction scheme:

(3a) $\phi\text{-CH-CH}_3 \rightarrow C_6H_5 + C_2H_4$

(3b) $C_6H_5 + \phi\text{-CH}_2\text{-CH}_3 \rightarrow C_6H_6 + \phi\text{-CH-CH}_3$

(4a) $H + \phi\text{-CH}_2\text{-CH}_3 \rightarrow C_8H_{11}$

(4b) $C_8H_{11} \rightarrow C_6H_7 + C_2H_4$

(4c) $C_6H_7 \rightarrow C_4H_3 + C_2H_4$

(4d) $H + C_4H_3 \rightarrow C_4H_4$

Disintegration of the ethylbenzyl leads to the formation of phenyl and ethylene, the former stripping a hydrogen atom from ethylbenzene to form benzene and ethylbenzyl.

Since, as the temperature gets higher, the production of ethylene by far exceeds that of benzene reactions (4a-4d) are proposed, in which the aromatic ring is destroyed and two molecules of ethylene are produced. Biacetylene as well as the three radicals C_8H_{11}, C_6H_7, and C_4H_3 have been detected in the low pressure experiments. Again, kinetic parameters have been estimated and allocated to the various reaction steps (Table I).

For verification of the calculations of the ex-

ER No	$_{10}$log A	E	ER No	$_{10}$log A	E
(1)	15.3	305.4	(4a)	11.0	46
(1a)	16.0	347.3	(4b)	13.0	105
(2)	7.82	29.3	(4c)	13.0	105
(2a)	13.0	125.5	(4d)	13.0	105
(3)	14.85	125.5	(5)	11.0	0
(3a)	14.85	182	(6)	10.34	0
(3b)	11.0	31.4	(7)	11.9	0
(4)	10.5	21.0			

Table I. Kinetic (Arrhenius) parameters for all reaction steps ER of the comprehensive reaction mechanism. Preexponential Factor A in $sec.^{-1}$ or (l/mol·sec) resp., Activation Energy in (kJ/mol).

In Chemical Reaction Engineering—Houston; Weekman, V., et al.;
ACS Symposium Series; American Chemical Society: Washington, DC, 1978.

tended reaction scheme a rather large variety of experimental data were available from the NPA runs. Two sets of experiments were performed, one up to temperatures of 720°C and conversions of ethylbenzene to 13% and the second up to temperatures as high as 830°C according to conversions of approx. 75%.The flow of the reaction gas was constant in all these experiments the reaction time varied, due to different temperatures, between 2 and 3 msec. Good agreement was obtained with the experimental data for the experiments covering the temperatures up to 750°C. This is shown in Figures 4-7, in which for ethylbenzene, styrene, benzene and ethylene conversions at specific reaction times are plotted against the reaction temperature. The dotted lines represent the calculations with the extended reaction scheme. No agreement could be obtained for the production of methane and toluene where larger amounts were obtained in the experiments than resulted from the calculations. However it should be noted that the absolute amounts of both substances were relatively low in this temperature range. For further testing of the reaction scheme we calculated certain quotients of molar quantities of species and compared them with the experimental data. Some of them are shown in Figures 8-10. The hydrogen-styrene ratio should be unity as both species are produced in the same reaction chain exclusively, which is confirmed by the experimental results over the whole temperature range, as shown in Figure 8.

Figure 9 shows the branching of reactions (3) and (3a). Again good agreement is obtained between the calculations and the experiments. As the temperature increases, the chain reactions (3) and (4) decrease in terms of relative conversions. The second branching within the reaction scheme is the concurring reactions (4) and (4a), which can be expressed by the ethylene styrene ratio. In Figure 10 the experimental values are compared with the calculations. The agreement is again very satisfactory which means that the aromatic ring is destroyed even at relatively low temperatures.

For the methane and toluene formations the calculated values were too small compared with the calculations, and it seems that this has to be taken into account by the addition of further reaction steps. Probably the two substances are formed in a catalytic process on the reactor walls, which needs a more complicated mechanism.

As shown in Figure 4 the calculation of the overall reaction rates with the extended scheme agrees

In Chemical Reaction Engineering—Houston; Weekman, V., et al.;
ACS Symposium Series; American Chemical Society: Washington, DC, 1978.

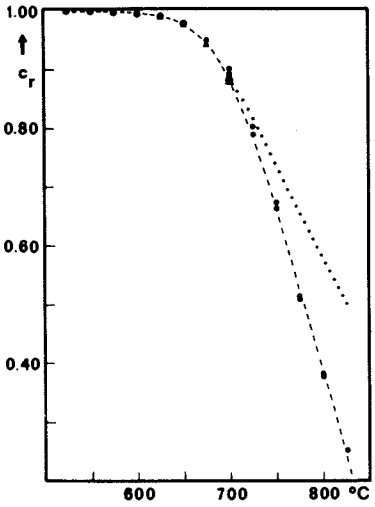

Figure 4. Ethylbenzene

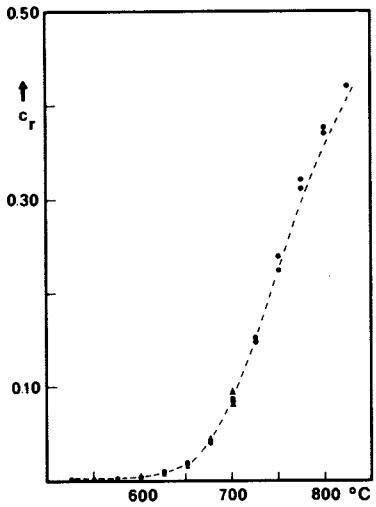

Figure 5. Styrene

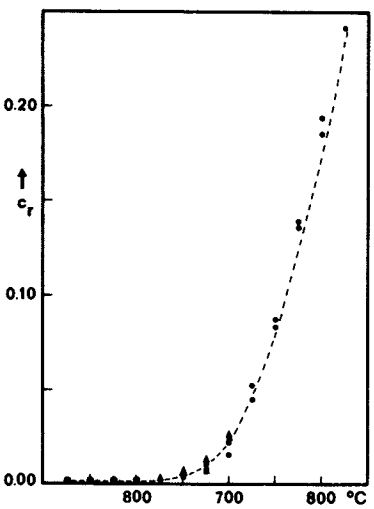

Figure 6. Benzene

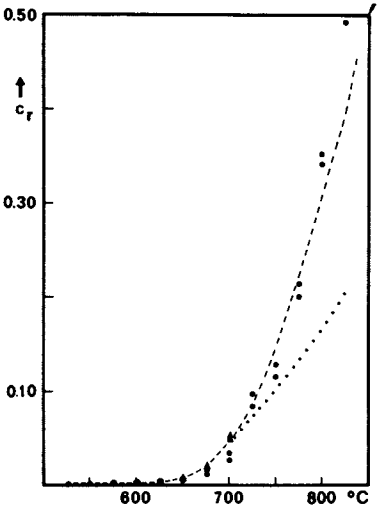

Figure 7. Ethylene

Figures 4–7. Comparison of the decomposition of ethylbenzene and yields of different products or ratios of them in relative molar concentrations at various temperatures in the NPA (● ▲ experiments at different runs) with calculations of the extended (· · ·) and comprehensive (– – –) reaction schemes

In Chemical Reaction Engineering—Houston; Weekman, V., et al.;
ACS Symposium Series; American Chemical Society: Washington, DC, 1978.

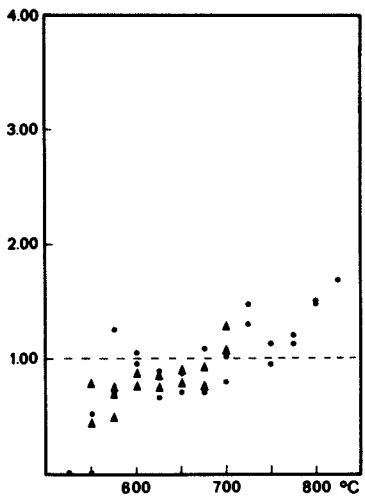

Figure 8. Hydrogen/styrene

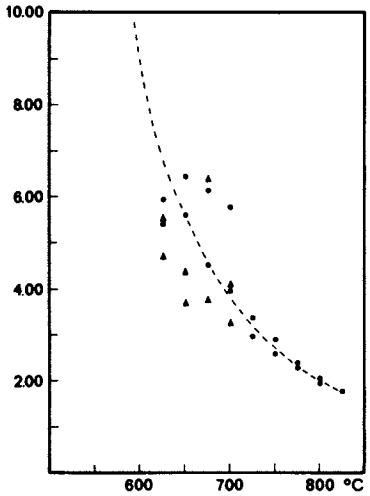

Figure 9. Styrene/benzene

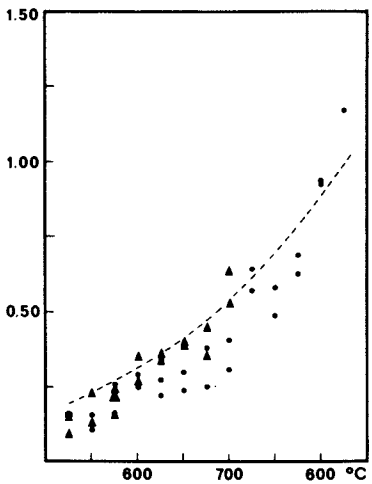

Figure 10. Ethylene/styrene

Figures 8–10. Comparison of the decomposition of ethylbenzene and yields of different products or ratios of them in relative molar concentrations at various temperatures in the NPA (● ▲ experiments at different runs) with calculations of the extended (· · ·) and comprehensive (– – –) reaction schemes

In Chemical Reaction Engineering—Houston; Weekman, V., et al.;
ACS Symposium Series; American Chemical Society: Washington, DC, 1978.

well with the experiments covering temperatures up to 750^0C. Above this temperature the experimental rates are appreciably higher and accompanied by an increase in benzene and ethylene concentrations. To account for this we introduced a second initiation reaction:

(1a) $\phi\text{-}CH_2CH_3 \rightarrow C_6H_5 + C_2H_5$

in which ethylbenzene is split in the α-position. Phenyl undergoes reaction (3a) and ethyl disintegrates as follows:

(2a) $C_2H_5 \rightarrow C_2H_4 + H$

Both reactions have been allocated kinetic constants (see Table I) and added to the extended reaction scheme. As shown in Figures 4 and 5 calculations now fitted in much better with the experimental data up to temperatures of 825^0C. Benzene and ethylene production gives very good agreement with the calculation as can be seen from Figures 6 and 7.

In a series of preliminary experiments in the NPA conversion-time runs have been performed at 675^0C simply by changing the flow rate. Special care has been take to keep the temperature constant. Deviations could not be prevented at low flow rates, i.e. high conversions. The results are shown in Figures 11-13. Deviations at higher conversions may be due to a decrease in temperature or inhibition reactions. The agreement at short reaction times is remarkably good, and induction periods were in all cases of the same shape in both the calculations and the experiments.

Summarising and Concluding Remarks

For the pyrolysis of ethylbenzene a reaction scheme could be set up by firstly selecting the most simple reaction scheme, taking into account the main products of the reaction at low temperatures. Secondly, on raising the temperature and the conversion the number of species in the reaction mixture gets more abundant, the reaction scheme was improved by adding new reactions for which experimental evidence could be obtained from the LPA experiments. Then all reaction steps were allocated kinetic constants, which either were taken from the literature or estimated from analogous reactions. Minor alterations of some of the kinetic constants were made for better agreement with the experimental data. In this way, grad-

In Chemical Reaction Engineering—Houston; Weekman, V., et al.;
ACS Symposium Series; American Chemical Society: Washington, DC, 1978.

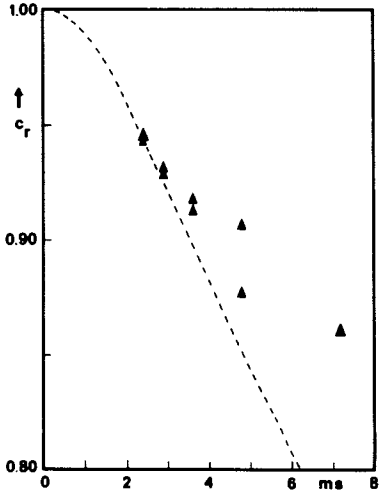

Figure 11. Ethylbenzene

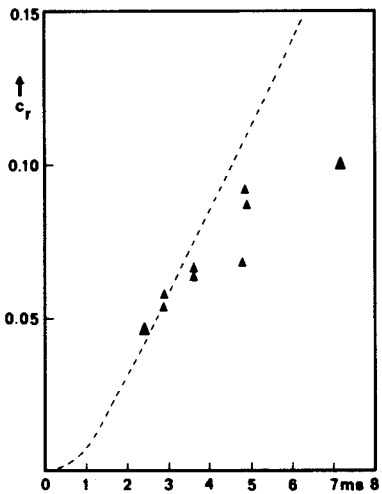

Figure 12. Styrene

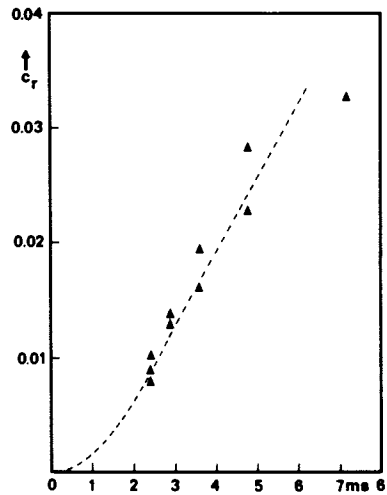

Figure 13. Benzene

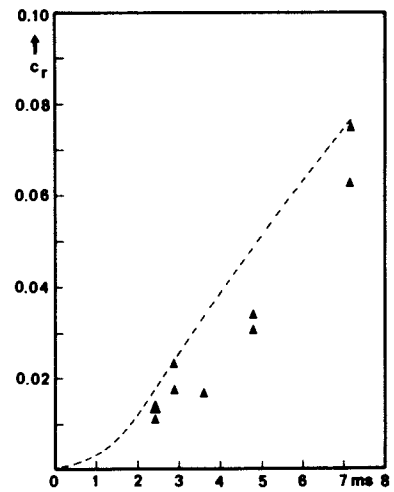

Figure 14. Ethylene

Figures 11–14. Comparison of relative molar concentrations against time of different species at 675°C with calculations of the comprehensive mechanism

ually, the reaction mechanism, which finally consists of 15 reaction steps, has been developed up to reaction temperatures of 825^{0}C and conversions of nearly 80%. Care was taken to ensure that each radical could react within a termination reaction. Therefore some more termination reactions than those formulated above were originally introduced into the calculations. Some of them could later be dropped, when it was found that they were of only minor importance to the calculation.

For the reaction chosen the agreement of the calculations and experimental results was good. The distribution of all main products could be calculated within a relatively large temperature range.

The method outlined appears to be more generally applicable to complicated reactions and provides kinetic results of good quality, involving an effort which is justifiable in many cases. Also it gives an insight into the course of a reaction, showing how the individual elementary reactions contribute to the process. Furthermore the reaction mechanism can be compressed by dropping certain reaction steps which are of minor interest, or by combining several steps into one equation with appropiate constants, which may be help save computer time. In this way it seems possible to modify a reaction mechanism to suit a special problem without sacrificing accuracy of the results obtained.

Literature Cited

(1) Gear W.C., "Numerical Initial Value Problems in Ordinary Differential Equations" Prentice-Hall Inc., New York, 1972.
(2) Benson S.W., "Thermochemical Kinetics", John Wiley, New York, 1968
(3) Benson S.W., O'Neal H.E., "Kinetic Data on Gas Phase Minimolecular Reactions" NSRDS-Nat.Bur.of Standards 21, Washington, 1970
(4) Kerr J.A., Parsonage M.J., "Evaluated Kinetic Data on Gas Phase Hydrogen Transfer Reactions of Methyl Radicals" Butterworth, London, 1976
(5) Kerr J.A., Parsonage M.J., "Reactions of Atoms and Radicals with Alkenes, Alkynes and Aromatic Compounds" Butterworth, London, 1972
(6) Kondratiev V.N., "Rate Constants of Gas Phase Reactions" NSRDS-Nat.Bur.of Standards, Washington, 1972

In Chemical Reaction Engineering—Houston; Weekman, V., et al.;
ACS Symposium Series; American Chemical Society: Washington, DC, 1978.

27

Aromatic Sulfonation in a Cyclone Reactor, a Stirred Cell, and a Cocurrent Tube Reactor; Influence of Mass Transfer on Selectivity

ANTONIE A. C. M. BEENACKERS

Department of Chemical Engineering, Twente University of Technology, Enschede, P.O. Box 217, The Netherlands

For mass transfer, followed by a fast chemical reaction of type

$$A(G) \longrightarrow A(L) \quad (1)$$

$$A(L) + zB(L) \longrightarrow zI(L); \qquad r_B = -zk_1 c_A c_B \quad (2)$$

$$A(L) + I(L) \longrightarrow I'(L); \qquad r_{I'} = k_2 c_A c_I \quad (3)$$

Van de Vusse [1] pointed out that selectivity with respect to I increases with an increase of the mass transfer coefficient (k_L). In light of this observation, we have developed a new reactor of cyclonic type in which, due to strong centripetal forces on the gas bubbles, a very high k_L is realized [2]. This paper deals with the selectivities obtained in sulfonation of benzene with sulfur trioxide. Both neat benzene and benzene diluted with 1,2-dichloroethane were used. This reaction was selected as a model reaction for industrially important aromatic sulfation (e.g. detergents). We studied the reaction in three reactor types that greatly differ in mass transfer characteristics, i.e. in a stirred cell reactor (low k_L), a co-current gas-liquid tube reactor (intermediate k_L) and in the cyclone reactor (high k_L).

Reaction Kinetics; Regime of Mass Transfer with Chemical Reaction

We have discussed reaction mechanism and kinetics of sulfonation of benzene (B) with SO_3 (A) in aprotic media [3] and have concluded that the reaction proceeds according to Van de Vusse kinetics (1-3), with k_1 (25°C) >9.4 m^3/kmol s and $z = \frac{1}{2}$. Pyrosulfonic acid (I) and Ar S_3O_9H (I′) are both unstable and react with benzene to give the desired product benzenesulfonic acid (P) and the unwanted product diphenyl sulfone (X), respectively

$$I(L) + B(L) \longrightarrow 2P(L) \quad (4)$$

$$I'(L) + B(L) \longrightarrow X(L) + H_2S_2O_7\ (L) \quad (5)$$

Reaction (4) is slow with respect to mass transfer and thus of negligible influence on absorption rate. Reaction (5) consumes only minor amounts of benzene (all experimentally observed selectivities are (often much) above 70% based on benzene). Therefore this reaction also does not influence absorption rate appreciably. For reaction sequence (1-3), the relation between mass transfer parameters and conversion rate is – in general – complex. However, as long as observed selectivity η is high, the influence of reaction (3) on SO_3 absorption rate is an effect that may be neglected in the first, rough estimation of the regime of absorption with reaction [4] which characterizes the system. Which regime occurs, mainly depends on the numerical values of the dimensionless groups Ha, E_∞ and $mk_L E/k_G$. Due to uncertainties in the kinetic rate constant, in local liquid viscosity in the interface diffusion zone (to be discussed later), and in SO_3-solubility, a prediction of the regime characterizing sulfonation of benzene, solved in 1,2-dichloroethane, is not free of speculation. In case of no liquid viscosity increase at the interface during reaction, Table I gives numerical estimations of the relevant parameters for atmospheric sulfonation at

© 0-8412-0401-2/78/47-065-327$05.00/0

% benzene by volume	Ha	$1 + \frac{D_B \bar{c}_B}{z D_A m (c_A)_G}$	$\frac{k_G}{m k_L}$
100	> 4	5.6	0.7
30	> 2.2	2.4	0.7
10	> 1.3	1.4	0.7
5	> 0.9	1.2	0.7

Table I. Estimated mass transfer parameters for sulfonation of benzene, solved in 1,2-dichloroethane with gaseous sulfur trioxide (10 mol % in nitrogen) at 20°C and 10^5 Pa in a conventional bubble contactor with $\mu = 0.7\ 10^{-3}$ s Pa and k_l the minimum value of 9.4 m^3/kmol s. For hydrodynamical and physical constants applied, see reference No [3].

20°C with a mixture of SO_3 and nitrogen containing 10 mol % SO_3 (typical for our experiments in cyclone and tube reactor) in a conventional bubble column. In our stirred cell sulfonation experiments, k_L was found to be a factor of 10 lower than the value $1.2\ 10^{-4}$ [m/s] used in calculating Table I. Therefore $Ha \gg 1 + D_B \bar{c}_B / z D_A m (c_A)_G$ in the stirred cell. This means that the reaction is instantaneous with respect to mass transfer in that reactor.

Influence of Mass Transfer on Selectivity

As first pointed out by Van de Vusse [1], the observed selectivity η' for fast reactions of type (1-3) is influenced by the value of k_L. 'Fast' implies $Ha > 0.5$ and not much smaller than E_∞ [5]. Some experimental results are available for chlorination [1,6-9]. A numerical analysis [10], an analog simulation [1] and trial and error procedures [6,8,10] by which approximate solutions can be obtained, have been presented.

As in our sulfonation experiments, there is often much doubt about the exact values of the relevant parameters (c, m, ρ, μ, D, T) at the interface, mainly because local interface conditions differ from bulk conditions. Because of this difficulty, explicit rough approximate relations for η' are sophisticated enough to discuss experimental results and are therefore very useful. Harriott [5] derived such a simple model for the intermediate regime between fast and instantaneous reaction. Our experiments are mainly in the instantaneous regime. Based on film theory, we derived for this regime [3]

$$(1 - \eta') \cong \frac{k_2 D_A}{2z} \frac{[D_B \bar{c}_B / D_l + \bar{c}_l]}{k_L^2 E_\infty^2} \qquad (6)$$

for $(1 - \eta') \ll 1$.

Equation (6) shows the manner in which the selectivity is favoured in the instantaneous regime by a high value of k_L, provided that the selectivity is not much smaller than one. The latter condition is always fulfilled in our experiments.

Experimental

The stirred cell reactor was of the Danckwerts type [4, page 180]. The reactor was filled with degassed (diluted) benzene and kept under its own vapour pressure. The experiment was then started by connecting the space above the liquid to a thermostrated (30°C) container, filled with degassed stabilized liquid sulfurtrioxide, which was also under its own vapour pressure. Due to the difference in partial pressure of reaction mixture and liquid SO_3, the latter evaporated and flowed via a flow controller and a rotameter to the cell reactor where it absorbed into the liquid.

Figure 1 is a sketch of the cyclone reactor. The liquid is fed tangentially into it (A). A gas mixture of SO_3 and N_2 is introduced into the reactor via a porous section of the cylindrical wall. The liquid phase is the continuous phase in the reactor, except near the cyclone-axis. Here, a gaseous core is found, due to a strong centripetal field, generated by the rotating liquid. This field causes gas bubbles to spiral from the wall to the cyclone-axis. Gas leaves the reactor via the upper outlet which is known as the vortex. Liquid leaves the reactor via the bottom outlet which

In Chemical Reaction Engineering—Houston; Weekman, V., et al.;
ACS Symposium Series; American Chemical Society: Washington, DC, 1978.

is referred to as the apex. Cone E prevents gas entrainment with the liquid. Liquid entrainment through the vortex varied between 12 and 20% depending on gas and liquid velocities. Liquid conversion per pass through the reactor was small. Therefore the system was operated batch wise with respect to the liquid, by recycling reaction mixture over the reactor. Absorption efficiency of SO_3 was ≅ 100%.

The diameter of the cocurrent gas-liquid tube reactor was 8 10^{-3} m. Gas and liquid were introduced via a T-piece of the same diameter.

Results and Discussion

Mass Transfer in Absorption without Reaction. We measured k_L in the stirred cell with an O_2 - H_2O system (figure 2). Forced convection k_L in the reaction mixtures was calculated from this result according to [11]

$$Sh \sim Re^n Sc^{1/3} \tag{7}$$

with n = 1.1. Reaction effects were neglected in this procedure. However, in reaction experiments, as will be explained in a later section, a local increase of viscosity at the interface caused by pyrosulfonic acid accumulation, produced a lower k_L than calculated this way.

We measured k_L in a cyclone reactor with simultaneous absorption of CO_2 and O_2 in a hydroxide solution [2]. Figure 3 gives results. The figure shows that k_L reaches extremely high values in this reactor (k_L is on the order of 10^{-4} m/s in conventional reactors as the stirred tank [13], the bubble column [14], the bubble cap plate [15] and the packed column [16, 17].

Slugflow is obtained in the tube reactor in the range of gas and liquid velocities, we applied in sulfonation [18, Figure 10.3]. k_L values realized in this flow regime have been reported by Gregory and Scott [19]. From this reference we calculated [3] k_L in our tube reactor (see Figure 3).

Mass Transfer in Stirred Cell Reactor during Sulfonation. The actual k_L during sulfonation follows experimentally from

$$k_L = \frac{J}{c_{Ai} E} \tag{8}$$

As derived earlier, sulfonation of benzene is instantaneous in a stirred cell reactor. Therefore [4]:

$$c_{Ai} E \cong c_{Ai} + \frac{2 D_B \bar{c}_B}{D_A} \tag{9}$$

Because of uncertainties in c_{Ai}, only an approximate k_L during sulfonation can be obtained this way. Experiments were carried out with both neat and diluted benzene (5.3 and 30 vol% benzene

initial reaction mixture	$\bar{T}$ [°C]	J [10^{-3} kmol/m^{2}s]	(1-η) -	k_L [10^{-5} m/s]	$c_{Ii}-\bar{c}_I$ [kmol/m^3]	x_{Ii} -	T_i [°C]	$k_2 D_A$ [m^5/kmol s^2]
5.3 vol%	35	0.15	0.031	≈2	≈3.6	≈0.5	51	3.0 10^{-11}
30 vol%	25	0.092	0.107	≈1	≈4.1	≈0.7	44	0.67 10^{-11}
	35	0.13	0.137	≈1.5	≈3.75	≈0.6	53	1.9 10^{-11}
	45	0.23	0.187	≈2.2	≈4.25	≈0.8	67	4.2 10^{-11}
100% B	28	0.35	0.25	≈1.5	≈8.75	≈1	78	14 10^{-11}

Table II. Estimated values for gas-liquid interface pyrosulfonic acid concentration rise ($c_{Ii}-\bar{c}_I$), surface temperature rise ($T_i-\bar{T}$) and reaction rate constant ($k_2 D_A$) in stirred cell reactor sulfonation experiments.

In Chemical Reaction Engineering—Houston; Weekman, V., et al.;
ACS Symposium Series; American Chemical Society: Washington, DC, 1978.

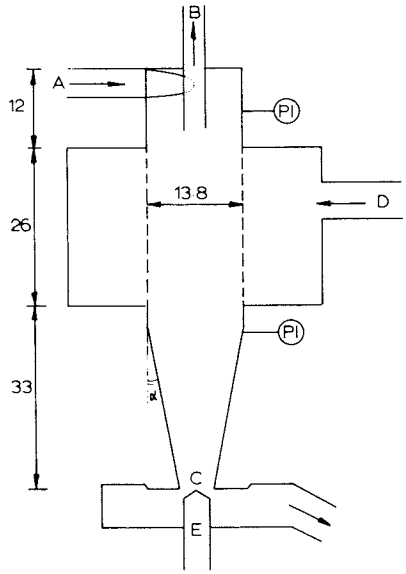

Figure 1. Cyclone reactor. Unit of length: 10^{-3} m. (A) liquid inlet (4 10^{-3} m), (B) gas outlet (vortex) (3 10^{-3} m), (C) liquid outlet (apex) (8.66 10^{-6} m^2), (D) gas inlet, (E) cone (120°C), (PI) pressure indicator, (a) 8°C.

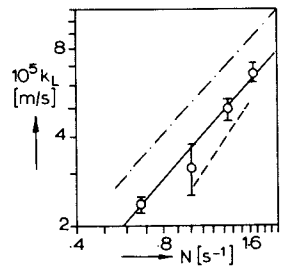

Figure 2. k_L in stirred cell reactor. (○), (——) our measurements (O_2 in H_2O at 25°C); (– – –) Jhaveri and Sharma [12]; (– · –) SO_2 in both 1,2-dichloroethane and benzene, with Equation 7.

In Chemical Reaction Engineering—Houston; Weekman, V., et al.;
ACS Symposium Series; American Chemical Society: Washington, DC, 1978.

in 1,2-dichloroethane respectively). Stirrer speed (N) varied between 0 and 2 rev/s. k_L showed to be independent of N and to be appreciably lower than without reaction. The average values of k_L are summarized in Table II. Table II also shows that both the interface pyrosulfonic acid concentration (c_{li}) and the interface temperature (T_i) are much higher than in the bulk of the liquid. The first quantity (c_{li}) has been approximated with

$$c_{li} - \bar{c}_l = \tfrac{1}{2}\, \eta J/k_L \tag{10}$$

The second quantity (T_i) has been estimated from the simple film model according to Danckwerts [4]

$$T_i - \bar{T} = JD_B\, (\Delta H_a + \Delta H_r) / \lambda_S k_L \tag{11}$$

The influence of pyrosulfonic acid concentration on viscosity is neither known nor measurable because of the instability of this intermediate [3]. We measured the viscosity of a reaction mixture at 23.5°C as a function of benzenesulfonic acid concentration. The relationship obtained is:

$$\ln(\mu(x_p)/\mu(o)) = 8.85\, x_p \tag{12}$$

Without measurements, our best possible assumption is that pyrosylfonic acid has the same influence on viscosity as sulfonic acid. Recalling from eqn. (7) that

$$k_L \sim (D/\mu)^{2/3}$$

and applying the Stokes-Einstein equation results in

$$k_L \sim \mu^{-4/3} \tag{13}$$

It follows from x_{li} (Table II) and eqns (12,13) that k_L is appreciably lowered by viscosity effects that occur during reaction. In practice this tendency is counteracted by both the interface temperature rise and free convection, driven by density and/or surface tension gradients. Both effects lower the extent of interface viscosity increase. Thus, a k_L is obtained which is independent of stirrer speed and lower than that for forced convection in the absence of interface viscosity effects as given in Figure 2.

Selectivity in Stirred Cell Reactor. Observed $1 - \eta$ is always $\ll 1$. Therefore eqn. (6) is expected to be applicable though its accuracy is probably low due to the discussed interface viscosity increase. From eqn. (6)

$$1 - \eta \sim 1/k_L^{\,2} \tag{14}$$

Figure 4 shows $(1-\eta)$ to be nearly independent of N. Even the abcense of stirring does not lower selectivity significantly. This fact is in agreement with, and additional argument for, our preceding conclusion that k_L is independent of stirrer speed.

Figure 4 shows that by-product formation increases with initial benzene concentration. Taking as a first approximation $D_B = D_l$, $\bar{c}_l \ll \bar{c}_B$ and $1 - \eta' \cong 1 - \eta$ (allowed for $\zeta \ll 1$) we obtain from eqn. (6) with $z = \tfrac{1}{2}$:

$$1 - \eta \cong k_2 D_A \bar{c}_B / (k_L E_\infty)^2 \tag{15}$$

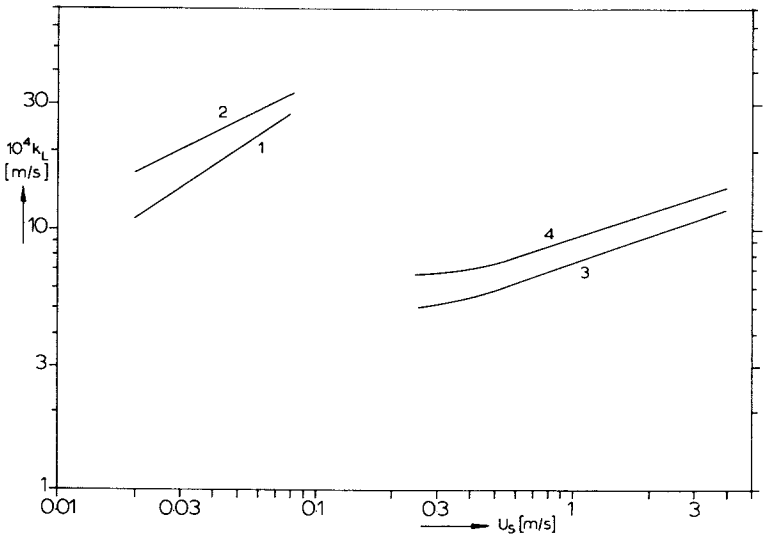

Figure 3. k_L *as* $f(U_s)$ *for* CO_2 *in 2.07M NaOH solution in a cyclone reactor with* $v_i = 5.97$ *m/s (1) and 9.15 m/s (2) and in tube reactor for* $U_L = 1$ *m/s (3) and 1.75 m/s (4)*

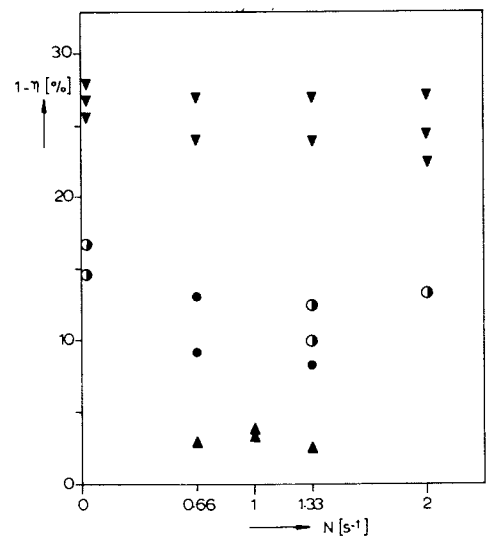

Figure 4. By-product formation in sulfonation of benzene with gaseous sulfur trioxide in a stirred-cell reactor in relation to initial benzene concentration and stirrer speed. (▲) 5.3 vol % benzene in dichloroethane, $T \cong 35°C$, $\zeta \cong 0.8$; *(○) 30 vol % benzene in dichloroethane,* $T \cong 25°C$, $\zeta \cong 0.09$; *(○) 30 vol % benzene in dichloroethane,* $T \cong 35°C$, $\zeta \cong 0.1$; *(▲) 100 vol % benzene in dichloroethane,* $T \cong 28°C$, $\zeta \cong 0.005$.

In Chemical Reaction Engineering—Houston; Weekman, V., et al.;
ACS Symposium Series; American Chemical Society: Washington, DC, 1978.

Combining with equation (8) gives

$$k_2 D_A \cong (1 - \eta)\, J^2/(\bar{c}_B c_{A_i}^2) \qquad (16)$$

With this equation, the value of $k_2 D_A$ has been estimated from the experimental results (Table II). Figure 5 shows log $k_2 D_A$ as a function of $1/T_i$. Fitting the experimental data to

$$k_2 D_A = k_\infty D_A e^{-\Delta E/RT_i} \qquad (17)$$

results in

$$k_\infty D_A = 4.5\ m^5/kmol\ s^2$$

and $\Delta E = 30.7\ 10^6$ J/kmol

The obtained value for ΔE is likely for this consecutive reaction because Bosscher [20] found the approximate same value for ΔE in a chemically, very similar reaction in sulfonation of chlorobenzene. Assuming at the interface: $D_A \cong 10^{-10} m^2/s$, it follows from eqn. (17) that k_2 (25°C) ≅ $1.7\ 10^{-2}$ m^3/kmol s. Reaction rate constant for the first reaction (eqn. (2)) has been shown to be [3]:

$$k_1(25°C) > 9.4\ m^3/kmol\ s$$

Hence, in homogeneous sulfonation, no diphenyl sulfone will be obtained.

Selectivity in the Cyclone and in the Tube Reactor. Differential selectivity (η') was measured as a function of ζ. About 25 experimental runs were carried out. Table III shows the range between which the operation parameters were varied. Observed η' depended mainly on initial benzene concentration and on gas load (U_s). The results are summarized in Figure 6. Figure 6 also shows results from tube reactor experiments ($1 < U_L < 1.8$ m/s; $0.04 < f_A < 0.08$; $\zeta < 0.33$). The Figure shows that by-product formation is much less in these reactors than in the stirred cell reactor. However, the difference is less than may be expected from eqn. (14) with k_L from Table II and Figure 3 respectively. Therefore, k_L is probably also lowered by interface viscosity effects in the cyclone and in the tube reactor during sulfonation of 30 vol. % bezene and of neat benzene. Additional arguments support this hypothesis [3]. This does not exclude the possibility that the value of the mass transfer coefficient, as measured in the cyclone and in the tube reactor with the (O_2-)CO_2-aqueous NaOH system, remains a relative measure of the actual k_L in those reactors during sulfonation, provided that gas and liquid loads are similar in both types of experiment. Figure 7 presents average values of $1-\eta'$ as a function of this liquid-side, mass transfer coefficient in both the cyclone and the tube reactor (from Figure 3, partly by extrapolation). Thus presented, the ($1-\eta'$) values fall on a single line within the experimental error.

$\bar{T}$ [°C]	Initial vol % benzene in liquid phase -	U_s [m/s]	v_i [m/s]	f_A -	ζ -
20	10	0.02 - 0.04	3.5 - 6.8	0.09 - 0.11	0.13 - 0.46
	30	0.01 - 0.38	3.3 - 7.9	0.06 - 0.13	0.07 - 0.42
	100	0.01 - 0.21	2.8 - 6.6	0.08 - 0.13	0.01 - 0.05
40	30	0.01 - 0.08	2.7 - 7.9	0.09 - 0.12	0.04 - 0.51
	100	0.01 - 0.02	2.4 - 7.6	0.11 - 0.12	0.01 - 0.05

Table III. Scheme of sulfonation experiments in cyclone reactor.

In Chemical Reaction Engineering—Houston; Weekman, V., et al.;
ACS Symposium Series; American Chemical Society: Washington, DC, 1978.

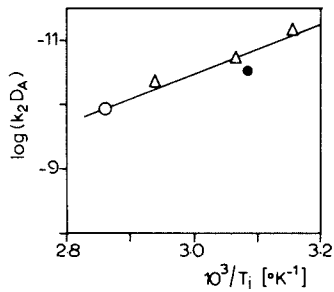

Figure 5. k_2D_A as a function of surface temperature from averaged experimental results. (●) 5.3 vol % benzene; (△) 30 vol % benzene; (○) neat benzene.

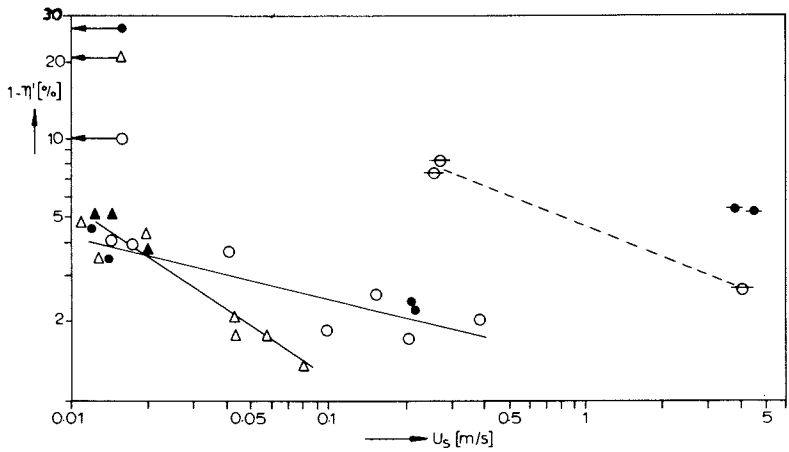

Figure 6. By-product formation in sulfonation of benzene (average values). (●, ⊖, ←●) neat benzene at ≅ 20°C in cyclone reactor (●), tube reactor (⊖), and stirred-cell reactor (←●, ζ ≅ 0.05, T = 25°C) respectively. (○, ⊖, ←○) 30 vol % benzene in 1,2-dichloroethane at ≅ 20°C in cyclone reactor (○), tube reactor (⊖), and stirred-cell reactor (←○, ζ ≅ 0.1, T = 25°C) respectively. (▲) neat benzene at ≅ 40°C in cyclone reactor (ζ ≅ 0.04). (△, ←△) 30 vol % benzene at ≅ 40°C in cyclone reactor (△, ζ ≅ 0.1) and stirred-cell reactor (←△, ζ ≅ 0.15, T = 45°C).

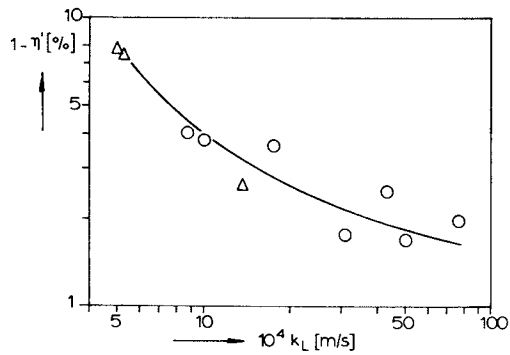

Figure 7. By-product formation (1 − η') in sulfonation of 30 vol % benzene in 1,2-dichloroethane at 20°C, as a function of k_L as measured with the system O_2-CO_2-hydroxide. (○) in cyclone reactor, (△) in tube reactor.

In Chemical Reaction Engineering—Houston; Weekman, V., et al.;
ACS Symposium Series; American Chemical Society: Washington, DC, 1978.

Sulfonation of 10 vol.% benzene results in 100 % selectivity in a cyclone reactor (see Table IV). Compared to 30 vol. % benzene sulfonation, the term

$$1 + \frac{D_B \bar{c}_B}{z D_A m \bar{c}_{AG}}$$

decreases from 2.4 to 1.4 (Table I). Apparently this is sufficient to produce a substantially higher k_L (by lowering of c_{Ii}) and thus for a far better selectivity. Comparison of the 10 vol. % bezene cyclone experiments with the 5.3 vol. % benzene sulfonation in the stirred cell reactor shows that minimum by-product formation is found in the cyclone reactor even though the higher benzene concentration favours sulfone formation. At these low $\bar{c}_B$ values the difference in η possibly follows from eqn. (14) with k_L from Table II and Figure 3 respectively.

U_s [m/s]	v_i [m/s]	f_A -	ζ -	η' -	$\bar{T}$ [°C]
0.025	6.80	0.105	0.259	1.00	23.0
0.030	3.46	0.107	0.327	1.00	20.0
0.042	5.89	0.088	0.459	0.995	20.6

Table IV. Sulfonation of 10 vol. % benzene in 1,2-dichloroethane in a cyclone reactor at ± 20°C.

Nomenclature

A	sulfur trioxide
B	benzene
c	concentration, kmol/m^3
d	diameter, m
D	diffusion coefficient, m^2/s
E	enhancement factor, i.e., factor by which rate of absorption is increased by reaction (2)
E_∞	enhancement factor when reaction (2) is instantaneous
ΔE	activation energy, J/kmol
f	mol fraction in gas feed
G	gas phase
Ha	Hatta number ($\sqrt{k_1 D_A c_B / k_L^2}$)
ΔH_a	heat of absorption, J/k mol
ΔH_r	heat of reaction, J/kmol
I	pyrosulfonic acid (benzenesulfonic acid, monoanhydride with sulfonic acid)
I'	$C_6H_5S_3O_9H$ (benzenesulfonic acid, monoanhydride with disulfuric acid)
J	absorption rate per unit area, kmol/m^{2}s
k_1, k_2	reaction rate constants, defined in eqns. (2) and (3), m^3/kmol s
k_G	gas phase mass transfer coefficient, m/s
k_L	liquid phase mass transfer coefficient, m/s
k_∞	pre-exponential factor in eqn. (17)
L	liquid phase
m	solubility $(c_{Ai})_L/(c_{Ai})_G$
N	speed of revolution of impeller, rev/s
P	benzene sulfonic acid
r	rate of formation, kmol/m^{3}s
R	gas constant, J/kmol°K
Re	Reynolds number; in stirred cell: $\rho N d^2/\mu$ with d = diameter of stirrer
Sc	Schmidt number ($\mu/\rho D$)
Sh	Sherwood number ($k_L d/D$)
T	temperature, °K, °C
U_L	superficial liquid velocity, m/s
U_s	superficial gas velocity; in cyclone reactor related to porous wall area; in tube reactor as usual, m/s
v	liquid velocity, m/s
x	molfraction in liquid
X	diphenyl sulfone
z	stoichiometric coefficient from equation (2)
ζ	conversion of benzene
η	selectivity, fraction of converted benzene that is converted to benzenesulfonic acid
η'	differential selectivity $(-r_P/r_B)$
λ	thermal conductivity, W/m°C
μ	viscosity, s Pa
ρ	liquid density, kg/m^3

Subscripts

A	sulfur trioxide
B	benzene
G	gas phase
i	at interface; in inlet
I	pyrosulfonic acid
L	liquid phase
P	benzenesulfonic acid
S	solvent

Superscript

–	in bulk of liquid

In Chemical Reaction Engineering—Houston; Weekman, V., et al.;
ACS Symposium Series; American Chemical Society: Washington, DC, 1978.

Literature Cited

[1] Van de Vusse, J.G., Chem. Eng. Sci., (1966), 21, 631

[2] Beenackers, A.A.C.M., and van Swaaij, W.P.M. "Chem.React. Eng., Proc. Eur., 6th, Int., 4th, Symp.", p.VI 260, Dechema, Frankfurt (M), 1976

[3] Beenackers, A.A.C.M., "Ph. D.Thesis", Twente University of Technology, Enschede, 1977

[4] Danckwerts, P.V., "Gas-Liquid Reactions", McGraw Hill, London, 1970

[5] Harriott, P., Can. J. Chem. Eng., (1970), 48, 109

[6] Teramoto, M., Nagayasu, T., Matsui, T., Hashimoto, K. and Nagata, S., J. Chem. Eng. Jpn., (1969), 2, 186

[7] Inoue, H. and Kobayashi, T., "Chem. React. Eng., Proc. Eur. Symp., 4th", 147, Pergamon, Oxford, 1968 (pub. 1971)

[8] Pangarkar, V.G. and Sharma, M.M., Chem. Eng. Sci., (1974), 29, 561

[9] Nakao, K., Hashimoto, K. and Otake, T., J. Chem. Eng. Jpn., (1972), 5, 264

[10] Teramoto, M., Hashimoto, K. and Nagata, S., J. Chem. Eng. Jpn., (1973), 6, 522

[11] Hikita, H., Ishikawa, H. and Murakami, Y., Bull. Univ. Osaka Prefect., Ser. A., (1970), 19, 34

[12] Jhaveri, A.S. and Sharma, M.M., Chem. Eng. Sci., (1967), 22, 1

[13] Koetsier, W.T., "Ph. D. Thesis", Twente University of Technology, Enschede, 1973

[14] Calderbank, P.H. and Moo-Young, M.B., Chem. Eng. Sci., (1961), 16, 39

[15] Porter, K.E., King, M.B. and Varshney, K.C., Trans. Inst. Chem. Eng., (1966), 44, T274

[16] Danckwerts, P.V. and Sharma, M.M., Chem. Eng. (London), (1966), 44, CE244

[17] Gianetto, A., Specchia, V. and Baldi, G., AIChE J., (1973), 19, 916

[18] Govier, G.W., and Aziz, K., "The flow of complex mixtures in pipes", van Nostrand Reinhold Comp., New York, 1972

[19] Gregory, G.A., and Scott, D.S. in: "Co-current Gas-Liquid Flow", (Edited by E.Rhodes and D.S. Scott), Plenum Press, New York, 1969

[20] Bosscher, J.K., "Ph. D. Thesis", Gemeentelijke Universiteit, Amsterdam, 1967

In Chemical Reaction Engineering—Houston; Weekman, V., et al.;
ACS Symposium Series; American Chemical Society: Washington, DC, 1978.

28

Axial Mixing of Liquid in Packed Bubble Columns and Perforated Plate Columns of Large Diameter

PETER MAGNUSSEN and VOLKER SCHUMACHER

BASF Aktiengesellschaft, Amoniaklaboratrium, 6700 Ludwigahafen, West Germany

In many cases bubble columns are used for gas-liquid-reactions. Their construction is very simple, but it is difficult to precalculate their optimal design.

The simplest form of a bubble column is a vertical tube in which a gas distributor is placed at the bottom; packed or plate bubble columns are also used. The gas bubbles rise through the liquid phase, which may flow through the column either cocurrent or countercurrent to the gas. As a result of the short residence time of the gas bubbles in the liquid phase, bubble column reactors are preferred for reactions which require a short gas and a long liquid reaction time. Therefore the residence time distribution of the liquid phase is a characteristic factor for the design of the reactor. The dependence of the residence time distribution upon the column diameter has to be known for any scale-up of bubble columns.

The residence time distribution of a reactor is a function of the axial mixing within the reactor. The extreme cases are: 1) the ideal continuous stirred tank reactor (CSTR) with complete mixing and, 2) the ideal plug flow reactor (PFR) without any backmixing of the liquid during its flow through the reactor. The behavior of real reactors lies between these extremes. It may be described by comparison to a stirred tank cascade of as many tanks as necessary to obtain the behavior of the real reactor; the result of this comparison is called "number of equivalent tanks". In this model the CSTR equals 1 ideal tank and the PFR is equivalent to a cascade with an infinite number of tanks. This description corresponds to the mathematical cell model.

The dispersion model is another way of characterizing the residence time distribution of a real reactor. In this model it is assumed that axial mixing is super-

In Chemical Reaction Engineering—Houston; Weekman, V., et al.;
ACS Symposium Series; American Chemical Society: Washington, DC, 1978.

imposed upon plug flow through the reactor. This axial mixing widens the residence time curve and is characterized by the Peclet-number Pe (in German this is usually called Bodenstein-number Bo) which is defined by equation (1):

$$Pe = \frac{u \cdot L}{D_{ax}} \qquad (1)$$

u = superficial liquid velocity
L = length of the reactor (height of the bubble column)
D_{ax} = mixing coefficient

In this equation D_{ax} is the total axial mixing coefficient and is independent of the mixing mechanism (i.e. molecular diffusion, backmixing etc.). The mixing coefficient $D_{ax} = 0$ in an ideal PFR yields $Pe = \infty$. The boundary value for the ideal CSTR with infinite mixing approximates $Pe = 0$.

Several equations are used to compare both models. A simple approximation is given by equation (2):

$$\text{number of equivalent tanks } n = \frac{Pe}{2} + 1 \qquad (2)$$

At small Pe-numbers additional correction terms may be used.

Both models may be used to describe the residence time distribution in bubble columns. The residence time behavior depends upon the column L/D ratio . Bubble columns of large L/D ratios may be compared with PFRs; bubble columns of small L/D ratios are similar to CSTRs. The objective of our work was to determine the relationship between axial mixing and column diameter with an end of finding a way to reduce axial mixing in large diameter bubble columns.

Literature about axial mixing in bubble columns is quite extensive, i.e. (1), (2), (3). Unfortunately most of the publications refer to column diameters of less than 200 mm. Only a few studies have been done on bubble columns of large diameter. Argo and Cova (4) as well as Towell and Ackermann (5) have studied empty bubble columns up to a diameter of 1 m. No literature is known about packed columns of this size. The largest diameter packed columns studied by Carleton et al. (6) and by Hoogendoorn et al. (7) had a diameter of less than 0.5 m.

In our studies we have investigated the residence time behavior in large diameter bubble columns with and without packings (fig.1). We have used several columns

In Chemical Reaction Engineering—Houston; Weekman, V., et al.;
ACS Symposium Series; American Chemical Society: Washington, DC, 1978.

with heights from 1 to 4 m and diameters from 40 mm to 1000 mm. Different packings of Raschig-rings and Pall-rings varying in size from 10 to 50 mm were used as well as perforated plates which are described later. All measurements have been made with air and tap-water in countercurrent flow at ambient temperature. The water flow rate was maintained at 40 $m^3/m^2.h$.The superficial air velocity was varied from 0.01 to 0.1 m/s.

Several testing methods are known for measuring residence time distributions in a reactor. It was necessary to select a method which was suitable for all columns studied in this work.

Steady state methods used for measuring axial mixing consist of injecting a tracer in the middle of the studied interval and measuring the upstream concentration. There are problems in large packed columns as it is very difficult to get a homogeneous dispersion of the tracer and to obtain an average sample profile without disturbing the liquid flow in the column.

Unsteady state methods for measuring axial mixing consist of injecting a tracer at the reactor inlet and measuring the response function at the outlet. In this investigation the pulse method was used. This method was selected because only small amounts of tracer substance had to be prepared. Imposing a step concentration change would have required much greater amounts of tracer liquid; for example in a column of 1 m diameter 36 m^3/h would be required.

The measurements were done by adding a sudden pulse of concentrated sodium hydroxide solution to the water inlet.The concentration of the sodium hydroxide at the column outlet was measured by a pH-meter. pH measurement is highly accurate at small concentrations because of the logarithmic concentration function. Daily tests were done to compensate for changes in pH indication caused by changing water composition.

In order to interpret the experimental residence time curves , comparison may be made with an ideal stirred tank cascade. Interpolation methods are known to get the number of equivalent tanks from the normalized residence time curves (8). This is only possible if the experimental residence time distribution is an ideal one. In many cases this is not true. Furthermore the residence time curves we get from our experimental arrangement comprise not only the residence time behavior of the bubble column itself but also the behavior of the liquid and gas distributors. These additional effects must not be neglected. In order to determine the effects of the distributors

In Chemical Reaction Engineering—Houston; Weekman, V., et al.;
ACS Symposium Series; American Chemical Society: Washington, DC, 1978.

as well as the approach effects in the bubble phase, every test was run in two columns of differing lengths (L_1 and L_o) using identical liquid and gas distributors (fig.2). The difference in the curves obtained from the columns with heights L_1 and L_o allows one to calculate the residence time behavior of a column with height $L = L_1 - L_o$. The analysis was done by the moments method of Levenspiel and Smith (9). The first moment η is the center of the curve corresponding to the mean residence time. The second moment s^2 is related to the dispersion of the residence time curve by axial mixing. The partial differential equations may be converted by LaPlace-transformation into linear equations from which the Pe-number may be calculated without retransformation.

It should be noted that the choice of the boundary conditions for the calculation of the response function is very important. Most published proposals for boundary conditions derive from two residence time distribution curves recorded simultaneously upstream and downstream of the studied interval. Starting from the boundary conditions suggested by van der Laan (10) we have developed new boundary conditions applicable to the residence time curves of two columns with different heights. The resulting equation for calculating the Pe-number is shown in figure 3. This equation is true when the tracer is added and the response function is measured outside of the test interval. It is assumed that mixing above the liquid level and beyond the gas sparger is negligible compared to the mixing within the bubble column itself.

The influence of the boundary conditions at high Pe-numbers is small. At small Pe-numbers, as obtained in CSTRs, the effect may be of considerable magnitude. This must be taken into account when comparing small Pe-numbers calculated from different works.

The results of our studies show a rapid increase of axial mixing corresponding to a rapid decrease of Pe-number with increasing column diameter (fig.4). For example, an empty bubble column of a height of 4 m and a diameter of 40 mm yields a Pe-number of 16 which corresponds to a 9 stage tank cascade. A bubble column of the same height with an increased diameter of 1 m yields Pe = 0.6 which is comparable to a CSTR: The total liquid holdup of 3 m^3, which had a mean residence time of 6 minutes, was homogeneously colored 20 seconds after adding a dye to the water input.

Compared to the influence of column diameter the effect of gas velocity is fairly small (fig.5). An in-

In Chemical Reaction Engineering—Houston; Weekman, V., et al.;
ACS Symposium Series; American Chemical Society: Washington, DC, 1978.

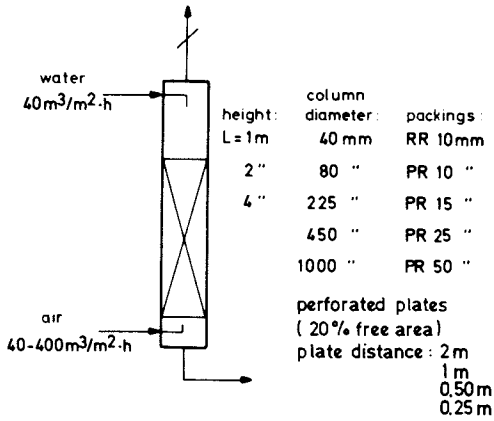

Figure 1. Survey of tested bubble columns

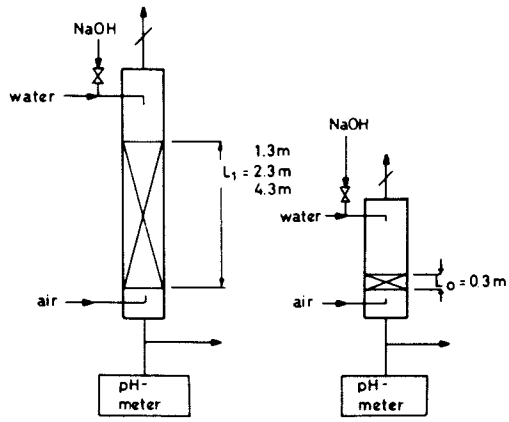

Figure 2. Experimental arrangement for the measurement of residence time distribution

$$\frac{\Delta S^2}{\Delta^2 \Omega} = \frac{2}{\left(1-\frac{L_0}{L_1}\right)^2 Pe^2}\left[Pe\left(1-\frac{L_0}{L_1}\right) + e^{-Pe} - e^{-Pe\frac{L_0}{L_1}}\right]$$

$$Pe \equiv \frac{u \times L_1}{D}$$

Figure 3. Calculation of Pe number

In Chemical Reaction Engineering—Houston; Weekman, V., et al.;
ACS Symposium Series; American Chemical Society: Washington, DC, 1978.

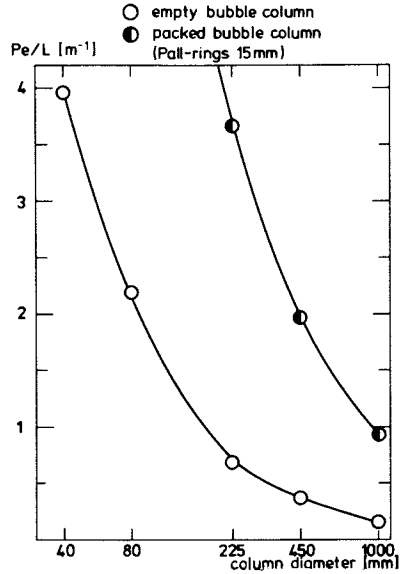

Figure 4. Axial mixing in bubble columns—effect of diameter

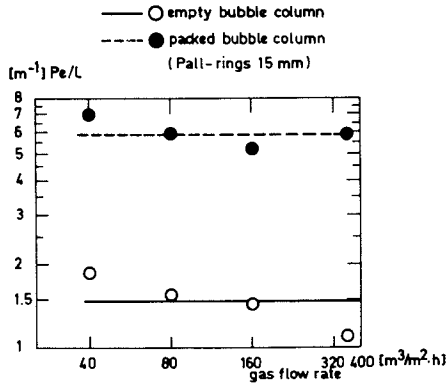

Figure 5. Axial mixing in bubble columns —effect of gas flow rate

In Chemical Reaction Engineering—Houston; Weekman, V., et al.;
ACS Symposium Series; American Chemical Society: Washington, DC, 1978.

crease of the gas flow rate in empty bubble columns by a factor 10 (from 40 to 400 $m^3/m^2.h$) decreases the Pe-number by only 40 %. In packed bubble columns the effect is even smaller. Therefore all data given in this work are mean values averaged over all gas flow rates.

The logarithmic scale diagram (fig.6) shows the linear relation of Pe-number to the column diameter. The slope of -1 agrees well with the published values from other works which vary from -1 to -1.5.

Packed bubble columns show a reduction of axial mixing which increases with decreasing size of packing. In packed bubble columns the relationship between Pe-number and column diameter is the same as in empty bubble columns.The axial mixing is inversely proportional to the column diameter. The opposite effect is observed with narrow columns where the packing size is large compared with the column diameter. In this case wall effects occur. Some liquid streams run through the column much faster than others resulting in a widening of the residence time curve decreasing the Pe-number.

By inserting 50 mm packings in a 1 m diameter column the Pe-number is decreased. This may be caused by statistical nonuniformities of the packing. Dye added to the water input shows the formation of channels; other parts of the liquid remain much longer in dead water regions. The resulting extension of the residence time curve yields the extremely low Pe-number.

This example shows that packings of usual technical size do not diminish axial mixing in large bubble columns but may have the opposite effect. An inhibition of axial mixing is possible only by using unusually small packing. In some cases the cost of this packing may be prohibitive especially when expensive construction materials have to be used. We have tried to find a less expensive way of reducing axial mixing by the use of perforated plates.

Perforated plates that fit into bubble columns like sieve trays are still used in cocurrent bubble columns (11). Usually the resultant free area of the openings is very small, i.e. 1 - 5 % of the total plate area. These plates may totaly suppress backmixing by forming a gas buffer beyond each plate which prevents liquid backflow. Such plates cannot be used in countercurrent flow in as much as the required pressure drop through the holes prevents the liquid downflow. Several possibilities have been suggested for the utilization of perforated plates in countercurrent bubble columns, i.e. special kinds of downcomers with or without control valves (12) (13) or additional pulsing

In Chemical Reaction Engineering—Houston; Weekman, V., et al.;
ACS Symposium Series; American Chemical Society: Washington, DC, 1978.

of the liquid holdup (14).

Instead of these more complicated apparatus we have used simple perforated plates of greater free area. Holes of 10 mm diameter with a resulting free area of 20% of the total plate area allow an undisturbed countercurrent flow at the flow rates mentioned above. We used 1,3,7 or 15 plates at a column height of 4 m forming 2,4,8 or 16 compartments with a height of 2, 1, 0.5 or 0.25 m each.

Despite the large free area of the plates we obtained a remarkable reduction in axial mixing (fig.7). For example, 7 plates fitted into a 450 mm diameter column decrease mixing (and increase the Pe-number) by a factor 6. This is a greater effect than could be obtained by using 15 mm Pall-ring packing. Only 3 plates are necessary in a 1 m diameter column to give the same decrease in axial mixing. On the other hand the efficiency of the plates in reducing axial mixing decreases with smaller column diameters.

In contrast to packed bubble columns, the decrease of Pe-number with increasing column diameter is much less in perforated plate bubble columns than in empty ones. This is true if the plate distance H is constant varying only the column diameter D. At constant values of H/D as shown by the dotted lines in figure 7 the same slope is found as for empty bubble columns.

The packing and plate efficiency is compared in figure 8, where the increase of Pe-number is plotted versus the column diameter. It is seen that the plate efficiency increases rapidly while the packing efficiency is independent of the column diameter.

Summary

Residence time distributions have been measured in empty, packed and perforated plate bubble columns with diameters from 40 mm to 1 m.

In empty bubble columns the axial mixing as expressed by the Pe-number is nearly independent of the gas flow rate. Mixing increases rapidly with increasing column diameter, the Pe-number is inversely proportional to the column diameter.

The reduction of axial mixing by use of packings depends on the size of the packing. For good efficiency small packings have to be used. The dependence of axial mixing on the column diameter is the same as in empty bubble columns.

The use of perforated plates in large bubble columns reduces axial mixing. The plate efficiency increases with increasing column diameter.

In Chemical Reaction Engineering—Houston; Weekman, V., et al.;
ACS Symposium Series; American Chemical Society: Washington, DC, 1978.

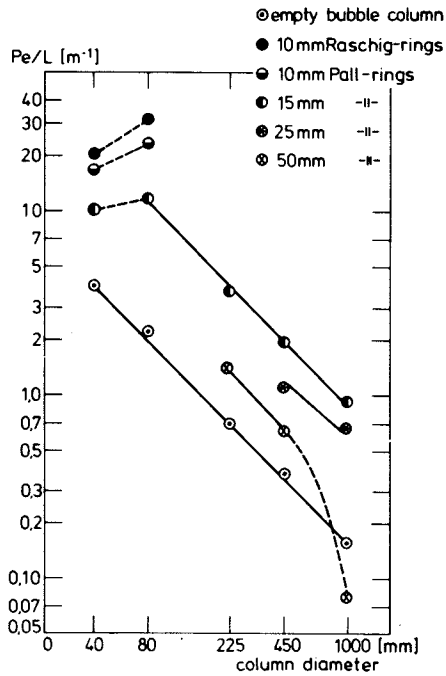

Figure 6. Axial mixing in bubble columns —effect of packings

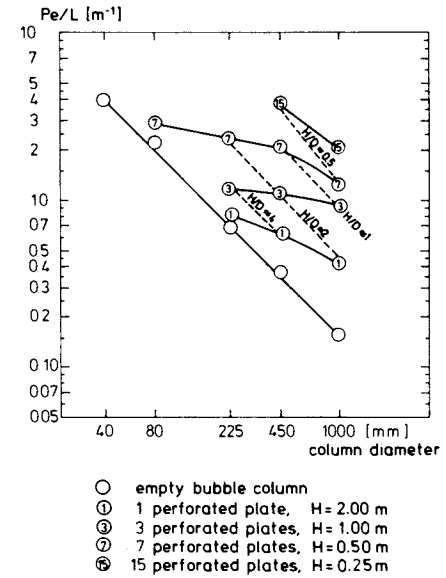

Figure 7. Axial mixing in bubble columns—effect of plates

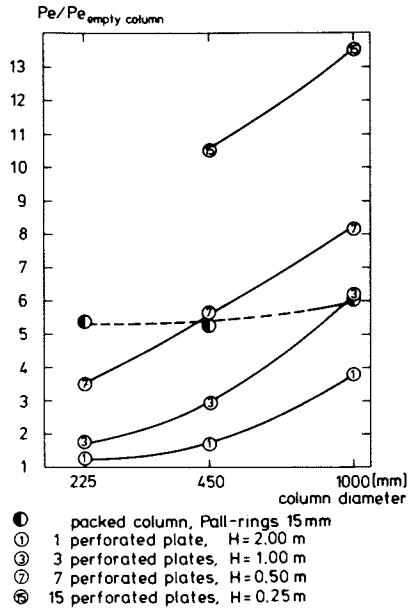

Figure 8. Comparison of plate efficiency and packing efficiency at varying diameter

In Chemical Reaction Engineering—Houston; Weekman, V., et al.;
ACS Symposium Series; American Chemical Society: Washington, DC, 1978.

Literature cited:

(1) Kölbel H., Dechema Monographie (1972) 68, 35-73
(2) Mashelkar R.A., British Chemical Engineering (1970) 15 (10), 1297 - 1301
(3) Tadaki T., Maeda, S., Kagaku Kogaku (1964) 2, 195-198
(4) Argo W.B., Cova D.R., I & EC Process Design and Development (1965) 4 (4), 352-359
(5) Towell G.D., Ackerman G.H., 2nd Internat Symp. Chem. React. Engng., Amsterdam (1972)
(6) Carleton A.I., Flain R.I., Rennie I., Valentin F.H.H., Chemical Engineering Science (1967) 22, 1839-1849
(7) Hoogendoorn C.I., Lips I., Canadian Journal of Chemical Engineering 1965 (June), 125-131
(8) Pippel W., Chemische Technik (1965) 17, 729-738
(9) Levenspiel O., Smith W.H., Chemical Engineering Science (1957) 6, 227-233
(10) van der Laan E.Th., Chemical Engineering Science (1958) 7, 187-191
(11) Blass E., Koch K.H., Chemie Ingenieur Technik (1972) 44, 913-921
(12) Kastanek F., Zahradnik J., Coll. Czech. Chem. Communications (1973) 38, 3725-3741
(13) Judat A., Judat H., (Bayer AG) West German OLS 2 331 195 (1975)
(14) Hackl A., Dechema Monographie (1974) 73 (1410 - 1431), 37-49

29

Computer-Aided Development of the Cyclohexane Oxidation Process

J. A. DE LEEUW DEN BOUTER, L. L. VAN DIERENDONCK, and W. O. BRYAN
CRO/DSM, P.O. Box 18, Geleen, The Netherlands

1. INTRODUCTION

Within the scope of its program aimed at process improvements, the Corporate Department for Research and Patents of DSM is now seeking ways of optimizing the cyclohexane oxidation route towards cyclohexanone (anone) and cyclohexanol (anol). These products are intermediates in the preparation of caprolactam. Caprolactam is polymerised to nylon-6. As DSM has a great interest in the world production of caprolactam, much effort is put into research and optimization of the various process steps. In the oxidation of cyclohexane, the efficiency is relatively low, which is the reason why research into and optimization of this process step was taken in hand. The flowsheet of the oxidation section is shown in fig. 1. Fresh cyclohexane is mixed with the recycled cyclohexane from the top of the cyclohexane distillation column. The mixture is fed to the condensation section to exchange heat with the vapour stream from the reactors. Next, the cyclohexane is oxidized with air in a cascade of stirred reactors. The oxidate leaving the reactors undergoes an after-treatment in a decomposition reactor, while the acids formed as byproduct in the oxidation section are neutralized in a mixer-settler unit. In the cyclohexane distillation section non-converted cyclohexane is separated from cyclohexanol, cyclohexanone and byproducts.

DSM studied the catalysed process in the years before 1960. Steeman et al. (1) on the basis of experimental work, calculated the optimum degree of cyclohexane conversion to be 7-8 % at an efficiency of 75 %.

Alagy et al. (2), introducing boric acid (metaborate) into the oxidation section, achieved efficiency figures in the range 85-90 %. The metaborate used by these authors reacts with cyclohexanol (anol) to form an ester, thereby preventing oxidation of anol to anone, and, as a consequence, suppressing the anone concentration. Since the bulk of the byproducts is formed via anone, the use of boric acid therefore brings in this

© 0-8412-0401-2/78/47-065-348$05.00/0

In Chemical Reaction Engineering—Houston; Weekman, V., et al.;
ACS Symposium Series; American Chemical Society: Washington, DC, 1978.

case an improvement in efficiency.

The new process variant investigated at DSM is also based on suppression of the anol and anone concentrations, which is achieved by leaving out the catalyst. Application of appropriately chosen conditions counteracts decomposition of the cyclohexyl-hydroperoxide intermediate (PER), thus lowering the anol and anone concentrations and as a consequence improving the efficiency. Depending on the degree of cyclohexane conversion, efficiencies of 85-95 % can now be obtained. Of course, the degree to which the overall efficiency is increased after the decomposition of the peroxide depends on the selectivity of the peroxide conversion step, but this will not be considered here.

The process improvement has been thoroughly evaluated in bench-scale experiments and afterwards been tried out in a commercial plant process. All operations involved were conducted in gear with computer model calculations. On the basis of the laboratory experiments a kinetic model was developed on an analog computer. Next, a reactor model based on the kinetic model was worked out on a digital computer. In the following step, a model of the new process variant was set up by means of the DSM flowsheet simulation system TISFLO. Finally, the process model was used for optimizing the process. The various stages of the investigations and the supporting activities are schematically shown in Table I.

Table I. Survey of the work done on improvement of the CH-oxidation process

Experimental	Model calculations
Bench scale experiments	Analog simulation of the reaction kinetics. Digital simulation of a gas-liquid reactor. Simulation of an actual plant for test-run planning
Test runs in an existing plant	Correction of several quantities in the model after the test runs. Optimization of the design.

The present paper briefly outlines the development of the computer models and some of the results achieved with these.

2. KINETIC MODEL

In bench-scale batch experiments, cyclohexane was oxidized with air in a stirred autoclave. To describe the change in the concentrations of the principal oxidation products, we postulated the following reaction scheme:

In Chemical Reaction Engineering—Houston; Weekman, V., et al.;
ACS Symposium Series; American Chemical Society: Washington, DC, 1978.

$$R + O_2 \xrightarrow{k_1} PER \qquad (2.1)$$

$$PER \xrightarrow{k_2} ANOL + \tfrac{1}{2} O_2 \qquad (2.2)$$

$$PER \xrightarrow{k_3} ANONE + H_2O \qquad (2.3)$$

$$2\ PER \xrightarrow{k_4} ANOL + ANONE + H_2O + \tfrac{1}{2} O_2 \qquad (2.4)$$

$$ANOL + \tfrac{1}{2} O_2 \xrightarrow{k_5} ANONE + H_2O \qquad (2.5)$$

$$ANONE + 3/2\ O_2 \xrightarrow{k_6} \text{"acids"} \qquad (2.6)$$

This scheme is practically analogous to those put forward by Steeman et al. (1), Alagy et al. (2) and Vasey et al. (3). The diversity of byproducts, such as acids, esters, heavies, lights, CO, CO_2 and alkanes, are included under "acids". Reaction (2.1) is regarded as the sum of two radical reactions:

$$R^{\cdot} + O_2 \longrightarrow ROO^{\cdot} \qquad (2.7)$$

$$ROO^{\cdot} + R \xrightarrow{k_p} PER + R^{\cdot} \qquad (2.8)$$

The cyclohexyl radicals are generated during the breakdown of the PER according to the reactions (2.2), (2.3) and (2.4). Along the same lines as followed by Emanuel (4), it can be derived that the rate of this auto-oxidation system is proportional to the square root of the radical-generating components.

Simplification of the radical reaction equations yields the following expression for the formation rates of the various components:

$$-\left(\frac{d[CH]}{dt}\right) = k_1 \cdot [O_2] \cdot \left([PER] + [PER] \cdot [ANON]\right)^{\frac{1}{2}} \qquad (2.9)$$

On the basis of the above reasoning, the following differential equations can be set up:

$$\frac{d[PER]}{dt} = k_1 \cdot [O_2] \cdot \left([PER] + [PER] \cdot [ANONE]\right)^{\frac{1}{2}} - (k_2 + k_3) \cdot [PER] - k_4 \cdot [PER] \cdot [ANONE] \qquad (2.10)$$

$$\frac{d[OL]}{dt} = k_2 \cdot [PER] + k_4 \cdot [PER] \cdot [ANONE] - k_6 \cdot [ANOL] \cdot [O_2] \qquad (2.11)$$

$$\frac{d[ANONE]}{dt} = k_3 \cdot [PER] + k_4 \cdot [PER] \cdot [ANONE] + k_6 \cdot [ANOL] \cdot [O_2] - k_7 \cdot [ANONE] \cdot [O_2] \qquad (2.12)$$

In Chemical Reaction Engineering—Houston; Weekman, V., et al.;
ACS Symposium Series; American Chemical Society: Washington, DC, 1978.

$$\frac{d[\text{"acids"}]}{dt} = k_7 \cdot [\text{ANONE}][O_2] \qquad (2.13)$$

$$\frac{d[O_2]}{dt} = -k_1 \cdot [O_2] \cdot ([\text{PER}] + [\text{PER}] \cdot [\text{ANONE}])^{\frac{1}{2}} -$$

$$\tfrac{1}{2} \cdot k_5 \cdot [\text{ANOL}] \cdot [O_2] - 1\tfrac{1}{2} \cdot k_6 \cdot [\text{ANONE}] \cdot [O_2] + \tfrac{1}{2} \cdot k \cdot [\text{PER}] +$$

$$+ \tfrac{1}{2} \cdot k_4 \cdot [\text{PER}] \cdot [\text{ANONE}] \qquad (2.14)$$

For the O_2-consuming reactions the product of $k \cdot [O_2]$ is fitted. Equation (2.14) allowed us to calculate the stoichiometric oxygen need of the reactions. This need can be related to an independent supply of air to the reactors.
The factor F_{O_2} is defined as

$$F_{O_2} = \frac{O_2 \text{ supply}}{O_2 \text{ consumed in the stoichiometric conversion}}$$

The k-values were fitted for those experiments in which $F_{O_2} > 1$. For this case a zero-order description in O_2 is valid. When $F_{O_2} < 1$, all O_2-consuming reactions were multiplied by the factor F_{O_2}. This means that in this case a first-order reaction in O_2 is assumed.

The example shown in Fig. 2 serves to illustrate to what extent the laboratory experiments are covered by the model.

3. MODEL OF THE GAS-LIQUID REACTOR

With regard to the gas-liquid reactor the following assumptions have been made:
- the liquid phase and the gas phase are perfectly mixed,
- the issuing gas stream is in physical equilibrium with the issuing liquid stream,
- the reactor operates adiabatically,
- the compositions, flowrates, temperatures and pressures of the feed streams are known.

In calculating the physical equilibrium, we made use of gas-liquid equilibrium constants, which are defined as

$$\left(K = \frac{y}{x}\right)_i$$

where K_i is a function of the temperature, pressure and composition of the liquid (x_i).

The dependence of K on the liquid concentrations was brought into account in that the activity coefficients were calculated with the aid of Wilson's equation. The Wilson constants for several binary systems were derived from experimental figures by means of non-linear regression.

In Chemical Reaction Engineering—Houston; Weekman, V., et al.;
ACS Symposium Series; American Chemical Society: Washington, DC, 1978.

The component balance for each individual component can be written as:

$$(F_G \cdot y_F + F_L \cdot x_F = L \cdot x + G \cdot y - V \cdot r)_i \qquad (3.2)$$

The enthalpy balance of the reactor reads:

$$F_G \cdot H_G^F + F_L \cdot H_L^F = L \cdot H_L + G \cdot H_G - Q_r \qquad (3.3)$$

Solution of the set of equations (3.1), (3.2) and (3.3) yields the model of the gas-liquid reactor. Except for the terms $(V \cdot r)_i$ and Q_r, the above set of equations is equal to that defining an adiabatic flasher. Supplementation of an adiabatic flash standard calculation routine with these terms provided a program for the gas-liquid reactor. After the temperatures, compositions and flowrates of the issuing vapour and liquid streams have been calculated, the effective reactor volume can be determined.

4. SIMULATION OF A PLANT OXIDATION SECTION BY MEANS OF TISFLO

For further evaluation of the process, the reactor model was incorporated in a flowsheet calculation routine executed with the standard flowsheet simulation program TISFLO. TISFLO is a component of TIS (Technological Information System), a system developed by DSM (5,6) for executing chemical process calculations. The flowsheet model on which the calculations were carried out is illustrated in fig. 1. The flowsheet may comprise either one reactor or several reactors connected in series.

The independent variables in the simulations were so chosen as to correspond with the control variables in the plant. These independent variables were:

- the pressure,
- the flowrate of the feed stream to the first reactor,
- the temperature of the first reactor,
- the air feed to each reactor.

We can now calculate the following characteristic data: degree of cyclohexane conversion, oxidation efficiency and production level. With the aid of the flowsheet simulation program the mass and heat balances can be determined and a scenario is prepared for undertaking experiments in an existing plant equipped with two series-connected reactors. The program comprised six experiments, with a planned maximum duration of 24 h each. The pressure during the experiments was kept constant. The plant was run at two feed flow rates with simultaneous variation of air supply and temperature. Checking the model was done with reference to the temperatures measured in the reactors and to the analyses of samples taken of the liquid and vapour streams from the reactors. The

In Chemical Reaction Engineering—Houston; Weekman, V., et al.;
ACS Symposium Series; American Chemical Society: Washington, DC, 1978.

calculated reactor temperatures according to the model were found to deviate by a few degrees from those recorded in the plant, but after introduction of the heat of reaction of each part reaction proper agreement was obtained.

An important finding made during the calculation was that set point changes give rise to instable situations. In fig. 3 we have plotted the reactor temperature versus the air flow rate for two temperatures of the first reactor. A change over from situation A to situation D should be conducted along the path ABCD, i.e. by first reducing the air feed and then lowering the temperature of the first reactor, and not the other way about, because this would give rise to an instable situation leading to a blow out of the reaction. This instability was demonstrated in the plant.

5. OPTIMIZATION

The optimizing calculations were carried out on the simplified flowsheet model illustrated in fig. 4, where RE_n represents a series of gas-liquid reactors, and WW denotes the heat exchanger. The equipment following the reactors is indicated by one block, OPW. Stream 5 is the offgas from the reactor and stream 7 the product from the top of the cyclohexane distillation column.

Because of the complexity of the process and the great many variables involved, the optimization was carried out by means of a sensitivity analysis. The cost function is composed of the following factors:

(a) raw materials consumption (cyclohexane and caustic),
(b) condensation of reactor offgas (costs calculated from energy consumption and investments),
(c) distillation of the cyclohexane recycle stream (ditto),
(d) investment in reactors (cost per cu.m. of reactor volume).

The variables that play an important role in the reactor section are:

(1) fresh cyclohexane feed,
(2) air flow rate to each reactor,
(3) production level,
(4) degree of cyclohexane conversion,
(5) oxidation efficiency,
(6) temperature of first reactor,
(7) flowrate of cyclohexane recycle stream,
(8) flowrate of reactor feed stream,
(9) pressure,
(10) number of reactors,
(11) split of all components over section OPW (see fig. 4),
(12) split of all components over the heat exchanger (WW/offgas),
(13) reactor volume.

In Chemical Reaction Engineering—Houston; Weekman, V., et al.;
ACS Symposium Series; American Chemical Society: Washington, DC, 1978.

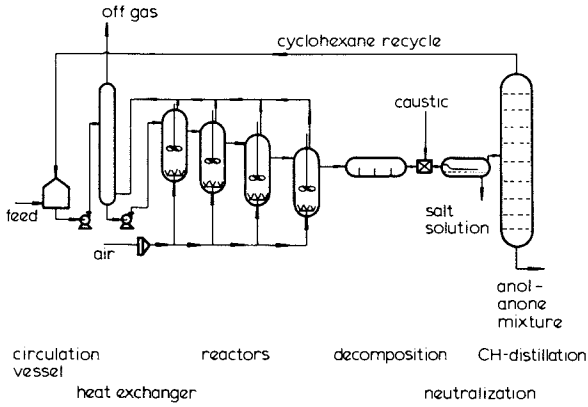

Figure 1. Flowsheet for the cyclohexane oxidation section

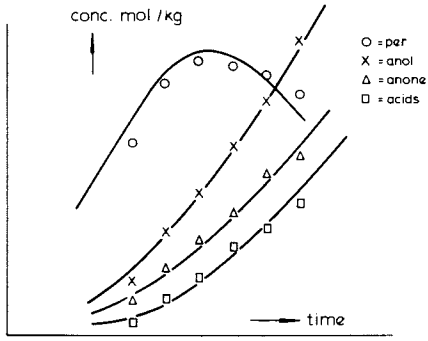

Figure 2. Comparison of a batch experiment with the model on the analog computer

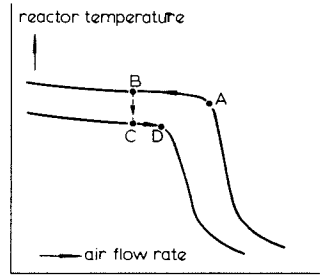

Figure 3. Reactor-temperature as a function of the air flowrate at two reactor feed temperatures

In Chemical Reaction Engineering—Houston; Weekman, V., et al.;
ACS Symposium Series; American Chemical Society: Washington, DC, 1978.

Before starting on the optimization, we determined the number of degrees of freedom by analyzing the interrelations between the variables. Specifying fixed values for:
- the split of the components over section OPW,
- the split of the components over section WW.

We found that there are six more degrees of freedom to be selected from the above list. The optimization is carried out in two steps. In our first optimizing effort, we selected as variable factors those that had an unambiguous effect on the cost function: the number of reactors and the air feed to each reactor.

This optimization was carried out by using fixed values for the reactor volume, the pressure, the degree of conversion, and the production. The influence of the way in which the air is distributed over the reactors is illustrated in fig. 5. As can be seen here a distribution pattern ensuring that $F_{O_2} = 1$ is to be preferred to the situation where the air feed rates to all reactors are equal. It is also seen that the cost function decreases with an increase in the number of reactors. For practical reasons the number of reactors was in all cases taken equal to six.

In the second optimizing step, we fixed the number of reactors, the volume of each reactor, the air feed to the reactors (in compliance with the requirement $F_{O_2} = 1$ for each reactor). As the remaining three degrees of freedom we chose: the pressure, the temperature of the first reactor and the flowrate of the cyclohexane recycle. To determine the optimum working point of a given reactor configuration, we calculated the cost function at two temperature levels of the first reactor ($T_1 < T_2$) and three pressure levels ($P_1 < P_2 < P_3$) as a function of the cyclohexane recycle flowrate (see fig. 6).

The two principal factors opposing each other are: the use of more raw materials when the recycle rate is low (as a result of low selectivity), and the high cost of distillation when the recycle rate is high.

It appeared that for each of the six combinations of P and T there exists an optimum production capacity and also that the production increases with the flowrate of the cyclohexane recycle stream.

6. FINAL REMARKS

The optimizing calculations are based on the kinetic model and the reactor model outlined in paragraphs 2 and 3. Notwithstanding that the research work had progressed so far as to enable the plant reactor performance to be fairly accurately predicted from the results of batch experiments we considered it desirable to build a complete pilot installation comprising recirculation, neutralization and saponification units. The

In Chemical Reaction Engineering—Houston; Weekman, V., et al.;
ACS Symposium Series; American Chemical Society: Washington, DC, 1978.

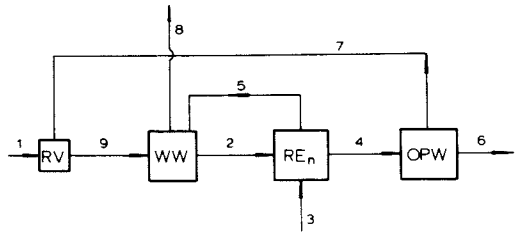

Figure 4. Flowsheet representation of the cyclohexane oxidation section

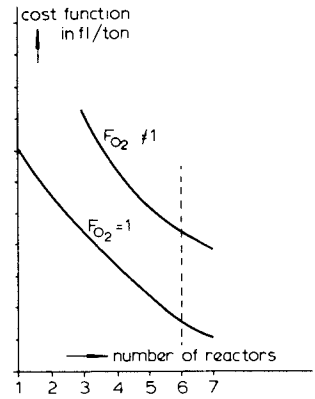

Figure 5. Results of the first optimization

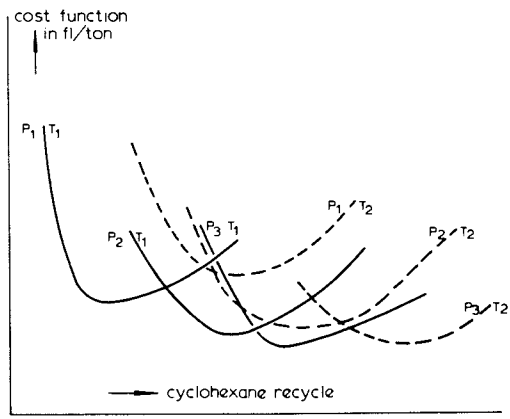

Figure 6. Results of the second optimization

In Chemical Reaction Engineering—Houston; Weekman, V., et al.;
ACS Symposium Series; American Chemical Society: Washington, DC, 1978.

principal objectives underlying this decision were:
a) checking the results of optimizing calculations by downscaling from plant to semi-technical scale,
b) examining if the recycle streams have an effect on the efficiency,
c) production of oxidation liquid for further research of the decomposition step and the neutralization of acids,
d) testing the quality of caprolactam prepared from anone made in the pilot plant,
e) availability of an installation for carrying out research on behalf of plants all over the world under conditions obtaining there,
f) offering the possibility of training operating staff.

The results of the optimizing calculations have also been used for determining what costprice reduction can be realized. The new procedure has appeared to be applicable to both new and existing installations. The cost of rebuilding and the loss of production during rebuilding will normally be more than offset by the gain in profit and efficiency.

We have shown how the development of processes in the chemical industry is supported by means of mathematical models. Recognizing that the basic kinetic model still has several weak points, we are convinced that these have hardly any effect on the trends disclosed by the optimization, and also that the results of our study will contribute towards improved operation of the reactor section in existing plants as well as towards more exact design of new installations.

LIST OF SYMBOLS

		dimension
R	cyclohexane	
PER	cyclohexyl hydroperoxide	
ANONE	cyclohexanone	
ANOL	cyclohexanol	
$R^{\cdot}$	cyclohexyl radical	
$ROO^{\cdot}$	cyclohexyl hydroperoxide radical	
F_{O_2}	oxygen factor (see eq. 2.14)	-
K	gas liquid equilibrium constant (eq. 3.1)	-
x	mole fraction in the liquid	-
y	mole fraction in vapour	-
T	temperature	C
P	pressure	kPa
F	feed rate	kmoles/hr
L	liquid flowrate from reactor	kmoles/hr
G	gas flowrate from reactor	kmoles/hr
V	liquid volume in reactor	m^3
r	reaction rate $(\frac{d}{dt})$	kmoles/$(hr.m^3)$

In Chemical Reaction Engineering—Houston; Weekman, V., et al.;
ACS Symposium Series; American Chemical Society: Washington, DC, 1978.

H	enthalpy	kJ/kmoles
Q_r	heat of reaction	kJ/kmoles

INDICES

F	feed
G	gas phase
L	liquid phase

7. LITERATURE CITED

1. Steeman J.W.M. et al. Chem. Eng. Sci (1960) 14 39.
2. Alagy J. et al. Ind. Eng. Chem. Proc. Des. Developm. (1974) 13 317.
3. Vasey C.H. et al. Symp. 'Oxidation in Chemistry', Manchester, april 1975.
4. Emanual' N.M. et al. 'The Oxidation of cyclohexane', Pergamon Press, Oxford (1966).
5. de Leeuw den Bouter J.A., Swenker A.G. Symp. 'Computer application in process development' 2-3/4 '74 Erlangen.
6. de Leeuw den Bouter J.A., Swenker A.G. Symp. 'Computers in the design and erection of chemical plants' 1-4 sept. 1975 Karlsbad.

In Chemical Reaction Engineering—Houston; Weekman, V., et al.;
ACS Symposium Series; American Chemical Society: Washington, DC, 1978.

30

Detailed Analysis of CO_2-Interphase Mass Transfer in a Bubble Column to Prove the Validity of a Design Model

W.-D. DECKWER and I. ADLER

Institut für Technische Chemie, TU Hannover, Callinstr. 3, 3000 Hannover 1, West Germany

A. ZAIDI

Institut für Technische Chemie, TU Berlin, Strasse des 17, Juni 135, 1000 Berlin 12, West Germany

The common treatment of bubble column reactors is based on the axial dispersion model. Two-phase dispersion models were first developed for several kinds of extraction equipment, and these models were also overtaken to describe the behaviour of gas-liquid contactors like bubble columns (1-3). The favorable application of bubble columns presents the performance of gas-liquid reactions which take place in the slow reaction regime of mass transfer theory. In this absorption regime bubble columns provide for sufficient interfacial areas for mass transfer and at the same time the liquid volume needed for the reaction is large enough. In industry high conversions are desired. Thus the molar gas flow rate may vary considerably along the column since the reaction product is usually non-volatile and the mass capacity of the gas phase is small compared to that of the liquid phase. For that reason design models proposed for extractors are not a realistic description of bubble columns. Recently a theoretical model for bubble columns of industrial size was proposed which accounts for variations of gas flow rate and pressure (4). There it was demonstrated by numerical simulations that even at isobaric conditions the gas flow rate has to be considered as variable since gas volume decrease by absorption leads to increased gas residence time which in turn improves the conversion. Simpler models like those for extractors can be applied only if the column operates at elevated pressures and if, in addition, the gas shrinkage due to absorption is small.

When the absorption and reaction of isobutene in sulfuric acid was studied in a tall bubble column it was found that the conversions measured at the column exit could be explained reasonably only on the base of this improved model (5). However, the comparison of experimental and predicted concentration profiles would present a better mean to prove the validity of a parti-

© 0-8412-0401-2/78/47-065-359$05.00/0

cular model and to discriminate among rival models. Obvious experimental difficulties did not allow the determination of concentration profiles for the absorption and reaction of isobutene. Therefore the absorption and desorption of CO_2 in water was studied. Owing to the large interphase mass transfer due to the high CO_2 solubility the CO_2-water system is very appropriate to simulate conditions which are encountered in industrial applications of bubble columns as reactors.

Experimental

The investigations were carried out in a bubble column (BCI) of 20 cm I.D. and a height of 723 cm. The experimental set up is shown in Figure 1. The column was made from glass and could be operated at cocurrent and countercurrent flow. The gas was sparged by 56 nozzles of 1 mm I.D. Tap water was used as liquid phase and its temperature was maintained at 16 °C. The liquid flow rate was 3 m^3/h for all runs reported here. Another bubble column (BCII) of smaller size was used to regenerate the liquid phase which was recycled. Gas samples were withdrawn from several axial positions by means of a special device. The samples were analyzed on their CO_2-content. For some measurements liquid phase concentration profiles were determined too. The manometric method was used to measure local values of the gas hold up along the column. The interfacial area was obtained from photographic pictures which were taken from the gas-liquid dispersion at 350 and 610 cm above the sparger.

A detailed description of the experimental arrangement and the applied analytical techniques is given elsewhere (7). Typical experimental conditions for absorption and desorption measurements are presented in table 1. The overall CO_2-balance was fulfilled within 3 per cent for all runs.

Gas Hold up and Interfacial Area

The majority of experimental results on bubble columns was obtained from conditions at which the applied concentrations of the transfer components are kept low. Hence the molar gas flow rate can be assumed as sufficiently constant. From table 1 it can be discerned that in this study the mole flow rate of the gas phase varies considerably. Therefore all fluiddynamic properties reveal marked local dependencies. From the measured local gas hold up the concentration profiles and the bubble size distributions axial profiles of the in-

In Chemical Reaction Engineering—Houston; Weekman, V., et al.;
ACS Symposium Series; American Chemical Society: Washington, DC, 1978.

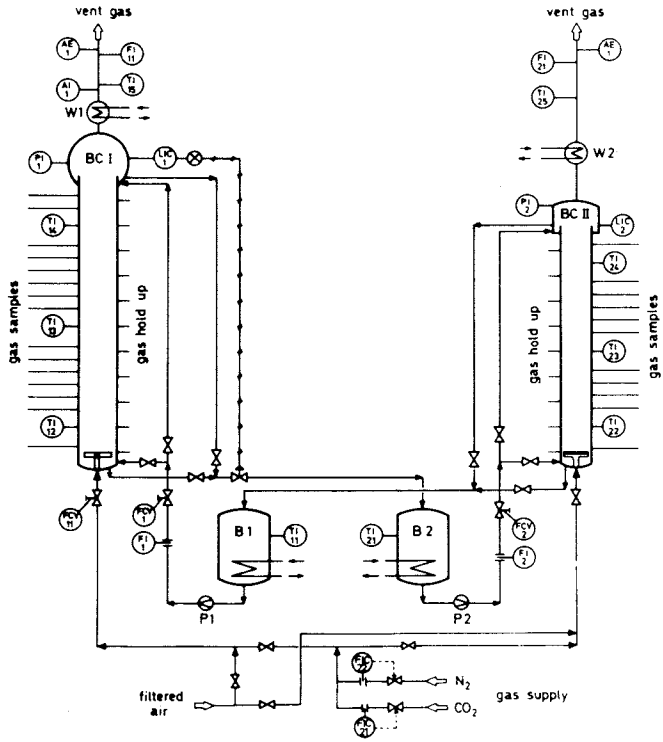

Figure 1. Experimental set-up

Table 1: Operational conditions of typical experimental runs

No. W	flow	x_o	x_1	u_{Go} cm/s	u_{G1} cm/s	P_{Li} Torr	$\bar{\varepsilon}_G$	d_s mm	f_B	$10^2 k_L$ cm/s
1	↑↓	0.	0.59	0.48	1.68	691	0.038	3.08	3	0.61
2		0.	0.45	1.00	2.94	601	0.070	2.94	3	0.57
3		0.	0.36	1.55	3.75	559	0.073	2.56	2	0.50
4		0.	0.33	1.90	4.50	514	0.130	2.79	2	0.53
5		0.	0.17	4.26	7.65	501	0.150	2.50	2	0.47
6	↑↑	0.	0.51	0.50	1.60	733	0.032	3.15	3	0.91
7		0.	0.39	1.00	2.63	670	0.060	3.10	4	0.73
8		0.	0.33	1.53	3.55	662	0.089	2.79	3	0.71
9		0.	0.24	2.51	4.95	612	0.091	2.90	4	0.69
10		0.	0.17	4.00	7.20	581	0.155	2.56	4	0.75
11	↑↓	0.76	0.12	0.71	0.30	102	0.013	4.50	2	2.09
12		0.65	0.14	1.05	0.65	118	0.025	3.76	2	1.80
13		0.75	0.20	1.44	0.78	119	0.032	3.65	2	1.14
14		0.69	0.23	1.77	1.13	103	0.049	3.10	3	0.82
15		0.56	0.21	1.96	1.72	111	0.076	2.83	3	0.92
16		0.42	0.20	2.58	3.06	94	0.120	2.68	2	0.96

In Chemical Reaction Engineering—Houston; Weekman, V., et al.;
ACS Symposium Series; American Chemical Society: Washington, DC, 1978.

terfacial area, the linear gas velocity, the mean bubble rise velocity and frequency factors for coalescence and break up of bubbles could be obtained. These data offer a sophisticated insight on the behaviour of gas-liquid dispersion at high interphase mass transfer rates, and they are discussed in detail in refs. (7,8). For the purpose of this paper it will suffice to point out that the measured local values of the gas hold up ε_G are described by a regression function of the dimensionless axial coordinate z:

$$\varepsilon_G(z) = \bar{\varepsilon}_G \varphi(z) \quad (1)$$

with

$$\varphi(z) = a_o + a_1 z + a_2 z^2. \quad (2)$$

$\bar{\varepsilon}_G$ presents the integral value (see table 1) which is obtained from the local values by:

$$\bar{\varepsilon}_G = \sum_i \varepsilon_G(z_i) \Delta z_i. \quad (3)$$

Since the mean Sauter diameter d_s was found to be approximately independent on z the interfacial area a is calculated from the smoothed hold up data by:

$$a(z) = 6 \bar{\varepsilon}_G \varphi(z)/d_s. \quad (4)$$

Model Assumptions

The measured fluiddynamic properties and the reasons outlined in (4) recommend the evaluation of the experimental concentration profiles on the base of the following assumptions:

(1) Henry's law is valid:

$$Px = Hc_L = p \quad (5)$$

(P = total pressure, x = mole fraction, H = Henry's constant, c_L = liquid phase concentration, p = partial pressure)

(2) oxygen and nitrogen are inerts
(3) axial dispersion in liquid phase
(4) plug flow in gas phase
(5) neglect of radial dispersion
(6) pressure depends linear on z:

In Chemical Reaction Engineering—Houston; Weekman, V., et al.;
ACS Symposium Series; American Chemical Society: Washington, DC, 1978.

$$P = P_T [1 + \alpha(1-z)] \quad (6)$$

where P_T is the pressure at column top

(7) gas hold up and interfacial area vary with z
(8) gas velocity u_G is variable
(9) neglect of reaction of CO_2 with water
(10) gas phase resistance to mass transfer can be neglected.

Owing to their low solubility the amounts of O_2 and N_2 transfered from one phase to the other is always less than 2 % of the exchanged CO_2. Thus assumption (2) is justified with sufficient accuracy. The dispersion coefficients of the liquid phase D_L were calculated from (6):

$$D_L = 2.7\, d^{1.4}\, u_G^{0.3} \quad (7)$$

(d = column diameter).

Eqn (7) was established from measured data in the used columns and its significance was confirmed by other investigators (9,10). The available information on gas phase dispersion coefficients (11) justifies assumption (4). If merely linear processes occur radial dispersion effects need not be accounted for (12). Since the model eqns applied in this study are non-linear and furthermore measured tracer distributions in the liquid phase show marked radial profiles particularly at countercurrent flow (13) a two-dimensional description may be more pertinent. CO_2 concentration measurements at different radial positions did,however,not yield any significant differences. Therefore the one-dimensional model is thought to be a sufficient approximation. Although gas hold up may vary considerably along the column the value of α in eqn(6) can be taken as approximately constant. α represents the ratio of the maximum hydrostatic head to the pressure at the top of the bubble column:

$$\alpha = \frac{\rho g (1 - \bar{\varepsilon}_G) L}{P_T} \quad (8)$$

The variation of the gas hold up and the interfacial area are taken into account by eqns (1) and (4), respectively. Assumption (8) accounts for a variable gas velocity. Therefore an additional relation is required. This is obtained from a balance on the inerts which yields:

In Chemical Reaction Engineering—Houston; Weekman, V., et al.;
ACS Symposium Series; American Chemical Society: Washington, DC, 1978.

$$u_G\, P(1-x) = u_{Go} P_T (1+\alpha)(1-x_o) \qquad (9)$$

The index o refers to conditions at column inlet. Assumption (10) must not be fulfilled actually as the liquid side mass transfer coefficient can be substituted by the overall transfer coefficient.

Model Equations

The governing differential balance equations are not derived here as this is outlined for similar problems in detail in ref. (4). Consideration of eqn (9) leads to eqn (10) for the CO_2-balance of the gas phase:

$$\frac{dx}{dz} = -St_G \varphi(z)(1-x)^2 \left(\beta(z)x - \frac{p_L}{P_T}\right). \qquad (10)$$

For the partial pressure of CO_2 in the liquid phase p_L one obtains on the base of the made assumptions:

$$\frac{d^2 p_L}{dz^2} + a\,\frac{Pe_L}{1-\bar{\varepsilon}_G \varphi(z)}\,\frac{dp_L}{dz} = \frac{Pe_L\, St_L \varphi(z)}{1-\bar{\varepsilon}_G \varphi(z)}\,(P_T \beta(z) x - p_L). \qquad (11)$$

In eqns (10) and (11) the following dimensionless quantities were introduced:

$$St_G = k_L \frac{6\bar{\varepsilon}_G}{d_S} \frac{L}{u_{Go}(1+\alpha)(1-x_o)} \frac{RT}{H} \qquad (12)$$

$$\beta(z) = 1+\alpha(1-z) \qquad (13)$$

$$Pe_L = \frac{u_L L}{D_L} \qquad (14)$$

$$St_L = k_L \frac{6\bar{\varepsilon}_G}{d_S} \frac{L}{u_L}. \qquad (15)$$

Here k_L presents the liquid side mass transfer coefficient, L the entire column length, R the gas constant, T the temperature, and u_L the superficial liquid velocity.
The initial condition for eqn (10) is

$$x(0) = x_o \qquad (16)$$

The boundary conditions for eqn (11) are for the case of cocurrent flow (a = -1):

In Chemical Reaction Engineering—Houston; Weekman, V., et al.;
ACS Symposium Series; American Chemical Society: Washington, DC, 1978.

$$p_L(0) = p_{Li} + \frac{1-\bar{\varepsilon}_G \varphi(0)}{Pe_L} \frac{dp_L(0)}{dz} \quad (17)$$

$$\frac{dp_L(1)}{dz} = 0 \quad (18)$$

and for countercurrent flow (a = +1):

$$\frac{dp_L(0)}{dz} = 0 \quad (19)$$

$$p_L(1) = p_{Li} - \frac{1-\bar{\varepsilon}_G \varphi(1)}{Pe_L} \frac{dp_L(1)}{dz} \quad (20)$$

The index i refers to inlet conditions.
The differential eqns (10) and (11) were solved numerically by the method of Lee (14) which is well suited to solve non-linear boundary value problems with non-constant coefficients. However, as will be discussed later it was not possible to obtain convergence for certain parameter combinations, particularly at high values of k_L. It is assumed that this has to be attributed to stiffness of the system of differential equations. Since D_L depends on gas velocity (see eqn (7)) and this varies considerably along the column preliminary computations were carried out with different values of D_L calculated from u_{Go} and u_{G1} (gas velocity at outlet), respectively. These calculations revealed that computed gas phase profiles are practically not effected by D_L for the possible range of variation. Therefore D_L was calculated from eqn (7) with the mean gas velocity which is defined by

$$\bar{u}_G = \int_0^1 u_G(z)\,dz \quad (21)$$

where the local values of $u_G(z)$ are obtained from eqn (9) by consideration of eqn (6) and the measured gas phase profile. The liquid side mass transfer coefficient is now the only quantity which is unknown. It was thought that these k_L-values can simply be determined by fitting model predictions to experimental gas phase profiles. No special optimization procedure was applied. Since only one parameter had to be determined and the computations were fast enough a trial-and-error method was sufficient.

In Chemical Reaction Engineering—Houston; Weekman, V., et al.;
ACS Symposium Series; American Chemical Society: Washington, DC, 1978.

Description of Measured Profiles

When using constant values of k_L the model equations could not describe reasonably the experimental profiles. This is shown in fig. 2 for desorption measurements. The curves for $f_B = 1$ refer to k_L-values which are constant over the entire column. Though experimental and theoretical results can be brought in agreement nearby the top of the column, the calculated mole fractions are always considerably too low close to the bottom. Further increase of k_L did not improve the agreement but led usually to stiffness since convergence could not be obtained any more. As the theoretical profiles indicate that mass transfer is too small merely near the gas distributor increased k_L-values were applied there. Favorable and consistent results for all runs could be obtained if the constant mass transfer coefficient was replaced by a profile which is shown in fig. 3. For reasons of simplification integer values of f_B were taken only: $2 \leq f_B \leq 4$ (see table 1). Thus a striking agreement between the measured data and the model predictions (full drawn curves) is obtained as can be seen from fig. 1. Fig. 4 and 5 present CO_2 profiles of the gas and liquid phase, respectively, for the case of absorption runs at countercurrent flow. Once again a sufficient agreement is observed.

It is interesting to note that the gas phase concentration can run through a minimum value. Though this minimum is very flat it is reproducible and was also found for other runs. Such extreme values in gas concentration were not observed experimentally before, however, they were already predicted theoretically from numerical studies for the case of cocurrent flow (4). For the countercurrent absorption run presented in fig. 4 the minimum results from the rather high inlet concentration of CO_2 in the liquid phase, see fig. 5. Due to the hydrostatic head the concentration of CO_2 in the gas phase decreases to a lower value than that one which corresponds to the inlet partial pressure in the liquid phase. Therefore at column top small amounts of CO_2 desorb from the liquid phase which is supersaturated against gas phase. Though the observed minima are irrelevant for any technical application they present a justification of the applied model since simpler models are not able to describe the measured profiles.

If constant values of the hold-up and the interfacial area ($\varphi(z) = 1$) were applied in the calculations a reasonable fitting of the measured profiles could not be obtained. This is shown in fig. 6 where the dotted lines indicate theoretical profiles with the smallest

In Chemical Reaction Engineering—Houston; Weekman, V., et al.;
ACS Symposium Series; American Chemical Society: Washington, DC, 1978.

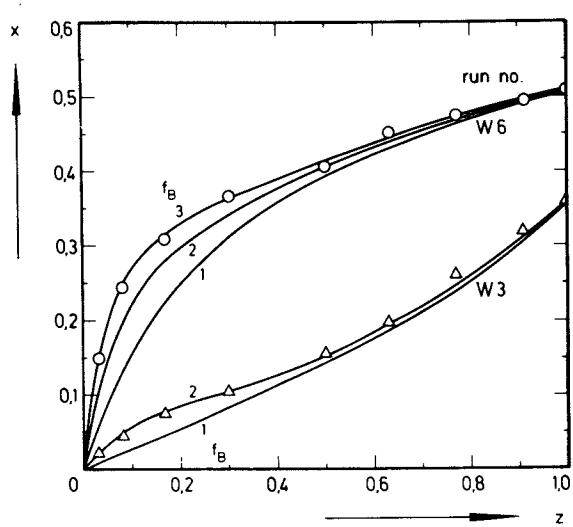

Figure 2. Measured and calculated gas phase mole fraction of CO_2 for different values of f_B

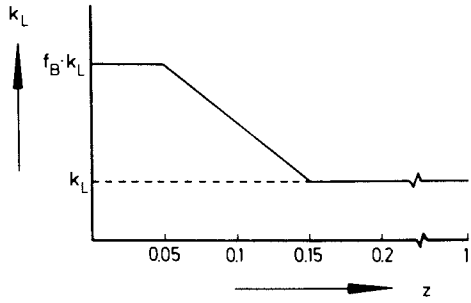

Figure 3. Applied profile of liquid phase mass transfer coefficient

In Chemical Reaction Engineering—Houston; Weekman, V., et al.;
ACS Symposium Series; American Chemical Society: Washington, DC, 1978.

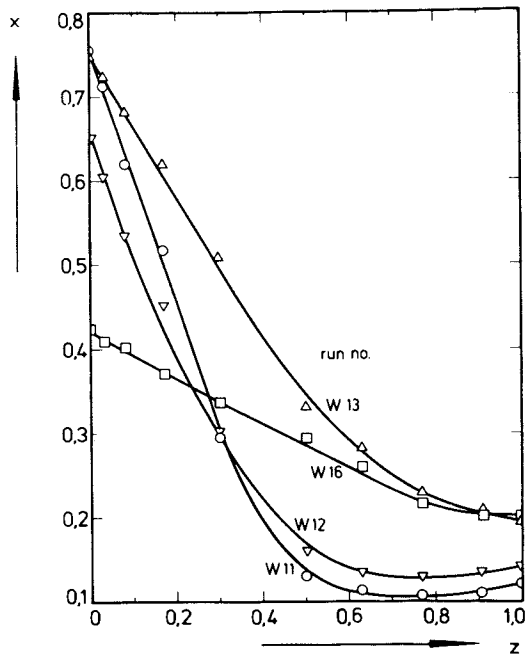

Figure 4. Measured and calculated gas profiles at countercurrent absorption

In Chemical Reaction Engineering—Houston; Weekman, V., et al.;
ACS Symposium Series; American Chemical Society: Washington, DC, 1978.

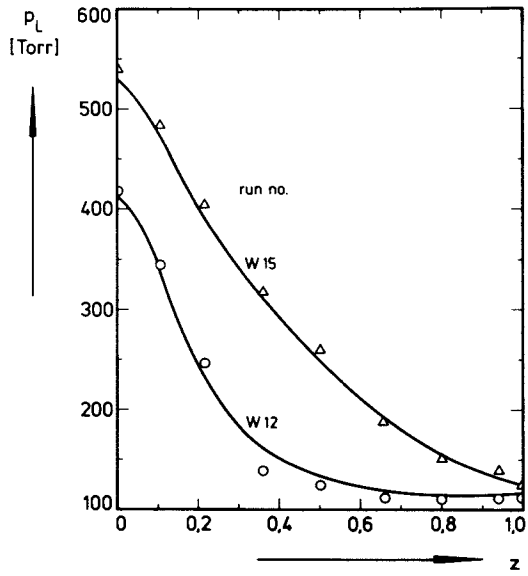

Figure 5. Measured and calculated profiles of liquid phase partial pressure of CO_2

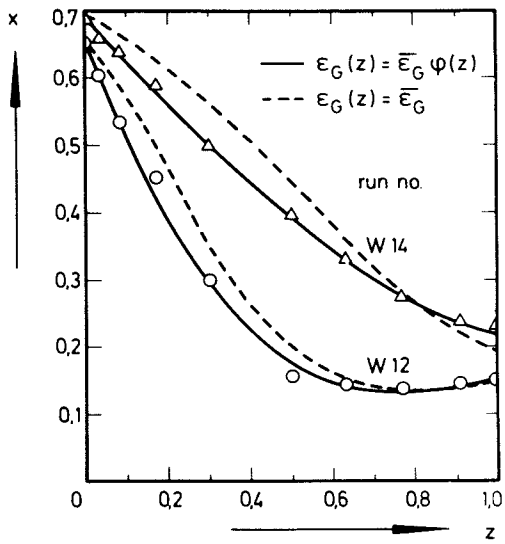

Figure 6. Measured and calculated gas profiles

In Chemical Reaction Engineering—Houston; Weekman, V., et al.;
ACS Symposium Series; American Chemical Society: Washington, DC, 1978.

attainable deviation (k_L = 0.0235 cm/s and f_B = 2 for run 12, k_L = 0.0133 and f_B = 3 for run 14). This observation leads to the conclusion that the proposed model is able to describe the measured profiles only because φ (z) is known with sufficient accuracy too.

The k_L- and f_B-values determined from matching theoretical predictions to experimental results are given in table 1. Since the important hydrodynamic properties are locally dependent it is understood that the mass transfer coefficient is also a function of z. The obtained k_L-data are in the reasonable range. However, contrary to previous findings at low interphase mass transfer (6) they differ largely for absorption and desorption runs. Furthermore cocurrent desorption yields surprisingly higher values than countercurrent flow. The dependency of k_L on the operating conditions and particularly on the frequency factors of bubble coalescence and break up (8) will be discussed together with further measurements in a following paper (15).

Conclusion

The findings of this study on a bubble column of industrial length and a diameter sufficiently large not to involve wall effects confirms the significance of the applied model which accounts for the hydrostatic head and gas flow variations. However, the excellent agreement between experimental and theoretical results could only be obtained with consideration of detailed information on the hydrodynamic parameters. Unfortunately such exact knowledge on hydrodynamic properties is seldom available. This fact will certainly not permit the widespread application of the proposed model in industry at the present time. Therefore further studies at operating conditions prevailing in industry are needed which are focused on measurements inside the equipment and which are evaluated on the base of realistic models. It can be expected that only from such studies reasonable guidelines may be developed which provide for a reliable design of bubble columns.

Acknowledgement

The authors gratefully acknowledge support from Deutsche Forschungsgemeinschaft and Stiftung Volkswagenwerk.

Literature Cited

(1) Pavlica, R.T., Olson,J.H., Ind.Eng.Chem.(1970) 62 45
(2) Mhaskar,R.D., Chem.Engng.Sci. (1974)29 897
(3) Szeri,A., Shah,Y.T., Madgavkar,A., Chem.Engng.Sci. (1976) 31 225
(4) Deckwer,W.-D., Chem.Engng.Sci. (1976) 31 309
(5) Deckwer,W.-D., Chem.Engng.Sci. (1977) 32 51
(6) Deckwer, W.-D., Burckhart,R., Zoll,G., Chem.Engng. Sci. (1974) 29 2177
(7) Deckwer, W.-D., Zaidi,A., Adler,I., Chem.-Ing.-Techn. (1976) 48 1075
(8) Deckwer,W.-D., Zaidi,A., Adler,I., Preprints Eur. Congr.: Transfer Processes in Particle Systems, Nuremberg,Germany, 1977, ed. by H.Brauer and O.Molerus
(9) Baird,H.M.I., Rice,R.G., Chem.Engng.J. (1975) 9 171
(10) Subramanian,G., Tien,C., Can.J.Chem.Engng. (1975) 53 611
(11) Towell,G.D., Ackerman,G.H., Proc. ISCRE 2, B3-1, Amsterdam 1972
(12) Serpemen,Y., Deckwer,W.-D., Ind.Eng.Chem.Fundam. (1974) 13 399
(13) Göhler,P., Dr.-Ing. thesis, TU Berlin, 1973
(14) Lee,E.S.: "Quasilinearisation and Invariant Imbedding" Academic Press, New York, 1968
(15) Deckwer,W.-D., Zaidi,A., Adler,I., Chem.Engng.J., in preparation

31

Determination of Fluid Dynamic Parameters in Bubble Column Design

TH. PILHOFER, H. F. BACH, and K. H. MANGARTZ

Lehrstuhl A für Verfahrenstechnik, Technische Universität München, West Germany

Bubble columns are applied to many processes. They are employed in the same way for chemical synthesis (1) as also in waste water cleaning (2). Quite recently, their use for microbial processes has become increasingly important (3). In spite of the variety of these applications and the number of known experimental studies, the design and scale-up of a bubble column is still a difficult task. In this paper, results of experiments are presented, which are concerned with the determination of fluiddynamic parameters for column design.

The description of a process, taking place in a bubble column, requires the selection of a suitable model. In most cases the application of the one-dimensional dispersion model has proven satisfactory. When a differential mass balance is made around a differential segment of the column, disregarding radial dependencies, the following equations result for the case of counter-current:

$$\frac{dc_G}{dt} = - u_D \cdot \frac{dc_G}{dx} - k_L \cdot a \cdot (c_G^* - c_F) + D_D \cdot \varepsilon \cdot \frac{d^2 c_G}{dx^2} \qquad (1)$$

$$\frac{dc_F}{dt} = u_F \cdot \frac{dc_F}{dx} + k_L \cdot a \cdot (c_G^* - c_F) + D_C \cdot (1-\varepsilon) \cdot \frac{d^2 c_F}{dx^2} \qquad (2)$$

The linear velocities of the continous and disperse phase, u_C and u_D, can be adjusted arbitrarily, whereas the mass transfer coefficient k_L depends first of all on the system's physical properties. On the other hand the fluiddynamic parameters like interfacial area a, gas holdup ε and the dispersion coefficients D_D and D_C are influenced strongly by the phases throughputs. It is therefore necessary to prepare appropriate correl-

© 0-8412-0401-2/78/47-065-372$05.00/0

In Chemical Reaction Engineering—Houston; Weekman, V., et al.;
ACS Symposium Series; American Chemical Society: Washington, DC, 1978.

ations for the calculation of these parameters in order to solve equation (1) and (2). The following statements are concerned with this problem.

First of all, the lay-out of the gas distributor will be treated. Its task is to generate swarms of bubbles. If a sieve tray is used, one should be aware of the fact, that all the holes must be in operation. Otherwise, undesired circulations come into existence. Furthermore, weeping must be avoided when using large openings. This is most important, if the liquid tends to incrustate or solidify.

These phenomena are caused by the mechanism of the particle formation on the sieve tray. The openings work in the jetting region and not in the bubbling region (4). Therefore, to obtain a fully working sieve tray, so much a gas throughput has to be presented, that all openings work at least at the beginning of the jetting region. The minimum gas load relative to each hole can be determined by the following equations (4):
Small hole diameters:

$$We_L = \frac{w_L^2 \cdot d_L \cdot \rho_D}{\sigma} = 2 \qquad (3)$$

Large hole diameters:

$$Fr'_L = \frac{w_L^2}{d_L \cdot g} \cdot \left(\frac{\rho_D}{\Delta\rho}\right)^{5/4} = 0,37 \qquad (4)$$

The validity of both equations is separated by the following value of the hole diameter:

$$d_O = 2,32 \cdot (\sigma/\rho_D \cdot g)^{0,5} \cdot (\rho_D/\Delta\rho)^{5/8} \qquad (5)$$

These equations are valid for gas/liquid systems as well as for liquid/liquid systems (4).

The swarms of bubbles produced by the distributor moves upward through the liquid. Now, the nature of the bubble motion is most important for the development of the process in the column. At low gas velocities the bubble hardly hinder each other and the swarm rises upward in a regulated manner. This is called the "bubbly flow regime"(5). Presuming a constant bubble size, there is a maximum value of gas throughput within this bubbly flow regime, that can be determined by flooding point calculations (6). If the throughputs are increased beyond this point, a flow alteration takes place. In order to reach higher buoyancy forces for gas transport, bubble clusters or plugs are formed. This is called the "churn turbulent regime" (5).

In Chemical Reaction Engineering—Houston; Weekman, V., et al.;
ACS Symposium Series; American Chemical Society: Washington, DC, 1978.

For these two flow regimes figure 1 shows schematically typical curves for the dependency of the gas holdup on the gas velocity. During bubbly flow the gas holdup increases superproportionally with the gas throughput. With the beginning formation of bubble clusters, these curves are shifted to the right because of the continuously increasing bubble size. This results in a subproportional rise of the gas holdup with gas throughput. It is therefore necessary to distinguish between these two flow regions.

At the moment it is not possible to specify the limits of both regimes. For a rough approximation the following calculation may be carried out: Wallis (5) recommends the following equation for the motion of a swarm of bubbles in the bubbly flow regime:

$$w_R/w_\infty = (1 - \varepsilon) \qquad (6)$$

Using a batch-type liquid, for the relative velocity the following holds:

$$w_R = u_D / \varepsilon \qquad (7)$$

The flooding condition is:

$$du_D / d\varepsilon = 0 \qquad (8)$$

From equation (6) and (7) we get at the flooding point a gas holdup of 0,5 and the relationship:

$$u_D = 0{,}25 \cdot w_\infty \qquad (9)$$

For a usual rise velocity of a single bubble of 23 cm/s, from equation (9) a maximum linear gas velocity of 5,7 cm/s arises. At higher gas velocities only the churn turbulent regime exists. Yet, experiments show, that flow alteration may already occur at lower gas throughputs.

At hte moment equation (6) may be recommended for the calculation of the gas holdup in the bubbly flow regime. A better correlation can be obtained, if equations for the motion of solids are modified in a convenient way. This has already been achieved for the motion of droplet swarms (7).

Though the churn turbulent regime is the more significant region, there are no equations generally applicable to determine the gas holdup. Beyond this, most experiments have been carried out with air/water systems. In our experiments preference was therefore given to the variation of the system's physical properties. Four liquids were used under different temperatures; experiments under pressure are still going on but not yet evaluated. For example, in figure 2 measurements of the gas holdup at different linear gas

In Chemical Reaction Engineering—Houston; Weekman, V., et al.;
ACS Symposium Series; American Chemical Society: Washington, DC, 1978.

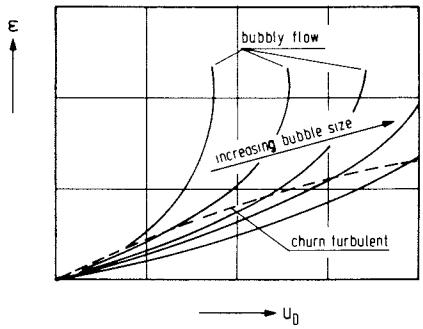

Figure 1. Dependency of the gas holdup on the linear gas velocity for different flow regions

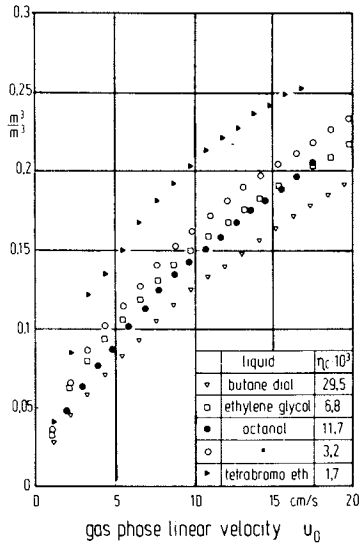

Figure 2. Measured gas holdup values for four different liquids as a function of gas linear velocity

In Chemical Reaction Engineering—Houston; Weekman, V., et al.;
ACS Symposium Series; American Chemical Society: Washington, DC, 1978.

velocities with different liquids are plotted.

Evaluating our own measurements and considering the results of Küsters (8) and Hammer/Rähse (9), using columns with the same dimensions, the following equation for the dependency of the gas holdup from the linear gas velocity and the physical properties holds:

$$\frac{\varepsilon}{1-\varepsilon} = 0{,}115 \left(u_D^3 / (\nu_C \cdot g \cdot \Delta\rho / \rho_C) \right)^{0{,}23} \qquad (10)$$

Equation (10) is valid for a column with an inner diameter of 100 mm and a clear liquid height greater than 1200 mm. In a further step we therefore examined, wether gas holdup is influenced by the column dimensions. In figure 3 gas holdup measurements are plotted versus gas linear velocity. The experiments were carried out in columns with inner dimensions larger than 150 mm and clear liquid heights higher than 1000 mm. Furthermore, the employed gas distributors caused a churn turbulent flow already at low gas throughputs. It can be seen, that all the values are described by one regression line with satisfactory accuracy. Consequently, there is no dependency of gas holdup from column dimensions. Because of the agreement of the exponent of the gas linear velocity in equation (10) with the results of figure 3, equation (10) can be recommended for gas holdup calculations. It is possible, that the constant value of 0,115 must be corrected insignificantly, as equation (10) has been derived for a column of 100 mm inner diameter whereas figure 3 refers to columns with a diameter equal or greater than 150 mm. The mentioned dependencies comply well with the results of Riquarts's considerations (10) for fluidized beds.

An additional fluiddynamic parameter to be determined is the interfacial area a:

$$a = 6 \cdot \varepsilon / d_{32} \qquad (11)$$

In equation (11) the gas holdup can be determined by equation (10) or resp. (6). Further informations are needed with regard to the medium bubble size d_{32}.

Unfortunately there is not much experimental data on bubble sizes resp. bubble size distributions due to the complicated measuring methods. For our measurements a new electric measuring device (11),(12) was used. A partial stream of the disperse fluid two-phase system is sucked off by a vertical funnel connected with a glass capillary. The capillary diameter is chosen so, that most of the bubbles are deformed to plugs. These are detected twice by a suitable light sensing means that informs on the length of the plugs. If the plug

In Chemical Reaction Engineering—Houston; Weekman, V., et al.;
ACS Symposium Series; American Chemical Society: Washington, DC, 1978.

cross-section is determined by additional calibration procedures, the volume of each particle can be calculated; it is an advatage of this measuring method to enable high measuring frequencies.

In figure 4 measured mean bubble sizes are shown for the aeration of xylene and propanol by nitrogen. The measurements took place in a column of 225 mm diameter. The measuring height was 850 mm above the gas distributor, which was formed as a sieve tray with different hole diameters. It can be seen, that the sauter mean diameter d_{32} is almost independent of the gas throughput. Küsters (8) got similar results.

More detailed information results from an analysis of bubble size distributions. These have been approximated by a logarithmic normal distribution so that the value of the sauter mean diameter remained the same as before. The central values d_{50} and the standard deviations σ_ξ, calculated in the way mentioned before, are plotted in figure 5. The dependency of the central values of the gas throughput is basically the same as on single holes. After the transition of all holes in the jetting region ($u_D \approx 1$ cm/s) a strong decrease of d_{50} appears, which flattens with higher gas throughputs. Yet, it must be considered, that the standard deviations at first increase strongly with gas holdup, before reaching a constant value. With respect to the parallels to single orifices, a further aspect must be noted: the bubbles, emerging from the sieve plate, should be not larger than a certain maximum value; otherwise they are no longer stable and devide into smaller particles. According to Mersmann (13), the maximum stable particle diameter results from the relation:

$$d_{max} = 3 \cdot \sqrt{\sigma \cdot \Delta\rho \cdot g} \qquad (12)$$

Taking all experiments into account, if particles collapse, a churn turbulent flow region already appears at lower gas throughputs. In sieve plate design, this aspect has to be checked additionally. For the determination of the size of the emerging bubbles, well-known methods like that of Ruff (14) can be used.

In determining mean bubble sizes in columns, there is still a lack of suitable correlations. Even our results do not enable more precise statements. Therefore we recommend to determine mean bubble sizes from equation (12). According to our calculations there is an accuracy of $\pm$ 30 % with respect to measured values, if the liquid viscosity is lower than 10 cP.

Finally, the determination of the dispersion coefficients in both phases is to be treated. The

In Chemical Reaction Engineering—Houston; Weekman, V., et al.;
ACS Symposium Series; American Chemical Society: Washington, DC, 1978.

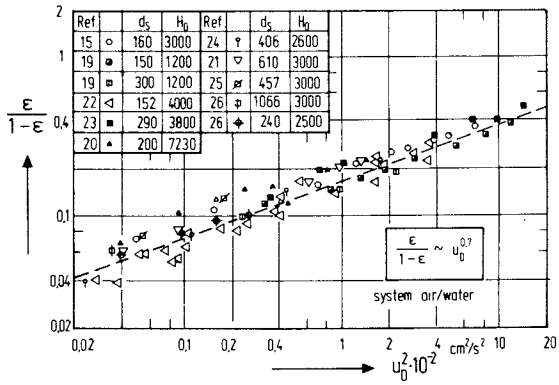

Figure 3. Dependency of gas holdup on column dimensions for the system air/water

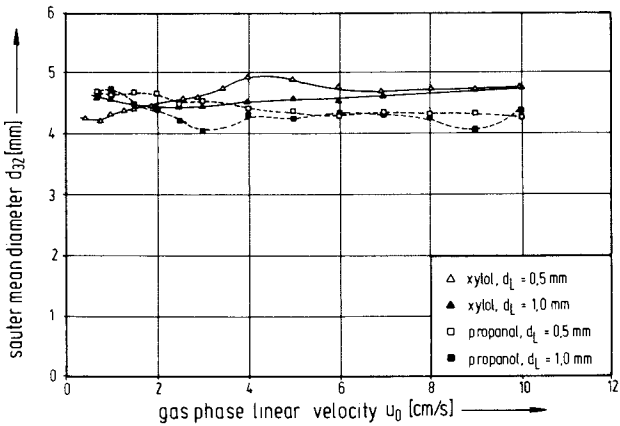

Figure 4. Sauter mean bubble diameter as a function of gas linear velocity for the aeration of xylene and propanol

In Chemical Reaction Engineering—Houston; Weekman, V., et al.;
ACS Symposium Series; American Chemical Society: Washington, DC, 1978.

dispersion coefficient of the liquid phase has been measured frequently, but mostly in air/water systems. For this, corrobated equations have been presented (15) (16). Therefore, our investigations were focussed on the influence of liquid phase properties. Preliminary tests showed, that the dispersion coefficient depends in the same way on the gas throughput as the gas hold-up. Therefore, mainly the influence of the liquid viscosity was studied. Referring to figure 6, there is a clear dependency of the liquid phase dispersion coefficient on the liquid viscosity. Additionally, figure 6 shows lines for the relation between dispersion coefficient and gas throughput according to Hikita and Kikukawa (17). This equation agrees with our experimental data and can be recommended generally. It is:

$$D_C = (0,15 + 0,69 \cdot u_D^{0,77}) \cdot d_S^{1,25} \cdot (10^{-3}/\eta_C) \qquad (13)$$

Up to now, there are only few measurements of the gas phase dispersion coefficient; i.e. see the paper of Towell/Ackermann (18). In our experiments we applied a new method based on frequency analysis for the measurement of gas phase dispersion. There is an insoluble gas tracer, varying in time in a sinous mode so that the describing equations (1) and (2) are decoupled because of the absence of mass transfer. The shortened equation (1) can be solved theoretically, allowing the determination of the gas phase dispersion coefficient as a function of the amplitude ratio of the tracer concentrations between two measuring points. Three liquids were used in the experiments. As a result, figure 7 shows the gas phase dispersion coefficient as a function of the relative velocity w_R. The measured points can be described by the following equation:

$$D_D = 0,002 \cdot w_R^{3,56} \qquad (14)$$

This equation can be recommended for design purposes. The relative velocity can be determined by applying equation (10) and (7) for the churn turbulent regime, neglecting the liquid velocity. Additionally, it is to consider, that equation (14) is valid only for a column diameter of 100 mm. However, there is a strong dependency of the gas phase dispersion coefficient on the column diameter. In comparing our results with literature data, we got the following dependency:

$$D_D \sim d_S^{1,5} \qquad (15)$$

This fact is to be taken into account in determining gas phase dispersion coefficients for column diameters other than 100 mm.

In Chemical Reaction Engineering—Houston; Weekman, V., et al.;
ACS Symposium Series; American Chemical Society: Washington, DC, 1978.

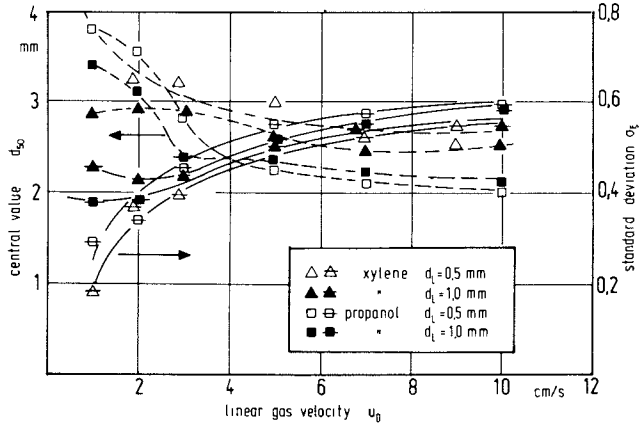

Figure 5. Central values and standard deviations for the approximation of bubble size distributions by log normal distributions

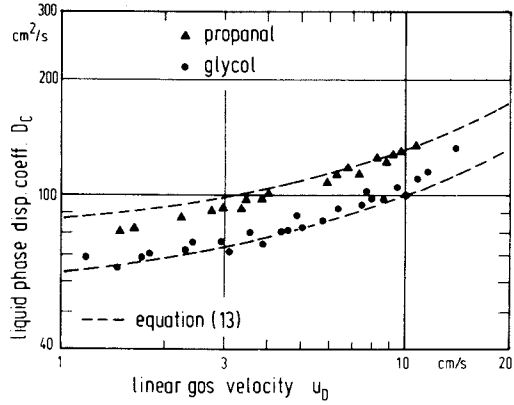

Figure 6. Liquid phase dispersion coefficient as a function of linear gas velocity

In Chemical Reaction Engineering—Houston; Weekman, V., et al.;
ACS Symposium Series; American Chemical Society: Washington, DC, 1978.

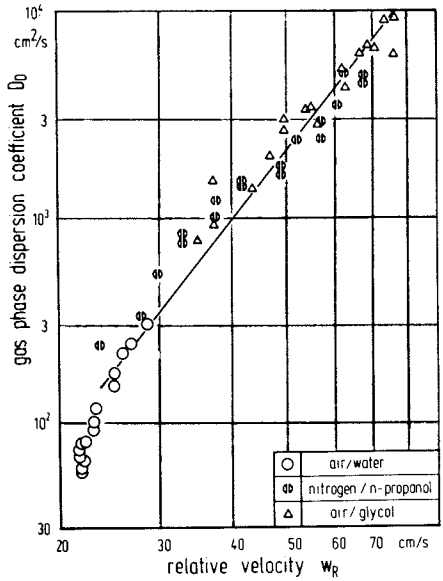

Figure 7. Gas phase dispersion coefficient as a function of the relative velocity between gas and liquid

In Chemical Reaction Engineering—Houston; Weekman, V., et al.;
ACS Symposium Series; American Chemical Society: Washington, DC, 1978.

Nomenclature:

a	m^2/m^3	interfacial area
c	kmol/kmol	concentration
c^*	" / "	equilibrium concentration
d_L	m	hole diameter
d_{32}	m	sauter mean diameter
d_S	m	column diameter
d_{50},	m	central value
Fr	---	dimensionless mod. Froude-number
D	m^2/s	dispersion coefficient
g	m/s^2	gravitational acceleration
H_0	m	clear liquid height
k_L	m/s	mass transfer coefficient
t	s	time
u	m/s	linear velocity
w	m/s	velocity
We	---	dimensionless Weber-number
x	m	length
ε	m^3/m^3	gas holdup
η	kg/ms	dynamic viscosity
ν	m^2/s	kinematic viscosity
ρ	kg/m^3	density
$\Delta\rho$	"/"	density difference
σ	N/m	surface tension
	---	standard deviation

subscripts:

C	continuous phase
D	disperse phase
F	liquid
G	gas
L	hole
∞	referring to single bubbles

Literature cited:

(1) Mashelkar R.A., Brit. Chem. Eng, (1970), 15, 1297
(2) Ploos v. Amstel J.J.A., Rietema K., Chem. Ing. Techn., (1970), 42, 981
(3) Todt J., Lücke J., Schügerl K., Renken A., Chem. Engng. Sci., (1977), 32, 369
(4) Ruff K., Pilhofer Th., Mersmann A., Chem. Ing. Techn., (1976), 48, 759
(5) Wallis G.B., ASME Int. Dev. Heat Trans., (1962), 319
(6) Lapidus L., Elgin J.C., AIChE J., (1957), 3, 63
(7) Pilhofer Th., Chem. Ing. Techn., (1976), 48, 273
(8) Küsters W., Ph.D. Diss. TH Aachen Germany 1976
(9) Hammer H., Rähse W., Chem. Ing. Techn., (1973), 45, 968
(10) Riquarts H.P., Verfahrenstechnik, (1977), 11, 164
(11) Pilhofer Th., Jekat H., Miller H.D., Müller J.H., Chem. Ing. Techn., (1974), 46, 913

In Chemical Reaction Engineering—Houston; Weekman, V., et al.;
ACS Symposium Series; American Chemical Society: Washington, DC, 1978.

(12) US Pat. 3.818.200
(13) Mersmann A., Verfahrenstechnik,(1976),10,641
(14) Ruff K., Chem.Ing.Techn.,(1972),44,1360
(15) Ohki Y., Inoue H., Chem.Engng.Sci.,(1970),25,1
(16) Badura R., Deckwer W.D., Warnecke H.J., Langemann H., Chem.Ing.Techn.,(1974),46,399
(17) Hikita H., Kikukawa H., Chem.Eng.J.,(1974),8,191
(18) Towell G.D., Ackermann G.H., 2.Int.Symp.Chem. React.Eng., Amsterdam 1972, Preprints B3
(19) Kastanek F., Nyvlt V., Rylek M., Coll.Czech.Chem. Comm.,(1974),39,528
(20) Deckwer W.D., Burckhart R., Zoll G., Chem.Engng. Sci.,(1974),29,2177
(21) Freedman W., Davidson J.F., Trans.Instn.Chem. Engrs.,(1969),47,251
(22) Akita K., Yoshida F., Ind.Eng.Chem.Proc.Des.Dev. (1973),12,76
(23) Reith T., Chem.Engng.Sci.,(1968),23,619
(24) Towell G.D., Strand C.P., Ackermann G.H., AIChE - I.Chem.E.Symp.Ser.,(1965),10,97
(25) Fair J.R., Ind.Eng.Chem.Proc.Des.Dev.,(1962),1,33
(26) Jekat H., Ph.D.Diss. TU München Germany 1976

In Chemical Reaction Engineering—Houston; Weekman, V., et al.;
ACS Symposium Series; American Chemical Society: Washington, DC, 1978.

Catalyst Effectiveness Factor in Trickle-Bed Reactors

M. P. DUDUKOVIĆ and P. L. MILLS

Chemical Reaction Engineering Laboratory, Department of Chemical Engineering, Washington University, St. Louis, MO 63130

Observed rates in a number of trickle-bed reactors employed in hydrodesulfurization and hydrotreating of heavy residuals indicate that they operate in the regime free of major gas-liquid mass transfer limitations (1,2,3,4,5). Due to the fact that often the liquid reactants are nonvolatile or dilute at the operating conditions used the reaction is frequently liquid reactant limited and confined to the catalyst effectively wetted by liquid. Since porous packing, typically 1/32" to 1/8" (0.08 cm to 0.318 cm) extrudates is most often employed it is clear that reaction rates may be affected both by internal pore fill-up with liquid and by internal diffusional limitations. Catalyst effectiveness factors from 0.5 to 0.85 have been generally reported (1,3,5,6,7,8).

In order to interpret or predict trickle-bed performance attempts have been made to account for liquid maldistribution, deviation from plug flow and for incomplete wetting of catalyst particles (4,9,10,11,12). It has been shown that liquid phase deviation from plug flow does not have significant effects on conversion in commercial and pilot scale trickle-bed reactors (13). Application of Mears' (14) criterion confirms the insignificance of dispersion effects. Incomplete catalyst wetting (i.e. contacting efficiency, catalyst utilization) as affected by the hydrodynamic regime in the bed was singled out as the most important parameter which determines reactor performance (12). One may distinguish between reactor scale incomplete contacting caused primarily by flow maldistribution and global hydrodynamic effects, and particle scale incomplete contacting which is determined by local viscous, inertia and surface forces. When transport effects control the overall reaction rate reactor hydrodynamics has a dominant effect on reactor performance. When kinetics masked by internal diffusion controls the rate single particle phenomena determine reactor performance to a great degree.

The purpose of this paper is to summarize previous interpretations of the effect of incomplete catalyst wetting on trickle-bed performance and to develop a model for the effectiveness factor for partially wetted catalyst pellets. In the case of a reaction

© 0-8412-0401-2/78/47-065-387$05.00/0

confined to the wetted portion of the catalyst only the wetted volume of the pellet contributes to reaction and the supply of liquid reactant occurs only across the wetted external surface of the pellet. Under these conditions the catalyst effectiveness factor is a function of the ratio of the maximal kinetic rate and maximal rate of internal diffusion, of the external contacting efficiency and of internal pore fill-up. An approximate equation describing this relationship and based on the work of Aris (15) can be incorporated in the trickle-bed reactor performance equation. Solutions to more rigorous models representing the effectiveness of partially wetted pellets were sought also in order to assess the validity of the approximate models.

Review of Previous Models

Most of the previously used expressions to account for incomplete catalyst wetting in trickle-beds are summarized in Table I. All of these, with the exception of the last one, are based on the assumptions of a) plug flow of liquid, b) no external mass transfer limitations, c) isothermal conditions, d) first order irreversible reaction with respect to the liquid reactant, e) nonvolatile liquid reactant, f) no noncatalytic homogeneous liquid phase reaction.

Satterfield (5) suggested comparing the apparent rate constant, k_v, obtained from trickle bed data to the rate constant, k_{tc}, determined in perfectly mixed slurry reactors, as a measure of trickle bed effectiveness. The ratio k_v/k_{tc} less than unity was interpreted on the basis of liquid deviations from plug flow (10) and of incomplete catalyst wetting (8,16). Ross (12) in treating the data from commercial and pilot plant hydrodesulfurization reactors assumed that liquid space time is the basic parameter in reactor performance. This asserts that performance and the apparent rate constant are proportional to liquid holdup as shown in equation (1). Bondi (17) developed an empirical expression (2a) in interpreting data for the hydrodesulfurization of heavy gas oil. This expression relates the space time required to achieve 50% conversion, $\tau_{\frac{1}{2}}$, to the analogous space time at complete wetting, $\tau_{\frac{1}{2}}^{c}$, and to liquid superficial velocity, U_L. This can also be written as equation (2b) in terms of previously defined constants. Henry and Gilbert (11) extended Ross' (12) formula by incorporating into it an available correlation for liquid holdup which resulted in expression (3). Finally, Mears (4) hypothesized that the apparent rate constant, k_v, is proportional to the true rate constant on completely wetted catalyst, k_{tc}, to the catalyst effectiveness factor, η_T, and to the contacting efficiency, η_{CE}, *i.e.* to the fraction of the external catalyst area contacted by liquid. By incorporating the correlation of Puranik and Vogelpohl (18), which was developed for incomplete contacting in absorbers packed with different packing size and shape, Mears (4) arrived to expression (4). Sylvester and Pitayagulsarn (19) reproduced the model of Suzuki and Smith

In Chemical Reaction Engineering—Houston; Weekman, V., et al.;
ACS Symposium Series; American Chemical Society: Washington, DC, 1978.

Table I
Suggested Performance Equations for Trickle-Bed Reactors

$$\ln \frac{1}{1-X} \propto \frac{k_{tc} H_{TL}}{LHSV} \tag{1}$$

$$\tau_{\frac{1}{2}} = \tau_{\frac{1}{2}}^{c} + \frac{A'}{U_L^b} \tag{2a}$$

$$\frac{1}{k_v} = \frac{1}{k_{tc}} + \frac{A}{U_L^b} \; ; \; 0.5 < b < 0.7 \tag{2b}$$

$$\ln \frac{1}{1-X} \propto \frac{k_{tc} L_m^{1/3}}{(LHSV)2/3} \tag{3}$$

$$\ln \frac{1}{1-X} \propto L_m^{0.32} (LHSV)^{-0.68} d_p^{0.18} \nu^{-0.05} (\sigma_c/\sigma)^{0.21} \eta_T \tag{4}$$

$$\ln \frac{1}{1-X} = \Lambda_3 \omega \tag{5}$$

where

$$\Lambda_3 = \frac{N_{B_o}}{2} [1 + 4\Lambda_2/N_{B_o} - 1] \tag{5a}$$

$$\Lambda_2 = \frac{1}{1/\Lambda_1 + 1/N_{st}} \tag{5b}$$

$$\Lambda_1 = \frac{1}{f} [\phi_T \coth \phi_T - 1] \tag{5c}$$

(20) for gas solid catalytic reactions and applied it to three phase systems in trickle beds. Incomplete wetting was accounted for by assuming only a portion of the reactor, i.e. an effectively smaller volume, to be contributing to reactant conversion. This is again equivalent to assuming that a primary parameter is liquid space time. When the external mass transfer limitations and axial dispersion effects are neglected the model expressed by equations (5) is reduced to Ross' (12) expression (1) multiplied with catalyst effectiveness factor.

Recently (21) another approximate model for the catalysts effectiveness factor in trickle bed reactor has been proposed. In this model the effectiveness factor for a partially wetted catalyst pellet in a trickle-bed reactor for a reaction occurring only in the liquid filled pore region of the pellet is defined by:

$$\eta_{TB} = \frac{\text{(actual rate on a partially wetted pellet)}}{\begin{pmatrix}\text{ideal maximum rate at bulk conditions} \\ \text{on a completely wetted pellet}\end{pmatrix}} =$$

$$= \frac{\text{(actual rate per unit volume of partially wetted pellet)}}{\text{(ideal maximum rate per unit volume of completely wetted pellet}} \times$$

(fraction of pellet actually internally wetted) (6)

Using Aris' (15) definition for the modulus of irregular particles the following modified modulus was obtained:

$$\phi_{TB} = \frac{\eta_i}{\eta_{CE}} \phi_T \tag{7}$$

which results in the expression for the effectiveness factor given below:

$$\eta_{TB} = \eta_{CE} \frac{\tanh \left(\frac{\eta_i}{\eta_{CE}} \phi_T\right)}{\phi_T} \tag{8}$$

Expression (8) reduces to the product of $\eta_{CE}\ \eta_T$, as used by Mears (4) under two conditions.

$$\phi_T >> 1;\ \eta_{TB} \sim \frac{\eta_{CE}}{\phi_T} = \eta_{CE}\ \eta_T \tag{9a}$$

In this case the internal pore diffusional limitations are severe and thus reaction occurs only in a narrow zone (shell) close to the exterior surface. The utilization of the pellet is directly proportional to the size of this zone which in turn is directly related to the fraction of external area wetted.

$$\eta_i/\eta_{CE} = 1;\ \eta_{TB} = \eta_{CE}\ \eta_T \tag{9b}$$

The second case implies that the pores in the catalyst pellets are not interconnected and that the fraction of internal wetting corresponds directly to external wetting. This in general is not the case when dealing with real catalysis and hydrocarbon feeds which readily wet internal pore structures (22).

For small modulii i.e. very slow reactions such as typical of hydrodesulfurizers expression (12) reduces to:

$$\eta_{TB} \simeq \eta_i \left[1 - \frac{1}{3} \left(\frac{\eta_i}{\eta_{CE}} \phi_T\right)^2\right] \tag{9c}$$

and catalyst utilization is directly proportional to fraction of internal pore fill up.

This shows that for large modulii η_{CE} is the dominant variable, for small modulii η_i becomes the important parameter.

One of the questions to be answered is how well expression (8) for the effectiveness factor compares to the results computed on the basis of a more rigorous model for a partially wetted pellet.

In Chemical Reaction Engineering—Houston; Weekman, V., et al.;
ACS Symposium Series; American Chemical Society: Washington, DC, 1978.

Mathematical Model For Reaction In Partly Wetted Catalyst Pellets

It is instructive to consider first a simpler problem, namely that of a reaction on a partly externally but completely internally wetted catalyst pellet. This case is of interest in particular for hydrocarbon feeds which presumably readily wet the internal pore structure. Clearly if the kinetic rate is very slow the reduction in the "supply area" i.e. external area wetted through which reactants arrive to the pellet will hardly affect pellet utilization but for higher kinetic rates a reduction in utilization due to incomplete external wetting should become apparent.

The solution for the problem in cartessian coordinates for slab geometry is presented here. The governing equations are:

$$\frac{\partial^2 u}{\partial x^2} + \frac{\partial^2 u}{\partial y^2} - \phi^2 u = 0 \tag{10}$$

$$\frac{\partial u}{\partial x} = 0 \text{ at } x = 0 \text{ for } y_0 \leq y \leq 1 \tag{11}$$

$$-\frac{1}{Bi_m}\frac{\partial u}{\partial x} + u = 1 \text{ at } x = 0 \text{ for } 0 \leq y \leq y_0 \tag{12}$$

$$\frac{\partial u}{\partial y} = 0 \text{ at } y = 0 \text{ and } y = 1 \tag{13}$$

where u is the dimensionless reactant concentration. Clearly, numerically $y_0 = \eta_{CE}$.

One method of solution may be outlined as follows. Divide the region of interest into two subregions by line parallel to x axis at $y = y_0$. Let $u = u_1$ and $u = u_2$ in region 1 and 2, respectively, and solve by separation of variables the corresponding differential equations and boundary conditions. This results in an infinite series of $\cos(\lambda_n(1-x))$ for u_1 and a series of $\cos(n\pi x)$ for u_2. The eigenvalues λ_n are the roots of the transcendental equation $\lambda_n \tan\lambda_n = Bi_m$, the six first values are tabulated (23) the others can readily be obtained. The expression for the effectiveness factor takes the following form:

$$\eta_{TB} = \frac{y_0\left[1 + \frac{1}{y_0}\frac{\tanh(\phi_T(1-y_0))}{\phi_T}\right]}{\frac{\phi_T}{\tanh\phi_T} + \frac{\phi_T^2}{Bi_m}} + \sum_{n=1}^{\infty} a_n \frac{\sin\lambda_n}{\lambda_n}\left[\frac{\tanh(p_n y_0)}{p_n^2} + \frac{\tanh(\phi_T(1-y_0))}{\phi_T p_n}\right] \tag{14}$$

In Chemical Reaction Engineering—Houston; Weekman, V., et al.;
ACS Symposium Series; American Chemical Society: Washington, DC, 1978.

The coefficients a_n are found by the solution of an infinite set of linear algebraic equations (infinite matrix) which results when one requires $u_1 = u_2$ and $\frac{\partial u_1}{\partial y} \frac{\partial u_2}{\partial y}$ at the artificial boundary $y = y_0$.

$$\sum_{j=1}^{\infty} \alpha_{ij} a_j = b_i \; ; \; i = 1,2,\ldots\infty \tag{15}$$

where:

$$\alpha_{ij} = \frac{\sin \lambda_j}{\lambda_j}\left[\frac{\phi_T}{p_j} + \frac{\tanh(q_j y_0)}{\tanh(q_T(1-y_0))}\right] \tag{16a}$$

for $j = 1,2,3\ldots\infty$

$$\alpha_{ij} = \frac{2\lambda_j \sin \lambda_j}{\lambda_j^2-(i-1)^2\pi^2}\left[\frac{1}{p_j} + \frac{\tanh p_j y_0}{q_{i-1}\tanh q_{i-1}(1-y_0)}\right] \tag{16b}$$

for $i = 2,3,4\ldots\infty$, $j = 1,2\ldots\infty$

$$b_1 = -\gamma \sin \phi_T \; ; \quad b_i = -\frac{2\gamma\phi_T}{q_i^2} \sinh \phi_T; \; i = 1,2,3\ldots\infty \tag{16c}$$

$$p_j = \sqrt{\phi_T^2 + \lambda_j^2} \quad ; \quad q_i = \sqrt{\phi_T^2 + i^2\pi^2} \tag{16d}$$

$$\gamma = \frac{Bi_m}{Bi_m \cosh \phi_T + \phi_T \sinh \phi_T} \tag{16e}$$

The infinite set of equations (15) has unique solutions since $\sum_{i=1}^{\infty}\sum_{j=1}^{\infty} |\alpha_{ij}|$ converges and $\sum_{i=1}^{\infty} |b_i|$ converges (24,25). The solutions for a_n of increasing accuracy are obtained by truncating the infinite matrix after various, increasing number of terms which is a method often employed in solution of mixed boundary value problems (26,27). When $y_0 = \eta_{CE} = 1.0$ all $a_n \equiv 0$ and the value for the effectiveness factor reduces properly to the expression for a totally wetted slab.

For $y_0 \simeq 0$ also $\eta_{TB} = 0$ as expected. Solutions for effectiveness factors in other geometries of interest such as partially externally wetted sphere or cylinder of finite length can also be developed but are omitted here for brevity and will be presented elsewhere.

In Chemical Reaction Engineering—Houston; Weekman, V., et al.;
ACS Symposium Series; American Chemical Society: Washington, DC, 1978.

In the limit of no external mass transfer resistance ($Bi_m \to \infty$) the Robin type boundary condition (12) becomes a simpler Dirichlet condition of u = 1. This problem was solved also.

Discussion

A study was performed to ascertain the effect of matrix truncation on calculated values of the catalyst effectiveness for both the Dirichlet and Robin conditions. The results are summarized in Table II for a Thiele modulus of 1.0, an external contacting efficiency of 0.5 and for matrices of size N x N. The answers seem to be accurate on the first two decimal places and the results for $Bi_m = 10^4$ and $Bi_m = \infty$ computed from two different expressions agree well.

Table II
Effect of Matrix Truncation on Calculated Effectiveness Factors

Biot Number	Catalyst Effectiveness N = 30	N = 40	N = 50
10^{-2}	0.49610×10^{-2}	0.49610×10^{-2}	0.49610×10^{-2}
10^{-1}	0.46356×10^{-1}	0.46356×10^{-1}	0.46356×10^{-1}
1.0	0.28018	0.28019	0.28019
10^{1}	0.57047	0.57051	0.57053
10^{2}	0.64285	0.64312	0.64326
10^{3}	0.65199	0.65251	0.65282
10	0.65292	0.65347	0.65380
∞	0.65302	0.65358	0.65391

It is also of interest to compare the above derived solution for the effectiveness factor to the approximate form of Aris (15) and Mears (4). For an infinite Biot number for liquid-solid transport this comparison is presented in Figure 1. Mears' approximation deviates drastically from the true values at low and intermediate modulii and becomes a good approximation only in the region of strong internal diffusional limitations i.e. high modulii. As expected the actual effectiveness factor in kinetically controlled regime (small modulii) is much greater than predicted by the product of the effectiveness factor for totally wetted pellet and fraction of external area wetted as suggested by Mears (4). Aris' formula (15) also deviates substantially from the computed values especially at intermediate modulii. However, this expression represents a useful lower bound on the effectiveness factor and is expected to be in closer agreement with computed results for other geometries.

In Figure 2 a comparison of the effect of the liquid-solid Biot number and incomplete contacting on effectiveness factor is presented. External mass transfer limitations are more pronounced even at relatively high degree of external wetting ($\eta_{CE} > 0.5$) for higher modulii which is to be expected since by reducing the area for supply of reactants the reactant flux cannot keep up with

In Chemical Reaction Engineering—Houston; Weekman, V., et al.;
ACS Symposium Series; American Chemical Society: Washington, DC, 1978.

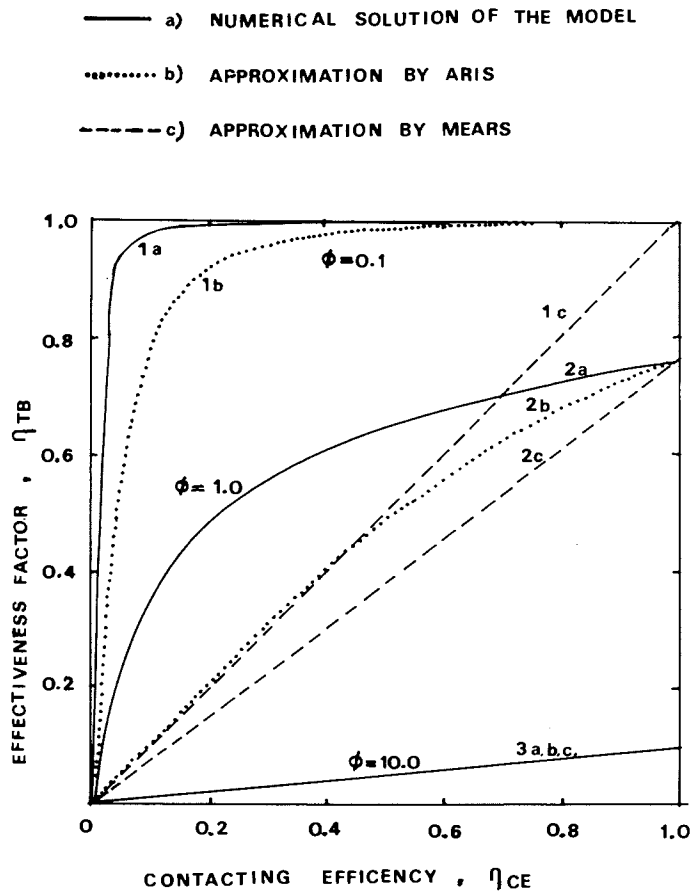

Figure 1. Catalyst effectiveness in partly externally wetted slab

In Chemical Reaction Engineering—Houston; Weekman, V., et al.;
ACS Symposium Series; American Chemical Society: Washington, DC, 1978.

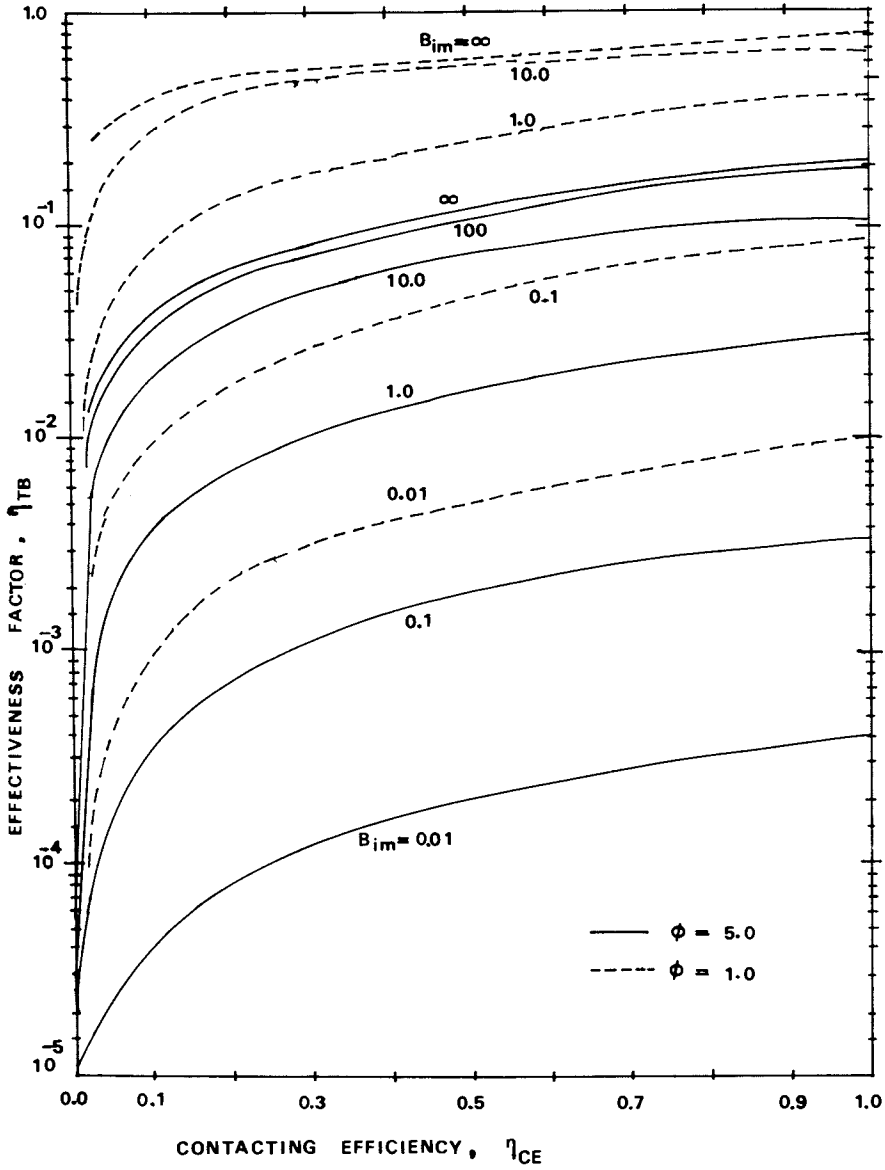

Figure 2. Contacting efficiency and effectiveness factor

In Chemical Reaction Engineering—Houston; Weekman, V., et al.;
ACS Symposium Series; American Chemical Society: Washington, DC, 1978.

reaction demands at higher kinetic rates. Figure 3 represents the effect of incomplete external contacting and Biot number on effectiveness factor in a different form.

The models for catalyst effectiveness in trickle bed reactors developed in this paper require explicit measurements or predictions of external contacting, η_{CE}, and pore fill-up, η_i. In laboratory conditions this can be accomplished by tracer techniques (22,28). Fractional pore fill up may be determined by the difference in first moments of the impulse response tracer tests performed on two beds of same particle size and shape when one bed consists of porous the other of nonporous particles. Fractional pore fill-up can also be assessed from the measured volumetrically static holdup. External contacting is measured by adsorbable tracer tests on beds of nonporous particles (28). In industrial conditions η_{CE} and η_I would have to be evaluated from correlations. Unfortunately at present the existing correlations for η_{CE} are unsatisfactory since they were developed for fixed bed adsorbers with larger packing and correlations for η_I are nonexistent but may be developed in the future.

Conclusions

Catalyst effectiveness factor in trickle-bed reactors is a function of the Thiele modulus, ϕ_T, incomplete external wetting, η_{CE}, and fractional pore fill-up, η_i. Exact formulas for representation of the effectiveness factor in partially internally and externally wetted pellets can be derived only if the geometry of the wetted region and its boundary is known. In this paper a solution is derived for the case of total internal and partial external wetting. This seems to be the case in a number of trickle-bed reactors.

A lower bound for the general case is also presented.

Acknowledgement

The authors are grateful to the National Science Foundation for partial financial support of this work (Grant No. ENG 57406A).

Nomenclature

$Bi_m = \frac{k_f L}{D_{eff}}$ - Biot number for liquid-solid mass transfer, dimensionless

D_{eff} - effective diffusivity of the liquid reactant in catalyst particle, $cm^2 s^{-1}$

d_p - diameter of catalyst pellet, cm

E_z - axial dispersion coefficient, $cm^2 s^{-1}$

$f = \frac{U_L d_p}{2D_{eff}(1-\varepsilon)}$ - parameter in equation (5c), dimensionless

H_{TL} - total liquid holdup, cm^3 liquid/cm^3 reactor, dimensionless

In Chemical Reaction Engineering—Houston; Weekman, V., et al.;
ACS Symposium Series; American Chemical Society: Washington, DC, 1978.

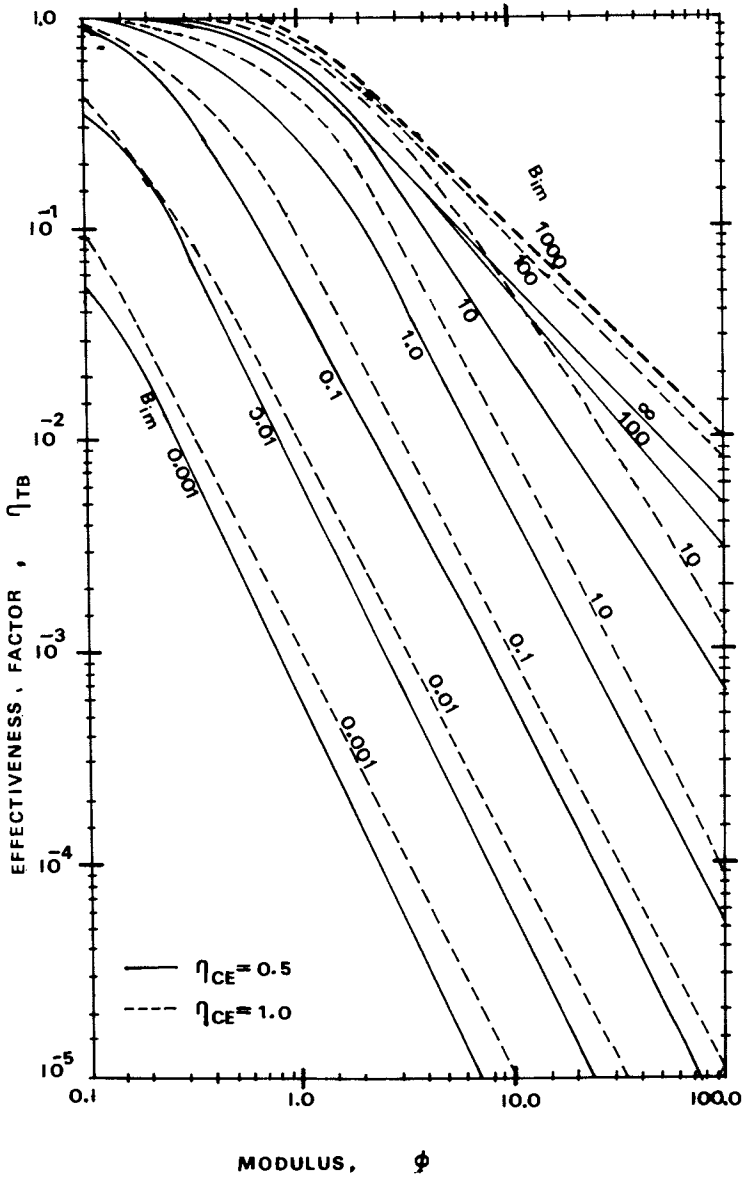

Figure 3. Contacting efficiency and effectiveness factor

In Chemical Reaction Engineering—Houston; Weekman, V., et al.;
ACS Symposium Series; American Chemical Society: Washington, DC, 1978.

k_f - external mass transfer coefficient, cm s^{-1}
k_v - reaction rate constant, cm^3 liquid/cm^3 catalyst and second, s^{-1}
k_{tc} - true reaction rate constant, cm^3 liquid/cm^3 catalyst s^{-1}
L_m - liquid superficial mass velocity, g $cm^{-2}s^{-1}$
LHSV - liquid hourly space velocity, hr^{-1}
$N_{Bo} = \frac{U_L d_p}{2E_z}$ - Bodenstein number for axial dispersion in question (5a), dimensionless
$N_{st} = \frac{3(1-\varepsilon)k_f}{U_L}$ - Stanton number in equation (5b), dimensionless

Greek Letters

ε - bed porosity, cm^3 voidage/cm^3 reactor, dimensionless
η_{CE} - external contacting efficiency, dimensionless
η_i - fractional pore fill-up, dimensionless
η_T - catalyst effectiveness factor, dimensionless
η_{TB} - catalyst effectiveness factor in trickle-bed reactors, dimensionless
ν - kinetic viscosity, cm^2s^{-1}
σ - surface tension of liquid, dyne cm^{-1}
σ_c - critical surface tension of the solid, dyne cm^{-1}
τ_{i_2} - actual space time required to reach fifty percent conversion, s
$\tau_{i_2}^c$ - space time at complete wetting required for fifty percent conversion, s
ϕ_T - Thiele modulus, dimensionless
ϕ_{TB} - modified modulus in trickle-beds, dimensionless
$\omega = \frac{2z}{d_p}$ - axial coordinate, dimensionless

Literature Cited

1. Le Nobel, J. W., Choufoer, J. H., "Fifth World Petr. Cong. Proc. Sect III," Paper 18, Fifth World Petr. Cong., Inc., New York, 1959.
2. Van Deemter, J. J., "Proc. Third Eur. Symp. Chem. Reaction Eng.," p. 215, Pergamon Press, 1964.
3. Adlington, D., Thompson, E., "Proc. Third Eur. Symp. Chem. Reaction Engr.," p. 203, Pergamon Press, 1964.
4. Mears, D. E., 3rd Int. Symp. Chem. React. Eng., Adv. Chem. Ser., (1974) 133, 218.
5. Satterfield, C. N., AIChE J., (1975) 21(2).
6. Van Zoonen, D., Douwes, C. Th., J. Inst. Petroleum, (1963), 49, 383.

In Chemical Reaction Engineering—Houston; Weekman, V., et al.;
ACS Symposium Series; American Chemical Society: Washington, DC, 1978.

7. Satterfield, C. N., Mah, Y. H., Sherwood, T. K., Inst. Chem. Eng. Symp. Ser., (1968) 28, 22.
8. Germain, A. H., Lefebure, A. G., L'Homme, G. A., 3rd Int. Symp. Chem. React. Eng., Adv. Chem. Ser., (1974)133, 164.
9. Cecil, R. R., Mayer, F. X., Cart, E. N., Jr., "Fuel Oil Hydrodesulfurization Studies in Pilot Plant Reactors," paper presented at the 68th AIChE Annual Meeting, Los Angeles, Calif., Dec. 1-5, 1968.
10. Murphree, E. V., Voorhies, A., Jr., Mayer, F. X., Ind. Eng. Chem. Process Des. Develop., (1964) 3(4), 381.
11. Henry, H. C., Gilbert, J. B., Ind. Eng. Chem. Process Des. Develop., (1973) 12(3), 328.
12. Ross, L. D., Chem. Eng. Progr., (1965) 61(10), 77.
13. Schwartz, J. G., Roberts, G. W., Ind. Eng. Chem. Process Design Develop., (1973) 12, 262.
14. Mears, D. E., Chem. Eng. Sci., (1971) 26, 1361.
15. Aris, R., Chem. Eng. Sci., (1957) 6, 262.
16. Koros, R. M., "Fourth Int. Chem. React. Symp. Proceedings," Vol. 1, p. IX 372, Dechema, Frankfurt, 1976.
17. Bondi, A., Chem. Tech., (1971) 1, 185.
18. Puranik, S. S., Vogelphhl, A., Chem. Eng. Sci. (1974) 29,501.
19. Sylvester, N. D., Pitayagulsarn, P., Can. J. Chem. Eng., (1974) 52, 539.
20. Suzuki, M., Smith, H. M., (1970) AIChE J., 16(5), 882.
21. Dudukovič, M. P., AIChE J., 1977 (in press).
22. Colombo, A. J., Baldi, G., Sicardi, S., Chem. Eng. Sci., (1976) 31, 1101.
23. Carslaw, H. S., Jaeger, J. C. "Conduction of Heat in Solids" Oxford University Press, Oxford (1959).
24. Reisz, F., "Les Systemes d'equations lineaires a une infinite d'inconnues," Gauther-Villars, Paris, 1913.
25. Whittaker, E. T., Watson, G. N., A Course of Modern Analysis, Cambridge University Press, Cambridge, 1935.
26. Sell, M. G., Jr., Hudson, J. C., Int. J. Heat Mass Transfer (1966) 9, 11.
27. Snedonn, I. N., "Mixed Boundary Value Problems in Potential Theory," Wiley, New York, 1966.
28. Schwartz, J. G., Weger, E., Dudukovič, M. P., AIChE Jr., (1976) 22(5).

In Chemical Reaction Engineering—Houston; Weekman, V., et al.;
ACS Symposium Series; American Chemical Society: Washington, DC, 1978.

33

Modeling the Slugging Fluidized Bed Reactor

J. RAGHURAMAN and O. E. POTTER

Department of Chemical Engineering, Monash University,
Clayton 3168, Victoria, Australia

In some industrial, and nearly all pilot-plant, fluidized bed reactors the aspect ratio is such that slugging behaviour can be expected, as Davidson and his co-workers have suggested. Scale-up therefore frequently involves a jump from slugging-bed behaviour to freely bubbling bed behaviour.

Slugging behaviour occurs when the bubbles present in the bed have diameters approaching that of the vessel. By 'freely bubbling' is meant that there are many bubbles present, each bubble being of a diameter much less than that of the vessel.

Fryer and Potter (1,2,3) have compared the counter-current backmixing model with experimental results and the predictions of other models and have demonstrated that the countercurrent backmixing model is appropriate to the freely bubbling bed and has advantages over other models which have been proposed. Raghuraman and Potter (4) have extended the concepts of the countercurrent backmixing model to the slugging fluidized bed, basing the analysis on the solids mixing model of Thiel and Potter (5,6). Comparison of the predictions of the new model with the experimental data of Hovmand and Davidson (7,8) and Hovmand, Freedman and Davidson (9) shows better agreement with experiment than is exhibited by the two-phase model of Hovmand and Davidson.

In this paper an extension of the new model is described. This extension of the model has the aim of facilitating a detailed dynamic investigation of the slugging fluidized bed reactor whether of the catalytic type or of the type exhibiting reaction between gas and solid as in mineral roasting and fluidized bed combustion. The extended model reported here seeks to describe the cyclic variations which occur due to slugging in a steady-state catalytic system.

Although the studies completed and proposed have direct application only to slugging fluidized bed reactors there will be insights given into the behaviour of freely bubbling beds. Potter (10) has recently reviewed the modelling of fluidized bed reactors.

© 0-8412-0401-2/78/47-065-400$05.00/0

Model of Davidson and Co-workers Hovmand and Davidson (8) proposed a two-phase model and compared the predictions of that model with the experimental data of Hovmand and Davidson (7) and Hovmand, Freedman and Davidson (9). The model assumes co-current piston-flow of bubble gas ($U-U_{mf}$) and dense-phase gas (U_{mf}), with total mixing occurring when slugs coalesce. This latter assumption has not been justified as yet. The new model retains the account of gas-exchange given by Hovmand and Davidson (8).

Gas exchange due to diffusion and bulk-flow are additive.

$$\frac{Q}{V_S} = \frac{1}{Dm}\left[U_{mf} + \frac{16\varepsilon_{mf} I}{1+\varepsilon_{mf}}\left(\frac{D_G}{\pi}\right)^{1/2}\left(\frac{g}{D}\right)^{1/4}\right] \qquad \ldots(1)$$

In equation (1) m is a shape-factor for the slug, given by :

$$m \doteq \frac{4V_S}{\pi D^3} = \frac{L_S}{D} - 0.495\left(\frac{L_S}{D}\right)^{1/2} + 0.061 \qquad \ldots(2)$$

L_S is slug-length. I is surface integral tabulated in Table I.

Table I

Value of Surface Integral I

L_S/D	0.3	0.5	1.0	2.0	3.0	4.0	5.0
I	0.13	0.21	0.39	0.71	0.98	1.24	1.48

The authors also give an expression for gas-exchange which takes into account interaction between diffusion and bulk-flow but recommend for use the gas-exchange rate calculated by equation (1).

The slug-rise velocity, with respect to stationary solids ahead, is given by Kehoe and Davidson (11)

$$U_S = 0.35\,(gD)^{\frac{1}{2}} \qquad \ldots(3)$$

and the rise velocity of continuously generated slugs is given by:

$$U_{SA} = U-U_{mf} + 0.35\,(gD)^{\frac{1}{2}} \qquad \ldots(4)$$

The exchange coefficient, Q/V_S, is used by Davidson and co-workers for gas exchange between the slug and the rest of the bed, or dense phase.

The New Model, Time-Averaged Thiel and Potter (4,6) have shown that mixing of solids in round-nosed slugging beds can be accounted for by assuming that the slug is followed by a wake of well-mixed solids which takes up about two-thirds of the inter-slug material. The remainder of the inter-slug material is in piston-flow.

Thus the model adopts the gas-exchange rate as given in equation (1) but considers it applicable to gas exchange between

In Chemical Reaction Engineering—Houston; Weekman, V., et al.;
ACS Symposium Series; American Chemical Society: Washington, DC, 1978.

wake and slug, Q/V_S being relabelled K_{BC}. So far as gas-exchange between wake and the piston-flow region is concerned, this is considered to be determined by the solids movement, allowance being made for gas flow U_{mf}, with respect to stationary solids.

The solids phase flows in and out of the wake, which is of volume $f_w V_S$, at a volumetric rate, $U_S \pi D^2/4$. This exchange can be expressed in terms of an exchange coefficient, namely the volume of solids phase exchanged with the wake per unit slug volume per unit time, $(U_S \pi D^2/4)/V_S$. If there were no flow of gas through the solids phase, then the gas-exchange rate would be $(\varepsilon_{mf} U_S \pi D^2/4)/V_S$.

Following Stewart and Davidson (12) the flow out of the slug nose and in at the base of the slug will be $U_{mf} \pi D^2/4$. So, the net volume of gas exchanged between the particulate piston-flow region and the wake per unit time will be $(U_S \varepsilon_{mf} - U_{mf}) \pi D^2/4$.

$$K_{CP} = \frac{(U_S \varepsilon_{mf} - U_{mf})\pi D^2}{4 V_S} \qquad ...(5)$$

If the fraction of the bed-volume occupied by slugs is ε_B, then :

$$\varepsilon_B = \frac{V_S}{V_S + TD(\pi D^2/4)} \qquad ...(6)$$

where T is the ratio of mean inter-slug spacing to column diameter. Therefore, equation (5) may be alternatively presented :

$$K_{CP} = \frac{(1-\varepsilon_B)}{TD\ \varepsilon_B}\left[U_S \varepsilon_{mf} - U_{mf}\right] \qquad ...(7)$$

Figure 1 illustrates the gas-exchange process.

For first-order steady-state chemical reaction, the material balances on reactant gas, on a time-averaged basis, are as follows :

Slug
$$U_{GB}\frac{dC_B}{dz} = K_{BC}(C_C - C_B)\varepsilon_B \qquad ...(8)$$

Wake
$$U_{G_C}\frac{dC_C}{dz} = K_{CP}(C_P - C_C)\varepsilon_B + K_{BC}(C_B - C_C)\varepsilon_B - k\, f_w\, \varepsilon_B\, C_C \qquad ...(9)$$

Piston-flow region
$$U_{GP}\frac{dC_P}{dz} = K_{CP}(C_C - C_P)\varepsilon_B - k\left[1-\varepsilon_B(1+f_w)\right] C_P \qquad ...(10)$$

Here the wake fraction is given by :

$$f_w = w(\pi D^2/4)TD/V_S \qquad ...(11)$$

In Chemical Reaction Engineering—Houston; Weekman, V., et al.;
ACS Symposium Series; American Chemical Society: Washington, DC, 1978.

w is the proportion of the inter-slug material which is well-mixed and has been estimated by Thiel and Potter to be 0.7 ± 0.2. The boundary conditions are given by Raghuraman and Potter (4).

On average, $$U = U_{GB} + U_{GC} + U_{GP} \quad ...(12)$$

where $$U_{GB} = U-U_{mf},\ U_{GC} = f_w \varepsilon_{mf} U_{GB}$$

and $$U_{GP} = U_{mf} - \varepsilon_{mf} f_w (U-U_{mf}) \quad ...(13)$$

At $$z = 0,\ C_B = C_0 \quad ...(14)$$

and $$-U_{GP}C_P + (U-U_{GB})C_0 = U_{GC}C_C \quad ...(15)$$

At $$z = H,\ C_C = C_P \quad ...(16)$$

The exit gas concentration is given by :

$$U\,C_H = U_{GB}C_B + U_{mf}\,C_C \quad ...(17)$$

The New Model, Mechanistic Cyclic Form In this form we follow each slug, the wake of the slug, and the piston-flow region from formation at the bottom of the fluidized bed to the top of the bed where the slug bursts. Thus the steady-state is approached from an initial state in which the bed is fluidized with non-reacting gas and then reacting gas is admitted at zero time. Only the final steady-state solutions are presented here for comparison with the time-averaged version, the two-phase model of Hovmand and Davidson and the experimental data.

The cycle time is the time for the slug to rise through the inter-slug length i.e. TD/U_S. At the beginning of each cycle a new slug is admitted at the bottom of the bed and slugs above are renumbered. Figure 2 shows the progressive situations in the bed as slugs are formed and rise to the top. Special conditions obtain at the bottom during the first cycle as the wake and piston flow regimes are formed behind slug 1, and at the top. It is assumed that when a slug bursts the flow in the top section becomes piston-flow since there is no slug above to produce mixing. New slug formation and slug bursting are not necessarily in phase and this is taken into account in the calculation.

Referring again to Figure 2, it is seen that at $t = 0^-$ a new slug, numbered 0 is just about to detach itself from the distributor and at $t = 0^+$ it has detached, being renumbered at the moment of detachment from 0 to 1; also 1 is renumbered to 2 and so on. Since the bed does not contain, in general, an integral number of interslug regions, a fractional amount α remains at the top of the bed at the time when the new slug is detaching itself from the distributor. In Figure 2 this fraction α is approximately one-third. At $t = \tau/3$, slug 0 is forming, all slugs have risen by one-third of the interslug spacing and slug 5 has just reached the top of the bed and bursts, as illustrated, a moment later.

In Chemical Reaction Engineering—Houston; Weekman, V., et al.;
ACS Symposium Series; American Chemical Society: Washington, DC, 1978.

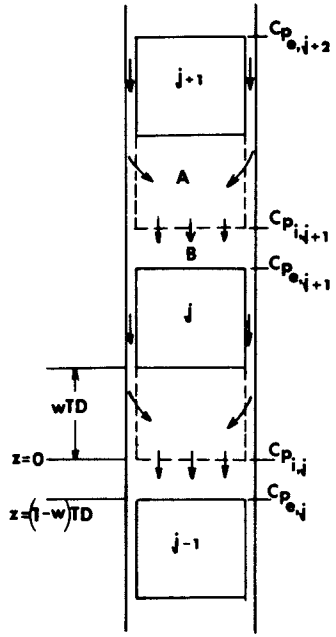

Figure 1. Slugging fluidized bed. (A) well-mixed wake region; (B) piston-flow region.

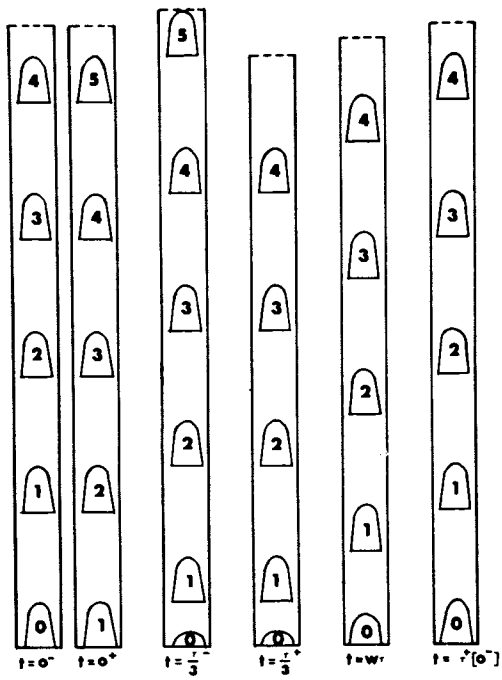

Figure 2. The mechanistic model portrayed over one time cycle

In Chemical Reaction Engineering—Houston; Weekman, V., et al.;
ACS Symposium Series; American Chemical Society: Washington, DC, 1978.

The length of the well-mixed region behind a slug is wTD. Therefore at time wτ, fraction w of a new slug 0 has formed and the length of the inter-slug material behind slug 1 is wTD. As the rest of the inter-slug material, behind slug 1, falls into place, a piston-flow region is commenced until at $t = \tau^+$ the situation has returned to that depicted for $t = 0^-$.

Due to the fraction of TD remaining at the top of the bed, the top section is out of phase with the formation of new slugs at the bottom of the bed. Thus, referring to Figure 2, at time $t = \tau/3$ the top-most slug bursts, leaving a length TD of particulate phase or inter-slug material, lying above slug 4 which has now become the top-most slug. As time increases to wτ, the length of this inter-slug (or should we now say "above-slug") material decreases. At wτ the new wake region behind slug 1 is complete. At τ the piston-flow region behind slug 1 is also complete and the slug detaches. At the top of the bed, the length of inter-slug material will have fallen to one-third of TD. The behaviour now repeats itself and is thus cyclical.

The model briefly described above is now considered from a chemical reaction point of view. Fresh reactant gas is supplied at a steady flow U and of this U_{mf} flows continually through the bed while $(U-U_{mf})$ acts gradually to raise the bed above the new slug and, in a sense, only enters the bed, as reactant in the new slug at the moment of its detachment. The steady-state results presented here have been approached from an initial state in which the bed is cycling as above with no reactant gas present, the process starting when the entering gas instantaneously has its reactant concentration adjusted to C_o.

Consider a general cell, j. Cells, as depicted in Figure 1, are counted from the bottom upwards, so that (j+1) is above cell j and (j-1) below it.

Material Balances on general cell, j

Slug

$$0 = \frac{dC_{B,j}}{dt} + K_{BC}(C_B - C_C)_j \qquad \ldots(18)$$

Wake

$$0 = \varepsilon_{mf} f_w \frac{dC_{C,j}}{dt} + K_{BC}(C_C - C_B)_j \qquad \ldots(19)$$

$$+ K_{CP}(C_{C,j} - C_{P,e,j+1}) + kf_w C_C$$

Piston-Flow Region of Particulate Phase Since piston-flow obtains, accumulation terms can, in this case, be ignored - although qualifications would be made to this statement if space permitted. However there remains a distance - velocity lag which needs to be taken into account. If z is the length dimension and z = 0 at the bottom of the well-mixed wake,

In Chemical Reaction Engineering—Houston; Weekman, V., et al.;
ACS Symposium Series; American Chemical Society: Washington, DC, 1978.

$$\left(U_S - \frac{U_{mf}}{\varepsilon_{mf}}\right)\frac{dC_{P,j,z}}{dz} + kC_{P,j,z} = 0 \qquad \ldots(20)$$

and

$$\frac{C_{P,j,z}}{C_{P,j,0}} = \exp\left|\frac{-kz}{\left(U_S - \frac{U_{mf}}{\varepsilon_{mf}}\right)}\right| \qquad \ldots(21)$$

Note that $C_{P,j,z}$ is related to $C_{P},j,0$ at time $[z/(U_S-U_{mf}/\varepsilon_{mf})]$ earlier.

Material Balances on Cell 1 The slug-balance is the same as equation (18). The wake and piston-flow regions are no longer of constant dimensions but of dimensions which vary with time. The wake begins to form immediately and when it has grown to full size, the piston-flow region commences to form.

Wake

$$0 = \frac{\varepsilon_{mf} f_w}{\tau w}\frac{d}{dt}(tC_{C1}) + K_{BC}(C_{C1}-C_{B1}) - \frac{f_w}{w\tau D}\left[U_{mf}C_o + (U_S\varepsilon_{mf} - U_{mf})C_{P_{e,2}}\right] + \frac{k f_w}{\tau w} tC_{C1} \qquad \ldots(22)$$

Piston-flow Region This region commences to form at time $w\tau$ and the region extends from $z = 0$ to $z = [(t/\tau)-w]TD$. Equation (21) applies with this proviso.

Material Balances on Top-most Region When a slug reaches the top of the bed and bursts, it leaves behind a well-mixed wake region and piston-flow region and it is assumed that flow is piston-flow thereafter. This material falls around the rising top-most slug and of course disappears entirely at the moment of slug bursting, only to be replaced by the inter-slug material below the bursting slug. Equation (21) applies. When $0 \leq t \leq \alpha\tau$, the top-most region decreases in length from $z = \alpha TD$ to $z = 0$; when $\alpha\tau \leq t \leq \tau$, the new top-most region decreases in length from $z = TD$ to $z = \alpha TD$.

Results and Discussions

The above equations were solved with the boundary condition that $C_{Pi,j} = C_{Cj}$ and the initial condition that at $t = 0$, $C_{B1} = C_{0}, jC_{C1} \cong jC_{0}$ and all other concentrations are zero. The exit concentration is given by :

In Chemical Reaction Engineering—Houston; Weekman, V., et al.;
ACS Symposium Series; American Chemical Society: Washington, DC, 1978.

$$U_{CH} = (U-U_{mf})C_{B,N}\ (t=\alpha\tau) + U_{mf}\left[\int_0^{\alpha\tau} C_{P,N+1,i}\,dt + \int_{\alpha\tau}^{\tau} C_{P,N,i}\,dt\right] \quad ..(23)$$

The entire calculations were repeated until steady state was achieved.

Figures 3 and 4 show the experimental data on decomposition of ozone given by Hovmand and Davidson (8), the predictions of the Hovmand-Davidson model, the predictions of the time-averaged countercurrent backmixing model and of the mechanistic cell model of this paper. The same value of T was used in both the versions of the new model. It can be seen that the new model in both its forms has a superior predictive capacity to that of the Hovmand-Davidson model. At high values of k the experimental data show better conversion than predicted by the model. This is to be expected as the models do not take into account the bubbling region at the bottom of the bed before the transition to slugging behaviour occurs. It will be possible to allow for this by using the countercurrent backmixing model for freely bubbling beds, in this region.

Conclusion

A model has been formulated which follows the cyclical behaviour of the slugging fluidized bed and adequately incorporates mixing of the solids. The results for the steady-state agree with a previously formulated time-averaged model. The new mechanistic model provides a point of departure for stability studies and for the analysis of fluidized bed combustion and roasting of ores.

Nomenclature

C_o = reactant concentration at inlet, moles cm^{-3}
C_B = reactant concentration in slug gas, moles cm^{-3}
C_C = reactant concentration in cloud-wake gas, moles cm^{-3}
C_H = reactant concentration in exit gas, moles cm^{-3}
C_P = reactant concentration in piston-flow region moles cm^{-3}
D = column diameter
D_G = gas phase reactant diffusivity, $cm^2\ s^{-1}$
f_w = ratio of wake volume [solids plus associated gas] to slug volume
g = gravitational acceleration, cm s^{-2}
H = height of the expanded bed, cm
H_{mf} = height of incipiently fluidized bed, cm
I = integral given in Table I
k = first order reaction rate constant based on unit volume of solids and associated gas at ε_{mf}, s^{-1}
k' = $k\ H_{mf}/U$
K_{BC} = volumetric rate of gas exchange between slug and cloud-wake per unit slug volume, s^{-1}
K_{CP} = volumetric rate of gas exchange between cloud-wake and piston-flow region per unit slug volume, s^{-1}
L_S = length of slug, cm

In Chemical Reaction Engineering—Houston; Weekman, V., et al.;
ACS Symposium Series; American Chemical Society: Washington, DC, 1978.

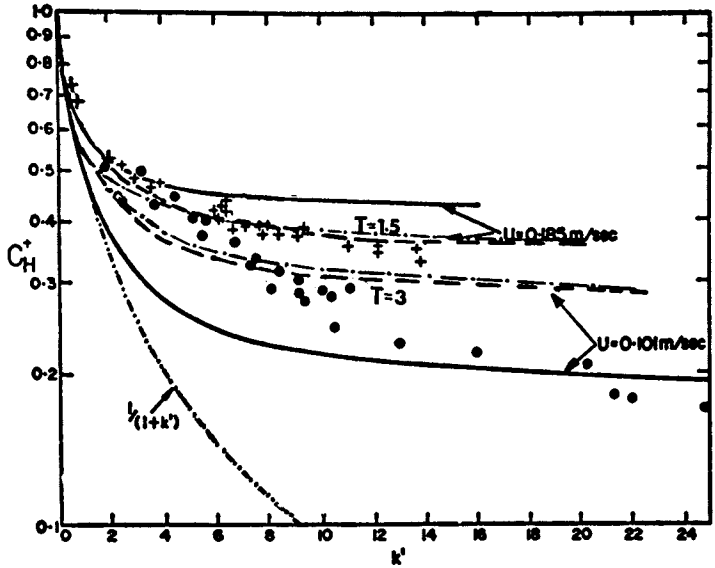

Figure 3. Comparison of the mechanistic model with experimental data, the model of Hovmand and Davidson, and the time-averaged model.

(– · –) *Mechanistic model*
(——) *Hovmand and Davidson*
(– – –) *Time-averaged model*
(– · · –) *CSTR*

$U_{mf} = 3\ cm\ s^{-1}$; $H_{mf} = 255\ cm$; $\epsilon_{mf} = 0.48$; $D = 46\ cm$; $D_G = 0.2\ cm^2\ s^{-1}$ + $U = 0.185\ m\ s^{-1}$; ● $U = 0.101\ m\ s^{-1}$

In Chemical Reaction Engineering—Houston; Weekman, V., et al.;
ACS Symposium Series; American Chemical Society: Washington, DC, 1978.

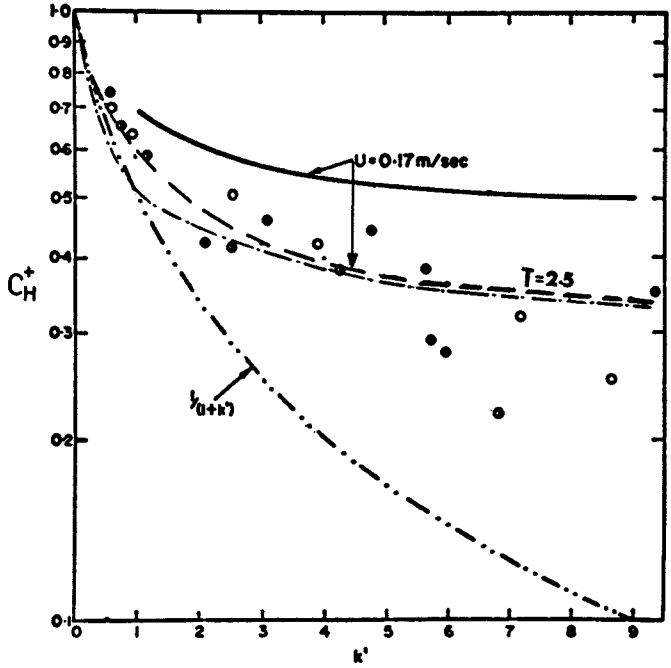

Figure 4. Comparison of the mechanistic model with experimental data, the model of Hovmand and Davidson, and the time-averaged model.

(- · -) *Mechanistic model*
(——) *Hovmand and Davidson*
(– – –) *Time-averaged model*
(- · · -) *CSTR*

$U_{mf} = 1$ *cm* s^{-1}; $H_{mf} = 130$ *cm;* $\epsilon_{mf} = 0.5$; D = *10 cm;* $D_G = 0.2$ *cm*^{2} s^{-1}.

In Chemical Reaction Engineering—Houston; Weekman, V., et al.;
ACS Symposium Series; American Chemical Society: Washington, DC, 1978.

m = shape factor for slug, equation (2)
Q = volumetric rate of gas exchange between slug and particulate phase, $cm^3\ s^{-1}$
T = ratio of interslug spacing to column diameter
U = superficial velocity of fluidizing gas $cm\ s^{-1}$
U_{GC} = superficial velocity of cloud-wake gas $cm\ s^{-1}$
U_{GP} = superficial velocity in piston-flow region, $cm\ s^{-1}$
U_{mf} = superficial gas velocity at incipient fluidization $cm\ s^{-1}$
U_S = rise velocity of an isolated slug, $cm\ s^{-1}$
U_{SA} = rise velocity of continuously generated slugs with respect to vessel, $cm\ s^{-1}$
V_S = slug volume, cm^3
w = ratio of wake volume to volume of interslug material
z = height above the distributor, cm.

Greek Letters

ε_B = fraction of bed volume occupied by slugs
ε_{mf} = voidage of bed at incipient fluidization.

Literature Cited

1. Fryer, Colin and Potter, O.E., Ind. Eng. Chem. Fund. (1972) 11, 338.
2. Fryer, Colin, and Potter, O.E., "Proc. Internat. Symp. on Fluidization and its Applications", p.440, Soc. Chim. Ind., Toulouse, (1973).
3. Fryer, Colin, and O.E. Potter, A.I.Ch.E. Jl., (1976), 22, 38.
4. Raghuraman, J. and Potter, O.E., submitted for publication.
5. Thiel, W. and Potter, O.E., submitted for publication.
6. Potter, O.E. and Thiel, W., "Fluidization Technology", ed. D. Keairns, 185, Vol. II, Hemisphere Publ. Corp.,Washington, (1976).
7. Hovmand, S. and Davidson, J.F., Trans. Inst. Chem. Engrs., (1968), 46, T190.
8. Hovmand, S. and Davidson, J.F.,"Fluidization", ed. J.F. Davidson and D. Harrison, Ch.5, Academic Press, London,(1971).
9. Hovmand, S., Freedman, W. and Davidson, J.F., Trans. Inst. Chem. Engrs. (1971), 49, 149.
10. Potter, O.E., to be published in Catalysis Reviews - Science and Engineering.
11. Kehoe, P.W.K. and Davidson, J.F., 'Chemeca 70', Chem. Eng. Conf. Australia, Butterworth & Co. (Aust.), (1970), Sec. 1, 97.
12. Stewart, P.S.B. and Davidson, J.F., Powder Technology, (1967), 1, 61.

In Chemical Reaction Engineering—Houston; Weekman, V., et al.;
ACS Symposium Series; American Chemical Society: Washington, DC, 1978.

34

Modeling of a Trickle-Bed Reactor: The Hydrogenation of 2-Butanone on a Ruthenium Catalyst

A. GERMAIN, M. CRINE, P. MARCHOT, and G. A. L'HOMME

Laboratoire de Chimie Industrielle et de Génie Chimique, Université de Liège, Rue A. Stévart, 2, B-4000 Liège, Belgique

It is generally accepted now that the trickle-bed reactor operating mechanisms depend strongly on the volatility of the processed liquid. When its vapor pressure is very low, the chemical reaction can only occur on the irrigated catalyst particles and the reactor production increases with the catalyst wetting efficiency i.e. with the liquid flow rate (L.F.R.). In that case the rather empirical models which have been developped (1,2) allow the reactor design estimation or at least the correlation and extrapolation of experimental measurements. Such low volatilities are frequently met in hydrotreating heavy petroleum fractions. But when the processed liquid is volatile, the chemical reaction can occur on the non irrigated particles as on the irrigated ones. Because of the comparatively weaker transfer resistance in the gaseous phase, the more efficient catalyst particles are the non irrigated ones. So it happens that the highest specific reaction rates are observed at the lowest wetting efficiency i.e. at the lowest L.F.R. That paradoxical behaviour appeared during various experimental investigations about the operation of trickle-bed reactors with test chemical reactions (3,4,5,6,7). In these studies, the production increase at low L.F.R. is explained by the appearance of dry catalyst particles on which the reaction rate can be faster, for the diffusion inside their pores is easier.

Yet, till now, a quantitative treatment of these phenomena is lacking. In addition, several observations remain completely unexplained : dry zones formation even with prewetted beds, stationnary operation slow settling, hysteresis... That is the reason why we have chosen to investigate the hydrogenation of 2-butanone into 2-butanol on a ruthenium supported catalyst. Indeed this chemical reaction can be studied over a large

© 0-8412-0401-2/78/47-065-411$05.00/0

range of temperature using a ketone aqueous solution which enables to modify strongly the reactant volatility.

Experimental Set-up

A simplified diagram of the experimental apparatus is given on Figure 1. It consists of a jacketed reactor through which hydrogen and the ketone aqueous solution flow cocurrently down. The reactor is provided with an axial thermocouple well and a sliding thermocouple, and with sampling valves allowing the inlet and outlet flows analysis. An inert bed, realized with alumina pellets similar to the catalyst pellets, ensures the preheating and a good distribution of the liquid. Six small 1/16" pipes provide a good liquid spreading at the top of the column. The essential reator features and the experimental conditions variation range are given in Table 1. All the experiments were realized on a completely prewetted bed obtained by flooding. So it is possible to record well reproducible measurements, without any hysteresis effect. An operating stationnary state is reached during the hour which follows the settling of the flow rates and of the heating fluid temperature. Further details are given by Germain (8).

Table I. EXPERIMENTAL VARIABLES

a. BED PARAMETERS	
DIAMETER, m	0.040
HEIGHT OF LOWER ALUMINA LAYER, m	0.114
HEIGHT OF UPPER ALUMINA LAYER, m	0.086
HEIGHT OF CATALYST LAYER, m	0.250
WEIGHT OF CATALYST LAYER, kg	0.280
b. CATALYST (0,5% Ru on γ-Al_2O_3)	
BULK FORM	COATED CYLINDER
BULK DIMENSIONS, HEIGHT, mm	3.2
DIAMETER, mm	3.2
PELLET APPARENT DENSITY, $kg.m^{-3}$	1470
PELLET POROSITY, %	54
c. RANGE OF VARIABLES	
TOTAL PRESSURE	atmospheric
TEMPERATURE, K	269 - 326
LIQUID SUPERFICIAL MASS FLOW RATE, $kg.m^{-2}.s^{-1}$ (L.F.R.)	0.135 - 1.13
GAS SUPERFICIAL MASS FLOW RATE, $kg.m^{-2}.s^{-1}$	$2.5\ 10^{-4}$ - $7.7\ 10^{-4}$
2-BUTANONE CONCENTRATION, $mol.m^{-3}$	0.245 - 0.893

In Chemical Reaction Engineering—Houston; Weekman, V., et al.;
ACS Symposium Series; American Chemical Society: Washington, DC, 1978.

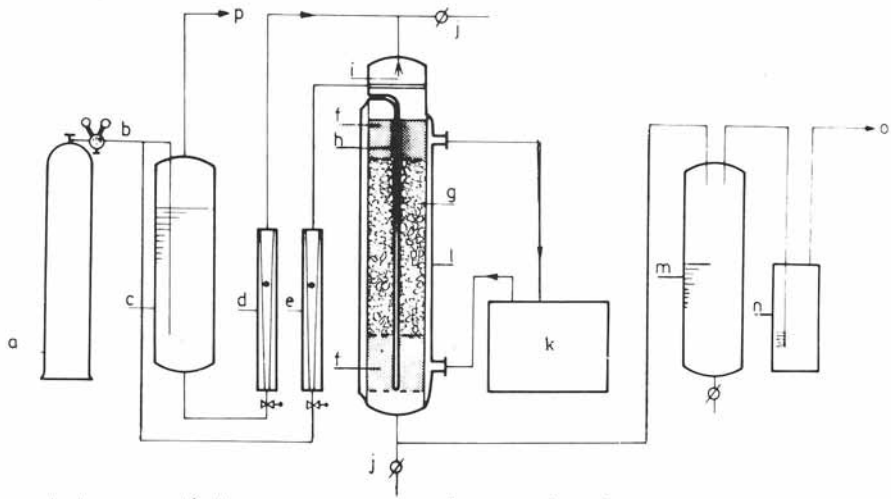

Figure 1. Butanone hydrogenation in trickle-bed reactor

In Chemical Reaction Engineering—Houston; Weekman, V., et al.;
ACS Symposium Series; American Chemical Society: Washington, DC, 1978.

Experimental Result

We have determined the intrinsic reaction rate equation for the hydrogenation of the 2-butanone into the 2-butanol on $Ru-Al_2O_3$ in a preliminary kinetic investigation using a perfectly agitated slurry reactor. After some corrections due to a partial diffusional resistance at the liquid-solid interface, this equation takes the form :

$$r = 3.27\ 10^{-5} \exp\left[5367.9(1/313 - 1/T)\right].C_K.P_H^{0,5} \quad [1]$$

Contrary to what we observed for the hydrogenation of α-methylstyrene on $Pd-Al_2O_3$ in a countercurrent trickle-bed reactor (4), the temperature control appears very easy in the present investigation. If the liquid and the gas are preheated, the jacket heat transfer is sufficient to ensure the isothermicity of the catalytic bed. Hot spots or dry catalyst particles are not observed, corroborating the assumption that the hot spot formation is related to the drying of some catalyst particles.

As shown on Figures 2 and 3, the L.F.R. appears to be a very important parameter in the operation of this trickle-bed reactor; however its influence on the reactor production depends on the catalytic bed temperature. At low temperature ($T<297$ K), the specific reaction rate increases with the L.F.R., while at high temperature the opposite effect is observed. At 326 K for instance, the specific reaction rate is increased by a factor 3 when the L.F.R. is lowered from 1.2 to 0.2 $kg.m^{-2}s^{-1}$. There is a temperature where the reactor production is nearly independent of the L.F.R. even if the latter is varied over a rather wide range. Clearly the apparent activation energy of the reaction rate is a L.F.R. function. At the lowest L.F.R. investigated it amounts about 12 $kcal.mol^{-1}$; at the highest it is much smaller, about 6.5 $kcal.mol^{-1}$ showing that different phenomena play the prominent part at high or low L.F.R. At low L.F.R., it is probable that the reaction implies a diffusionnal step in the gaseous phase; this is a highly activated process due to the high latent heat of vaporization of the ketone.

At the opposite of the usual observations the gas flow rate influence, measured at 315 K, is not negligible. The specific reaction rate is approximatively proportionnal to the 0.4 power of the gas flow rate, implying, at least, a diffusionnal step in the gaseous phase (Figure 3).

It has been proposed (3,4,5) to explain such kind

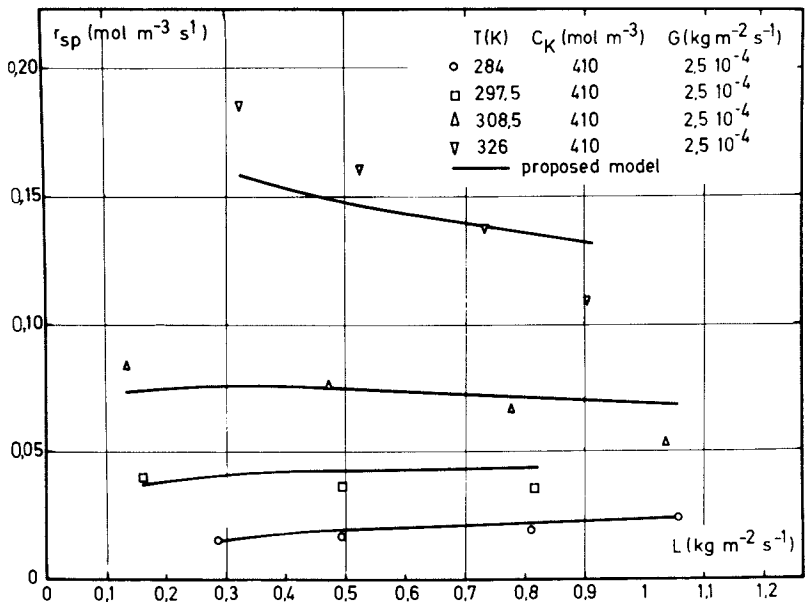

Figure 2. Superficial liquid velocity dependence of reaction rates

In Chemical Reaction Engineering—Houston; Weekman, V., et al.;
ACS Symposium Series; American Chemical Society: Washington, DC, 1978.

of results by assuming incomplete wetting of the catalyst particles at low L.F.R. and considering that the dry catalyst is more active than the wetted one at high temperature, but less active at low temperature due to ketone transfer limitation in the gaseous phase.

In table II, we compare our experimental results with the effective reaction rates $r_{L,e}$ and $r_{G,e}$. These are calculated using the intrinsic rate equation [1] and assuming diffusion limitations respectively in the liquid and gas filled pores of the catalyst, but excluding external concentration gradients (the tortuosity factor is set equal to 4). We see that $r_{L,e}$ is always smaller than $r_{G,e}$ but always larger than the experimental rates measured in the trickle-bed reactor. So, it is not useful to assume the existence of dry catalyst particles, which in fact have never been observed in this study. But to explain the L.F.R. dependence of the reaction rate we must assume the existence in the completely wetted bed of *different types of areas*, the activity of which is determined by different mass transfer processes. That is why we have to look for a more sophisticated topological description of the liquid distribution in the catalytic bed.

Table II. EXPERIMENTAL AND CALCULATED SPECIFIC REACTION RATES

T(K)	$r_{G,e}$	$r_{L,e}$	r_{exp}		
			L = 0.269	L = 0.809	L = 1.078
284	59.8	5.54	2	2.8	3.2
308.5	243	14.5	11.2	9.1	6.9
326	609	28	26	17.5	8.9
r in $mol.s^{-1}.gr.Ru^{-1}$			L in $kg.m^{-2}.s^{-1}$		

$r_{G,e}$ calculated effective reaction rate on the dry catalyst, without any external mass transfer limitation

$r_{L,e}$ calculated effective reaction rate on the wetted catalyst without any external mass transfer limitation

r_{exp} experimental reaction rate in the trickle-bed reactor

In Chemical Reaction Engineering—Houston; Weekman, V., et al.;
ACS Symposium Series; American Chemical Society: Washington, DC, 1978.

Topological Model of the Liquid Distribution in a Trickle-Bed

A close visual inspection of an operating trickle-bed reactor allows to define three types of zones characterized by different local values of their interfacial specific areas.

We distinguish (Figure 4) : (i) the catalyst particles covered by a trickling film (F zones);

(ii) the catalyst particles partially or totally covered by the stagnant or nearly stagnant liquid forming the menisci localized at the contact points between the particles (S zones);

(iii) the catalyst particles soaked up by the liquid because of capillarity (C zones). (*)

The liquid repartition between F and C zones is fixed on one hand by the liquid kinetic energy and on the other hand by the energy used to overcome the local dewetting forces. We consider the catalytic bed as a set of transport cells, each formed by one S zone and its own collection of adjacent F and C zones. A force balance established on a cell leads to a stability criterion for the F zones. At this scale the acting forces are (Figure 5): Δp, the stagnation force resulting from the conversion of the liquid kinetic energy into static pressure; Δs, resulting from the difference of the gas-solid and liquid-solid surface tension; Δf, resulting from gas-liquid surface tension heterogeneities on the film (9).

For a laminar film flow and neglecting the curvature effects of the interfaces and the pressure drop of the gas flow, we obtain :

$$p = 0.592.\Phi_L.\rho.\sin^{-2}\alpha.\ a^{-1}.\left(\frac{g}{\rho\mu}\right)^{1/5}.\ .\ (\sigma_{LG} + DS - \sigma_{LG}\cos\theta)^{-3/5} \quad [2]$$

giving the existence probability of F zones.

Peculiar catalyst dispositions drive the liquid (F zones) along preferential directions stable in time; this kind of anisotropic transport is a percolation process. The S zones liquid renewal is determined by the values of the kinetic and potential energy of

(*) Residence time distribution measurements by the tracer method realized on the operating reactor have shown that the total liquid hold-up is not compatible with the existence of dry zones. That is the reason why these are not taken into account in the preceeding classification.

In Chemical Reaction Engineering—Houston; Weekman, V., et al.;
ACS Symposium Series; American Chemical Society: Washington, DC, 1978.

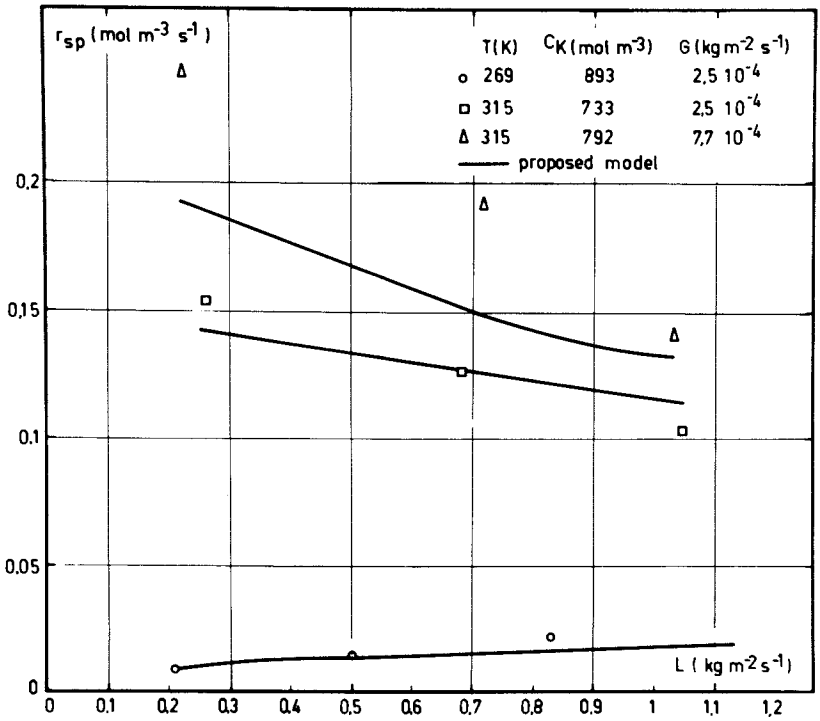

Figure 3. Superficial liquid velocity dependence of reaction rates

In Chemical Reaction Engineering—Houston; Weekman, V., et al.;
ACS Symposium Series; American Chemical Society: Washington, DC, 1978.

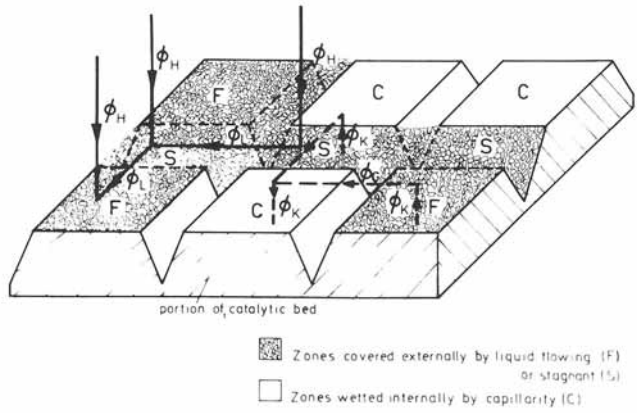

Figure 4. Representation of reactants mass transfers

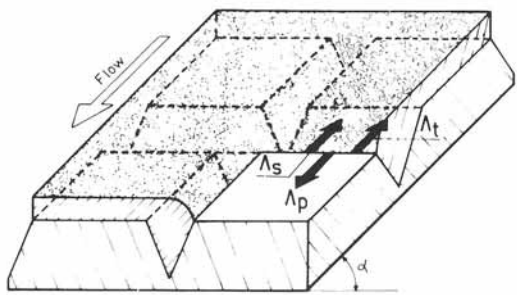

Figure 5. Force balance on transport cell

In Chemical Reaction Engineering—Houston; Weekman, V., et al.;
ACS Symposium Series; American Chemical Society: Washington, DC, 1978.

the liquid itself; this kind of isotropic transport is a diffusionnal process. (*)

The percolation theory (10,11,12,13) allows to establish analytical correlations (obtained by Monte Carlo simulations) giving the F and S zones spatial distributions, regarding to their magnitudes and assuming the liquid flow continuity between them.

Modelling the S zones as liquid bridges between two spheres of the same characteristic dimension (14) gives their interfacial specific areas. The dynamic holdups are computed assuming a viscous dissipation on the F zones and a nearly complete dissipation of the liquid kinetic energy in the S zones (15). That provides a quantitative description of the reactor wetting efficiency (16).

Mathematical Model of Mass Tranfers in a Trickle-Bed Reactor

The trickle-bed reactor performances can be expressed in terms of mass transfers between F, C and S zones, in the gaseous and liquid phases, as shown on Figure 4. In the liquid phase the mass transfer limitations arise from the hydrogen absorption into F and S zones (Φ_H) and from its transport between these zones (Φ_L). In the gaseous phase the transfer limitations arise from the ketone vaporization on the F and S zones (Φ_K), from its transport (Φ_G) and its condensation onto the C zones (Φ_K).

These transfer phenomena are described by the following equations (**).

$$(\Delta C_K)_{ln} \cdot k_G \cdot a \cdot h = \Phi_G \cdot \Delta C_K \qquad [3]$$

(material balance for the ketone vaporizatcn and condensation)

$$r_C \cdot h = \Phi_G \cdot \Delta C_K \qquad [4]$$

(material balance for the ketone consumption on the C zones)

$$(\Delta C_H)_{ln} \cdot k_{LS} \cdot a \cdot h = \Phi_L \cdot \Delta C_H \qquad [5]$$

(material balance for the hydrogen absorption on the S zones)

(*) In a diffusionnal process the stochastic scattering of one particle is a property of the particle studied while in a percolation process the stochastic scattering of a particle is a property of the scattering medium.

(**) S zones are considered as inactive because of strong external hydrogen transfer limitations.

In Chemical Reaction Engineering—Houston; Weekman, V., et al.;
ACS Symposium Series; American Chemical Society: Washington, DC, 1978.

$$r_F \cdot h = k_{LF} \cdot a. h .(\Delta C_H)_F + \Phi_L \cdot \Delta C_H \quad [6]$$

(material balance for the hydrogen consumption on the F zones)

where h is the length of a transfer zone, supposed to be equal to d_p; k_G the mass transfer coefficient in vapor phase at low gas flow rate (17); k_{LS} the mass transfer coefficient at low liquid flow rate (18); k_{LF} the mass transfer coefficient in a thin stagnant liquid film.

The vapor-liquid interface data must be estimated under transfer conditions. The ketone behaves like an hydrophobic material and tends to be rejected from the water phase by preferentially concentrating on the surface. In such a case the bulk concentrations are very different from the surface concentrations and so are the activity coefficients (19). It is reasonable to suppose that in vapor pressure relations for mixtures, surface compositions play a more important role than bulk compositions. That is why we have correlated the vapor phase compositions to the surface concentrations by mean of the UNIFAC method of activity coefficients determination (20) and by the relation of Tamura et al (21) giving the surface tension for aqueous mixtures. So we compute maximum correction values for surface tension (DS) and ketone vapor pressure (PVAP) corresponding to a non equilibrium state where bulk and surface composition are equal. The adjusted corrections (Table III) amount to about 15% of their maximum values.

Table III. ADJUSTED CORRECTIONS FOR SURFACE TENSION (DS) AND KETONE VAPOR PRESSURE (DVAP) IN TRANSFER CONDITIONS

T(K)	DS($N.m^{-1}$)	DVPA
269	$5.38\ 10^{-5}$	0.046
284	$5.47\ 10^{-5}$	0.062
308.5	$5.62\ 10^{-5}$	0.142
315	$5.66\ 10^{-5}$	0.152
326	$5.72\ 10^{-5}$	0.233

Assuming the existence of a stationnary state related to the initial conditions, we compute the reactant concentration at the catalyst external surface in F and C zones and, consequently, their specific production. The specific reaction rates calculated using this model are

shown by the continuous lines on Figures 2 and 3. It can be seen that the agreement with the experiments is fair even at the highest temperature.

Conclusion

The prediction of the performances of a trickle-bed reactor is possible knowing only the intrinsic rate equation, if a good description of the topological liquid distribution is available. This one can be obtained using the percolation theory and resolving the local forces balances at the gas-liquid and liquid-solid interfaces. For the hydrogenation of 2-butanone, we could obtain calculated values of the conversion in satisfactory agreement with the experiments, provide that we take into account all the possible mass transfer processes between all the different types of bed areas. So for the first time the description of the liquid distribution in a trickle-bed catalytic reactor is sufficiently detailed to allow the quantitative prediction of the performances of such a reactor using a volatile liquid reactant.

List of symbols

a	geometric specific surface area (m^{-1})
C_K	ketone concentration (mol m^{-3})
d_p	equivalent particule diameter (m)
DS	gas-liquid surface tension correction (Nm^{-1})
g	gravity acceleration (m s^{-2})
h	length of a transfer zone (m)
k_G	ketone mass transfer coefficient in vapor phase (m s^{-1})
k_{LS}	hydrogen mass transfert coefficient in liquid phase (m s^{-1})
k_{LF}	hydrogen mass transfert coefficient in a thin stagnant liquid film (m s^{-1})
p	existence probability of F zones (adim.)
p_H	hydrogen pressure (atm)
PVAP	ketone vapor pressure correction factor (adim.)
r	intrinsic reaction rate (mol(gr Ru)$^{-1}$)
r_C	apparent specific reaction rate on C zones (mol $m^{-3}s^{-1}$)
r_F	apparent specific reaction rate on F zones (mol m^{-3} s^{-1})
r_{SP}	experimental specific reaction rate in the trickle-bed (mol $m^{-3}s^{-1}$)
T	temperature (K)
α	mean orientation angle of liquid-solid interface
ΔC_H	difference between inlet and outlet hydrogen liquid concentration on a transfer zone (mol m^{-3})
$(\Delta C_H)_F$	hydrogen concentration difference across the liquid film (mol m^{-3})

In Chemical Reaction Engineering—Houston; Weekman, V., et al.;
ACS Symposium Series; American Chemical Society: Washington, DC, 1978.

ΔC_K difference between inlet and outlet ketone vapor concentration on a transfer zone (mol m^{-3})
$(\Delta C_K)_{ln}$ logarithmic mean driving concentration difference for ketone transfer (mol m^{-3})
$(\Delta C_H)_{ln}$ logarithmic mean driving concentration difference for hydrogen transfer (mol m^{-3})
Φ_G gas superficial velocity (m s^{-1})
Φ_L liquid superficial velocity (m s^{-1})
θ apparent contact angle
μ liquid viscosity (kg m^{-1} s^{-1})
ρ_L liquid density (kg m^{-3})
σ_{LG} gas-liquid surface tension (N m^{-1})

Literature cited

(1) HENRY, H.C. and GILBERT J.B., Ind. Eng. Chem. Process Design Devel., (1973) 12,328.
(2) MEARS, D.E.,"Chem. Reaction Eng. II",Adv. in Chem. Ser., (1974) 133,218.
(3) WARE, C.H., Ph. D. Thesis, Univ. of Pennsylvania, (1959).
(4) SEDRICKS, W. and KENNEY,C.N., Chem. Eng. Sci.,(1973) 28,559.
(5) GERMAIN, A.H., LEFEBVRE, A.G. and L'HOMME, G.A."Chemical Reaction Engineering II", Adv. in Chem. Series, (1974) 133,164.
(6) HANIKA, J., SPORKA, K., ULBRICHOVA, Z., NOVAK, J., and RUZICKA, V., Coll. Zech. Chem. Commun., (1974) 9,210.
(7) SATTERFIELD, C.N., PELOSSOF, A.A. and SHERWOOD,T.K., A.I.Ch.E. J. , (1969) 15,226.
(8) GERMAIN A., Collection des Publications de la Faculté des Sciences appliquées, Université de Liège (1977) 65,1.
(9) ZUBER, N., STAUBE, F.W., Int. J. Heat Mass Transfer, (1966) 9,897.
(10) BROADBENT, S.R. and HAMMERSLEY, J.M., Proc. Camb. phil. Soc., (1957) 53,629.
(11) HAMMERSLEY, J.M., Proc. Camb. phil. Soc., (1957) 53, 642.
(12) SHANTE, V.K.S. and KIRKPATRICK, S., Adv.Phys.,(1971) 20, 325.
(13) KIRKPATRICK, S., Rev. Mod. Phys., (1973) 45,574.
(14) BUCHANAN, J.E., Ind. Eng. Chem. Fund., (1967) 6 ,400.
(15) HUTTON, B.E.T. and LEUNG, L.S., Chem.Eng. Sci.; (1974) 29,1681.
(16) CRINE, M., MARCHOT, P. and L'HOMME,G.,to be published.
(17) PETROVIC, L.J. and THODOS, G., Ind. Eng. Chem. Fund., (1968) 7,274.

In Chemical Reaction Engineering—Houston; Weekman, V., et al.;
ACS Symposium Series; American Chemical Society: Washington, DC, 1978.

(18) GOTO,S. and SMITH, J.M., A.I.Ch.E. J. , (1975) 21, 706.
(19) REID, R.C., PRAUSNITZ, J.M. and SHERWOOD, T.K., "The Properties of Gases and Liquids", 612, Mc Graw Hill, New York (1977).
(20) *Op. cit.*, 347.
(21) TAMURA, M., KURATA, M. and ODANI, H., Bull. Chem. Soc. Japan, (1955) 28, 83.

In Chemical Reaction Engineering—Houston; Weekman, V., et al.;
ACS Symposium Series; American Chemical Society: Washington, DC, 1978.

35

Determination of the Extent of Catalyst Utilization in a Trickle Flow Reactor

B. BAKER, III

Shell Development Company, Westhollow Research Center, P. O. Box 1380, Houston, TX 77001

This study concerns trickle flow reactors for hydrotreating heavy oil. In these reactors, sulfur and nitrogen are removed, and certain compounds in the oil are saturated with hydrogen. Vapor (mostly H_2) and liquid (oil) are passed cocurrently downward over a fixed bed of small catalyst particles. The liquid flows over the particles in films and rivulets; the vapor flows through the remaining voids. As discussed below, these hydrodynamical conditions may lead to incomplete catalyst wetting, axial dispersion, and restricted interphase mass transfer and may therefore result in incomplete catalyst utilization. Since the catalyst is fairly expensive and the conditions of temperature and pressure require expensive reactor vessels, there is considerable incentive to ensure that maximum utilization of the catalyst is obtained.

It appears that these effects may be more serious in the process development scale units (PDU), due to their low velocities and short lengths, than in the commercial units they simulate. Hence conversions in these units may not be suitable targets for commercial performance. The assessment of this latter possibility is the objective of this study.

In this study a trickle flow reactor is considered to be obtaining maximum catalyst utilization if it is operating in plug flow with the catalyst fully contacted and there are no interphase mass transfer limitations external to the catalyst particles.* An illustrative conversion (desulfurization) for a fully contacted plug flow reactor with no mass transfer limitations is plotted as a function of LHSV in Figure 1.**

---

*Improving catalyst utilization by decreasing the size of the catalyst particles or changing particle porosity, i.e., improving intraparticle mass transfer, is not considered.

**In Figure 1, overall conversion is assumed to be represented by a second-order equation; this does approximately fit experimental desulfurization data. Therefore, the lowest line is simply the second order plug flow reactor equation.

© 0-8412-0401-2/78/47-065-425$05.00/0

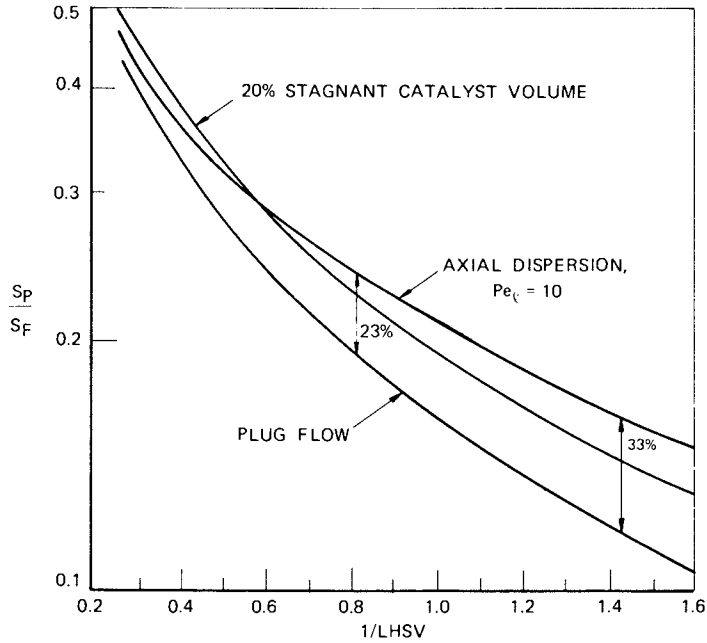

Figure 1. Conversion in trickle flow reactor with second-order kinetics—effect of axial dispersion and incomplete catalyst contacting

In Chemical Reaction Engineering—Houston; Weekman, V., et al.;
ACS Symposium Series; American Chemical Society: Washington, DC, 1978.

Incomplete Catalyst Wetting. It has been widely reported in the literature that liquid contacting is not complete in trickle flow reactors (1,2,3,4,5). All of the catalyst particles may not be wetted on an individual basis because of the tendency of the liquid flow to occur in rivulets. Data (1) on non-porous particles indicate that wetting is at a maximum at a particle size of around 4 mm and decreases as the particle size increases or decreases from this value. An improvement as the liquid velocity is increased is also indicated. The data would suggest that in a commercial heavy oil unit containing 1.5 mm extrudate catalyst, nearly all the particles may be wetted but that in a PDU* simulating the commercial unit having only a 30 cm/hr liquid superficial velocity, liquid contacting may be only 80% or less. The effect of not contacting 20% of the catalyst, as illustrated in Figure 1,** is to increase the effective space velocity so that less conversion is obtained compared to the fully contacted case. Other studies (2) indicate that in some cases 66% of the catalyst is not contacted. Thus, there is considerable interest to establish or not this is really the case in PDU containing porous catalyst particles diluted with smaller diameter, non-porous inert particles.

Axial Dispersion. It has also been reported that axial dispersion (backmixing) is much more pronounced in two-phase flow in packed beds than in single-phase flow (6) and that this may effect conversion in trickle flow reactors (7). In particular, the short PDU are more likely to be affected than the longer commercial units since the axial concentration gradient caused by the reaction is much steeper. The conclusions in (6) indicate that the axial dispersion coefficient decreases as the particle size is decreased so that the adverse length effect in a PDU can be partially offset by diluting the catalyst bed with small inert particles. Dilution also serves to lengthen the bed, which reduces the axial concentration gradient. A very rough estimate of the effect of axial dispersion from the above studies indicates that for the commercial unit above, there would be no axial dispersion effect but that there might be an axial dispersion effect in the above PDU with a liquid axial Peclet number of about 10. The effect of axial dispersion of this magnitude on conversion is

*In the PDU, the 1.5 mm extrudate catalyst particles, which are cylinders 1.5 mm in diameter and 4.5 mm in length, are diluted with an equal volume of approximately spherical, non-porous inert particles, 1.0 mm in diameter.

**The effective LHSV is the apparent LHSV divided by 0.8; otherwise the identical second order plug flow reactor equation is plotted for this case.

In Chemical Reaction Engineering—Houston; Weekman, V., et al.;
ACS Symposium Series; American Chemical Society: Washington, DC, 1978.

also illustrated in Figure 1.* Again it is of interest to examine if axial dispersion is influencing PDU results.

Interphase Mass Transfer. There are a number of interphase mass transfer steps that must occur in a trickle flow reactor. The mass transfer resistances can be considered as occurring at the more or less stagnant fluid layer interfaces, i.e., on the gas and/or the liquid side of the gas/liquid interface and on the liquid side of the liquid/solid interface. The mass transfer correlations (8) indicate that the gas/liquid interface and the liquid/solid interface mass transfer resistances decrease with higher liquid velocity and smaller particle size. Thus, in the PDU, the use of small inert particles partially offsets the adverse effect of low velocity. These correlations indicate that for this system, external mass transfer limitations are more likely to occur in the PDU than in the commercial reactor because of the lower liquid velocity, but that probably there is no limitation in either. If a mass transfer limitation were present, it would limit conversion in a way similar to that shown for axial dispersion and incomplete catalyst wetting illustrated in Figure 1. Due to the uncertainty in the correlations and in the physical properties of these systems, particularly the molecular diffusivities, it is of interest to examine if external mass transfer is influencing the PDU results.

Selection of a System to Determine Maximum Catalyst Utilization

In order to determine maximum catalyst utilization, a small-scale system that eliminated wetting problems, axial dispersion, and mass transfer limitations was necessary. In addition, results directly applicable to heavy oil hydrotreating were desired. The liquid full (flooded bed) upflow reactor with an external hydrogen equilibrator shown in Figure 2 was selected. Only dissolved hydrogen passes through the reactor, eliminating the gas phase. A high liquid recycle rate and an efficient equilibrator prevent hydrogen depletion of the liquid in the system. The high liquid recycle rate also insures adequate external mass transfer. Since the reactor is completely well mixed, there can be no axial dispersion effect. Furthermore, with this arrangement, switching between trickle flow and liquid full operation can be accomplished without disturbing the catalyst bed.

Although the system could have been operated in a continuous mode, it was decided to operate it in a batch mode. In the batch high-recycle mode the reactor mass balance is that for a stirred-tank batch reactor and thus over a period of time is analogous to the mass balance for a plug flow reactor over a distance along

*The calculations follow (7) for a second order reactor with axial dispersion.

In Chemical Reaction Engineering—Houston; Weekman, V., et al.;
ACS Symposium Series; American Chemical Society: Washington, DC, 1978.

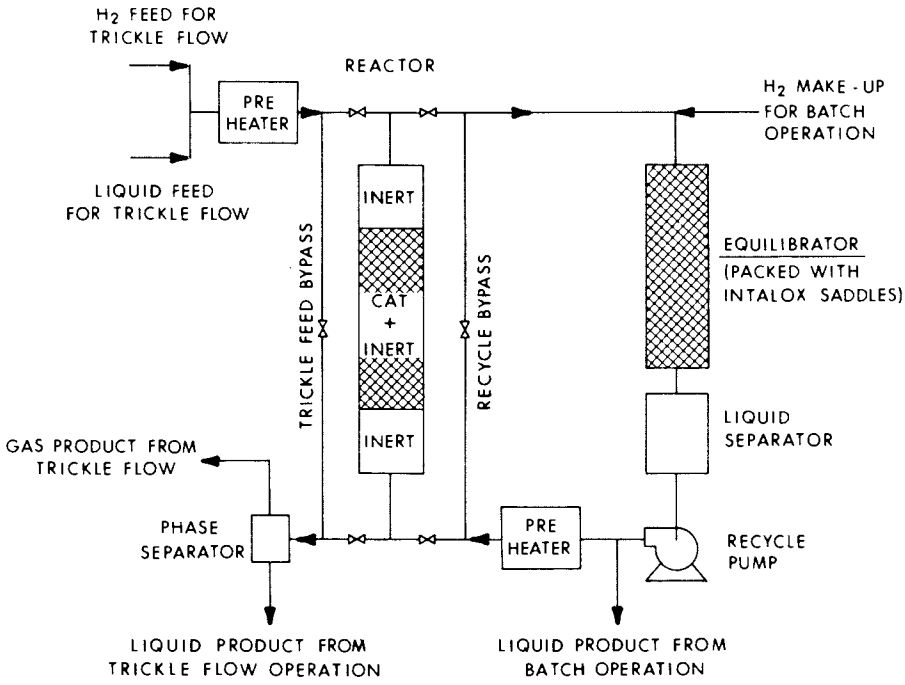

Figure 2. Experimental system for determining maximum catalyst utilization

In Chemical Reaction Engineering—Houston; Weekman, V., et al.;
ACS Symposium Series; American Chemical Society: Washington, DC, 1978.

the reactor. In the continuous high-recycle mode, the mass balance equation for a continuous-stirred tank reactor (CSTR) would be operative. When numerous reactions occur over a spectrum of reaction rates, as for a heavy oil feed, it is difficult to relate measurements of overall conversion (desulfurization, H_2 uptake) between a CSTR and a plug flow reactor.

The conditions for insuring that the batch recycle reactor is analogous to a once-through reactor, in addition to operating at the same temperature and pressure, are as follows:

1. $\left.\text{LHSV}\right|_{\text{batch}} = \left.\text{LHSV}\right|_{\text{trickle}}$ where

$$\left.\text{LHSV}\right|_{\text{batch}} = \frac{V_{\text{batch, } \ell\text{, std}}}{V_{\text{cat}} \cdot t_{\text{batch}}} \quad \text{and}$$

$$\left.\text{LHSV}\right|_{\text{trickle}} = \frac{F_{\text{trickle, } \ell\text{, std}}}{V_{\text{cat}}}$$

2. $$\frac{V_{\text{batch, g, reac}}}{V_{\text{batch, } \ell\text{, reac}}} = \frac{F_{\text{trickle, g, reac}}}{F_{\text{trickle, } \ell\text{, reac}}}$$

The first criterion is simply the well-known analog between a plug flow continuous reactor and a well-stirred batch reactor mentioned above. The second criterion is the analogy between a continuous one-stage equilibrium flash and a batch equilibrium flash. Since some of the gas dissolves in the liquid and some of the liquid vaporizes, this criterion insures that the vaporization conditions are the same as well as insuring that the concentration of any reaction inhibiting reaction products, namely, H_2S are the same.

Other considerations were (1) The equilibrator was designed to replace at least 99% of the dissolved H_2 lost from the liquid per pass through the reactor. (2) The amount of dissolved H_2 was estimated from flash calculations, but there were no data to establish the H_2 uptake at the high recycle rates being considered. To ensure that the liquid was not excessively depleted of H_2 before reequilibration and that the equilibration was adequate, batch experiments were run at the same LHSV at several recycle rates to establish a recycle rate high enough to insure no significant decrease in conversion because of H_2 depletion. (3) It was established by calculation that the time required to change the concentration profiles inside the catalyst particles was extremely small compared to the length of the batch experiment so that the profiles at a certain point along the once-through trickle reactor can be duplicated at a corresponding time in the batch experiment. (4) By operating the system without catalyst, it was established that homogeneous reactions do not occur over the much longer exposure to reaction temperature and pressure in the batch experiment to any significant extent.

In Chemical Reaction Engineering—Houston; Weekman, V., et al.;
ACS Symposium Series; American Chemical Society: Washington, DC, 1978.

Apparatus. The system was constructed by modifying an existing trickle-flow once through PDU reactor. A 2.5 cm diameter reactor was packed with a mixture of 100 cm^3 of 1/16-inch extrudate catalyst and 100 cm^3 of 1.0 mm silicon carbide non-porous inerts, producing a 60 cm long catalyst bed. There were 25 cm long sections of inerts above and below the catalyst. Isothermal conditions were maintained throughout the bed within about 5°C. The 8 cm diameter equilibrator vessel contained a 60 cm long bed of 1 cm Intalox saddles.

Procedure. The unit was brought up and lined-out as a normal trickle flow reactor. After a three-four day lineout period, the reactor reached steady-state as indicated by constant product quality.

At this time liquid was added to the batch side of the reactor and the batch side was pressured with H_2. The batch liquid was circulated through the recycle bypass around the reactor, and brought to the desired equilibration temperature. The system was then switched to the batch mode by the following procedure. The trickle flow liquid/gas feed flow was switched out of the reactor into the trickle bypass and the batch liquid recycle flow was switched out of its bypass into the reactor. Lined-out batch conditions were reached in 2-3 minutes. The length of the batch experiment required from 8-16 hours, depending on the LHSV desired. At the end of this period, the batch liquid recycle flow was switched out of the reactor back into its recycle line and the trickle flow liquid/gas feed flow was switched from the trickle bypass back into the reactor. The batch recycle liquid was then sampled. Meanwhile the trickle flow run was continued. It was found that 24-48 hours were required for the trickle flow run to again reach steady-state.

There were three series of experiments performed. The characteristics of the feed used in all of the experiments are shown in Table I. The same bed of catalyst was used in Series 1 and 2. In

Table I

CHARACTERISTICS OF FEED
USED IN THE EXPERIMENTS

Specific Gravity	0.8868
Carbon, %w	85.19
Hydrogen, %w	12.04
Sulfur, %w	2.04
Nitrogen, %w	0.13
MW	374
50%w Distilled, °C	450

Series 3, a more active catalyst was used in order to study high conversions. The average set of conditions for each series is

In Chemical Reaction Engineering—Houston; Weekman, V., et al.;
ACS Symposium Series; American Chemical Society: Washington, DC, 1978.

shown in Table II. In Series 1, the batch vapor and liquid were equilibrated at 230°C and the liquid reheated to the 365°C

Table II

REACTOR CONDITIONS DURING COMPARISONS OF TRICKLE AND BATCH OPERATIONS

	Series 1		Series 2		Series 3	
	Trickle	Batch	Trickle	Batch	Trickle	Batch
Reactor						
Temperature, °C	365	365	365	365	360 350	360 350
Pressure, kg/cm^2	48.5	66.8	66.8	66.8	66.8	66.8
Equilibrator						
Temperature, °C	-	230	-	365	- -	360 350
H_2/Oil Feed Ratio, moles H_2/mole oil						
Inlet	2.84	-	2.84	-	2.94 2.84	- -
Outlet	1.85	-	1.85	-	1.85 1.85	- -
Start	-	2.05	-	2.05	-	2.05
End	-	1.92	-	1.92	-	1.92

reaction temperature after the recycle pump, since it was felt at the time that the recycle pump could not tolerate liquid at 365°C. This in turn required a compensating change in pressure and resulted in a somewhat less precise comparison. Later it was found that the modified pump would operate on liquid at the higher temperature so that in Series 2 and 3, the batch vapor and liquid were equilibrated at the same temperature as the reactor.

Results and Discussion

The system described above has considerable versatility in examining questions of maximum catalyst utilization. However, its use in the present study was limited to the question of whether or not maximum utilization was being obtained in the 60 cm long, 2.5 cm diameter PDU reactors used to simulate a heavy oil hydrotreater. These normally operate at a LHSV around 1.0 hr^{-1}, with a H_2/oil feed ratio of 1.5-3.0 moles H_2/mole oil. Approximate conversions obtained are desulfurization 60-90%, denitrogenation 20-50%, and H_2 uptake 0.7-1.0 moles H_2/mole oil.

Series 1. The results from Series 1 using diluted catalyst are shown in Figure 3 (top). For both desulfurization and H_2 uptake, as well as denitrogenation (not shown), there were no differences

In Chemical Reaction Engineering—Houston; Weekman, V., et al.;
ACS Symposium Series; American Chemical Society: Washington, DC, 1978.

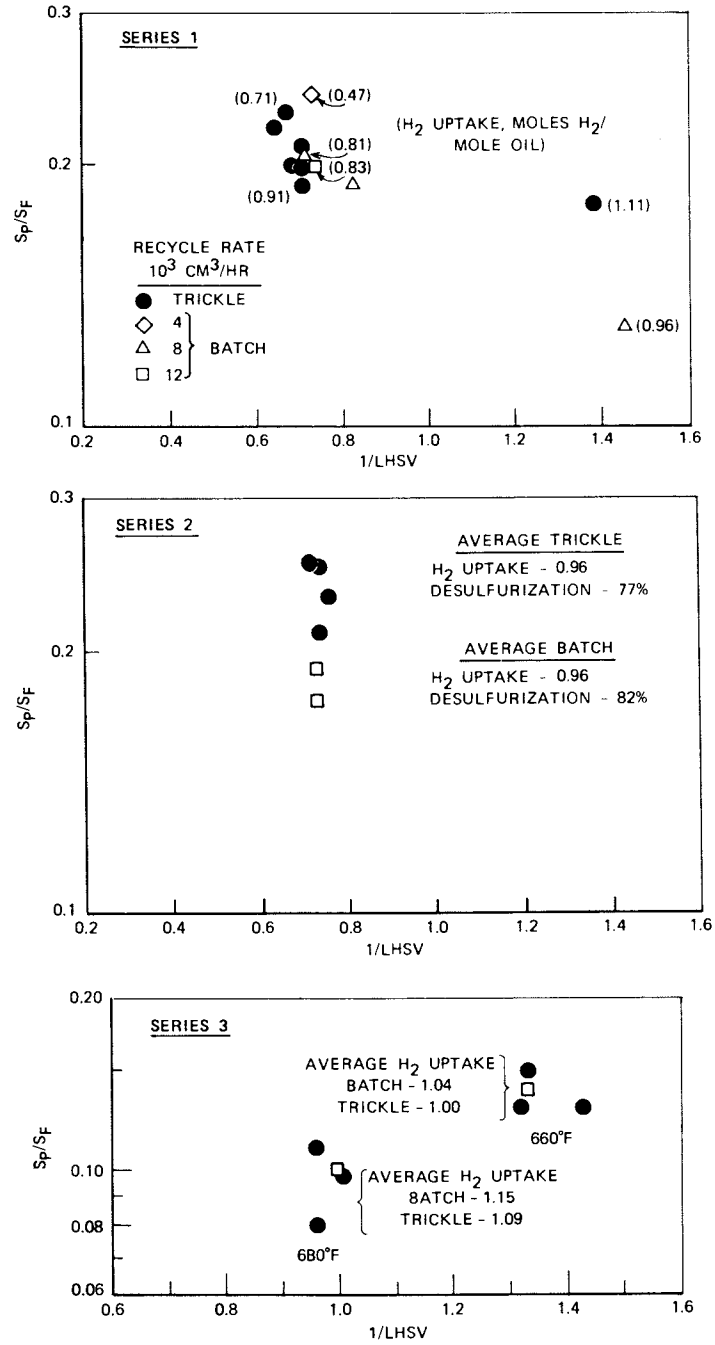

Figure 3. Comparison of trickle flow and batch operation—desulfurization and H_2 uptake

evident between the trickle flow and batch results at LHSV=1.3 for recycle rates $\geq$ 8000 cm^3/hr. The effect of the batch liquid recycle rate was studied by performing runs at recycle rates of 4000, 8000, and 12,000 cm^3/hr. Only at the lowest rate of 4000 cm^3/hr was any decrease in conversion or H_2 uptake evident, indicating that a recycle rate $\geq$ 8000 cm^3/hr was sufficient to prevent excessive H_2 depletion in the recycle liquid at these reactor conditions. The desulfurization results indicated a substantial difference between the single trickle and batch comparison at LHSV=0.7. The denitrogenation and H_2 uptake results did not confirm a difference, however.

Series 2. The results from Series 2 on the same diluted bed of catalyst are shown in Figure 3 (middle). No differences in denitrogenation (not shown) or H_2 uptake between the trickle and batch runs at LHSV $\sim$ 1.3 hr^{-1} were evident. There was a small difference in desulfurization, which is probably not significant considering the experimental scatter.

Series 3. In order to make further comparisons at higher conversion and lower space velocity, a few experiments were run using a diluted bed of more active catalyst. The reaction rates for this more active catalyst are equivalent to the first catalyst at a 17°C lower temperature. The results shown in Figure 3 (bottom), indicate no significant differences in desulfurization, H_2 uptake, or denitrogenation (not shown).

Conclusions

A modified process development unit apparatus has been utilized in this study in which, for the same 200 cm^3 packed bed of catalyst, normal once-through trickle flow operation can be compared to liquid-full batch operation. In the latter, the possibilities of incomplete catalyst wetting, axial dispersion, and interphase mass transfer limitations are not present and thus, maximum catalyst utilization is obtained. Comparison of the results of the two modes of operation for the specific system of interest leads to the following conclusions:

1. Diluted bed* heavy oil hydrogenation trickle flow process development units at least 60 cm long obtain maximum catalyst utilization at up to 90 percent desulfurization at LHSV as low as 0.75 hr^{-1}. Maximum catalyst utilization for denitrogenation and hydrogen uptake at these conditions is also obtained.
2. The conversions measured in these units are, therefore, suitable targets for commercial unit performance.

*Diluted with an equal volume of 1.0 mm diameter silicon carbide inerts.

In Chemical Reaction Engineering—Houston; Weekman, V., et al.;
ACS Symposium Series; American Chemical Society: Washington, DC, 1978.

Generalization

It is known that in some trickle flow systems, incomplete catalyst contacting, axial dispersion, and external mass transfer limitations do occur. Studies using this same approach could be used to examine a wider variety of systems, including in particular, reactions in which extremely high conversion, > 99% is desired. This approach may also be useful in establishing the conditions, if any, under which a reactor might better be designed as a packed bed in gas/liquid upflow rather than in trickle flow (gas/liquid downflow).

Nomenclature

E	axial dispersion coefficient, cm^2/hr
L	reactor length, cm
LHSV	v_ℓ/L, liquid hourly space velocity, hr^{-1}
Pe	vL/E axial Peclet number
S	sulfur concentration, w%
t_{batch}	time of batch reaction, hr
v	superficial velocity cm/hr
V	volume, cm^3
V_{batch}	volume in entire batch system, cm^3

Subscripts

cat	catalyst
F	feed
g	gas or vapor
ℓ	liquid
P	product
reac	at reactive conditions after flash
std	at standard conditions, 1 atm, 15.6°C

Literature Cited

1. Wiffels, J. B., et al., "Chemical Reaction Engineering - II," Adv. in Chem., Series 133, Hulburt, H. M., Ed., p. 151, ACS Publishers, Washington, D.C., 1974.
2. Schwartz, J. G., et al., "Fourth International Symposium on Chemical Reactor Engineering Preprints," p. 382, DECHEMA Publishers, Frankfurt, FRG, 1976.
3. Hoffman, H., Int. Chem. Eng., (1977) 17, 19.
4. Satterfield, C. N., AIChE J., (1975) 21, 209.
5. Montagna, A. and V. T. Shah, Ind. Eng. Process D/D, (1975) 14, 479.
6. Furzer, I. A. and R. W. Michell, AIChE J., (1970) 16, 380.
7. Mears, D. E., CES, (1971) 26, 1361.
8. Goto, S. and J. M. Smith, AIChE J., (1975) 21, 706.

In Chemical Reaction Engineering—Houston; Weekman, V., et al.;
ACS Symposium Series; American Chemical Society: Washington, DC, 1978.

36

Two-Phase Theory and Fluidized Bed Reactor Models

P. N. ROWE

Department of Chemical and Biochemical Engineering, University College of London, Torrington Place, London WCIE, 7JE, England

The concept of two fluid phases in a bubbling fluidised bed and its application to a reactor model originates in the work of Johnstone and colleagues at the University of Illinois (1,2). Since then numerous and different modifications have been made to the basic model (3) but practically all these variants assume that the interstitial flow (the interstitial or dense phase) is the minimum fluidisation value. Flow in the form of bubbles (the bubble or cloud phase) is the difference between interstitial and total flow. This is simply formulated

$$Q_B/A = U - U_{mf} \qquad (1)$$

A few models concede that interstitial flow may be greater than indicated by Eq. 1 and introduce a multiplier of U_{mf} that is greater than unity.

This formulation of the two-phase theory is over-simplified and in the first part of this paper a more rigorous expression is derived to take account of the reduction in cross sectional area of the interstitial phase as the bed fills with bubbles and also of gas expansion which must occur as pressure falls with bed height. In many cases these corrections can be ignored when the expression reduces to Eq. 1.

In addition, especially with finely divided powders, the particles constituting the dense phase can expand, increase the phase voidage and hence its permeability. In these circumstances the local interstitial gas velocity exceeds U_{mf} and more gas passes in this phase than Eq. 1 allows. The consequences of this for overall conversion in a fluidised bed chemical reactor are examined in the second part of the paper by considering the predictions of an appropriate model.

The Two-Phase Theory Examined

Gas in a bubbling fluidised bed can be thought of as divided into three phases; that flowing interstitially (the dense phase), that associated with the bubble wakes and that in the essentially empty space of the bubbles. If f is the fraction of bed volume

© 0-8412-0401-2/78/47-065-436$05.00/0

occupied by a given phase and U_G is the absolute gas velocity,

$$Q_i = U_{Gi}\ A\ (1-f_B-f_W)\ \varepsilon_i \quad (2)$$

$$Q_W = U_{GW}\ A\ f_W \varepsilon_W \quad (3)$$

$$Q_B = U_B\ A\ f_B \quad (4)$$

The sum of these three flows is equal to the total flow. Three assumptions are introduced: (i) $f_W = f_B/3$ that is, the wake associated with each bubble is about 1/3 its own volume, (ii) $U_{GW} = U_B$ that is, gas associated with the wake travels at the bubble velocity, (iii) $\varepsilon_i = \varepsilon_W$ that is, the particle voidage in the wake is essentially the same as in the dense phase. Neglecting any gas expansion, a volumetric flow balance leads to

$$U_{Gi} = \left[\varepsilon_i\ (3-4f_B)\right]^{-1} \left[3U-(3+\varepsilon_i)\ Q_B/A\right] \quad (5)$$

or

$$Q_i/A = U - Q_B\ (3+\varepsilon_i)/3A \quad (6)$$

Particles move upwards in the bubble wakes at bubble velocity and, assuming that none is lost, there must be an equal volumetric flow rate downwards in the dense phase. That is

$$-U_{Si} = Q_B/A\ (3-4f_B) \quad (7)$$

The relative velocity between gas and particles in the dense phase follows from Eqs. 5 and 7

$$U_{G/S} = \left[U-Q_B/A\right]\ 3/\varepsilon_i(3-4f_B) \quad (8)$$

Now assume that the dense (and wake) phase voidage remains constant at its minimum fluidisation value. If the voidage does not change then the permeability is unlikely to change and the interstitial gas velocity must be maintained at U_{mf} if the bed is to remain fluidised without a net force lifting particles out of the bed. Thus, $U_{G/S} = U_{mf}/\varepsilon_{mf}$ and Eq. 8 becomes

$$Q_B/A = U-U_{mf}\ (3-4f_B)/3 \quad (9)$$

This is the simplest way in which the two-phase theory can be expressed and differs from the usual expression by the multiplier of U_{mf} which, it should be noted, is less than unity. It reflects the fact that as the bed fills with bubbles there is less cross-sectional area available for interstitial flow. Gas in the wake phase forms a small proportion of the whole and it makes little practical difference whether it is included with the interstitial or with the bubble phase. As a consequence of assumption (ii) it is included here with the bubble phase.

The term $(3-4f_B)/3$ is often not very different from unity

In Chemical Reaction Engineering—Houston; Weekman, V., et al.;
ACS Symposium Series; American Chemical Society: Washington, DC, 1978.

for f_B is rarely as big as 0.5. The numbers 3 and 4 in Eq.9 arise from the assumption that the wake volume is 1/3 of the bubble volume and small changes around this make little difference. The bubble fraction, f_B, is related to bubble flow rate and average rise velocity through Eq. 4 so it can be eliminated from Eq. 9 with the introduction of U_B. If and only if the dense phase voidage remains constant at ε_{mf}

$$f_B = 1 - (H_{mf}/H) \qquad (10)$$

when it can be measured directly.

Because of pressure drop through the bed there must be gas expansion and increased volumetric flow with height. Fluidised beds are of uniform temperature so the expansion must be isothermal and

$$(Q_H - Q_D)/Q_D = H(1-\varepsilon_i)\,\rho_p g/p_H \qquad (11)$$

where the suffix D denotes the distributor plane and H, a plane height H above it. The increase is small for most laboratory scale equipment with bed heights only a few tens of centimeters but it is not negligible for typical industrial dimensions even with light powders of bulk density, $(1-\varepsilon)\rho_p$ less than that of water as Figure 1 shows.

The effect of gas expansion on Eq.9 affects only the term U so that it becomes

$$(Q_B/A)_H = U_D \left[1+(H(1-\varepsilon_i)\rho_p g)/p_H\right] - U_{mf}\,(3-4f_B)/3 \qquad (12)$$

This is a refined version of the "true volume ideal two-phase theory" (4).

The amount of gas that flows interstitially can differ from Eq. 12 only if the dense phase permeability changes which in practice means change of voidage with a given powder. This certainly happens with fine powders where the voidage changes with gas velocity, U, and usually depends on the particle size distribution and is particularly influenced by proportions at the smaller end of the particle size range. This effect can be incorporated in Eq. 12 by introducing a further multiplier of U_{mf}, a coefficient, greater than unity, that is some function of gas velocity and may also vary with height. The nature of this coefficient is not well understood but it can be approximated in some cases by a constant.

Experimental work with one particular powder (a typical industrial grade of catalyst) shows that with fine powders ($d_p \lesssim 60\mu m$) more gas flows interstitially than Q_{mf} and thus is strongly dependent on the fines content ($d_p < 45\mu m$) of the powder. Figure 2 summarises recent experimental results (5) and shows that as much as 30% of the gas flow can occur interstitially. This is the kind of information from which the remaining factor to be included in Eq. 12 can be estimated.

Fluidised Bed Reactor Model

Most fluidised bed reactor models incorporate the two-phase

In Chemical Reaction Engineering—Houston; Weekman, V., et al.;
ACS Symposium Series; American Chemical Society: Washington, DC, 1978.

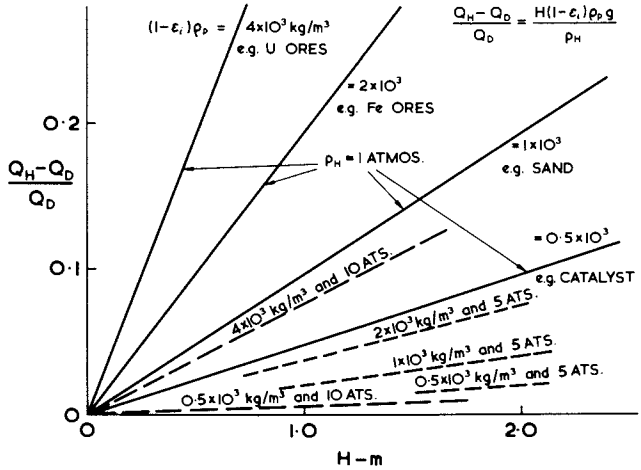

Figure 1. Increase in volumetric gas flow with bed height

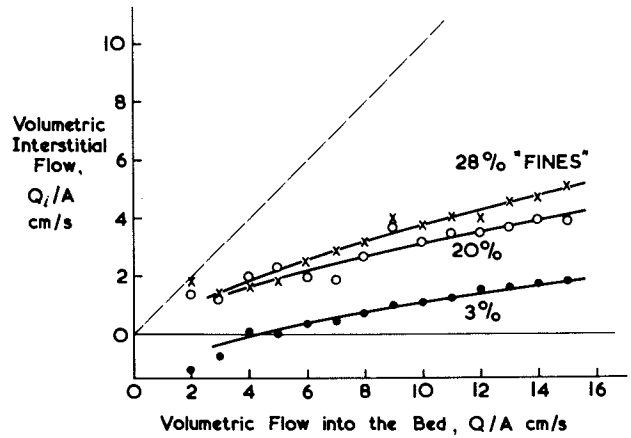

Figure 2. How the interstitial flow increases with gas velocity and "fines" content. At low gas velocities, downward particle movement (balancing upward flow as wakes) can result in a net downward interstitial gas flow.

In Chemical Reaction Engineering—Houston; Weekman, V., et al.;
ACS Symposium Series; American Chemical Society: Washington, DC, 1978.

theory in the form

$$Q_B/A = U - U_{mf} \qquad (13)$$

The correction of this to Eq. 9 is slight when U/U_{mf} is not very much greater than unity for then f_B is small. It is also slight when $U/U_{mf} >> 1$ for then the proportion of gas flowing interstitially is negligible.

The additional correction for gas expansion implied by Eq.12 may be more important. The result is a net mass transfer from the interstitial to the less efficient bubble phase and hence an overall reduction in the expected performance. Again, if $U_D >> U_{mf}$ the effect is negligible. In reactor modelling this correction cannot be sensibly considered without additionally taking into account change in gas volume as a result of chemical reaction. In many reactions reduction in volume occurs (e.g. oxidation of benzene to maleic anhydride, hydrofluorination of UO_2), in some there is no change (e.g. chlorination of saturated hydrocarbons, hydrogen reduction of ores) and in some there is volume increase (e.g. oxidation of ethylene, catalytic cracking). If this is to be taken into account then the extent of reaction must be known which may require an iterative calculation to follow the consequence of the model. It is not possible to generalise the treatment this correction requires. In many cases the modification will be negligible and it is easy to judge from Eq. 11 and the known chemistry whether or not it is important. The only consequent correction to the reactor model is to replace the bubble phase flow of Eq.13 by that of Eq. 12 with additional correction of the multiplier of U_D to account for volume change by chemical reaction.

Interstitial flow greater than Q_{mf} as indicated by Figure 2 is likely to be a much more important correction than those mentioned above whenever fine particles are involved. Since this includes most gas phase solids catalysed organic reactions, it is an important category. With fine powders the interstitial gas velocity is small compared with bubble velocity, clouds form around the bubbles and are little bigger than their parents so that gas/solid contacting in the bubble phase is very poor. An appropriate model for this situation is one in which interstitial gas moves in plug flow reacting readily with the solids, there is no reaction in the bubble phase but exchange between the two phases as bubbles rise through the bed. This is similar to the model of Davidson and Harrison (6) where first order reaction kinetics is additionally assumed.

Calculations have been made using this model assuming a superficial gas velocity, U = 0.5 m/s and neglecting volume change by expansion and by chemical reaction (or assuming the two effects cancel). The reactor diameter is assumed larger than any bubble so that no slugging occurs. The powder U_{mf} =.002 m/s and its voidage, ε=0.38 which corresponds to a typical commercial catalyst. The mean bubble rise velocity is assumed given by

In Chemical Reaction Engineering—Houston; Weekman, V., et al.;
ACS Symposium Series; American Chemical Society: Washington, DC, 1978.

$$U_B = \frac{g^{3/8}}{\sqrt{2}} K_V \frac{8}{11} (U-U_{mf})^{1/4} H^{3/8} \qquad (14)$$

with $K_V = 1.3$ (4). The first order rate constant was assumed to be 50 s^{-1} (fast reaction) and 0.5 s^{-1} (slow reaction) with some intermediate values. The interstitial gas flow was taken as Q_{mf} and 0.3Q with two equal steps between. The only remaining quantity needed is the main model parameter, the exchange coefficient between the two phases, q_E/V_B.

There are means of estimating the exchange coefficient from the known physics of a bubbling fluidised bed and Davidson and Harrison show one method (6). Various methods of estimation indicate a typical value of order 1 s^{-1} but differ by a factor of two or more. This parameter also conceals some of the idealisations of the model such as the assumption that no reaction occurs in the bubble phase. Consequently in this treatment the exchange coefficient is regarded as an arbitrary variable changing by an order of magnitude from 0.2 to 2.0 s^{-1}. It is therefore likely to span the values experienced in practice.

Figures 3 to 8 show the results of calculation as a plot of concentration of a reactant species against bed height. Figure 3 shows one extreme, a high chemical rate constant (K = 50 s^{-1}) and a high rate of interphase gas exchange (q_E/V_B = 2.0 s^{-1}). The reactor performance approaches the plug flow case (but with rate controlled by the exchange coefficient, not the chemical kinetics) and the prediction not very sensitive to the proportion of gas flowing interstitially. Even so, the bed height needed to achieve a given level of conversion is materially reduced as the interstitial flow proportion increases.

Figure 4 refers to a slow chemical reaction (K = 0.5 s^{-1}) and the same high gas exchange rate (q_E/V_B = 2.0 s^{-1}). Markedly less conversion occurs than would in a plug flow reactor with this chemical rate constant so performance is still dominated by the rate of phase exchange. The effect of interstitial flow proportion is similar to the previous case but reaction to near completion would be virtually unobtainable even if 50% of the gas flowed interstitially and continued to exchange at this very high rate. Of course, if it all flows interstitially it is a plug flow reactor and 99% conversion occurs in a height of 4.6 m.

Figure 5 shows the fast reaction (K=50 s^{-1}) with a low phase exchange coefficient (q_E/V_B = 0.2 s^{-1}). Performance is now limited by the exchange rate and the extent of conversion is largely determined by the proportion that flows interstitially. This is a case where for a catalyst such as referred to in Figure 2, the conversion achievable would largely depend on the fines content.

Figure 6 refers to a slow reaction (K=0.5 s^{-1}) and a low exchange coefficient (q_E/V_B = 0.2 s^{-1}). Comparison with Figure 5 shows that an extreme change in chemical rate produces only a small change in reactor performance if the phase exchange rate is low. The proportion of interstitial gas flow is important in determining the bed height needed for a given conversion but shows that it is

In Chemical Reaction Engineering—Houston; Weekman, V., et al.;
ACS Symposium Series; American Chemical Society: Washington, DC, 1978.

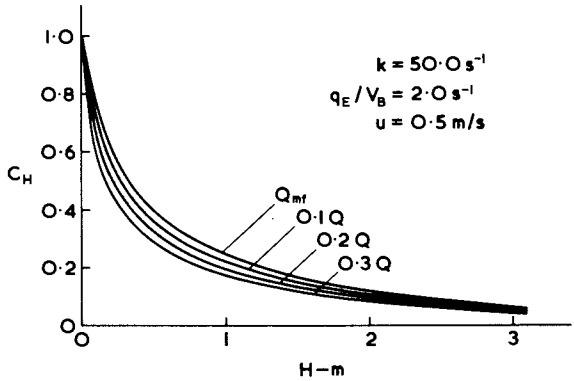

Figure 3. Predicted variation of composition with bed height—fast reaction; fast exchange

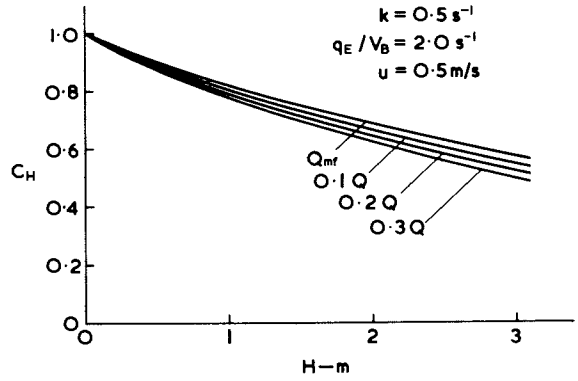

Figure 4. Predicted variation of composition with bed height—slow reaction; fast exchange

In Chemical Reaction Engineering—Houston; Weekman, V., et al.;
ACS Symposium Series; American Chemical Society: Washington, DC, 1978.

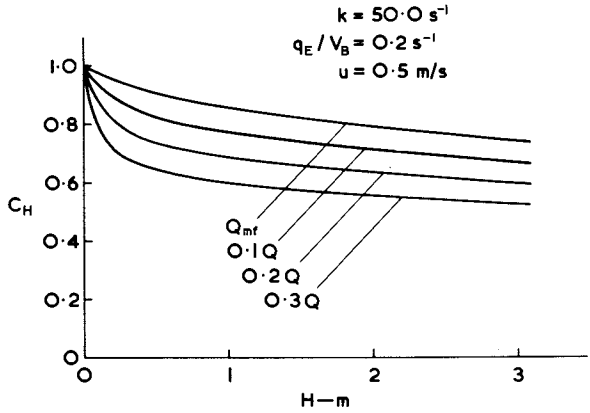

Figure 5. Predicted variation of composition with bed height—fast reaction; slow exchange

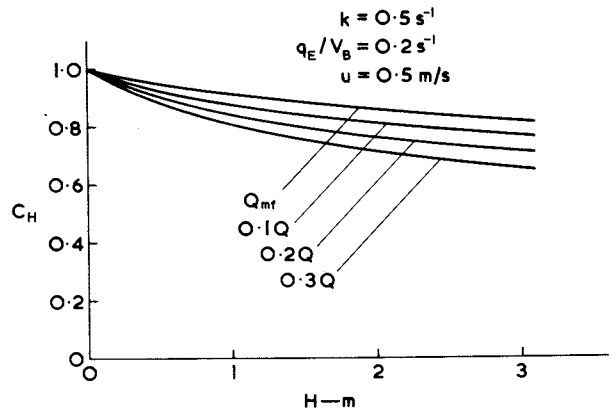

Figure 6. Predicted variation of composition with bed height —slow reaction; slow exchange

In Chemical Reaction Engineering—Houston; Weekman, V., et al.;
ACS Symposium Series; American Chemical Society: Washington, DC, 1978.

powerless to improve the maximum achievable conversion if the exchange rate is low (unless, of course, nearly all flows interstitially).

Figures 7 and 8 show some intermediate values which probably correspond to more realistic values for the exchange coefficient. In these cases the proportion of interstitial flow is important in determining the bed height needed.

Conclusions

In cases where the dense phase permeability remains constant at its minimum fluidisation value, the amount of gas flowing in this phase will in all cases be less than that predicted by the usually formulated two-phase theory. This will generally affect reactor performance adversely although the effect will usually be small. The reason for this is that bubbles reduce the cross-sectional area available for interstitial flow and gas expansion causes a net transfer to the bubble phase.

With fine powders such as fluidised catalysts the dense phase permeability does in fact increase with gas velocity and the above corrections become negligible in many cases. In a chemical reactor the degree of conversion then becomes importantly dependent on the proportion of gas that flows interstitially but is dominated by the rate of exchange between the two phases.

It is not possible to generalise the consequences because of complex interaction between the three main variables, reaction rate constant, interstitial flow proportion and interphase exchange rate. Particular examples of model calculations are given in Figures 3 to 8. It appears that exchange rate will determine the maximum degree of conversion that is attainable in practice but, within practical limits, the depth of bed needed depends largely on the proportion of gas flowing interstitially.

List of Symbols

A	cross sectional area of the fluidised bed	m^2
C_H	concentration of reactant at height H	kg/m^3
d_p	average particle diameter	μm
f_B	fraction of total bed volume occupied by bubbles	
f_W	fraction of total bed volume occupied by bubble wakes	
g	gravitational acceleration	m/s^2
H	bed height above the distributor plane	m
H_{mf}	bed height at minimum fluidisation	m
K	first order rate constant	s^{-1}
K_V	velocity coefficient (Eq. 14)	
p_H	gas pressure at height H	N/m^2
Q	volumetric gas flow into the bed	m^3/s
Q_B	volumetric gas flow in the form of bubbles	m^3/s
Q_D	volumetric gas flow across the distributor plane	m^3/s
Q_H	volumetric gas flow across a horizontal plane at height H	m^3/s

In Chemical Reaction Engineering—Houston; Weekman, V., et al.;
ACS Symposium Series; American Chemical Society: Washington, DC, 1978.

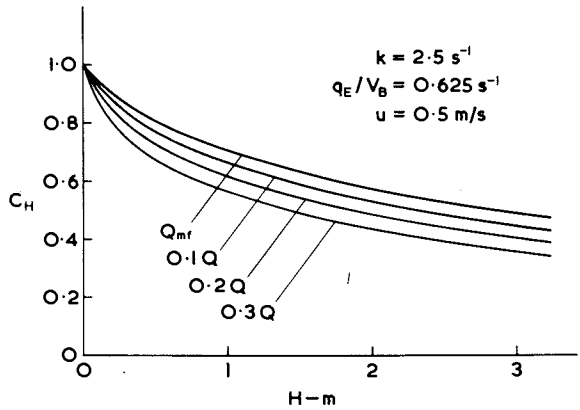

Figure 7. Predicted variation of composition with bed height—intermediate reaction; intermediate exchange

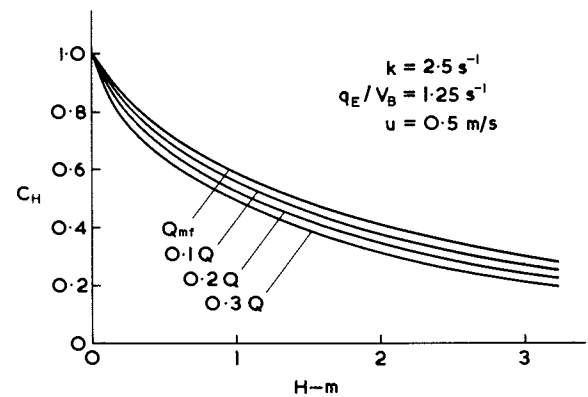

Figure 8. Predicted variation of composition with bed height—intermediate reaction; fast exchange

In Chemical Reaction Engineering—Houston; Weekman, V., et al.;
ACS Symposium Series; American Chemical Society: Washington, DC, 1978.

Q_i	volumetric interstitial gas flow	m^3/s
Q_W	volumetric gas flow as part of bubble wakes	m^3/s
q_E	phase exchange rate	m^3/s
U	superficial gas velocity into the bed = Q/A	m/s
U_B	average bubble rise velocity	m/s
U_D	superficial gas velocity across the distributor plane = Q_D/A	m/s
U_{Gi}	superficial gas velocity in the dense phase	m/s
$U_{G/S}$	average relative velocity between interstitial gas and particles	m/s
U_{GW}	velocity of gas in the wake phase	m/s
U_{mf}	superficial minimum fluidisation velocity	m/s
U_{Si}	average (vertical) velocity of particles in the dense phase	m/s
V_B	average bubble volume	m^3
ε_i	voidage of the dense phase	
ε_W	voidage of the wake phase	
ρ_p	individual particle density	kg/m^3

Literature Cited

(1) Toomy, R.D. and Johnstone, H.F., Chem. Eng. Prog.(1952)48,220.
(2) Johnstone, H.F., Batchelor, J.D. and Shen, C.-Y., AIChE Jnl, (1955) 1, 318.
(3) Kunii, D. and Levenspiel, O."Fluidisation Engineering", John Wiley, New York, (1962).
(4) Rowe, P.N. and Yacono, C.X.R., Chem. Eng. Sci.(1976) 31, 1179.
(5) Rowe, P.N., Santoro, L. and Yates, J.G., Chem. Eng. Sci., to be published.
(6) Davidson, J.F. and Harrison, D."Fluidised Particles",p.97, Univ. Press, Cambridge, (1963).

In Chemical Reaction Engineering—Houston; Weekman, V., et al.;
ACS Symposium Series; American Chemical Society: Washington, DC, 1978.

Multiphase Kinetic Studies with a Spinning Basket Reactor

E. C. MYERS and K. K. ROBINSON

Amoco Oil Company, P.O. Box 400, Naperville, IL 60540

The study of multiphase catalytic process such as petroleum hydrotreating requires laboratory reactors that ensure good contact between gas, liquid, and solid phases at high temperatures and pressures. Numerous reactors have been developed for process studies and fall mainly into two categories: fixed bed and agitated (gradientless). For multiphase catalytic systems, the experimental studies are normally performed in a trickling fixed bed reactor. This type reactor is subject to problems with catalyst contacting and flow maldistribution unless certain precautions are taken. External mass transport limitations are also possible, particularly with the more active catalysts that are currently available. Vigorous gas-liquid-catalyst contacting will often remedy this situation. Weekman (1) concluded that the gradientless reactors are far superior to the fixed bed in terms of sampling ease, temperature maintenance, mass transport, and other operating variables.

Although several gradientless reactors are available for studies of gas-phase reactions (2-6), none of them are suitable for studying multiphase systems, particularly at the high pressure required in such petroleum processes as distillate hydrotreating. Russian workers (7) did report a gradientless multiphase reactor but it was only suitable for atmospheric pressure operation. Now we have developed a high-pressure version to study hydrotreating reactions. It comprises a spinning basket held in a 500 cc stirred autoclave. Baffles around the basket ensure good mixing and contacting of the liquid and also eliminate vortexing at the gas-liquid interface. The flow pattern of the oil approximates that obtained in a single perfectly mixed reactor because the vaporized hydrocarbons which exit in the off-gas stream are recycled.

The spinning basket reactor was used to study the desulfurization kinetics of a model sulfur compound--dibenzothiophene in white oil. This study is confirming data for an earlier study by Frye and Mosby (8) with a trickle bed type reactor and actual petroleum fractions. There is good agreement between the two kinetic studies. This current study has achieved a further

© 0-8412-0401-2/78/47-065-447$05.00/0

In Chemical Reaction Engineering—Houston; Weekman, V., et al.;
ACS Symposium Series; American Chemical Society: Washington, DC, 1978.

refinement in the kinetic model; competitive adsorption effects by the reactant sulfur compound are accounted for.

Experimental

Materials. The feedstock was white oil spiked with dibenzothiophene. The white oil was obtained from the Whiting refinery of Amoco Oil Company. The dibenzothiophene (Eastman Chemicals) and the hydrogen (Liquid Carbonic) were used as received.

The hydrodesulfurization catalysts were 1/16" cylindrical extrudates of commercial cobalt-molybdenum on alumina.

Spinning Basket Reactor Description. The spinning catalyst basket of the reactor is shown in Figure 1. The catalyst is held in place by wire mesh in an annular space inside the basket, where internal baffles are between the catalyst space and the center support shaft. The basket is also surrounded by a baffle system which directs the fluid flow and prevents liquid vortexing. A 500 cc autoclave designed and built by Autoclave Engineers serves as the basis for the reactor system and is equipped with a packless magnetic drive to rotate the basket.

Good contacting is provided by the liquid and entrained gas bubbles flowing rapidly past the catalyst. This highly turbulent gas-liquid mass is a liquid continuous bubble swarm. Backmixed (gradientless) operation is assured by good mixing in the reactor. The flow pattern, shown in Figure 2, is as follows: (1) Fluid enters near the center of the basket through the cutouts at the top and bottom; (2) the fluid inside the basket rotates at the same rate as the basket and moves by centrifugal force into the catalyst; (3) fluid exits the catalyst and moves up or down between the basket and autoclave wall; (4) the fluid moves into the spaces above and below the basket where it then re-enters the basket.

Process Description. The overall flow scheme is shown in Figure 3. Hydrogen is metered to the reactor from the pilot plant feed system. Liquid feed is pumped to the reactor by a Whitey pump which regulates the flow rate.

Hydrogen, hydrogen sulfide, and vaporized oil are removed from the vapor space above the spinning basket. It is heated to reaction temperature to prevent condensation and refluxing, then cooled to room temperature in a condenser where it enters a separator. The liquid hydrocarbon is recycled with an air driven Haskel pump to the reactor. The uncondensed gas, hydrogen and hydrogen sulfide, passes through the unit pressure control valve to the wet test meter, which measures the gas flow rate.

The liquid exits the reactor to a high-pressure separator with an overflow pipe positioned inside. Liquid level in the reactor is maintained at the same level as the top of the over-

In Chemical Reaction Engineering—Houston; Weekman, V., et al.;
ACS Symposium Series; American Chemical Society: Washington, DC, 1978.

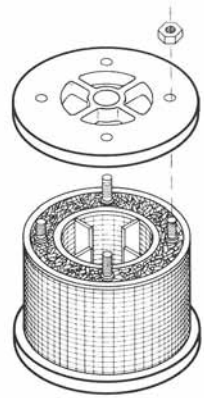

Figure 1. Annular catalyst basket

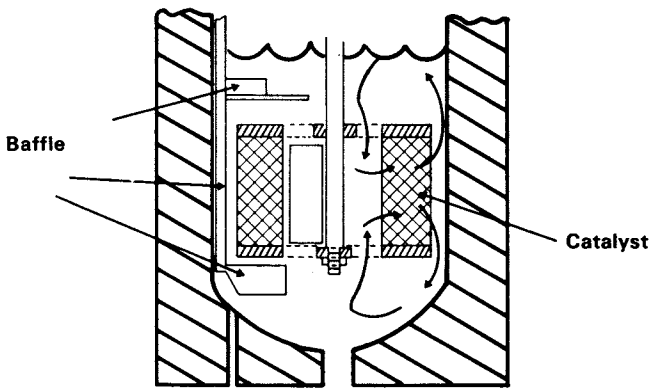

Figure 2. Multiphase spinning basket reactor

In Chemical Reaction Engineering—Houston; Weekman, V., et al.;
ACS Symposium Series; American Chemical Society: Washington, DC, 1978.

flow pipe in the separator. The liquid overflows from the pipe into the body of the separator. The liquid level in the body of the separator is maintained below the top of the overflow pipe.

Results and Discussion

The studies which we will examine can be subdivided into two areas: (1) Development of the reactor system, (2) a kinetic study on the hydrodesulfurization of dibenzothiophene.

Reactor Development--Catalyst Basket. The reactor internals and flow scheme were designed at Amoco Oil Research and Development. Two types of spinning baskets were designed and built, the initial design used a cross-shaped paddle, while a later one adopted an annular shape. The latter improved design was used in all test work.

The improved design was an annular-shaped basket (Figure 1), with a basket capacity of 35 cc (∿25 gm catalyst). The baffle was designed to include a large ring above the basket to prevent vortexing and baffle extensions added below the basket to decelerate the liquid and allow it to enter the middle of the basket. Mixing and contacting performance of the improved basket-baffle design was tested with air and water at ambient pressure and temperature in a plexiglass mockup of the reactor. The plexiglass mockup studies showed the flow patterns satisfied the requirements for effective mixing and contacting in the spinning basket reactor. A high degree of gas entrainment was observed in the liquid phase and resembled a bubble swarm.

Reactor Development--Overall System. A second portion of the overall development was the system design for feeding oil and hydrogen and removing liquid product and off-gas. For analysis of the data, the residence time distribution of the liquid must be clearly defined; the spinning basket reactor should approximate a single backmixed reactor. Highly vaporized feeds work against this objective, however. To maintain the partial pressure of the reaction species (e.g. hydrogen sulfide) at the desired level, hydrogen is constantly fed and withdrawn from the reactor. As hydrogen is withdrawn, so is the vaporized liquid. This results in the residence time of the lighter components being less than the rest of the reaction mixture. To prevent this, vaporized liquid leaving the reactor with the gas stream should be condensed and then recycled back to the reactor. This controls and defines the residence time distribution of the liquid in the reactor by requiring all of it which enters to exit the reactor as liquid assuming hydrocracking reactions are negligible. More specifically, the off-gas is cooled to ambient temperature to condense the light hydrocarbons before being vented. Then the light hydrocarbons are returned to the reactor with an air-driven recycle pump.

In Chemical Reaction Engineering—Houston; Weekman, V., et al.;
ACS Symposium Series; American Chemical Society: Washington, DC, 1978.

Liquid level in the reactor was controlled with an overflow pipe located in an external separator. All liquid then exits through the overflow pipe into the separator; the level is measured with a differential pressure transmitter and maintained slightly below the overflow tip.

Kinetic Study--Dibenzothiophene Desulfurization. Earlier work at Amoco by Frye and Mosby (8) studied the rate of reaction of single sulfur compounds in light catalytic cycle oil. Conclusions from that study were (1) the reaction kinetics are first order in hydrogen and reactant sulfur; (2) hydrogen sulfide inhibits the reaction; (3) overall energy of activation is around 28-30 kcal.

A reaction kinetic study with a model sulfur compound, dibenzothiophehe, was performed in the spinning basket reactor. A mixture of dibenzothiophene in white oil was hydrodesulfurized over a wide range of reaction conditions, varying temperature, pressure, space velocity, and hydrogen sulfide level.

The stoichiometry for hydrodesulfurization of dibenzothiophene may be written as follows:

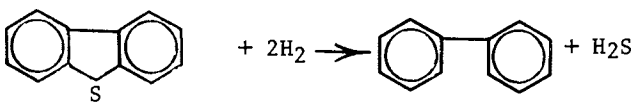

dibenzothiophene biphenyl

The kinetic study of dibenzothiophene desulfurization had two objectives:

1. Evaluate reactor performance to determine the minimum agitation rate which leads to kinetically controlled conditions.
2. Confirm earlier desulfurization kinetics developed by Frye and Mosby on selected sulfur compounds using a trickle bed reactor; refine their kinetic model if necessary.

Agitation Tests. The observed reaction rate should represent the catalytic kinetics unclouded by phenomena such as the transfer of hydrogen at the gas-liquid interface or reaction species through the stagnant film surrounding the catalyst.

The minimum stirring rate is usually established from a simple diagnostic test in which conversion is measured for various levels of agitation. Agitation rate was varied between 500 to 1000 rpm and desulfurization level measured. Results of the agitation tests are listed in Table I. Raising agitation

In Chemical Reaction Engineering—Houston; Weekman, V., et al.;
ACS Symposium Series; American Chemical Society: Washington, DC, 1978.

rate from 500 to 700 rpm increases the desulfurization conversion by 2.6%. By raising the agitation rate further to 1000 rpm, a smaller 1.4% increase in conversion was observed. It was concluded that 750 rpm should be an adequate agitation rate since high speeds put stress on the stirrer mechanism and eventually lead to bearing failure.

TABLE I
EFFECT OF AGITATION RATE ON PERFORMANCE

Feedstock	Press., psig	Temp., °F	WHSV Wo/hr-Wc	Agitation rpm	Desulfurization %
Dibenzothiophene	300	540	2.10	500	68.0
in White Oil	300	540	2.06	750	70.6
.5% S	300	540	2.06	1000	72.0

Kinetic Study. The experimental method consisted of changing a single process variable (such as temperature or total pressure) and then observing the effect on conversion. Generally, the effect of each variable was observed by making two excursions from a set of base conditions. Table II summarizes the experimental results.

TABLE II
DIBENZOTHIOPHENE IN WHITE OIL

Pressure, psig	Temperature, °F	WHSV Wo/hr-Wc	H_2 Rate ft^3/hr	Desulfurization, %
300(*)	540(*)	2.0(*)	0.42(*)	74.6
*	*	6.25	.87	40.0
*	*	1.69	.37	76.5
*	*	.62	.23	94.5
*	523	*	.37	63.0
*	545	*	.46	76.0
*	566	*	.36	89.0
100	*	*	.46	52.0
500	*	*	.40	82.0
*	*	*	.10	62.5
*	*	*	1.5	85.5
*	523	1.17	.31	80.4
*	566	4.4	.99	84.5

*Base Conditions

Kinetic Modelling. If the reaction were strictly first order in dibenzothiophene, then a plot of reaction rate versus

In Chemical Reaction Engineering—Houston; Weekman, V., et al.;
ACS Symposium Series; American Chemical Society: Washington, DC, 1978.

sulfur concentration would yield a straight line. Figure 4 shows that this relationship does not hold. Frequently catalytic kinetics can be described using a Hougan-Watson kinetic model, an extension of the earlier Langmuir-Hinshelwood forms.

The general form of the model parallels the earlier work by Frye and Mosby (8) on single sulfur compounds in petroleum fractions. The basic difference is that competitive adsorption of the reactant is accounted for which helps to describe the non-first order behavior. The kinetic model is

$$-r_{DB} = \frac{k\, P_{DB} P_{H_2}^{\,n}}{(1 + K_{DB}P_{DB} + K_{HS}P_{HS})^{m}}$$

where $-r_{DB}$ = rate of reaction, g moles/sec-gm catalyst
k = rate constant
P_i = partial pressure of species i, atm
K_i = adsorption constant of species i, atm^{-1}
DB = dibenzothiophene
H_2 = hydrogen
HS = hydrogen sulfide
n,m = integer constants, 1 or 2

The two integer constants, n and m, for hydrogen partial pressure and the adsorption term were assigned values of 1 or 2. This results in four possible models to describe the experimental data. The data were fitted with the four models by non-linear regression techniques. The results are summarized in Table III.

TABLE III
KINETIC MODEL SUMMARY

Model	Integer Powers n	m	Fitted Constants $k \times 10^6$	K_{DB}	K_{HS}	Std. Dev. of Rate $\sigma \times 10^8$
A	1	1	4.64	607.9	9.5	.64
B	1	2	2.47	90.0	1.4	.81
C	2	2	.147	89.1	2.7	1.25
D	2	1	.32	671.8	2.2	1.14

Models A and B which were first order in hydrogen partial pressure gave the best fit. Figures 5 and 6 show fitted vs. observed reaction rates for these two models. Furthermore, the statistical significance of the three fitted parameters, k, K_{DB}, and K_{HS}, was considerably better for models A and B. Unfortunately the data do not allow discrimination on the power for the adsorption term.

In Chemical Reaction Engineering—Houston; Weekman, V., et al.;
ACS Symposium Series; American Chemical Society: Washington, DC, 1978.

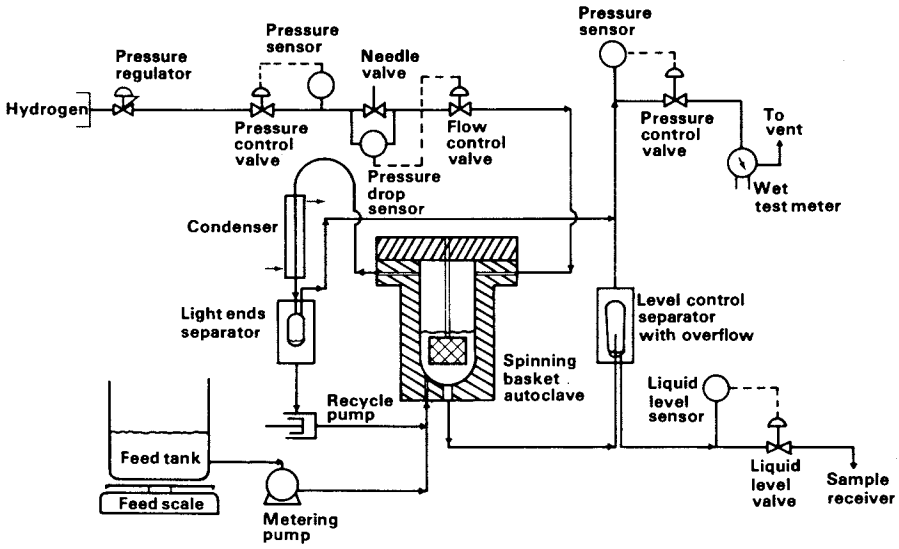

Figure 3. Process flow diagram

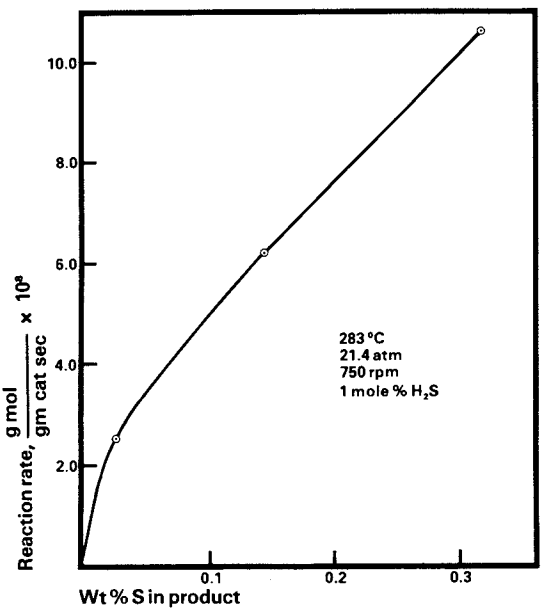

Figure 4. Reaction rate as a function of product sulfur

In Chemical Reaction Engineering—Houston; Weekman, V., et al.;
ACS Symposium Series; American Chemical Society: Washington, DC, 1978.

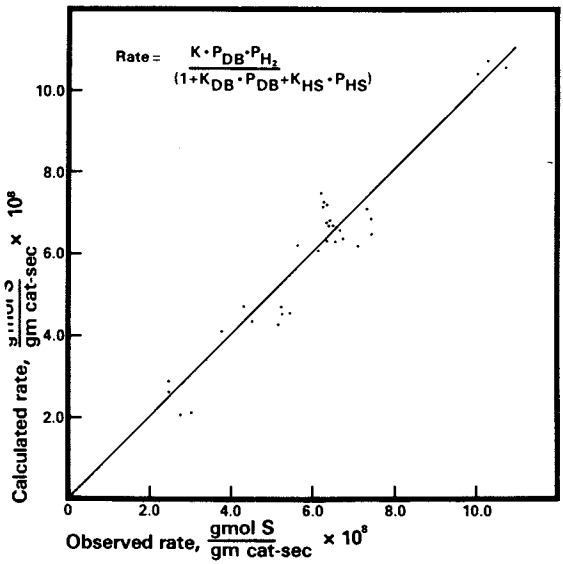

Figure 5. Calculated vs. observed rate—single site model

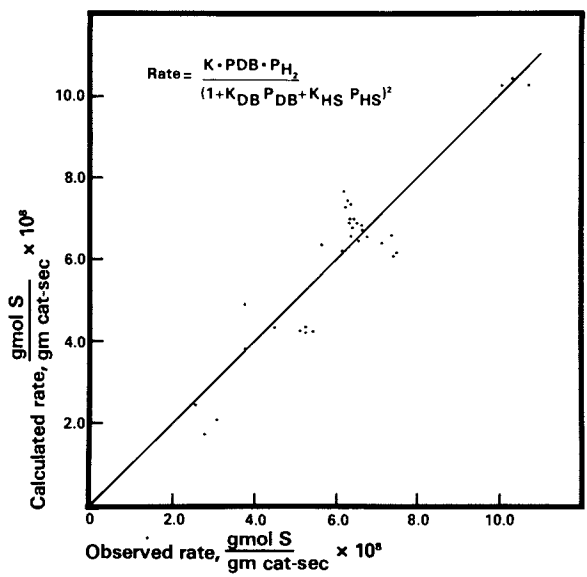

Figure 6. Calculated vs. observed rate—dual site model

In Chemical Reaction Engineering—Houston; Weekman, V., et al.;
ACS Symposium Series; American Chemical Society: Washington, DC, 1978.

An unsuccessful attempt was made to fit the activation energies for the kinetic and adsorption constants. The parameters were all highly intercorrelated since the experiments were not designed to uncouple the temperature effects. As an alternate approach the overall temperature response was determined by plotting rate versus reciprocal temperature in Figure 7 and the slope, $-\Delta E/R$, calculated. Figure 7 shows the overall temperature response by least squares fit to be 28.0 kcal.

The overall energy of activation includes the effect of temperature on the vapor pressure of dibenzothiophene. As discussed by Frye and Mosby (8), the apparent energy of activation for a liquid-vapor system is a combination of several factors which include the adsorption enthalpies of dibenzothiophene and hydrogen, the latent heat of vaporization and the reaction activation energy. If we assume that the enthalpy of vaporization is 13 kcal/mole, then the activation energy is about 15 kcal/mol. This also suggests that film diffusion effects are not controlling the observed reaction rate. With the exception of the reaction order for the dibenzothiophene, good qualitative agreement exists with the results of both studies. The discrepancy in the apparent reaction order could be explained by the differences in the reaction environment. In contrast to white oil, light catalytic cycle oil is highly aromatic. These aromatics competitively adsorb and inhibit the desulfurization reaction. At high aromatics concentration, the dibenzothiophene adsorption would be masked by aromatic adsorption. Apparent first order kinetics with respect to dibenzothiophene would then be observed.

Conclusions

The Amoco annular spinning basket reactor system is a useful tool for studying the fundamental kinetics of liquid-vapor-solid catalyzed reaction systems. We believe it is generally superior to trickle bed systems for the study of pure compound kinetics in liquid-vapor-solid catalyzed systems. A desulfurization kinetic study with dibenzothiophene in white oil was successfully completed. The results of the study compare favorably with an earlier study performed in a trickle bed reactor by Frye and Mosby (8).

Abstract

A spinning basket reactor has been developed for studying multiphase reactions at high pressure. Studies have been performed on the hydrodesulfurization of various petroleum fractions and a model sulfur compound. Hydrogen and liquid feed are continuously fed to the reactor and contacted with the catalyst which is held in a rotating annular basket. The

In Chemical Reaction Engineering—Houston; Weekman, V., et al.;
ACS Symposium Series; American Chemical Society: Washington, DC, 1978.

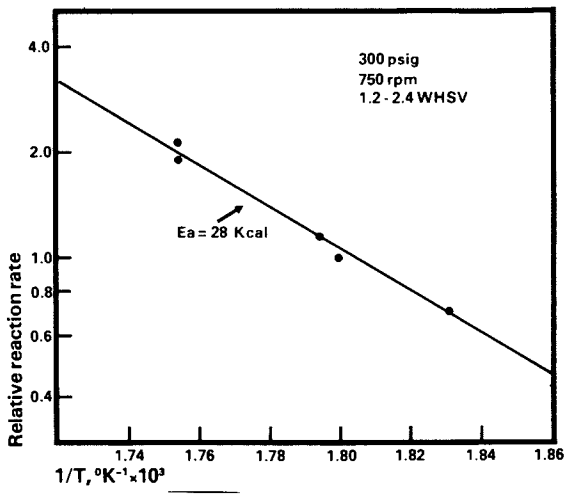

Figure 7. Reaction rate vs. reciprocal temperature

In Chemical Reaction Engineering—Houston; Weekman, V., et al.;
ACS Symposium Series; American Chemical Society: Washington, DC, 1978.

residence time distribution of the oil approximates a single backmixed reactor by recycling the light hydrocarbons which exit in the off-gas stream. A catalyst basket-baffle design was developed which assures good mixing and contacting and eliminates vortexing at the gas-liquid interface. Plexiglass mock-up studies provided guidance in the design of the reactor internals.

Desulfurization kinetics were studied with a model sulfur compound system, a dibenzothiophene in white oil. Tests on basket agitation rate indicate that mass transfer and contacting effects are small above 750 rpm. The reaction kinetics agreed well with earlier work. The Langmuir-Hinshelwood kinetic model was further refined to account for competitive adsorption effects due to dibenzothiophene as well as hydrogen sulfide.

Literature Cited

1. Weekman, V. W., AIChE J., 20, 833 (1974).
2. Carberry, J. J., Ind. Eng. Chem., 56, 39 (1964).
3. Tajbl, D. J.; Simons, J. B.; and Carberry, J. J.; Ind. Eng. Chem. Fundam., 5, 171 (1966).
4. Bennett, C. O.; Cutlip, M. B.; and Yang, C. C.; Chem. Eng. Sci., 27, 2255 (1972).
5. Berty, J., Chem. Eng. Prog., 70, Vol. 6, 78 (1974).
6. Mahoney, J. A., J. of Cat., 32, 247 (1974).
7. Tikhonov, G. F.; Shestov, G. K.; Temkin, O. N.; and Flid, R. M.; "Gradientless Reactor Suitable for Studying the Kinetics of Liquid Phase Reactions in Gas-Liquid Systems," Kinetika, Kataliz, 7, No. 5, 914, Sept-Oct (1966).
8. Frye, C. G., and Mosby, J. F., "Kinetics of Hydrodesulfurization," Chem. Eng. Prog., 63, No. 9, 66 (1967).

In Chemical Reaction Engineering—Houston; Weekman, V., et al.;
ACS Symposium Series; American Chemical Society: Washington, DC, 1978.

38

Carbon Monoxide Oxidation in an Integral Reactor: Transient Response to Concentration Pulses in the Regime of Isothermal Multiplicities

SE H. OH, KENNETH BARON, JAMES C. CAVENDISH, and L. LOUIS HEGEDUS
General Motors Research Laboratories, Warren, MI 48090

The idea of deliberate unsteady state operation of chemical reactors for performance improvement has received considerable attention in the literature of the past decade. Typically, periodic variations of one or more system parameters have been used (e.g., 1, 2, 3, 4). Extensive discussion of this subject is given in the book of Douglas (5) and in a review article by Bailey (6).

Most of the earlier theoretical and experimental studies in the area of unsteady state operation have two common features. First, the parameter variations considered were periodic in nature (i.e., sine wave, square wave, or sawtooth). Secondly, it has been widely assumed, with the exception of recent studies by Sincic and Bailey (7) and Wandrey and Renken (8), that the systems under consideration have a unique (and stable) steady state within the range of parameter variation.

In this paper we investigate the possibility of enhancing the conversion of an isothermal, integral catalytic reactor in the multiple steady state regime by means of a single inlet concentration perturbation. This study is essentially a follow-up of the earlier work by Hegedus et al. (9) on CO oxidation over Pt, where wide ranges of stable steady state multiplicities were observed under isothermal conditions.

Experimental Part

Spherical, alumina-supported Pt catalyst pellets were used in the experiments (see Table I for the catalyst properties). The catalyst was aged for 1000 hours in the exhaust gas of a dynamometer-mounted V-8 automobile engine. The pellets were found to be surrounded by a partially impervious poison layer with a reduced diffusivity (10). A detailed description of the techniques used to characterize the catalyst can be found elsewhere (9).

© 0-8412-0401-2/78/47-065-461$05.00/0

For the catalyst used here, both the noble metal impregnation profile and the poison profile were found to be reasonably sharp along the pellet radius, so that the catalyst pellets can be visualized as a composite material with four different layers, as shown in Fig. 1 (e.g., 10). Zones 2 through 4 of the pellet were originally impregnated by Pt, zone 1 being left unimpregnated. Zone 3 represents a poisoned layer without pore plugging, while zone 4 is partially obstructed (thereby reducing its effective diffusivity) and poisoned. The dimensions of these zones are also given in Table I. We chose such a complex catalyst in this study because this catalyst was shown to exhibit a wide range of steady state multiplicities (9).

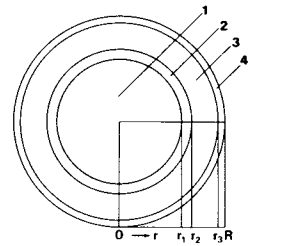

Figure 1. Cross section of an aged catalyst pellet

Table I

Catalyst Properties

Pt (w%)	0.06 (est.)	ρ_s (g/cm^3)	3.61
Pt dispersion (%)	40 (est.)	ρ_p (g/cm^3)	1.16
a_2 (cm^2 Pt / cm^3 pellet)	2352 (est.)	R (cm)	0.1766
Pb (w%)	1.31	r_3 (cm)	0.1759
P (w%)	0.39	r_2 (cm)	0.1753
V_{macro} (cm^3/g)	0.070	r_1 (cm)	0.1562
V_{micro} (cm^3/g)	0.515	$D_1=D_2=D_3$ (cm^2/sec)*	0.0589
$\bar{r}_{macro}$ (Å)	13099	D_4 (cm^2/sec)	0.00393
$\bar{r}_{micro}$ (Å)	220	$\varepsilon_{p,1}=\varepsilon_{p,2}=\varepsilon_{p,3}$	0.679
s (m^2/g)	57	$\varepsilon_{p,4}$	0.045 (est.)

*Computed from the random pore model of Wakao and Smith [Smith (11)], and given here at 1 atm and 838 K. D varies with the 1.4th power of T.

The integral reactor used in our experiments has been described previously (9). The reactive section (total volume 10

In Chemical Reaction Engineering—Houston; Weekman, V., et al.;
ACS Symposium Series; American Chemical Society: Washington, DC, 1978.

cm^3), packed with the Pt-alumina catalyst, was sandwiched between two catalytically inactive SiC layers which serve as a heat transfer medium and also help to provide a fully developed flow pattern through the reactor section. The stainless steel reactor tube was heated to the desired temperature by an electric furnace, and both the inlet and outlet temperatures of the reactive section were monitored using thermocouples. Also, electrochemical and infrared analyzers were used to measure inlet and outlet O_2 and CO concentrations, respectively.

CO concentration pulses were injected to the reactor inlet using four solenoid valves which, when energized, allowed a second (supplemental) CO stream (instead of the main CO stream) to feed the reactor for a predetermined period of time. The pulse amplitudes were varied by adjusting the concentrations in the main and supplemental CO streams. Pressure perturbations during the solenoid operation were negligibly small.

Theoretical Part

In our experiments the inlet CO concentrations were kept low enough (about 0.3 vol. %) to ensure near-isothermal operation. Furthermore, a large excess of O_2 (2 vol. %) was employed; thus we need to consider only the conservation of CO in the mathematical model. While the diffusion-reaction model was found to be adequate in analyzing the steady state behavior of the CO-Pt system (9), in this study we will use a transient model which also includes the accumulation of CO over the catalytic surface.

The importance of including surface phenomena in the transient model of porous catalyst particles has been pointed out, e.g., by Sheintuch and Schmitz (12). Experimental work by Lehr et al. (13) and by Denis and Kabel (14, 15) seems to support this argument. Elnashaie and Cresswell (16, 17) also employed a mathematical model which accounts for adsorption, desorption, and surface reaction in studying porous catalyst pellets.

The balance equation for CO in the intrapellet gas phase is

$$\varepsilon_p(r)\frac{\partial c}{\partial t} = \frac{1}{r^2}\frac{\partial}{\partial r}\left[D(r)r^2 \frac{\partial c}{\partial r} \right] - a(r)\,\tilde{R}_a \qquad (1)$$

where $\tilde{R}_a$ represents the net rate of CO adsorption on the Pt active sites.

The conservation of adsorbed CO over the Pt surface can be expressed, in terms of its surface fractional coverage Θ, as

$$N_s \frac{d\Theta}{dt} = \tilde{R}_a - \tilde{R}_s \qquad (2)$$

where N_s represents the CO concentration over the active sites corresponding to a complete monolayer coverage, and $\tilde{R}_s$ is the rate of the surface reaction. For our computations, N_s was

taken to be 2×10^{-9} mol CO/cm^2 Pt based on the assumption of 1:1 stoichiometry between Pt surface atoms and CO molecules.

The most general case requires solving Eqs. (1) and (2) simultaneously, with the given rate expressions $\tilde{R}_a$ and $\tilde{R}_s$. In the present study, however, the chemisorption process on the Pt surface is assumed to rapidly equilibrate according to the Langmuir isotherm. This assumption seems reasonable because CO adsorption on Pt is a fast, non-activated process (18, 19), and the desorption rate also appears to be reasonably fast at our reaction temperatures [around 200°C or higher (18, 20, 21)].

It is convenient to eliminate $\tilde{R}_a$ between Eqs. (1) and (2) to yield

$$\varepsilon_p(r)\frac{\partial c}{\partial t} + N_s a(r)\frac{d\Theta}{dt} = \frac{1}{r^2}\frac{\partial}{\partial r}\left[D(r)\, r^2 \frac{\partial c}{\partial r} \right] - a(r)\tilde{R}_s \qquad (3)$$

From the Langmuir isotherm relationship

$$\frac{d\Theta}{dt} = \left(\frac{\partial \Theta}{\partial c} \right)\left(\frac{\partial c}{\partial t} \right) = \frac{K}{(1 + Kc)^2}\frac{\partial c}{\partial t} \qquad (4)$$

and thus Eq. (3) becomes

$$\left[\varepsilon_p(r) + N_s a(r) \frac{K}{(1 + Kc)^2} \right] \frac{\partial c}{\partial t} = \frac{1}{r^2}\frac{\partial}{\partial r}\left[D(r) r^2 \frac{\partial c}{\partial r} \right] - a(r)\tilde{R}_s \qquad (5)$$

It should be noted that in deriving Eq. (4), O_2 adsorption on Pt was assumed to be negligibly small compared to CO adsorption.

The dynamic behavior of the individual catalyst pellets can then be simulated by solving Eq. (5) for the four different layers shown in Fig. 1. The boundary conditions for Eq. (5) are

$$\frac{\partial c}{\partial r}(0) = 0 \qquad (6)$$

$$\frac{\partial c}{\partial r}(R) = \frac{k_m}{D(R)}\left[c_\infty - c(R) \right] \qquad (7)$$

In addition, the continuity of both the flux and concentration of CO is imposed at the zone interfaces (that is, $r = r_1$, r_2 and r_3). For the particular catalyst considered here, D, ε_p and a are taken to be piecewise constant with the following properties:

$$D_1 = D_2 = D_3 >> D_4 \qquad (8)$$

$$\varepsilon_{p,1} = \varepsilon_{p,2} = \varepsilon_{p,3} >> \varepsilon_{p,4} \qquad (9)$$

$$a_1 = a_3 = a_4 = 0\ ,\ a_2 = \text{finite} \qquad (10)$$

where the numbers in the subscripts refer to various layers of the catalyst pellet (see Fig. 1).

In Chemical Reaction Engineering—Houston; Weekman, V., et al.;
ACS Symposium Series; American Chemical Society: Washington, DC, 1978.

Independent experiments with a recycle reactor in our laboratory (22) indicated that under similar operating conditions the maximum rate of CO oxidation at 200°C occurs at a CO concentration of 0.04 vol. %. Since it follows directly from the Langmuir isotherm that $\Theta = 0.5$ at the CO concentration corresponding to the peak rate, the adsorption equilibrium constant can be estimated to be

$$K = 3.118 \exp (16000/R_g T) \ , \ \frac{cm^3}{mol} \qquad (11)$$

with the heat of adsorption taken to be 16000 cal/mol (23).

With the assumption of chemisorption equilibrium invoked here, the surface reaction becomes the rate determining step, and thus R_s in Eq. (5) can be reasonably approximated by the empirical rate expression [Eq. (12)] which was found to be adequate in describing the steady state behavior of CO oxidation under our operating conditions (9). That is,

$$\tilde{R}_s \approx \frac{k_o T \exp (-15000/R_g T)\ c\ c_{O_2}}{[1 + 4.5 \times 10^5 T \exp (2000/R_g T) c]^2} \ , \ \frac{\text{mol CO}}{cm^2 \text{ Pt sec}} \qquad (12)$$

where the pre-exponential factor k_o is on the order of 10^{12}.

The system of partial differential equations describing the various layers of the individual pellets [Eqs. (5) through (7)] was first reduced to a large set of ordinary differential equations in the time domain by using Galerkin's method employing piecewise continuous rational basis functions. Galerkin's method of this type has proven to be effective in solving composite catalyst pellet problems (9, 10).

The numerical integration of the resulting set of ordinary differential equations presents a considerable challenge, since the system exhibits a rapid overshoot followed by a slow transient, as will be shown later. Due to the widely different time constants inherent in our problem, we used the GEARIB code (24), which is well suited to handle such stiff problems. The detailed description of the numerical technique can be found elsewhere (25).

The integral reactor was simulated by a cascade of axial mixing cells. The Reynolds number for our typical operating condition is about 50, and the corresponding Peclet number (based on the particle diameter) is about 2 (26). If the number of mixing cells is chosen by $N_{cell} = Pe\ L/4R$, then each layer of pellets amounts to a mixing cell (27). Since our integral reactor is about 8 pellet diameters long, 8 mixing cells were used in the computations.

The conservation equation for CO around the jth mixing cell is

$$Q [c_\infty(j-1) - c_\infty(j)] + 3 k_m V_{cell} \frac{(1-\epsilon)}{R} [c(R, j) - c_\infty(j)] = 0 \qquad (13)$$

In Chemical Reaction Engineering—Houston; Weekman, V., et al.;
ACS Symposium Series; American Chemical Society: Washington, DC, 1978.

This equation allows us to determine the exit concentration of the jth cell, $c_\infty(j)$, from the known inlet concentration $c_\infty(j-1)$ and the solution of the single-pellet equations. It should be noted that the accumulation of mass in the interpellet space was neglected in Eq. (13), since its time constant is typically 80 times smaller than that of the intrapellet transients. The external mass transfer coefficient of CO, k_m, of Eqs. (7) and (13) was estimated from the de Acetis-Thodos correlation, as given in Smith (11).

Results and Discussion

It has been shown in the earlier paper (9) that isothermal CO oxidation over Pt-alumina catalysts with appreciable intrapellet diffusion resistances can exhibit a wide range of steady state multiplicities in the conversion-temperature, conversion-inlet CO concentration, and conversion-mass flow rate domains. Fig. 2 shows the steady state CO conversion as a function of reactor inlet temperature for a fixed set of concentrations (~0.3 vol. % CO, ~2 vol. % O_2). The details of the experimental conditions of Fig. 2 and the subsequent figures are given in Table II. Hegedus et al. (9) pointed out that the hysteresis envelope shown in Fig. 2 corresponds to the highest and lowest stable steady state conversions, and also demonstrated the existence of several intermediate stable steady states within the envelope of the hysteresis loop. They also have shown that each of these multiple conversion levels can be achieved by a properly chosen sequence of steady state operations.

Table II

Description of Various Experimental Conditions

	Fig. 2	Fig. 3	Figs. 4, 5	Figs. 6, 7
k_o	-	-	1.07×10^{12}	1.10×10^{12}
T_{in} (°C)	varies	varies	212	212
ϵ	0.4	0.4	0.4	0.4
$c_{O_2,in}$ (%)	2.07	2.01	2.02	2.00
c_{in} (%)	0.297	0.316- 0.108- 0.316	varies	0.321- 0.076- 0.321
Pulse Duration (sec)	-	3	3	varies
Q_p (g/sec)	0.089	0.094	0.094	0.093

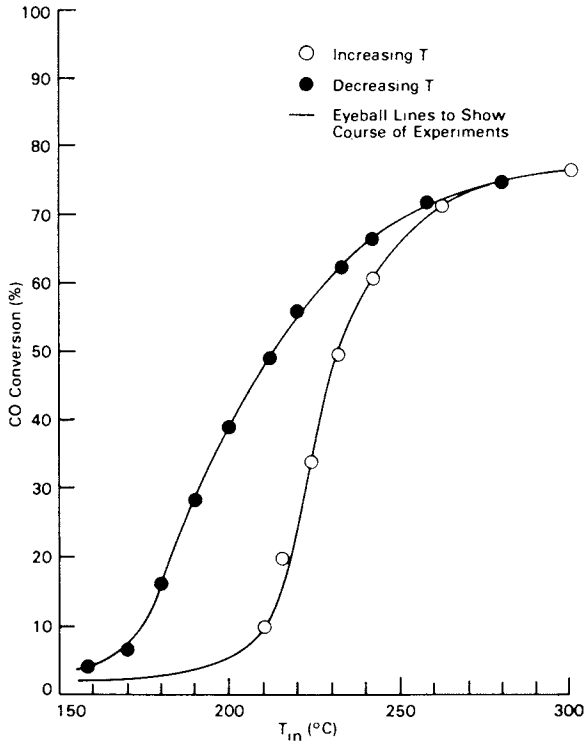

Figure 2. Steady state hysteresis in the conversion-inlet temperature domain

In Chemical Reaction Engineering—Houston; Weekman, V., et al.;
ACS Symposium Series; American Chemical Society: Washington, DC, 1978.

In the present study we investigate the possibility of enhancing the reactor conversion in the regime of multiple conversions by means of deliberate perturbations of the initial steady state. For all the results reported here, the reactor was initially set to operate at the lowest conversion steady state, and the reactor inlet CO concentration was perturbed by temporarily reducing the CO concentration to a lower value, while maintaining the total flow rate, the reactor pressure, and oxygen concentration essentially unperturbed. Before each pulse, the reactor was cooled down to a temperature well below the hysteresis loop of Fig. 2 and then slowly heated up to a desired temperature to establish the lowest conversion state.

Fig. 3 shows the steady state conversion data at various temperatures before and after the inlet concentration pulse. In this experiment, the inlet CO concentration was reduced from 0.316 vol. % to 0.108 vol. % for the duration of 3 sec. It can be readily seen that the steady state conversion is enhanced upon pulsing in the multiple conversion regime, while the reactor quickly returns to the original conversion level at temperatures outside the hysteresis loop (e.g., T_{in} = 145°C or 299°C).

It is interesting to note that the hysteresis loop of Fig. 2 can be made to superimpose reasonably well with Fig. 3 if the latter is shifted to the left by approximately 10°C along the temperature axis. This small shift of the hysteresis loop (without changing its shape or area significantly) seems to be associated with the difficulty in exactly reproducing the chemical state of the catalyst at the beginning of each experiment. Allowing for this, the data of Fig. 3 may be taken to represent the outer boundaries of the hysteresis envelope.

In order to examine in more detail the conversion enhancement in the multiple conversion regime, we investigated the effects of pulse amplitude and duration at a temperature which falls in the middle of the hysteresis loop in the conversion-temperature plane (see Fig. 2). Fig. 4 shows the observed time variations of CO conversion for various pulse amplitudes at T_{in} = 212°C. In each case of Fig. 4, a pulse of 3 sec duration was injected at time t = 0 to the reactor which had been previously stabilized at the lowest conversion steady state. As expected, the degree of conversion enhancement was found to increase with increasing pulse amplitudes. Also, it appears that the reactor already attained the highest conversion level (about 40%) with the pulse amplitude of 0.321-0.076-0.321, and thus the even larger pulse amplitude of 0.317-0-0.317 did not provide any further conversion enhancement.

The computational results shown in Fig. 5 are in reasonably good agreement with the experimental data of Fig. 4, except at the early portion of the transients. It can be seen that the transient model predicts a larger overshoot followed by a somewhat faster stabilization to a new conversion level when compared with the experimental data. This difference in time be-

In Chemical Reaction Engineering—Houston; Weekman, V., et al.;
ACS Symposium Series; American Chemical Society: Washington, DC, 1978.

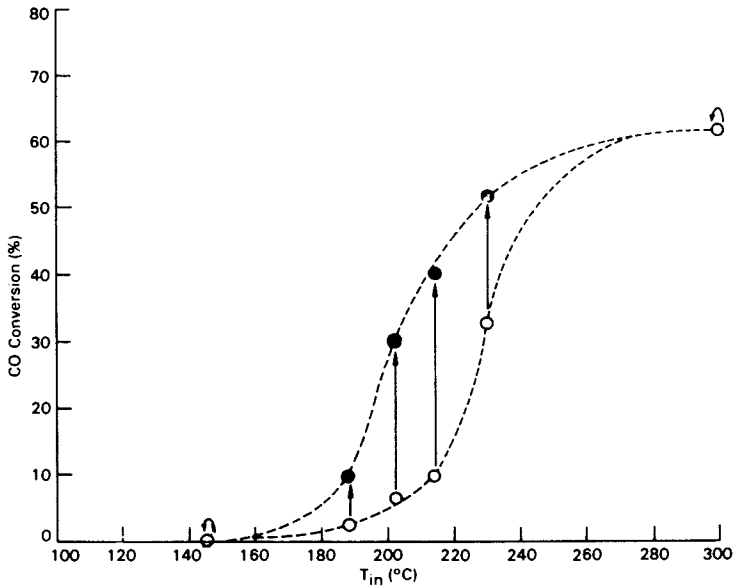

Figure 3. Steady state conversion performance with pulsing at various temperatures. Pulse amplitude = 0.316–0.108–0.316. Pulse duration = 3 sec.

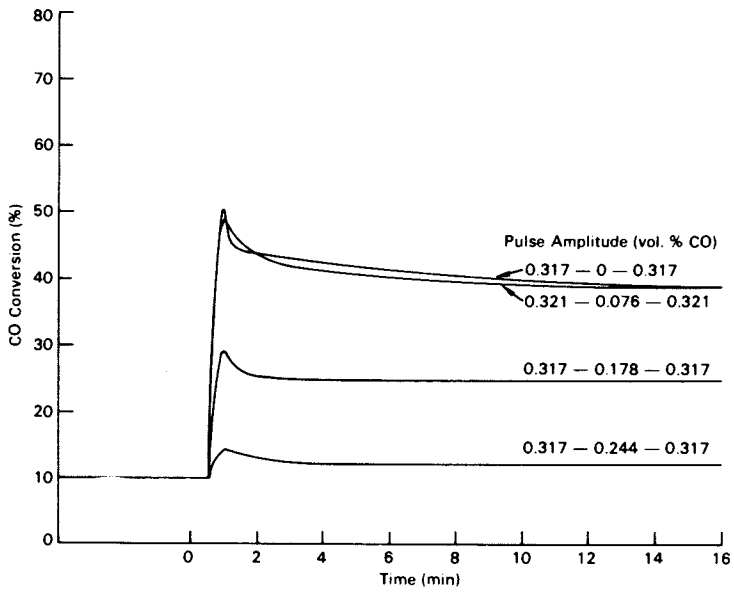

Figure 4. Effects of pulse amplitude on conversion enhancement (experiments). Pulse duration = 3 sec. T_{in} = 212°C.

In Chemical Reaction Engineering—Houston; Weekman, V., et al.;
ACS Symposium Series; American Chemical Society: Washington, DC, 1978.

havior may be attributed to the nonidealities of our experimental system, such as the transportation lag (about 30 sec, see Fig. 4) and signal dispersion effects between the reactor exit and the CO analyzer, and within the CO analyzer. Therefore, no attempts were made in this study to match the transient response of the early period (i.e., near t = 0) during which rapid changes in CO concentration occur. Instead, we focused our attention on the ultimate steady state which the system assumed as the result of the perturbation.

Although only three different conversion levels are shown in Fig. 5, computations with other pulse amplitudes indicated that conversion enhancement to other intermediate conversion levels is also possible. For example, with a pulse amplitude of 0.317-0.174-0.317, the model predicted a final CO conversion of 30.9%.

We also conducted some experiments at the same inlet temperature as before (T_{in} = 212°C) to investigate the effects of pulse duration. The pulse amplitude of 0.321-0.076-0.321 was used, and the experimental data are shown in Fig. 6 for various values of pulse duration. Conversion enhancement was observed for the durations of 1 sec or longer, and virtually no further enhancement was achieved when the pulse duration was increased beyond 2 sec.

The simulation results shown in Fig. 7 provide a good qualitative comparison with the experimental data of Fig. 6. The curve for the pulse durations of 2 sec and 6 sec exhibits a slower response than the other curves for shorter durations. This behavior seems to be consistent with the experimental observation (Fig. 6). The computed reactor response with the pulse duration of 1.05 sec is also included in Fig. 7 to show the sensitivity of the system and to illustrate the existence of some additional intermediate stable steady states.

It is of interest to discuss the predictions of a diffusion-reaction model which accounts for no surface accumulation phenomena [that is, the model with N_S = 0 in Eq. (5)]. We found that such a model was inadequate in describing the transient behavior of our system: the simulation based on the operating conditions of Fig. 6 predicted a conversion enhancement to the highest conversion level even with the very short pulse duration of 0.25 sec. In view of the small characteristic response time (about 0.1 sec) for intrapellet diffusion, surface phenomena seem to play a key role in determining the transient response of supported catalysts (12, 14, 15, 28). This, of course, does not invalidate the use of the simpler diffusion-reaction model for the description of steady state behavior, as shown in our previous paper (9).

To our knowledge, the present work is the first observation of conversion enhancement upon perturbations in the regime of isothermal steady state reactor multiplicities, although transitions between stable steady states have been reported by

In Chemical Reaction Engineering—Houston; Weekman, V., et al.;
ACS Symposium Series; American Chemical Society: Washington, DC, 1978.

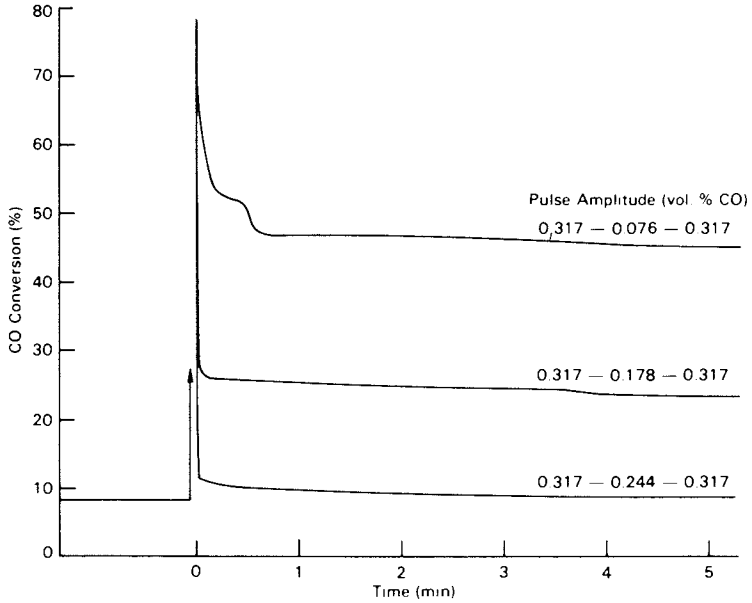

Figure 5. Effects of pulse amplitude on conversion enhancement (theory). Pulse duration = 3 sec. T_{in} *= 212°C.*

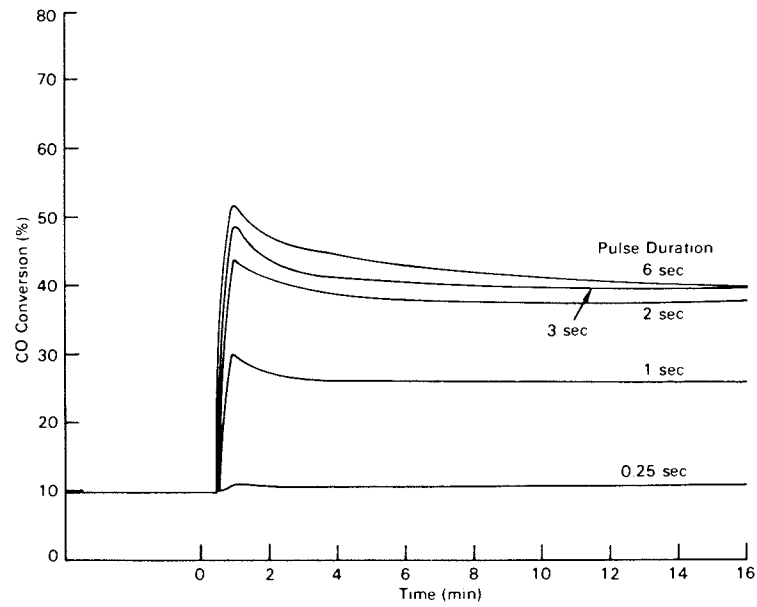

Figure 6. Effects of pulse duration on conversion enhancement (experiments). Pulse amplitude = 0.321–0.076–0.321. T_{in} *= 212°C.*

In Chemical Reaction Engineering—Houston; Weekman, V., et al.;
ACS Symposium Series; American Chemical Society: Washington, DC, 1978.

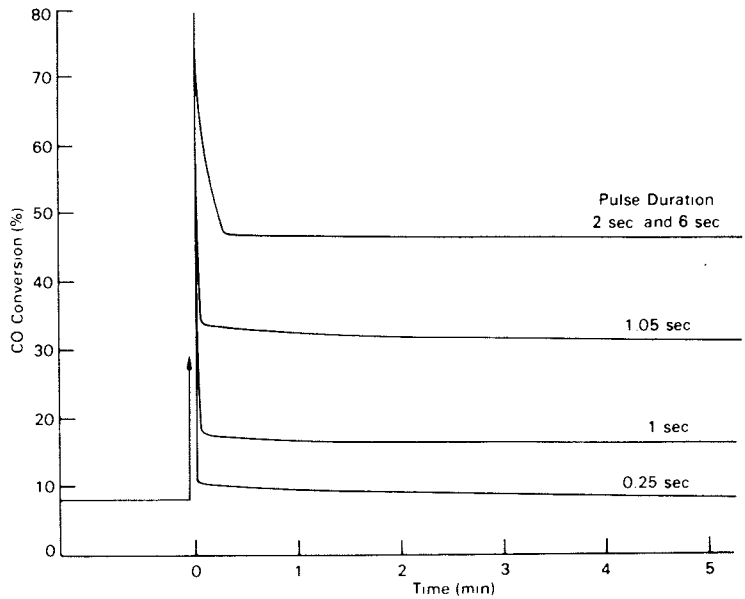

Figure 7. Effects of pulse duration on conversion enhancement (theory). Pulse amplitude = 0.321–0.076–0.321. T_{in} *= 212°C.*

Root and Schmitz (29), and Votruba et al. (30) for adiabatic reactor systems. Adiabatic reactor multiplicities were also investigated by Aris and Schruben (31), who computed the ultimate conversions achieved from various initial conditions.

Besides its practical implications in improving reactor conversion performance by deliberate inlet concentration perturbations, this study also serves to confirm the existence of the isothermal reactor multiplicities and the intermediate stable steady states reported in our earlier paper (9).

Acknowledgement

The reactor experiments were carried out by E. Miller.

Nomenclature

a (cm^2 Pt/cm^3 pellet)	local Pt surface area
c (mol/cm^3)	CO concentration in the intrapellet gas phase
c_{O_2} (mol/cm^3)	O_2 concentration
c_∞ (mol/cm^3)	CO concentration far away from catalyst pellet
D_i (cm^2/sec)	effective diffusivity of CO in Zone i
k_m (cm/sec)	mass transfer coefficient of CO
k_o	kinetic pre-exponential in Eq. (12)
K	CO adsorption equilibrium constant
L (cm)	length of the integral reactor
N_{cell}	number of mixing cells
N_s (mol/cm^2 Pt)	saturation CO concentration of active sites
Pe	Peclet number
Q (cm^3/sec)	gas volumetric flow rate
$\bar{r}_{macro\ or\ micro}$ (Å)	integral averaged pore radii
r (cm)	pellet radial coordinate
R (cm)	pellet radius
$\tilde{R}_a$ (mol/cm^2 Pt sec)	net rate of CO adsorption on Pt
$\tilde{R}_s$ (mol/cm^2 Pt sec)	surface reaction rate
R_g	gas constant
s (m^2/g)	BET surface area of support
t (sec)	time
T (K or °C)	temperature
V_{cell} (cm^3)	volume of a mixing cell
$V_{macro\ or\ micro}$ (cm^3/g)	pellet macro or micro pore volumes

$\epsilon_{p,\,i}$	pellet void fraction in Zone i
ρ (g/cm^3)	gas density
ρ_p (g/cm^3 pellet)	pellet density
ρ_s (g/cm^3 solid)	pellet solid density
Θ	fractional surface coverage of CO

Literature Cited

1. Douglas, J. M., D. W. T. Rippin, Chem. Eng. Sci. (1966), 21, 305.
2. Douglas, J. M., Ind. Eng. Chem. Proc. Des. Devel. (1967), 6, 43.
3. Lee, C. K., J. E. Bailey, Chem. Eng. Sci. (1974), 29, 1157.
4. Wandrey, C., A. Renken, GVC/AIChE Joint Meeting (1974), 1, A3-3.
5. Douglas, J. M., "Process Dynamics and Control," Prentice-Hall, Englewood Cliffs, N.J., 1972.
6. Bailey, J. E., Chem. Eng. Commun. (1973), 1, 111.
7. Sincic, D., J. E. Bailey, Chem. Eng. Sci. (1977), 32, 281.
8. Wandrey, C., A. Renken, Chem. Eng. Sci. (1977), 32, 448.
9. Hegedus, L. L., S. H. Oh, K. Baron, AIChE J. (1977), in press.
10. Hegedus, L. L., J. C. Cavendish, Ind. Eng. Chem. Fund. (1977), in press.
11. Smith, J. M., "Chemical Engineering Kinetics," McGraw-Hill, New York, 1970.
12. Sheintuch, M., R. A. Schmitz, Cat. Rev.-Sci. Eng. (1977), in press.
13. Lehr, C. G., S. Yurchak, R. L. Kabel, AIChE J. (1968), 14, 627.
14. Denis, G. H., R. L. Kabel, AIChE J. (1970), 16, 972.
15. Denis, G. H., R. L. Kabel, Chem. Eng. Sci. (1970), 25, 1057.
16. Elnashaie, S. S. E. H., D. L. Cresswell, Can. J. Chem. Eng. (1973), 51, 201.
17. Elnashaie, S. S. E. H., D. L. Cresswell, Chem. Eng. Sci. (1974), 29, 753.
18. Hayward, D. O., B. M. W. Trapnell, "Chemisorption," Butterworths, London, 1964.
19. Morgan, A. E., G. A. Somorjai, J. Chem. Physics (1969), 51, 3309.
20. Bonzel, H. P., J. J. Burton, Surf. Sci. (1975), 52, 223.
21. Bonzel, H. P., R. Ku, Surf. Sci. (1972), 33, 91.
22. Chou, T. S., J. C. Schlatter, unpublished results, 1976, General Motors Research Laboratories.
23. Hori, G. K., L. D. Schmidt, J. Catalysis (1975), 38, 335.
24. Hindmarsh, A. C., Lawrence Livermore Laboratory Report UCID 30130, 1976.
25. Cavendish, J. C., S. H. Oh, to be presented in 70th Annual Meeting of AIChE, New York, November 1977.
26. Froment, G. F., Adv. in Chem. Series (1972), 109, 1.
27. Wei, J., Adv. in Catalysis (1975), 24, 57.
28. Unni, M. P., R. R. Hudgins, P. L. Silveston, Can. J. Chem. Eng. (1973), 51, 623.
29. Root, R. B., R. A. Schmitz, AIChE J. (1969), 15, 670.
30. Votruba, J., V. Hlavacek, J. Sinkule, Chem. Eng. Sci. (1976), 31, 971.
31. Aris, R., D. L. Schruben, Chem. Eng. J. (1971), 2, 179.

In Chemical Reaction Engineering—Houston; Weekman, V., et al.;
ACS Symposium Series; American Chemical Society: Washington, DC, 1978.

Limit Cycle Phenomena during Catalytic Oxidation Reactions over a Supported Platinum Catalyst

M. B. CUTLIP
Department of Chemical Engineering, University of Connecticut, Storrs, CT 06268

C. N. KENNEY
Department of Chemical Engineering, University of Cambridge, Cambridge, England CB2 3RA

Oscillatory phenomena during isothermal or nearly isothermal catalytic reactions have been observed for carbon monoxide and hydrogen oxidation over various forms of platinum catalysts. Recent research has concentrated mainly on carbon monoxide oxidation perhaps as a result of continuing interest in automotive emission control and the rather unique aspects of this reaction.

Carbon monoxide oxidation over platinum is discussed in considerable detail by Wei (1) and Carberry (2). The kinetics are unusual in that the rate is first order with respect to carbon monoxide at low concentrations and negative first order at high concentrations. There is general agreement with the following sequence of elementary steps involved in this reaction:

$$CO + S \underset{k_{-1}}{\overset{k_1}{\rightleftarrows}} CO - S \qquad \text{step (1)} \qquad (1)$$

$$O_2 + 2S \underset{k_{-2}}{\overset{k_2}{\rightleftarrows}} 2\,O - S \qquad \text{step (2)} \qquad (2)$$

$$CO - S + O - S \xrightarrow{k_3} CO_2 + 2S \qquad \text{step (3)} \qquad (3)$$

$$CO + O - S \xrightarrow{k_4} CO_2 + S \qquad \text{step (4)} \qquad (4)$$

where S in step (1) represents two platinum surface atoms for a bridged adsorbed CO species and one surface atom for a linear adsorbed CO species. It is well known that steps (1) and (2) are very nearly irreversible at low temperatures as they are the basis for platinum titration procedures which utilize hydrogen (3) and carbon monoxide (4). Unfortunately there is little agreement as to the relative importance of carbon dioxide production via the Langmuir-Hinshelwood step (3) and the Eley-Rideal step (4).

A thorough review of multiplicity and oscillatory phenomena

© 0-8412-0401-2/78/47-065-475$05.00/0

by Schmitz (5) summarizes the previous work prior to 1974. Limit cycles have recently been observed for carbon monoxide oxidation by McCarthy (6) using supported platinum on α alumina pellets and by Plichta (7) using platinum foil. Gradientless reactors were used in both studies, and transients in product CO_2 were observed by continuous infrared analysis.

Attempts at modeling the oscillations by using steps (1) - (4) with idealized kinetics have not been successful. Plichta (7) obtained oscillations by considering step (1), step (2) and step (4) where the activation energy of step (4) was assumed to be linearly dependent upon the surface coverage of the adsorbed atomic oxygen. Unfortunately the resulting model did not satisfactorily represent the results. Pikios (8) analyzed a kinetic scheme similar to steps (1) to (3) and also assumed changes in activation energy of step (3) due to surface coverage in order to obtain oscillations. Eigenberger (9) has shown with a modeling approach that oscillations may result when a non-reactive species reversibly adsorbs on the catalyst surface. Thus an additional step may be considered for carbon monoxide oxidation as follows:

$$A + S \underset{k_{-5}}{\overset{k_5}{\rightleftarrows}} A - S \qquad \text{Step (5)} \qquad (5)$$

where A is a species such as O_2 which reversibly chemisorbs but does not react.

Experimental Considerations

Reactor System. A general purpose reactor system shown in Figure 1 was used in this work to study catalytic oxidation reactions over supported platinum catalyst pellets. This equipment allowed up to six precise gas mixtures to be prepared and made available for feed to the reactor. The switching valve directed a desired gas mixture flow to the reactor while another gas mixture flow was precisely measured by the bubble flow meter. A switch interchanged the reactor and flow meter streams so that the reactor could be subjected to step changes in flow and/or composition enabling a wide variety of experiments to be performed.

The reactor was made from a 304 stainless-steel cylinder 69.8 mm in diameter and 50.8 mm in length. The catalyst pellets were placed in seven 9.53 mm in diameter holes in the cylinder and were retained by screens. The two end closures were sealed by standard copper vacuum gaskets which were gold plated.

A metal bellows recycle pump described by Hanson (10) was used to maintain a recycle ratio in excess of 30 to 1 so that completely mixed or gradientless reactor performance was obtained. The reactor, metal bellows pump, and recycle lines were contained in a forced convection oven held at the reaction temperature. An orifice plate in the recycle line enabled the recycle ratio to be measured by a pressure transducer. Reactor/recycle line gas volume was found to be 52 cm^3.

In Chemical Reaction Engineering—Houston; Weekman, V., et al.;
ACS Symposium Series; American Chemical Society: Washington, DC, 1978.

Inlet and outlet analyses were obtained by an on-line magnetic-deflection mass spectrometer equipped with a fast response continuous inlet system. An electronic peak select unit allowed up to four mass numbers to be continuously monitored.

Catalyst. The catalyst was 10g of 0.5% platinum by weight, deposited on the surface of 1/8 inch in diameter γ alumina pellets and obtained from Engelhard Ltd., Cinderford, England. The properties of the catalyst are summarized in Table I. Catalyst deactivation was not observed during the experimental studies.

Experimental Results

Steady State Multiplicity During CO Oxidation. Rates were measured for various oxygen-rich feed compositions at a fixed feed flow rate of 100 cm^3/min. Regions of multiple steady state reaction rates were determined by maintaining feed composition and flow rate constant and varying the reactor temperature in a programmed manner.

Typical results for a 2% CO and 3% O_2 in argon feed composition are shown in Figure 2. This hysterisis curve was generated by starting at a low temperature and obtaining rates at increasing temperatures until the temperature at which the rate jumped to the high rate. The reactor was then slowly cooled for additional rate measurements to the temperature at which the high rate was extinguished. These "jump" temperatures result when the fractional surface coverages of adsorbed carbon monoxide and oxygen undergo dramatic changes. Cutlip (11) has discussed these results in more detail. All combinations of feed compositions between 0.5 to 3% CO and 2 to 4% O_2 exhibited regions of steady state multiplicity bounded by varying jump temperatures.

At any temperature in the region of the two steady states, the low rate could also be established by switching to the reactor a mixture of 10% CO in argon until the catalyst was saturated with the CO, then switching to the feed mixture. Pretreatment with 5% O_2 in argon until CO_2 was no longer produced gave the high rate steady state. These results indicate that the initial coverages of the platinum surface dictate the final rate in the multiple steady state region with the low rate occuring at high coverages of carbon monoxide and the high rate occuring at high coverages of oxygen.

External gradients were experimentally eliminated by increasing the recycle ratio until the characteristic "jump" temperatures were no longer affected. Extensive calculations of interphase and intraphase heat and mass transfer also indicate the absence of gradients.

It is significant that no oscillations were observed when

In Chemical Reaction Engineering—Houston; Weekman, V., et al.;
ACS Symposium Series; American Chemical Society: Washington, DC, 1978.

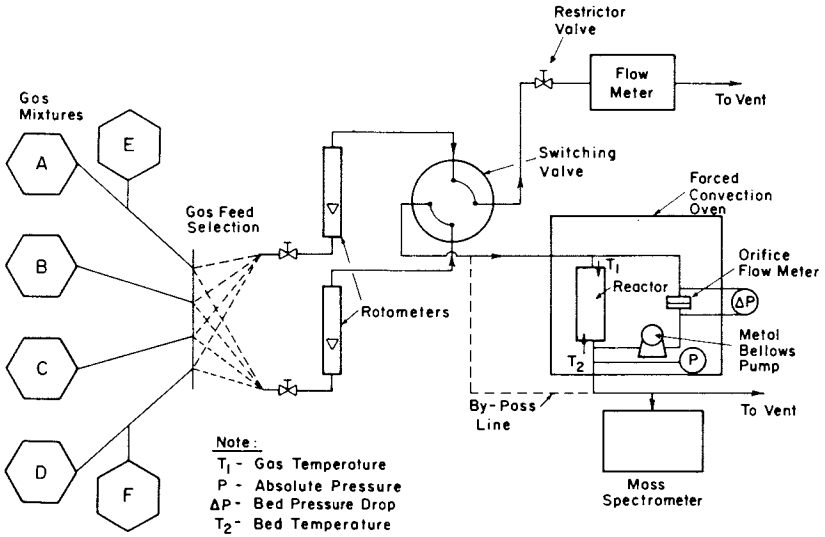

Figure 1. Experimental system

Table I - Catalyst Properties

Platinum Dispersion	
A. H_2 Chemisorption	46.7 ± 3.7%
B. H_2 Desorption	48.0%
C. CO Titration in Situ (4)	43%
D. Thickness of Impregnated Layer	0.03 mm
BET and Pore Size Determinations	
A. Average Pore Radius	20.1 Å
B. Total Pore Volume	.23 cm^3/g
C. Σ Pore Areas	212 m^2/g
D. BET Area	227 m^2/g
Pellet Density	1.98 g^2/cm^3

In Chemical Reaction Engineering—Houston; Weekman, V., et al.;
ACS Symposium Series; American Chemical Society: Washington, DC, 1978.

the reactor was operated in a gradientless manner. This may be due to the low experimental turnover rates of this work which tend to minimize undesirable gradients. A comparison of turnover rates is given in Table II. Anomalous oscillations were occasionally noted when recycle rates were low or when it was thought that trace hydrocarbons were inadvertently added to the recycle stream from the surfaces of new metal tubing or fittings.

Table II - Approximate Turnover Rate Comparison

	Rate (molecules / sec site)	Temperature (°C)	Ratio to This Work
This Work	.01	130	1
Plichta (7)	.60	230	60
McCarthy (6)	40	210	4000

Limit Cycles During Simultaneous CO and 1 - Butene Oxidation. Subsequent rate measurements were made for a mixture of 2% CO, 3% O_2 and 1% 1-butene in argon. As this mixture was introduced to the reactor at temperatures above the previously determined multiple steady state region, very dramatic concentration oscillations were obtained as shown in Figure 3 for a temperature of 150°C and a feed rate of 100 cm^3/min at NTP. This limit cycle was characterized by a periodic rapid rate of oxidation of CO and 1-butene with a period of 31 minutes yielding minima in the reactant concentrations and a corresponding maximum in product CO_2 concentration. The spontaneous oscillations once established were quite reproducible with only minor variations attributed to flow rate and temperature fluctuations. Gas phase temperature variations within the reactor were not detected.

The effect of temperature was investigated with increments of 5°C increases from the 150°C base temperature at a fixed feed rate of 100 cm^3/min. At 160°C, the period and amplitudes of the oscillations were decreased as indicated in Figure 4. The time-averaged rates of both CO and 1-butene oxidation were increased, and the oscillations became more sinusoidal. At 165°C oscillation amplitudes were very small and the period was reduced to 0.78 minutes. Thus it is apparent that temperature has a very strong influence on the oscillations.

The reactor space time was also varied at the base temperature of 150°C. Figure 5 shows the oscillations obtained when the flow was reduced from 100 cm^3/min to 75 cm^3/min at NTP. Two relative maxima per cycle are evident for all of the reacting species and product CO_2. Further reduction of the feed flow rate to 60 cm^3/min at NTP yielded the complex limit

In Chemical Reaction Engineering—Houston; Weekman, V., et al.;
ACS Symposium Series; American Chemical Society: Washington, DC, 1978.

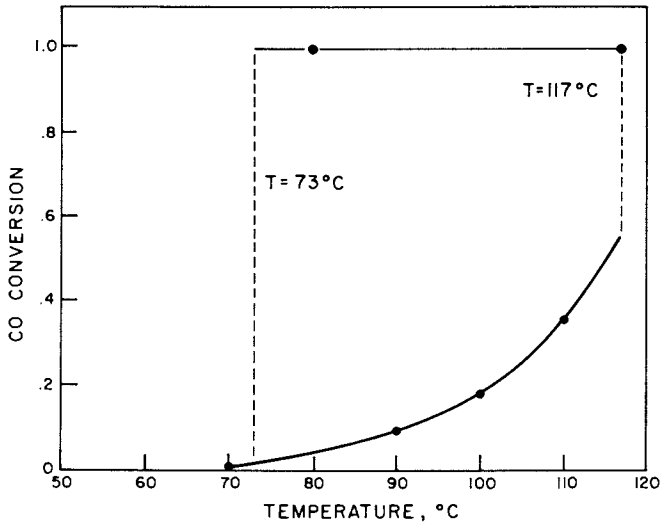

Figure 2. Multiple steady states for 2% CO, 3% O_2 feed at 100 cm^3/min NTP

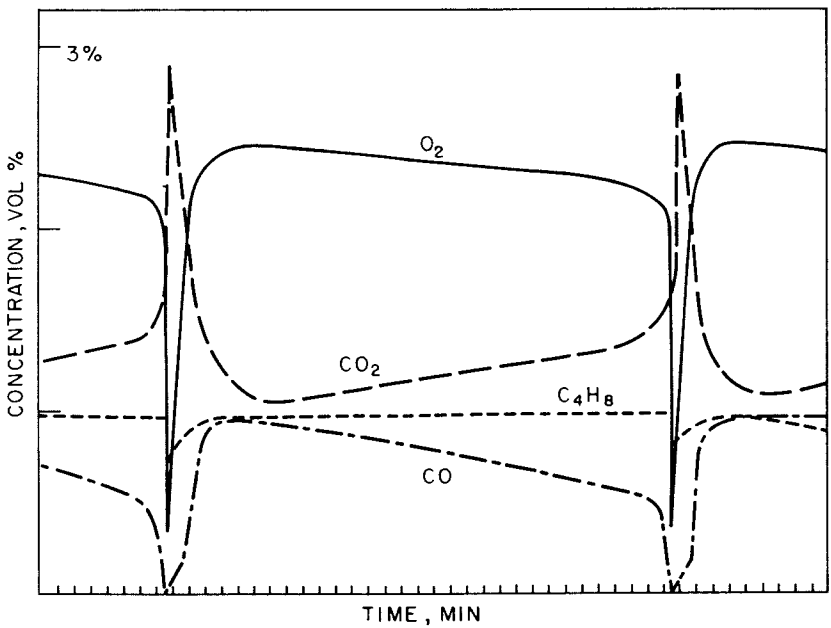

Figure 3. Oscillations at T = 150°C and feed at 100 cm^3/min NTP

In Chemical Reaction Engineering—Houston; Weekman, V., et al.;
ACS Symposium Series; American Chemical Society: Washington, DC, 1978.

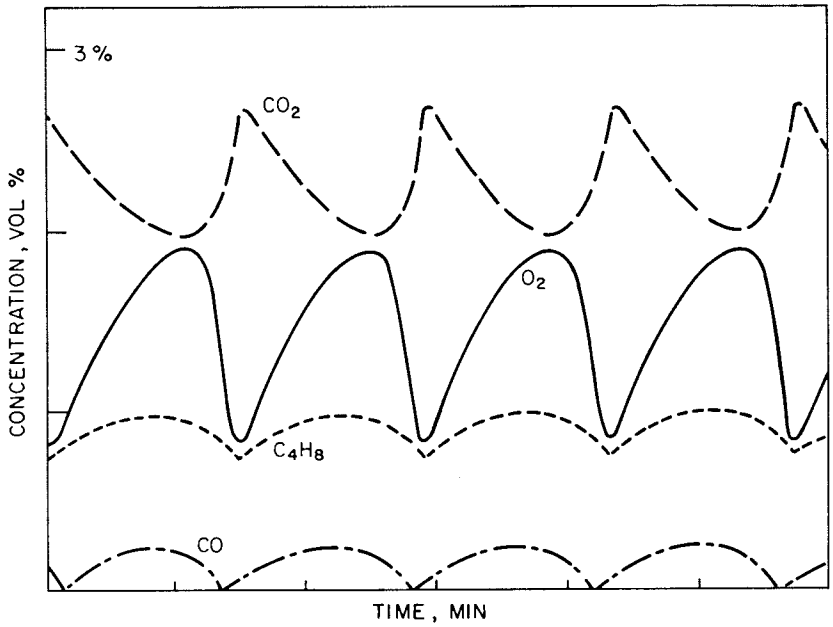

Figure 4. Oscillations at T = 160°C and feed at 100 cm³/min NTP

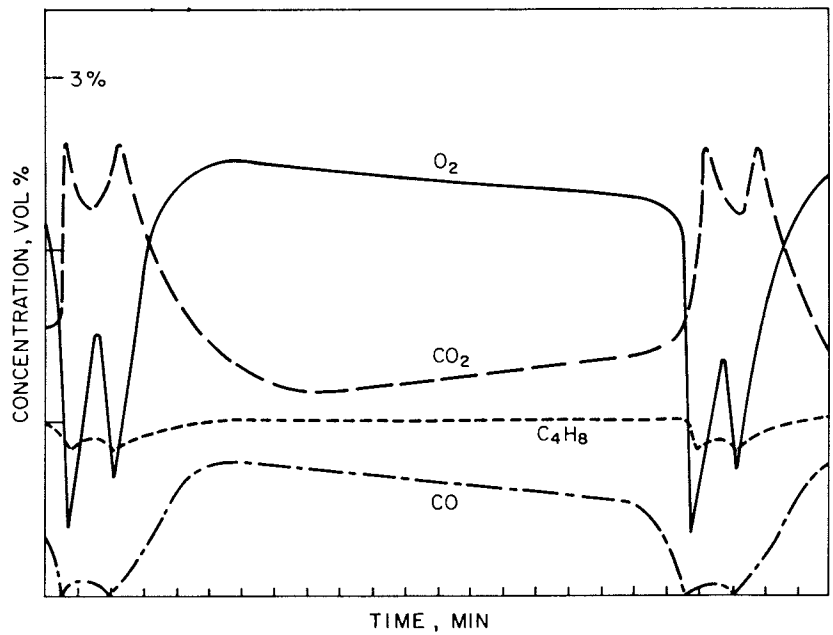

Figure 5. Oscillations at T = 150°C and feed at 75 cm³/min NTP

In Chemical Reaction Engineering—Houston; Weekman, V., et al.;
ACS Symposium Series; American Chemical Society: Washington, DC, 1978.

cycle of Figure 6 where seven relative maxima per cycle were found.

Additional experimental data are summarized in Table III in order of increasing flow rate at NTP for the 2% CO, 3% O_2 and 1% 1-butene in argon feed mixture. These experimental results in the regions of oscillations indicated that at fixed reactor space time, higher temperatures resulted in period and amplitude decreases for all components of the reacting system. At constant temperature, space time decreases also resulted in period and amplitude decreases. The time-averaged rates of oxidation of both CO and 1-butene increased with temperature and with reduction in space time. Reactor material balances suggested that 1-butene oxidation was essentially complete to CO_2 and H_2O.

Discussion of Results

These oscillatory phenomena are best understood by first considering the steady state multiplicity which is observed in the absence of 1-butene.

Our interpretation is that carbon monoxide is very strongly adsorbed at the lower temperatures, and thus almost completely covers the platinum surface. As the reactor temperature is slowly increased, more and more oxygen is adsorbed. Thus the overall reaction rate increases gradually until the surface reaction of equation (3) achieves a critical rate causing the various elementary steps to collectively produce a high overall rate where most of the carbon monoxide is removed from the reactor. At this point the catalyst has appreciable coverage of adsorbed oxygen, little adsorbed carbon monoxide and a significant proportion of vacant sites. As the reactor is cooled, the high rate continues but falls gradually until the rate is reduced sufficiently for carbon monoxide to again be chemisorbed in sufficient amounts to extinguish the reaction rate.

A proposed explaination for the oscillations during the introduction of 1-butene requires significant adsorption of the 1-butene on the platinum:

$$B + S \underset{k_{-5}}{\overset{k_5}{\rightleftarrows}} B\text{-}S \qquad \text{step (5)} \qquad (6)$$

where B refers to the 1-butene. At low temperatures, the 1-butene covers some of the platinum surface and thus increases the temperature required to initiate the "jump" to the high rate of CO oxidation. During the "jump", CO is removed both from the gas phase and the catalyst surface. This allows the 1-butene to adsorb on the platinum surface with some oxidation, but the adsorption eventually quenches the high rate of CO oxidation. CO then begins to adsorb on the platinum and accumulates causing the entire process to be repeated.

In Chemical Reaction Engineering—Houston; Weekman, V., et al.;
ACS Symposium Series; American Chemical Society: Washington, DC, 1978.

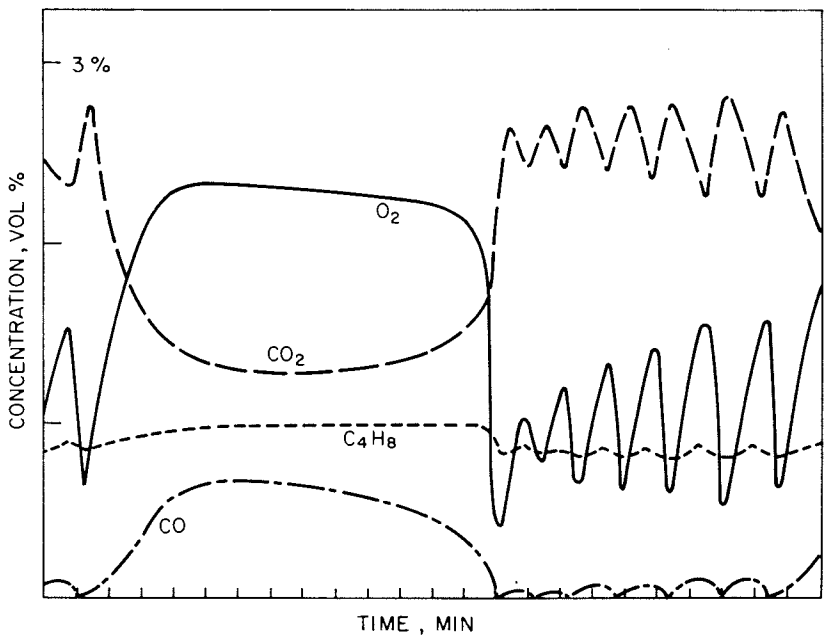

Figure 6. Oscillations at $T = 150°C$ *and feed at 60* cm^3/min *NTP*

Table III
Data for Feed Mixture of
2% CO, 3% O_2 and 1% 1-C_4H_8 in Argon

Point	Flow Rate cm^3/min	Reaction Temp. °C	CO %			O_2 %			CO_2 %			C_4H_8 %			Period min.	Relative Maxima Per Cycle	Time-averaged CO Oxidation gmole/g sec x 10^7	Time-Averaged C_4H_8 Oxidation gmole/g sec x 10^8
			max.	min.	avg.	max.	min.	avg.	max.	min.	avg.	max.	min.	avg.				
1	60	150	0.67	0.00	0.32	2.36	0.36	1.68	2.83	1.23	1.94	0.96	0.81	0.91	21	7	0.687	0.327
2	60	155	0.06	0.00	0.05	1.03	0.73	0.89	2.73	2.57	2.63	0.82	0.78	0.80	1	1	0.797	0.774
3	75	150	0.83	0.00	0.59	2.53	0.38	2.24	2.63	1.13	1.41	1.00	0.76	0.98	19	2	0.720	0.0475
4	75	155	0.09	0.00	0.05	1.44	0.75	1.13	2.71	2.32	2.55	0.88	0.82	0.83	1.18	1	0.996	0.763
5	75	160	0.05	0.00	0.03	0.93	0.79	0.82	2.60	2.53	2.58	0.80	0.78	0.79	0.88	1	1.01	1.02
6	94.7	160	0.08	0.00	0.06	1.18	0.84	1.00	2.67	2.43	2.56	0.88	0.83	0.86	0.88	1	1.25	1.11
7	100	150	0.93	0.00	0.76	2.46	0.32	2.29	2.76	1.04	1.26	0.97	0.77	0.96	31	1	0.845	0.102
8	100	155	0.73	0.00	0.38	2.35	0.42	1.80	2.83	1.23	1.83	0.99	0.72	0.92	15	5	1.10	0.446
9	100	160	0.25	0.00	0.18	1.88	0.79	1.48	2.55	1.93	2.14	0.95	0.76	0.86	1.5	1	1.24	0.693
10	100	165	0.08	0.06	0.07	1.00	0.95	0.96	2.53	2.51	2.52	0.80	0.80	0.80	0.78	1	1.32	1.22
11	115.8	165	0.12	0.05	0.10	1.08	0.92	1.03	2.53	2.43	2.48	0.87	0.77	0.80	0.63	1	1.49	1.35

In Chemical Reaction Engineering—Houston; Weekman, V., et al.;
ACS Symposium Series; American Chemical Society: Washington, DC, 1978.

An additional elementary step must be added to equations (1) - (4) and (6) to account for the surface reaction of the 1-butene. Numerical simulations with an elementary step modeling approach discussed elsewhere, Cutlip (11), have confirmed limit cycles for this group of elementary steps when combined with dynamic material balance equations for the reactor. We are continuing experimental and modeling investigations on these interesting phenomena.

Conclusions

1. The multiple steady state regions for carbon monoxide oxidation in oxygen rich feed mixtures can be generated by catalyst pretreatment with oxygen which leads to a high reaction rate and by pretreatment with carbon monoxide which leads to a low reaction rate. This is additional evidence that the platinum has appreciable adsorbed oxygen at the high rate and significant adsorbed carbon monoxide at the low rate.

2. No oscillations were observed for carbon monoxide oxidation. This may have resulted from the low turnover rates of this work which may have enabled gradientless reactor operation to be achieved with more certainty.

3. The dramatic oscillations observed during simultaneous carbon monoxide and 1-butene oxidation can be interpreted by including reversible adsorption and surface oxidation of the 1-butene occuring simultaneously with the elementary steps describing the carbon monoxide oxidation. Activation energies of surface rate processes which vary with surface coverages need not necessarily be used in modeling the experimental oscillations.

4. Multiple steady state and limit cycle experiments may well contain valuable quantitative information regarding surface rate processes in catalytic reactions and may contribute to improved dynamic catalytic models for process optimization and control.

Acknowledgements

Financial support was provided by the U. K. Science Research Council, the U. S. National Science Foundation and the University of Connecticut Research Foundation. Catalyst properties were evaluated in the laboratory of J. B. Butt, Northwestern University.

Abstract

Isothermal kinetic studies of carbon monoxide oxidation

which included the introduction of 1-butene were made in a gradientless reactor containing 10 grams of 0.5% platinum on alumina catalyst. In the absence of 1-butene, multiple steady state regions were found for oxygen rich feed streams, but no oscillations or limit cycles were observed. The addition of 1-butene to a feed mixture which previously had given a multiple steady state region yielded very dramatic oscillations (limit cycles) which can be explained by a proposed sequence of elementary steps occuring on the platinum surface.

Literature Cited

1. Wei, J. and Becker, E. R., Adv. in Chem. (1975) 143, 116
2. Carberry, J. J., "Chemical and Catalytic Reaction Engineering," McGraw-Hill, New York, 1976.
3. Benson, J. E. and Boudart, M., J. Catal. (1965) 4, 704.
4. Wentrcek, P., Kimoto, K, and Wise, H., J. Catal. (1973) 31, 279.
5. Schmitz, R. A., Adv. in Chem. (1975) 148, 156.
6. McCarthy, E., et at., J. Catal. (1975) 39, 29.
7. Plichta, R. J., "Oscillations in the Oxidation of Carbon Monoxide on an Unsupported Platinum Catalyst," Ph. D. Thesis, University of Illinois, 1976.
8. Pikios, C. A., and Luss, D., Chem. Eng. Sci. (1977) 32, 191.
9. Eigenberger, G., Preprints, 4th International/6th European Symposium of Chemical Reaction Engineering, Fed. Re. Germany, April, 1976.
10. Hanson, F. V., and Benson, J. E., J. Catal. (1973) 31, 471.
11. Cutlip, M. B., Hawkins, C. J., and Kenney, C.N., Chicago Meeting, A. I. Ch. E., December, 1976.

In Chemical Reaction Engineering—Houston; Weekman, V., et al.;
ACS Symposium Series; American Chemical Society: Washington, DC, 1978.

Kinetic Modeling for Oscillatory Catalytic Reactions

M. SHEINTUCH

Department of Chemical Engineering, Technion, Israel Institute of Technology, P.O. Box 4910, Haifa, Israel

R. A. SCHMITZ

Department of Chemical Engineering, University of Illinois at Urbana-Champaign, 108 Roger Adams Laboratory, Urbana, IL 61801

In a recent publication reviewing the status of research into intrinsic oscillations in solid-catalyzed reactions (1), we emphasized the potential exploitation of combined theoretical and experimental studies of oscillatory behavior for obtaining new insights into catalytic reaction mechanisms and kinetics. In the present paper, we elaborate further on the subject of formulating and analyzing kinetic models which account for oscillatory behavior, and we present some new experimental information for the oscillatory oxidation of CO on a platinum foil. As in reference 1, the analysis here is applied to models describable by two first-order differential equations. The laboratory data reported were obtained from an isothermal gradientless CSTR of void volume 460 cm^3 into which there was inserted a platinum foil of area 200 cm^2. Continuous measurements were made of the CO_2 concentration in the effluent stream. The experimental system is described in detail elsewhere (2, 3).

Positive Feedback and Capacity Effects.

Well-known theorems of Bendixon and Poincaré lead to the conclusion that sustained periodic solutions can be ruled out for a second-order differential system of the form $\bar{\bar{L}}\, d\bar{x}/dt = \bar{F}(\bar{x})$ if it is impossible throughout the parameter space for the trace of the matrix $\bar{\bar{L}}^{-1}\bar{\bar{J}}$, (where $\bar{\bar{J}}$ is the Jacobian of $\bar{F}$) to change sign from negative to positive values with $\bar{F}(\bar{x}) = 0$ and with the determinant of $\bar{\bar{L}}^{-1}\bar{\bar{J}}$ positive. Therefore, the magnitude of the capacity elements in $\bar{\bar{L}}$ and the magnitude and signs of partial derivatives in $\bar{\bar{J}}$ are crucial in ascertaining the possibility of oscillatory states. Notice that in general there is no need for "positive feedback" or "autocatalycity" to exist; that is to say, it is not necessary for the existence of oscillatory states that either $\partial F_1/\partial x_1$ or $\partial F_2/\partial x_2$ become positive.

The following simpler mathematical form applies to two models to be considered here.

© 0-8412-0401-2/78/47-065-487$05.00/0

$$\begin{pmatrix} 1 & 0 \\ 0 & \ell_c \end{pmatrix} \frac{d}{dt} \begin{pmatrix} x_1 \\ x_2 \end{pmatrix} = \begin{pmatrix} F_1 (x_1, x_2) \\ F_2 (x_1, x_2) \end{pmatrix} \quad (1)$$

The underlying kinetic models and reaction mechanisms are described later. In both models, the variable x_1 represents a gas-phase concentration, x_2, a surface concentration, and ℓ_c is a surface capacitance factor. Therefore, the function $F_1(x_1\ x_2)$ accounts for flow terms (in a CSTR species balance equation) as well as chemisorption and perhaps other reaction terms. The function $F_2\ (x_1, x_2)$, on the other hand, accounts only for surface rate processes. The variable x_2 is a "latent" variable, not measurable in situ in the unsteady state presently.

For this system, the above criterion requires that the quantity $[\partial F_1/\partial x_1 + (1/\ell_c)\partial F_2/\partial x_2]$ changes sign in order for periodic states to be possible. Hence one of the partial derivatives must become positive; that is, positive feedback must exist. Furthermore, in our experimental system, ℓ_c was very small. (We estimated its value to be as low as 0.01.) Thus the term containing the derivative $\partial F_2/\partial x_2$ in the above expression dominates, and our attention appropriately focused on those reaction mechanisms and kinetic models for which $\partial F_2/\partial x_2$ could be positive and hence for which the latent variable could accelerate the rate of CO conversion.

It is worth mentioning that this small value of ℓ_c might be expected to lead to relaxation oscillations. Such oscillations would be typified by sudden jumps in the latent variable x_2 with corresponding jumps in the rate of change of x_1.

Results of Analysis of Two Models

The results of an analysis of two models, hereafter referred to as models 1 and 2, fashioned from the set of reactions listed in Table I are described briefly here. Assumptions made throughout are that oxygen is present in excess in the gas phase and therefore constant at its feed value, and that the effect of the surface capacitance is important only in the product $\ell_c\ dx_2/dt$ -- all other terms containing surface capacitances are neglected.

In model 1 it is further assumed that reaction 1 in Table I is in equilibrium, that the reverse rate of reaction 2 is negligible, and that reactions 5, 6 and 7 do not occur. We consider two subcases, models 1a and 1b, each of which invokes the assumption that the rate-determining steps are chemisorption of oxygen and the formation of CO_2 -- the formation of CO_2 occurring only by way of reaction 3 in model 1a and only by way of reaction 4 model 1b. The rate expressions and equations for these models are given in Table I. In both cases, x_1 represents the reduced concentration of CO in the gas phase, and x_2 the fractional surface coverage by chemisorbed oxygen. Under the assumptions stated, both cases yield mathematical descriptions of the form given in equation (1)

In Chemical Reaction Engineering—Houston; Weekman, V., et al.;
ACS Symposium Series; American Chemical Society: Washington, DC, 1978.

TABLE I. SUMMARY OF CO OXIDATION MODELS

Stoichiometric Reactions

(1) $A_1 + s \rightleftharpoons A_{1s}$
(2) $A_2 + s \rightleftharpoons A_{2s}$
} chemisorption of CO and O_2

(3) $2A_1 + A_{2s} \longrightarrow 2A_3 + s$
(4) $2A_{1s} + A_{2s} \longrightarrow 2A_3 + 3s$
} formation of CO_2

(5) $2A_1 + A_{2s} + s \longrightarrow 2A_3 + s'$
(6) $2A_{1s} + A_{2s} + s \longrightarrow 2A_3 + 3s'$
(7) $s' + A_{1s} \longrightarrow s + A_3$
} surface oxidation and reduction

Intrinsic Rate Expressions

Model 1

Equil: $\theta_1(x_1,x_2) = K_1x_1(1-x_2)/(1+K_1x_1)$

$R_2 = k_2C_{2,F}[(1-x_2)/(1+K_1x_1)]$

$R_3 = k_3C_{1,F}x_1x_2f_3(\mu,x_2)$

$R_4 = k_4\theta_1(x_1,x_2)x_2f_4(\mu,x_2)$

$R_5 = 0$

$R_6 = 0$

$R_7 = 0$

where $x_1 = C_1/C_{1,F}$

$x_2 = \theta_2$

Model 2

(1) Equil: $\theta_1(x_1,x_2) = K_1x_1(1-x_2)/(1+K_1x_1)$

(2) Equil: $\theta_2(x_1,x_2) = K_2'C_{2,F}(1-x_2)/(1+K_1x_1)$

(3) $R_3 = k_3C_{1,F}x_1\theta_2\ (x_1,x_2)$

(4) $R_4 = k_4\theta_1(x_1x_2)\theta_2(x_1,x_2)$

(5) $R_5 = k_5C_{1,F}x_1\theta_2(x_1,x_2)$

(6) $R_6 = k_6\theta_1(x_1,x_2)\theta_2(x_1,x_2)$

(7) $R_7 = k_7[\theta_1(x_1,x_2)]^{\nu}x_2$

where $x_1 = C_1/C_{1,F}$

$x_2 = \theta_{s'}$

Equations

Model 1

Balance on total CO:

$$\frac{dx_1}{dt} = 1-x_1 - \frac{2\tau a_v}{C_{1,F}} R_m$$

Balance on chemisorbed O_2:

$$\ell_c \frac{dx_2}{dt} = \frac{a_v\tau}{C_{1,F}} (R_2-R_m)$$

where m = $\begin{cases} 3 & \text{model 1a} \\ 4 & \text{model 1b} \end{cases}$

Model 2

Balance on total CO:

$$\frac{dx_1}{dt} = 1-x_1 - \frac{a_v\tau}{C_{1,F}} [2(R_m+R_n) - R_7]$$

Balance on oxidized sites:

$$\ell_c \frac{dx_2}{dt} = \frac{\tau a_v}{C_{1,F}} (R_n - R_7)$$

where m = $\begin{cases} 3 & \text{model 2a} \\ 4 & \text{model 2b} \end{cases}$

n = $\begin{cases} 5 & \text{model 2a} \\ 6 & \text{model 2b} \end{cases}$

In Chemical Reaction Engineering—Houston; Weekman, V., et al.;
ACS Symposium Series; American Chemical Society: Washington, DC, 1978.

(This model is a special version of a more general model described in Table 4 of reference 1.) The main result of our analysis of model 1 is that if the functions f_3 and f_4 (see rate expressions R_3 and R_4 for model 1 in Table 1) in models 1a and 1b respectively are assumed to be unity, then neither case can yield oscillatory states according to the criterion stated earlier. This is somewhat surprising at first glance because model 1b, which includes reaction 4, gives a positive feedback effect due to CO inhibition by chemisorption on active sites. However, this positive effect is offset by the negative feedback effect of the chemisorption of oxygen. We found further that if a kinetic model is formulated so as to account for a positive feedback effect of chemisorbed oxygen by taking f_3 and f_4 to be the quantity $(1-x_2)^\mu$, then the value of μ must be at least 2 for oscillatory states to be possible. An inhibition effect of such high order is not kinetically plausible unless it is incorporated in an exponential form, $\exp(-\mu x_2)$, wherein the chemisorbed oxygen has the effect of increasing the activation energy for the rate of formation of CO_2. Such dependencies of activation energies on surface coverage are supported from theoretical considerations and have been observed experimentally.

If this activation energy dependence on x_2 is incorporated into the kinetic model in either of the two subcases, the condition that $\partial F_2/\partial x_2 > 0$ requires that the following inequality be satisfied:

$$-(4 - m) - (1 - x_2)/x_2 + \mu (1 - x_2) > 0 \qquad (2)$$

where m has the value 3 in model 1a and 4 in model 1b.

As inequality (2) indicates, oscillations are possible for model 1 if μ is greater than some critical value. We calculated the critical values to be 4 and 1 for models 1a and 1b respectively. Thus reaction 4 is more likely to lead to oscillatory states than is reaction 3, according to this model The magnitudes of the critical values appear to be quite reasonable. The analysis of other variations of this model are described in reference 1 and some computer simulations of oscillatory states are presented later in this paper. Important items of information obtainable through a more extensive analysis are that (1) the model admits multiple steady states (2) the added inclusion of a surface coverage-dependent chemisorption equilibrium constant for CO, to account for a decrease in the enthalpy of CO adsorption with oxygen coverage, enhances the possibility of oscillatory states and (3) the assumption of a dissociated form of chemisorbed oxygen decreases the likelihood of satisfying inequality (2). It should be noted here that although this model with the activation energy dependence on oxygen surface ocverage permits oscillatory states, it is not capable of describing all of the experimentally observed features of oscillatory behavior (1). Therefore, no claim is made that this model is generally satisfactory. The main conclusion to be drawn is that if one is to base a mathematical description of

In Chemical Reaction Engineering—Houston; Weekman, V., et al.;
ACS Symposium Series; American Chemical Society: Washington, DC, 1978.

CO oxidation on the reaction steps and rate expressions underlying this model, as is the currently popular approach, then the incorporation of an activation energy dependence on surface coverage seems reasonable as does the assumption of more than one rate-determining step -- at least over certain ranges of conditions.

In model 2 the oxidation and reduction of surface sites, as represented by reactions 5, 6 and 7 in Table I, are taken into account. In order to retain a second-order differential model, we invoke the assumption that both chemisorption steps (reactions 1 and 2) are in equilibrium. We further assume that the inhibition effect of chemisorbed oxygen is negligible. The rate-determining steps, therefore, are reactions 3 through 7, the rate expression for which are listed in Table I. Here x_1 is the reduced gas-phase concentration of CO, as in the previous model, and x_2 is the fraction of oxidized sites. Oxidized sites are assumed to be inactive. Notice that the oxidation rates in expressions R_5 and R_6 are assumed to be proportional to the CO_2 formation rates in expressions R_3 and R_4 respectively. This assumption was prompted by the results of oxidation studies reported by Ostermaier et al. (4). Notice also that the reaction order ν in the expression for R_7 is unspecified. In the analysis of this model, we are interested in the critical value of ν beyond which oscillatory states are possible. Again we consider two subcases. In the first of these, model 2a, reactions 4 and 6 do not occur, and in the second, model 2b, reactions 3 and 5 do not take place. Both subcases lead to mathematical descriptions of the form given in equation (1), and the criterion for oscillations stated earlier is readily applied. Our analysis by this approach led to critical values of ν of 2 and 3 for models 2a and 2b respectively. That is to say that ν must have values greater than these in order for oscillatory states to be possible. From a fundamental viewpoint, the required high order of the surface reduction step is bothersome. The important point, however, is that the oxidation and reduction of catalytic sites during reaction can indeed lead to oscillations. Alternate rate expressions or reaction steps, perhaps more realistic ones which account for the migration of oxidized sites into the bulk of the metal, would lead to more plausible explanations of oscillations. We are conducting further investigations into the effects of variations of this model.

A conclusion to be drawn from the results of analysis of the two models described here is that some accounting for insidious mechanistic details in catalytic reactions, more than is usually necessary for reaction engineering purposes, is apparently necessary in order to describe oscillatory behavior. The models each possessed mechanisms of positive feedback resulting from the role of a surface species -- as was shown to be necessary from the direct application of well-known theorems.

In Chemical Reaction Engineering—Houston; Weekman, V., et al.;
ACS Symposium Series; American Chemical Society: Washington, DC, 1978.

Some Experimental Observations and Computed Results

Due to space limitations, we do not present an extensive array of computed and experimental results, but instead show a sufficient sample to give an appreciation of key features.

Figure 1 shows limit cycles computed from model 1a with $f_3(\mu,x_2) = \exp(-\mu x_2)$. (Our computations for model 1a are far more extensive than for other models, but results for the others do not seem to be significantly different from those of model 1a.) Notice that the axes of the phase plane are CO concentration and the rate of CO conversion. We used this rate on the vertical axis because its instantaneous values could be computed in experiments directly from strip chart data of CO_2 concentration versus time.

As the value of τ is increased the cycles in Figure 1 approach a relaxation cycle. For example, the left half and the bottom portion of the cycle for τ = 20 sec. closely follow the branches of the steady rate curve (dashed curve in Figure 1) for CO conversion. (Notice that the steady rate curve, computed from the steady-state equation for this model is multivalued at lower CO concentrations and that the upper branch shows a decreasing rate with increasing CO concentration. The decreasing rate has been well established through recent years, but the multivalued geometric nature, caused by the form of $f_3(\mu,x_2)$ employed, has not been substantiated. Steady state solutions, according to the steady species balance for CO, would be the points of intersection of the rate curve with straight lines of negative slope -- the supply lines.)

Decreasing the capacitance factor, ℓ_c has the same qualitative effect on model predictions of limit cycles as increasing τ.

Experimental limits cycles in the rate-concentration plane are shown in Figure 2. The important points regarding this figure are: (1) the amplitude of the oscillatory states were found to increase as τ is decreased -- in conflict with the theoretical curves of Figure 1; (2) stable nonoscillatory states were obtained at residence times below 49 sec. and above 130 sec.; (3) multipeak cycles were observed at lower residence times as the bifurcation to stable states was approached. (See the insert in Figure 2 and the time trace in Figure 3.) Multipeak cycles require a higher dimensional space for their representation and are indicative that more than two rate-determining reaction steps are involved under some conditions.

Figure 4 presents an example of another experimental observation -- that of a multiplicity of limit cycles -- which has not previously been reported and is not predicted by the models described earlier. When such multiplicity was encountered, we were able to reach either of the two periodic reactor states by means of appropriate feed concentration changes. It is interesting to note that the period of the single-peak cycle (curve b in Figure 4) is very nearly half that of the complex cycle, curve

In Chemical Reaction Engineering—Houston; Weekman, V., et al.;
ACS Symposium Series; American Chemical Society: Washington, DC, 1978.

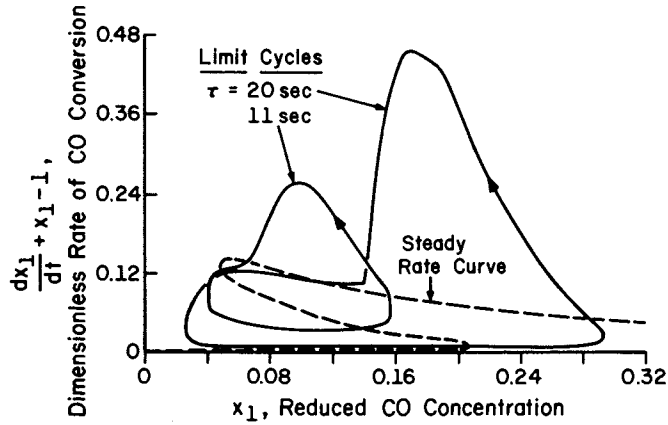

Figure 1. Simulated limit cycles for model 1a with $f_s(\mu,x_2) = exp(-\mu x_2)$. *Parameter values:* $\mu = 8$; $l_c = 0.08$; $K_1 = 10$; $a_v k_3 = 0.01$ sec^{-1}, $a_v k_2 C_{2,F} = 0.12$ sec^{-1}.

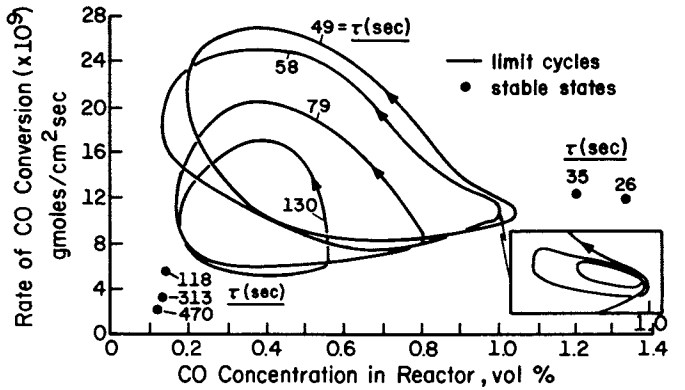

Figure 2. Experimental limit cycles for reactor temperature of 217°C; feed composition: 1.95% CO, 19% O_2, *and 79%* N_2 *(by vol). Insert shows a magnification of multipeak cycle at the high concentration extreme for* $\tau = 58$ *sec.*

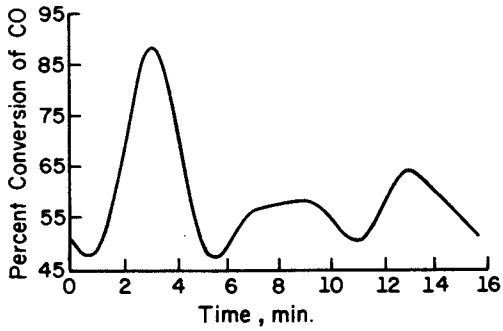

Figure 3. One period of a three-peak cycle for τ = 49 sec with experimental conditions given in Figure 2

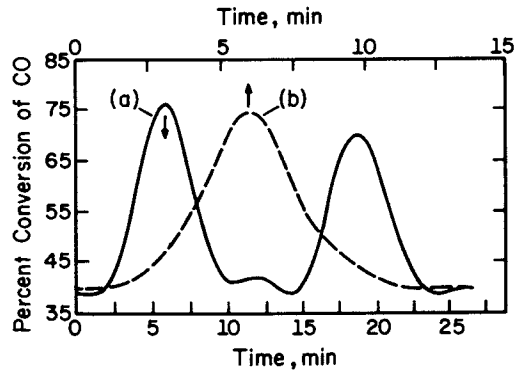

Figure 4. Multiplicity of periodic states—(a) multipeak cycle and (b) simple cycle—at reactor temperature of 217°C, residence time of 82.6 sec and feed state: 2.15% CO, 12.9% O_2, 85% N_2

In Chemical Reaction Engineering—Houston; Weekman, V., et al.;
ACS Symposium Series; American Chemical Society: Washington, DC, 1978.

(a), which contains two large peaks.

Even a more intriquing type of behavior was observed in one single run at a reactor temperature of 271°C and a feed composition of 1.99% CO, 19.3% O_2, and 79.7% N_2. In this run our data gave strong evidence that "chaotic" states existed at residence times below 29 sec. Such states are characterized by sustained time-dependent but nonperiodic behavior. Prior theoretical work suggests that such behavior may be intrinsic in differential systems of order three and higher (5) and might generally be accompanied by such phenomena as multipeak cycles and multiple periodic states (6). There are, of course, competing explanations for chaotic outputs, including the simple one that the reactor state under certain conditions is very sensitive to small extrinsic disturbances. We are strongly inclined toward accepting the existence of intrinsic chaotic states in this system, but the matter requires considerably more deliberation and careful experimentation than we have given it thus far.

In conclusion we should comment further on two points. (1) Theoretical and experimental results are not in agreement. Models which we have examined here serve mainly to exclude certain mechanisms and rate expressions. Still the principal features incorporated separately to account for oscillatory behavior, namely an activation energy dependence on surface coverage and metal oxidation and reduction certainly are realistic features. We feel that some alternate method of describing them or of including both effects simultaneously (or perhaps including other rate processes) to obtain qualitative agreement with experimental information will likely shed new light on the kinetics of CO oxidation and perhaps on catalytic oxidation reactions in general. (2) As is nearly always the case with catalytic reaction experiments, we faced, in our laboratory work, the problem of a changing and nonreproducible catalytic activity. The information shown in Figures 2 and 3 was obtained during a relatively stable activity period and could be reproduced quite accurately over a period of a few days. After regeneration of the catalyst, the qualitative features shown and described for those figures were usually preserved, but all quantitative information was altered. The changing activity makes it particularly difficult to state conclusively that such phenomena as the multiple limit cycles shown in Figure 3 and the chaotic behavior (which incidentally was observed on only one occassion -- on the third day following catalyst regeneration) described above are truly behavioral traits and not simply the effect of transient activity levels. Unfortunately theoretical and experimental studies and the understanding of the causes and effects of insidious activity changes have not yet reached to the point at which questions relating to such matters can be answered with assurance.

In Chemical Reaction Engineering—Houston; Weekman, V., et al.;
ACS Symposium Series; American Chemical Society: Washington, DC, 1978.

Nomenclature

A_1, A_2, A_3	chemical components CO, O_2, and CO_2 respectively, in the gas phase
A_{1s}, A_{2s}	chemisorbed components CO and O_2 respectively
a_v	catalyst area per unit void volume
C_1	gas phase concentration of CO in the reactor
$C_{1,F}, C_{2,F}$	concentrations of CO and O_2 in the feed stream
f_3, f_4	functions of μ and x_2 used in rate expressions R_3 and R_4 for model 1
F_1, F_2	elements in the vector $\bar{F}$
$\bar{F}$	vector of functions of $\bar{x}$
$\bar{J}$	Jacobian matrix
K_1	dimensionless chemisorption equilibrium constant, $K'_1/C_{1,F}$
K_1', K_2'	chemisorption equilibrium constants for CO and O_2
k_j	reaction velocity constant for the jth reaction
$\bar{L}$	matrix of capacitance factors
ℓ_c	surface chemisorption capacity factor for CO, $M_s a_v/C_{1,F}$
m	index defined where used
M_s	concentration of active sites (moles/area)
n	index defined where used
q	volumetric flow rate at reactor temperature
R_j	rate expression for the jth reaction in Table I
s	active surface site
s'	oxidized (inactive) surface site
t	dimensionless time, time/τ
V	void reactor volume
$\bar{x}$	general vector of state variables
x_1, x_2	dimensionless state variables defined in Table I for specific models

Greek Letters

θ_1, θ_2	fraction of sites occupied by chemisorbed CO and O_2 respectively
$\theta_{s'}$	fraction of sites in the oxidized state
μ	parameter used as reaction order or as coefficient in exponent in reactions 3 and 4 of model 1
ν	order of reaction 7 with respect of CO coverage in model 2
τ	residence time, V/q

In Chemical Reaction Engineering—Houston; Weekman, V., et al.;
ACS Symposium Series; American Chemical Society: Washington, DC, 1978.

Acknowledgment

This work was supported by grants from the National Science Foundation and the Gulf Oil Corporation.

Literature Cited

1. Sheintuch, M. and Schmitz, R. A., Cat. Rev.-Sci. & Eng. (1977) 15, 107.
2. Plichta, R. T. and Schmitz, R. A. (in press).
3. Sheintuch, M., Ph.D. Thesis, Univ. of Ill., Urbana (1977).
4. Ostermaier, J. J., Katzer, J. R. and Manogue, W. H., J. Cat. (1976) 41, 277.
5. Rössler, O. E., Z. Naturforsch., (1976) 31a, 259.
6. May, R. M., J. Theor. Biol. (1975) 51, 511.

41

Theoretical and Experimental Study of Self-Sustained Oscillations in a Stirred Tank Reactor

P. HUGO and H.-P. WIRGES*

Institut für Technische Chemie, Technische Universität Berlin Strasse des 17. Juni 135, 1000 Berlin 12, West Germany

1. Mathematical model

The dynamics of temperature and conversion within a cooled continuous-flow stirred tank reactor (CSTR) can be obtained from the material and energy balances. For a simple first order chemical reaction they are in a dimensionless form

$$\frac{du}{d\Theta} = -u + Da_0(1-u)\exp\left[\frac{v}{1+\varepsilon v}\right] \tag{1a}$$

$$\frac{1}{B}\frac{dv}{d\Theta} = -\mu^* v + Da_0(1-u)\exp\left[\frac{v}{1+\varepsilon v}\right] \tag{1b}$$

where u, v, Θ are the dimensionless conversion, temperature difference and time, respectively, defined by

$$u = 1 - \frac{c}{c_E}\ ;\quad v = \frac{E}{RT_0^2}(T - T_0) \text{ and } \Theta = \frac{t}{\tau} \tag{2}$$

T_0 is the stationary temperature of the cooled reactor in the absence of a chemical reaction

$$T_0 = \frac{T_E + \mu T_k}{1+\mu} \quad (3) \quad \text{with} \quad \mu = \frac{k_w F}{\dot{m} c_p} \tag{4}$$

as a dimensionless heat transfer coefficient.

The type of reaction and the reaction conditions are represented by four dimensionless parameters

$$B = \frac{E(-\Delta H)\, c_E}{R\,\rho\, c_p\, T_0^2}\ ;\quad \varepsilon = \frac{RT_0}{E}\ ;\quad \mu^* = \frac{1+\mu}{B}\ ;\quad Da_0 = k(T_0)\cdot\tau$$

(5a) (5b) (5c) (5d)

* Present address: Bayer AG, Werk Ürdingen, 4150 Krefeld.

In Chemical Reaction Engineering—Houston; Weekman, V., et al.;
ACS Symposium Series; American Chemical Society: Washington, DC, 1978.

This choice of the dimensionless parameters is useful for a mathematical description of stability.

2. Steady state and stability

At a steady state the solutions of Eq. (1) are:

$$u_s = \frac{Da_s}{1 + Da_s} \qquad u_s = \mu^* v_s \qquad (6a), (6b)$$

where

$$Da_s = Da_0 \exp\left[\frac{v_s}{1 + \varepsilon v_s}\right] \qquad (6c)$$

So the steady state u_s, v_s depends on three parameters Da_0, μ^*, ε. The reaction number B is lumped together with the cooling parameter by Eq. (5c).

Provided a highly exothermic reaction occurs, a steady state may be unstable.

Stability considerations [1,2,3,4] lead to the definition of the two stability parameters

$$2\alpha = B\left[\frac{u_s}{(1+\frac{\varepsilon u_s}{\mu^*})^2} - \mu^*\right] - \frac{1}{1-u_s} \qquad (7),$$

$$\beta = B\left[\frac{\mu^*}{1-u_s} - \frac{u_s}{(1+\frac{\varepsilon u_s}{\mu^*})^2}\right] \qquad (8)$$

whose signs determine whether a steady state is stable or not.

A steady state is stable if $\alpha < 0$ and $\beta > 0$; instabilities of the type $\beta < 0$ correspond to multiplicity phenomena [1]. For $\beta > 0$ and $\alpha > 0$ oscillatory instabilities can be observed if

$$\frac{B}{(1+\frac{\varepsilon u_s}{\mu^*})^2} > 6{,}75 \qquad (9)$$

Such sustained oscillations (limit cycles) of the temperature and the conversion are mostly due to a unique steady state solution of Eq. (1) which is unstable to small perturbations. The region of parameter space for which instabilities occur can be plotted into a so-called stability diagram. Fig. 1 gives μ^* versus u_s with Da_0 as a fixed parameter. The curves $\alpha = 0$ and $\beta = 0$ calculated from Eqs. (7) and (8) are drawn into this diagram. It will be used here to present the results for a lot of numerical calculations concerning limit cycles in the region $\alpha > 0$, $\beta > 0$.

3. Numerical calculations

Several attempts have been made [3, 5 - 8] to describe limit cycles by approximate solutions of the balance equations (1).

In Chemical Reaction Engineering—Houston; Weekman, V., et al.;
ACS Symposium Series; American Chemical Society: Washington, DC, 1978.

However the range of validity of such approximate solutions is small. The application is either limited to comparatively small B-values or to the neighbourhood of the borderline $\alpha = 0$.

To find out a better description of limit cycles, extensive numerical calculations were carried out for B-values from 10 to 30 and $\varepsilon = 0$ to 0.02075. Details of these calculations are presented in [9].

As an example Fig.2 shows a temperature oscillation computed under rather extreme conditions. Typical for the temperature oscillations is the asymmetry of the oscillation due to the law of Arrhenius.

From the numerical calculations the computed frequency is obtained by

$$\omega_{comp} = \frac{2\pi}{\Delta\Theta} \tag{10}$$

$\Delta\Theta$ is the dimensionless time difference between two succeeding maxima of temperature.

From the maxima and minima of the temperature oscillations a modified amplitude A can be calculated

$$A = \frac{1}{2}\left[\frac{v_{max}}{1 + \varepsilon v_{max}} - \frac{v_{min}}{1 + \varepsilon v_{min}}\right] \tag{11}$$

Further a time averaged conversion $\bar{u}$ was calculated:

$$\bar{u} = \frac{\omega}{2\pi} \int_0^{2\pi/\omega} u \, d\Theta \tag{12}$$

In the subsequent sections these results will be compared with approximate solutions and empirical correlations.

4. Frequency of limit cycle

For fixed values B, ε and by varying μ^* and Da_o several frequencies were computed. From these data pairs of parameters μ^*, Da_o were selected which gave the same frequency. Fig. 3 and 4 show the result for $\varepsilon = 0.02075$ and B = 15 and 30.

The values ω_{comp} were compared with approximate solutions. The linearized theory [1] gives

$$\omega_L = \sqrt{\beta - \alpha^2} \tag{13}$$

This approximation is useful for small α-values but fails in the center of the region $\alpha > 0$. We found empirically that the simple equation

$$\omega_{Lo} = \sqrt{\beta} \tag{14}$$

gives in most cases a sufficient approximation.

A better fit of the data of the computer simulation was obtained by the regression equation

In Chemical Reaction Engineering—Houston; Weekman, V., et al.;
ACS Symposium Series; American Chemical Society: Washington, DC, 1978.

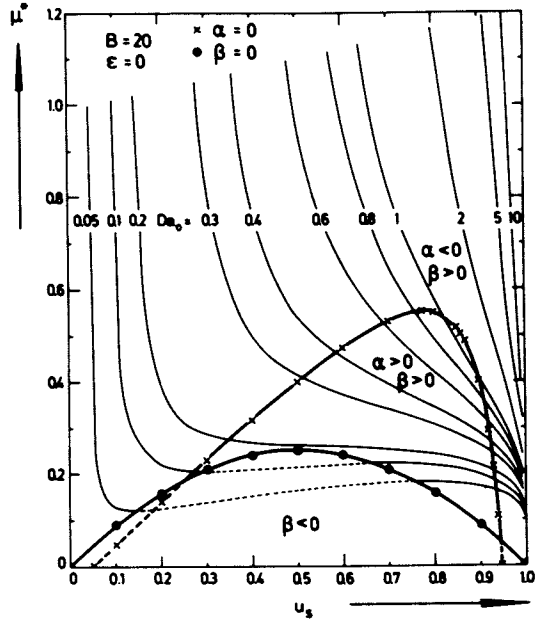

Figure 1. Stability diagram ($B = 20, \epsilon = 0$)

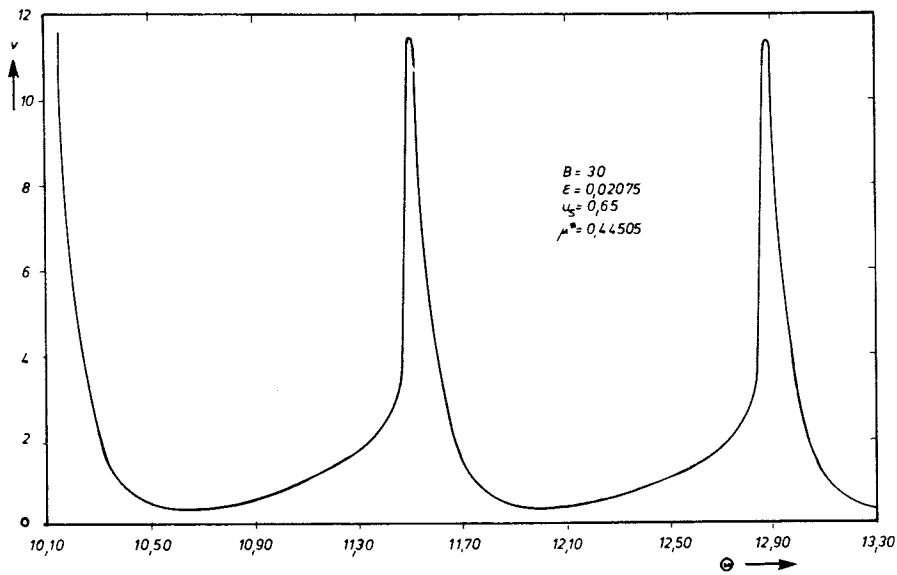

Figure 2. Typical temperature oscillation from computer simulation ($B = 30, \epsilon = 0, 02075, \mu^* = 0, 44505, u_s = 0, 65$)

In Chemical Reaction Engineering—Houston; Weekman, V., et al.;
ACS Symposium Series; American Chemical Society: Washington, DC, 1978.

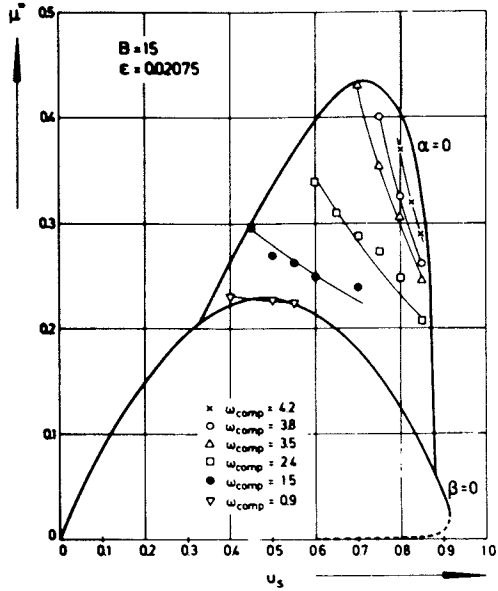

Figure 3. Stability diagram with curves of equal frequency (B = 15, ε = 0, 02075)

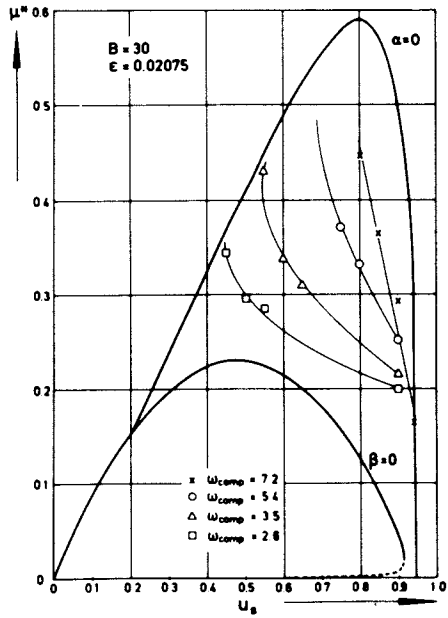

Figure 4. Stability diagram with curves of equal frequency (B = 30, ε = 0, 02075)

In Chemical Reaction Engineering—Houston; Weekman, V., et al.;
ACS Symposium Series; American Chemical Society: Washington, DC, 1978.

$$\omega_R = 9.6 - 35.7\ u_s + 23.9\ u_s^2 + 20.5\ \mu^* u_s - 0.2\ B\mu^* + 0.23\ B\ u_s + 10.6\ u_s\varepsilon \qquad (15)$$

Within the range $\alpha > 0$, $\beta > 0$ and

$0.40 < u_s < 0.95 \quad 0 < \varepsilon < 0.03 \quad 10 < B < 30 \quad 0.2 < \mu^* < 0.6$

the maximum percentage error $(\omega_{comp} - \omega_R)/\omega_{comp}$ was $\pm$ 10%.

Table I: Comparison of some representative frequencies.

5. Amplitude of temperature oscillations

A lot of more severe difficulties arise if the amplitude of the temperature is to be predicted. Several proposed approximations [3], [5], [6], [7] are only useful in a small range, namely in the neighbourhood of the borderline $\alpha = 0$ and for comparatively small B-values.

The asymmetric behavior of the temperature oscillations can approximately be accounted for by setting

$$\Delta v = v - v_s = -\ln(1 - a\cos\omega\Theta) \quad \text{where} \qquad (16)$$

$$a = \tanh(A) \qquad (17)$$

Fig. 5 and 6 show curves of equal a-values for $\varepsilon = 0.02075$ and $B = 15$ and $B = 30$. These diagrams illustrate that small temperature amplitudes are restricted to a very small zone near the borderline $\alpha = 0$. All analytical approximations must fail in the main part of the region $\alpha > 0$, $\beta > 0$ where the a-values are very near to 1.

A regression method was applied selecting about 500 representative data from the computer simulation. The best fitting was found by

$$A_R = -11.5 - 54.4\ \mu^* + 57.2\ u_s + 0.76\ B - 57.2\ \varepsilon - 56.5\ u_s^2 - 0.012\ B^2 + 51.1\ \mu^* u_s \qquad (18)$$

which is valid in the same range of the parameters as Eq.(15). As far as $A < 5$ the maximum percentage error $(A - A_R)/A$ was about $\pm$ 30%.

To our own surprise a comparatively simple semi-empirical approximation works quite well in the range of high temperature amplitudes. From Eq. (1) a coupling equation can be obtained by elimination the dimensionless reaction rate

$$\frac{d\varphi}{d\Theta} + \varphi = v\ ; \quad \varphi = \frac{Bu - v}{B\mu^* - 1} \qquad (19)$$

In Chemical Reaction Engineering—Houston; Weekman, V., et al.;
ACS Symposium Series; American Chemical Society: Washington, DC, 1978.

Table I: Comparison of some representative frequencies

parameters		ω_{comp} Eq.(10)	ω_L Eq.(13)	ω_{Lo} Eq.(14)	ω_R Eq.(15)
B=10 ε=0	u_S=0,80 μ^*=0,280	2,406	2,449	2,451	2,210
B=10 ε=0	u_S=0,80 μ^*=0,2509	1,917	2,118	2,132	1,800
B=10 ε=0	u_S=0,60 μ^*=0,261	0,938	0,561	0,717	0,868
B=30 ε=0,02075	u_S=0,80 μ^*=0,3118	4,961	3,447	5,013	5,280
B=30 ε=0,02075	u_S=0,75 μ^*=0,310	4,325	2,060	4,100	4,511
B=30 ε=0,02075	u_S=0,60 μ^*=0,3038	3,159	imagin.	2,485	2,981
B=30 ε=0,02075	u_S=0,55 μ^*=0,2716	2,394	imagin.	1,705	2,580

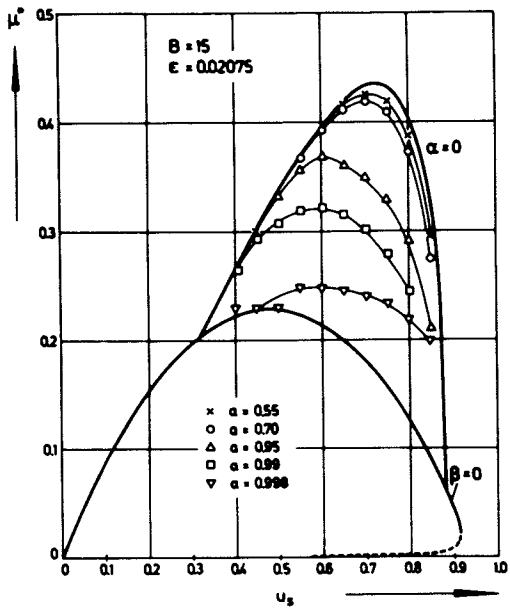

Figure 5. Stability diagram with curves of equal temperature amplitude ($B = 15, \epsilon = 0, 02075$)

From several numerical calculations we found that the oscillations of φ are considerably smaller than those of v. This effect is demonstrated for a typical limit cycle with a high temperature amplitude in Fig. 7.

So we tested the approximation $\varphi(v_{extr}) = v_s$ where the corresponding conversion u is obtained from Eq. (1b) by setting $\frac{dv}{d\Theta} = o$. One gets

$$(B\mu^* - 1)v_s = B - v_{extr} - \frac{B\mu^*}{Da_{extr}} \cdot v_{extr} \qquad (20)$$

$$Da_{extr} = Da_o \exp\left[\frac{v_{extr}}{1 + \varepsilon v_{extr}}\right] \qquad (21)$$

The first and the third intersection of the curve $\varphi(v_{extr})$ with the line $\varphi = v_s$ (see Fig. 7) yield approximate values for v_{min} and v_{max} which are used to calculate A from Eq. (11).

Table II: Comparison of some representative amplitudes of temperature

6. Time averaged conversion

A short comment should be made to the time-averaged conversion. By an approximate solution [9] we obtained

$$\bar{u} > u_s \quad \text{for} \quad \bar{v} < 2$$
$$\text{and} \quad \bar{u} < u_s \quad \text{for} \quad \bar{v} > 2$$

From our numerical calculations we found that this rule is valid even at high B-values. From the practical point of view the increase of conversion $(\bar{u} - u_s)$ in the range $\bar{v} < 2$ is comparatively small. The severe problems of a reactor with self-sustained oscillation makes it unrealistic to use this way for increase of conversion.

7. Experimental results

In the experimental part of this study the catalytic decomposition of hydrogen peroxide by $Fe(No_3)_3 \cdot 9\ H_2O$ in a nitric acid solution was used as a model reaction. This reaction has the advantage ob being first order [10, 11]. The concentrations of Fe^{3+} and H^+ remain constant during the reaction. The following rate expression was obtained by kinetic experiments:

$$r = 1{,}6 \cdot 10^{18} \cdot \frac{c_{Fe^{3+}}}{c_{H^+} + 0{,}01} \cdot c_{H_2O_2} \cdot \exp\left(-\frac{14620}{T}\right) \quad \frac{\text{g-mole}}{\text{litre} \cdot \text{sec}} \qquad (22)$$

In Chemical Reaction Engineering—Houston; Weekman, V., et al.;
ACS Symposium Series; American Chemical Society: Washington, DC, 1978.

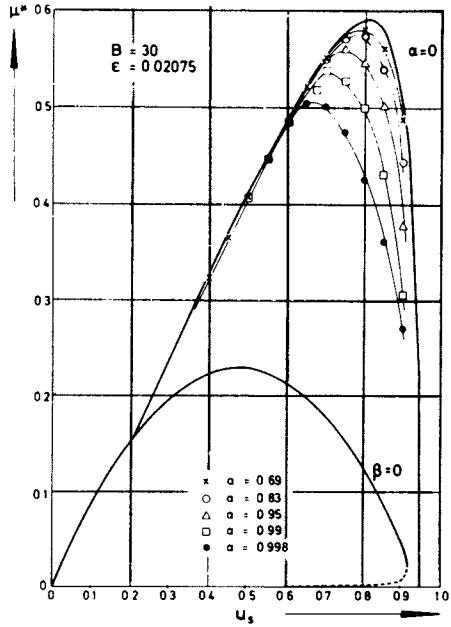

Figure 6. Stability diagram with curves of equal temperature amplitude (B = 30, ε = 0, 02075)

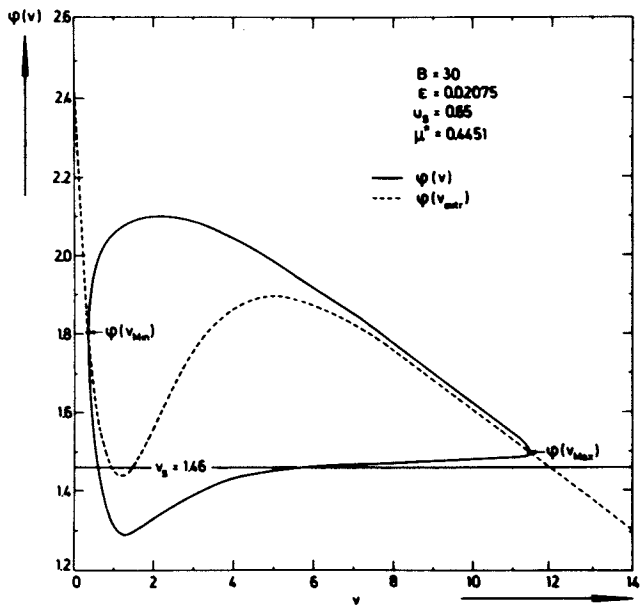

Figure 7. Limit cycle φ(v) for B = 30, ε = 0, 02075, μ = 0, 445, and u_s = 0, 65*

In Chemical Reaction Engineering—Houston; Weekman, V., et al.;
ACS Symposium Series; American Chemical Society: Washington, DC, 1978.

The values of the activation energy (E = 121,5 kJ/g-mole) and of the reaction enthalpy (-ΔH = 94,8 kJ/g-mole) are high enough to fulfil Eq.(9) so that the oscillatory behaviour of temperature and conversion in the CSTR can be observed for a wide range of operating conditions (see Table III).

The acid/hydrogen peroxide solution and the catalyst were pumped in two feed streams via rotameters into the reactor. The liquid phase volume (V = 500 ml) was kept constant with an outlet valve. The extent of the reaction was followed by titration of hydrogen peroxide and by sensing the temperature with a thermocouple.

Table III Range of experimental conditions

800 ml/h	<	$\dot{v}_{H_2O_2}$	<	2400 ml/h
101 ml/h	<	$\dot{v}_{Fe^{3+}}$	<	305 ml/h
665 s	<	τ	<	1800 s
300,8 k	<	T_o	<	305,6 k
15,2	<	B	<	27,9
4,2 g-mole/l	<	$c_E^{H_2O_2}$	<	7,5 g-mole/l
0,08g-mole/l	<	c_{H^+}	<	0,12g-mole/l
		$c_{Fe^{3+}}$	=	0,02g-mole/l

Fig. 8 gives an impression of the frequency and the amplitude of the measured oscillations. The oscillation of the temperature is extremely asymmetric.

The Figures 9 and 10 show a comparison of the experimental data of the oscillation period and the temperature amplitude with the computed results. The basis of these plots is a refined mathematical model that takes the evaporation of water into account. The main assumption is to consider the oxygen stream to be saturated with water vapour. On this condition the heat per unit time removed from the reactor is given by

$$\dot{Q}_{ev} = \Delta_v H \cdot \gamma \cdot \dot{n}_{o_2}; \quad \text{with } \gamma = \frac{P_{H_2O}}{760 - P_{H_2O}} \tag{23}$$

As $\dot{n}_{O_2}$ is proportional to the reaction rate, the following expression for the heat balance could be derived

$$\frac{1}{B}\frac{dv}{d\Theta} = -\mu^* \cdot v + Da_o(1-u)[1-\xi\cdot\gamma(v)] \cdot \exp\frac{v}{1+\varepsilon v} \tag{24}$$

$$\xi = \frac{1}{2}\frac{(\Delta_v H)}{(-\Delta H)} = 0{,}215 \tag{25}$$

In Chemical Reaction Engineering—Houston; Weekman, V., et al.;
ACS Symposium Series; American Chemical Society: Washington, DC, 1978.

Table II: Comparison of some representative amplitudes of temperature

parameters		computer A_{comp} (a)	Eq.(18) A_R	Eq.(20) A
B=10 ε=0	u_S=0,80 μ^*=0,297	0,275 (0,268)	0,44	1,22
B=10 ε=0	u_S=0,6 μ^*=0,261	2,21 (0,976)	2,67	1,79
B=30 ε=0,02075	u_S=0,80 μ^*=0,573	1,19 (0,827)	1,11	1,44
B=30 ε=0,02075	u_S=0,70 μ^*=0,467	3,82 (0,9990)	2,82	3,84
B=30 ε=0,02075	u_S=0,65 μ^*=0,445	4,45 (0,99973)	3,19	4,33

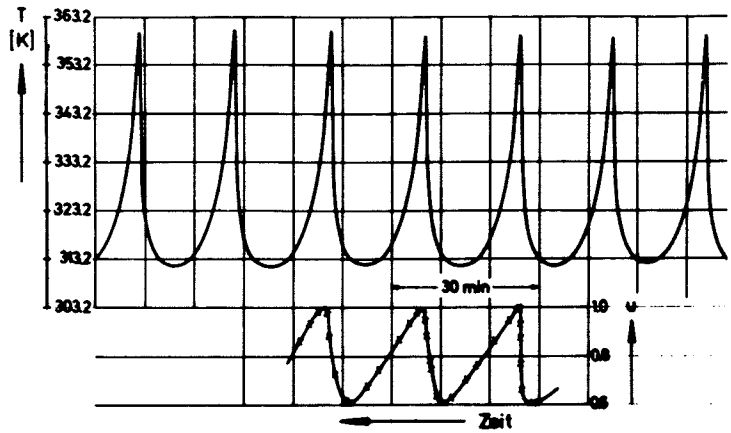

Figure 8. Measured oscillations of temperature and conversion

In Chemical Reaction Engineering—Houston; Weekman, V., et al.;
ACS Symposium Series; American Chemical Society: Washington, DC, 1978.

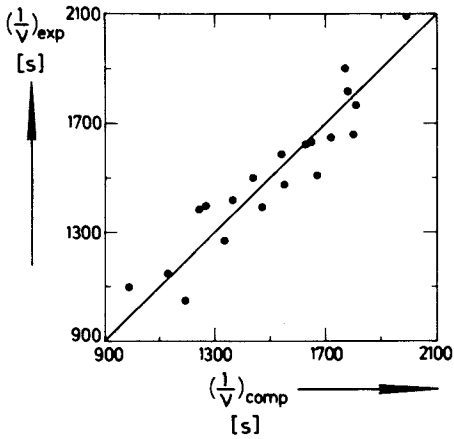

Figure 9. Experimental period of oscillation in comparison with computer period

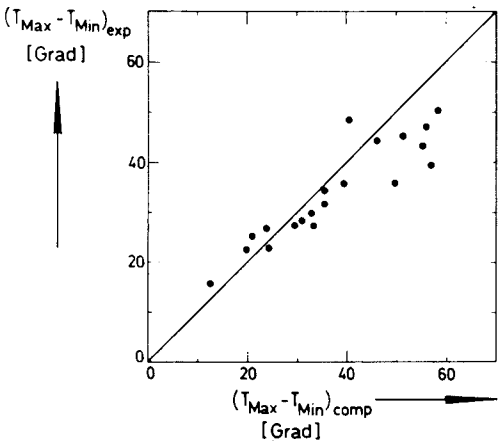

Figure 10. Experimental temperature difference ($T_{max} - T_{min}$) vs. computed results for the refined mathematical model

In Chemical Reaction Engineering—Houston; Weekman, V., et al.;
ACS Symposium Series; American Chemical Society: Washington, DC, 1978.

The parameter $\gamma(v)$ was determined from the temperature dependence of $P_{H_2O}(v)$.

On the basis of the refined heat balance (24) and Eq.(1a) a lot of computer simulations were performed that led to a good agreement between numerical calculations and experimental findings as per Fig. 9 and 10.

Abstract

The oscillatory behaviour of temperature and conversion in a cooled continuous-flow stirred tank reactor with a first order exothermic liquid phase reaction was studied.

Approximate analytical relationship were developed to predict the period and the amplitude of the limit cycle in a wide range of operation conditions. These theoretical results were linked to experimental findings.

The agreement between theoretical computations and experimental observations was good.

Notation

a	modified dimensionless amplitude of temperature, Eq. (17)
A	dimensionless amplitude of temperature, Eq. (11)
B	reaction number, Eq. (5a)
c	concentration
c_p	specific heat of reaction mixture
Da	Damköhler number Eq. (5d)
E	Activation energy
F	area for heat transfer to the coolant
$(-\Delta H)$	heat of reaction
$\Delta_V H$	heat of evaporation
$k(T_o)$	rate constant at T_o
k_w	heat transfer coefficient
$\dot{m}$	mass transfer coefficient
$\dot{n}_{O2}$	molar flow rate of oxygen
P_{H_2O}	water vapour
$\dot{Q}_{ev}$	heat per unit time by evaporation
r	reaction rate
R	universal gas constant
T	temperature
u	degree of conversion Eq. (2)
$\overline{u}$	time average of u Eq. (12)
v	dimensionless temperature difference Eq. (2)
V	volume of the reaction phase
$\dot{v}$	volume flow rate

In Chemical Reaction Engineering—Houston; Weekman, V., et al.;
ACS Symposium Series; American Chemical Society: Washington, DC, 1978.

Greek symbols

α	stability parameter, Eq. (7)
β	stability parameter, Eq. (8)
γ	dimensionless pressure ratio, Eq. (23)
ϵ	reciprocal of the dimensionless activation energy, Eq.(5b)
Θ	dimensionless time, Eq. (2)
μ	dimensionless heat transfer coefficient, Eq. (4)
μ^*	dimensionless cooling parameter, Eq. (5c)
$\frac{1}{\nu}$	oscillation period
ξ	dimensionless heat ratio, Eq. (25)
ρ	density of the reaction mixture
τ	mean residence time
ω	dimensionless frequency

Subscripts

comp	from computer solution
exp	referring to experimental data
E	entrance of reactor
k	coolant
L	by linearized equations
Lo	by linearized equations and $\alpha = o$
R	from regression equation
s	steady state
o	referring to T_o, Eq. (3)

"Literature Cited"

[1] WICKE,E., "Grundlagen der chem.Prozessregelung"p.54, Editors Oppelt and Wicke,Oldenbourg Verlag, München 1964
[2] HOFMANN,H.and HOFFMANN,U., Ind.Chim.Belge (1967)32, 326
[3] GILLES,E.D., the same book as [2], p. 111
[4] UPPAL,A., RAY, W.H. and POORE,A.B., Chem.Engng.Sci. (1974) 29, 967 and (1976) 31, 205
[5] DOUGLAS,J.M.and GAITONDE,N.Y.,Ind.Engng.Chem.Fund.(1967)6,265
[6] LUUS,R.and LAPIDUS,L., Chem.Engng.Sci.,(1966) 21, 159
[7] HUGO,P., Proc.4th Europ.Symp.on Chemical Reaction Engng., Brussels 1968, p. 459
[8] BEEK,J., Chem. Engng.Sci. (1977) 32, 265
[9] WIRGES,H.-P., Dissertation TU Berlin, 1977
[10] HAFKE,C., Diplomarbeit, TH Darmstadt, 1964
[11] HOFMANN,H., Proc.Third Europ.Symp. on Chemical Reaction Engng. Pergamon Press, Oxford 1965, p. 283

In Chemical Reaction Engineering—Houston; Weekman, V., et al.;
ACS Symposium Series; American Chemical Society: Washington, DC, 1978.

42

Effect of Periodic Operation on the Selectivity of Catalytic Reactions

A. S. AL-TAIE and L. S. KERSHENBAUM

Department of Chemical Engineering and Chemical Technology, Imperial College, London S.W.7, England

In recent years there has been a good deal of work which revealed that unsteady-state operation of chemical reactors often proves superior to the conventional steady-state operation. The subject has been extensively reviewed by Bailey (1) who classified the periodic operation according to the ratio of the cycle time to the dominant time constant of the system.

In spite of the numerous publications showing the potential of such periodic operations especially in the field of complex reactions, experimental studies are virtually non-existent. Of the few experimental works, Renken et al. (2) compared the performance of a tubular reactor in which a single reaction, the hydrogenation of ethylene, took place, under periodic operation and at steady-state. He reported an improvement of 60% in conversion. In another publication, Renken et al. (3) showed experimentally that periodic operation can be used to eliminate the temperature problems associated with highly exothermic reactions, e.g. the oxidation of ethylene over a silver catalyst. In other experimental work Unni et al. (4) showed that periodic variation of reactant composition improved the rate of oxidation of SO_2 over a vanadium oxide by as much as 30%. Denis and Kabel (5) studied the cyclic operation of a heterogeneous reactor for the vapour phase dehydration of ethanol and observed that adsorption/desorption played a predominant role in the transients of the system.

The above-mentioned work has dealt primarily with single reaction systems. Although much of the theoretical work has indicated that the real potential of periodic operation is in the improvement of selectivity in complex reaction systems, no experimental work has yet been reported to confirm these findings. In this work an experimental investigation has been conducted on the effect of cycling the inlet feed compositions on the performance of an isothermal heterogeneous fixed-bed catalytic reactor in which a complex reaction is taking place. The reaction system studied was the hydrogenation of butadiene over a commercial nickel catalyst.

© 0-8412-0401-2/78/47-065-512$05.00/0

Experimental

The experimental system is outlined in Fig. 1 and consists of three main parts - a reactants feed system, the fixed-bed catalytic reactor, and the gas analysis system.

All feed gases were supplied by the British Oxygen Co.; 1, 3-Butadiene was stated to be 99.6% pure, Hydrogen and Nitrogen were 99.9% pure. Normal, trans, and cis Butenes used for calibration purposes were 99.8% pure. The feed gases were thoroughly mixed in a jet mixer before entering the reactor. This also served to damp out any pressure waves during periodic operation. The periodic variation of the reactant composition was achieved by actuating two solenoid valves through an autotimer which gave two signals which, in these experiments, were 180° out of phase. The reactants stream after passing through the mixer entered the preheater, which was immersed along with the reactor in a water bath maintained at 70 (± 0.5)°C by a controlled heater unit.

The reactor was made of 10 mm ID brass tube and had a length of 0.25 m. Four copper-constant thermocouples, placed at intervals of 5 cm along the reactor axis, were connected to a Data Logger with a punch tape output. The reactor was packed with a commercial 23% Ni on Kieselguhr catalyst supplied by Harshaw Chemical Company. It was crushed to mesh size 18-22 (mean diameter 778 microns) and diluted by an inert packing of the same dimension (dilution ratio 3:2 by volume) which effectively eliminated any bulk temperature rise along the reactor. In addition, the feed gas always contained 60% diluent (nitrogen) which further reduced bulk temperature rises and minimized local hot spots on the catalyst. The catalyst was found to be active at temperatures greater than 30°C and no activation was required. It was normally stored under a blanket of nitrogen when not in use.

The effluent stream from the reactor could be either sent to a wet-test meter, or diverted to the vent. Provisions were also made for sampling of the product stream in a gas chromatograph during the steady-state runs or the collection of an effluent sample in a special purpose collection chamber during the cyclic runs. Similarly there was a by-pass arrangement for the analysis of the reactants stream for the steady-state runs and a reactant collection chamber for the cyclic runs.

The steady-state gas analyses were done by conventional chromatography, but for the periodic runs, the inlet and exit analyses were performed on an integrated sample. Any discrete-sample analytical technique such as chromatography has certain disadvantages under transient operation. These disadvantages are amplified when one is dealing with periodic operation at high frequencies, especially when the dead-time and elution time are large compared with the period of the input signal. In this work, we overcome these difficulties by collecting the reactor exit gas over many periods to calculate mean compositions. A modified water-displacement method was used; this assured that the product was being collected at a constant flow rate, despite variations

In Chemical Reaction Engineering—Houston; Weekman, V., et al.;
ACS Symposium Series; American Chemical Society: Washington, DC, 1978.

in liquid level in the collection chamber (6). The collected sample was then analyzed by chromatography using a column packed with 33% dimethyl-sulpholane on chromosorb P. The collection and sampling procedure was tested by comparing analyses of known compositions under non-reactive conditions. The error in the compositions was less than ± 0.8%.

The experimental runs were divided into two main categories, steady-state and periodic runs. The purpose of the steady-state runs was to obtain experimentally the value and conditions of maximum steady-state yield. The yield under periodic operating conditions was always compared with this maximum achievable under steady-state conditions. During each of these runs the reactant flow rates were set to the required value. After allowing time for the system to reach the steady-state, the effluent volumetric flow rate was measured by the wet-test meter. Effluent samples and feed gas samples were then analysed in the chromatograph. The temperature profile along the reactor was continuously monitored to check on the isothermality of the reactor. Steady-state runs were conducted at four residence time levels: 0.273, 0.352, 0.54 and 1.33 seconds. For each residence time, a set of ten runs were made at different H_2:C_4H_6 ratios, keeping the diluent composition (nitrogen) always constant at $\sim$ 60%. For all runs, the operating conditions were a temperature of 70°C (± 0.5°C) and a pressure of 1 psig (1.07 bar).

In the case of the periodic runs, the flow rates of the two reactants H_2 and C_4H_6 were divided into two sections. A portion of the feed of each reactant was fed at a constant rate and the balance in a periodic mode. The nitrogen flow rate was maintained at $\sim$ 60% of the total volumetric rate throughout each set of cyclic runs. The cycling policy was such that the mean composition, the overall volumetric flow rate and residence time, temperature and pressure were identical to those at the corresponding optimum steady state conditions.

Each periodic run was started by adjusting the flow rates of the fixed portions of the reactants to the required value. Then the flow rates of the cycled sections were set, by switching in turn, one of the solenoid valves, keeping the other switched off. The cycle time was set by programming the autotimer drum to give the required cycle time. A 15 minute interval was adequate for the system to reach pseudo-steady-state. The product sample was then collected, and the temperature profile along the reactor axis was continuously monitored to check the isothermality of the reactor.

Reactor Performance. In the absence of detailed economic data, the performance of a chemical reactor can be measured in terms of conversion, selectivity, yield, or some combination of these. The choice of a suitable performance index will depend upon the particular application, although maximum selectivity generally corresponds to negligible conversion i.e. small product-

In Chemical Reaction Engineering—Houston; Weekman, V., et al.;
ACS Symposium Series; American Chemical Society: Washington, DC, 1978.

ion rate of the desired products. Objective functions considered in this work were: (i) yield; (ii) selectivity subject to the constraint that the yield is equal to the maximum achievable at steady-state; (iii) the difference in production rate of desired and undesired products (7). (The yield is defined here as the moles of the desired intermediate produced per mole of reactant fed to the reactor).

For the competing/consecutive hydrogenation of butadiene, the conversion, selectivity, and yield can be calculated from experimental measurement of the mole fraction of each component in the exit and inlet gas streams. In all cases, care was taken to correct for fractional volume shrinkage upon reaction, which would otherwise have introduced a systematic error into the calculation.

For fair comparisons of the reactor performance under steady state and periodic operation, certain conditions or constraints must be satisfied. The periodic operation performance index should be compared to its optimum steady state counterpart, as there is no point in using periodic operation to achieve something which can otherwise be realized through the conventional steady-state mode of operation. The same amount of reactants should be used under both modes of operation. The same reaction conditions, e.g. pressure, temperature and residence time should apply.

Theoretical

The hydrogenation of Butadiene proceeds according to the following elementary steps (Bond (8)).

$$C_4H_6 + s \underset{k_{-1}}{\overset{k_1}{\rightleftharpoons}} (C_4H_6)_s \qquad (C_4H_8)_s + H_2 \xrightarrow{k_{s_2}} (C_4H_{10})_s$$

$$(C_4H_6)_s + H_2 \xrightarrow{k_{s_1}} (C_4H_8)_s \qquad (C_4H_{10})_s \underset{k_4}{\overset{k_{-4}}{\rightleftharpoons}} (C_6H_{10}) + s$$

$$(C_4H_8)_s \underset{k_3}{\overset{k_{-3}}{\rightleftharpoons}} C_4H_8 + s$$

From the mechanism it can be seen that material is added to or depleted from the gas phase by adsorption/desorption with the exception of hydrogen which is assumed to be consumed directly from the gas phase. In formulating a theoretical model for the system it was assumed that the adsorption/desorption kinetics played an important role in the dynamics of the periodic operation and these kinetics were incorporated into the dynamic equations. Furthermore, it was assumed that there was neither bulk nor pore diffusional heat and mass transfer resistances, that the reactor was isothermal (both in the bulk gas phase and locally) and that the flow pattern in the reactor could be approximated by plug flow. Most of the above assumptions (i.e. plug flow, bulk isothermal conditions, no pore diffusion limitations) could be

In Chemical Reaction Engineering—Houston; Weekman, V., et al.;
ACS Symposium Series; American Chemical Society: Washington, DC, 1978.

verified by simple independent experiments or by well accepted correlations. Under these conditions and assuming that the adsorption/desorption follows the Langmuir monolayer theory, differential mass balances on the gas and solid phases yield

Gas phase:

$$\frac{\partial x_i}{\partial z} + \frac{\varepsilon}{v}\frac{\partial x_i}{\partial t} = \frac{-(P\theta_v x_i k_i - k_{-i}\theta_i)(1-\varepsilon)\rho_c}{v\rho_m} \quad ; \quad i = 1,3,4 \qquad (1)$$

Hydrogen, i = 2, is removed directly from the gas phase and hence

$$\frac{\partial x_2}{\partial z} + \frac{\varepsilon}{v}\frac{\partial x_2}{\partial t} = \frac{r_{s_2}(1-\varepsilon)\rho_c}{v\rho_m} \qquad (2)$$

Adsorbed phase:

$$\frac{\partial \theta_i}{\partial t} = \frac{(P\theta_v x_i k_i - k_{-i}\theta_i) + r_{si}}{y_m} \qquad (3)$$

where r_{si} is the rate of surface reaction of component i, where

$$\begin{bmatrix} r_{s_1} \\ r_{s_2} \\ r_{s_3} \\ r_{s_4} \end{bmatrix} = \begin{bmatrix} -1 & 0 \\ -1 & -1 \\ +1 & -1 \\ 0 & +1 \end{bmatrix} \begin{bmatrix} R_{s_1} \\ R_{s_2} \end{bmatrix} \qquad (4)$$

$$R_{s_1} = k_{s_1} P\theta_1 x_2$$
$$R_{s_2} = k_{s_2} P\theta_3 x_2$$

The adsorption/desorption rate constants were experimentally measured using a chromatographic technique (9) and the surface reaction rate constants were obtained independently from a non-linear regression of the data from the steady state runs. The set of coupled hyperbolic partial differential equations (1)-(4) were solved numerically by the method of characteristics. The high degree of coupling in the different characteristic directions required that an iterative method be used for the numerical solution (6).

Results

Steady-State Runs. Four levels of residence times were employed: 0.273, 0.352, 0.54 and 1.33 seconds. Each set of runs was conducted over a wide range of ratio of reactants in the feed stream, keeping the nitrogen composition constant throughout at ∿ 60%, and the water bath temperature at 70°C. The objective of these runs was to establish experimentally the conditions for optimum steady-state yield, and to determine the kinetics

In Chemical Reaction Engineering—Houston; Weekman, V., et al.;
ACS Symposium Series; American Chemical Society: Washington, DC, 1978.

of the reactions. The results of these steady-state runs are presented in Figs. 2 to 4 in the form of conversion, selectivity, and yield vs. H_2:Butadiene ratio. From Fig. 4, it can be seen that the optimum yield value for each residence time occurs at a given H_2:Butadiene ratio which is sharply defined. The values of the conversion and selectivity which correspond to the maximum yield can be read from Figs. 2 and 3.

It is more convenient to transform these steady state data into a plot which is independent of residence times and feed composition. Levenspiel (10) gave a general time-independent plot for second-order series-parallel reactions. However, it can be shown that such a plot is also valid for Langmuir-Hinshelwood kinetics, if the denominators are the same for both reactions. Figs. 5 and 6 show universal, time-independent plots for steady-state yield and selectivity vs. conversion for all residence times and H_2:Butadiene ratios less than 6 (runs at the higher ratios were difficult to reproduce because of uncertainties in chemical analyses caused by the high dilution). It can be seen from these two plots that the optimum steady-state yield is 30% and the corresponding conversion and selectivity are 50% and 60% respectively.

The steady-state data were also used to estimate the best values of the surface rate constants, k_{s_1} and k_{s_2}. This was achieved by a non-linear weighted least squares estimation technique, given the experimentally obtained values of the adsorption/desorption rate constants. These constants were subsequently used in the simulation of the cyclic runs.

Cyclic Runs. Having established the inlet ratio of H_2:Butadiene for which the steady-state yield is maximised for a given residence time, the cyclic runs were carried out such that the mean value of the feed compositions were as near as possible to their optimum steady-state values. The mole fractions of H_2 and Butadiene were cycled out of phase in a symmetrical square wave fashion. Such symmetrical wave forms need not be the optimum periodic operation. Indeed, Farhad Pour et al. (7) demonstrated theoretically that it was possible to obtain further improvement in the selectivity of series-parallel reactions in a CSTR when asymmetrical rather than symmetrical square waves are considered. Theoretically the search for the optimum wave modulation, or the number of switches over one cycle time, can be computed by search methods or optimisation routines. However, in this work we arbitrarily limited ourselves to symmetrical square waves which are 180° out of phase accepting that such a configuration may, indeed, be quite far from the optimum periodic mode.

The periodic operation was conducted over the whole range of disturbance amplitude, λ(0-100%) and cycle time, τ_p (2-30 seconds). Two levels of residence time were employed, 0.27 and 0.54 seconds. Typical results for these periodic runs are presented in Figs. 7-9 in the form of time average conversion, selectivity and yield

In Chemical Reaction Engineering—Houston; Weekman, V., et al.;
ACS Symposium Series; American Chemical Society: Washington, DC, 1978.

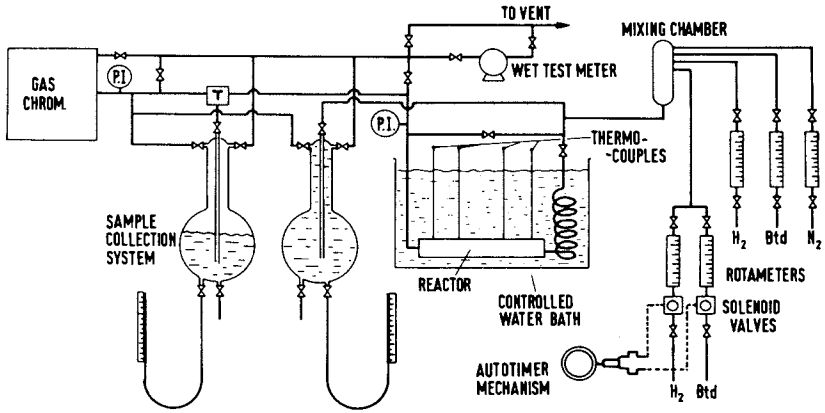

Figure 1. Diagram of experimental system

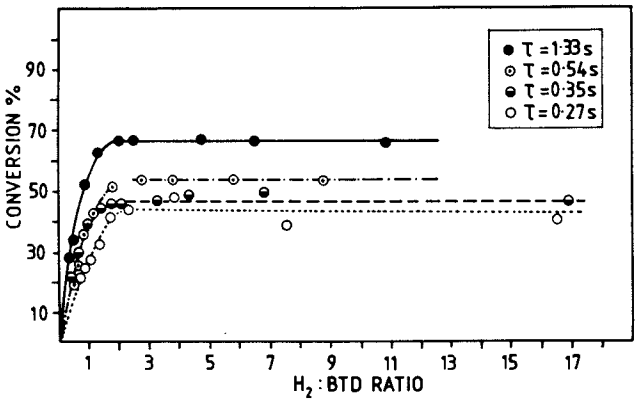

Figure 2. Steady-state conversion of C_4H_6

In Chemical Reaction Engineering—Houston; Weekman, V., et al.;
ACS Symposium Series; American Chemical Society: Washington, DC, 1978.

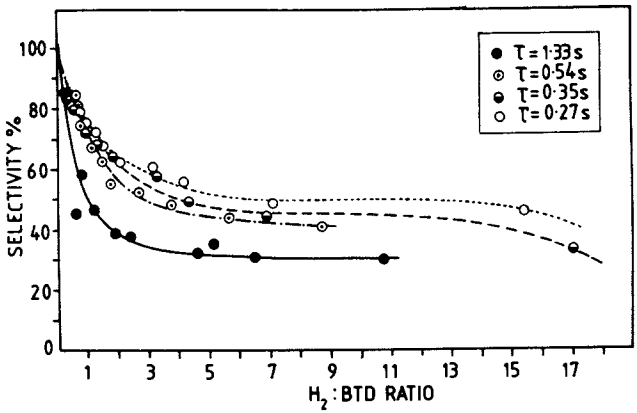

Figure 3. Steady-state selectivity

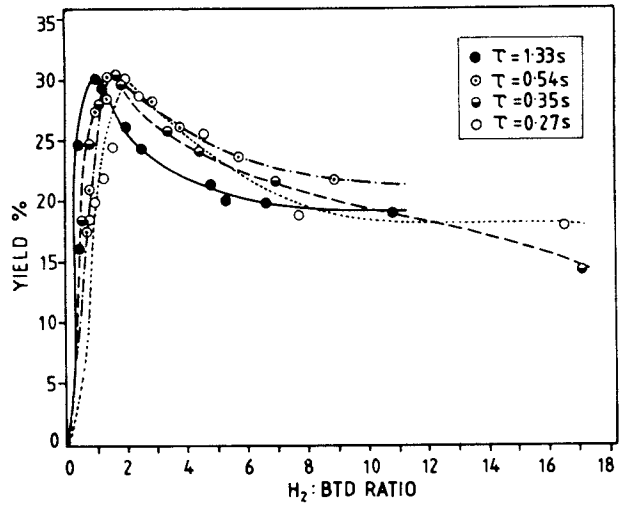

Figure 4. Steady-state yield of C_4H_8

In Chemical Reaction Engineering—Houston; Weekman, V., et al.;
ACS Symposium Series; American Chemical Society: Washington, DC, 1978.

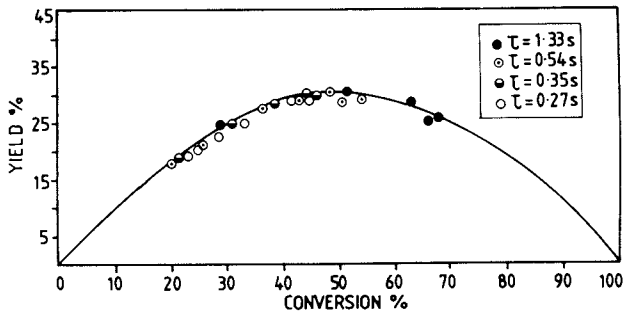

Figure 5. Composite plot of yield vs. conversion

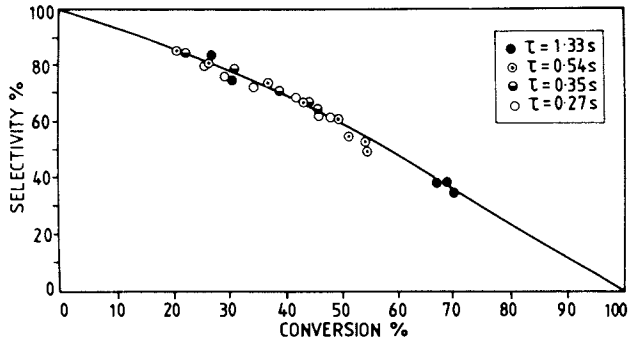

Figure 6. Composite plot of selectivity vs. conversion

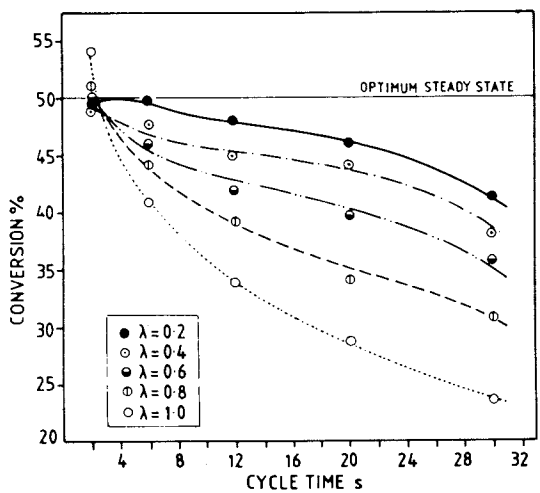

Figure 7. Mean conversion under periodic operation

In Chemical Reaction Engineering—Houston; Weekman, V., et al.;
ACS Symposium Series; American Chemical Society: Washington, DC, 1978.

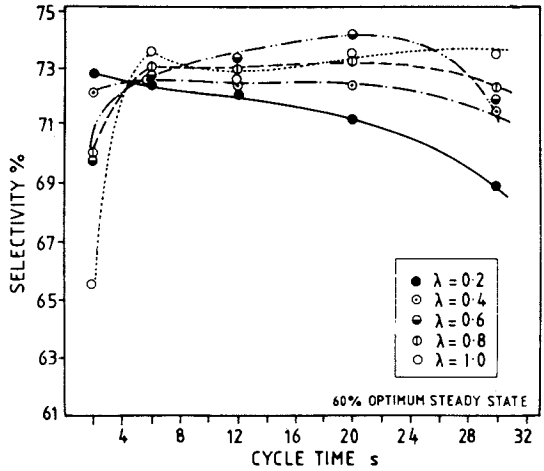

Figure 8. Mean selectivity under periodic operation

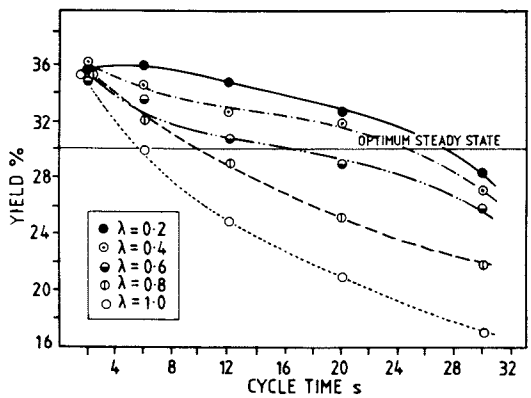

Figure 9. Mean yield under periodic operation

In Chemical Reaction Engineering—Houston; Weekman, V., et al.;
ACS Symposium Series; American Chemical Society: Washington, DC, 1978.

for one residence time. They are compared to the corresponding steady-state values at optimum yield given in the previous section. It can be seen that relatively high improvements in either yield, selectivity or both can be obtained depending on the choice of amplitude, cycle time and the reactor residence time.

Faced with this wide spectrum of improvements we must state our objective clearly. Choosing yield as a performance index, it can be seen that as much as 20% improvement in yield is possible depending on the choice of amplitude, cycle time and residence time. On the other hand, improving the selectivity alone is meaningless, as this can lead to infinitesimal conversion. Consequently, for a meaningful comparison between steady-state and periodic operation we should impose the constraint that the reactor performance is measured under identical yield values corresponding to the optimum steady-state. Selectivities attainable under periodic operation for each residence time and amplitude show that an increase of up to 24% can be achieved while maintaining the yield at its optimum steady-state value. Thus, periodic operation is capable of improving both the quality and the quantity of a desired product over its best steady-state value. This is reminiscent of the work of Cannon et al. (11) who observed that, depending on the choice of the liquid flow time and the vapour flow time, it is possible to improve either the efficiency or the capacity of a distillation column by periodic operation.

To complete the picture over the whole range of frequencies, a set of runs was made under conditions of slow cycling ($\tau_p \rightarrow \infty$). In all cases, the conversion and yield under slow cycling was always inferior to the optimum steady-state values This is to be expected as their response surfaces are concave.

A typical result of the simulation of the reactor behaviour corresponding to conditions in Figs. 7-9 is shown in Fig. 10. These result from the numerical solution of the dynamic equations (1) - (4) with the relevant rate constants for adsorption/desorption and surface reaction, equilibrium constants and catalyst capacity obtained by independent experimental measurements (no fitting of the periodic data was attempted). The results clearly indicate a general agreement with the experimental data. The simulations are described and discussed in detail elsewhere (6, 12).

Discussion

The results presented above illustrate that significant improvement can be achieved in the performance of reactors with complex reactions. Furthermore, this performance could be explained by postulating that the kinetics of adsorption/desorption played an important role in the system dynamics in general and in this improvement, in particular. Nevertheless, there are other models which could also be consistent with this behaviour,

In Chemical Reaction Engineering—Houston; Weekman, V., et al.;
ACS Symposium Series; American Chemical Society: Washington, DC, 1978.

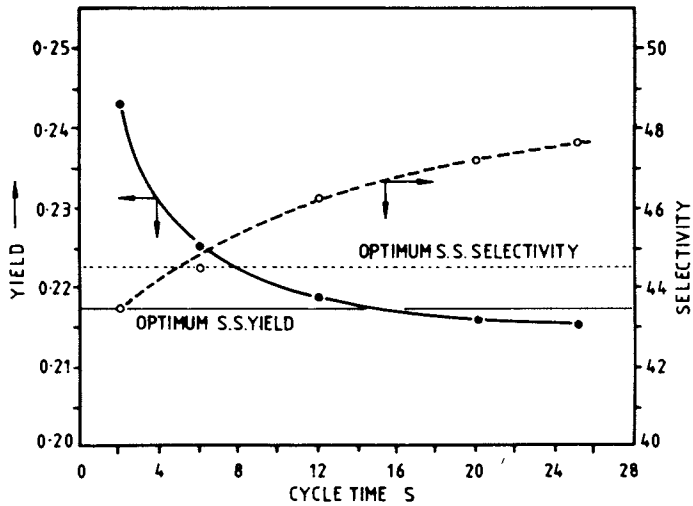

Figure 10. Simulation of mean yield and selectivity under periodic operation

In Chemical Reaction Engineering—Houston; Weekman, V., et al.;
ACS Symposium Series; American Chemical Society: Washington, DC, 1978.

and an attempt was made to confirm that the adsorption effects were indeed predominant. A set of step and pulse responses was performed under both reactive conditions (i.e. with both reactants present) and under non-reactive conditions. It was seen that, in both cases, the form of the responses and the mean and spread of the response curves were nearly identical. This implied that the same process (adsorption/desorption) was responsible for the dynamics of the system under both reactive and non-reactive conditions. Furthermore, it appeared that local thermal effects were not the main factor in the improvement of performance, although they may have been a contributing factor. Having postulated a mechanism for the reactor dynamics, possible reasons for the improvement in the reactor conversion, yield and/or selectivity can be discussed qualitatively. It can be argued that under cyclic operation the catalyst bed is capable of holding more reactant (Butadiene) for short periods of time than at the corresponding steady-state. Hence over the hydrogen-rich half of the cycle it is possible to hydrogenate more of the Butadiene. Similarly, because of the strong Butadiene adsorption Butenes are desorbed before they have a chance to react further to Butane with consequent increases in selectivity.

Conclusion. The work has demonstrated experimentally that significant improvement in the yield and/or selectivity can be obtained by operating a reactor with competing/consecutive reactions in a periodic mode. The main cause of this improvement appears to be the resonance induced by the adsorption/desorption kinetics during periodic operation.

Notation

k_i	adsorption rate constant	kmol/kg.s.bar
k_{-i}	desorption rate constant	kmol/kg.s
k_{s1}, k_{s2}	surface reaction rate constants	kmol/kg.s.bar
P	total pressure	bar
r_{si}	net rate of surface reaction	kmol/kg.s
R_{s1}, R_{s2}	rate of surface reaction for hydrogenation of butadiene, butene	kmol/kg.s
t	time	s
v	linear gas velocity	m/s
x_i	mole fraction of component i	
y_m	capacity of catalyst	kmole/kg
ε	voidage	
θ_i	surface coverage for component i	
λ	amplitude	
ρ_c	catalyst density	kg/m^3
ρ_m	molar gas density	$kmol/m^3$
τ	mean residence time	s
τ_p	period of input disturbance	s

Subscript i refers to component: 1=C_4H_6; 2=H_2; 3=C_4H_8; 4=C_4H_{10}

In Chemical Reaction Engineering—Houston; Weekman, V., et al.;
ACS Symposium Series; American Chemical Society: Washington, DC, 1978.

Literature Cited

(1) Bailey J.E., Chem. Eng. Commun., (1973), 1, 111.
(2) Renken A., Helmrich H. and Schügerl K., Chem. Ingr. Techn., (1974), 46, 647.
(3) Renken A., Müller M. and Wandrey C., Proc. 4th Intl. Conf. Chem. Reac. Eng., (1976), Heidelberg, 107.
(4) Unni M.P., Hudgins, R.R. and Silveston P.L., Can. J. Chem. Eng., (1973), 51, 623.
(5) Denis G.H. and Kabel R.L., A.I.Ch.E. Jl. (1970), 16, 972.
(6) Al-Taie A.S., Ph.D. Thesis, University of London, 1977.
(7) Farhad-pour F.A. and Gibilaro L.G., Chem. Eng. Sci., (1975), 30, 735.
(8) Bond G.C., "Catalysis by Metals", Academic Press, N.Y. (1962).
(9) Smith J.M. and Schneider P., A.I.Ch.E. Jl., (1962), 14, 762.
(10) Levenspiel O., "Chemical Reaction Engineering", Wiley, (1972).
(11) Cannon M.R., Oil and Gas J., (1956), 55, 68
(12) Al-Taie A.S. and Kershenbaum L., in press

In Chemical Reaction Engineering—Houston; Weekman, V., et al.;
ACS Symposium Series; American Chemical Society: Washington, DC, 1978.

43

Dynamic Studies of Acetylene Hydrogenation on Nickel Catalysts

M. R. BILIMORIA and J. E. BAILEY

Department of Chemical Engineering, University of Houston, Houston, TX 77004

Several benefits including improved selectivity, increased conversion, and reduced sensitivity may in some cases be realized by intentional periodic operation of chemical reactors [1-6]. These alterations in reactor performances arise because, in dynamic operation, the governing rate processes may assume different relationships than can occur in the more constrained steady state case. Thus, in addition to revealing promising new operational policies for chemical reactors, unsteady-state reaction studies may provide valuable insights into the fundamental properties of the reaction system.

This study focuses on the vapor-phase catalytic hydrogenation of acetylene to ethylene and ethane:

$$C_2H_2 + H_2 \longrightarrow C_2H_4$$

$$C_2H_4 + H_2 \longrightarrow C_2H_6$$

Bond [7], Komiyama and Inoue [8], and several others have studied this reaction sequence using nickel catalysts, and Bond et al. [9] have reported that the ethylene selectivity S varies with hydrogen partial pressure p_{H_2} according to

$$S = 1 - Kp_{H_2}^n \text{ where } K = \text{a constant and } 0<n<1. \qquad (1)$$

Since S is a convex function of p_{H_2}, it appears that fluctuations in p_{H_2} will have a beneficial effect on ethylene selectivity. This hypothesis has been corroborated in simulation studies based upon the kinetics of Komiyama and Inoue [8]. Lee's calculation [10] indicates that substantial improvements in ethylene selectivity may be obtained by cycling the feed hydrogen concentration to a perfectly mixed, isothermal continuous flow reactor with a

© 0-8412-0401-2/78/47-065-526$05.00/0

period of the order of one-half the mean reactor residence time. Although intrapellet diffusional effects were considered by Lee, it is important to note that other dynamic phenomena which might occur within the porous catalytic solid were totally neglected in his model.

Experimental Materials and Methods

The reaction was conducted at a pressure of 108.2 kN/m^2 in a continuous-flow, spinning basket (104.7 rad/s) stainless steel reactor with a mean residence time of 66 s. Nearly isothermal operation at 439 K was maintained by automatic on-off control of a heater in an air-cooled jacket surrounding the reactor. The gases used in the experiments were Linde Lab 145 Atomic absorption grade acetylene (>99.6%), prepurified grade hydrogen (>99.99%) and prepurified grade nitrogen (>99.997%). Acetylene feed to the reactor was maintained constant at 0.5 cm^3/s, whereas the flow-rates of hydrogen and inert nitrogen were adjusted in a complementary manner so as to maintain total gas feed rate of 5 cm^3/s.

In periodic experiments, the inlet hydrogen flow rate u(t) was varied in a bang-bang fashion as follows:

$$u(t) = \begin{cases} 1.625 \text{ cm}^3/\text{s} & \text{for } 0 \leq t < \gamma\tau \\ 0.250 \text{ cm}^3/\text{s} & \text{for } \gamma\tau \leq t < \tau. \end{cases} \quad (2)$$

Here τ is the length of one cycle or period, and γ is the fraction of τ for which the hydrogen feed rate is at the upper level. The manipulated input u is evaluated at subsequent times according to the periodicity rule

$$u(t) = u(t + \tau) \qquad \text{for } t \geq 0 \quad (3)$$

The mean or time-average hydrogen flow rate is

$$\bar{u} = 0.25 + 1.375\gamma \text{ cm}^3/\text{s} \quad (4)$$

and the nitrogen feed flow-rate w(t) is specified by

$$w(t) = 4.5 - u(t) \quad \text{cm}^3/\text{s}. \quad (4)$$

These variations in feed hydrogen and nitrogen concentrations were generated without any appreciable pressure fluctuations and at constant volumetric flow by a dosing system composed of a multichannel electronic timer, metering valves, and solenoid valves as shown in Figure 1.

The catalysts used in the experiments, Harshaw Ni-0707T (Catalyst I) and Girdler G52 (Catalyst II), were crushed to a size of 0.84-1.2 mm and pretreated by soaking in 5% (wt.) solution of $Na_2S_2O_3$ in H_2O for 24 h as recommended by

Komiyama and Inoue [9]. Before each run, the catalyst was activated "in situ" in a hydrogen stream at 477 K for 6 h.

From time to time, the effluent concentrations from the reactor were measured using a 0.25 cm^3 sampling valve and a flame-ionization type gas chromatograph with a Porapak N column and nitrogen carrier at 313 K. The resulting peaks from the chromatograph were recorded on a strip-chart and integrated automatically by a digital integrator. The product gas stream was also monitored continuously by a variable-filter infra-red analyzer with a flow-through cell, and acetylene, ethylene and ethane were detected at 3.05, 5.25 and 6.55 (all μm), respectively.

The reactor is said to be in a periodic state when all the state variables satisfy the condition

$$x_i(t) = x_i(t + \tau) \qquad \text{for } t > t_p \tag{6}$$

where t_p is defined as the start-up time required to reach periodic conditions. The oscillating effluent concentrations may be damped by a surge tank (see Figure 1) to obtain a time-invariant process effluent which may be directly compared to the products of steady-state reactor operation. The time-average effluent concentrations may also be calculated using

$$\bar{x}_i = \frac{1}{\tau} \int_{t_p}^{t_p+\tau} x_i(t)dt \tag{7}$$

and sets of instantaneous concentration data which span the period. These computed values were consistently in good agreement with direct surge-tank measurements.

Results and Discussion

The experimental results are presented in Figures 2 through 8. Figure 2 is a comparison of steady-state compositions with time-average values obtained by cycling with different periods for Catalyst I. This catalyst showed negligible fouling with almost constant activity, a result consistent with conventional B.E.T. surface-area measurements which gave values of ~125 - 129 m^2/g before and after reaction. The data show that periodic operation results in increased conversion for τ=60 s, τ=180 s and τ=300 s, with the maximum effect obtained for the longest period. In addition, the data for τ=300 s show a significant improvement in both ethylene and ethane yields. This dependence on cycling period is quite different from Lee's predictions (optimum period ≈ 1/2 mean residence time = 33 s) and suggests that the catalyst phase dynamics cannot be neglected for this system.

The instantaneous concentration-time profiles obtained during periodic operation with Catalyst I for τ=300 s are shown in Figure 3. All these curves were obtained by making 15 discrete

In Chemical Reaction Engineering—Houston; Weekman, V., et al.;
ACS Symposium Series; American Chemical Society: Washington, DC, 1978.

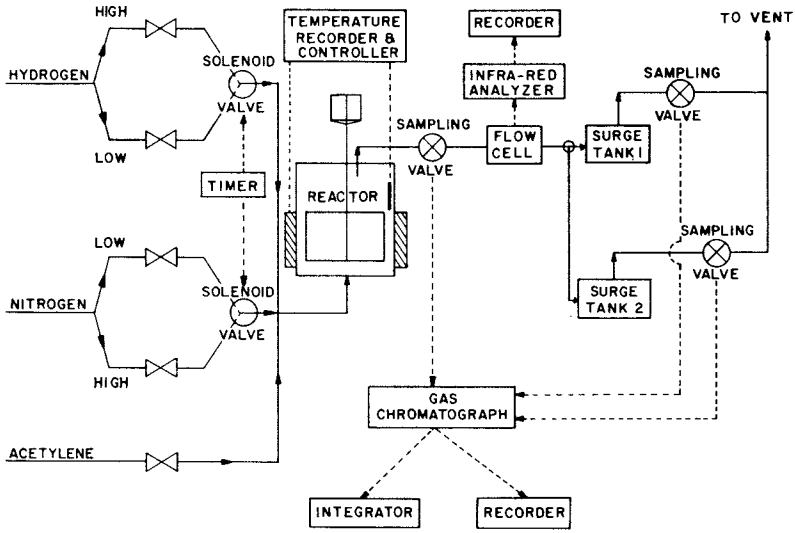

Figure 1. Experimental reaction system highlighting cyclic feed makeup apparatus and effluent analysis equipment

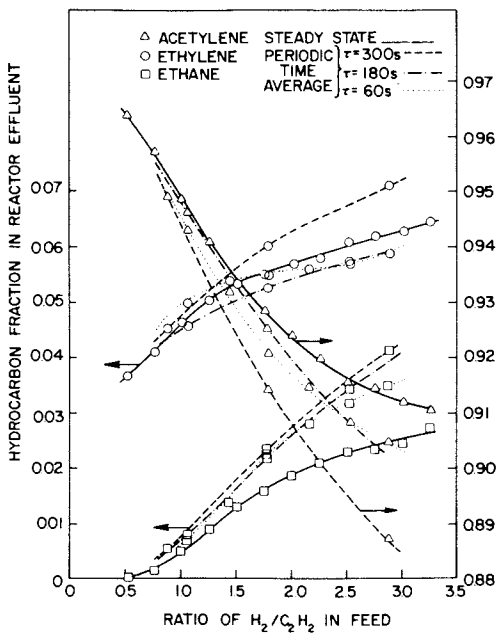

Figure 2. Steady-state (solid line) and periodic (broken lines—see legend) effluent hydrocarbon distributions for various time-average hydrogen/acetylene feed ratios for Catalyst I

In Chemical Reaction Engineering—Houston; Weekman, V., et al.;
ACS Symposium Series; American Chemical Society: Washington, DC, 1978.

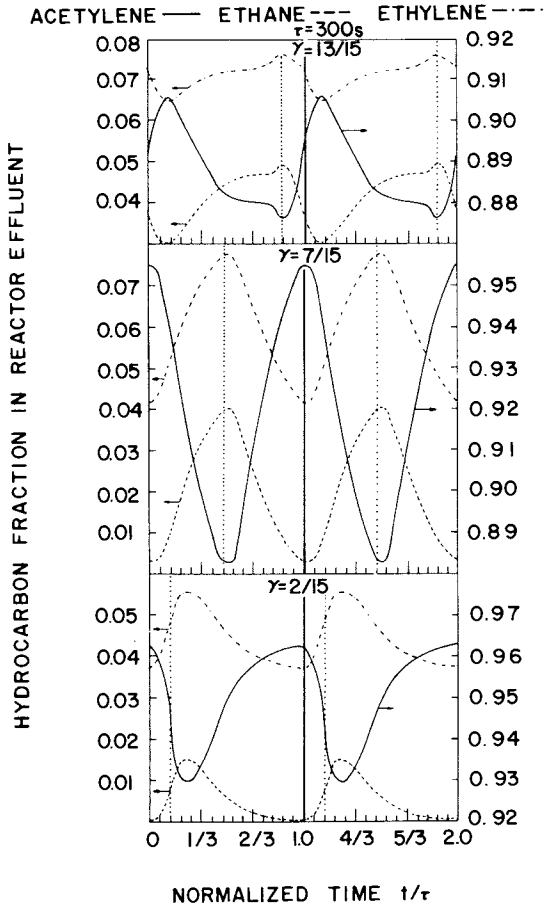

Figure 3. Instantaneous effluent compositions for cycling with Catalyst I and a period of 300 s. Different sets of data correspond to different mean hydrogen feed rates.

In Chemical Reaction Engineering—Houston; Weekman, V., et al.;
ACS Symposium Series; American Chemical Society: Washington, DC, 1978.

measurements at different times during one period using the gas chromatographic method already described. These data show the effect of varying γ for a constant τ. As expected, the wave-form for each component shows a maximum variation in amplitude for $\gamma \approx 1/2$. The wave-forms for $\gamma = 13/15$ show unusual discontinuities just before the hydrogen is switched to the lower level, and it is this set of operating conditions that gives rise to the largest differences between periodic time-average and steady-state behavior for all three hydrocarbons. For $\gamma = 7/15$ and $\gamma = 2/15$, the profiles indicate that acetylene conversion continues to increase for a short time after the hydrogen feed rate is switched to the lower level. Similar overshoots are also observed for both ethylene and ethane.

These observations reinforce the hypothesis that such phenomena are a direct consequence of capacitances within the solid catalyst phase with a response time of the order of several minutes. In an attempt to better understand this unexpected behavior, another series of unsteady-state experiments was conducted with Catalyst I. A step increase in hydrogen feed concentration showed an overshoot in the instantaneous ethylene concentration followed by a very slow approach to steady-state (see Figure 4). On the other hand, a step decrease in feed hydrogen resulted in a relatively very rapid and monotonic decline to the final steady-state ethylene concentration. It should be noted that the sum of all hydraulic and mixing lags for this system is of the order of 75 s and the diffusional relaxation time (R^2/D_e) is much smaller than one second. Hence, the extremely slow response observed in the step-up experiment and its asymmetry compared to the step-down result suggest that non-linear dynamics of the gas phase-catalyst surface interaction play a major role in unsteady reactor behavior.

A more complete set of experiments was done with Catalyst II which gave higher absolute conversions than Catalyst I for the same feed conditions. However, this catalyst, which had a higher nickel content and more acid sites than Catalyst I, was found to be subject to severe fouling. In order to keep track of the gradual decline in catalyst activity, the sequence of experiments was modified in such a way that periodic experiments were sandwiched in between steady-state experiments. Figure 5 shows a comparison of steady-state and periodic time-average data for ethane on Catalyst II. The results show an increasing trend in ethane selectivity due to cycling which was counter to the gradual decline in catalyst activity due to drastic fouling. The steady-state region shown on this figure indicates the attainable set of ethane compositions by steady-state operation throughout the entire useful life of this catalyst and hence includes effects which are a direct consequence of the fouling. Figure 5 clearly demonstrates that in spite of fouling, periodic operation of chemical reactors gives rise to product compositions which are unavailable in any steady-state operation.

In Chemical Reaction Engineering—Houston; Weekman, V., et al.;
ACS Symposium Series; American Chemical Society: Washington, DC, 1978.

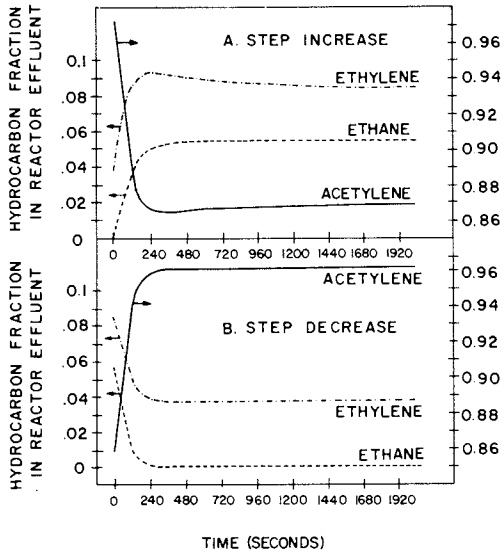

Figure 4. The results of a step-up in feed hydrogen mole fraction (A) show overshoots and much longer transients than the reverse step-down experiment (B) for Catalyst I

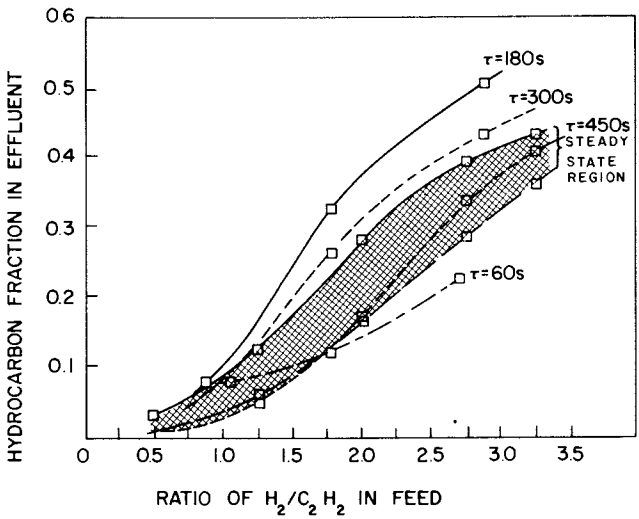

Figure 5. The shaded region shows the domain of ethane yields obtained in several different steady-state experiments at different stages of deactivation of Catalyst II. The curves show ethane yields obtained by cycling feed hydrogen concentration with different periods.

In Chemical Reaction Engineering—Houston; Weekman, V., et al.;
ACS Symposium Series; American Chemical Society: Washington, DC, 1978.

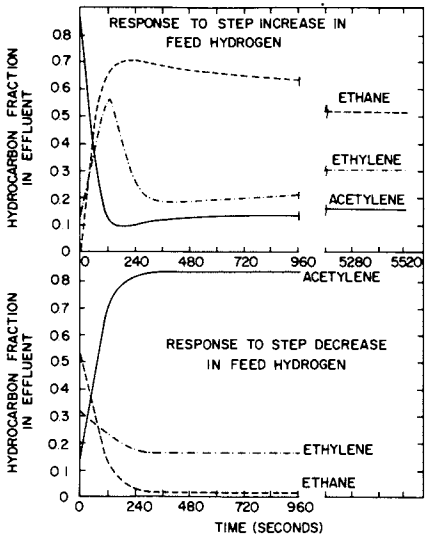

Figure 6. Feed hydrogen step-up (A) for Catalyst II produces a damped oscillation in effluent ethylene in contrast to a step-down in feed hydrogen (B)

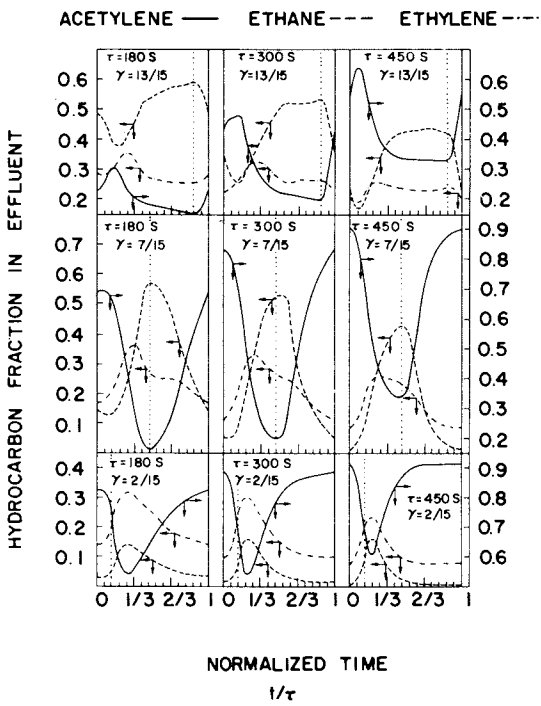

Figure 7. Instantaneous effluent compositions for feed hydrogen cycling with Catalyst II for nine sets of periods (τ) and mean hydrogen feed rates (directly related to γ: see Equation 4)

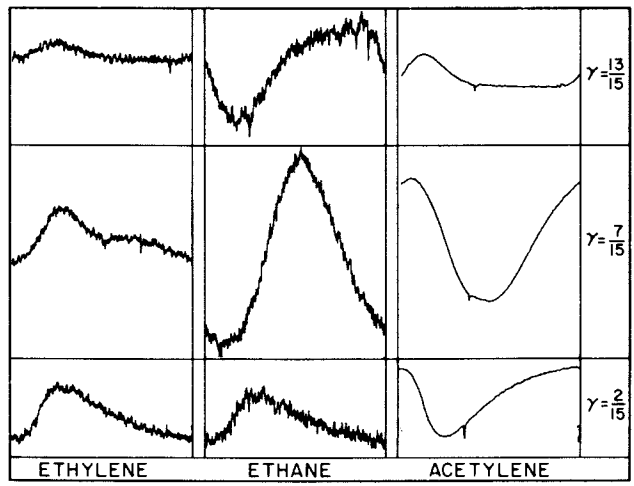

Figure 8. Periodic effluent concentrations for three different switching fractions as measured continuously using the ir analyzer (τ = 180 s, Catalyst II)

In Chemical Reaction Engineering—Houston; Weekman, V., et al.;
ACS Symposium Series; American Chemical Society: Washington, DC, 1978.

Step response experiments for this catalyst show that when the reactor is subjected to a step increase in feed hydrogen, the ethylene concentration profile exhibits damped oscillations, while ethane and acetylene show an overshoot and an undershoot, respectively, followed by a slow monotonic approach to the final steady-state value. On the other hand, an asymmetric response was again observed for a step decrease in feed hydrogen (Figure 6).

Figure 7 shows the results of a parametric study of the instantaneous concentration-time profiles obtained by cyclic operation with Catalyst II for different τ's and γ's. All these curves were obtained from gas chromatographic measurements. Once more, as with Catalyst I, for $\gamma = 2/15$ and all three τ's the profiles tend to overshoot the switching point. As expected, for a fixed value of γ, the peaks in the wave-forms tend to become sharper as τ increases, and this effect is most clearly seen in the bottom row of diagrams. The curves for $\gamma = 7/15$ are different in that acetylene and ethane seem to follow the switch from high to low hydrogen feed rate fairly well although they tend to overshoot the reverse switching point. The behavior of ethylene for these cases is dramatically different. In the case of $\gamma = 13/15$ all three components follow the high to low hydrogen switch very well, but show a considerable lag for the reverse operation. These rather unusual response patterns have been confirmed by continuous infra-red measurements (see Figure 8).

The results obtained in these unsteady-state studies clearly show that the dynamics of the gas phase-catalyst surface interaction cannot be neglected when determining a periodic control strategy. Further, catalyst surface capacitance should not generally be neglected when investigating stability and control of catalytic reactors. Similar conclusions have resulted recently from several studies of self-oscillating isothermal catalytic reactions [11]. Features observed in dynamic experiments such as these will undoubtedly contribute to improved understanding of catalyst behavior.

Acknowledgments

We are grateful to Dr. Duane D. Bruns for his help in the design and fabrication of the reactor. We are also grateful to the National Science Foundation, the Camille and Henry Dreyfus Foundation, and the University of Houston for financial support to this work.

Literature Cited

1. Bailey, J. E., Chem. Eng. Comm. 1, 111 (1973).
2. Bailey, J. E. and F. J. M. Horn, JOTA 7, 378 (1971).
3. Bailey, J. E. and F. J. M. Horn, Chem. Eng. Sci. 27, 109 (1972).
4. Renken, A. et al., Proc. AIChE/GVC Mtg. Munich, p. A3-1 (1974).

5. Renken, A., Chem. Eng. Sci. 27, 1925 (1972).
6. Renken, A. et al., 4th Int./6th Europ. Symp. Chem. React. Eng., Heidelberg, p. III-107 (1976).
7. Bond, G. C., J. Chem. Soc., p. 2705, 4288, 4738, (1958).
8. Komiyama, H. and Inoue, H., J. Chem. Eng. Jap. 1, 142 (1968).
9. Bond, G. C. et al., Trans. Far. Soc. 54, 1537 (1958).
10. Lee, C. K., MS Thesis, Univ. of Houston (1972).
11. Sheintuch, M. and Schmitz, R. A., Cat. Rev., in press.

In Chemical Reaction Engineering—Houston; Weekman, V., et al.;
ACS Symposium Series; American Chemical Society: Washington, DC, 1978.

44

Multiple Steady States of a Moving Bed Reactor—Theory and Experiment

KLAUS THOMA and DIETER VORTMEYER

Institut B für Thermodynamik, Technische Universität München, 8000 München 2, Arcisstr. 21, West Germany

A moving bed chemical reactor is characterized by a cc- or countercurrent movement in the presence of chemical reactions. Furthermore heat and mass is exchanged between the two phases. Due to the solid movement the reactors are difficult to model in laboratory experiments.

The only experiments known to us are reported by Weekman and Nace (1). These authors were mainly interested in the behaviour of an isothermal moving bed reactor with respect to catalytic cracking and used for their experiments more or less free falling particles in a cocurrent gas stream.

In the present paper model experiments are reported under defined conditions for gas and solid flow by countercurrent operation. In this situation the energetic feedback by the effective heat conduction is increased through the countercurrent movement. Interesting stability problems arise concerning ignition/extinction phenomena.

In principle these effects are rather similar to those encountered in fixed bed reactors (2), (3), (4) although the situation gets a new dimension by the solid movement. A simplified theoretical investigation of a countercurrent moving bed reactor was presented by Schaefer, Vortmeyer and Watson (5). The work neglects heat conduction in both phases, the only feedback mechanism being the movement of one phase against the other. Three solutions were obtained for certain parameter ranges. The upper and lower solutions were stable and the middle one unstable.

It is interesting to note that the governing equations for a moving bed are identical with the two phase model of a liquid/liquid spray column which was investigated theoretically by Luss and Amundson (6).

The aim of our work was to design a laboratory model of a moving bed reactor and to compare experimental results with numerically predicted multiple steady state solutions of the governing equations.

© 0-8412-0401-2/78/47-065-539$05.00/0

Design of a moving bed reactor

The most difficult problem was to obtain a defined steady movement of the solid. A movement due to gravitational force only results in a stick-slip flow (Yoshida et al (7)) which makes the desired measurement uncorrect, if not impossible. Therefore the catalyst particles were surrounded by a fine wire cloth. This tubular arrangement of 2.5 m length was pulled mechanically through a stainless steel tube (length 4.95 m, inner diameter 5 cm, wall thickness in the reaction section 0.2 mm). This tube was closed at both ends. A 24 cm long central part of this tube was the reaction section (fig. 1). A vacuum and thermal insulation together with additional heaters kept radial heat losses low. The solid was moved through the reaction section with a speed of 5 mm/min.

The gas mixture enters and leaves the reactor shortly before and shortly after the reaction section as indicated in fig. 1. Since both ends of the long catalyst storage pipe were closed the gas could only move through the reaction section. Temperature profiles within the reaction section were measured by a movable thermocouple within a thin axial tube.

In the reaction section ethane was oxidized by a $Pd\text{-}Al_2O_3$ catalyst. Overall chemical reaction rates were determined experimentally in a differential reactor as a function of concentration and temperature by Simon (8), (9).

Theory

With regard to a fixed bed the moving bed reactor has two more operational parameters. They are the preheat temperature T_{S_0} and the mass flow rate $\dot{m}_S$ of the solid. Because of the increased number of variables calculations had to be made in advance in order to find the interesting experimental range where multiplicity could be expected.

The following steady state model equations were solved:

Energy balances

solid:

$$\lambda_0^{eff} \frac{d^2T_S}{dx^2} - |\dot{m}_S| c_S \frac{dT_S}{dx} - hS(T_S-T_F) - \alpha_1(T_S-T_W) = -\Delta H \cdot r \qquad (1)$$

gas:

$$|\dot{m}_F| c_F \frac{dT_F}{dx} - hS(T_F-T_S) - \alpha_2(T_F-T_W) = 0 \qquad (2)$$

Concentration balance:

$$\frac{1}{\rho_F} |\dot{m}_F| c_{tot} \frac{dy}{dx} = r \qquad (3)$$

In Chemical Reaction Engineering—Houston; Weekman, V., et al.;
ACS Symposium Series; American Chemical Society: Washington, DC, 1978.

Some underlying assumptions are
i) piston flow
ii) only slight heat losses to the wall
iii) no concentration diffusion.

In fact without the term $\dot{m}_S c_S dT_S/dx$ in equation (1) we have a set of equations which has been used successfully by various authors for the modelling of fixed bed chemical reactors. Another interesting aspect can be shown by re-writing equations (1) and (2) if heat conduction and heat losses are neglected:

$$- \frac{|\dot{m}_F c_F \; \dot{m}_S c_S|}{hS} \frac{d^2T_F}{dx^2} + (|\dot{m}_F| c_F - |\dot{m}_S| c_S) \frac{dT_F}{dx} = - \Delta H \cdot r \qquad (4)$$

$$T_S = T_F - \frac{|\dot{m}_F| \cdot c_F}{hS} \frac{dT_F}{dx} \qquad (5)$$

The first term in equation (4) represents the dispersion (feedback) process caused by the countercurrent movement of solid and fluid.

Boundary conditions

The adjustment of the bc's to the experimental situation is somewhat problematic. Due to the particular way how the gas is fed into and taken out of the reactor the flow condition within inlet and exit cross-sections are rather undefined. Within a zone of at least 1 cm width at both sides of the reaction section there are radial and axial flow components. More details on the conversion of radial inlet flow to axial flow in packed beds can be found in a paper by Szekely and Poveromo (10).

For mathematical reasons, however, clear cut bc's are needed. We therefore simply choose

i) $x = 0 \qquad T_S(0) = T_{S_o}$

$$x = L \begin{cases} T_F(L) = T_{F_o} \\ \left(\frac{dT_S}{dx}\right)_L = 0 \\ y(L) = y_o \end{cases}$$

These conditions exclude heat fluxes across inlet and exit sections. A more sophisticated choice of bc's would be an extension of the Danckwert's conditions:

In Chemical Reaction Engineering—Houston; Weekman, V., et al.;
ACS Symposium Series; American Chemical Society: Washington, DC, 1978.

ii) $x = 0$ $\quad \dot{m}_S c_S (T_{S_0} - T_S(0)) = \lambda_0^{eff} \left(\frac{dT_S}{dx}\right)_0$

$x = L_- \quad \dot{m}_F c_F (T_{F_0} - T_F(L)) = \lambda_0^{eff} \left(\frac{dT_S}{dx}\right)_{L_-}$

$y(L) = y_0$

$x = L_+ \quad T_F(L_+) = T_{F_0}$

In contrast to i) now heat fluxes across inlet and exit sections are included. These fluxes preheat the inflowing gas and solid. Calculations will show negligible differences in the results from the two sets of bc's.

The numerical procedure

Solutions of the stationary model equations were obtained by the collocation method (11). The following expansions in Legendre polynomials for the temperatures and the concentration were assumed:

$$T_S(x) = \sum_{i=1}^{N} a_i P_i(x) \tag{6}$$

$$T_F(x) = \sum_{i=1}^{N} b_i P_i(x) \tag{7}$$

$$y(x) = \sum_{i=1}^{N} c_i P_i(x) \tag{8}$$

For some cases an expansion up to N = 17 was necessary. Using equations (6), (7), (8) the system of equations may be written in the following matrix form:

$$\bar{\bar{A}} \cdot \bar{\xi} = \bar{r}(\bar{\xi})$$

where $\bar{\xi}$ is the solution vector and $\bar{r}$ contains the nonlinear parts of the differential equations. The nonlinearity was solved with a simple iteration procedure. As Reilly and Schmitz (12) pointed out such a procedure will give only stable solutions.

Calculated region of multiple solutions

Table I summarizes the data for which a range of multiplicity was found by calculation. The table also includes numbers for the various heat transport coefficients of equations (1) and (2). These coefficients are determined experimentally:

In Chemical Reaction Engineering—Houston; Weekman, V., et al.;
ACS Symposium Series; American Chemical Society: Washington, DC, 1978.

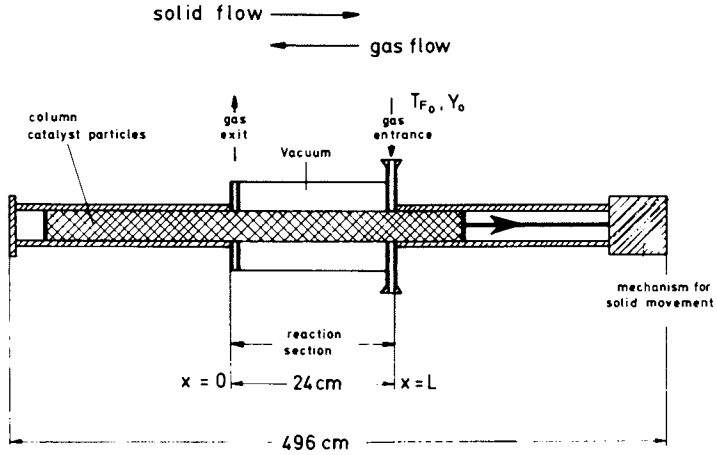

Figure 1. Moving bed reactor

Table I: Data for numerical calculations

T_{S0}	=	383 K
y_0	=	0.0055
T_W	=	300 K
$\dot{m}_S$	=	285.6 kg/m^2/hr
L	=	0.24 m
λ_0^{eff}	=	1.39 W/m/K
ε	=	0.427
d_p	=	0.43 cm

Re	α_1	α_2	W/m^3/K
3.95	0.33	0.007	
4.82	1.66	0.99	
6.16	4.12	1.06	

h determined by $Nu = 0.89\ Re^{0.41}$

c_F	=	1048 J/kg/K at 573 K
c_S	=	932 J/kg/K at 573 K
ρ_F	=	1.29 kg/m^3 at standard conditions
$(1-\varepsilon)\cdot\rho_S$	=	952 kg/m^3
S	=	1012 1/m
ΔH	=	$-1.425 \cdot 10^9$ J/kmole
c_{tot}	=	1/22.414 kmole/m^3 at standard conditions

Kinetic data from Simon (8), (9).

In Chemical Reaction Engineering—Houston; Weekman, V., et al.;
ACS Symposium Series; American Chemical Society: Washington, DC, 1978.

Under various conditions the reaction section was heated only by a hot gas stream. Temperature profiles were measured and fitted to the equations.

The calculated results are presented in fig. 2 where the inlet gas temperature T_{F_0} is plotted against the ratio of "flow capacities" $\beta = \dot{m}_F c_F / \dot{m}_S c_S$. Already Luss and Amundson (6) found this parameter to be the most important one besides inlet conditions when they analysed a countercurrent liquid/liquid spray column. Inlet gas concentration y_0 and the preheat temperature T_{S_0} of the solid are parameters of the graph. The shaded area is the range of predicted multiple solutions, while outside either we find a unique upper or lower steady state. The limiting curves marked with i) or ii) are obtained from the two different sets of bc's. The experiments were performed in the range $0.9 \leq \beta \leq 1.4$. It is seen that the range of multiple solutions is centered around $\beta = 1$. The calculations were done for the experimentally accessible range of β and T_{F_0}.

Experimental results

The measurements were performed according to the calculated data. The following procedure was adapted (fig. 3): For a preheat solid temperature of $T_{S_0} = 383$ Kelvin the reactor was started in the lower steady state by choosing a suitable inlet temperature T_{F_0}. This temperature then was gradually increased along the path 1→2 in fig. 3. The reactor remained in the lower steady state until at point 2 ignition occurs. The reactor remains ignited if T_{F_0} is further increased. The extinction procedure goes along path 3→4. While lowering the gas inlet temperature the reactor remains ignited until point 4 is reached where extinction takes place.

If the experimental reactor behaves like theoretical predictions the ignition/extinction experiments should exhibit a pronounced hysteresis. Fig. 4 shows that this is in fact the case. The conversion of ethane is plotted against T_{F_0} with other parameters kept constant. The numbers 1 to 4 in fig. 3 correspond to those of fig. 4. Fig. 5 contains temperature profiles of the upper and lower steady state. Due to the movement of the solid they lie much closer together than one would expect from fixed bed reactor behaviour. The final fig. 6 is concerned with an experimental check of the calculated range of multiplicity. A series of ignition/extinction experiments were performed at three different ratios of β {0.902, 1.09, 1.381}. The black points in fig.6 represent states where the reactor may either be in the upper or lower state while the bright points are unique states. The shaded area again is the calculated one with bc i) from fig. 2.

In Chemical Reaction Engineering—Houston; Weekman, V., et al.;
ACS Symposium Series; American Chemical Society: Washington, DC, 1978.

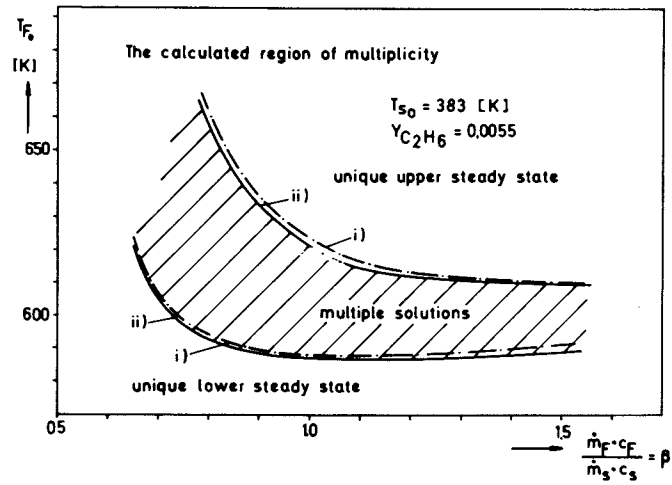

Figure 2. Regions of multiplicity and uniqueness calculated for boundary conditions i and ii

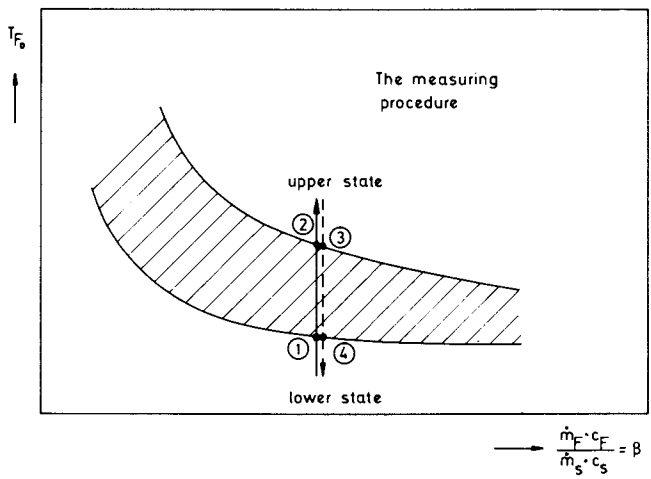

Figure 3. Measuring procedure

In Chemical Reaction Engineering—Houston; Weekman, V., et al.;
ACS Symposium Series; American Chemical Society: Washington, DC, 1978.

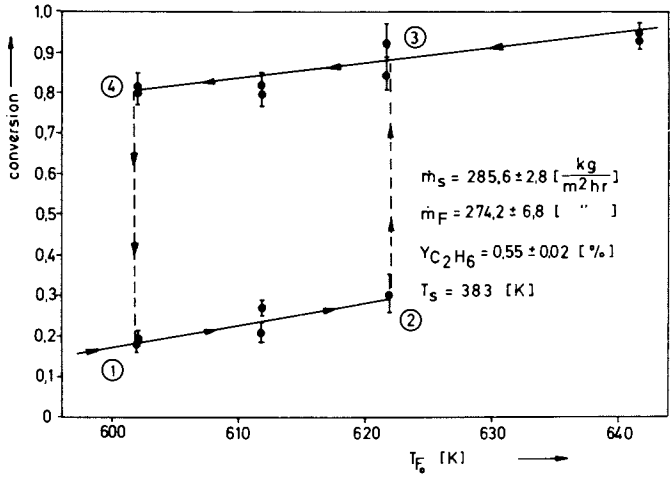

Figure 4. Measured conversion of ethane as a function of the gas inlet temperature T_{F_o}

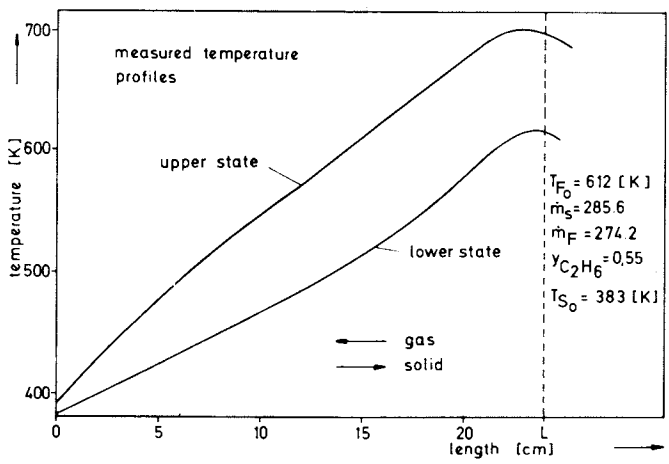

Figure 5. Upper and lower temperature profiles in the region of multiplicity

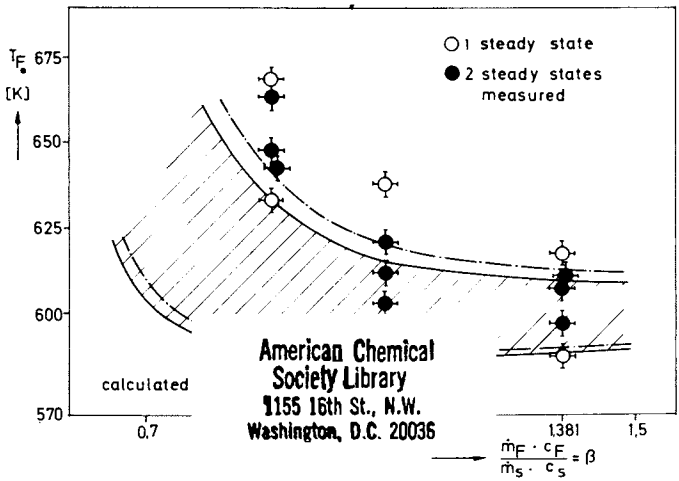

Figure 6. Measured and calculated ranges of multiplicity and uniqueness

Discussion

The agreement between computed and measured results is good for $\beta > 1$. At $\beta = 0.902$ larger deviations are observed. This may be due to a growing discrepancy between model assumptions and experimental reality if smaller values of β are approached. This was done by keeping $\dot{m}_S$ constant and lowering the gas velocity to 5.5 cm/s NTP at $\beta = 0.902$. In the range of low gas velocities effects of heat losses usually become more pronounced, a fact that is also observed in fixed bed experiments. In order to test this point of view we have replaced in bc i) the exit temperature gradient $(dT_S/dx)_L = 0$ by a negative gradient estimated from our measurements. The dotted line in fig. 6 is calculated for a gradient of $(dT_S/dx)_L = -3$ K/cm. A marked shift of the upper limiting curve to higher gas inlet temperatures is observed which gives a better fit to the data. This shows that indeed heat losses may be responsible for the observed differences between theory and experiment at $\beta = 0.902$.

Conclusions

The two-phase model of a moving bed chemical reactor with countercurrent operation was solved numerically. Due to the increased feedback by the countercurrent movement a broad range of multiplicity was obtained. Experiments confirmed the predicted results.

This work was sponsored by the Deutsche Forschungsgemeinschaft (SFB 153).

Nomenclature

$\bar{A}$	linear part of the system of diff. equations in matrix form
C_F	specific heat of gas (const. press.) J/kg/K
C_S	specific heat of solid, J/kg/K
C_{tot}	concentration of the gas mixture (at standard conditions), kmole/m^3.
ΔH	reaction enthalpy, J/kmole
d_p	diameter of catalyst particle, m
h	heat transfer coefficient, J/m^2/hr/K
L	length of the reaction section, m
$\dot{m}_F$	mass velocity of gas, kg/m^2/hr
$\dot{m}_S$	mass velocity of solid, kg/m^2/hr
P_i	Legendre polynomial
r	reaction rate, kmole/m^3/hr
$\bar{r}$	nonlinear part of the diff. equ. in vector form
S	surface area per unit bed volume, 1/m
T_F	temperature of the gas, K

In Chemical Reaction Engineering—Houston; Weekman, V., et al.;
ACS Symposium Series; American Chemical Society: Washington, DC, 1978.

T_{F_o} inlet temperature of the gas, K
T_S temperature of the solid, K
T_{S_o} inlet temperature of the solid, K
T_W wall temperature, K
x axial distance, m
y mole fraction of ethane
y_o mole fraction of ethane at the entrance

Greek letters

α_1 coefficient describing heat losses to the wall $J/m^3/hr/K$
α_2 " "
ε void fraction of the bed
λ_o^{eff} effective thermal conductivity of the solid column J/m/hr/K
ρ_F density of the gas, kg/m^3
ρ_S density of the solid, kg/m^3
ξ solution vector, containing the expansion coeff.

Literature cited

(1) Weekman, V.W., Nace, D.M., AIChE J.,(1970),16,397.
(2) Van Heerden, C., Chem.Eng.Sci.,(1958),8,133.
(3) Amundson, N.R., Canad.J.Chem.Engng.,(1965), 43, 49.
(4) Wicke, E., Padberg, G., Arens, H., Proc.Europ. Symp. Chem.Reaction Eng., 4th, Brussels (1968).
(5) Schaefer, R.J., Vortmeyer, D., Watson, C.C., Chem. Eng.Sci.,(1974),29,119.
(6) Luss, D.L., Amundson, N.R., I&EC Fund.,(1967),6,437.
(7) Yoshida, S., Tamura, S., Kunii, D., Int.J.Heat Mass Transfer (1966), 9,865.
(8) Simon, B., thesis, Techn.Universität München (1976).
(9) Simon, B., Vortmeyer, D., Chem.Eng.Sci., in Press.
(10) Szekely, J., Poveromo, J.J., AIChE J.,(1975),21,769.
(11) Finlayson, B.A., "The method of weighted residuals a. variational principles", Acad. Press (1972).
(12) Reilly, M.J., Schmitz, R.A., AIChE J., (1966),12,153.

In Chemical Reaction Engineering—Houston; Weekman, V., et al.;
ACS Symposium Series; American Chemical Society: Washington, DC, 1978.

45

Cell Model Studies of Radial Flow, Fixed Bed Reactors

J. M. CALO

Department of Chemical Engineering, Princeton University, Princeton, NJ 08540

The radial flow, fixed bed reactor (RFBR) was originally developed to handle large gas flow rates in the catalytic synthesis of ammonia. Since then, RFBRs have been used, or considered for, catalytic reforming, desulfurization, nitric oxide conversion, catalytic mufflers, and other processes in which fluids must be contacted with solid particles at high space velocities. The principal advantages of the RFBR over the more conventional tubular, axial flow, fixed bed reactor (AFBR) have been outlined elsewhere (1, 2). Although usually cylindrical in geometry, spherical RFBRs have also been considered (3).

Perhaps the first published analysis of an RFBR was by Raskin, et al. (4), who developed a quasicontinuum distributed parameter model for a radial ammonia synthesis reactor. General conclusions were limited, however, since the model was specifically concerned with ammonia synthesis and later carbon monoxide conversion (5), where both processes are second order and reversible. However, these authors did note that "radial reactors are anisotropic", i.e., they observed higher ammonia yields for centripetal radial flow (CPRF -- periphery to the center) than for centrifugal radial flow (CFRF -- center to periphery) (4).

In the present work, a packed bed cell model is used to calculate temperature and concentration profiles in the adiabatic RFBR for exothermic catalytic reactions with interphase resistance to mass and heat transfer. In particular, differences between the RFBR and the AFBR, operated at the same space velocity, are explored with respect to uniqueness, multiplicity, and stability of the steady state, profile location, selectivity in parallel and series reactions, and transient behavior.

RFBR Cell Model

Following Vanderveen, et al. (6), the mass and energy conservation equations for the fluid and the particle in the jth cell for a first order, irreversible, exothermic reaction are

$$M_j\left(v_{j-1} - v_j\right) - \left(v_j - \hat{v}_j\right) = a_1\left(dv_j/dt\right) \qquad [1]$$

© 0-8412-0401-2/78/47-065-550$05.00/0

$$H_j(y_{j-1} - y_j) - (y_j - \hat{y}_j) = a_2(dy_j/dt) \quad [2]$$

$$(v_j - \hat{v}_j) - k_j\hat{v}_j = a_3(d\hat{v}_j/dt) \quad [3]$$

$$(y_j - \hat{y}_j) + \beta k_j\hat{v}_j = a_4(d\hat{y}_j/dt) \quad [4]$$

subject to the inlet conditions $v_0 = v_0(t) = 1.0$ and $y_0 = y_0(t) = 1.0$ and appropriate initial conditions (see Notation and Vanderveen, et al. (6) for parameter definitions).

In radial flow, the fluid interstitial velocity, u_j, is a function of position in the bed, and hence, cell number, j. The interphase mass and heat transfer coefficients vary approximately as $Re^{0.6}$ (6, 7), and thus M_j and H_j are functions of $Re^{0.4}$ which increase in CPRF and decrease in CFRF with bed depth. k_j is also a function of u_j due to its dependence on k_g.

With the assumption of constant mean fluid density throughout the bed (5), the continuity equation for cylindrical geometry integrates to $ur = U_1R_1 = U_2R_2$; while for spherical geometry, $ur^2 = U_1R_1^2 = U_2R_2^2$. Integration of the velocity, $u = \pm dr/dt$ (+ for CFRF and - for CPRF), from the bed entrance to the bed exit yields the space time distribution along the bed length. Results of this calculation reveal that in radial flow the local residence time near the outer periphery of the bed is increased at the expense of residence time near the inner core of the bed as compared to axial flow at the same total space time.

The steady state temperature profiles presented in Figure 1 were determined by an initial value cell-by-cell calculation for the same feed conditions, average space velocity, and bed depth. All the parameter values are those of Vanderveen, et al. (6) except as otherwise noted. As can be seen, the CPRF profile appears earlier, and the CFRF profile appears later in the bed than the axial flow profile as a result of residence time reapportionment. This "early-late" phenomenon is accentuated by decreasing aspect ratio and by spherical over cylindrical geometry at the same aspect ratio.

Uniqueness, Multiplicity, and Stability

Algebraic manipulation of the steady state forms of the conservation equations [104] in the same manner as Ervin and Luss (8) yields

$$\hat{y}_j - y_{j-1} = (M_j+1)k_j(\hat{y}_{m,j} - \hat{y}_j)/M_j \equiv G_j(\hat{y}_j) \quad , \quad [5]$$

where $\hat{y}_{m,j}$ is the maximum particle temperature in the jth cell (8). Equation [5] can be rewritten as

$$1 = G_j(\hat{y}_j)/(\hat{y}_j - y_{j-1}) \equiv F_j(\hat{y}_j) \quad [6]$$

and the steady states of the system are determined by the intersection of the horizontal line at unity and the function $F_j(\hat{y}_j)$. For small $\hat{y}_j$, $dF_j(\hat{y}_j)/d\hat{y}_j$ is negative, and if

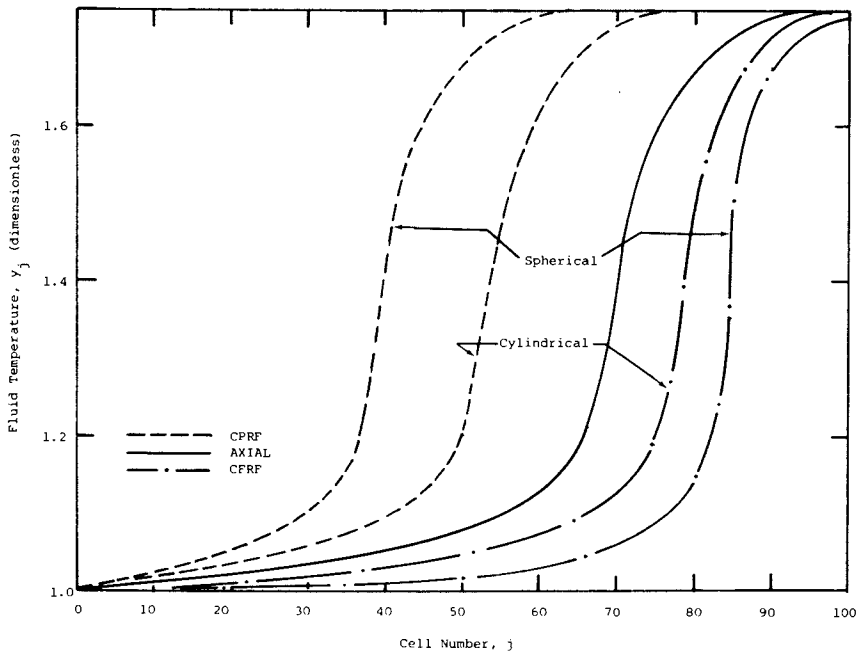

Figure 1. Unique steady state temperature profiles for CPRF and CFRF ($\rho = 0.25$) and axial flow ($P_o = 9kP_a$, $T_o = 667$ K, $T_o = 667$ K, $\beta = 5$, $M/H = 1.67$)

In Chemical Reaction Engineering—Houston; Weekman, V., et al.;
ACS Symposium Series; American Chemical Society: Washington, DC, 1978.

$$dF_j(\hat{y}_j)/d\hat{y}_j < 0 \quad , \quad \hat{y}_j \epsilon (\hat{y}_{m,j}, y_{j-1}) \qquad [7]$$

then this is a sufficient condition for uniqueness of the steady state. If condition [7] is violated, then $F_j(\hat{y}_j)$ will exhibit extremum at

$$\hat{y}_j \pm = \left[\gamma(\hat{y}_{m,j} + y_{j-1}) \pm Q_j\right]/2(\hat{y}_{mj} + \gamma - y_{j-1}) \qquad [8]$$

where $Q_j = \left[\gamma^2(\hat{y}_{m,j} + y_{j-1})^2 + 4\gamma y_{j-1}\hat{y}_{m,j}(y_{j-1} - \gamma - \hat{y}_{m,j})\right]^{\frac{1}{2}}$

In order to insure condition [7], the argument of Q_j must be negative, or

$$\gamma < \inf_{1 \le j \le n} 4\left[y_{j-1} + A_j y_{j-1}^2/(y_m - y_{j-1})\right] \quad , \qquad [9]$$

where $A_j = (M_j+1)/(H_j+1)$. A_j varies with bed position in radial flow and can either increase or decrease with j for CPRF or CFRF depending on whether M_j/H_j is greater than, or less than, unity. More conservative lower bounds for the RHS of inequality [9] can be obtained by setting A_j equal to its minimum value in the bed and $y_{j-1} = 1$:

$$\gamma < 4\left[1 + (A_{1(n)}/(y_m - 1))\right] \qquad [10]$$

For M/H > 1, inequalities [9] and [10] are identical for CPRF since the minimum A_j occurs in the first cell where $y_{j-1} = 1$. For CFRF, however, the RHS of inequality [9] will always be greater than the RHS of inequality [10] since the latter is the lower bound. Thus for M/H > 1, CPRF increases the range of parameter space for which multiplicity can occur, and CFRF decreases the range, as compared to axial flow at the same total space time. The opposite is true for M/H < 1. Again, this effect becomes more pronounced for decreasing aspect ratio and for spherical over cylindrical geometry at the same aspect ratio.

Condition [9] is sufficient but not necessary to insure uniqueness of the steady state. If it is violated, multiple steady states will exist in cells for which $F_j(\hat{y}_j+) > 1 > F_j(\hat{y}_j-)$. Typical behavior of the $F_j(\hat{y}_j)$ curves with cell number is illustrated in Figure 2, which shows that for M/H > 1, y_{j-1} increases with bed depth, and $\hat{y}_{m,j}$ increases, but less rapidly, to y_m. Simultaneously, the $F_j(\hat{y}_j)$ curve rises, $\hat{y}_j-$ approaches $\hat{y}_j+$, and at some point in the bed, $\hat{y}_j+ = \hat{y}_j- \equiv \hat{y}_{j,t}$ and $F_j(\hat{y}_j+) = F_j(\hat{y}_j-) \equiv F_j(\hat{y}_{j,t})$ -- the trifurcation point. If $F_j(\hat{y}_{j,t}) > 1$, multiple steady states exist for some catalyst particles in the bed in the region where $F_j(\hat{y}_j+) > 1 > F_j(\hat{y}_j-)$. However, if $F_j(\hat{y}_{j,t}) < 1$, then all catalyst particles have a unique steady state, and the reactor profile is unique. $F_j(\hat{y}_{j,t}) < 1$ is both a necessary and sufficient condition for uniqueness of the steady state.

In radial flow, $F_j(\hat{y}_{j,t})$ cannot be calculated a priori as in

In Chemical Reaction Engineering—Houston; Weekman, V., et al.;
ACS Symposium Series; American Chemical Society: Washington, DC, 1978.

axial flow because the values of A_j and k_g (in k_j) at the trifurcation point are not known. Nevertheless, it can be shown that the lowest interstitial velocity in the bed, i.e., at the outer periphery, yields an upper bound in evaluating $F_j(\hat{y}_j,t)$. Thus, if $F_j(\hat{y}_j,t)_{u.b.} < 1$, then this is a sufficient, but not necessary condition for uniqueness of the steady state.

The difference in behavior between the $F_j(\hat{y}_j)$ curves for CPRF and CFRF in Figure 2 is due to the scale factor effect of $(M_j+1)/M_j$ and k_g (in k_j). These velocity-dependent terms are larger for CPRF and smaller for CFRF in the initial portion of the bed, and they cause the $F_j(\hat{y}_j)$ curves to rise faster from cell to cell in CPRF. Therefore, if multiple steady states exist, the region of multiplicity will be shifted toward the bed entrance in CPRF and toward the bed exit in CFRF. This effect can be better appreciated in Figure 3, which is a plot of $F_j(\hat{y}_j+)$ and $F_j(\hat{y}_j-)$ as a function of j for the same conditions as in Figure 2. As shown, the $F_j(\hat{y}_j+)$ and $F_j(\hat{y}_j-)$ branches cross unity and coalesce at the trifurcation point first for CPRF, next for axial flow, and last for CFRF.

The open interval $[F_j(\hat{y}_j+), F_j(\hat{y}_j-)]$ is a measure of the parameter space for which multiplicity can occur. CPRF presents a larger interval and CFRF a smaller interval than axial flow at the same average space velocity. Thus, in general, CFRF suppresses multiplicity and CPRF promotes multiplicity as compared to axial flow at the same average space velocity. In all the calculations performed, however, CPRF never induced multiplicity nor did CFRF completely suppress multiplicity when compared to the "equivalent" axial flow case. On the other hand, the possibility that conditions may exist under which this could occur has not been eliminated. It should be noted that Hlavacek and Kubicek (1) concluded that CPRF, and not CFRF, tends to suppress multiple solutions for the quasicontinuum axial dispersion model without interphase transport resistance.

A stability analysis of the transient equations [1-4] yields the same necessary and sufficient set of conditions for asymptotic stability as obtained by Vanderveen, et al. (6), viz.

$$b_{j1} > 0 \; ; \; b_{j2} > 0 \; ; \; b_{j1}b_{j2}b_{j3} > b_{j1}^2 b_{j4} + b_{j3}^2 \; ; \; b_{j4} > 0 \; , \quad [11]$$

except, of course, that for radial flow, M and H are functions of j. The fourth condition, $b_{j4} > 0$, is simply condition [7], i.e., $dF_j(\hat{y}_j)/d\hat{y}_j < 0$. Thus all steady states on the positive slope branch of $F_j(y_j)$ are unstable with respect to small perturbations. Steady states on the high and low temperature branches with negative slope have a chance of being stable if in addition they satisfy the first three conditions in [11].

For gas-solid systems with $a_4/a_3 >> 1$, the first two conditions in [11] imply the slope condition (6,8,9). Condition [7] is stronger than the slope condition if

$$(1 + H_j)M_j/(H_j(M_j + \delta_j)) > 1 \quad , \quad [12]$$

In Chemical Reaction Engineering—Houston; Weekman, V., et al.;
ACS Symposium Series; American Chemical Society: Washington, DC, 1978.

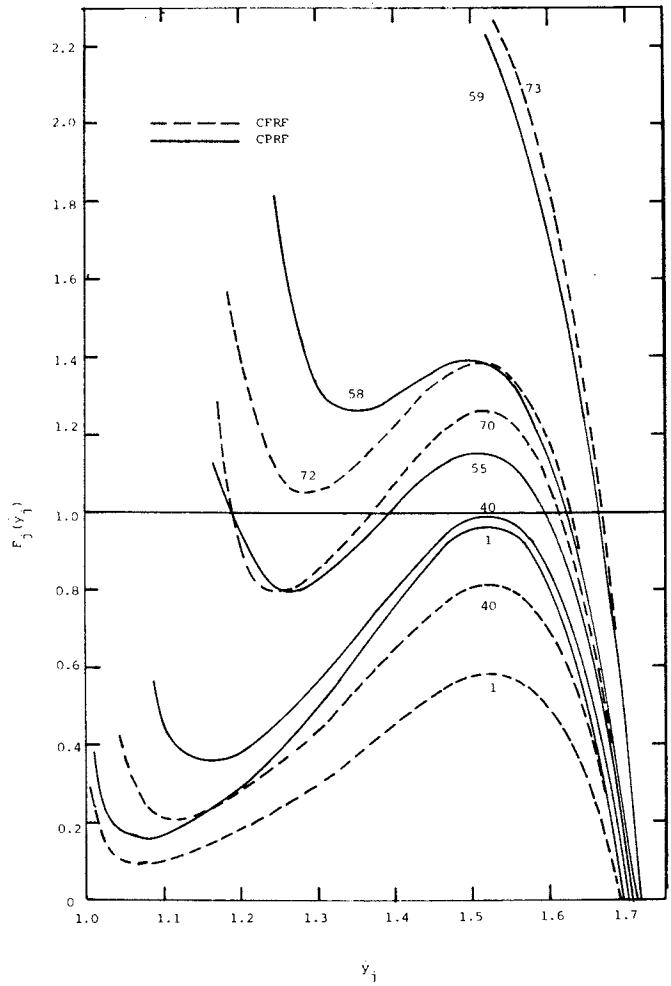

Figure 2. $F_j(\hat{y}_j)$ *curves as a function of cell number for CPRF and CFRF* ($\rho = 0.5$). ($P_o = 9kP_a$, $T_o = 667°K$, $\hat{T}_o = 667°K$, $\beta = 7.5$, $M/H = 1.1133$). *The curves are labeled with cell numbers.*

In Chemical Reaction Engineering—Houston; Weekman, V., et al.;
ACS Symposium Series; American Chemical Society: Washington, DC, 1978.

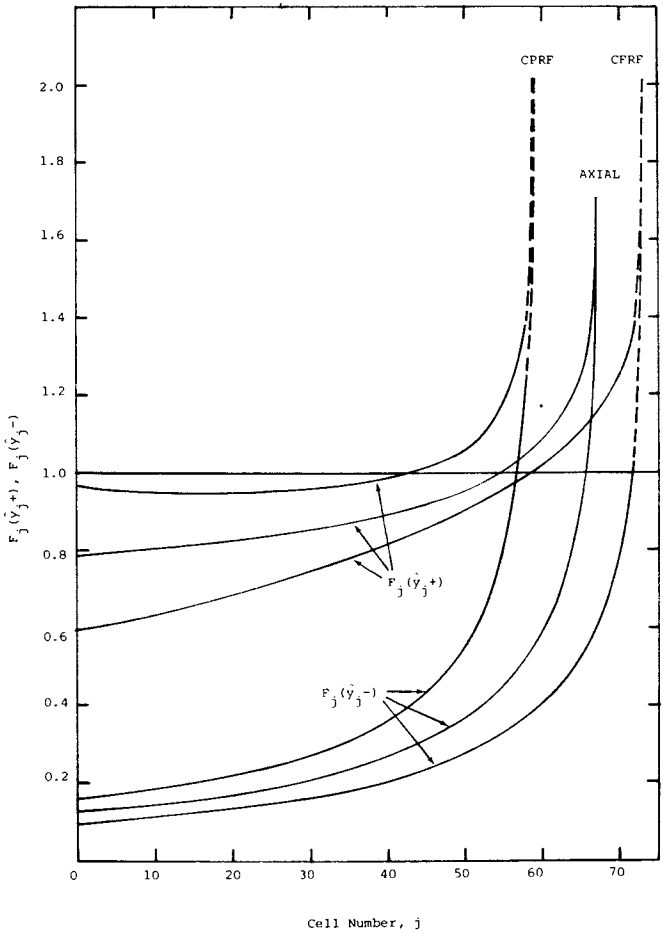

Figure 3. $F_j(\hat{y}_j+)$ *and* $F_j(\hat{y}_j-)$ *as a function of cell number for CPRF, CFRF, and axial flow for the same conditions as in Figure 3. The CPRF and CFRF curves are dashed to* $F_j(\hat{y}_j,t)_{u.b.}$ *since the* $F_j(\hat{y}_{j,t})$ *are not known.*

In Chemical Reaction Engineering—Houston; Weekman, V., et al.;
ACS Symposium Series; American Chemical Society: Washington, DC, 1978.

which is always satisfied for M/H > 1, and thus condition [7] implies the first, second, and fourth conditions in [11]. For M/H < 1 and $\delta_j \simeq 1$, inequality [12] is not satisfied, and the slope condition will be stronger. In any case, for a steady state on the negative slope branches of $F_j(\hat{y}_j)$ to be stable, the third condition in [11] must also be satisfied, and as has been pointed out (6,8), this condition is a complex expression with no obvious physical meaning.

A comparison of relative magnitudes of condition [12] for M/H > 1 reveals that radial flow tends to destabilize the bed at the outer periphery and stabilize the bed at the inner core to a greater extent than axial flow at the same total space velocity.

Selectivity Effects

The reapportionment of residence time in radial flow is analogous to variable volume CSTRs in series. As such, radial flow would be expected to affect product selectivity in series and parallel reactions. For two parallel first order, exothermic reactions, the particle equations [3, 4] become

$$\left(v_j - \hat{v}_j\right) - \left(k_{1j} + k_{2j}\right)\hat{v}_j = 0 \qquad [13]$$

$$\left(y_j - \hat{y}_j\right) + \left(\beta_1 k l_j + \beta_2 k_{2j}\right)\hat{v}_j = 0 \qquad [14]$$

The results of a typical calculation are presented in Figure 4. For the parameters chosen (see figure caption), CPRF increased the yield of R and decreased the yield of S, while CFRF acted in the opposite sense. Thus, in this case, the yield of R varied 6.2% and that of S 6.7% simply according to whether the reactor was operated in CPRF or CFRF.

For two series first order, exothermic reactions, the particle mass balance is the same as Equation [3], but the particle energy balance (Eq. [4]) becomes

$$y_j - \hat{y}_j + \beta_1 k_{1j}\hat{v}_j + \beta_2 k_{2j}\hat{w}_j = 0 \quad , \qquad [15]$$

where $\hat{w}_j$ is the fraction of intermediate. Also, additional particle and fluid mass balances are required for the intermediate. The results of a typical calculation for this case are presented in Figure 5. As compared to axial flow, and for the parameter values chosen (see figure caption), CPRF increased the yield of product S and decreased the yield of intermediate R, while CFRF again acted in the opposite sense. The yield of S varied 9.5% and that of R 77.3% simply according to flow direction in cylindrical radial flow. Also, when the crossover point for R and S is near the reactor exit in axial flow, CPRF can yield a product with S > R, while CFRF yields a product with R > S. This occurs when the crossover point moves toward the bed entrance in CPRF, increasing S over R, and moves out of the reactor exit in CFRF, thereby increasing R over S.

Of course, differences in selectivity due to flow direction in an RFBR are extremely sensitive to the specific kinetic parameters.

In Chemical Reaction Engineering—Houston; Weekman, V., et al.;
ACS Symposium Series; American Chemical Society: Washington, DC, 1978.

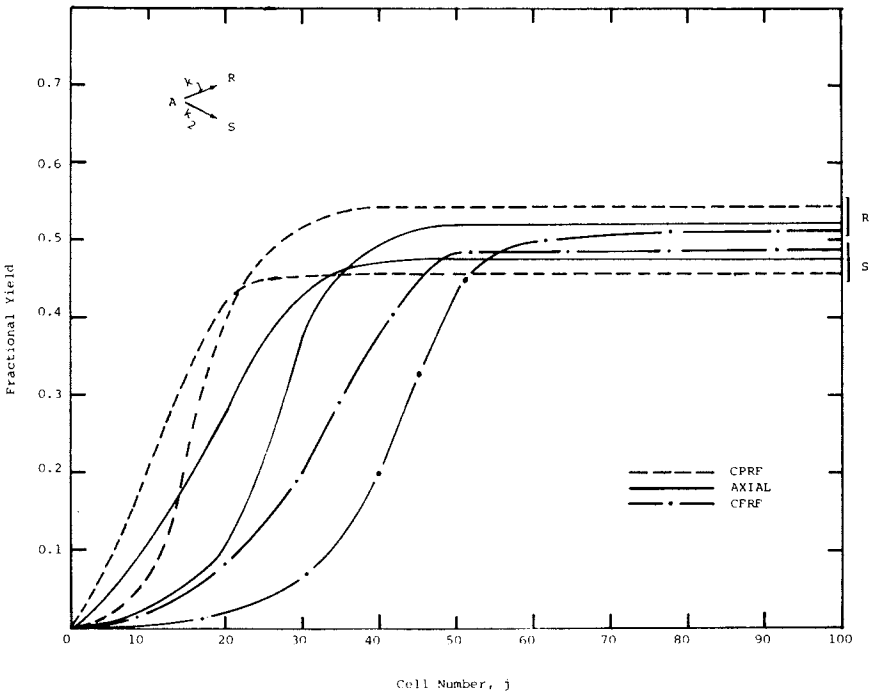

Figure 4. Fractional yield as a function of cell number for two parallel first-order, exothermic reactions in CPRF, CFRF ($\rho = 0.25$), and axial flow ($\gamma_2/\gamma_1 = 2$, $\beta_1/\beta_2 = 2$, $\gamma_1 = 18.33$, $\beta_1 = 5$, $k_2/k_1 = 7.5$ (at feed conditions), $P_o = 9kP_a$, $T_o = 667°K$, $\bar{T}_o = 667°K$, $M/H = 1.67$)

In Chemical Reaction Engineering—Houston; Weekman, V., et al.;
ACS Symposium Series; American Chemical Society: Washington, DC, 1978.

However, it is conceivable, depending on the reaction system, that selectivity effects in radial flow could be significant.

Transient Behavior

When multiple steady states exist, steady state profiles can be determined only by a transient analysis. Typical results of the numerical solution of the transient simple cell equations [1-4] are presented in Figure 6. Here fluid temperature profiles are presented for CPRF and CFRF for cylindrical geometry (ρ = 0.25), and axial flow for the same average space velocity at 5, 15, and 30 minutes after start up. The feed and initial conditions are noted in the figure caption. Several interesting features are apparent. The incipient profiles at 5 minutes are much closer together than at 30 minutes. In each case the reaction zone is formed within 15 minutes, and the profile then creeps steadily toward the bed exit. It is quite evident that the CFRF profile creeps the most, and the CPRF profile the least. It is also interesting to note that all the CFRF and axial flow profiles significantly overshoot the maximum adiabatic fluid temperature, y_m, while the CPRF profile also does but to an almost imperceptible extent. The creep behavior is directly related to the degree of temperature overshoot, since it is caused by cooling of the over-temperature cells to less than or equal to y_m, which, of course, cannot be exceeded at steady state. Thus in Figure 6, the axial flow and CFRF profiles continue to creep until the cells near the bed exit cool.

The degree of overshoot, and hence, profile creep, is a function of the initial bed temperature, $\hat{y}_{j0}$. A study was conducted in which the initial bed temperature was varied keeping all the other parameters constant. As $\hat{y}_{j0}$ was increased from 1.0 to 1.17, the profiles for all three flow modes ignited closer to the bed entrance. All the profiles were stationary at 30 minutes from start up except for the CFRF profile for $\hat{y}_{j0} = 1.17$, which overshot the maximum adiabatic fluid temperature and was still creeping. Also, for $\hat{y}_{j0} = 1.17$ the CPRF and axial flow profiles were the closest together, while the CFRF was farthest from the other two and moving away. Thus, for initial bed temperatures exceeding the feed temperature, steady state multiplicity tends to accentuate the "early-late" reaction zone phenomenon observed for the unique steady state profiles.

Conclusions

In general, CPRF is the better mode of operation for the RFBR when multiple steady states are possible. In addition to expediting the approach to steady state, the establishment of the CPRF profile early in the bed is an advantage in cases where the reaction zone gradually creeps toward the bed exit due to catalyst deactivation. When only unique steady states are possible and/or for parallel and series reactions, the preferred flow mode may depend on other considerations.

In Chemical Reaction Engineering—Houston; Weekman, V., et al.;
ACS Symposium Series; American Chemical Society: Washington, DC, 1978.

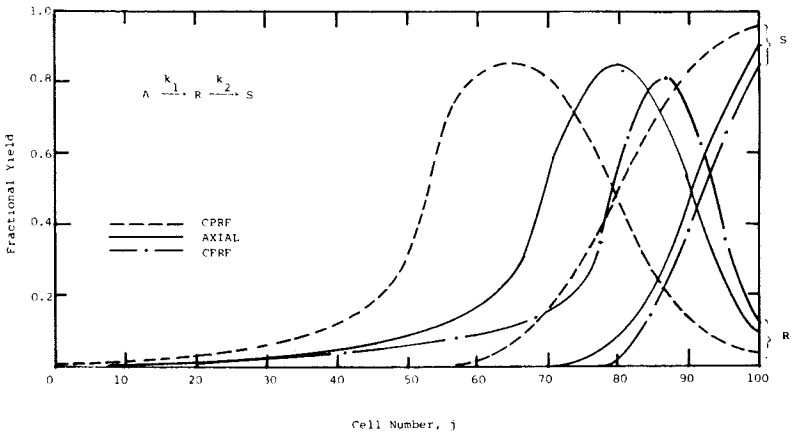

Figure 5. Fractional yield as a function of cell number for two first-order, exothermic series reactions in CPRF, CFRF ($\rho = 0.25$), and axial flow ($\gamma_2/\gamma_1 = 1.55$, $\gamma_1 = 18.33$, $\beta_1 = \beta_2 = 5$, $k_2/k_1 = 1.0$ (at feed conditions), $P_o = 9kP_a$, $T_o = 667°K$, $\bar{T}_o = 667°K$, $M/H = 1.67$)

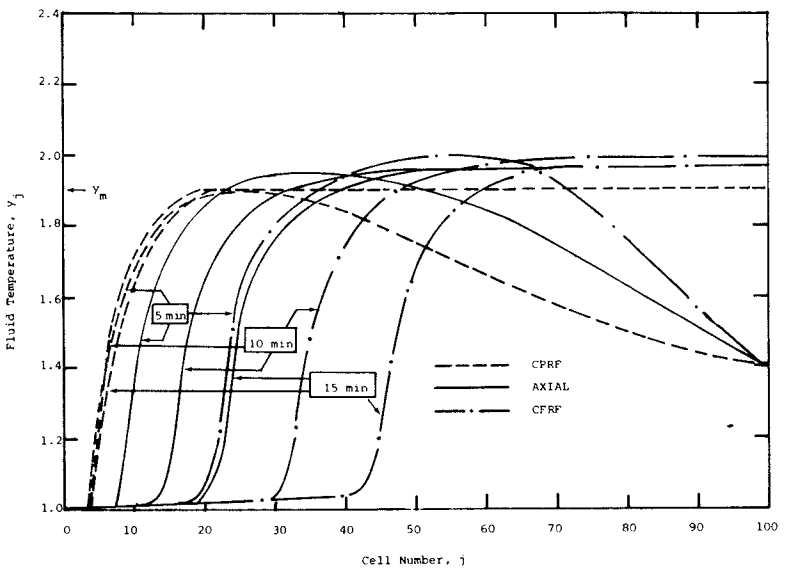

Figure 6. Transient behavior of temperature profiles in CPRF, CFRF ($\rho = 0.25$), and axial flow ($\rho = 0.25$, $P_o = 11kP_a$, $T_o = 667°K$, $\bar{T}_o = 883°K$, $\beta = 5$ $M/H = 1.67$)

In Chemical Reaction Engineering—Houston; Weekman, V., et al.;
ACS Symposium Series; American Chemical Society: Washington, DC, 1978.

Notation [see also Vanderveen, et al. (6)]

A_j = defined in text
F_j = defined by Eq. [6]
G_j = defined by Eq. [5]
H_j = dimensionless HTU for heat transfer
k_j = dimensionless rate constant
M_j = dimensionless HTU for mass transfer
Q_j = defined in text
R,r = radius
U,u = interstitial fluid velocity
v,w = reactant mole fraction
$y = T/T_0$ (dimensionless temperature)

$\beta = (-\Delta H)k_g/h_f T_0$
$\gamma = (-\Delta E)/R_g T_0$
$\delta_j = k_j/(1 + k_j)$
$\rho = R_1/R_2$

Subscripts and Superscripts

j = cell number
m = maximum
n = last cell
0 = feed conditions
^ = particle phase
1 = inner radius
2 = outer radius

Literature Cited

1. Hlavacek, V., and Kubicek, M., Chem. Eng. Sci. (1972), 27, 177.
2. Dudukovic, M. P., and Lamba, H. S., 80th AIChE National Meeting, Boston (1975), paper #576.
3. Cimbalnik, Z., et al., 2nd CHISA Cong., Czechoslovakia (1965).
4. Raskin, A. Ya., et al., Theor. Found. Chem. Tech. (1968), 2, 220.
5. Raskin, A. Ya., and Sokolinskii, Yu. A., Khim Prom. (1969), 45, 520.
6. Vanderveen, J. W., Luss, D., and Amundson, N. R., AIChE J. (1968), 14, 636.
7. Wicke, E., Chem. Ing. Tech. (1965), 37, 892.
8. Ervin, M. A., and Luss, D., AIChE J. (1970), 16, 979.
9. Liu, S.-L., and Amundson, N. R., IEC Fund. (1962), 3, 200.

In Chemical Reaction Engineering—Houston; Weekman, V., et al.;
ACS Symposium Series; American Chemical Society: Washington, DC, 1978.

46

Flow Control Operation of a Plug-Flow Tubular Reactor with High Heat Diffusivity

YU. P. GUPALO, V. A. NOVIKOV, and YU. S. RYAZANTSEV

The Institute for Problems in Mechanics, USSR Academy of Sciences, Moscow, USSR

1. Formulation of the problem

It is known that controlled operation of chemical reactors at naturally unstable conditions should be of interest in the design of some commercial reactors because the unstable or so-called intermediate states may offer a desirable compromise between a state of very low activity or conversion on the one hand and a state of poor selectivity on the other [1]. In the present paper the model of a tubular reactor with negligible mass diffusivity and high diffusivity of heat is considered.

The dimensionless equations with the boundary and initial conditions governing the unsteady mass and heat transfer in the one-dimensional plug flow tubular reactor with high heat diffusivity can be written in the form

$$\frac{\partial \xi}{\partial \tau} + v\frac{\partial \xi}{\partial x} = (1 - \xi)g \exp\left(-\frac{\beta}{\theta}\right) \qquad (1.1)$$

$$\frac{d\theta}{d\tau} = \omega v(\theta_0'' - \theta) + \omega g \exp\left(-\frac{\beta}{\theta}\right) \int_0^1 (1 - \xi)dx \qquad (1.2)$$

$$x = 0, \qquad \xi(0, \tau) = 0 \qquad (1.3)$$

$$\tau = 0, \qquad \xi(x,0) = \xi_0(x), \quad \theta(0) = \theta_0 \qquad (1.4)$$

$$\xi = \frac{c - c}{c_0}, \quad x = \frac{X}{L}, \quad \theta = \frac{T}{T^*}, \quad T^* = \frac{hc}{C_g g}$$

$$\tau = \frac{t}{\tau^*}, \quad \tau^* = \frac{L}{u^*}, \quad v = \frac{u}{u^*}, \quad \beta = \frac{E}{RT^*}, \quad g = k_0\tau^*$$

$$\alpha = \alpha_s \frac{S^*}{V^* c^*}, \quad \omega = \frac{\varepsilon_0 \rho_g C_g}{\rho^* c^*}$$

© 0-8412-0401-2/78/47-065-562$05.00/0

$$\rho_* c_* = \varepsilon_o \rho_g c_g + (1 - \varepsilon_o)\, \rho_s c_s$$

where X is a spatial coordinate ($0 \leq X \leq L$), L is a reactor length, t is a time, c is a concentration of reactive species in reactor volume, c_o is a feed concentration of reactive species, ξ is an extent, u is flow velocity, ε is the ratio of a bulk fluid volume to a total one, T is a temperature; V,S are a reactor volume and a surface of reactor walls, ρ_g , c_g are a density and a heat capacity of fluid; ρ_s , c_s are a density and a heat capacity of catalyst, T_o is a feed flow temperature, h is a heat of reaction, k_o is a pre-exponential factor for reaction rate, E is an activation energy, R is a gas constant, u* is characteristic reactant flow velocity.

In obtaining Eqs (1.1) and (1.2) mass diffusivity has been neglected; high diffusivity of heat and first order Arrhenius kinetics for one step exothermic chemical reaction has been assumed. These assumptions can serve as a fair approximation for some kinds of fluidized-bed reactor [2] . The Eq. (1.2) can be derived formally by integration over the total length of the reactor.

The solutions of the steady-state forms of Eqs (1.1) and (1.2) can be written as

$$\xi^{o}(x) = 1 - \exp\left[-x\frac{g}{v}\exp\left(-\frac{\beta}{\theta^{o}}\right)\right] \qquad (1.5)$$

$$\theta_o'' - \theta^{o} + 1 - \exp\left[-\frac{g}{v}\exp\left(-\frac{\beta}{\theta_o}\right)\right] = 0 \qquad (1.6)$$

The dependence of the steady-state temperature θ^{o} on parameter v for fixed values of θ_o'' , and g obtained from Eq. (1.6) are presented in Fig. 1, which shows that the multiplicity of the steady states in possible. For example three steady-state temperatures correspond to the value $v = v_{o.}$ It is known that the upper and lower steady states 0^{+}, 0^{-} are stable, meanwhile the intermediate steady state is unstable [3] .

2. The method of control

Consider the possibility of stabilization of the unstable intermediate steady state by the method of proportional control (see, for example [4]). Up to now the theory of chemical reactor control was focu-

In Chemical Reaction Engineering—Houston; Weekman, V., et al.;
ACS Symposium Series; American Chemical Society: Washington, DC, 1978.

sed primerely upon the control of a stirred reactor [2]. The first example of the analysis of the unstable steady state stabilization for distributed parameter reactor was given recently by Oh and Schmitz [1].

In the case under consideration the controlled variable is the temperature θ and the manipulated variable is the flow velocity v. The feed back relationship is as follows

$$v(\tau) = v_o \left\{ 1 + d\left[\theta(\tau - \tau_d) - \theta_2^o\right]\right\} \qquad (2.1)$$

where θ_2^o is intermediate steady-state temperature, τ_d is a time lag, d is stabilization parameter.

In view of (2.1) the Eq. (1.6) becomes, respectively,

$$\theta_o'' - \theta^o + 1 - \exp \frac{-g \exp(-\beta/\theta^o)}{v_o\left[1 + d(\theta^o - \theta_2^o)\right]} = 0 \qquad (2.2)$$

The relationship (2.2) shows that in the presence of control the upper and lower steady-state temperatures depend on parameter d and can be determined as the intersection points of curve 1, with lines $\theta^o = \theta_2^o + d(v-v_o)$, corresponding to different values of d (lines 2-7) in Fig. 1. The dependence of θ^o on d resulting from Eq. (2.2) are pointed out in Fig. 2. It can be seen that for $d > d_c$ the intermediate steady state turns to be the lower one and for $d > d_1$ it becomes the single steady state. The value of d_c can be obtained from the condition that the line $\theta^o = \theta_2^o + d_c(v-v_o)$ is tangent to the curve 1.

$$d_c = \frac{\beta}{\theta_2^{o2}} - \frac{v_o}{g} \exp\left[\frac{\beta}{\theta_2^o} + \frac{g \exp(-\beta/\theta_2^o)}{v_o}\right] \qquad (2.3)$$

If the inequality $d > d_c$ takes place the steady state $\theta^o = \theta_2^o$ should satisfy the so-called slope condition for stability. Therefore one can expect the considered system of reactor control to be effective as $d > d_c$. This qualitative conclusion requires rigorous approaches. In order to analyse the stability of steady state under control, we use the small perturbation method. By substituting $\theta(\tau) = \theta^o + \theta'(\tau)$ and $\xi(x,\tau) = \xi^o(x) + \xi'(x,\tau)$ into Eqs (1.1)-(1.4) and (2.1) one can obtain by the Laplace transform the solution for $\theta'(\tau)$ and $\xi'(x,\tau)$. It can be found that all the singularities of this solutions are poles and

In Chemical Reaction Engineering—Houston; Weekman, V., et al.;
ACS Symposium Series; American Chemical Society: Washington, DC, 1978.

are determined by the roots of characteristic equation.

$$\Psi(s) = s^2 + a_1 s \exp(-sv^\circ\tau_d) + a_2 s + a_3 \exp(-sv^\circ\tau_d) + a_4 + \left[a_5 \exp(-sv^\circ\tau_d) - a_6\right] s^{-1}\left[1 - \exp(-s)\right] = 0, \quad s = p/v^\circ \tag{2.4}$$

$$a_1 = \frac{v_0 d}{v^{\circ 2}}(\Theta^\circ - \Theta_0''), \quad a_2 = \omega - \frac{\omega\beta}{\Theta^{\circ 2}}\left[1 - \exp(-\frac{b}{v^\circ})\right] + \frac{b}{v^\circ}$$

$$a_3 = \frac{b\, v_0 d}{v^{\circ 2}}\left[\Theta^\circ - \Theta_0'' - 1 + \exp(-\frac{b}{v^\circ})\right]$$

$$a_4 = \frac{b\omega}{v^\circ}, \qquad a_5 = \frac{b^2 \omega v_0 d}{v^{\circ 3}} \exp(-\frac{b}{v^\circ})$$

$$a_6 = \frac{b^2 \omega \beta}{v^{\circ 2}\Theta^{\circ 2}} \exp(-\frac{b}{v^\circ})$$

(p - is the Laplace transform variable). The necessary and sufficient condition for stability of the controlled reactor to small perturbations is that the real parts of the roots of Eq. (2.4) are negative. Therefore the controlled reactor are stable if all the roots of the Eq. (2.4) lie in the right half-plane of the complex plane $s = x + iy$. We chose the countor $\Gamma = \Gamma_1 + \Gamma_2$ where Γ_1 is the right half-circle of large radius R with the centre located in Zero point and Γ_2 is the part of the imaginary axis $|y| \leq R$. It can be shown that the increament of argument $\Psi(s)$ on Γ_1 at $R \to \infty$ is equal to 2π for any value of a .

3. The ideal control

In the special case of ideal control by putting in Eq. (2.4) $\tau_d = 0$ one can obtain

$$\Psi(s) = s^2 + \Omega_3 s - \Omega_1 + \Omega_2(1 - e^{-s})/s \tag{3.1}$$

$$\Omega_1 = -a_3 - a_4, \quad \Omega_2 = a_5 - a_6, \quad \Omega_3 = a_1 + a_2$$

The function (3.1) depends on s as well as on three parameters $\Omega_1, \Omega_2, \Omega_3$. To analyse the stability of controlled reactor we have to find the domain in three-dimensional space ($\Omega_1, \Omega_2, \Omega_3$) in which

In Chemical Reaction Engineering—Houston; Weekman, V., et al.;
ACS Symposium Series; American Chemical Society: Washington, DC, 1978.

there are no roots of $\Psi(s)$ with positive real parts. To do this we consider the behaviour of the function $\Psi(s)$ on Γ_2. It can be seen that the real parts of roots of $\Psi(s)$ vanish for those values of Ω_1, Ω_2, Ω_3 which belong to the surface defined by the following equations

$$\Omega_1 = -y^2 + \Omega_3 \frac{y \sin y}{1 - \cos y}, \quad \Omega_2 = \Omega_3 \frac{y^2}{1 - \cos y} \qquad (3.2)$$

$$0 \leq y < \infty$$

The analysis of Eq. (3.2) reveals that for the domain S_D bounded by the surface (3.2) at $0 \leq y \leq 2\pi$ and plane $\Omega_1 = \Omega_2$ the increament of argument $\Psi(s)$ on Γ_2 is equal to -2π. Therefore the total increament on $\Gamma_1 + \Gamma_2$ is nought and S_D is the stability domain because it contains no roots of $\Psi(s)$ with positive real parts.

The results obtained permit to analyse the influence of the control on the intermediate steady state stability. The section of the stability domains and the point A corresponding to intermediate steady temperature $\theta^\circ = \theta_2^\circ$ for different values of parameter d are shown in Fig. 3. The section of stability domain corresponding to d = 0 is dashed in Fig. 3. It is seen that the intermediate steady state becomes stable when $d > d_c$. If $d = d_c$ the point A achieves the boundary of the stability domain. The value d_c can be obtained from the equation $\Omega_1^* = \Omega_2^*$, which is identical to Eq. (2.4). Thus the intermediate steady state becomes stable when it turns to be the lower steady-state. The numerical analysis shows that in the nonlinear case the value of d depends on the perturbation amplitude. For example if $d = d_2$ the intermediate steady state is stable as the temperature perturbations are less than $\Delta\theta$ (see Fig. 2).

4. The influence of time lag

It has been shown that if $d > d_c$ and $\tau_d = 0$ the controlled steady state is stable. To study the effect of time lag τ_d on stability we consider the increase of argument of function (2.4) on Γ_2 for different values of τ_d. The curves $W = \Psi(iy) = U + iV$ $(0 \leq y)$ on the Nyquist plane are shown in Fig. 4 for the case $\tau_{d_1} < \tau_{d_2} < \tau_{d_3}$. It can be found that for $\tau_d = \tau_{d_1}$ and $\tau_d = \tau_{d_2}$ the controlled steady state is

In Chemical Reaction Engineering—Houston; Weekman, V., et al.;
ACS Symposium Series; American Chemical Society: Washington, DC, 1978.

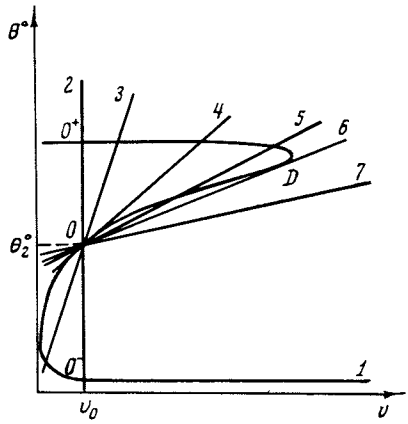

Figure 1. The steady-state diagrams for several values of the parameter d. *Curve 1 corresponds to the dependence of the steady-state temperature* θ° *on parameter* v *for fixed values of* θ_0'', β, *and* g. *Curves 2–7 are lines* $\theta^\circ = \theta_2^\circ + d(v - v_0)$ *corresponding to different values of the stabilization parameter* d.

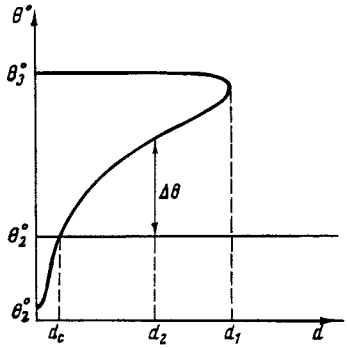

Figure 2. The dependence of the steady-state temperature θ° *on stabilization parameter* d

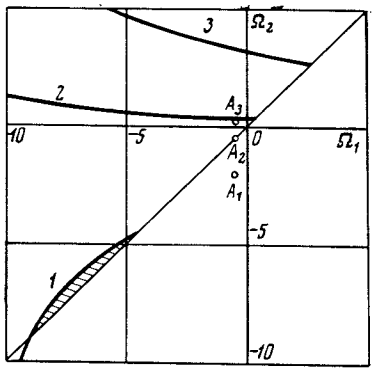

Figure 3. The sections of the stability domain. The points A correspond to the intermediate steady-state temperature $\theta^\circ = \theta_2^\circ$.

In Chemical Reaction Engineering—Houston; Weekman, V., et al.;
ACS Symposium Series; American Chemical Society: Washington, DC, 1978.

stable, and for $\tau_d = \tau_{d*}$ it is unstable. Thus the critical value of delay time τ_d^* exists. If $\tau_d = \tau_d^*$ the curve corresponding to $\Psi(iy)$ in the Nyquist plane goes through zero point. From this condition we can get the system of equations for obtaining τ_d^*

$$-y^2 + a_4 + \left[a_5 \cos(yv^\circ \tau_d^*) - a_6 \frac{\sin y}{y} - \right.$$

$$- a_5 \sin(yv^\circ \tau_d^*) \frac{1 - \cos y}{y} + a_1 y \sin(yv^\circ \tau_d^*) +$$

$$+ a_3 \cos(yv^\circ \tau_d^*) = 0 \qquad (4.1)$$

$$y\left[a_1 \cos(yv^\circ \tau_d^*) + a_2 + \left[a_6 - a_5 \cos(yv^\circ \tau_d^*) \frac{1 - \cos y}{y} - \right.\right.$$

$$\left.\left. - \left[a_3 + a_5 \frac{\sin y}{y}\right] \sin(yv^\circ \tau_d^*) = 0\right.\right.$$

The computing results of the solution of Eq. (4.1) in d, τ_d^* - plane are shown in Fig. 5. The curve $\tau_d^* = \tau_d^*(d)$ separates the instability domain from the stability domain (dashed one). It can be seen that the critical value of τ_d^* decreases if the stabilization parameter d grows. Therefore the upper limit of d is determined by the value of time lag τ_d.

5. Nonlinear analysis

The transient behavior of the reactor for finite perturbations was studied by computer simulation of Eqs (1.1)-(1.4). The curves 1 and 2 in the Fig. 6 demonstrate the transition from the lower stable state to stabilized intermediate one after beginning of the proportional control operation at $\tau = 0$. The curve 1 corresponds to the case of ideal control ($\tau_d = 0$). The curve 2 corresponds to nonideal control with parameters d and τ_d corresponding to the stability domain in Fig. 5. One can see that the curve 1 is monotonous and the curve 2 is not monotonous. In the case of nonideal control the damping oscillations of concentration and temperature near the intermediate steady values take place with the amplitude being dependent on the time lag value. The curve 3 corresponds to the case when the point (τ_d, d) belongs to the instability region in Fig. 5. It is seen that the reactor attains the upper steady state, which is stable (Fig. 6).

In Chemical Reaction Engineering—Houston; Weekman, V., et al.;
ACS Symposium Series; American Chemical Society: Washington, DC, 1978.

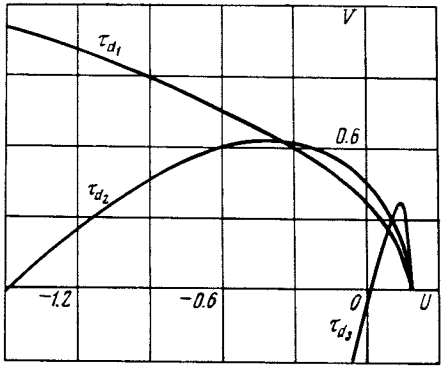

Figure 4. The curves $W = \psi(iy) = U + iV$, $0 \leqslant y$ *on the Nyquist plane for three values of the time lag*

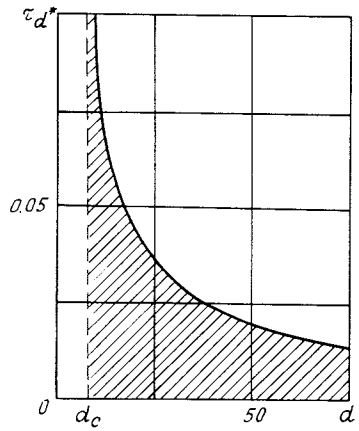

Figure 5. The stability domain (dashed) in τ_d, d *plane*

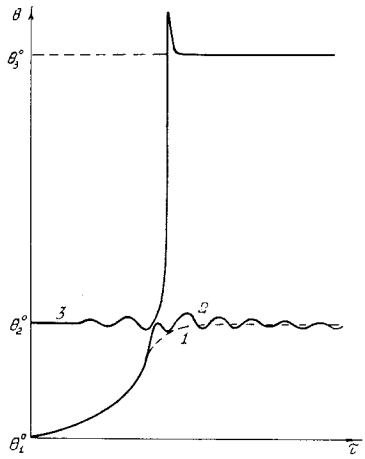

Figure 6. The transient behavior of the reactor temperature obtained by the computer simulation. Curve 1 corresponds to the ideal control ($\tau_d = 0$). *Curve 2 corresponds to non-ideal control with parameters d* and τ_d *from stability domain. Curve 3 corresponds to the parameters* d *and* τ_d *from instability domain at Figure 5.*

In Chemical Reaction Engineering—Houston; Weekman, V., et al.;
ACS Symposium Series; American Chemical Society: Washington, DC, 1978.

It was obtained also that for the points (τ_d, d) from the instability domain at $d > d_1$ only unstable steady state exists. In this case as the numerical calculations pointed out the sustained oscillations of the concentration and temperature are possible.

6. Conclusion

It is shown that the stabilization can be achieved by proportional flow-control method as long as the time lag in the control action does not exceed certain critical value. By numerical solution a restriction to be imposed on the control parameter for stability of an intermediate state at given disturbance level is defined.

By computer similation the transient behavior on nonlinear system is studied. It is shown that for zero time lag the stabilized intermediate steady state is achieved without oscillations. Under imperfect control operation damping oscillations of concentration profile and temperature near intermediate state can exist the amplitude being dependent on the time-lag value. For certain values of flow-control parameters sustained oscillations of concentration profile and temperature in the reactor are possible.

Literature Cited

1. Oh S.H., Schmitz R.A. Chem. Eng. Commun. (1974) 1, 199.
2. Borodulya V.A., Gupalo Yu.P. Matematicheskie modeli himicheskih reaktorov s kipyashim sloem. "Nauka i technika", Minsk, 1976.
3. Gupalo Yu.P., Ryazantsev Yu.S. PMTF (1969) 1, 82.
4. Aris R., Amundson N.R. Chem. Eng. Sci. (1958) 7, 121, 132, 148.
5. Schmitz Roger A. Advances in chemistry series (1975) 148, 156.

In Chemical Reaction Engineering—Houston; Weekman, V., et al.;
ACS Symposium Series; American Chemical Society: Washington, DC, 1978.

47

Use of Intensity Function Representation of Residence Time Variability to Understand and Improve Performance of Industrial Reactors

PHILIP T. WOODROW

Union Carbide Corporation, Chemicals and Plastics Division,
Research and Development Department, South Charleston, WV 25303

The application of residence time distribution theory is an established method for identifying process system fluid flow and mixing characteristics. Tracer data analysis via this theory can give valuable insight into a system's hydrodynamic characteristics. It has been applied to understand and improve industrial reactor performance. Two applications are discussed.

Introduction

Residence time distribution theory is appropriately applied when the experimental objective is to account for a system's fluid flow and mixing behavior. This is a vital objective because to predict and/or analyze process equipment performance one must know the amount of mixing, the manner in which fluid passes through the equipment, and the time that a given fluid element can be expected to remain in the system. Experimentally this information can be determined by admitting a tracer into the system and monitoring its behavior as it exits the system. Common tracer input forms are the pulse and step. "System" in this paper refers to systems with closed boundaries, i.e., a system where material can enter and exit only once.

Three assumed properties, inherent in residence time analysis, should be noted:

- Stationarity. The system's average physical properties are time independent. Although in reality the properties fluctuate around some average, these time fluctuation periods are very short compared to a particle's residence time. Hence, the system and its properties can be classified as quasi-steady which is necessary to perform meaningful residence time studies.
- Ergodicity. By injecting a sample with a large number of tracer molecules, the residence time density thus derived would be equivalent to the residence time density obtained from a large number of experiments using one tracer molecule.

© 0-8412-0401-2/78/47-065-571$05.00/0

- Although the tracer should be experimentally distinguishable, it must possess the same "mixing" properties as the system fluid.

Within the scope of residence time analysis, there are two fundamental functions and an additional derivable function. Although these are defined elsewhere (1), for purposes of completeness they are given here.

First, is the residence time density function, f(t). The physical interpretation of f(t) is given by the following: On viewing a particle which has just entered the system, the probability of its leaving within a time interval (t to t + dt) is equal to f(t)dt. Mathematically f(t) is constrained by:

$$\int_0^\infty f(t)dt = 1$$

f(t) is the system response to a unit impulse of tracer material.

Second, is the integral of the residence time density or cumulative density function, F(t), where

$$F(t) = \int_0^t f(t')dt' \qquad (t' \text{ is a dummy variable of integration})$$

with $F(0) = 0$ and $F(\infty) = 1$

F(t) gives the fraction of particles possessing a residence time of t or less. F(t) is the system response to a unit step of tracer material. There is also the compliment of F(t), F*(t), where

$$F^*(t) = 1 - F(t)$$

F*(t) gives the fraction of particles possessing a residence time exceeding t.

Finally, there is a function which indicates the escape probability for a particle which has stayed in the system for a period t. This function, the intensity function (2), $\lambda(t)$, is useful if one is interested in the probability of a particle leaving a system in the time interval (t, t + dt) given that the particle has already stayed in the system for a time t. This probability is denoted by $\lambda(t)dt$ and may be deduced via the following:

let: A be the event that a particle which has just entered a system leaves in the next time interval, dt.
B be the event of the particle not leaving before t.

In Chemical Reaction Engineering—Houston; Weekman, V., et al.;
ACS Symposium Series; American Chemical Society: Washington, DC, 1978.

C be the event that the particle will leave in the next interval, dt, given that it has not left before.

In probability terms therefore:

$$P(A) = P(B) \bullet P(C) = P(B) \bullet P(A/B)$$

In terms of the previous definitions:

$$P(A) = f(t)dt$$
$$P(B) = F^*(t)$$
$$P(C) = P(B/A) = \lambda(t)dt$$

Therefore:

$$f(t)dt = F^*(t)\,\lambda(t)dt$$

or: $\lambda(t) = f(t)/F^*(t) = -d/_{dt}(\ell n(F^*(t)))$

Also note that f(t) and $\lambda(t)$ are related by the following transformation:

$$f(t) = \lambda(t) \exp\left[-\int_0^t \lambda(t')dt'\right]$$

Hence, the intensity function is another way of exhibiting residence time variability and, as will be shown in the subsequent examples, yields flow mechanism insight and highlights distinct features of different distributions.

A common approach used in translating the abstract residence time data into more physically meaningful concepts is to compare the experimental distributions to distributions derived from idealized models. This approach has a drawback in that f(t) and/or F(t) functions derived from different physical models may appear to be quite similar. Because a large number of different models can lead to similar functions, the basic flow system features should be elucidated in more precise terms. For this reason the intensity function, $\lambda(t)$, is a more effective way of exhibiting residence time characteristics rather than densities or distributions. The intensity function can give a direct indication of stagnancy and/or bypassing according to the following:

- A system will exhibit bypassing if a fluid element can short-circuit from inlet to outlet. This would be seen by a peak in f(t) for t less than the apparent mean residence time. The intensity function (escape

probability) would decrease over some time interval before the apparent mean residence time.

- A system will exhibit stagnancy if a fluid element enters a region only weakly connected with the rest of the system. This would be indicated by slow decay of f(t) for t greater than the apparent mean residence time. Experimentally, this may be hard to discern. The intensity function would show a decrease over some time interval after the apparent mean residence time.

Case 1 - Plant Scale Reactor

Acetic acid is a commodity chemical produced by Union Carbide Corporation via the liquid phase oxidation of butane. While acetic acid is the principal product, methyl ethyl ketone and ethyl acetate are valuable by-products. Large scale gas-liquid reactors are used to practice this technology. In general the plant reactor performance was inferior in both productivity and selectivity when contrasted to pilot unit scale reactors carrying out the same reaction under equivalent conditions.

The inferior performance was manifested in high temperatures necessary to transfer the oxygen to the liquid phase for chemical reaction. The higher-than-desirable temperatures adversely affected reaction selectivity, producing undesirable quantities of non-usable by-products, e.g., carbon dioxide and water. If lower reaction temperatures could be achieved without lowering reactant feed rates, reaction selectivity would change to enhance both the acetic acid and valuable reaction by-product efficiencies. In addition, lower temperatures would decrease reactor metal corrosion rates and allow more stable and flexible control of the reaction system.

It was suspected that fluid bypassing was occurring in the plant reactors which would necessitate operation at higher temperatures to effect oxygen mass transfer and reaction. Residence time distribution studies using idealized reactor flow models strongly confirmed this suspicion.

Residence time testing of the plant reactors was infeasible due to severe conditions, safety considerations, and the necessity to determine what modifications could be made during an impending plant shut-down. Based on these constraints, a Plexiglas scale model of a plant reactor, previously constructed but utilized for visual mixing/flow pattern studies only, was the best available apparatus to perform additional work.

Because capital constraints prohibited radical reactor geometry changes, e.g., L/D ratio, low cost modification of reactor internals appeared to be the most expedient method for improving performance. An experimental plan was made to study

In Chemical Reaction Engineering—Houston; Weekman, V., et al.;
ACS Symposium Series; American Chemical Society: Washington, DC, 1978.

the effects of internals change on the residence time characteristics of the scaled-down plant reactor. The existing internal conffguration was studied as well as eight alternate configurations. For each configuration the system was pulsed with a highly conductive dye solution which afforded qualitative observation recording by motion pictures and quantitative residence time density data acquisition by conductivity measurement. Each experiment was replicated. The tracer injection was a pulse of such narrow width that for all intents and purposes the system saw it as an impulse. Hence, the output concentration response (after normalization) could realistically be regarded as the residence time density, f(t).

Figures 1, 2, and 3 exhibit the salient residence time study results. Figure 1 shows the residence time density, f(t), for three different configurations: the analog of the existing plant reactor and two alternate internal modifications (labelled A and B, respectively). Figure 2 exhibits the residence time distribution F(t) and Figure 3 exhibits the deduced intensity function $\lambda(t)$.

The intensity function curves clearly show the suspected plant reactor bypassing; some stagnancy is also indicated. The slight stagnancy of alternative A and the uniform behavior of alternative B are also shown. If ideal stirred tank behavior were superimposed on the plot it would be a horizontal line (this limiting behavior is discussed in the second case of intensity function utility presented later in this paper).

Comparison of the f(t) and F(t) behaviors does little to indicate which alternative is clearly indicative of well-mixed properties. The f(t) curve for the existing plant reactor does indicate bypassing. The corresponding $\lambda(t)$ curve confirms the bypassing.

Although all internal modification alternates are not shown here, the intensity function was of equal utility both in differentiating between alternatives and assisting in alternative choice for plant implementation. Alternative B was chosen as the recommended modification. Whereas one might feel that the moments of the f(t) curves should give quantities for differentiating between the observed performances, they gave no significant guidance in this case.

The recommended modification was made in a plant reactor. Follow-up data and analysis showed the modified reactor to allow lower temperature operation at the same raw material consumption rates as the unmodified reactors. Product analysis showed a significantly higher concentration of desirable and hence more profitable products. As a result the remaining reactors have been modified. The plant can now produce the same commodity amount with lower raw material requirements or conversely with the same raw material consumptions, more product can be produced.

In Chemical Reaction Engineering—Houston; Weekman, V., et al.;
ACS Symposium Series; American Chemical Society: Washington, DC, 1978.

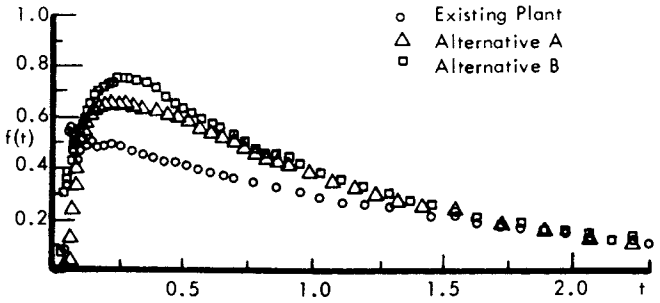

Figure 1. Salient residence time study results. Residence time density, f(t).

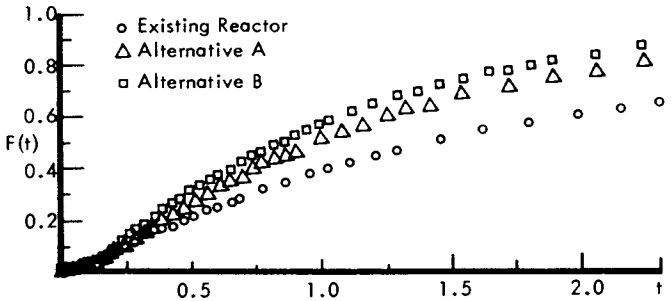

Figure 2. Salient residence time study results. Resident time distribution F(t).

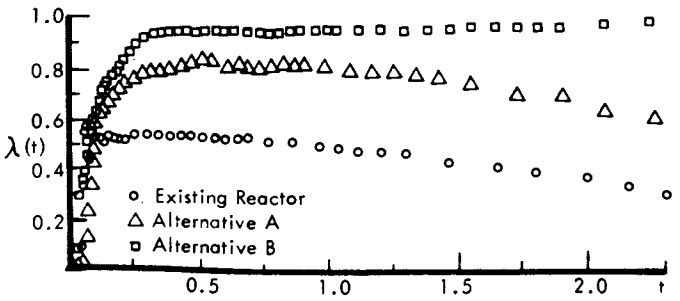

Figure 3. Salient residence time study results. Deduced intensity function λ(t).

In Chemical Reaction Engineering—Houston; Weekman, V., et al.;
ACS Symposium Series; American Chemical Society: Washington, DC, 1978.

Case 2 - Pilot Unit Scale Reactor

Early in the development of a new process, a productivity loss was encountered when the process was moved from the exploratory scale reactor to a larger pilot unit scale reactor. After study of many factors, the problem was resolved by installing a second impeller on the pilot reactor mixing shaft. While the action produced the desired results, it was not apparent why the one impeller system had performed below expectations. The traditional scale-up criterion of horsepower/unit volume for mixed vessels had been used when moving from the exploratory to pilot reactor. Historically this criteria had proved to be satisfactory.

In an effort to explain the second impeller effect, residence time data was collected for the one and two impeller reactors. Step testing was used and thus the response was in the form of the residence time distribution function F(t). For each system the residence time data was replicated twice. Figure 4 shows the average results for the respective reactors. While there is clearly a difference in F(t) behavior, there is no direct indication as to why the one impeller reactor yielded about half the productivity as the two impeller reactor.

The F(t) data were transformed to give the corresponding intensity function, $\lambda(t)$, curves shown in Figure 5. Comparison of the curves clearly shows a difference between the two reactors. The two impeller reactor exhibits well-mixed behavior whereas the one impeller reactor exhibits behavior indicative of a distributed system. This notion can be supported by examining a simple, transient, diffusion/convection flow model:

$$\frac{1}{Pe}\frac{\partial^2 y}{\partial z^2} - \frac{\partial y}{\partial z} = \frac{\partial y}{\partial t}$$

Solution with the following initial condition and boundary conditions gives f(t)

$$y(z, 0) = 0 \qquad z > 0$$
$$y(0, t) = \delta(t) \qquad t \geq 0$$
$$\lim_{z \to \infty} y(z, t) = \text{finite} \qquad t > 0$$

$$f(t) = y(1, t) = \left[\frac{Pe}{4\pi t^3}\right] \exp\left(-\frac{Pe}{4}\frac{(t-1)^2}{t}\right)$$

If one changes the inlet boundary condition to

$$y(0, t) = H(t) \qquad t \geq 0$$

In Chemical Reaction Engineering—Houston; Weekman, V., et al.;
ACS Symposium Series; American Chemical Society: Washington, DC, 1978.

F(t) can be derived:

$$F(t)=y(1,\ t)=\frac{\exp\left(\frac{Pe}{2}\right)}{2}\left\{\exp\left(-\frac{Pe}{2}\right)\operatorname{erfc}\left(\sqrt{\frac{Pe}{4t}}-\sqrt{\frac{Pe\ t}{4}}\right)+\exp\left(\frac{Pe}{2}\right)\operatorname{erfc}\left(\sqrt{\frac{Pe}{4t}}+\sqrt{\frac{Pe\ t}{4}}\right)\right\}$$

Evaluation of F(t) for high values of the Peclet number, Pe, can present problems. Use of the approximations given by Abramowitz and Stegun (3) resolve computational problems. The intensity function for the diffusion/convection model is formulated by

$$\lambda(t) = f(t)/(1 - F(t))$$

Figures 6, 7, and 8 show the behavior of f(t), F(t) and λ(t) for different values of Peclet number. The limiting cases of Pe = ∞ (zero diffusivity-plug flow) and Pe = 0 (infinite diffusivity - well-mixed behavior) are also shown.

By comparison of the intensity function results in Figure 5 to the curves shown in Figure 8, one can see directly the well-mixed behavior of the two impeller system versus the distributed behavior of the one impeller system. It was concluded that a well-mixed reactor was a necessary condition to ensure maximum productivity for the process under development. Hence, very firm mixing and fluid flow guidelines were established at the process development stage which reduced the risk of scale-up to plant equipment.

Conclusions and Recommendations

Based on the examples presented, it is clear that intensity function representation of residence time variability is a valuable tool for understanding and discerning fluid mixing characteristics. Effective utilization of this tool requires good experimental technique. Determination of residence time characteristics and use of intensity function representation/interpretation should be a critical step in the sequential development of exploratory, pilot unit and plant scale reactors.

Nomenclature

D	reactor diameter
L	reactor length
P( )	probability of event ( ) occurring
Pe	axial Peclet number (VL/D_a)
V	fluid velocity
D_a	axial diffusion coefficient
t^a	dimensionless time

In Chemical Reaction Engineering—Houston; Weekman, V., et al.;
ACS Symposium Series; American Chemical Society: Washington, DC, 1978.

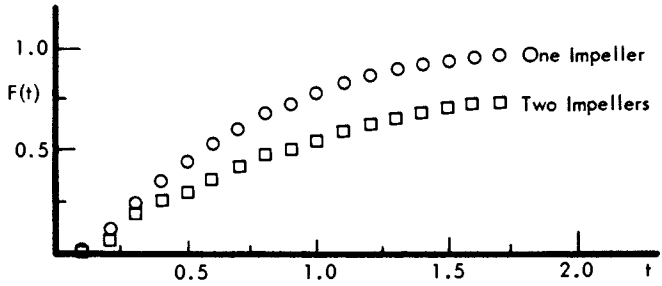

Figure 4. Residence time data. Residence time distribution function F(t).

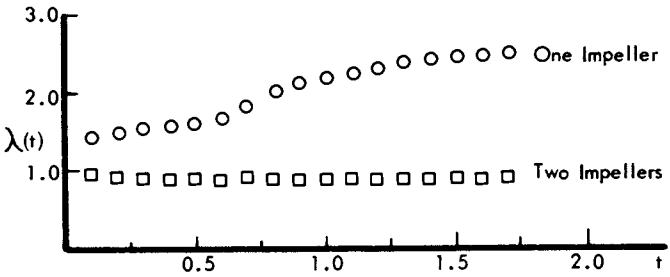

Figure 5. Residence time data. Intensity function λ(t).

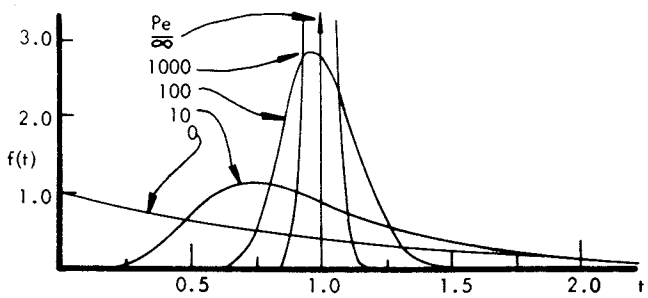

Figure 6. Behavior of f(t) for different values of Peclet number

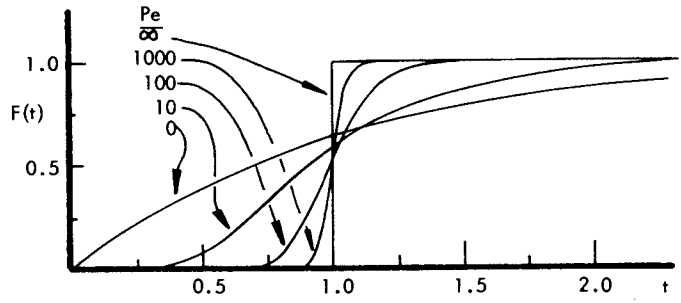

Figure 7. Behavior of F(t) for different values of Peclet number

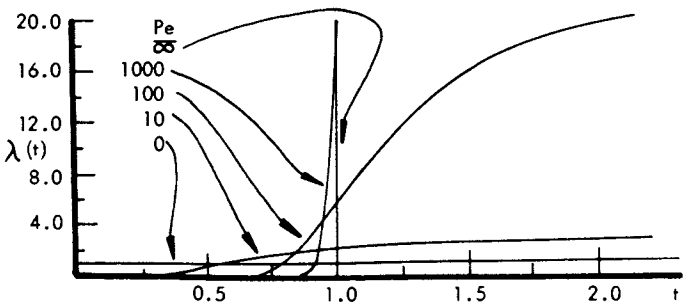

Figure 8. Behavior of λ(t) for different values of Peclet number

In Chemical Reaction Engineering—Houston; Weekman, V., et al.;
ACS Symposium Series; American Chemical Society: Washington, DC, 1978.

y	dimensionless concentration variable
z	dimensionless axial distance (Z = 1 corresponds to the bed outlet)
$\delta(t-t^*)$	unit impulse (Dirac delta function) at time t=t*
$H(t-t^*)$	unit step (Heaviside step function) at time t=t*

Literature Cited

1. Lapidus, L. and Seinfeld, J. H., "Mathematical Methods in Chemical Engineering, Volume 3: Process Modeling Estimation, and Identification", pp. 289-339, Prentice-Hall, Inc., Englewood Cliffs, 1974.
2. Naor, P. and Shinnar, R., I & EC Fundamentals (1963), 2, 278- 286.
3. Abramowitz, M. and Stegun, I. A., eds., "Handbook of Mathematical Functions", pp. 298-299, National Bureau of Standards, Washington, D. C., 1964.

In Chemical Reaction Engineering—Houston; Weekman, V., et al.;
ACS Symposium Series; American Chemical Society: Washington, DC, 1978.

48

Oxidation of SO_2 on Supported Molten V_2O_5-$K_2S_2O_7$ Catalyst

Kinetics under Varying Degree of Liquid Diffusion Influence

P. GRYDGAARD, H. JENSEN-HOLM, H. LIVBJERG, and J. VILLADSEN

Technical University of Denmark, 2800 Lyngby, Denmark

SO_2-oxidation rate data for a wide range of process conditions are presented. The rate data are combined with measurements of the composition of the V_2O_5-$K_2S_2O_7$ catalytic melt. It is shown that all available rate data can be explained if the $V^{(4)}$ content of the catalyst is assumed to increase with decreasing temperature and with increasing liquid diffusion resistance and if furthermore the availability of active $V^{(4)}$ compounds in the catalytic cycle is assumed to decrease with decreasing temperature, most probably by precipitation of some $V^{(4)}$ species.

SO_2-Oxidation Kinetics

Despite persistent research efforts over the last 40 years the active sulfovanadate complexes of the catalyst have not yet been identified. Under normal process conditions the rate determining step is almost certainly the reoxidation of a $V^{(4)}$ species Y in (2) or (4) in model 1 and model 2. The reduction of $V^{(5)}$ species X may be either (1) as proposed by Mars and Maessen [3] or (3) as proposed by Boreskov [4]. Both (1) and (3) are supposed to be fast equilibrium reactions, although a shift in rate determining step may be possible at very low operating temperature.

Model 1:

$$SO_2 + nX \rightleftarrows SO_3 + mY \quad (1)$$

$$mY + \tfrac{1}{2}O_2 \rightleftarrows nX \quad (2)$$

Model 2:

$$SO_2 + nX \rightleftarrows mY \quad (3)$$

$$mY + \tfrac{1}{2}O_2 \rightleftarrows nX + SO_3 \quad (4)$$

In terms of the degree of reduction $\varepsilon = \frac{V^{(4)}}{V_T}$ and with n=m=2 the equilibrium constants for (1) and (3) are

In Chemical Reaction Engineering—Houston; Weekman, V., et al.;
ACS Symposium Series; American Chemical Society: Washington, DC, 1978.

$$K_1 = \frac{\varepsilon^2}{(1-\varepsilon)^2} \frac{p_{SO_3}}{p_{SO_2}} = 2.3 \cdot 10^{-8} \exp\left(\frac{13600}{T}\right) \quad (5)$$

$$K_2 = \frac{\varepsilon^2}{(1-\varepsilon)^2} \frac{1}{p_{SO_2}} = 8.9 \cdot 10^{-10} \exp\left(\frac{17000}{T}\right) (atm^{-1}) \quad (6)$$

The ε data used in [3] to propose (5) did not have a sufficiently large variation of p_{SO_3} to discriminate between (5) and (6) while a thorough examination of all available ε-data in [1] including some with a 30-fold variation of p_{SO_3} points to (6) as the most likely equilibrium step. The statistical analysis of ε-data show that n=m=2 is far better than any other combination of integer exponents in model 1 as well as in model 2. Both (5) and (6) are based on diffusion free data obtained with either an equilibrated gas phase (no overall reaction takes place) or with liquids dispersed well enough to avoid diffusion effects. The variation of ε with liquid loading is shown in Fig. 1 which is based on [5]. Line C is described by (6).

A solubility of 4-6% $V^{(4)}$ in $K_2S_2O_7$ at 400-600°C is found in [7] and Boreskov [8] identified by ESR two $V^{(4)}$ species below 480°C. The existence of crystals of a precipitated $V^{(4)}$ compound is mentioned in [5,6,7].

$$Y_{liq} \rightleftarrows Y_{solid} \quad (7)$$

Precise measurement of the solubility of Y is difficult but qualitatively we know that $[Y_{solid}]$ increases below 450°C when the catalyst is reduced by SO_2, probably directly connected with the increase of ε by (5) or (6).

Arrhenius plots of the apparent rate constant for SO_2-oxidation invariably show a break at ~450°C and the apparent activation energy is often very high at low temperature [8,4]. This phenomenon is clearly connected with the lower oxidation level of V at low temperature, probably enhanced by liquid diffusion resistance and accompanied by inactivation of $V^{(4)}$. To improve the low temperature activity of vanadium catalyst, a primary goal if the cumbersome interabsorption converter design is to be avoided, our understanding of these complex phenomena must be advanced.

Experimental

190 SO_2-oxidation rate measurements were obtained in a recirculation reactor described in [2]. The experimental strategy is summarized in Table I.

Table I: Summary of rate measurements 1)

Series No.	No. of data points	Vanadium content 2)	
1	24	2.85	Orthogonal design at 480 C. O_2: 7.6-16%, SO_2: 2.1-6.5%, SO_3: 2.5-6%
2	16	2.85	Orthogonal design at 480 C. O_2: 20-48%, SO_2: 9-20%, SO_3: 7-17%
3	19	2.85	Orthogonal design at 530 C. O_2: 7-16%, SO_2: 2.9-6.5%, SO_3: 2.2-6%
4	18	2.85	440-550 C, 10 C temperature steps and standard gas composition
5	16	2.85	400-480 C, 10 C temperature steps and standard gas composition
6	12	1.37	380-460 C, 10 C temperature steps and standard gas composition
7	20	21.1	430-570 C, 10 C temperature steps and standard gas composition
8	12	7.87	400-480 C, 10 C temperature steps and standard gas composition
9	8	14.2	400-480 C, 10 C temperature steps and standard gas composition
10	8	24.2	380-450 C, 10 C temperature steps and standard gas composition
11	20	21.1	Orthogonal design at 480 C. O_2: 6-16%, SO_2: 3-6.8%, SO_3: 1.9-5.4%
12	17	21.1	Orthogonal design at 530 C. O_2: 7.2-15%, SO_2: 3-7%, SO_3: 2-5.2%

1) The support is controlled-pore glass (CPG, Electro-Nucleonics, Inc. Fairfield, N.J.) with porevolume 1.02 cm^3/g, porosity 69%, pore radius 1530 Å, particle size 20/30 mesh. The overall catalyst composition is K/V = 3.5 atom/atom. The standard gas composition is 10.7% O_2, 4.4% SO_2, 3.6% SO_3, balance N_2.

2) g V_2O_5/100 g support.

It was controlled by computations [2] that particle size, pore size, and recycle flow were chosen such that neither inter- nor intraparticle gas phase concentration gradients were of importance. Porous glass (CPG) was impregnated with an aquous solution of $VOSO_4$-$KHSO_4$, dried and activated for 2 days. 1.37-24.2 g V_2O_5/100 g support was used - the higher loadings by reimpregnation as discussed in [2].

Two types of measurements were made. In the first the temperature was decreased in small steps from one experiment to the next, but keeping constant gas composition. Some of the high temperature measurements were repeated to control that no deactivation had occurred. In the other type of measurement gas composition was changed isothermally using the orthogonal factorial design of figure 2. The centerpoints and also other points were frequently repeated to test for deactivation.

Determination of a feed flow and feed composition that yields a predetermined reactor gas composition requires an approximate knowledge of the rate at this composition. A few successive feed flow adjustments were sometimes necessary to give approximately the desired composition, but variations of 10% relative were

In Chemical Reaction Engineering—Houston; Weekman, V., et al.;
ACS Symposium Series; American Chemical Society: Washington, DC, 1978.

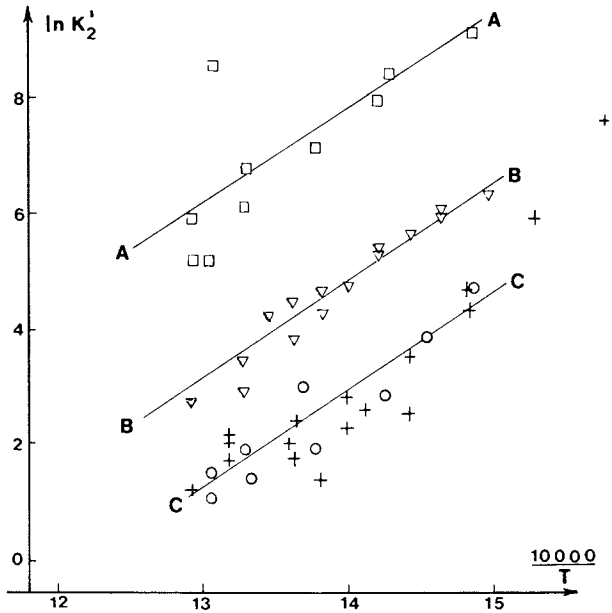

Figure 1. Vanadium reduction data obtained by ESR plotted as the equilibrium constant $K_2 = (1 - \epsilon)^2/\epsilon^2/P_{SO_2}$.

1. □ *unsupported melt,* K/V = 3.5 *[5]*
2. ▽ *industrial catalyst,* K/V = 2.5 *[5]*
3. ○ *finely dispersed supported melt,* K/V = 3.5 *[5]*
4. \+ – – – – *[4]*

The data of series 3 and 4 are included in the regression analysis of the present investigation.

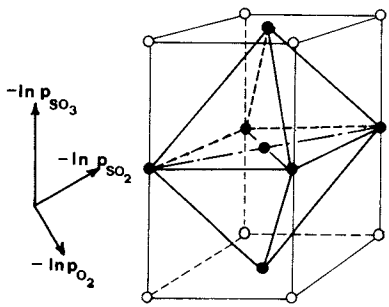

Figure 2. Orthogonal factorial design for reactor gas composition

allowed as long as the actual rate and composition were measured accurately. In this way the overall orthogonal factorial design for the 5 variables: V_2O_5 content, T, y_{O_2}, y_{SO_2}, y_{SO_3} was preserved sufficiently well to avoid unintentional cross correlation in the statistical analysis.

The effect of temperature and V_2O_5 content on the rate is shown in figure 3, an Arrhenius plot of turnover frequency N_{SO_2} for standard gas composition. In accordance with our previous results [2] N_{SO_2} is independent of V_2O_5 content below 3% V_2O_5. In this region there is no liquid diffusion resistance with the support that we have used. For 20% V_2O_5 liquid diffusion resistance is severe. The variation of apparent activation energy E_a with V_2O_5 content is interesting and has not previously been fully recognized. Above ~450°C E_a is independent of V_2O_5 content, changing from 24 kcal/mol for 450<T<500°C to 11 kcal/mol above 500°C. Below the break at ~450°C E_a depends strongly on V_2O_5 content, from 34 kcal/mol at 3% V_2O_5 to 50 kcal/mol at 20% V_2O_5.

Analysis of Purely Kinetic Data

In the following analysis we shall treat the data obtained with less than 3% V_2O_5 separately from the more or less diffusion restricted data with higher V-content.

If the individual rates of (1)-(4) can be described by simple power law kinetics in molar liquid concentrations of reaction species the following alternative rate expressions are derived from Model 1 and Model 2 respectively:

Model 1:

$$N_1 = k_1 \varepsilon_s^{\alpha_2} y_{SO_2}^{\alpha_1} (1-\varepsilon)^{\alpha_2} \left[1 - \frac{\varepsilon_s^{m-n} y_{SO_3} \varepsilon^m}{K_1 y_{SO_2} (1-\varepsilon)^n}\right] \quad (8)$$

$$N_2 = k_2 \varepsilon_s^{\beta_2} y_{O_2}^{\beta_1} \varepsilon^{\beta_2} \left[1 - \frac{K_1 \varepsilon_s^{n-m} (1-\varepsilon)^n}{K_p p^{\frac{1}{2}} y_{O_2}^{\frac{1}{2}} \varepsilon_m}\right] \quad (9)$$

Model 2:

$$N_1 = k_1 \varepsilon_s^{\alpha_2} y_{SO_2}^{\alpha_1} (1-\varepsilon)^{\alpha_2} \left[1 - \frac{\varepsilon_s^{m-n} \varepsilon^m}{K_2 p\, y_{SO_2} (1-\varepsilon)^n}\right] \quad (10)$$

In Chemical Reaction Engineering—Houston; Weekman, V., et al.;
ACS Symposium Series; American Chemical Society: Washington, DC, 1978.

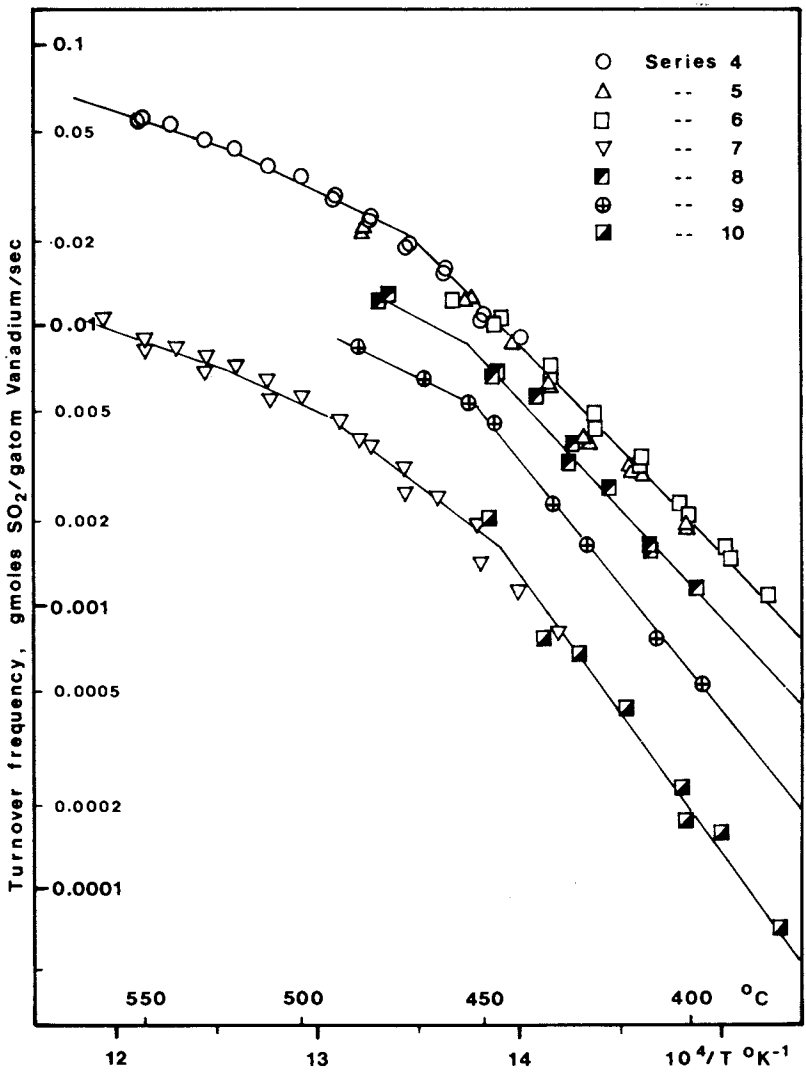

Figure 3. Arrhenius plot of measured reaction rate with gas composition approximately 10.7% O_2, 4.4% SO_2, and 3.6% SO_3. The uppermost curve is calculated by model 1 using parameter values from Table II.

$$N_2 = k_2\, \varepsilon_s^{\beta_2}\, y_{O_2}^{\beta_1}\, \varepsilon^{\beta_2} \left| 1 - \frac{K_2 \varepsilon_s^{n-m}\, y_{SO_3}\, (1-\varepsilon)^n}{K_p\, p^{-\frac{1}{2}}\, y_{O_2}^{\frac{1}{2}}\, \varepsilon^m} \right| \qquad (11)$$

y_i are gas molefractions. Henry's law constants and total vanadium concentration are included in k_1, k_2, and in the equilibrium constants K_1 and K_2. A fraction $1-\varepsilon_s$ of the total vanadium content V_T forms an inactive $V^{(4)}$ phase that is probably insoluble in the melt.

$$[V^4]_{liq} + [V^5] = \frac{2}{m} C_y + \frac{2}{n} C_x = \varepsilon_s V_T \qquad (12)$$

ε is the degree of reduction of the liquid phase: $[V^{(4)}]_{liq}/\varepsilon_s V_T$ and it is postulated that $[V^{(4)}]_{liq}/V_T$ cannot exceed a given solubility $S_y(T)$

$$\varepsilon_s \varepsilon \leq S_y \qquad (13)$$

The overall (or observed) degree of reduction ε_o is

$$\varepsilon_o = ([V^{(4)}]_{liq} + [V^{(4)}]_{solid})/V_T = 1-\varepsilon_s(1-\varepsilon) \qquad (14)$$

Arrhenius type expressions (with parameters to be determined from the statistical analysis) are supposed to hold for k_1, k_2, K_1, K_2, and S_y. All expressions are centered at 480 C:

$$(a_i \exp\, (\frac{E_i}{R_g}\, (\frac{1}{T} - \frac{1}{753})))$$

The computation by either model is done as follows: First ε_s is assumed to be 1. At steady state $N_1=N_2=$ the actual SO_2 turnover frequency N and for given parameters N, ε are calculated using either (8),(9) or (10), (11). If $\varepsilon \leq S_y$ no precipitation of $V^{(4)}$ occurs and the solution is correct. If $\varepsilon > S_y$ then $\varepsilon\varepsilon_s = S_y$ provides an extra equation which combined with the previous equations gives N, ε and ε_s for $\varepsilon_s < 1$.

Least squares applied to diffusion free rate data, series 1-6 of Table I, was combined with supposedly diffusion free vanadium reduction data (series 3 and 4 of Fig. 1). Both rate data and reduction data were obtained with K/V = 3.5 and essentially the same temperature - and gas composition range. 31 reduction data and 105 rate data are included in the regression. Parameter values that minimized SSQ were determined.

$$SSQ = SSQ_N + SSQ_\varepsilon = \sum_i [\ln(\frac{1}{c_j} N_{i,obs}) - \ln(N_{i,pred})]^2$$

In Chemical Reaction Engineering—Houston; Weekman, V., et al.;
ACS Symposium Series; American Chemical Society: Washington, DC, 1978.

$$+ \sum_i [\ln(\varepsilon_o)_{i,obs} - \ln(\varepsilon_o)_{i,pred}]^2 \qquad (16)$$

c_j is constant for series j, but may vary between series. It is included in the regression analysis (except for series 1 where $c_1 \equiv 1$) since small systematic variations (±10%) are expectable due to variations in catalyst sample impregnation and activation.

Both for model 1 and 2 a large number of (m,n) values were tried, but m=n=2 were the best with a residual comparable to the experimental error. The results are shown in Table II. The minimum SSQ is obtained only when (1) or (3) is close to equilibrium, a very satisfactory result since this was previsaged from the observations which lead to formulation of (5) and (6). As a consequence α_1, α_2, and the kinetic parameters of k_1 cannot be determined with any degree of confidence. Model 1 appears slightly better than model 2. The reason is that the SO_3 inhibition even far from equilibrium which is observed in the rate data (see Table III) is explained in model 1 through its influence on K_1. It is however, well possible that SO_3 affects the forward reaction rate of (4) in a manner which is not explained by the rate expression (11), and a discrimination between the two models cannot be made on the basis of our rate data.

Table II:
Estimated parameters for model 1 and 2 with m=n=2. 2σ confidence limits are included

	K_1 [1]	$k_2 = k_{20}\exp[\frac{E_2}{R_g}(\frac{1}{T}-\frac{1}{753})]$		β_1 and β_2	K_1, K_2
		k_{20} $\frac{\text{g mole}}{(\text{gatomV})\text{sec}}$	E_2 kcal/mole		
Model 1	>100	0.39±0.15	26.1±3	0.72±0.13 1.20±0.2	$(0.37\pm0.06)\exp[(13240\pm2000)(\frac{1}{T}-\frac{1}{753})]$
Model 2	>1000	0.64±0.4	27.8±5	0.66±0.15 1.59±0.4	$(5.6\pm4.0)\exp[(12000\pm3000)(\frac{1}{T}-\frac{1}{753})]$ (atm^{-1})

	$S_y = S_{yo}\exp[\frac{E_y}{R_g}(\frac{1}{T}-\frac{1}{753})]$		Standard error %	SSQ_ε	SSQ_N
	S_{yo}	E_y kcal/mole			
Model 1	0.48±0.05	7.2±2	11	0.8	0.6
Model 2	0.35±0.03	4.0±3	13	0.6	1.4

1) k_1, α_1, α_2 becomes indeterminate since the first step is close to equilibrium.

In Chemical Reaction Engineering—Houston; Weekman, V., et al.;
ACS Symposium Series; American Chemical Society: Washington, DC, 1978.

The equilibrium constants K_1 and K_2 of Table II are not directly comparable with those in (5) and (6), since the latter pair is based on measured ε_o and include precipitated $V^{(4)}$. At high T where no $V^{(4)}$ is precipitated the agreement is very good for K_1. For $\varepsilon_s<1$ K_2 of (6) is somewhat higher than in Table II and K_1 of (5) a factor 5 larger than the corresponding values from Table II in the whole temperature range.

Table III: Estimated parameters in a power law rate expression: $N=k\ y_{O_2}{}^a\ y_{SO_2}{}^b\ y_{SO_3}{}^c$. Data from series 1, 3, 11, and 12 of Table I. 2σ confidence limits are shown.

	480 C			530 C		
V_2O_5 Content	a	b	c	a	b	c
2.85%	0.74±0.12	0.50±0.08	-0.51±0.10	0.86±0.08	0.53±0.08	-0.30±0.06
21.1%	0.77±0.08	0.40±0.08	-0.37±0.06	0.81±0.16	0.50±0.14	-0.18±0.10

The observed change of E_a at 450°C is well predicted by both models (figure 3) a fact that gives credence to the postulated precipitation of a $V^{(4)}$ compound. The predicted precipitation is shown on figure 4 which agrees remarkably well with the ESR measurements of [8], assuming that "line B" of the reference corresponds to precipitated $V^{(4)}$. With the standard gas composition of our measurements a solid phase appears below 470°C, and at 380°C only 1/3 of the V is dissolved. Calculations with $S_y \equiv 1$ made it evident that neither of the two models could be used if the precipitation (or inactivation) mechanism was not included. From Table II the solubility S_{yo} at 480°C is .48 (model 1) and .36 (model 2) and the temperature dependence of S_y is small. Since a V_2O_5, 3.5-$K_2S_2O_7$ melt contains 17% vanadium (calculated as V_2O_5) the solubility of $V^{(4)}$ at 480°C is ∿17 S_y % or 8% (model 1) and 6% (model 2). Both results agree very well with the observed solubility (∿4-6%) in [7].

We conclude that a two step mechanism (1)-(2) or (3)-(4) combined with a precipitation step (7) explains the apparently conflicting experimental observations provided the data are essentially diffusion free.

Kinetics of The Liquid Diffusion Regime

X-ray microprobe investigation and scanning electron-microscopy show that above 3-5% V_2O_5 part of the melt agglomerates in the pore structure to form macroscopic

In Chemical Reaction Engineering—Houston; Weekman, V., et al.;
ACS Symposium Series; American Chemical Society: Washington, DC, 1978.

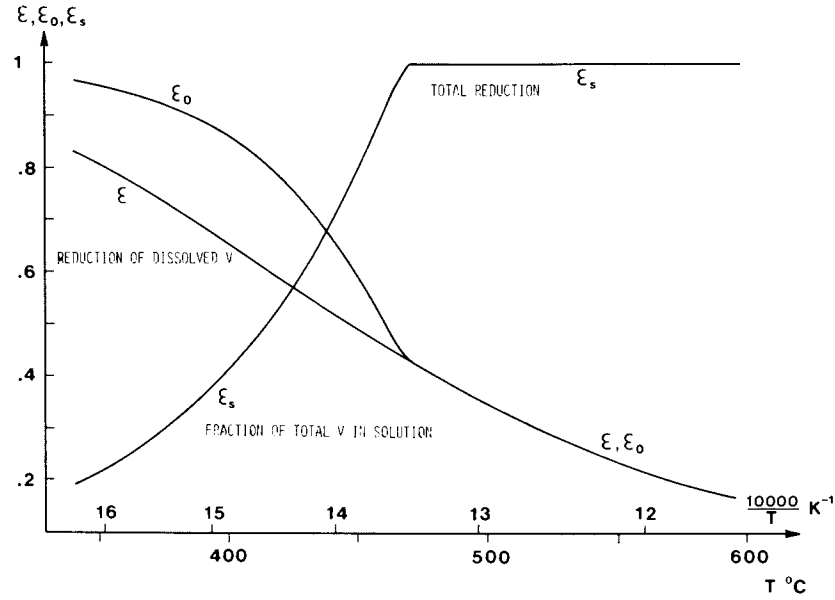

Figure 4. Prediction of vanadium reduction and precipitation of $V^{(4)}$ for standard gas composition using model 1 with parameter values from Table II.

clusters [1,2,9]. These clusters of size ∿0.025 mm are completely inactive, and the measured activity is related exclusively to a well dispersed liquid phase outside the clusters. Addition of further melt to the support leads to growth of the inactive clusters and actually to a decrease in active regions. This explains why E_a is independent of V_2O_5 content above 450°C. Table III compares the kinetics of catalysts with small and large V_2O_5 content. The reaction orders for the overall reaction are essentially the same which supports the theory that the reaction occurs in a well dispersed part of the catalyst independent of liquid loading.

The influence of V_2O_5 content on E_a below 450°C is remarkable and it points to the necessity of keeping the melt well dispersed - possibly by using only a small V_2O_5 content at low temperature. Since ε of the clusters is higher than in the rest of the melt due to the influence of liquid diffusion resistance on ε (figure 1) a relatively larger amount of vanadium will precipitate in the clusters. Consequently vanadium will diffuse from the active portion of the melt into the clusters. This may explain the unexpected low activity at low temperature for V_2O_5 rich catalysts.

We cannot yet give a quantitative treatment of the diffusion phenomena since our knowledge of reaction and liquid diffusion parameters and especially of the liquid distribution function is quite incomplete [1]. The following qualitative treatment does, however, prove that ε may increase significantly with film thickness if we assume a 3-step mechanism, whereas neither (1)-(2) nor (3)-(4) could lead to a similar conclusion since both assume a fast reduction step with C_y being the same in thick and thin films. Assume that

$$SO_2 + 2X \rightleftarrows 2Y, \quad 2Y \rightleftarrows 2Z + SO_3, \quad 2Z + \tfrac{1}{2}O_2 \rightleftarrows 2X \qquad (17\text{-}19)$$

$$\gamma_1 = \left(\frac{x^2 p_{SO_2}}{y^2}\right)_{eq} = \frac{k_1'}{k_1}, \quad \gamma_2 = \left(\frac{y^2}{z^2 p_{SO_3}}\right)_{eq} = \frac{k_2'}{k_2} \qquad (20\text{-}21)$$

$$\gamma_3 = \left(\frac{z^2 p_{O_2}^{\frac{1}{2}}}{x^2}\right)_{eq} = \frac{k_3'}{k_3} = \frac{1}{\gamma_1 \gamma_2 K_p} \qquad (22)$$

x is the concentration of a $V^{(5)}$ species and (y,z) the concentration of two different $V^{(4)}$ species. k_i and k_j' are forward and reverse reaction rate constants. Abbreviate p_{SO_2}, p_{SO_3}, and p_{O_2} by s_2, s_3, and o.

In Chemical Reaction Engineering—Houston; Weekman, V., et al.;
ACS Symposium Series; American Chemical Society: Washington, DC, 1978.

Assume the liquid phase kinetics (23) to (25)

$$k_1 x^2 s_2 - k_1 \gamma_1 y^2 = R_{obs} = \text{observed averaged rate/volume liquid} \quad (23)$$

$$k_1 \delta_1 y^2 - k_1 \delta_1 \gamma_2 z^2 s_3 = R_{obs} \quad (24)$$

$$k_1 \eta \delta_2 z^2 o^{\frac{1}{2}} - k_1 \delta_2 \gamma_3 x^2 = R_{obs} \quad (25)$$

Gas solubilities and total vanadium content V_T are incorporated into the rate constants. Thus $x+y+z=1$. The constants δ_1 and δ_2 are

$$\delta_1 = \frac{k_2}{k_1} \quad \text{and} \quad \delta_2 = \frac{k_3}{k_1} \quad (26)$$

Since k_1 and k_3 are scaled by the small gas solubilities they are much greater than k_2. Thus $\delta_2/\delta_1 >> 1$ and $\delta_1 << 1$. x, y, z, s_2, and s_3 are assumed to be constant through the film and only the forward reaction of (19) is assumed to be diffusion limited due to extreme low solubility of O_2. The effectiveness factor η is introduced to account for depletion of O_2 in thick films. (23) to (25) are easily solved to give

$$x = 1/(1 + \sqrt{a}(1+\sqrt{b})), \quad y = x\sqrt{a}, \quad z = x\sqrt{ab} \quad (27)$$

$$a = \frac{s_2}{(\delta_1+\gamma_1) - \dfrac{(\delta_1+\gamma_1)(1+\frac{\delta_2\gamma_3}{s_2}) - \gamma_1}{(1+\frac{\delta_2\gamma_3}{s_2}) + \frac{\delta_2 o^{\frac{1}{2}}\eta}{\delta_1\gamma_2 s_3}}} = \frac{y^2}{x^2} \quad (28)$$

$$b = \frac{(\delta_1+\gamma_1)(1+\frac{\delta_2\gamma_3}{s_3}) - \gamma_1}{\delta_1\gamma_2 s_3(1+\frac{\delta_2\gamma_3}{s_2}) + \delta_2\eta o^{\frac{1}{2}}} = \frac{z^2}{y^2} \quad (29)$$

We wish to study the case where reaction (17) is almost in equilibrium in thin films. This means that the first term in (23) >> the last term of (25) or $s_2 >> \delta_2\gamma_3$. Since also $\delta_1 << 1$ (28)-(29) can be reduced to

$$a = \frac{s_2}{\gamma_1} \quad \text{and} \quad b = \frac{\delta_1}{\delta_1\gamma_2 s_3 + \delta_2\eta o^{\frac{1}{2}}} \quad (30)$$

Since a is practically independent of η the same simple expression for a is obtained in thick films while b changes from

$$b(\eta=1) \sim \frac{\delta_1}{\delta_2 o^{\frac{1}{2}}} \quad \text{to} \quad b(\eta\sim 0) = \frac{1}{\gamma_2 s_3} \quad \text{since}$$

$$\delta_1/\delta_2 \quad (\text{and } \frac{\delta_1}{\delta_2} \frac{\gamma_2 s_3}{o^{\frac{1}{2}}}) << 1.$$

It is seen that b and consequently z may increase significantly from thin films (where $z\sim 0$) to thick films. As a consequence reaction (18) which is far from equilibrium in thin films is practically in equilibrium for thick films. Thus in thick films (17) to (19) collapse to Mars and Maessen's model (1)-(2). In thin films (18) and (19) can be combined and the model is identical to Boreskov's model [4] although he interprets Y as an adduct of SO_2 to a $V^{(5)}$ species.

List of Symbols

c_i	Correction parameter for rate data of series i
C_x, C_y	Molar liquid concentration, mole /cm^3
E_a, E_1, E_2, E	Activation energy, kcal/mole
k_1, k_2	Rate constants, mole/(gatomV)/sec
K_1, K_2	Equilibrium constants
K_p	$10^{(5005/T-4.743)}$ atm$^{-\frac{1}{2}}$, gas phase equilibrium constant for $SO_2+\frac{1}{2}O_2 \rightarrow SO_3$
N, N_1, N_2, N_{SO_2}	Turnover frequency, moles/(gatomV)/sec
p, p_i	Pressure, partial pressure, atm
R_g	Gas constant
S_y, S_{yo}	Solubility of $V^{(4)}$ defined in Eq.13
$SSQ, SSQ_\varepsilon, SSQ_N$	Sum of squares defined in Eq.16
T	Temperature
V_T	Total concentration of vanadium in liquid, (gatomV)/cm^3
$\alpha_1, \alpha_2, \beta_1, \beta_2$	Power law exponents
ε	Degree of reduction in the liquid phase $[V^{(4)}]_{liq}/V_T$
ε_o	Total fraction of vanadium reduced to $V^{(4)}$
ε_s	The fraction of total vanadium content which is dissolved in the liquid

In Chemical Reaction Engineering—Houston; Weekman, V., et al.;
ACS Symposium Series; American Chemical Society: Washington, DC, 1978.

Literature Cited

1. Villadsen, J. and Livbjerg, H., "Supported Liquid phase catalysts", Catal. Reviews, Chem.Eng. (1978)
2. Livbjerg, H., Jensen, K.F., and Villadsen, J., J. Catalysis (1976) 45 216
3. Mars, P. and Maessen, J.G.H., J. Catalysis 10 1 (1968)
4. Boreskov, G.K., Polyakova, G.M., Ivanov, A.A., Mastikhin, V.M., Dokl.Akad.Nauk. (USSR) 210(3) 626 (1973) (Engl. transl. p. 423)
5. Mastikhin, V.M., Polyakova, G.M., Zyulkovskii, Y., Boreskov, G.K., Kinetics and Catalysis (USSR) 14 1219 (Engl. transl.) (1970)
6. Hähle, S. and Meisel, A., Kinetics and Catalysis (USSR) 12(5) 1276 (1971) (Engl. transl. p. 1132)
7. Holroyd, F.P.B. and Kenney, C.N., Chem.Eng.Sci. 26 1971 (1971)
8. Boreskov, G.K., Davydova, L.P., Mastikhin, V.M., Polyakova, G.M., Dokl. Akad. Nauk. (USSR) 171(3) 648 (1966) (Engl. transl. p. 760)
9. Jensen-Holm, H., Ph.D. Thesis, Technical University of Denmark, Lyngby, To appear 1978.

In Chemical Reaction Engineering—Houston; Weekman, V., et al.;
ACS Symposium Series; American Chemical Society: Washington, DC, 1978.

INDEX

In Chemical Reaction Engineering—Houston; Weekman, V., et al.;
ACS Symposium Series; American Chemical Society: Washington, DC, 1978.

In Chemical Reaction Engineering—Houston; Weekman, V., et al.;
ACS Symposium Series; American Chemical Society: Washington, DC, 1978.

C

In Chemical Reaction Engineering—Houston; Weekman, V., et al.;
ACS Symposium Series; American Chemical Society: Washington, DC, 1978.

In Chemical Reaction Engineering—Houston; Weekman, V., et al.;
ACS Symposium Series; American Chemical Society: Washington, DC, 1978.

D

In Chemical Reaction Engineering—Houston; Weekman, V., et al.;
ACS Symposium Series; American Chemical Society: Washington, DC, 1978.

E

In Chemical Reaction Engineering—Houston; Weekman, V., et al.;
ACS Symposium Series; American Chemical Society: Washington, DC, 1978.

F

In Chemical Reaction Engineering—Houston; Weekman, V., et al.;
ACS Symposium Series; American Chemical Society: Washington, DC, 1978.

In Chemical Reaction Engineering—Houston; Weekman, V., et al.;
ACS Symposium Series; American Chemical Society: Washington, DC, 1978.

H

In Chemical Reaction Engineering—Houston; Weekman, V., et al.;
ACS Symposium Series; American Chemical Society: Washington, DC, 1978.

In Chemical Reaction Engineering—Houston; Weekman, V., et al.;
ACS Symposium Series; American Chemical Society: Washington, DC, 1978.

In Chemical Reaction Engineering—Houston; Weekman, V., et al.;
ACS Symposium Series; American Chemical Society: Washington, DC, 1978.

In Chemical Reaction Engineering—Houston; Weekman, V., et al.;
ACS Symposium Series; American Chemical Society: Washington, DC, 1978.

N

O

In Chemical Reaction Engineering—Houston; Weekman, V., et al.;
ACS Symposium Series; American Chemical Society: Washington, DC, 1978.

In Chemical Reaction Engineering—Houston; Weekman, V., et al.;
ACS Symposium Series; American Chemical Society: Washington, DC, 1978.

In Chemical Reaction Engineering—Houston; Weekman, V., et al.;
ACS Symposium Series; American Chemical Society: Washington, DC, 1978.

In Chemical Reaction Engineering—Houston; Weekman, V., et al.;
ACS Symposium Series; American Chemical Society: Washington, DC, 1978.

In Chemical Reaction Engineering—Houston; Weekman, V., et al.;
ACS Symposium Series; American Chemical Society: Washington, DC, 1978.

S

In Chemical Reaction Engineering—Houston; Weekman, V., et al.;
ACS Symposium Series; American Chemical Society: Washington, DC, 1978.

T

In Chemical Reaction Engineering—Houston; Weekman, V., et al.;
ACS Symposium Series; American Chemical Society: Washington, DC, 1978.

In Chemical Reaction Engineering—Houston; Weekman, V., et al.;
ACS Symposium Series; American Chemical Society: Washington, DC, 1978.

In Chemical Reaction Engineering—Houston; Weekman, V., et al.;
ACS Symposium Series; American Chemical Society: Washington, DC, 1978.